

Design and synthesis of small organic molecules to stabilize ALS-associated SOD1 mutants

Dissertation

For the award of the degree

“Doctor rerum naturalium”

of the Georg-August Universität Göttingen

within the doctoral program chemistry

of the Georg-August University School of Science (GAUSS)

submitted by

Robert Heinz Erich Schirmacher

from Münster, Germany

Göttingen, 2021

Thesis Committee

Prof. Franziska Thomas

Institute of Organic Chemistry, Centre for Advanced Materials, University of Heidelberg

Prof. Manuel Alcarazo

Institute of Organic and Biomolecular Chemistry, University of Göttingen

Prof. Ulf Diederichsen

Institute of Organic and Biomolecular Chemistry, University of Göttingen

Members of the Examination Board

Referee:

Prof. Franziska Thomas

Institute of Organic Chemistry, Centre for Advanced Materials, University of Heidelberg

Referee:

Prof. Manuel Alcarazo

Institute of Organic and Biomolecular Chemistry, University of Göttingen

Further members of the Examination Board

Prof. Ulf Diederichsen

Institute of Organic and Biomolecular Chemistry, University of Göttingen

Prof. Kai Tittmann

Department of Molecular Enzymology, University of Göttingen

Dr. Holm Frauendorf

Institute of Organic and Biomolecular Chemistry, University of Göttingen

Prof. Marina Bennati

Max-Planck Institute for Biophysical Chemistry Göttingen

Date of oral examination: 07.05.2021

This work was done under the supervision of Prof. Franziska Thomas and Prof. Ulf Diederichsen at the Center for Biostructural Imaging of Neurodegeneration of the University Medical Center and at the Institute of Organic and Biomolecular Chemistry of the Georg-August University Göttingen. Parts of this thesis were done in close collaboration with Prof. Kai Tittmann and Lisa-Marie Funk at the Department of Molecular Enzymology of the University of Göttingen between May 2016 and March 2021.

Declaration of Authorship

Hereby I declare that I prepared the doctoral thesis entitled “Design and synthesis of small organic molecules to stabilize ALS-associated SOD1 mutants” on my own and with no other sources and aids than quoted.

This dissertation is the result of my own work and includes nothing that is the outcome of work done in collaboration except where specifically indicated in the text. It has not been previously submitted, in part or completely, to any university or institution for any degree, diploma or other qualification.

Göttingen, 26.03.2021

Acknowledgments

I would like to thank my supervisors Prof. Franziska Thomas and Prof. Ulf Diederichsen for the opportunity to write my PhD thesis in their working groups. Their scientific input, generous assistance and fruitful discussions played a major role in the makings of this thesis. Their support will always be appreciated.

Moreover, Prof. Kai Tittmann earned a big thank-you for his outstanding collaboration during this thesis as well as for being part of the examination board. His experience, enthusiasm, and knowledge in the fields of molecular enzymology contributed highly to this project.

I would also like to thank Prof. Manuel Alcarazo for being the second supervisor of this thesis and for being a member of the examination board. Furthermore, I would like to thank Dr. Holm Frauendorf and Prof. Marina Bennati for being members of the examination board.

Special thanks go out to Lisa-Marie Funk for the great work in protein expression, biophysical assays and for answering the many questions regarding proteins throughout the entire duration of this thesis. Your commitment to the collaboration was outstanding. It is often said that without someone's help, the thesis would not have been possible – here it is nothing but the truth.

Furthermore, I would like to thank the entire working groups of Franziska Thomas, Ulf Diederichsen and Kai Tittmann for their general support, the nice atmosphere being around all of you, the refreshing group trips and the many small things that were not self-evident. I will think back of these times and always remember you with a smile.

My bachelor students Daniel Rösch, Jan-Philip Möller and Niklas Roszonwski as well as my lab rotational student Tobias Schmidt and Marvin Lange all did a tremendous job being part of my thesis. Thank you, a lot, for your support and commitment to the hard job of being a chemistry student in the BIN.

I would also like to acknowledge Angela Heinemann and Aoife Neville for being the best secretaries you could ever ask for. No question was left unanswered and your help and knowledge in administrative channels and ways was highly appreciated.

Another big thanks goes to my lab mate Viktoria – I felt that the journey that we both began at the same time would not have been possible without us being the great team that we were. Starting from being able to work nicely together in the lab to helping each other in biophysical questions to attending conferences all over the place – it was a pleasure working with you, especially on Fridays after one or the other Thirstday.

I would also like to thank my family for their years of support and love. This is especially true for the small sub-group of the Schirmachers residing in Göttingen, my wife Anastasiya and my small son Erik.

Contents

1 Abstract	1
2 Background	2
2.1 Amyotrophic Lateral Sclerosis	2
2.1.1 Epidemiology and clinical picture	2
2.1.2 Pathophysiology of ALS	3
2.1.3 Treatment of ALS – state of the art	6
2.2 Superoxide Dismutase 1 (SOD1)	8
2.3 Therapeutic approaches for SOD1 related ALS	13
2.4. Fluorescence Anisotropy	18
2.5 Microscale Thermophoresis (MST)	20
2.6 Isothermal Titration Calorimetry (ITC)	22
3 Aim of the work.....	24
4 Results and discussion	25
4.1 <i>In silico</i> studies and properties of the Lead Structures	25
4.1.1 Results for LS1	30
4.1.2 Results for LS2	33
4.1.3 Results for LS3	35
4.2 Synthesis of LS1	38
4.2.1 Synthesis of the molecular library based on the carboxylic acids of LS1	38
4.2.2 Synthesis of the molecular library based on LS1	45
4.2.3 HFIP in the Paal-Knorr synthesis of pyrroles.....	50
4.2.4 HFIP in the Paal-Knorr synthesis of furans and thiophenes.....	54
4.3 Synthesis of LS2	57
4.3.1 Sequence 1	58
4.3.2 Sequence 2	59
4.3.3 Direct approach for the disubstitution of LS2	64
4.3.4 Synthesis towards a colorimetric assay for binding observation between LS2 and SOD1	65
4.3.5 Summary of the advances towards LS2	67
4.4 Synthesis of the molecular library based on LS3	68
4.4.1 The fluorinated LS3	68
4.4.2 The non-fluorinated LS3	72
4.5 UV/VIS- and fluorescence properties of the Lead Structures	75
4.5.1 Optical properties of LS1	76
4.5.2 Optical properties of LS3	80
4.6 Protein Expression	82
4.7 Activity analysis	84

4.8 Binding studies of LS1 and LS3 to SOD1	87
4.8.1 Fluorescence Anisotropy of the LS1_C library	87
4.8.2 MST binding studies of LS1 and LS3	90
4.8.2.1 MST results for LS1	90
4.8.2.2 MST results for LS2	94
4.8.2.3 MST results for LS3	95
4.8.3 Results of ITC measurements.....	98
4.9 Protein crystallization.....	100
5 Summary and outlook.....	103
6. Experimental part	109
6.1 Ligand synthesis.....	109
6.1.1 Analytics.....	109
6.1.2 Synthesis procedures.....	111
6.1.2.1 Synthesis of the final ligands 1 – 24.....	111
6.1.2.2 Syntheses for chapter 4.2	142
6.1.2.3 Syntheses for chapter 4.3	196
6.1.2.4 Syntheses for chapter 4.4	208
6.2 Biological methods	210
6.2.1 Materials.....	210
6.2.2 Devices	212
6.2.3 Molecular biology protocols.....	214
6.2.3.1 Plasmid transformation	214
6.2.3.2 Plasmid DNA isolation.....	215
6.2.3.3 Determination of DNA concentration.....	215
6.2.3.4 DNA sequencing	215
6.2.3.5 PCR (Polymerase Chain Reaction).....	215
6.2.3.6 Horizontal agarose gel electrophoresis	216
6.2.4 Protein expression	216
6.2.4.1 hSOD1 wt and mutant expression	216
6.2.4.2 hSOD1 Purification	216
6.2.4.3 SDS-page analysis	217
6.2.4.4 Determination of protein concentration	217
6.2.4.5 Cofactor reconstitution	218
6.2.4.6 Activity assays	218
6.2.4.7 Size exclusion chromatography (SEC)	218
6.2.4.8 X-ray crystallography	219
6.3 Biophysical assays	220
6.3.1 UV/VIS and fluorescence measurements.....	220
6.3.2 Fluorescence Anisotropy.....	220

6.3.3 Microscale thermophoresis (MST)	221
6.3.4 Isothermal Titration Calorimetry (ITC)	223
6.4 Protein structure and ligand structure preparation for <i>in silico</i> screening	223
7 Bibliography	225
8 Appendix.....	233
8.1 Analytics	235
8.1.1 NMR and IR spectra.....	235
8.1.2 Mass spectra.....	325

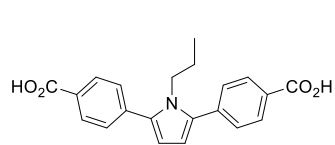
List of abbreviations and acronyms

5-HT _{2A}	5-hydroxytryptamine receptor 2A
AA	amino acid
Ac ₂ O	acetic anhydride
AcCl	acetyl chloride
ALS	Amyotrophic Lateral Sclerosis
Boc	tert-Butyloxycarbonyl
CuATSM	diacetylbis(N(4)-methylthiosemicarbazonato) copper II
CyPF- ^t Bu	(R)-1-[(S _p)-2-(Dicyclohexylphosphino)-ferrocenyl]ethyldi- <i>tert</i> -butylphosphin
DBU	diazabicycloundecen
DCC	(N,N′)-dicyclohexylcarbodiimide
DCM	dichloromethane
DMAP	4-dimethylaminopyridine
DMB	(3,3′)-dimethylbutyl
DMF	dimethylformamide
DMSO	dimethylsulfoxide
DTME	dithio-bis-maleimidoethane
DTNB	5,5′-dithiobis-(2-nitrobenzoic acid)
EDTA	ethylenediaminetetraacetic acid
equiv	equivalents
Et ₂ O	diethyl ether
Et ₃ N	triethylamine
EtOAc	ethyl acetate
EtOH	ethanol
fALS	familiar Amyotrophic Lateral Sclerosis
hCCs	Cytochrome c-type heme lyase
HEPES	(4-(2-hydroxyethyl)-1-piperazineethanesulfonic acid)
HFIP	1,1,1,3,3,3-hexafluoroisopropanol
HMDS	bis(trimethylsilyl)amine

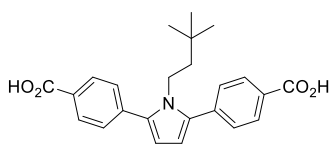
HPLC	high performance liquid chromatography
HR-MS	high resolution mass spectrometry
IC ₅₀	half maximal inhibitory concentration
iPrOH	isopropanol
IPTG	Isopropyl β-d-1-thiogalactopyranoside
IR	infrared
ITC	isothermal titration calorimetry
m/z	mass-to-charge ratio
MALS	multi-angle light scattering
MCH	methylcyclohexyl
MeCN	acetonitrile
MeLi	methyllithium
MeOH	methanol
MND	motor neuron disease
MST	microscale thermophoresis
MTBE	methyl <i>tert</i> -butyl ether
NaOAc	sodium acetate
nBuLi	n-butyllithium
NMR	nuclear magnetic resonance
PCR	polymerase chain reaction
PEG	poly(ethylene)glycol
ROS	reactive oxygen species
rpm	rounds per minute
sALS	sporadic Amyotrophic Lateral Sclerosis
SDS	sodium dodecylsulfate
SEC	size exclusion chromatography
SOD1	superoxide dismutase 1
TAE	Tris-acetate-EDTA
^t BuONO	tert-butyl nitrite
TCSPC	time correlated single photon counting

TFA	trifluoroacetic acid
TFB	4,4,4-trifluorobutyl
TFE	1,1,1-trifluoroethanol
THF	tetrahydrofuran
TLC	thin layer chromatography
TMSBr	trimethylsilyl bromide
TNB	2-nitro-5-thiobenzoate
Tris	tris(hydroxymethyl)aminoethan
TrtSH	triphenylmethanethiol
Xantphos	4,5-bis(diphenylphosphino)-9,9-dimethylxanthene
δ	chemical shift (NMR)

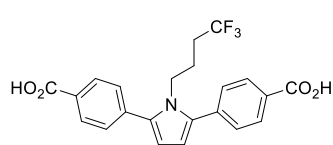
Compound index



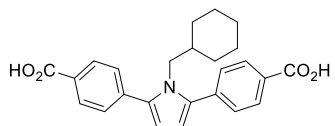
1
LS1_PRO_C



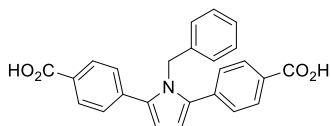
2
LS1_DMB_C



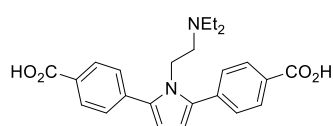
3
LS1_TFB_C



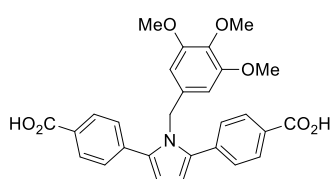
4
LS1_MCH_C



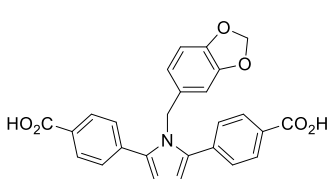
5
LS1_BN_C



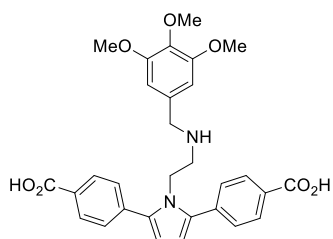
6
LS1_NEt_C



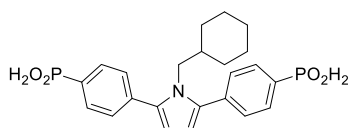
7
LS1_TMP_C



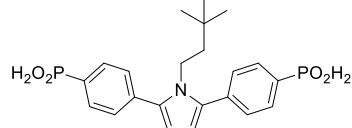
8
LS1_PIP_C



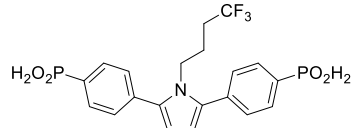
9
LS1_TMPN_C



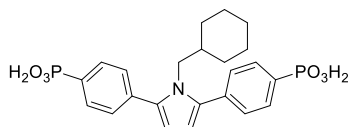
10
LS1_MCH_I



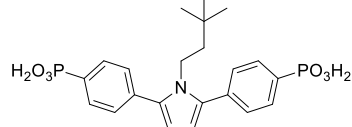
11
LS1_DMB_I



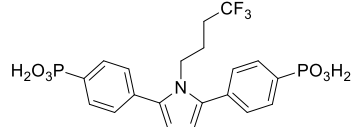
12
LS1_TFB_I



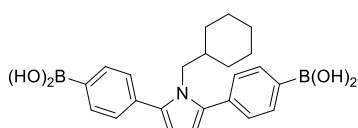
13
LS1_MCH_O



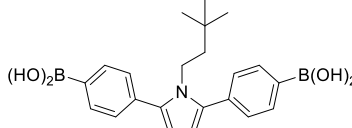
14
LS1_DMB_O



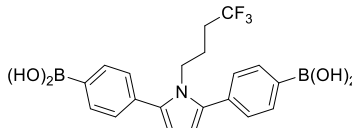
15
LS1_TFB_O



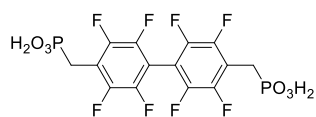
16
LS1_MCH_B



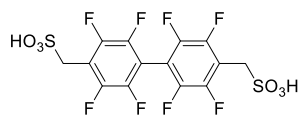
17
LS1_DMB_B



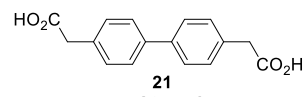
18
LS1_TFB_B



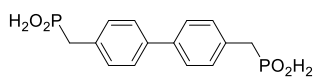
19
LS3_F_O



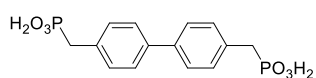
20
LS3_F_S



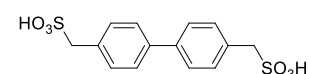
21
LS3_H_C



22
LS3_H_I



23
LS3_H_O



24
LS3_H_S

1 Abstract

Amyotrophic Lateral Sclerosis is a globally occurring neurodegenerative disease with serious implications for the patient's life as well as imposing a heavy economic burden both on the affected individuals and society. Due to higher exposure to risk factors and an increasing lifespan, total costs of Amyotrophic Lateral Sclerosis are expected to rise drastically in the near future. Since there are no causal treatments known and currently available medications only alleviate symptoms, more research in interdisciplinary fields of science is necessary.

This thesis focuses on the familiar type of Amyotrophic Lateral Sclerosis, more specifically the disease-induced aggregation of the well-studied protein Superoxide Dismutase 1, whose mutations account for 10-20 % of all ALS incidents in familiar Amyotrophic Lateral Sclerosis. Dissociation of SOD1 into aggregation prone monomers is currently viewed as one of the most important triggers for neuronal death. It is envisaged to stabilize the homodimer structure of the protein with a small molecule through an affinity-based approach in order to prevent aggregation and to restore the catalytic activity of pathological mutants. Using *in silico* design, several lead structures are elaborated as potential lead structures for protein-ligand binding. Upon rational variation of these structures, a small molecular library is synthesized to verify the computational results with biophysical techniques. After expression and purification of the protein, methods such as Isothermal Titration Calorimetry, Fluorescence Anisotropy, Microscale Thermophoresis as well as X-Ray Diffraction of protein-ligand-complex crystals are employed to obtain information about the biophysical properties of the synthesized ligands. It is demonstrated that some of the aforementioned small molecules show affinity-based binding to the protein of interest. Facile synthetic pathways to these molecules and strategies for their variation are outlined.

The significance of this work is that it expounds a rational approach for the development of novel, structurally diverse small molecules that exhibit the ability to bind the Superoxide Dismutase 1 in an affinity-based binding mode.

2 Background

2.1 Amyotrophic Lateral Sclerosis

2.1.1 Epidemiology and clinical picture

Amyotrophic Lateral Sclerosis (ALS), also known as motor neuron disease (MND) or Lou Gehrig`s disease is a fatal neurodegenerative disease that affects motor neurons in the spinal cord, the brain, and the motor cortex.^[1] It was first described in the 19th century by CHARCOT, a French neurologist.^[2] The annual incidence of ALS is 1 to 3 per 100.000 whereas the annual prevalence amounts to 3 to 8 per 100.000, implying that ALS is a rare neurodegenerative disease with a late onset (56 to 58 years).^[3,4] It is estimated that around 150.000 patients suffer from this disease, which makes ALS the third most common neurodegenerative disease. The gender ratio is approximately 1.5:1 in favor of men.^[5,6]

ALS has a very complex clinical picture, especially in the early stages of the disease, since muscle degeneration is one of the first symptoms that can manifest itself in a variety of consequences. If the first motor neuron is affected, spastic atrophies such as gait disorder, decreased dexterity or swallowing problems can be observed.^{[7][8]} Damage to the second motor neuron typically leads to muscle atrophy, cramps and ultimately to paralysis of arms and legs. When these symptoms start in the arms and/or legs, it is referred to as the "limb onset" that makes up for approx. 58-80% of all ALS cases. Speech and swallowing difficulties as the primary symptom are labeled as "bulbar onset", which adds up to approx. 28% of all cases. The bulbar onset is connected to shorter median survival rates than the limb-onset.^[4,6,9,10] Eventually, both of these pathways lead to serious impairments of patients due to them being unable to walk, stand or perform the most basic handwork. Weakening of the respiratory muscles leads to pneumonia, which is the prevailing reason for death of the affected persons. The median survival time is around 3 to 5 years from diagnosis, although a special form of ALS exists, the so-called chronically juvenile form that has a much longer survival time.^[11] Due to the symptoms being very generic and non-specific, the diagnosis is often made months or years after the actual disease onset.^[10]

2.1.2 Pathophysiology of ALS

ALS can be divided into two major groups, sporadic ALS (sALS) and familial ALS (fALS) (Figure 2.1.2-1).^[11–13] These two cases cannot be distinguished by molecular genetic techniques since their clinical picture is very similar. The exact cause for ALS is not known as of today, but it is generally accepted that genetic and environmental factors play a huge role in the course of the disease, no matter whether sALS or fALS is present.^[7] It is worth noting that genetic factors are much better understood than environmental factors, the consequence being that fALS can be described much more precisely than sALS.

Environmental factors that are being discussed controversially are smoking, exposure to air pollution, head injury, physical activity and sports as well as chronic exposure to certain substances such as lead, other heavy metals, or pesticides.^[14] The list is not exhaustive, though specific personal characteristics might be as relevant as the known environmental factors. In case of fALS, the autosomal dominant pathway of inheritance mainly consists of mutations in the following genes: *tardbp* (5%), *c9orf72*(40%), *vapb* (3%), *fus* (5%), and *sod1* (20%). A large contribution is attributed to unknown gene factors that could not be identified yet.^[13]

The sporadic form of ALS is significantly less explored in terms of genetic factors. Only 11% of all cases can be attributed to known genes, the majority of them are also linked to fALS. The vast majority of sALS-affected genes are unknown and their investigation will provide much needed knowledge towards potential treatment of ALS.^[13,15]

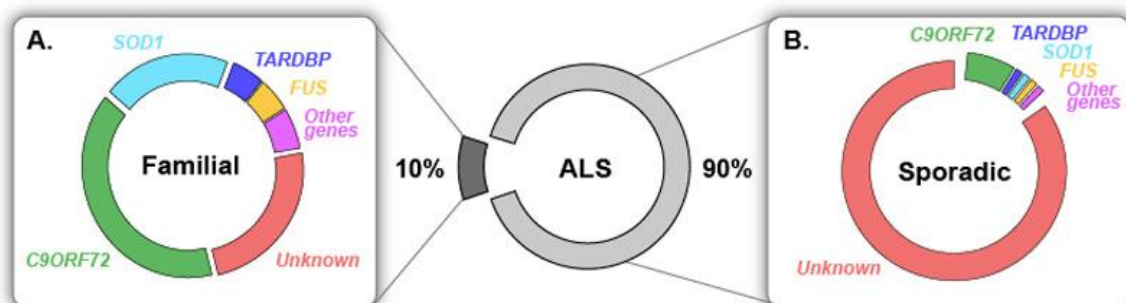


Figure 2.1.2-1. Etiology of ALS and the most common genetic factors for fALS (A) and sALS (B).^[13]

Copyright © Swiss Medical Weekly, CC BY 4.0 license

The interactions between symptoms, clinical pictures, gene mutations and their subsequent harmful effects on eukaryotic cells form a complex picture that is not fully understood so far. An overview of the mentioned mutations and their consequences is shown in Figure 2.1.2-2.^[15]

The discussed mutations lead, amongst other things, to a pathological accumulation of misfolded proteins such as TDP-43, FUS or SOD1.^[16–18] The protein degradation pathways are often malfunctional, leading to problems in proteostasis for a number of affected proteins.^[19] Protein clearance mechanisms are commonly compromised as well. Furthermore, transport between the nucleus and cytoplasm of eukaryotic cells can be affected, mainly caused by mutations in *c9orf72* and *gle1* genes.^[20,21] Mutations might also impair vesicle transport and axonal transport via disturbance of the cytoskeletal structure of the cell and its surrounding compartments, including oligodendrocytes. These mutations occur in a plethora of different genes; however, they are very rare and only make up for a small amount of ALS incidences. Interference with RNA and DNA homeostasis can occur *via* RNA-binding mutants, vitiation of repair mechanisms (especially for DNA) and altering of RNA metabolism. Moreover, transcription and translation processes can be disturbed. These changes in RNA/DNA behavior can be subsumed into one of the major factors of the ALS-related pathophysiological mechanism.^[22]

There are also mutations in the *ubqln2*-gene, attributed to the X-chromosomal inheritance that affect the degradation of ubiquitinated proteins leading to aggregates and neuronal damage.^[23] Furthermore, increased oxidative stress due to mitochondrial dysfunctions seems to play a role in fALS as well as sALS.^[24] A genetic factor that might be pertinent for both forms of ALS is the regulation of the glutamate homeostasis, which is dependent on a large number of genes, neurotransmitters and proteins.^[25] A reduced capacity of the glutamate transporter EAAT2 leads to an altered glutamate concentration on the NMDA receptors (N-Methyl-D-Aspartate) and AMPA receptors (Amino-3-hydroxy-5-methyl-4-isoxazolpropionic acid), resulting in excitotoxicity, overstimulation and ultimately in an efflux of calcium ions into the neuron, which is a risk factor for oxidative stress. The corresponding gene mutations can be found in ALS patients, though not everyone is affected by them.^[12,26] Mutations in SOD1 can also contribute to mitochondrial dysfunction; it is believed that these effects stem from protein aggregates rather than loss of enzymatic activity.^[27] Neuroinflammation,

affecting microglia, astrocytes, lymphocytes and macrophages has also been linked to ALS and various putative drugs are tested in clinical trials all over the world (Phase I to III).^[28]

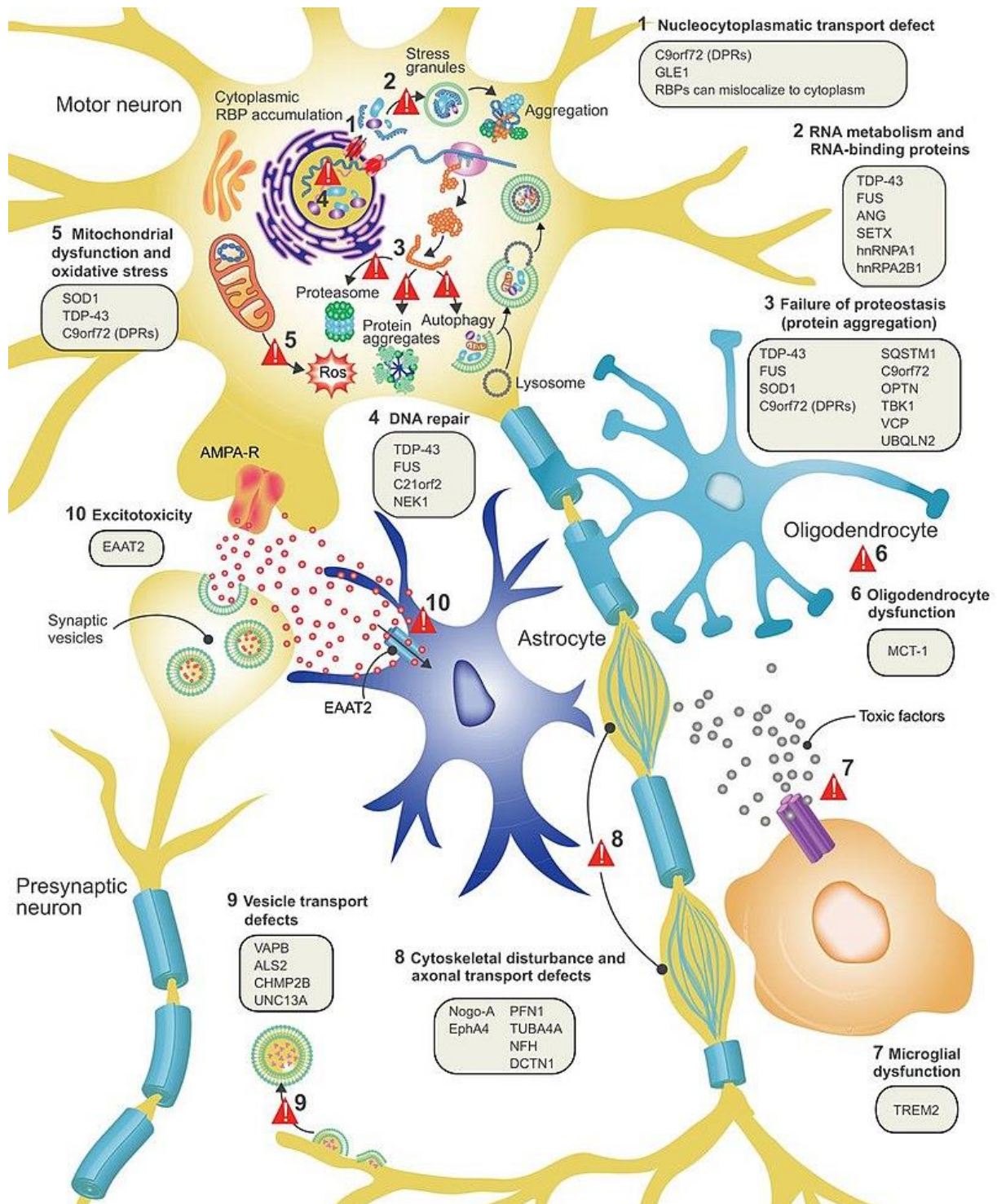


Figure 2.1.2-2. Overview of the most abundant gene mutations in ALS, their pathology and the overall proposed disease mechanisms.^[15] Copyright © Am. Lat. Scler., CC BY 4.0 license.

2.1.3 Treatment of ALS – state of the art

As of 2021, ALS cannot be cured and complementary treatments need to be used, which can be divided into two groups: medicinal and non-drug therapies.

Medicinal therapies

There are only two approved drugs available to treat symptoms of ALS: The glutamate-dependant sodium channel blocking-agent Riluzole, which was approved in 1995 as the first drug against ALS, and the antioxidant radical scavenger Edaravone, which was approved in the US and Japan in 2017.^{[29][30]}

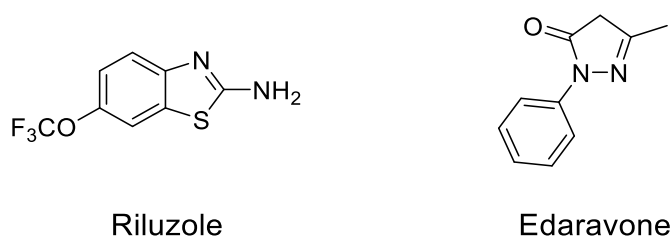


Figure 2.1.3-1. Structures of Riluzole and Edaravone.

Both of these have in common that they do not stop the progress of ALS but have the potential to slow it down significantly. Riluzole does that by blocking TTX-sensitive sodium channels, which can be associated with damage done to neurons while also increasing glutamate uptake, accelerating glutamate clearance from the synapse, as well as preventing presynaptic glutamate release.^[31] Whether the sodium channel blocking capacity or the intervention in the glutamate homeostasis is the prevailing factor for the retardation of ALS is currently under investigation. The mechanism by which Edaravone is active in ALS patients is unknown. Edaravone is known for its antioxidant potential and could possibly reduce oxidative stress in ALS patients, which is a known factor for neuronal death. Phase III clinical trials failed in Europe while being successful in Japan, this might be due to genetic variations between European and Asian population.

Recently a combination of two different drugs called AMX0035, consisting of sodium phenylbutyrate (PB) and tauroursodeoxycholic acid (TUDCA) was screened in a Phase II clinical trial with promising results.^[32] PB is a chemical chaperone, which accumulates misfolded or aggregated proteins, resulting in reduced neuronal stress. Furthermore, it is able to inhibit the histone deacetylase, resulting in an epigenetical regulation of gene expression.^[33] These two factors lead to a decrease in neuronal

death. TUDCA on the other hand is an antioxidant with neuroprotective properties that inhibits mitochondria apoptosis, decreases the amount of ROS and prevents neuronal death caused by oxidative stress.^[34] It is also well known from traditional Chinese medicine and therefore considered a safe substance with limited side effects. Masitinib, an inhibitor of the tyrosine-kinase, is screened in a Phase III clinical trial for the treatment of ALS since 2020 after a failed Phase III clinical trial in 2017.^[35]

More than 50 different substances have been proposed as a putative drug for the treatment of ALS since 1995. However, no substance was able to provide a cure for this disease, which reemphasizes its complexity and heterogeneity in symptoms, pathophysiology, and genetics.

Another approach that is discussed in the literature is a targeted gene therapy, which is being tested in clinical trials. The general concept of curing a neurodegenerative disease by means of a gene therapy was proven by the use of Zolgensma[®], a viral vector-mediated drug against Spinal Muscular Atrophy (SMA).^[36]

Apart from the drugs already discussed, substances to relieve the typical symptoms of ALS are also commonly used for the treatment of patients. Muscle relaxants from the benzodiazepine group (diazepam, clonazepam and others) or anticonvulsants such as gabapentin see frequent use. Swallowing problems that are one of the earliest symptoms of ALS can lead to pooling of saliva, which requires tricyclic antidepressiva or muscarin-receptor antagonists in order to improve the physical conditions of the patient.

Non-drug therapies

Another essential part of ALS treatment are the non-drug therapies that need to be started immediately after onset of the disease. Amongst them are physiotherapy, occupational therapies, changes in lifestyle, speech and breathing therapies and the usage of machines such as ventilators, wheelchairs, bracers or feeding tubes.

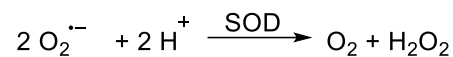
The result of these drastic courses of action that need to be taken is a heavy financial burden that is implied on the individual patient as well as on the society as a whole. ALS is considered one of the most cost intensive neurological diseases, even considering the low prevalence it still contributes to a high socioeconomic burden.

Numbers for Germany were collected in a study from 2020, which implies that up to 520.000.000 € need to be expended to fulfill the needs of ALS patients yearly.^[37] Since the most important risk factor for ALS is the age of an individual, numbers are expected to rise dramatically within the near future. This means that new medications and better methods for non-drug therapies are necessary.

2.2 Superoxide Dismutase 1 (SOD1)

Mutations in the gene that encodes for the protein Superoxide Dismutase 1 have been found in around 20% of all fALS cases as was discussed already.^[6] Since this is the protein of interest in this work, the different forms of humans SOD1 will be explained and its structure, its mutants, and importance for ALS will be depicted in this subchapter.

SOD1 is an ubiquitously expressed protein of many organisms that metabolizes oxygen and catalyzes the disproportionation of superoxide radicals into oxygen and hydrogen peroxide according to the following equation:



Superoxide radicals belong to the group of reactive oxygen species (ROS) and are often very harmful to cells; hence, the importance of SOD1 for the reduction of oxidative stress is highlighted.

Three different forms of SOD exist in humans: The mitochondrial manganese-based SOD (Mn-SOD), the extracellular SOD (EC-SOD) and the copper/zinc-containing SOD (Cu/Zn-SOD), which is located in the cytosol (this specific protein is also called SOD1).^{[38][39]} This protein was discovered in 1968 by McCord and Fridovich; this was considered a major breakthrough in the biochemistry of reactive oxygen species and oxygen metabolism in eukaryotic cells.^[40] Different forms of SOD have since been identified in almost every single aerobic organism, highlighting its importance for cell homeostasis.

The mechanism of the degradation of superoxide radicals into hydrogen peroxide and oxygen is also referred to as a “ping-pong mechanism” and is depicted in Figure 2.2-1.^[41,42]

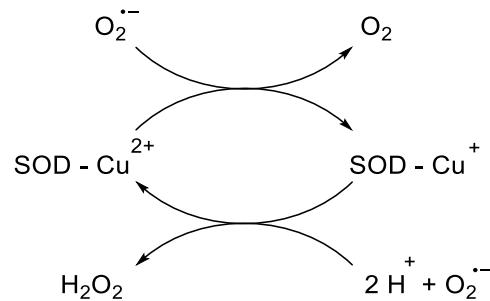


Figure 2.2-1. Ping-pong mechanism: The reactive center of the protein (the Cu^{2+} ion) is reduced to Cu^+ under simultaneous oxidation of the superoxide radical to hydrogen peroxide and reoxidation of the copper ion.

The structure of SOD1 and its most important properties are depicted in Figure 2.2-2.

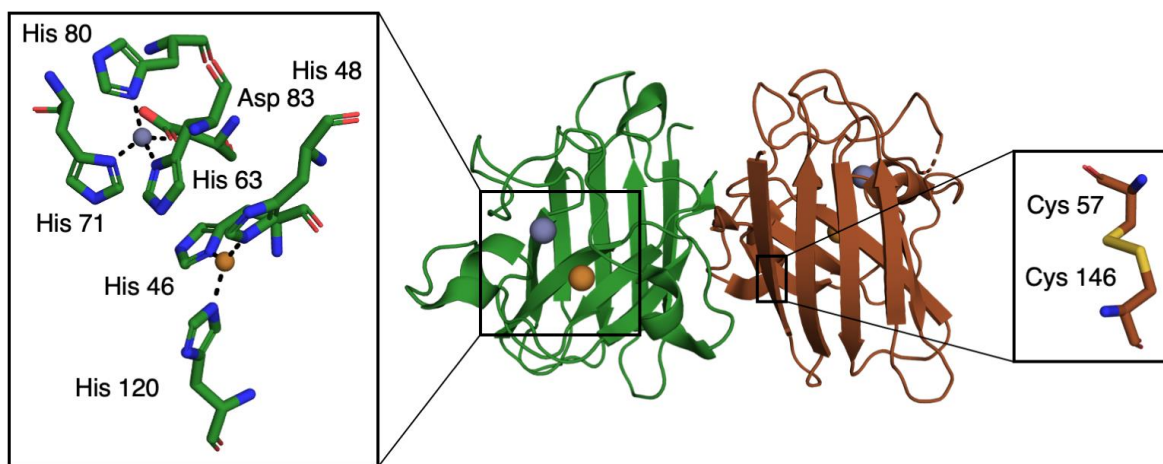


Figure 2.2-2: Structure of wt hSOD1. *Left:* metal binding sites in a SOD1 monomer with Cu^{2+} (grey) and Zn^{2+} (orange). *Middle:* Ribbon model of the SOD1 dimer. *Right:* Intra-monomeric disulfide bridge between Cys₅₇ and Cys₁₄₆. PDB-code: 2C9U. Picture taken from Niklas van den Bergh.

The fully metallized protein has a weight of 32 kDa and consists of two monomers that are connected through a large dimer interface that exhibits strong hydrophobic interactions. Each monomer consists of a beta-barrel structure with two metal binding sites. The Zn^{2+} ion plays a major role for the structural integrity of the monomer and is coordinated by three histidine and one asparagine residue, whereas the Cu^{2+} ion is coordinated by four histidine residues and is responsible for the catalytic activity of the protein.^[43] These two metals are connected *via* His₆₃ in the oxidized state. An

intramolecular disulfide bridge between Cys₅₇ and Cys₁₄₆ stabilizes the beta-sheet structure.^[44] Due to these structural properties, SOD1 is one of the most stable proteins known in the literature with a melting temperature of 85 – 95 °C and a dissociation constant of $K_d = 10 \text{ nM}$.^{[45][46]} The region between AA 122 and 143 is called the electrostatic loop, contributing to the active center of the protein. The zinc-binding region between AA 49 and 84 is called the zinc-loop and enhances the catalytic activity through a small canal that leads to the active center of the protein. The transit of negatively charged molecules is favored while preventing larger structures to interfere. The result is a very large enzymatic activity of around $10^9 \text{ M}^{-1}\text{s}^{-1}$ and the kinetics can be described as diffusion-controlled. ^[47]

More than 200 mutations – largely missense mutations, stop-codon and depletion mutations – are known for SOD1.^[48] The most common mutations for SOD1 are A4V, I113T and G93A.^[49] It is unclear whether every single mutation leads to ALS or whether a combination of mutations is required. Some of these mutations also retain their catalytic activity or show only a small decrease in their efficiency. This is why the loss of function of SOD1 is not attributed to ALS but more so a toxic gain of function, which could also be substantiated by animal trials in 1998.^{[50][51]} This undesirable gain of function can be rationalized by looking at the complex post-translational maturation of SOD1 that mainly consists of the following steps: N-terminal acetylation, transient complex formation with hCCS, chaperone-dependent Zn and Cu insertion, formation of the disulfide bridge between Cys₅₇ and Cys₁₄₆ and following homodimerization. Mistakes at any of these steps can either lead to misfolded SOD1 or promote the dissociation of the stable dimer into aggregation-prone monomers.^{[52][53]}

Figure 2.2-3 presents an overview about the most common ALS-related mutations of SOD1 and the affected regions of the protein.^[49] It is noteworthy that mutations can occur in every domain of the protein, i.e. on the dimer interface, the electrostatic loop, the zinc loop or in the beta-barrel structure. No correlation between the affected region and the consequences of different mutations can be observed, but the two most common mutations A4V and I113T are both located at the region of the dimer interface. The median onset of both mutations is comparable but the survival rate of I113T is more than three times higher than the survival rate of A4V. This means that A4V is one of the most deadly mutations of SOD1. Weakening of the dimer interface in the region of the respective mutation can be observed for both A4V and I113T, leading to rapid

dissociation of the homodimer into aggregation prone monomers due to weakening of attractive van-der-Waals interactions. Other mutations such as H46R or G37R have a significantly lower onset age but result in a drastically elevated survival time of around 17 years. Some mutations also occur in the sALS type, e.g. I113T. Most of the known mutations decrease the structural integrity of the protein, leading to, amongst other things, undesired changes in conformation. This is especially true for mutations near the metal binding sites such as H46R or G85R, where changes in the beta-barrel structure can be observed without altering the catalytic activity of the protein.^[54]

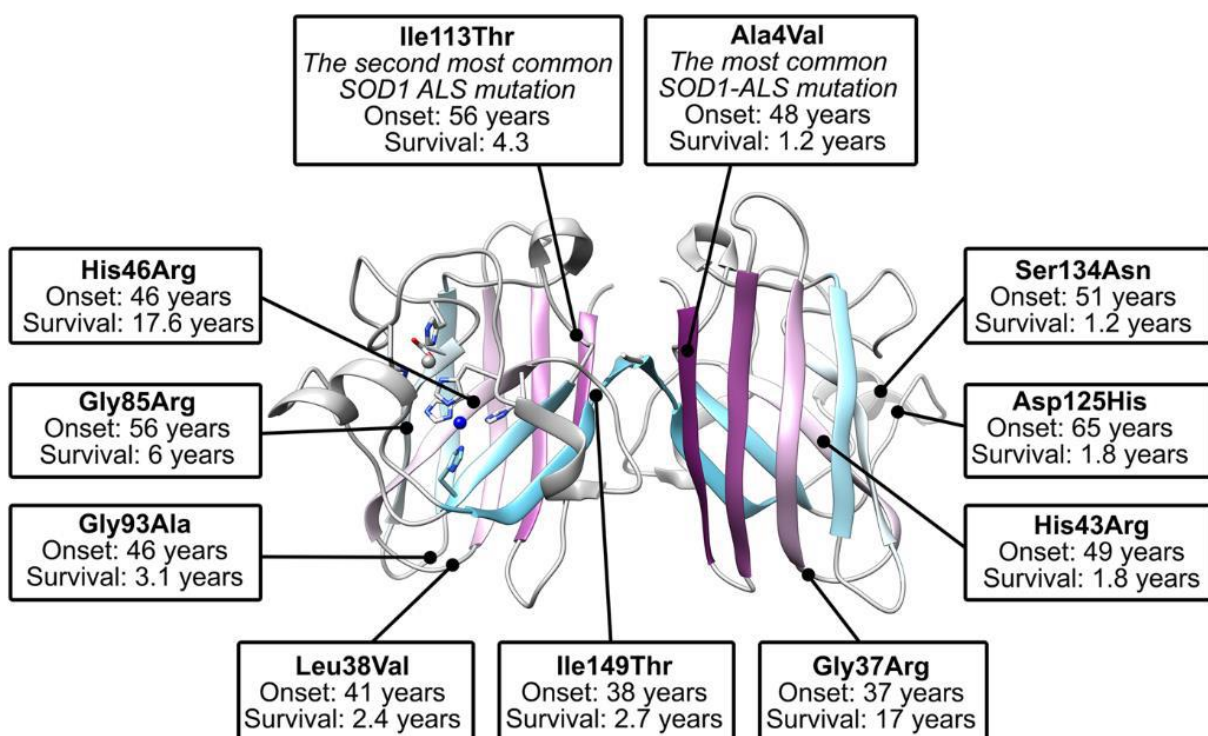


Figure 2.2-3. Overview of ALS-related SOD1 mutants.^[49] Copyright © The authors.

The commonly discussed aggregation pathways are depicted in Figure 2.2-4.

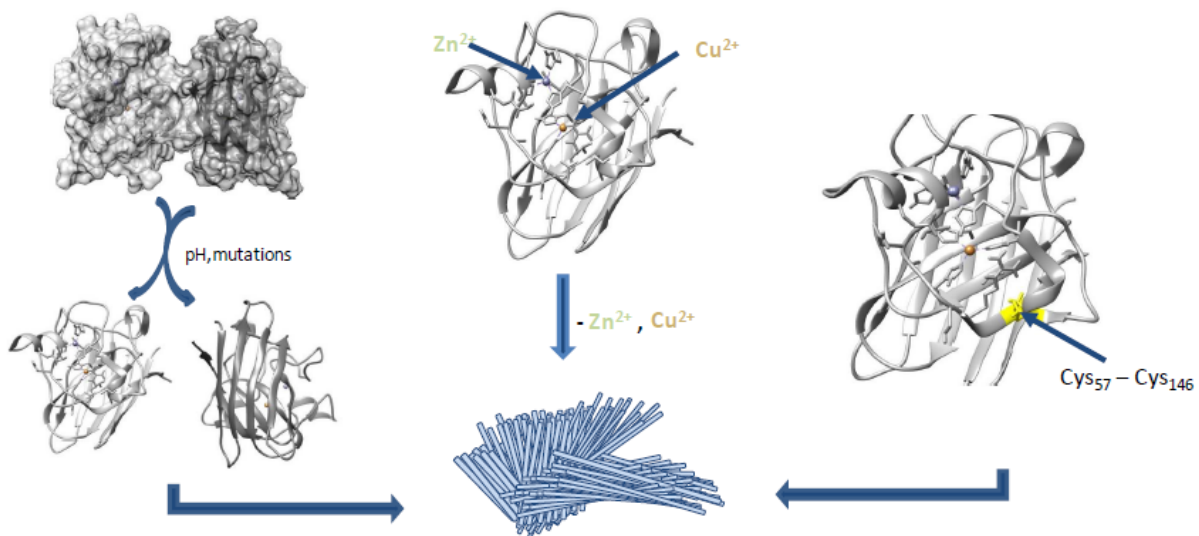


Figure 2.2-4. Aggregation pathways of SOD1. *Left:* Point mutations or a change in pH can lead to a smaller dimer interface with weaker hydrophobic interactions, leading to the dissociation of the dimer. *Middle:* Loss of metal ions due to weaker binding of the mutants through changes in complex geometry are believed to destabilize the quaternary structure. The resulting apo enzyme is prone to aggregation. *Right:* Reduction of the intra-monomeric disulfide bridge or mistakes in the maturation process of SOD1 are attributed with loss of stability of the dimer.

As was already described, aggregates seem to have a major impact in SOD1-related ALS. These soluble aggregates tend to form larger, insoluble amorphous (observed in fALS) or fibrilic structures that can interfere with a plethora of different components of the cell.^[55–57] These structures are similar to amyloid aggregates observed in other neurodegenerative diseases such as Alzheimer’s disease or frontotemporal dementia. Point mutations are generally believed to have an influence on the overall stability of a protein; therefore, they might be causing the formation of aggregates. A second discussed pathway is the lack of zinc and copper ions, resulting in a much less stable apo enzyme that is prone to aggregation.^[58–60] Many causes exist for the loss of metals such as faulty homeostasis, malfunction of chaperones or mutations in the respective metal binding sites. A third origin discussed for the aggregation of SOD1 is the reduction of the intramolecular disulfide bridge that results in a flexible zinc loop, significantly weakening the beta-barrel structure.^[61] In turn, a larger part of the protein is exposed to solvents and ROS, furnishing the aggregation of mutant SOD1. Effects of disulfide reduction on the melting temperature were also observed in the literature.^[62]

2.3 Therapeutic approaches for SOD1 related ALS

As previously depicted, one of the key factors in fALS is the dissociation of the SOD1-dimer into aggregation prone monomers that ultimately build up prion like structures.^[56,63,64] These aggregates have the potential to interfere with a plethora of different processes in the cell, which can lead to apoptosis, disturbance of homeostasis or other gain of toxic functions. A selection of possible harmful influences is shown in Figure 2.3-1.

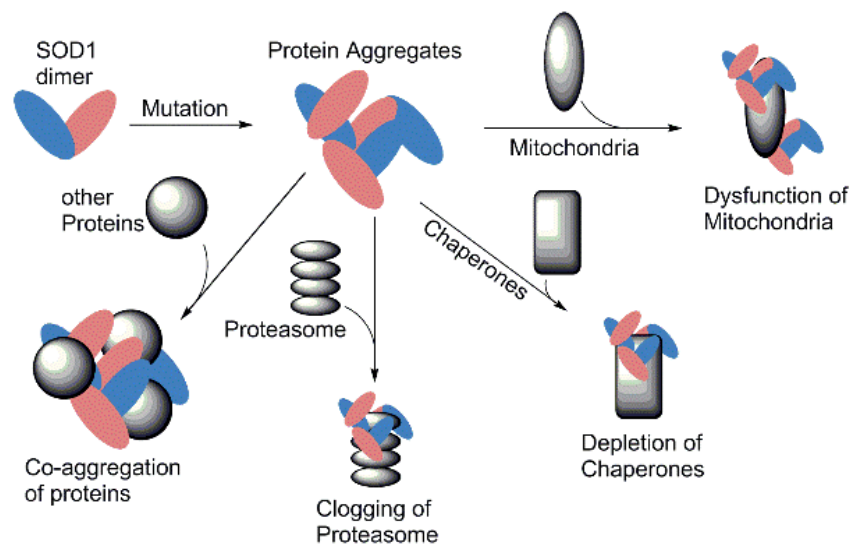


Figure 2.3-1. Harmful effects of SOD1-related aggregates in the cell.^{[65][66][67]}

The regulation of metal levels is a critical factor in protein maturation, folding and for its activity. Therefore, mutations that interfere with these processes are commonly found in ALS (e.g. G93A) and can be partially counteracted by increased metal intake. This is especially true for copper ions, since several mutants show a significantly decreased potential to interact with the SOD1-dependant human copper chaperone hCCS, leading to a decreased copper level and lower activity. Recent studies and clinical trials found a beneficial effect of metallated ATSM (CuATSM) for mutations that do not interfere in the metal-binding regions (e.g. G93A or G37R).^[68] Positive effects on the disease onset and progression were confirmed in mice and led to an increase in the survival rate of about 18 months compared to the placebo group.^[69,70] The molecular mechanisms are unclear; it is assumed that CuATSM increases metalation levels of unmetalated SOD1, thus preventing aggregation processes.

BIANCI *et al.* used cisplatin, a common anti-cancer drug, as a tool to prevent aggregation and to redissolve SOD1 oligomers and aggregates. Crystal structures indicated that each Cys₁₁₁ residue shows a high binding affinity to a cisplatin molecule, therefore preventing intermolecular disulfide bridges. It is noteworthy that binding of cisplatin at the dimer interface does not hamper the activity of the metalated protein. These findings could be validated by thermal shift assays, which showed a significant increase in the melting temperature of the protein.^[71] However, it was observed that cisplatin and other drug-like molecules that target Cys₁₁₁ covalently inhibit the maturation process by preventing interactions between SOD1 and its natural chaperone.^[72]

In 2004, LANSBURY *et al.* reported that an intersubunit disulfide bridge between two non-natural Cys₁₄₈ residues in each monomer was able to stabilize the monomer towards inhibition of dissociation (Figure 2.3-2). In order to realize this approach a valine moiety needed to be exchanged for a cysteine in both monomers by means of mutagenesis. The final protein was much more stable compared to wt hSOD1 *in vitro* as was shown by thermal shift studies.^[63]

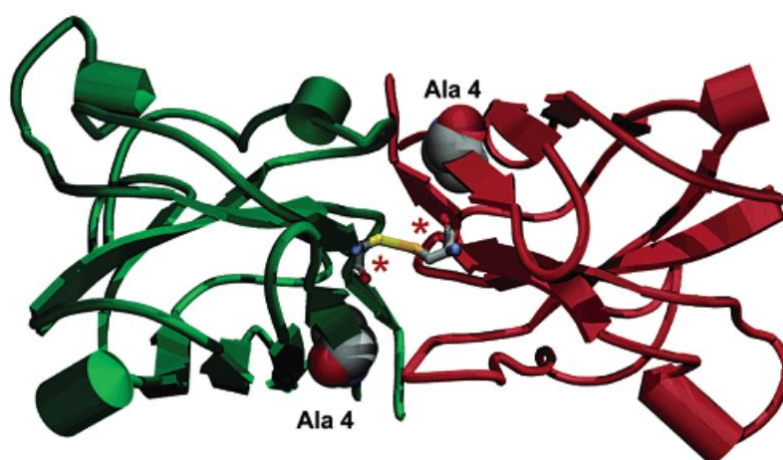


Figure 2.3-2. Ribbon style visualization of wt hSOD1 with the introduced disulfide bridge. Ala₄ is shown in space-filling mode and the red dot marks the original position of the AA that was mutagenized. Reprinted with permission from ^[63]© 2004 Am. Chem. Soc.

One year later, the same group discovered a new potential target area on the protein for binding to small molecules and over one million structures were tested for their suitability *in silico*. 20 different structures were identified to stabilize the protein when exposed to aggregation inducing conditions (Figure 2.3-3). The binding cavity was close to the already used Val₁₄₈ consisting of a hydrophobic surface and had the

potential to form hydrogen bonds with the surrounding AAs.^[73] This was one of the first approaches that made use of the binding affinity of a small molecule to a specific area of the protein. Mutagenesis of the surrounding AAs confirmed the importance of Val₇ and Val₁₄₈ in that those mutants did not benefit from the identified structures in terms of aggregation. Furthermore, it was deduced that the identified ligands needed to comprise of at least one aromatic moiety to bind to the protein in an affinity-based manner. Later the same group expanded their *in silico* studies to over 2 million substrates and presented an improved compound list. These molecules had higher binding affinities and showed an affinity for SOD1 in human blood plasma.^[74]

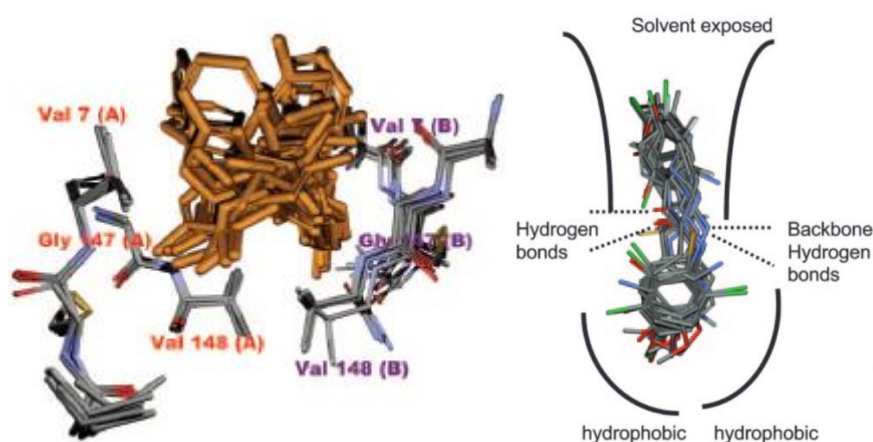


Figure 2.3-3. Left: Superposition of the backbone of three mutants (S134N, H46R, A4V), wt and apo-wt in the region of Val₁₄₈ and the best 20 hits from *in silico* screening. Right: Overlay of several docked structures showing a strong relation between the existences of an aromatic residue that resides deep in the cavity and a more variable, solvent exposed substructure.^[73] Copyright © The authors, CC BY 4.0 license.

Another potential binding site near Trp₃₂ was found by ANTONYUK *et al.* in 2013 when they tried to reproduce the findings of NOWAK *et al.* Crystal structure analysis revealed that several putative ligands (e.g. Uridine-5-monophosphate) did not bind at the expected Val₁₄₈ cavity but instead preferred binding near Trp₃₂.^[75,76] Moreover, the proposed ligands isoproterenol and 5-fluorouridine were found to be ineffective in stabilizing A4V and I113T mutants under aggregation inducing conditions. The authors concluded that crystal structure studies were the gold standard in ligand design and that *in silico* studies need to be validated by biophysical assays since their uncertainty is rather large. The same binding site was used later by POKRISHEVSKY *et al.* who expressed the Trp₃₂Ser mutant and found reduced aggregation compared to the wild

type. Additionally, the use of the anti-cancer drug 5-fluorouracil proved to be beneficial for the reduction of aggregation in said mutant.^[77,78]

AUCLAIR *et. al.* used a completely covalent approach for the stabilization of SOD1 in 2009 by employing a maleimide structure, which was supposed to tether the Cys₁₁₁ moieties of each monomer together, thus preventing the dissociation (Figure 2.3-4). They were able to show that a tethering of such sort was indeed stabilizing the dimer and could restore the catalytic activity of the G85R mutant. They concluded that the aforementioned cysteine residues were a potential target for therapeutics on a peptide basis. Even if a mutation showed unstable monomers, i.e. that no dimer was formed at all, they reported that usage of their maleimide-based structure would be able to overcome this and would still be able to tether monomers together, forming a functional dimer.^[79]

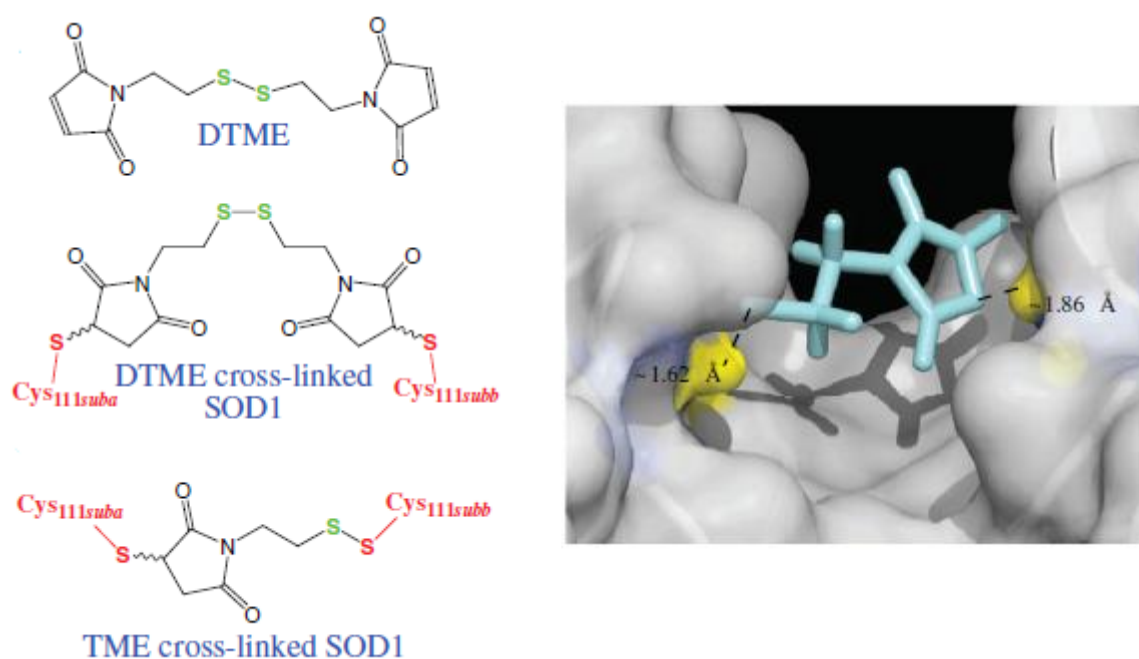


Figure 2.3-4. Left: The small molecule DTME/TME and the predicted binding modes between it and the Cysteine residues of the protein. Right: Model of TME (resulting from a thiol-exchange reaction between the cross-linked DTME and Cys₁₁₁) binding to both cysteines in each monomer.^[79] Copyright © The authors.

In 2018, HASNAIN *et. al.* introduced the cysteine-reactive molecule Ebselen for the maturation of SOD1 and its mutants. The selenium atom is able to form an S-Se bond in a disulfide reduced monomer, that is very reminiscent of a traditional disulfide bond, albeit much weaker in nature. Therefore, a proton exchange reaction leads to the

formation of a selenol compound that is oxidized back to Ebselen by H_2O_2 and the functional SOD1 monomer, which in turn folds to the functional dimer. The dimer can then bind two more Ebselen molecules, which stabilize the dimer against dissociation through a selenylsulfide bond and π - π -interactions. The authors showed that Ebselen promoted the formation of the disulfide-intact dimer, folding and zinc binding of SOD1 and its mutants. The mechanism of the Ebselen-promoted maturation of SOD1 is shown in Figure 2.3-5.^[80]

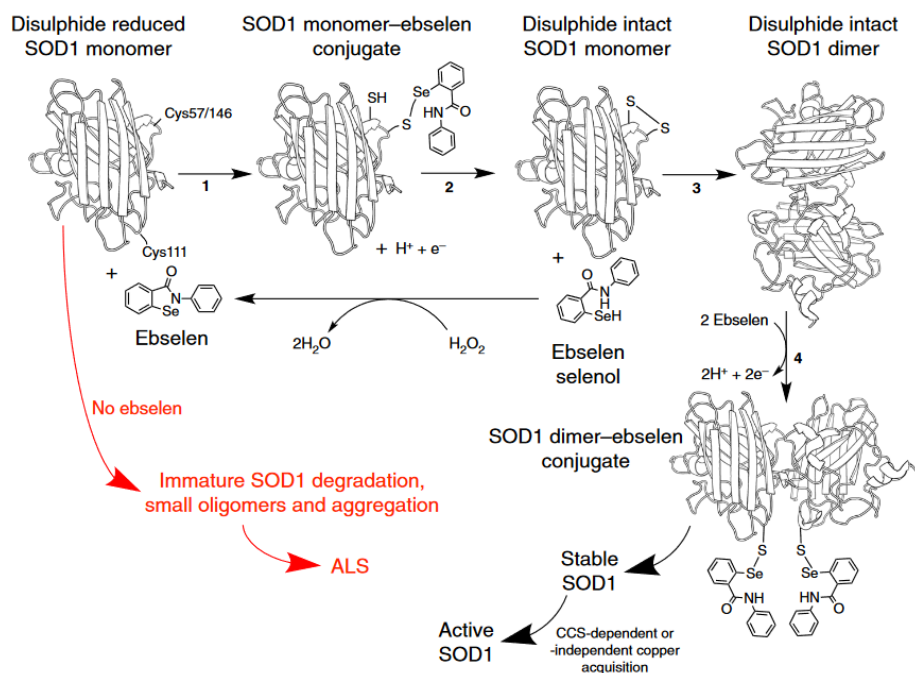


Figure 2.3-5. Mechanism of the Ebselen-promoted maturation of SOD1. The red part shows that the absence of Ebselen can lead aggregation of SOD1 and finally to ALS.^[80] Copyright © The authors. CC BY 4.0 license

In 2020, the group of HASNAIN reported variations of the Ebselen core structure to increase binding affinity to SOD1 through usage of several different interactions such as hydrogen bonds, charge- π -stacking or π - π -stacking (Figure 2.3-6, right). Many of the chosen ligands increased the melting temperature as could be seen in thermal shift assays and the binding modes were proven by crystal structures.^[81]

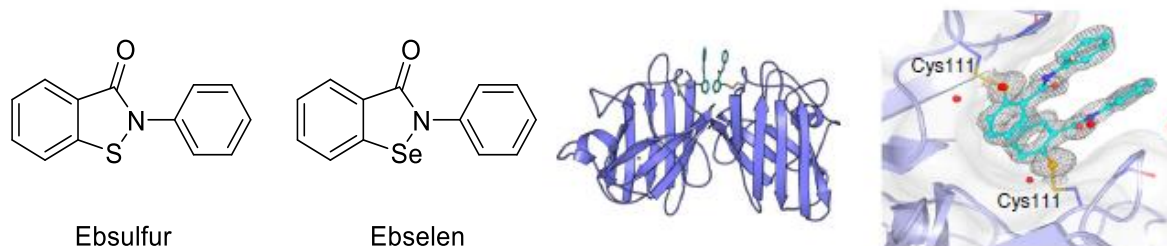


Figure 2.3-6. Left: Structure of Ebselen and Ebsulfur. Middle: Binding model of the small molecules and SOD1 at the dimer interface. Right: Electron density map of Ebselen bound to SOD1, showing proximal water molecules (in red) and a possible π - π -interaction between both covalently bound molecules.^[81] Copyright © The authors. CC BY 4.0 license.

2.4. Fluorescence Anisotropy

Fluorescence Anisotropy or Fluorescence Polarization is a method used to determine binding constants and reaction kinetics. It is based on the change in rotational freedom a molecule experiences upon binding to a larger structure like a protein.^[82]

In order to gain information about the binding process, one of the binding partners, preferably the smaller molecule, needs to be labeled with a fluorophore or needs to exhibit inherent fluorescence. The irradiation of a freely moving fluorophore with polarized light leads to the emission of depolarized light; this is because the typical fluorescence lifetime is in the range of nanoseconds while the Brownian motion and rotation of an unbound molecule is in the picosecond range. This means that any polarization of the irradiated light becomes depolarized before it can be re-emitted. When the ligand binds to a larger structure like a protein, the rotational freedom is hindered, proportional to the binding affinity and binding mode of the ligand to the protein. When the ligand-protein complex is then irradiated with polarized light, the timespan of rotation and fluorescence lifetime overlaps, which leads to the re-emission of polarized light (Figure 2.4-1). Afterwards, the difference between the free, unbound state compared to the bound state can be calculated. Titration of the two binding partners leads to a binding curve, which can be used to calculate K_d – values.

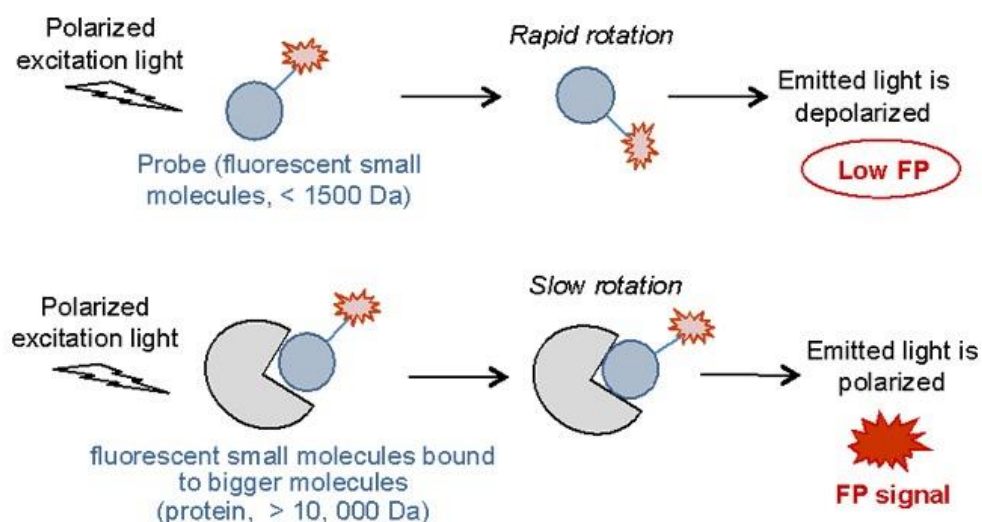


Figure 2.4-1. General scheme of a Fluorescence Anisotropy Assay.^[83] Copyright © The authors. CC BY 3.0 license.

Aside from requiring a fluorophore on one of the molecules, a few things need to be taken into consideration. First, the fluorophore emission spectrum must not overlap with the spectrum of the fluorescent amino acid tryptophan that is present in many proteins. Alternatively, one could use the fluorescence of said residue, but since the rotation of a protein is relatively small even in the unbound state, the differences between bound and unbound state are typically very small so that the assay becomes less accurate. Furthermore, the anisotropy is dependent on temperature and viscosity of the solvent, so a careful control of these parameters is essential. Moreover, the utilized fluorophore should have a fluorescence lifetime that is short compared to its rotational correlation time in order to allow the molecules to stay aligned during emission. However, if it becomes too small the changes in anisotropy might become too small to precisely detect them.^[84]

The requirement of having an inherent fluorescence was met by **LS1** as well as **LS3**. No information about the fluorescence lifetime of the excited states could be obtained, since the experiments needed to obtain these (time-correlated single photon counting [TCSPC] or cross correlation phase fluorometry) were beyond the scope of this thesis.^[85,86] This meant that every single result of the fluorescence anisotropy assay was to be taken conditionally and additional biophysical assays were absolutely needed to validate or negate those findings.

2.5 Microscale Thermophoresis (MST)

Microscale Thermophoresis is a fluorescence-based experiment that can be used to measure melting temperatures as well as K_d or IC_{50} – values of protein-ligand interactions.^[87,88] The general principle can be explained as follows: The observed molecule (ligand or protein) changes its physical properties such a size, hydration shell or shape upon binding to another molecule.^[89] These changes induce effects in secondary physical parameters such as the diffusion time, which can be recorded.

The underlying principle was already established in 1856 by Ludwig and is called thermophoresis (thermodiffusion, thermomigration or Ludwig-Soret-effect): Molecules or particles in general experience different responses to a temperature gradient depending on their physical properties and move along this gradient to constitute a new equilibrium.^[90] MST combines these two effects by establishing the temperature gradient by means of an IR-Laser that is focused to an area of approximately 25 μm radius. Upon experiencing this gradient, molecules start to move out of the irradiated area in which their velocity depends on the aforementioned properties size, shape, charge, and solvation shell. Either the protein or the ligand needs to be labeled with a fluorescent dye in order to observe changes in concentration that can be calculated from alterations of the fluorescence intensity inside the irradiated area. The new equilibrium is reached within seconds since the observed area is rather small and the temperature gradient is typically only a few $^{\circ}\text{C}$.

In order to measure the K_d -values of a protein-ligand interaction the fluorescently labeled protein is used in a set concentration, typically in the nM range, while the concentration of the ligand is varied from the mM to nM range. The thermophoresis of each measurement is fit into a titration curve from which biophysical parameters can be extracted.

The principle of an MST measurement and relevant curves are shown in Figure 2.5-1.

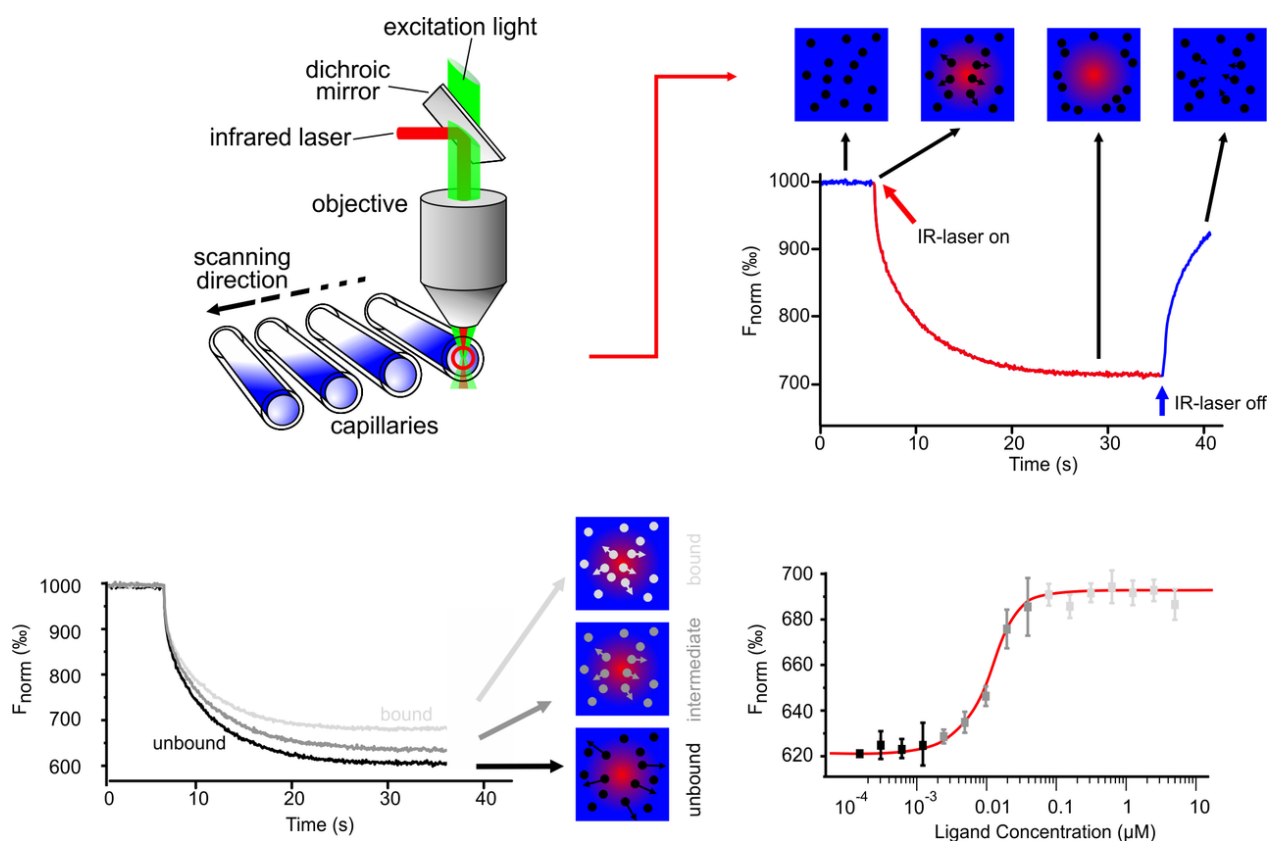


Figure 2.5-1. *Top left:* Basic construction of the experiment. The infrared laser constructs the temperature gradient while the fluorophore is excited by a second light source. *Top right:* MST trace of a single measurement and the different states of the experiment. *Bottom left:* Three MST traces of three individual measurements are plotted together. *Bottom right:* The MST signal plotted against the ligand concentration constitutes a binding curve, which gives information about binding properties.^[91] Copyright © The authors. CC BY 4.0 license.

Several differences in the fluorescence signals can be recorded during each individual experiment:

1. The initial fluorescence solely depends on the concentration of the labeled molecule since there is no irradiation at this point; this is used to normalize the obtained values.
2. When the IR irradiation starts, the temperature gradient is set almost immediately because the solvent molecules (most often water) rapidly absorb energy of this wavelength. In general, it can be assumed that the higher the decay of the fluorescence signal the stronger the protein-ligand interaction.
3. Thermophoresis occurs, in which the molecules move along the temperature gradient and the concentration of the labeled molecule is measured until a new

equilibrium is reached. The ratio of the initial fluorescence and the fluorescence at the equilibrium is typically used as the final value for each individual measurement.

4. The IR irradiation stops, and the molecule diffuses back into the now non-irradiated area. The fluorescence signal increases again since the concentration of the labeled molecules is increased through rediffusion.

2.6 Isothermal Titration Calorimetry (ITC)

Isothermal Titration Calorimetry is one of the biophysical measurements that was used in this thesis without the need of a fluorophore. Instead, the underlying physical principle is the formation or release of heat that occurs when a ligand is binding to its binding partner, in this case to a protein, which can be recorded. Using this data, several thermodynamic parameters of said interaction can be calculated.^[92]

An ITC-device consists of two identical cells that are made of inert material such as gold, located in an adiabatic shell (see Figure 2.6-1). The reference cell is filled with the same solvent that is used for the measurement, most often aqueous buffer, but in general, many solvents can be used. The sample cell is filled with the protein of interest and known quantities of the ligand are then titrated into the sample cell. Both cells are electrically connected in a way that the temperatures are kept consistent. Upon addition of ligand, the temperature of the sample cell can either increase or decrease, after which the heating device at the sample cell re-establishes the temperature of the reference cell. The ITC signal consists of the amount of energy (typically in kJ/mol) needed to maintain the temperature equilibrium after each addition of the ligand. These signals are then plotted against time, resulting in so-called “spikes”, each synonymous to one injection of the ligand solution. Upon integration of these signals with respect to time, the binding curve is obtained as the amount of total heat exchanged per injection. Analysis of the binding curve provides thermodynamic parameters such as K_d – values, affinity ($1/K_d$), stoichiometry of the reaction and reaction enthalpy ΔH .^[93]

ITC is one of the most sensitive biophysical measurements available and is often only used after other screening methods already established a promising ligand. This is due

to the large amount of time that is required for each measurement and the generally high amount of protein and ligand that is needed.

The general principle of ITC is summarized in Figure 2.6-1.

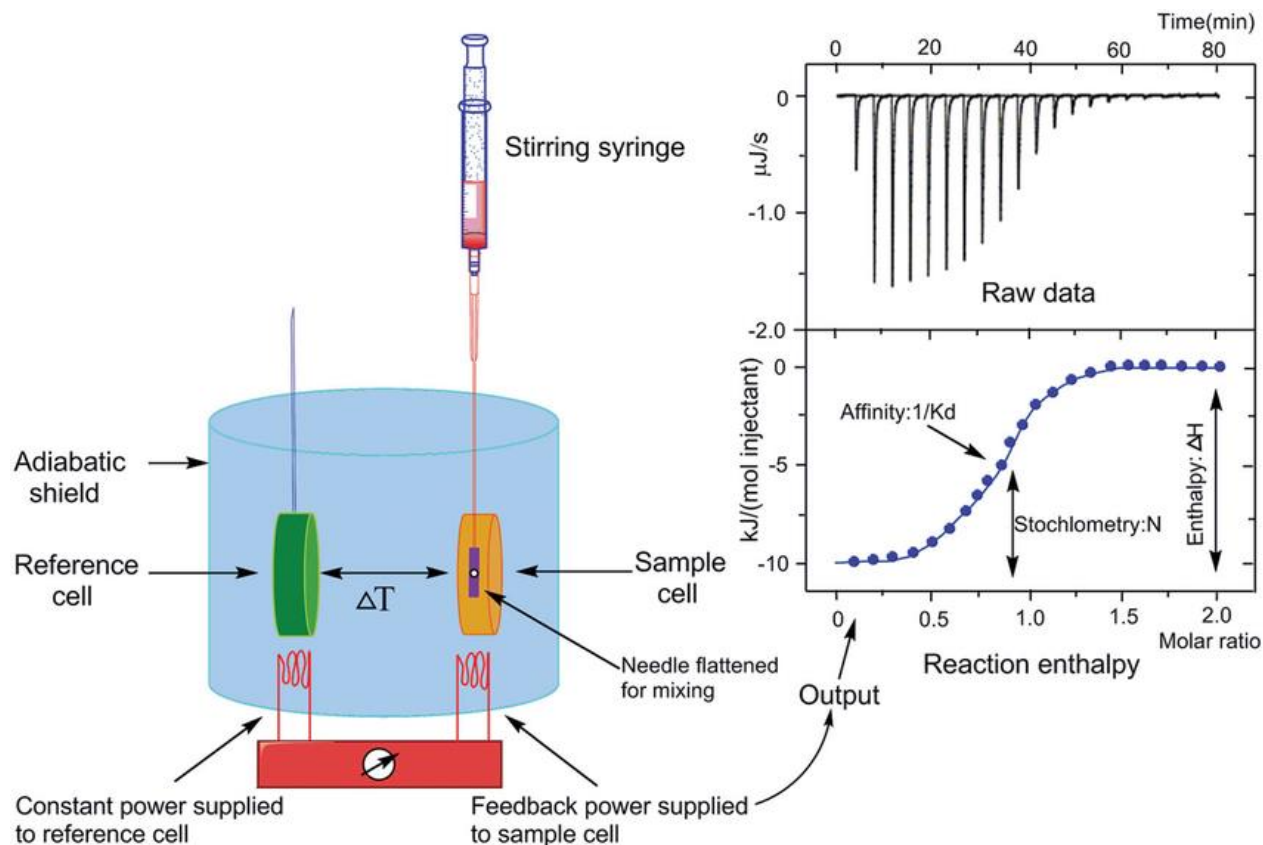


Figure 2.6-1. General principle of ITC. *Left:* Construction of the ITC device. *Right top:* Raw data obtained in the experiment showing the characteristic “spikes”. *Right bottom:* Integrated binding curve with several biophysical parameters that can be extracted from the measurement.^[94] Copyright © The authors. CC BY 4.0 license.

Due to the already described restrictions of the experimental procedure, ITC measurements were rarely used in the scope of this thesis and no screening of entire lead structures could be performed. Instead, ligands were chosen selectively to either validate already existing biophysical properties or to test the general viability of ITC for a series of compounds, e.g., their solubility in the chosen buffer. All ITC measurements were performed in the working group of Prof. Kai Tittmann, executed by Lisa-Marie Funk.

3 Aim of the work

Up to today, no literature-known ligand could be used as a therapeutic drug either due to missing affinity to the protein (e.g., the DTME approach), questionable reproducibility or low binding affinities and problematic solubilities of the lead compounds (e.g., the Ebselen derivatives).

The approach of this thesis aims to overcome the explained shortcomings by using an affinity-based stabilization through a small molecule that binds to the Cys₁₁₁ cavity and prevents the formation of aggregates (Figure 3-1). Furthermore, the molecules should be designed in a way that their water solubility for biophysical assays is high whilst opening up the possibility to change the solubility towards lipophilicity.

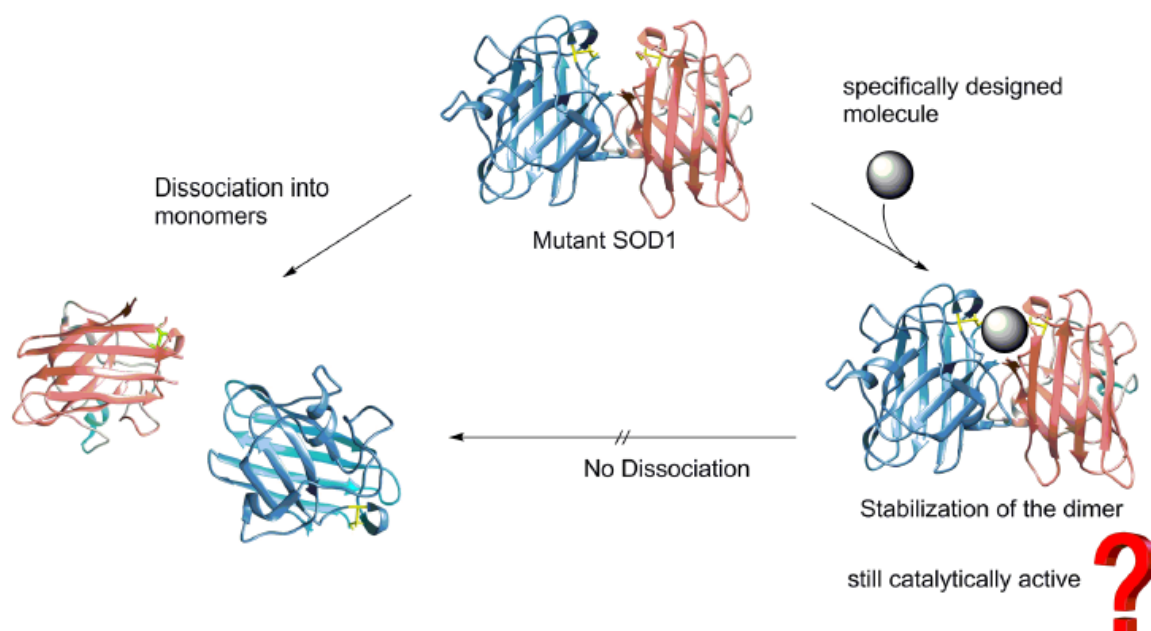


Figure 3-1. Approach of this thesis.

In order to attain this goal, the workflow needs to be divided into several steps:

1. *In silico* investigation of the Cys₁₁₁ cavity and design of ligands.
2. *In silico* binding studies with those ligands.
3. Synthesis of a small library of molecules to allow for a screening of substances with different properties.
4. Biophysical measurements to gain information about binding modes, K_d -values, aggregation properties and activity of the formed protein-ligand complexes.
5. Confirmation of the putative binding mode through X-ray crystallography.

4 Results and discussion

4.1 *In silico* studies and properties of the Lead Structures

A substantial simplification for the process of finding a suitable ligand to bind to a protein can arise from the existence of a natural binding ligand. An extremely well-studied example of this is 3,4,5-trimethoxyphenylethylamine, a naturally occurring phenylethylamine found in cacti. It binds to several receptors from the serotonergic system, e.g. to the 5-HT_{2A}-serotonin receptor, with a binding affinity of ca. 1.4 μ M.^[95] Based on the structure of this ligand, a plethora of non-natural molecules have been designed (see Figure 4.1-1). They found use as research chemicals, tools for biophysical studies (e.g. 25C-NBOMe) or recreational drugs (e.g. 2C-B).^[96]

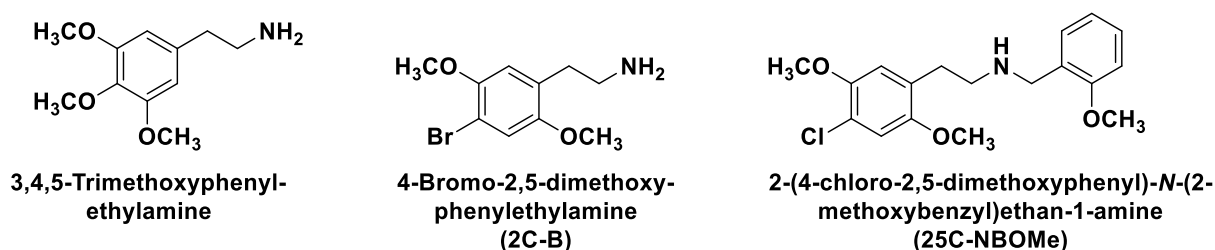


Figure 4.1-1. Comparison of different antagonists for the 5-HT_{2A}-serotonin receptor derived from the natural binding ligand 3,4,5-trimethoxyphenylethylamine.

Unfortunately, no natural ligand is known for SOD 1 except for several phosphate-binding sites near the metal ions, but those are not suitable for this project. Therefore, binding partners needed to be identified by a rational approach. For this, the general structure of the already described binding cavity needed to be further elucidated to find possible binding sites for small molecules.

Upon examining the cavity discussed above, it became obvious that most of the affected amino acids were non-polar amino acids like leucine, isoleucine, valine, and alanine. This was in accordance with the expectation to find these amino acids at the dimer contact interface, but unfortunately, these amino acids do not really offer any possibility for a protein-ligand interaction except for weak and unspecific non-polar interactions. However, two major amino acid contributors toward ionic interactions could be found: Arg₁₁₆ with its charged guanidine-group in the side chain and the often times also charged N-terminal end of the protein chain in proximity to the dimer contact interface and enclosed an area of approximately 14.45 Å length and 7.76 Å width

(Figure 4.1-2). This area was defined as the binding site for possible ligands and its impact on the selection of ligands could be described as follows:

1. The binding site mainly consists of non-polar amino acids, which means that the ligand should also be largely non-polar by its nature. At the same time, a certain solubility in water is desired in order to allow biophysical measurements to be performed without significant issues.
2. Ionic interactions are possible with the two charged guanidino groups of the Arg₁₁₆ as well as the charged N-terminal ends of the protein monomer.
3. The size of the area restricts the size of the ligand to approximately 14.4 Å in length and 7.8 Å in width. Considering that for ionic interactions to occur, the distance between the ligand and the charged group should not be larger than 4 Å and not smaller than 2 Å, a size between 12 and 15 Å is assessed as optimal. These values are only estimated though, since the actual orientation of the ligand in the binding site cannot be esteemed without *in silico* dockings, therefore it can be possible that the ligand binds in a diagonal manner (16.5 Å).
4. Since SOD1 is a homodimer, the binding site is C₂-symmetrical, which means that a possible ligand should preferably also have a symmetrical structure.

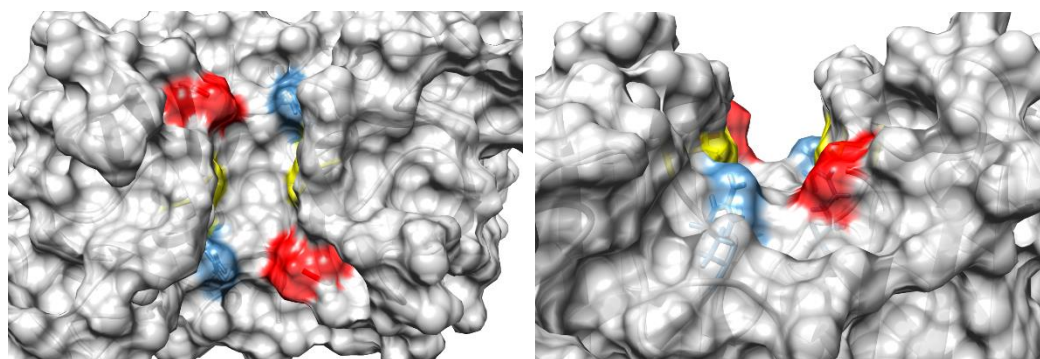


Figure 4.1-2. Structure of the upper binding cavity of SOD1 from the top (left) and from the side (right). Cys₁₁₁ in yellow, Arg₁₁₆ in blue and the N-terminal end of the protein monomer in red.

These constraints meant that the specific structure of the ligand was largely variable, which drastically reduced the chance to find a ligand with strong binding affinity on the spot. Instead, a rational approach needed to be implemented in a way to find the best balance between possible binding interactions of different structures and their expenditure of organic synthesis.

First, the required non-polar nature of the ligand was addressed: Considering the size of the area of the binding site, three different core structures were envisaged that featured the correct length of the molecule, a non-polar nature, and possibilities for modification and for the implementation of charged groups. These core structures are shown in Figure 4.1-3.

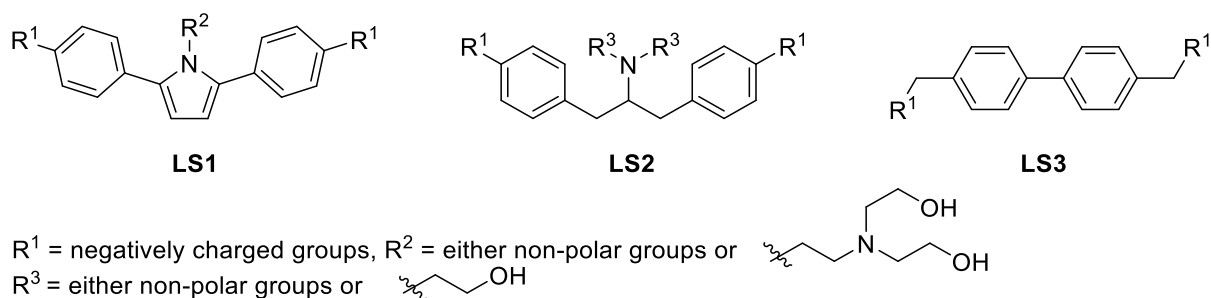


Figure 4.1-3. The resulting core motifs of the lead structures.

The next interaction that was considered was the ionic interaction of the already described Arg₁₁₆ and the N-terminal end of the protein monomer. Since both of these moieties were positively charged, a negatively charged group on the ligand was optimal. Organic acid groups offered a wide variety of properties that would allow for a biophysical screening in order to find the best structure. Moreover, the possibility of transforming the acid groups into esters would allow for the desired switch in solubility for *in vivo* experiments.

Table 4.1-1. Properties of the different acid groups chosen for *in silico* studies.

	pK_a	geometry	H-bond acceptors	H-bond donors
SO ₃ H (S)	-2.8	tetrahedral	2	1
PO ₃ H ₂ (O)	1.85	pyramidal	1	2
PO ₂ H ₂ (I)	2.10	pyramidal	1	1
CO ₂ H (C)	4.20	trigonal planar	1	1
B(OH) ₂ (B)	8.83	trigonal planar	0	2

These different acids could be distinguished by several factors. The most important property concerning the *in silico* screening was the pK_a -value, since the docking was

performed with the assumption that the acid groups were deprotonated with the only exception being the boronic acid. Biophysical measurements are often performed in aqueous buffer with a pH of around 7 to 8, in order to be as close to physiological conditions as possible. All of the above-mentioned acid groups possess pK_a-values that justified the assumption of being largely deprotonated at said conditions even though proteins tend to have structure-specific microenvironments.

Since binding affinity was supposed to arise from interactions between charged amino acid residues from Arg₁₁₆ and the N-terminal end of the protein monomer, the H-bond properties were examined. Carboxylic acids and phosphinic acids both have one H-bond acceptor- as well as one H-bond donor-group, even though the exact strength of these interactions could not be anticipated. Phosphonic acids have one more H-bond donor-group, whereas these values are swapped when looking at sulfonic acids. The only acid group without H-bond-accepting properties was the boronic acid. In screening these different options of interactions, one could hope to find a suitable ligand for binding to SOD1.

The geometry of the structures also differed from one another, albeit no specific binding probabilities could be derived from this property.

The last important factor was the ΔG -value, obtained from the mentioned *in silico* studies. It should be noted that these values were mostly used as a guideline for synthesis in order to determine, which structure should be synthesized first to maximize efficiency. Biophysical measurements are always authoritative concerning the binding properties, the *in silico* screening can only act as the first starting point to any research for protein-ligand interactions.

The ΔG -values for the investigated ligands are given in Table 4.1-2, the corresponding structures are given in Figure 4.1-4.

Table 4.1-2. ΔG -values from *in silico* studies (swissdock.ch and AutoDockVina were used).

Structure	ΔG (kcal/mol)	Structure	ΔG (kcal/mol)
LS1_MCH_S	-10.50	LS1_S_OH	-11.03
LS1_MCH_O	-12.95	LS1_O_OH	-13.73
LS1_MCH_I	-11.21	LS1_I_OH	-11.83
LS1_MCH_C	-10.68	LS1_C_OH	-10.78
LS2_S	-10.56	LS3_S	-10.49
LS2_O	-13.53	LS3_O	-13.11
LS2_I	-10.85	LS3_I	-11.11
LS2_C	-10.44	LS3_C	-10.75

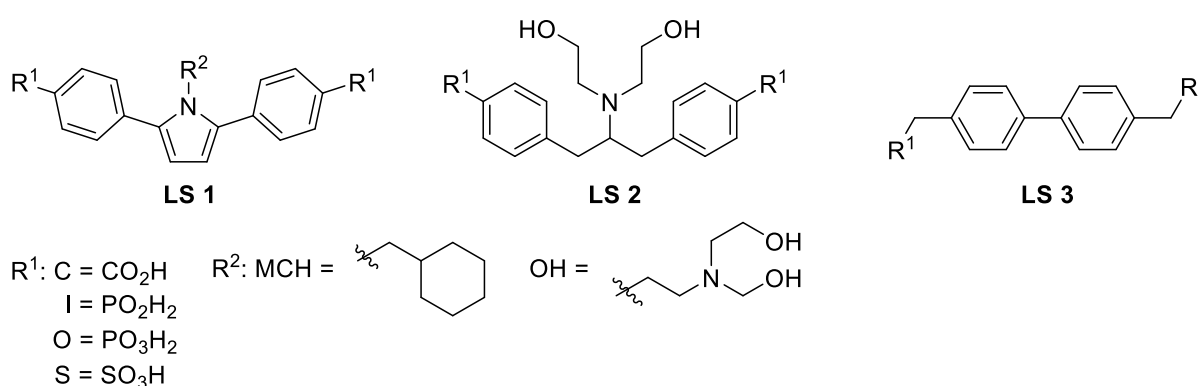


Figure 4.1-4. Structure depiction for Table 4.1-2.

The following trends could be observed from docking simulations:

1. Through all three lead structures, the phosphonic acids gave the best results in terms of overall docking score and the phosphinic acids always came second. The carboxylic acids and the sulfonic acids shared the third place.
2. The hydroxyalkane-substituted tertiary amines gave better results than the cyclohexylmethyl-substituted structures. This was somewhat arbitrary since the surrounding amino acids in the binding site were non-polar and a non-polar substitution was believed to increase the docking behavior. This might be attributed to the fact that non-polar interactions were quite hard to simulate with the standard docking routine and therefore could have been underestimated. Hydrogen bonds might also be overrepresented by the docking simulation because typically used force fields simulate hydrogen bonds in a more accurate fashion than hydrophobic interactions.

3. When comparing the best hits (the phosphonic acids), the following ranking of lead structures could be obtained: **LS1 > LS2 > LS3**.

It must be pointed out that binding conformations can be simulated much better than binding affinities using *in silico* studies. Therefore, the values obtained were only used as a guideline for synthesis and biophysical studies. Binding conformations and their impact on the overall proceeding of this work will be depicted in the following chapter.

4.1.1 Results for **LS1**

The resulting structures needed to be investigated in depth in order to gain information about the potential binding mode to the protein. The resulting docking information from the *in silico* screenings were visualized with *Chimera*. In this thesis, a selection of results will be presented.

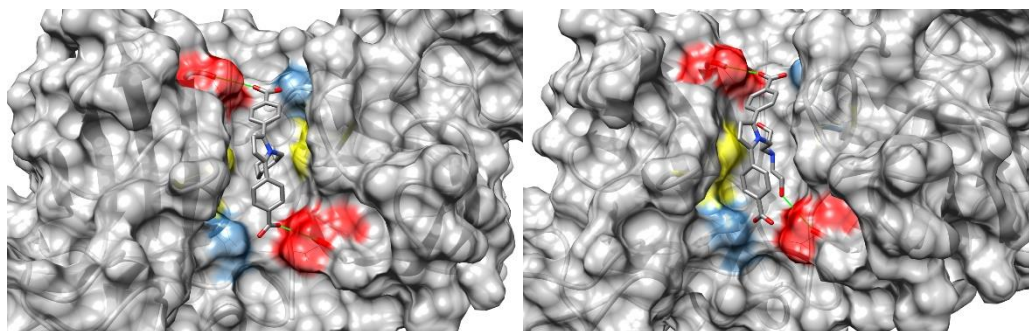


Figure 4.1.1-1. Results of the *in silico* docking for LS1_MCH_C (left) and LS1_C_OH (right). Cys₁₁₁ in yellow, Arg₁₁₆ in blue and the N-terminal end of the protein monomer in red.

First, LS1_MCH_C and LS1_C_OH were docked. As could be seen in Figure 4.1.1-1, both resulting binding modes were very similar, considering the whole protein was accessible as a possible binding site for the ligands. Both structures were binding at the desired location in the protein and the resulting interactions were very similar. The carboxylic acids produced two salt bridge like interactions with the N-terminal end of the protein monomer in case of the cyclohexylmethyl-substituted lead structure and one in case of LS1_C_OH, even though the distances for the latter also allowed for a second interaction that was not recognized by the program. In the same way, all carboxylic acids were also able to establish salt bridges to the Arg₁₁₆ residues concerning the distances between the respective atoms. Again, these interactions were not detected by the program. The biggest difference was seen with regard to the

N-substitution: While the alkyl moiety of LS1_MCH_C possibly gave rise to hydrophobic interactions, the OH-groups of the covalent approach were able to participate in hydrogen bonding with one of the N-terminal ends of the protein monomer.

In summary, the following points could be deduced from the first docking: The carboxylic acids were participating in salt bridges with the N-terminal end of the protein monomer. Interactions with the guanidine groups of Arg₁₁₆ seemed possible considering the distance; however, the program did not detect them. This could be interpreted that the size of the molecules was not perfectly aligned with the size of the binding site or that a second charged moiety needed to be installed to allow for more interactions between the ligand and the protein. The N-substitution gave the expected results in hydrophobic interactions for the alkyl-substituted lead structure and more hydrogen bonds for the hydroxyalkyl-substituted lead structure.

Next, the other acids were visualized to compare effects on the overall binding behavior of the ligand to the protein (Figure 4.1.1-2 for the phosphinic acids, Figure 4.1.1-3 for the phosphonic acids and Figure 4.1.1-4 for the sulfonic acids).

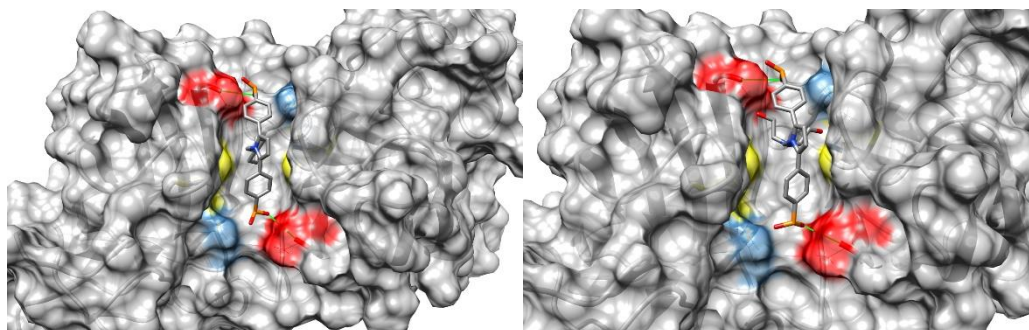


Figure 4.1.1-2. Results of the *in silico* docking for LS1_MCH_I (left) and LS1_I_OH (right). Cys₁₁₁ in yellow, Arg₁₁₆ in blue and the N-terminal end of the protein monomer in red.

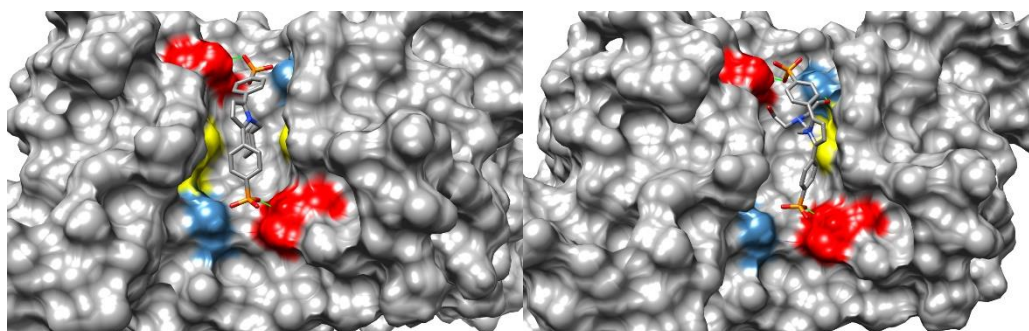


Figure 4.1.1-3. Results of the *in silico* docking for LS1_MCH_O (left) and LS1_O_covalent (right). Cys₁₁₁ in yellow, Arg₁₁₆ in blue and the N-terminal end of the protein monomer in red.

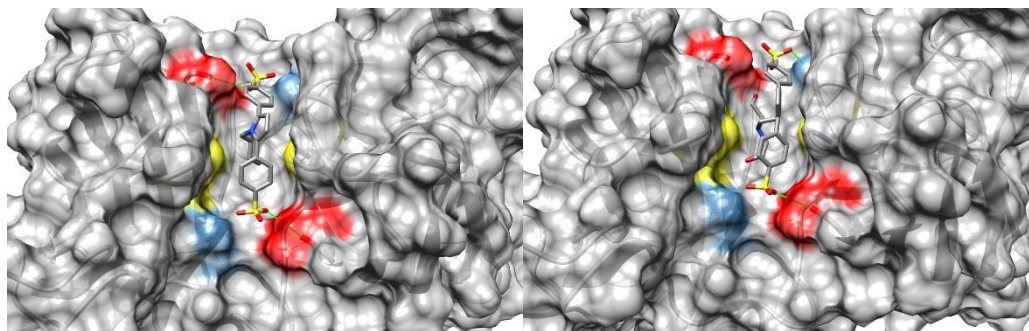


Figure 4.1.1-4. Results of the *in silico* docking for LS1_MCH_S (left) and LS1_S_OH (right). Cys₁₁₁ in yellow, Arg₁₁₆ in blue and the N-terminal end of the protein monomer in red.

As could be seen, the results were comparable to the already discussed results of the carboxylic acids.

For the cyclohexylmethyl-substituted lead structures, the docking always predicted possible hydrophobic interactions between protein and ligand and the orientation of the molecules was very similar in each iteration of the acids. The different acids always gave rise to binding with the N-terminal end of the protein monomer whilst also being in the correct distance for salt bridge interactions with the Arg₁₁₆ residues. Again, those interactions were not detected by the program.

The hydroxyalkyl-substituted lead structures also gave rise to interactions between the N-terminal end of the protein monomer and the acid groups while the sulfonic acid showed a possible salt bridge to one of the Arg₁₁₆ residues. The orientation of the substituent also differed significantly when comparing the phosphorous-based acids to the sulfonic acid, even though no new interactions arose from the different orientations according to the *in silico* results.

The strength of each of the confirmed interactions could not be deducted from the docking results other than comparing the final ΔG -values as was already discussed (Table 4.1-2).

4.1.2 Results for **LS2**

The first thing to recognize was that the phosphinic acid was the only investigated structure that did not bind at the desired binding site but instead showed a preferred binding to the lower part of the dimer contact surface (Figure 4.1.2-1). No efforts were made to elucidate these results further and this particular lead structure was declared a negative result.

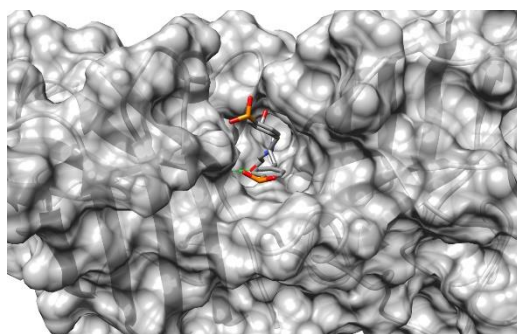


Figure 4.1.2-1. Results of the *in silico* docking for LS2_I.

The carboxylic acid and the sulfonic acid derivatives showed a different behavior than the corresponding **LS1**-structures: π - π stacking between the aromatic systems could be observed, giving rise to a different binding mode to the protein. Both acid groups as well as both alcohol groups were located at the same side of the binding site instead of crossing it diagonally. This resulted in one confirmed interaction for the carboxylic acid derivative (Figure 4.1.2-2) between a carboxylic acid and the N-terminal end of the protein monomer. The respective sulfonic acid showed three interactions, two hydrogen bonds between the two alcohol groups and the N-terminal end of the protein monomer and Arg₁₁₆, accompanied by the typical interaction of the acid group (Figure 4.1.2-3).

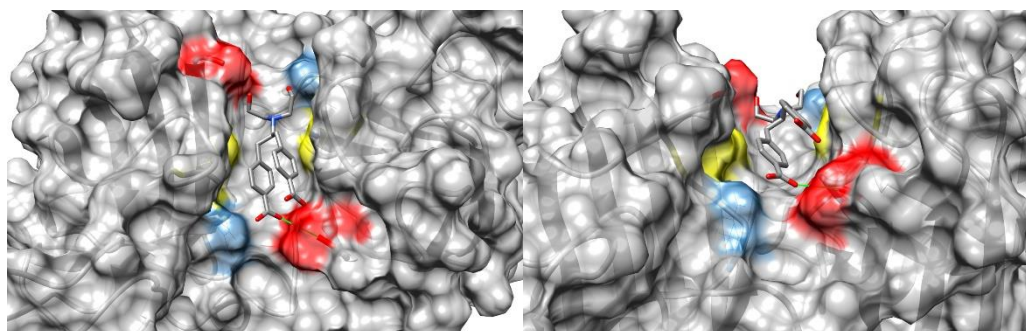


Figure 4.1.2-2. Results of the *in silico* docking for LS2_C. Cys₁₁₁ in yellow, Arg₁₁₆ in blue and the N-terminal end of the protein monomer in red.

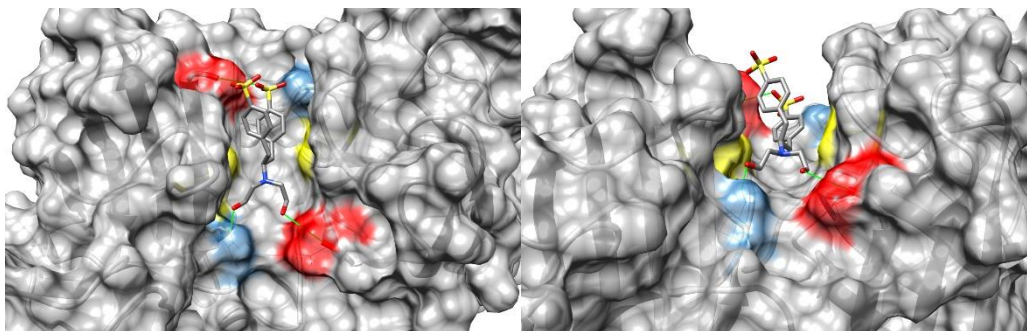


Figure 4.1.2-3. Results of the *in silico* docking for LS2_S. Cys₁₁₁ in yellow, Arg₁₁₆ in blue and the N-terminal end of the protein monomer in red, confirmed interactions in green.

The phosphonic acid showed a more similar binding mode compared to the **LS1**-derived structures already explained above (Figure 4.1.2-4). The two acid groups showed interactions to Arg₁₁₆ and the N-terminal end of the protein monomer as well as an unprecedented interaction between an alcohol group and a backbone amide moiety.

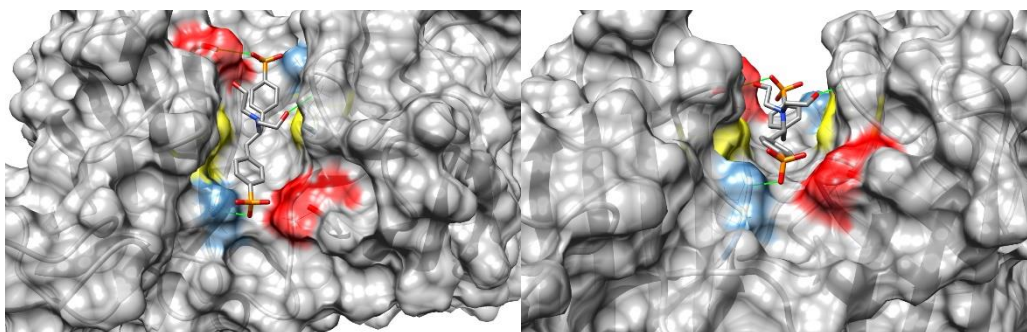


Figure 4.1.2-4. Results of the *in silico* docking for LS2_O. Cys₁₁₁ in yellow, Arg₁₁₆ in blue and the N-terminal end of the protein monomer in red, confirmed interactions in green.

4.1.3 Results for LS3

All derivatives of **LS3** were expected to cross the binding cavity in a diagonal manner to maximize potential binding interactions. This trend could be confirmed for all investigated structures.

The carboxylic acid derivative crossed the cavity from one *N*-terminal end of the protein monomer to its counterpart in the other monomer, giving rise to three confirmed interactions (Figure 4.1.3-1). The relative steric configuration of both carboxylic acid residues was not identical, indicating that further optimization might be needed. Unfortunately, no interactions to Arg₁₁₆ and the *N*-terminal end of the protein monomer were detected for a single carboxylic acid moiety. This reinforced the assumption that the carboxylic acid residue was not optimal for binding purposes.

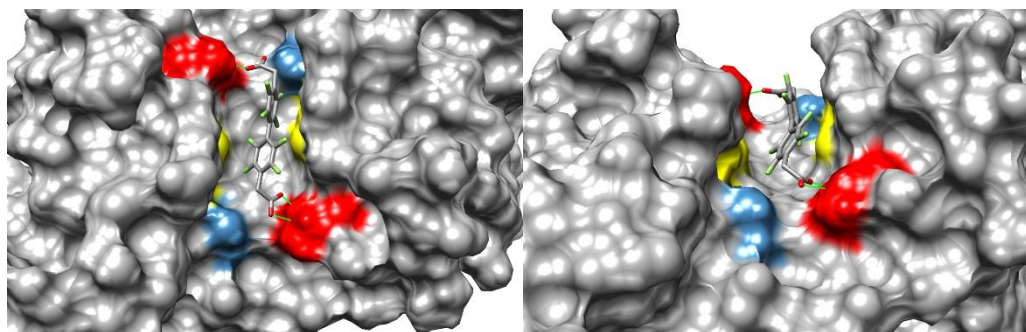


Figure 4.1.3-1. Results of the *in silico* docking for LS3_C. Cys₁₁₁ in yellow, Arg₁₁₆ in blue and the *N*-terminal end of the protein monomer in red.

The phosphinic acid bridged the cavity in the same manner, therefore the general binding mode was very similar to the one explained for the carboxylic acid (Figure 4.1.3-2). An important difference was the existence of two concurrent interactions between one acid residue and both possible binding partners.

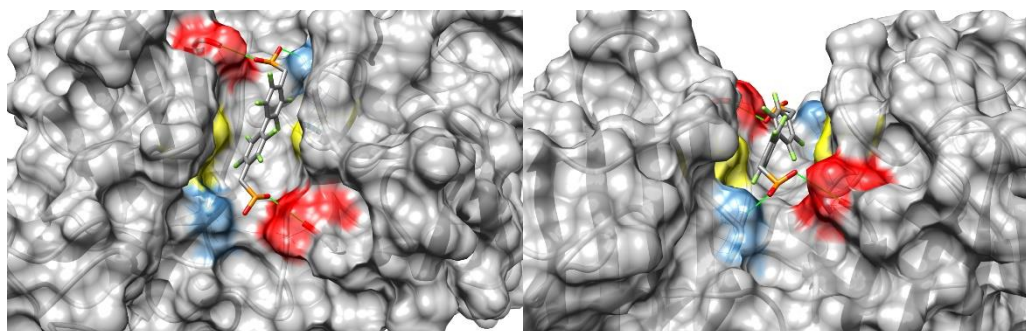


Figure 4.1.3-2. Results of the *in silico* docking for LS3_I. Cys₁₁₁ in yellow, Arg₁₁₆ in blue and the *N*-terminal end of the protein monomer in red.

The phosphonic acid derivative showed the same trend in crossing the binding cavity (Figure 4.1.3-3). Only one interaction could be confirmed, indicating a high affinity of the phosphonic acid to amines that can be explained by acid-base interplay between both binding partners.

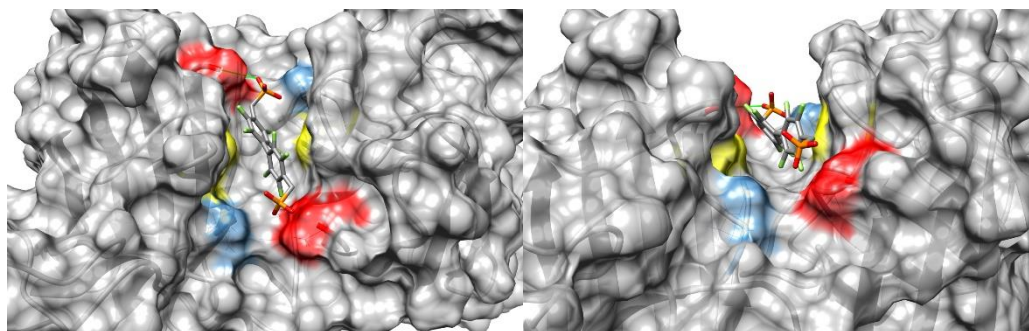


Figure 4.1.3-3. Results of the *in silico* docking for LS3_O. Cys₁₁₁ in yellow, Arg₁₁₆ in blue and the N-terminal end of the protein monomer in red.

The sulfonic acid derivative showed two confirmed interactions to the N-terminal end of the protein monomer while crossing the cavity in the same way as all other investigated structures (Figure 4.1.3-4).

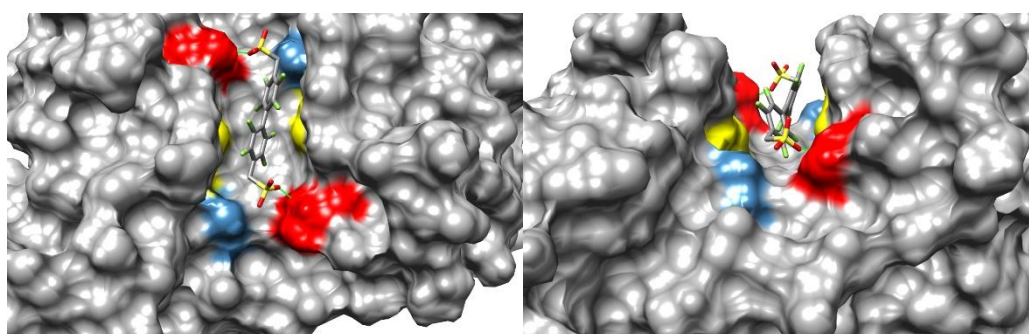


Figure 4.1.3-4. Results of the *in silico* docking for LS3_S. Cys₁₁₁ in yellow, Arg₁₁₆ in blue and the N-terminal end of the protein monomer in red.

In summary, all three lead structures studied herein showed the expected tendency of binding in the upper cavity near Cys₁₁₁. Putative interactions between the molecules and the protein could be confirmed. The binding mode was different between lead structures and acid residues within the lead structures; in turn, no clear picture can be drawn in that regard. It must be noted that the number of interactions did not say anything about the final ΔG -value since one would expect the phosphonic acids to be the worst of the aforementioned acids. In reality the opposite was true (see table 4.1-2), which again substantiated the suspicion that the *in silico* docking did not consider all possible interactions between ligand and protein. This is because the distances between the acid moieties and Arg₁₁₆ were small enough to allow for salt bridges in many cases.

Aliphatic and hydroxyl-substituted residues showed similar binding behavior that cannot be further elucidated by *in silico* studies alone. The most straightforward way to verify these interactions and to optimize the ligands would start with the synthesis of one lead structure and subsequent screening of the acid residues in biophysical assays. Crystal structure analysis would then allow to either confirm or invalidate the *in silico* findings, opening up the possibility to optimize the ligands in a rational way.

The general shortcomings of computational docking such as selection of force fields, selection of scoring functions, reduced flexibility of ligands, too rigid behavior of proteins as well as omitting the role of the solvent as potential hydrogen bond donor or acceptor can lead to imprecise binding predictions. This was observed in this thesis as well, since all investigated molecules showed the possibility of binding to other areas of the protein. The real binding modes, binding strengths and affinities can only be rationalized by biophysical assays.

4.2 Synthesis of **LS1**

Parts of this chapter have been published in “Robert H.E. Schirmacher, Daniel Rösch, Franziska Thomas, Hexafluoroisopropanol as solvent and promotor in the Paal-Knorr synthesis of N-substituted diaryl pyrroles, *Tetrahedron*, **2021**, 83, 131985.

4.2.1 Synthesis of the molecular library based on the carboxylic acids of **LS1**

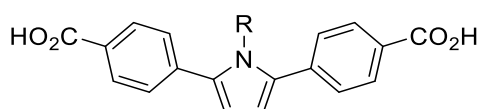


Figure 4.2.1-1. Structure of the carboxylic acid derivatives of **LS1**.

The first retrosynthetic task was to identify a common precursor for the different iterations of **R** that consisted of a plethora of alkyl or aryl groups as well as to plan a precursor for the synthesis of carboxylic acids. This was especially important since carboxylic acids were polar and generally more difficult to handle as solubility in organic solvents is reduced and purification often tedious. The transformation of the nitrile group into a carboxylic acid was chosen as the method of choice because the reaction tends to proceed smoothly in basic media and the nitrile precursors are commercially available, non-polar and therefore easy to handle (Figure 4.2.1-2).

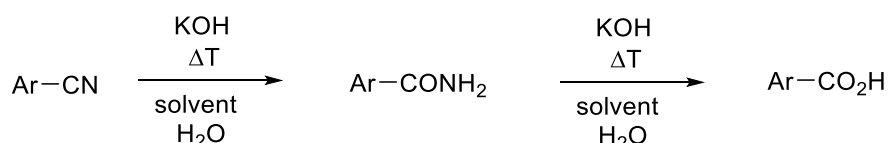


Figure 4.2.1-2. Synthesis of the carboxylic acid moiety from nitrile precursors (the amides are not isolated).

Having set the synthesis of the acid group, the main structural motif of **LS1**, the central 2,5-bis-aryl substituted pyrrole moiety with variable organic residues at the nitrogen atom had to be addressed. There is a broad variety of different organic reactions for the synthesis of pyrroles, both aryl- or alkyl-substituted and with the possibility of *N*-substitution.^[97] The most widely known literature approaches to bis-aryl-substituted pyrroles make use of palladium catalysts and require the already *N*-substituted pyrrole and a specific aryl precursor that is frequently pre-functionalized.^[97,98] The *N*-substituted pyrroles can conveniently be prepared by nucleophilic substitution with a

strong base and alkyl halides in moderate to good yields.^[99] A possible two-step sequence to the central motif is shown in Figure 4.2.1-3.

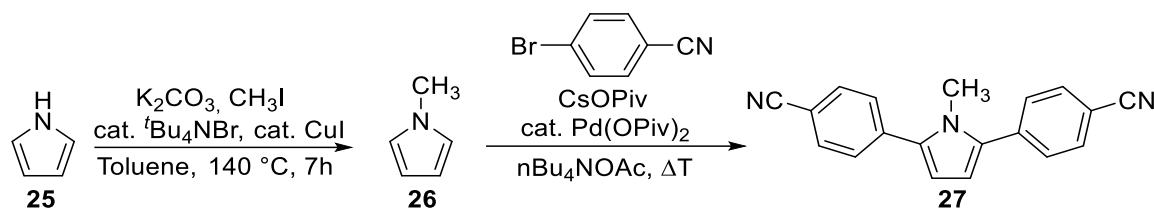


Figure 4.2.1-3. Two-step sequence for the synthesis of a possible precursor for **LS1**.

This reaction sequence has several drawbacks: First, the *N*-substituted precursors have to be synthesized for each variation of **R**. Each of these molecules has to be reacted with the appropriate aryl bromide to give rise to the desired core structural motif afterwards. Second, switching away from nitriles could possibly cause severe synthetic challenges since cross-coupling reactions of this type typically have a very limited functional group tolerance. Third, if the desired pyrrole precursor is supposed to exhibit chloride- or bromide-functionalized aromatic systems, the cross-coupling step itself could lead to polymerization due to double-couplings on the required 1,4-dihalide coupling partner.

Another literature-known approach to substituted heterocycles is the arylation of *N*-Boc protected pyrrole with *in situ*-generated diazonium ions (see Figure 4.2.1-4).^[100] Pyrrole is protected using a standard Boc-protocol and the coupling partner benzocaine was readily synthesized from 4-aminobenzoic acid. The diazonium ions were then generated by treatment of the free amine with ^tBuONO and MeSO₃H with additional CaCO₃ for pH control in water, followed by the addition of the protected pyrrole, acetone, and Cu(OAc)₂. When performing this reaction, no product formation was observed. Therefore, this pathway was abandoned for this project.

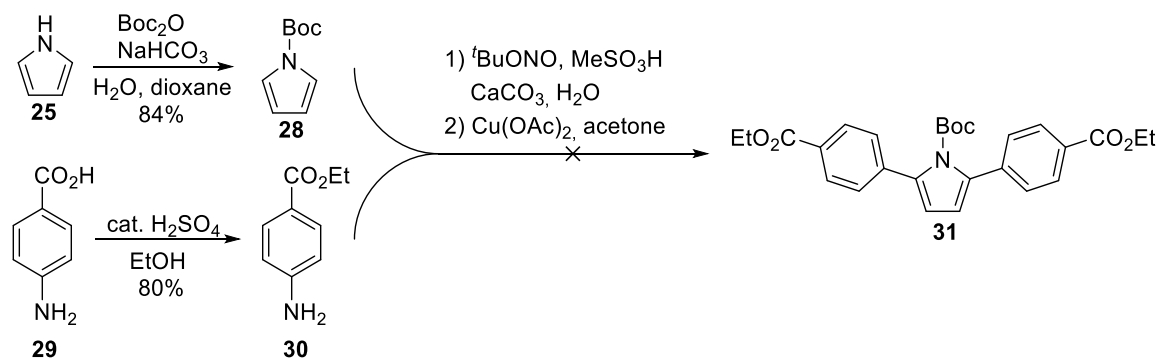


Figure 4.2.1-4. Unsuccessful reaction sequence utilizing *in situ*-generated diazonium ions.

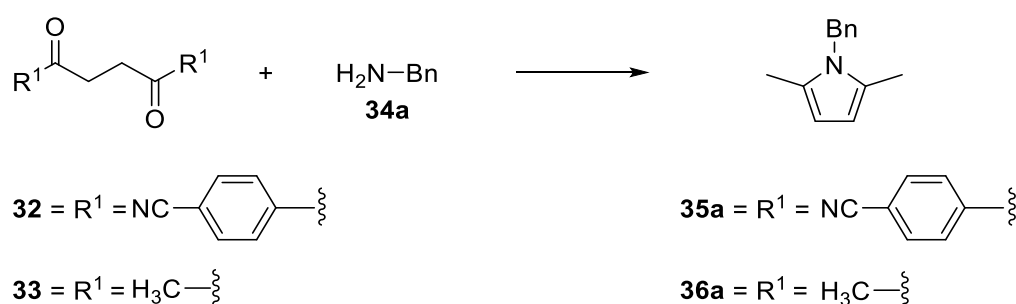
One of the most famous and well-known strategies for the synthesis of pyrroles is the Paal-Knorr pyrrole synthesis. Compared to modern techniques like the ones mentioned before, the Paal-Knorr reaction dates back to 1884 but experiences increasing attention in today's current research trends such as green chemistry or sustainable chemistry.^[101,102] The Paal-Knorr pyrrole synthesis includes the reaction of a 1,4-diketone and a primary amine, typically under acid or Lewis-acid catalysis. Commonly used solvents range from polar protic solvents such as EtOH or MeOH over polar aprotic solvents such as DMF or THF to nonpolar solvents, e.g. DCM or toluene. Novel approaches also make use of ionic liquids or deep eutectic solvents (DES) in order to increase the yields, minimize side products, increase reusability, and allow easy separation of the products.^[103,104]

However, initial tests with the highly insoluble 4,4'-succinyldibenzonitrile (**32**) were unfavorable in terms of product quality, yield and reaction control due to the use of high boiling solvents like DMF or DMSO (see Table 4.2.1-1, entries 1-2). Since the solubility of the diketone (**32**) was a major problem, solvent-free conditions were investigated; this improved the yield to 25% (Table 4.2.1-1, entry 3). Afterwards, the ionic liquid 1-butyl-3-methylimidazolium iodide and a deep eutectic solvent of choline chloride and urea were employed. Unfortunately, no conversion was observed, probably due to the poor solubility of **32** in those respective solvents (Table 4.2.1-1, entries 4-5). The poor solubility of **32** in common organic solvents can be attributed to two main factors: Firstly, π - π interactions between the electron-poor aromatic rings can lead to stacking in the solid phase, restricting the ability of the solvent to break these interplays. Secondly, the hydroxyl groups of the enol form of **32** can form hydrogen bonds with the nitrile moieties in an inter- or intramolecular fashion, further amplifying the structure of the molecule. Both of these effects result in an energy barrier the solvent needs to overcome in order to yield solvent-separated molecules.

Hexafluoroisopropanol is a very potent hydrogen bond donor due to its two TFB-groups adjacent to the alcohol, leading to a slightly acidic OH-group with a pKa of 9.3.^[105] On the other hand, the nucleophilicity is rather limited due to steric constraints, which makes HFIP a suitable solvent for Paal-Knorr reactions. This presumption was confirmed by achieving a yield of 74% after heating the reaction mixture at reflux for 2 days (Table 4.2.1-1, entry 6).

Next, the reaction between 2,5-hexandione (**33**) and benzyl amine was investigated, since **33** is a common model substrate for the optimization of reaction conditions in Paal-Knorr like reactions. The reaction in HFIP was completed almost instantly, giving quantitative yield of the desired pyrrole (Table 4.2.1-1, entry 7). Afterwards, the same reaction was carried out under literature known conditions (Table 4.2.1-1, entries 8-11) and their suitability was confirmed with excellent yields for every approach. The use of HFIP has several advantages though: The low boiling point meant that evaporation of the solvent after the reaction was feasible. In addition, the reaction was completed at the fastest rate compared to the other procedures.

Table 4.2.1-1. Optimization of the reaction conditions for the synthesis of 2,5-disubstituted pyrroles.



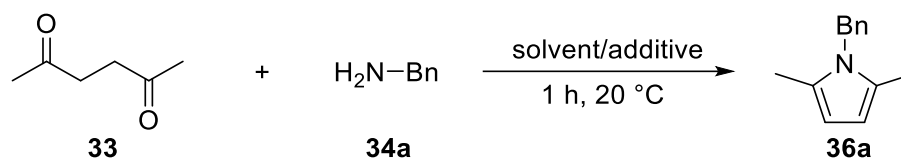
	32 / 33	34a equiv.	solvent	cat.	t (h)	T (°C)	yield (%) ^a
1	32	5	DMF	PTSA	12	100	0
2	32	5	DMSO	PTSA	24	130	12
3	32	neat	-	-	96	80	25
4	32	2.5	[BmIm] ^b	PTSA	24	100	0
5	32	2.5	CC/U ^c	-	24	80	0
6	32	1.5	HFIP	-	48	59	74
7	33	1.5	HFIP	-	< 0.1	r.t.	99
8	33	1.5	H ₂ O ^[106]	-	0.5	100	99
9	33	1.5	CC/U ^{c[104]}	-	12	80	98
10	33	1.5	[BmIm] ^{b[103]}	-	1	95	98
11	33	1.5	None ^[107]	-	1	100	99

^aYields refer to isolated compounds. ^b[BmIm] = 1-butyl-3-methylimidazolium iodide. ^cCC/U = 1:1 equimolar mixture of choline chloride and urea.

Thereafter, a catalytic approach was tested by running the same reaction in five different organic solvents at room temperature. Ethanol, the only protic solvent that was used, gave the best results (Table 4.2.1-2, entry 5). Addition of a catalytic amount of HFIP increased the yield by an additional 16% (Table 4.2.1-2, entry 6). This means that HFIP can be used as the acid additive in Paal-Knorr reactions instead of Bronsted- or Lewis-acids that are widely used in organic synthesis. The reason for the rate-accelerating properties is most likely the already described acidic character of the

hydroxyl group. It must be noted that the catalytic approach gave reduced yields compared to the approach in HFIP as the sole solvent; therefore, it should only be used as long as the solvent properties of HFIP are not required.

Table 4.2.1-2. Optimization of the catalytic activity of HFIP.



entry	34a equiv.	solvent	cat.	yield (%) ^a
1	1.5	DCM	-	45
2	1.5	EtOAc	-	41
3	1.5	Et ₂ O	-	39
4	1.5	Toluene	-	46
5	1.5	EtOH	-	56
6	1.5	EtOH	HFIP (5-mol%)	82

^aYields refer to isolated compounds.

In summary, a protocol for the synthesis of the desired 2,5-diaryl substituted pyrrole motif was established by employing hexafluoroisopropanol as solvent and reaction promotor in a Paal-Knorr pyrrole synthesis.

Having set out this critical reaction step, a retrosynthetic analysis of **LS1** is presented in Figure 4.2.1-5.

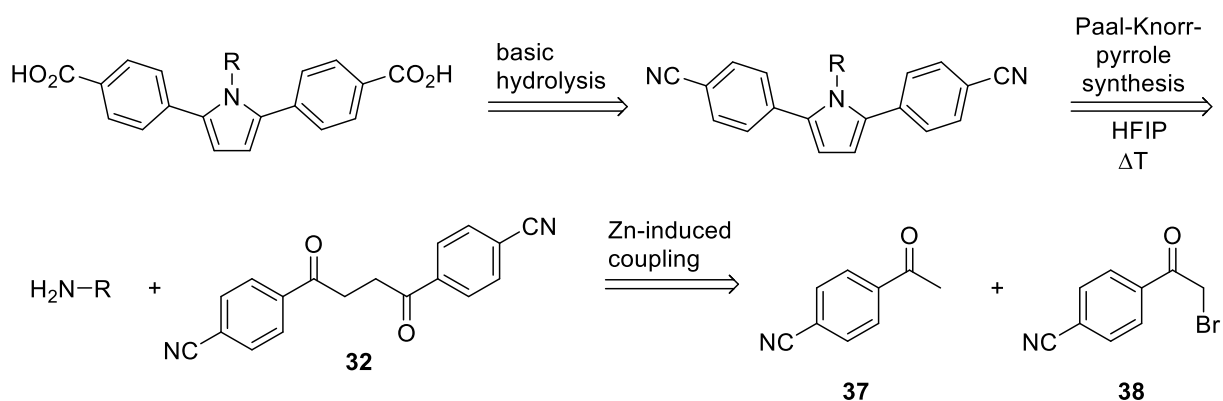


Figure 4.2.1-5. Retrosynthetic approach to the carboxylic acids of **LS1**.

The carboxylic acids can be synthesized *via* nitrile hydrolysis of the dicyanide precursors in a mixture of organic solvent and water. The dicyanide precursors can be synthesized utilizing the optimized reaction conditions from Table 4.2.1-1 employing the already described Paal-Knorr pyrrole synthesis. The necessary 1,4-diketone can

be conveniently prepared *via* Aldol reaction between a ketone and a bromoketone, followed by base-induced *in situ* nucleophilic substitution and ring opening. The proposed mechanism of this reaction is described in Figure 4.2.1-6.

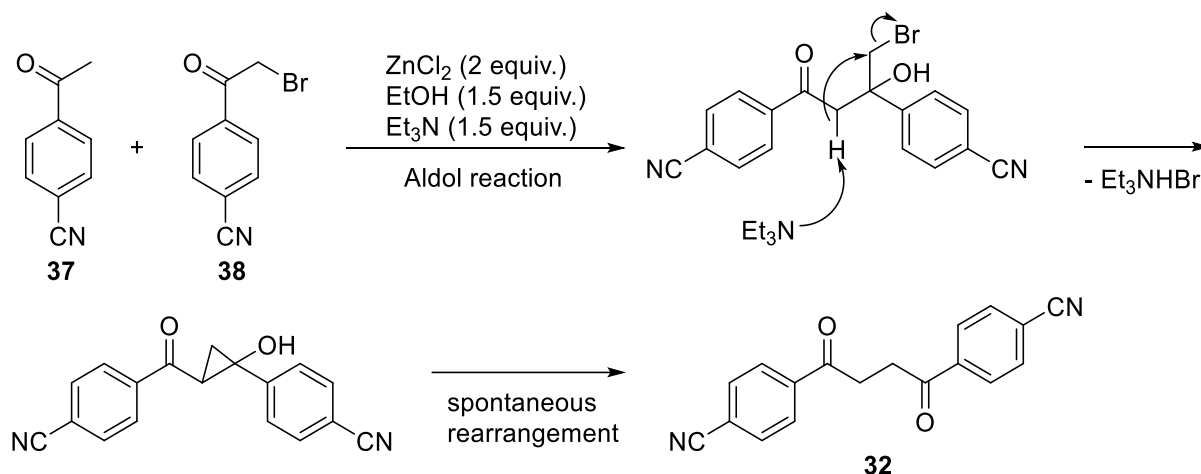


Figure 4.2.1-6. Reaction mechanism for the synthesis of 1,4-diketones utilizing zinc chloride, triethylamine, and ethanol.

In the first step, ketone (37) and bromoketone (38) were reacted to the desired 1,4-diketone structure using a condensation agent consisting of ZnCl₂, EtOH and Et₃N in toluene at room temperature for several days (Figure 4.2.1-7). Recrystallization of the precipitated solid afforded the general precursor (32) in 70% yield.^[108]

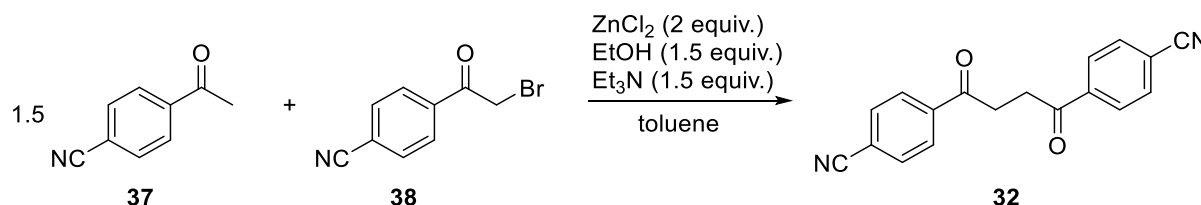


Figure 4.2.1-7. Synthesis of the 1,4-diketone precursor.

The already described Paal-Knorr-pyrrole syntheses followed by the literature-known base-promoted nitrile hydrolysis afforded each final structure in two individual steps (Figure 4.2.1-8).

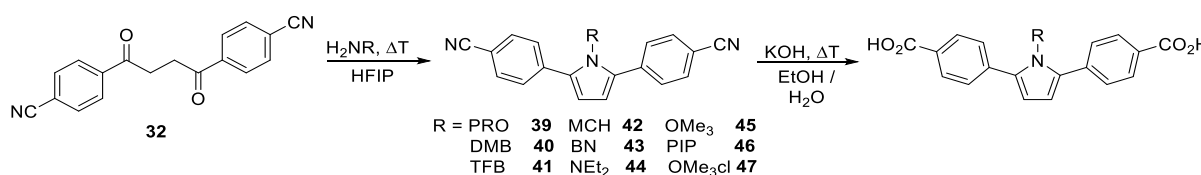


Figure 4.2.1-8. Two-step sequence to the carboxylic acids of LS1.

The following molecules were synthesized following the procedure described above (Figure 4.2.1-9):

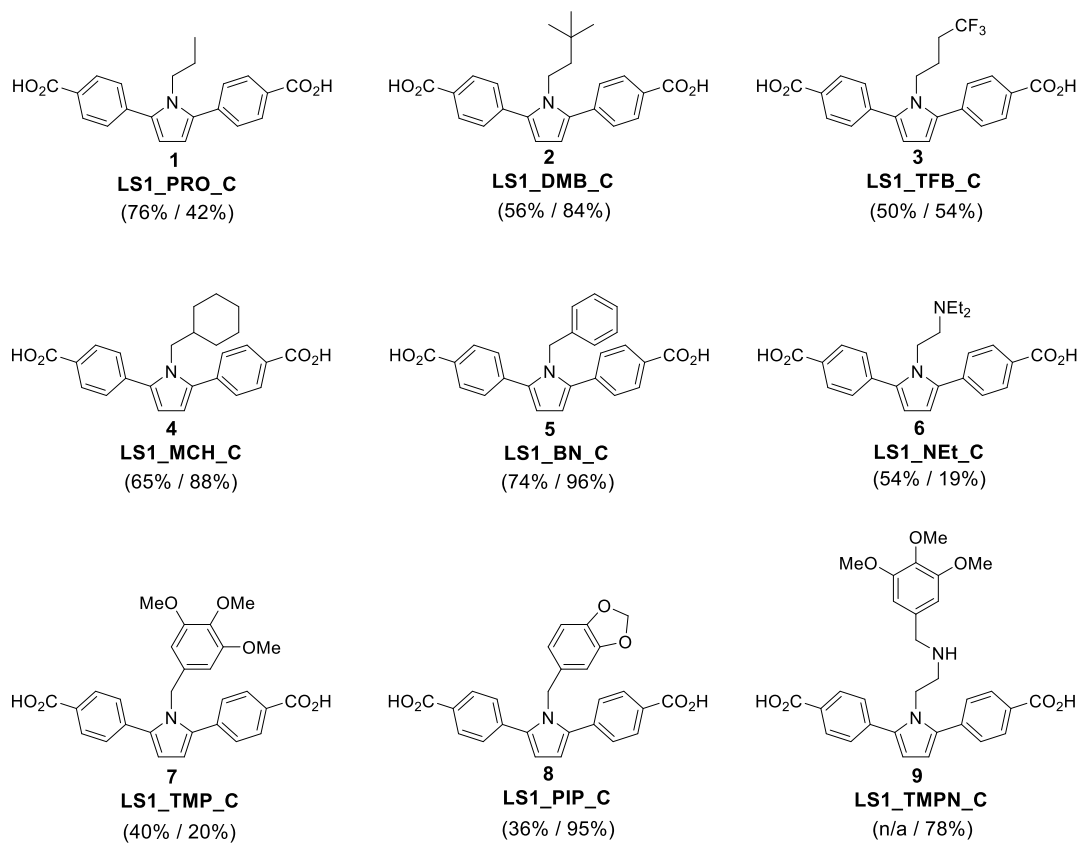


Figure 4.2.1-9. Overview of the synthesized carboxylic acids. Percentages in brackets indicate the isolated yields for (Paal-Knorr-pyrrole synthesis / nitrile hydrolysis).

4.2.2 Synthesis of the molecular library based on **LS1**

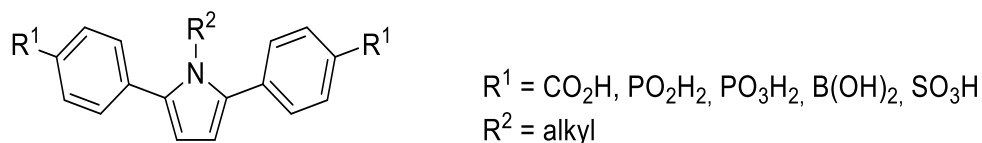


Figure 4.2.2-1. General structure of **LS1**.

The first retrosynthetic task for the diversification of the **LS1** based library was the introduction of a variety of different acid moieties to the two benzene moieties, preferably using only one conjoint precursor for all different acids in order to shorten the synthetic sequence. Fortunately, all desired moieties can be conveniently prepared from aryl bromides using literature known protocols.

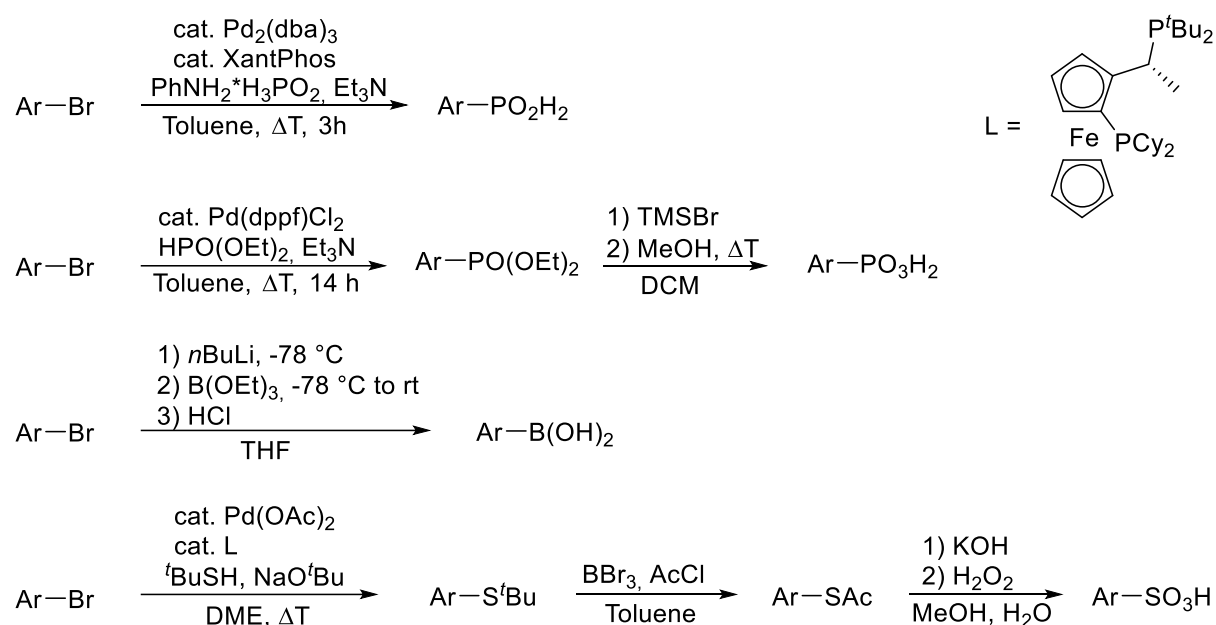


Figure 4.2.2-2. Synthesis of the acid moieties from two precursors.

As can be seen in Figure 4.2.2-2, the bromide functionality is well suited to the demands of the aforementioned syntheses. The phosphinic acids could be prepared in a single reaction step making use of a Palladium-catalysed cross coupling.^[109] Phosphonic acids also required a cross-coupling step, followed by the McKenna-reaction to saponify the phosphonate ester.^[109,110] Boronic acids could be synthesized by metalation at low temperatures, followed by quenching of the intermediate lithium salt with triethyl borate and subsequent acidic hydrolysis.^[111] Unfortunately, sulfonic acids are more difficult to obtain: First, the bromide can be converted to a protected thiol group, which is subsequently transformed to a thiol acetate, which can then be

oxidized with H₂O₂ after cleavage to produce the free sulfonic acid.^[112,113] However, the synthesis of sulfonic acids was not successful following this reaction pathway.

All of the synthesized acids were purified by acid-base extraction and precipitation from water at low pH values. Column chromatography, recrystallization and HPLC were performed if needed.

It should be noted that all of these reactions had to be carried out twice on the same molecule, which in turn drastically affected the yields.

With this in mind, a retrosynthetic analysis for the synthesis of the **LS1** derived library is presented (Figure 4.2.2-3).

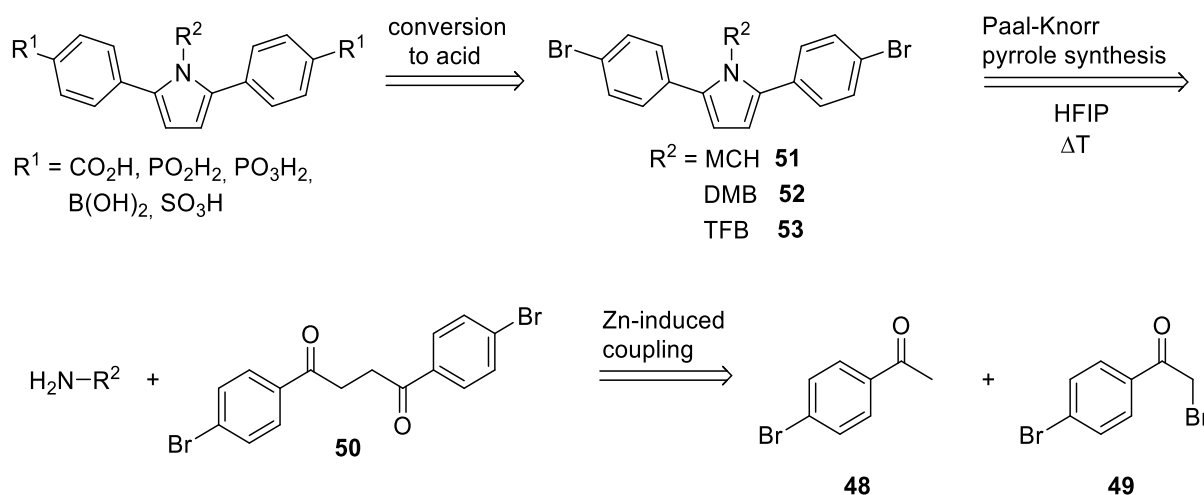


Figure 4.2.2-3. Retrosynthetic approach to **LS1**.

The general approach that was used for the dibromides was identical to the one used for the dicyanides (see Figure 4.2.1-5). The zinc-induced coupling produced the 1,4-diketone (**50**) in moderate yield (63%) after a reaction time of 7 days at room temperature. Followed by the already introduced Paal-Knorr pyrrole synthesis (the amines were also commercially available) this sequence yielded both of the two needed precursors in only four total steps for each alteration of **R**. Since three different alkyl residues were envisaged based on their performance in *in silico* screenings, eight individual reactions would allow the synthesis of the precursor molecules for the ensuing transformation into the acid moieties. Those summed up to 24 individual reaction steps – combination of these two sequences resulted in 32 individual reactions in order to generate the desired library of molecules for subsequent biophysical analysis.

An overview about the synthesized compounds and yields is given in Table 4.2.2-1. Since most of the reactions were performed similarly with the only variable being the primary amine and consequently the *N*-substitution, the reactions are not noted individually. Reactions already described in the previous chapter will be depicted again to present the entirety of the **LS1** – derived syntheses.

Table 4.2.2-1. Summarized yields of the library synthesis of **LS1**.

	32 (1,4-diketone CN ^a)	50 (1,4-diketone Br ^b)	PKS CN	PKS Br	CO ₂ H ^c	PO ₂ H ₂ ^d	PO ₃ H ₂ ^e	B(OH) ₂ ^f	SO ₃ H ^g
MCH	70%	63%	42 65%	51 78%	1 88%	10 53%	13 43%	16 68%	/
DMB	70%	63%	40 56%	52 43%	2 82%	11 64%	14 52%	17 48%	/
TFB	70%	63%	41 50%	53 61%	3 73%	12 53%	15 13%	18 41%	*

Reaction conditions: **a,b**) 1 bromoketone, 1.5 ketone, 2 ZnCl₂, 1.5 EtOH, 1.5 Et₃N, toluene, rt, 7 d; **c**) 1 **a**, 10 KOH, EtOH, H₂O, ΔT; **d**) 3 PhNH₂H₃PO₂, cat. Pd₂(dba)₃, cat. Xantphos, 3 Et₃N, 1 **b**, toluene, 90 °C, 3 h; **e**) 2 HPO(OEt)₂, 2 Et₃N, cat. Pd(dppf)Cl₂, 1 **b**, toluene, 110 °C, 12-16 h *then* 10 TMSBr, DCM, MeOH; **f**) 3 *n*BuLi, 1 **b**, THF, -78 °C *then* B(OEt)₃, HCl; **g**) 2 ^{DMBSH}, 2 NaO^tBu, cat. Pd(OAc)₂, cat. CyPF-^tBu, DME, 1 **b** 110 °C, 3 h *then* 6 BBr₃, 10 AcCl, toluene *then* 10 KOH, 10 H₂O₂, MeOH, H₂O. *reaction did not produce the desired product.

As shown in Table 4.2.2-1, the yields vary drastically, considering the reactions of the same acid group were done using the exact same protocol. The observed solubilities of the respective acids showed a broad variance, seriously restricting a clean work-up using acid-base extraction and subsequent precipitation. This might explain the low yields especially for the boronic acids. No efforts were spent to maximize yields, since only a very small amount of material was required to perform the biophysical measurements. Furthermore, the low yields could be compensated to some extent by producing ample starting material (the two 1,4-diketones (**32**) and (**50**)).

Another factor that needed to be taken into consideration was a side reaction that occurred during the synthesis of the sulfonic acid derivatives. Since this side reaction proved to make the timely synthesis of said molecules impossible, it will be explained shortly (see Figure 4.2.2-4): A literature-known transformation of aryl bromides to tert-butyl protected aryl thiols by means of a cross-coupling reaction was employed to synthesize the corresponding di-substituted pyrrole (**54**) in excellent yields.^[113] Lewis-acid promoted deprotection followed by immediate *in situ* acetate protection provided the reprotected pyrrole in moderate yields. Unfortunately, the used conditions allowed

a Friedel-Crafts-type acetylation at the pyrrole backbone. The obtained molecule (**55**) was unsuitable for further reactions since it would be very challenging to remove an aryl-acetate moiety from the pyrrole backbone. Possible reaction steps to achieve this transformation could be the oxidation of the ketone to an ester *via* a copper catalyzed reaction^[114] followed by a decarboxylation reaction. These steps would require harsh reaction conditions and were not tested during this thesis. The final reaction step – a base catalyzed deprotection followed by *in situ* oxidation using potassium hydroxide and hydrogen peroxide – was tested and delivered the desired sulfonic acid, albeit the acetylated one (**56**). No yield was determined since the purification was only performed using small amounts.

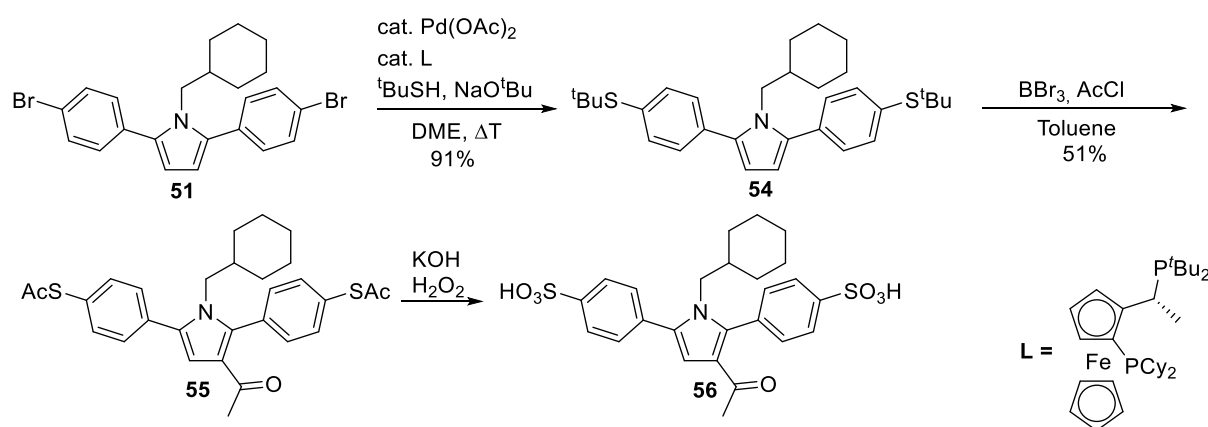


Figure 4.2.2-4: Pathways and side reactions concerning the synthesis of the sulfonic acids. These reactions were performed by DIANA MUKANOV in her master thesis.

It should be stated that in current studies, the acetylated pyrrole (**58**) is synthesized by palladium-catalyzed cross-coupling between the dibromide (**51**) and potassium thioacetate (**57**) in toluene (Figure 4.2.2-5). No side reactions on the pyrrole backbone were observed. It is noteworthy, that the same transformation of aryl bromides to aryl thioacetates was also successfully performed on the 1,4-diketone stage.

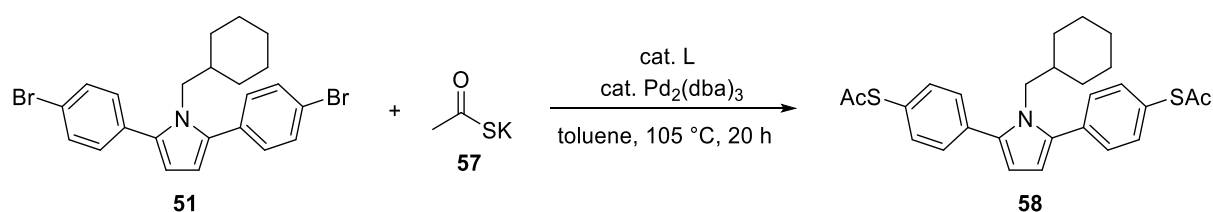


Figure 4.2.2-5: Alternative syntheses to the desired sulfonic acids. These reactions were performed by DIANA MUKANOV her master thesis.

In summary, the **LS1** based library of twelve different molecules was successfully synthesized; the resulting structures are depicted in Figure 4.2.2-6.

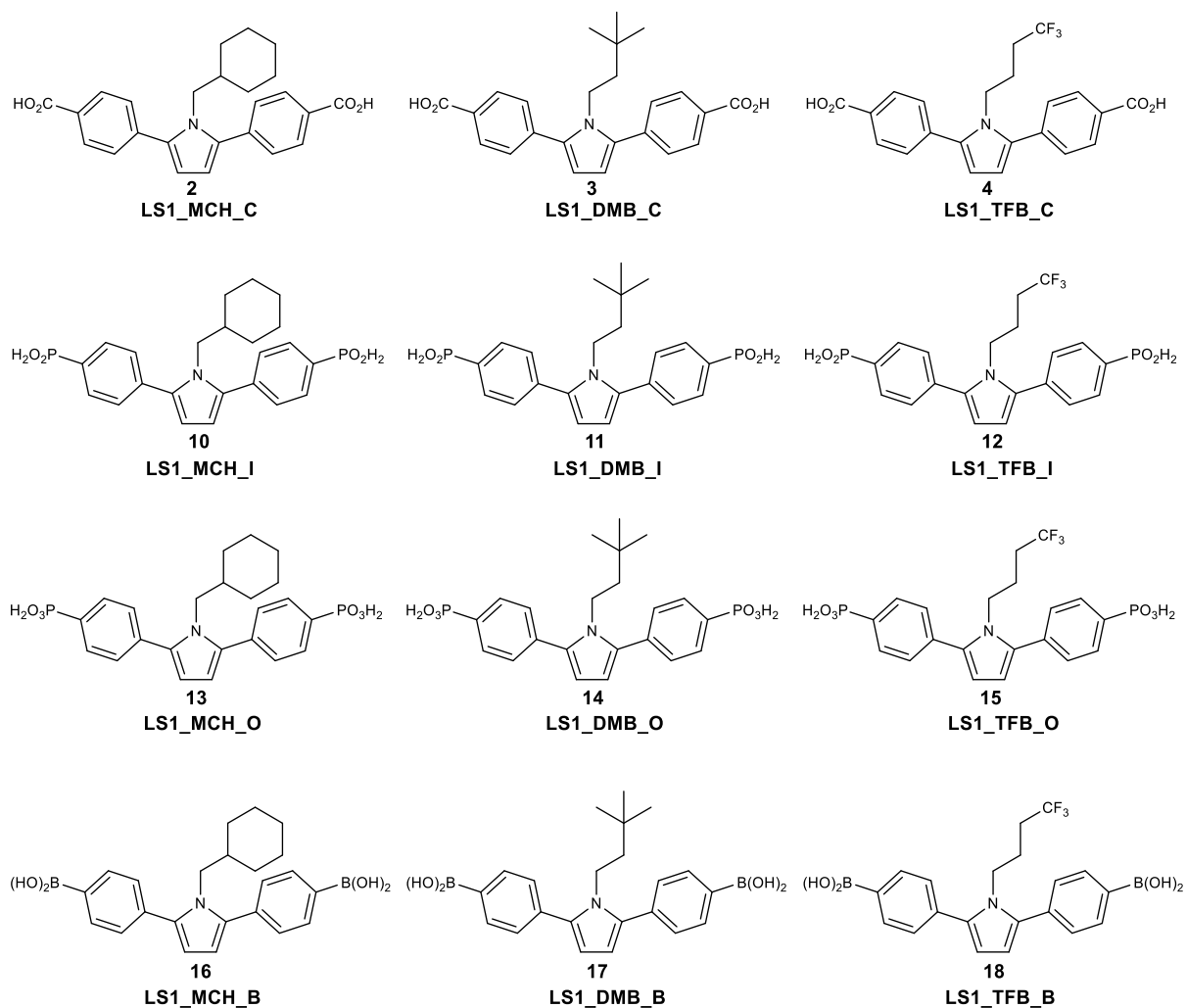


Figure 4.2.2-6. Overview about the synthesized molecular library based on **LS1**.

4.2.3 HFIP in the Paal-Knorr synthesis of pyrroles

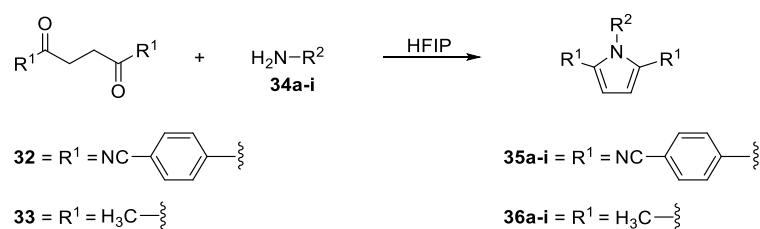
After optimizing the reaction conditions for the Paal-Knorr pyrrole synthesis in HFIP, the scope of the reaction protocol was investigated by reacting the two introduced diketones **32** and **33** with a range of different primary amines.

Generally, reactions with **33** were much faster than with **32** as expected, which is also reflected in much higher yields when using the alkyl over the aryl diketone. In addition, the reactions of **32** were run at reflux whereas **33** was reactive at room temperature for most of the amines.

The reaction between **32** and aliphatic amines **34a-f** gave isolated yields between 50% and 76%, representing average to good results for this reaction type (Table 4.2.3-1, entries 1-6). Aniline and its derivatives **34g-i** produced lower yields in the Paal-Knorr pyrrole synthesis (Table 4.2.3-1, entry 7-9) due to their lower nucleophilicity. The very electron-poor 4-nitroaniline showed no conversion at all under the chosen reaction conditions (Table 4.2.3-1, entry 9).

The reaction between **33** and aliphatic amines **34a-f** resulted in almost quantitative yields even at room temperature, highlighting the high reactivity of both reaction partners (Table 4.2.3-1, entries 10-15). Reactions using the less reactive aniline derivatives **34g-i** were conducted at reflux, giving very good yields between 88 and 90% (Table 4.2.3-1, entries 16-18).

Table 4.2.3-1. Reaction Scope of Paal-Knorr-Pyrrole Synthesis with Varying Amines.



entry	amine	32	yield	entry	amine	33	yield
1 ^a		32	35a , 74%	10 ^b		33	36a , 99%
2 ^a		32	35b , 76%	11 ^b		33	36b , 99%
3 ^a		32	35c , 56%	12 ^b		33	36c , 97%
4 ^a		32	35d , 50%	13 ^b		33	36d , 94%
5 ^a		32	35e , 65%	14 ^b		33	36e , 98%
6 ^a		32	35f , 76%	15 ^b		33	36f , 96%
7 ^a		32	35g , 61%	16 ^c		33	36g , 90% ^c
8 ^a		32	35h , 41%	17 ^c		33	36h , 88% ^c
9 ^a		32	35i , 0%	18 ^c		33	36i , 90% ^c

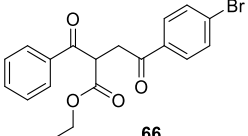
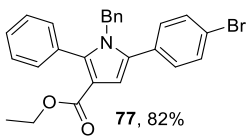
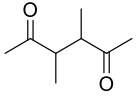
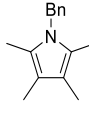
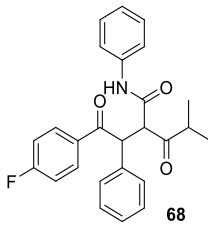
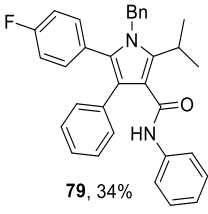
^a48 h, reflux; ^b5 min, room temperature; ^c15 min, reflux. Yields refer to isolated compounds.

The next step was the application of the optimized reaction conditions to a variety of 1,4-diketones, using **34a** as the primary amine. The results are depicted in Table 4.2.3-2.

Table 4.2.3-2. Reaction Scope of Paal-Knorr furan synthesis with varying 1,4-diketones.

entry	diketone	t (h)	yield
1		48	 35a, 74%
2 ^a		< 0.1	 36a, 99%
3		48	 69, 62%
4		48	 70, 82%
5		48	 71, 79%
6		48	 72, 66%
7		48	 73, 71%
8		48	 74, 79%
9		48	 75, 78%
10		72	 76, 74%

^a Reaction was performed at room temperature. Yields refer to isolated compounds.

entry	diketone	t (h)	yield
11	 66	72	 77, 82%
12 ^a	 67	< 0.1	 78, 82%
13	 68	72	 79, 34%

^a Reaction was performed at room temperature. Yields refer to isolated compounds.

The use of symmetrical aromatic diketones resulted in moderate to good yields of the desired pyrrole after two days of heating the reaction mixture to reflux (Table 4.2.3-2, entries 1 and 3-6). Surprisingly, the non-substituted **59** gave lower yields than the substituted derivatives, even if compared to the very electron poor para-nitro substituted diketone **61** (Table 4.2.3-2, entries 3 and 6). Non-branched mixed 1,4-diketones **62**, **63** and **64** gave comparable results to the symmetrical diketones, the same was true for the sterically more demanding branched 1,4-diketones **65** to **67** (Table 4.2.3-2, entries 10-12). It is reasonable to conclude that the electronic nature of the diketones plays an equally important role as the steric demand of the substrates, resulting in somewhat arbitrary results. The tetra-substituted Atorvastatin^[115] precursor **68** was unreactive when the optimized reaction conditions were employed. This problem could be overcome by increasing the temperature of the HFIP solution to 90 °C in a pressure tube. After heating for 3 days, dilution of the concentrated HFIP solution with a mixture of ⁱPrOH and acetone led to the crystallization of the product in 34% yield without the need of further purification (Table 4.2.3-2, entry 13).

In summary, the optimized reaction conditions employing HFIP as a solvent and reaction promotor were suitable for the production of the desired pyrrole precursors for subsequent library synthesis. Furthermore, the protocol could be expanded to a range of different diketones and primary amines, resulting in practically useful yields for almost all investigated reactions.

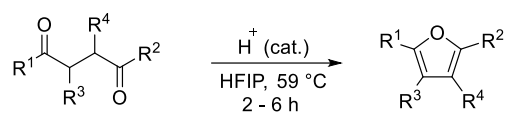
4.2.4 HFIP in the Paal-Knorr synthesis of furans and thiophenes

The use of HFIP as an acid catalyst in the synthesis of pyrroles led to the question whether this approach was beneficial for the synthesis of furans and thiophenes as well. Generally, the respective 1,4-diketone is dissolved in an appropriate solvent and heated under Brønsted- or Lewis-acid catalysis to give the furan compound.^[116] Unfortunately, heating of **32** in HFIP for prolonged times did not produce any furan, which probably meant that the acidic properties of HFIP were not strong enough for being a promising catalyst. Instead, heating of **32** in HFIP with a catalytic amount of hydrochloric acid resulted in the formation of the respective furan compound in 88% yield (Table 4.2.4-1, entry 1). All other 1,4-diketones resulted in yields ranging from 91% for the para-bromo substituted **50** to 55% for the tetra-substituted Atorvastatin precursor **68** (Table 4.2.4-1, entries 2-10).

The Paal-Knorr thiophene synthesis is synthetically more challenging than the furan synthesis since a sulfur atom needs to be introduced into the diketone prior to the nucleophilic attack. This means that the corresponding furan is a typical byproduct of thiophene synthesis since both of these processes happen on a similar time scale. Lawesson's reagent was used as the sulfur-source and was added to a solution of the diketone in HFIP, which was heated under reflux overnight. The diketones **46**, **99** and **100** reacted cleanly and gave good yields of the desired thiophenes (Table 4.2.4-2, entries 2-4), while diketones **97** and **103** gave inseparable mixtures of thiophenes and furans in a somewhat lower yield (Table 4.2.4-2, entries 1 and 5).

In summary, a new protocol for the Paal-Knorr synthesis of pyrroles, furans and thiophenes employing HFIP as solvent and reaction promotor was presented. This protocol is broadly applicable to a plethora of different diketone and/or amine compounds. The protocol shows deficiencies when it comes to sterically demanding substrates and requires mineral acid catalysts for the synthesis of furans. On the other hand, Paal-Knorr synthesis of 1,4-diketones with electron poor aromatic systems has scarcely been reported, probably due to a combination of solvation issues and the general lower reactivity, but several of these compounds were used successfully using the HFIP protocol.

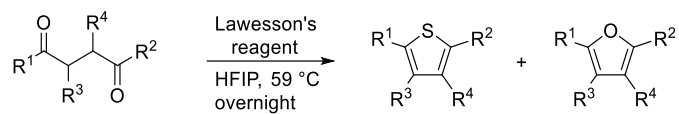
Table 4.2.4-1. Reaction scope of Paal-Knorr furan synthesis with varying 1,4-diketones.



entry	diketone	yield ^a
1	32	 80, 88%
2	59	 81, 80%
3	50	 82, 91%
4	61	 83, 85%
5	62	 84, 76%
6	63	 85, 87%
7	64	 86, 82%
8	65	 87, 70%
9	66	 88, 85%
10	68	 89, 55%

^aYields refer to isolated compounds.

Table 4.2.4-2. Reaction scope of Paal-Knorr thiophene synthesis with varying 1,4-diketones.



entry	diketone	yield ^a	
1 ^{a, b}	 59	 90, 56%	 81, 14%
	 50	 91, 83%	 82, not detected
3	 61	 92, 82%	 83, not detected
	 62	 93, 73%	 84, not detected
5 ^a	 65	 94, 39%	 85, 31%

^aYields were estimated from NMR integrals. All other yields refer to isolated compounds. ^b**90** has been purified by recrystallization giving a yield of 15%.

4.3 Synthesis of **LS2**

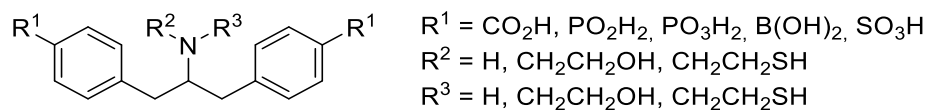


Figure 4.3-1. General structure of **LS2**. The amine can be mono- or disubstituted with an alkyl group, leading to two different variants of this backbone.

The retrosynthesis of **LS2** offered a more complex pattern of possible pathways compared to that of **LS1** since more than one structure was possible. In this chapter, the synthesis of the mono-*N*-substituted ligand is depicted. The synthesis of the di-*N*-substituted structure will be explained in a separate part of this thesis.

The alkyl residues R^2 and R^3 were designed to enable covalent binding to the protein if desired. To achieve this, the alcohol groups would be replaced with thiol groups, which could then form disulfide bridges with Cys₁₁₁ of the protein, tethering both monomers together.

It should be noted that the already established methods of synthesizing the acid groups from the respective bromides and/or nitriles were also valid for **LS2**, therefore no new synthetic pathways were needed to be explored in that regard. The retrosynthetic approach for the synthesis of **LS2** is shown in Figure 4.3-2.

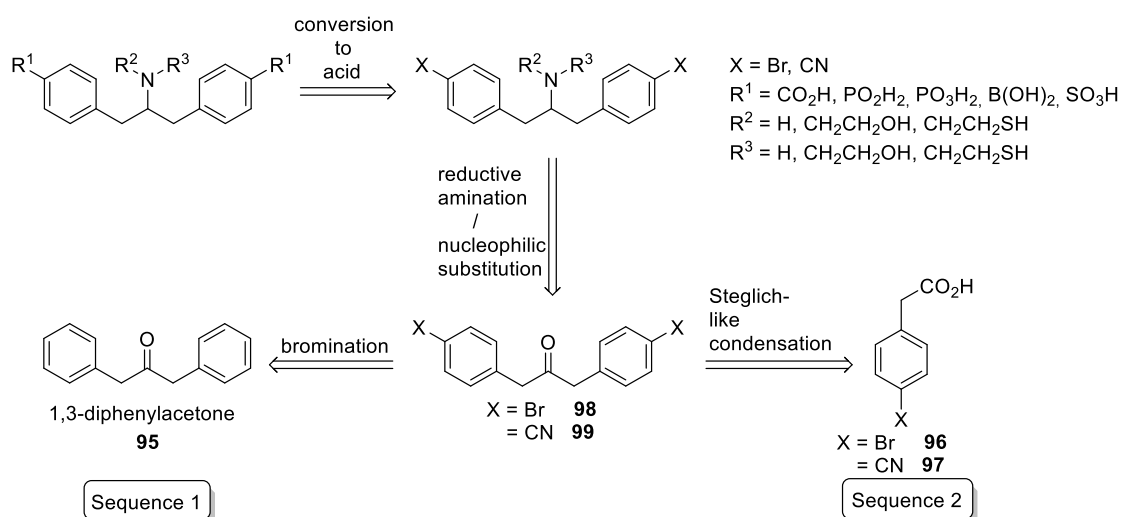


Figure 4.3-2. Retrosynthetic approach to **LS2**.

The conversion to the acid moieties can be conducted according to Figure 4.3-2 from halide/nitrile precursors. The substituted amine moiety is accessible from a ketone

moiety through reductive amination to give the primary amine, followed by a nucleophilic substitution. The ketone precursor can be synthesized *via* two different sequences: Sequence 1 starts with the ketone moiety already installed and introduces the halogen at the benzene moieties. Sequence 2 starts with a phenylacetic acid derivative, pre-functionalized with a halogen or nitrile. Both sequences are combined at the ketone stage.

4.3.1 Sequence 1

The first approach started with the backbone already set up by the commercially available 1,3-diphenylacetone and aimed to introduce the acid groups by brominating the benzene moieties followed by subsequent conversion to the acid groups.

First, different bromination methods, chosen from comprehensive arrays of literature known methods, were tested. Two reactions were selected: The NBS-mediated bromination in HFIP and the AlBr_3 catalyzed bromination with elemental bromine.^[117] Unfortunately, none of the reactions produced the desired product; also, no bromination in α -position to the ketone was observed (see Figure 4.3.1-1).

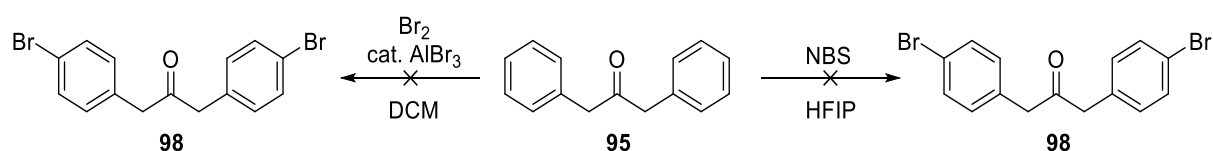


Figure 4.3.1-1. Failed bromination of 1,3-diphenylacetone.

The next reaction that was examined was the reductive amination since it would also be required if Sequence 2 was chosen. Once more, a plethora of different literature-known reactions was available to choose from: The reductive amination in TFE using NaBH_4 as a reducing agent as well as a sodium triacetoxyborohydride mediated process were tested.^[118,119] Further trials were performed by undergraduate students; however, all efforts to use secondary amines in this kind of reaction were unsuccessful. This was probably due to two factors: Firstly, the enol form of the ketone would result in a conjugated system, favoring it over the ketone form, reducing the reactivity in condensation reactions with amines. Secondly, the steric bulk by the two aromatic rings further impaired the reactivity.

Thus, the strategy needed to be split up in two parts: First, the synthesis of a free primary amine was performed, which was followed by a nucleophilic substitution to obtain the desired mono- and disubstituted products. The synthesis of the free primary amine is depicted in Figure 4.3.1-2.

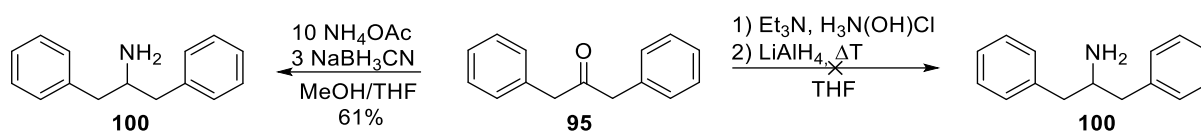


Figure 4.3.1-2. Reductive amination of 1,3-diphenylacetone.

The first reductive amination method that was tested was a two-step sequence: The ketoxime was synthesized by the reaction of the ketone with hydroxylamine-hydrochloride in the presence of triethylamine in good yields. However, the complete reduction with lithium aluminum hydride in refluxing THF only yielded a complex mixture of the ketoxime, hydroxylamine and free amine that was impossible to purify. Instead, the amine (**100**) was successfully obtained by the reaction of the ketone (**95**) with a large excess of ammonium acetate and sodium cyanoborohydride in a mixture of MeOH and THF in 61%. The resulting product was converted to the hydrochloride salt and recrystallized from *i*PrOH.

In summary, Sequence 1 did not produce the desired product, but a reductive amination strategy was established, including a purification method for the hydrochloride salts of similar products that would be beneficial for Sequence 2.

4.3.2 Sequence 2

Sequence 2 started from commercially available phenylacetic acid derivatives, functionalized with either a nitrile or a bromide moiety (**96** and **97**). Not many methods are known to produce 1,3-diaryl substituted acetones: One pathway is a Dakin-West like approach, starting from phenylacetic acid using NaOAc and Ac₂O under reflux, followed by distillation.^[120] Another approach makes use of a strong base to induce a Claisen condensation of a phenylacetic acid ester to produce α-β-keto ester which undergoes acidic saponification and subsequent decarboxylation.^[121] None of these reactions seemed to be suitable to generate large amounts of the precursor material, therefore a different, lesser-known reaction pathway was chosen. The respective

phenylacetic acid derivative was self-condensed in the presence of 0.6 equiv. of DCC and 0.3 equiv. of DMAP in anhydrous DCM, which produced the desired products (**98** and **99**) in moderate yields.^[122] This reaction path, reminiscent of Steglich-like reactions, is shown in Figure 4.3.2-1.

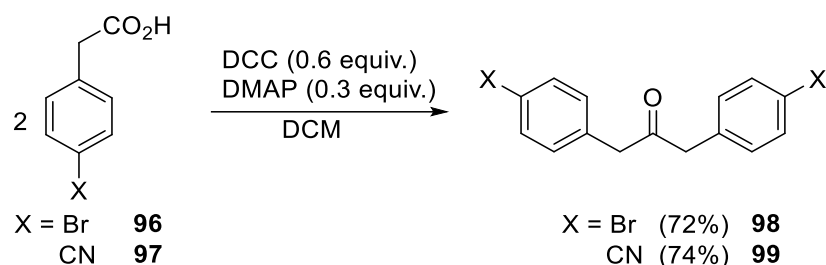


Figure 4.3.2-1. Steglich-like condensation of phenylacetic acid derivatives.

Once the ketone was synthesized, the reductive amination was performed as described for sequence 1 (Figure 4.3.2-2).

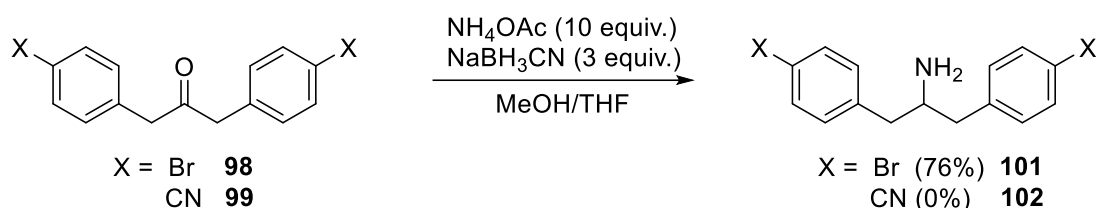


Figure 4.3.2-2. Primary amine synthesis by reductive amination as shown for Sequence 1.

The nitrile-substituted ketone derivative (**99**) did not undergo reductive amination but instead produced a complex mixture of products probably due to dimerization reactions between intermediate imides and nitriles. The bromide-substituted ketone derivative (**98**) was transformed to the insoluble hydrochloride salt (**101**) with moderate to good yields (ca. 60-80%). This presented a problem since there would be the need for a way to produce carboxylic acids from aryl bromides instead of using nitriles as a precursor. A reasonable reaction using metal-halogen exchange followed by quenching with CO_2 was proposed for this purpose (Figure 4.3.2-3)^[123]:

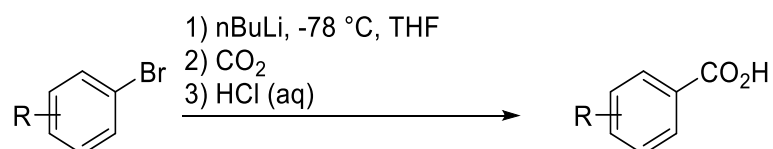


Figure 4.3.2-3. Alternative synthesis of carboxylic acids from aryl bromides.

The next step in Sequence 2 was a nucleophilic substitution with a suitable O-protected bromide, which led to the mono-substituted secondary amine (**103**) in moderate yields by refluxing the reaction mixture in MeCN in the presence of K_2CO_3 (Figure 4.3.2-4). The disubstituted, tertiary amine unexpectedly did not form during this reaction, even though secondary amines are usually more nucleophilic than primary amines. Steric bulk from the two 4-bromophenyl moieties might have been the reason for this outcome and changing the reaction conditions to higher boiling solvents such as toluene, stronger bases such as Cs_2CO_3 or increased amounts of reactants did not change the result.

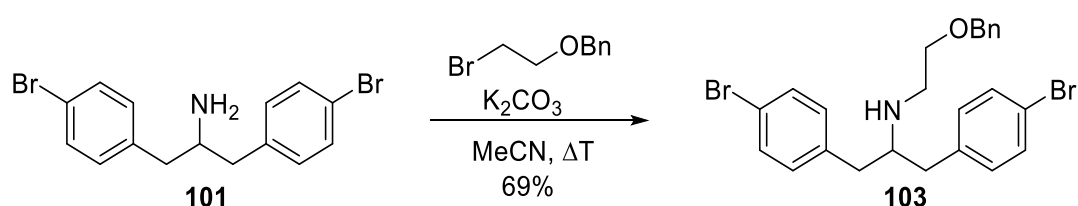


Figure 4.3.2-4. Nucleophilic substitution towards the mono-substituted precursor.

This precursor was now ready for the implementation of the different acid groups in the manner already described in the previous chapter. The only acid that was synthesized was the carboxylic acid using the conditions from Figure 4.3.2-3. The complete reaction sequence for the synthesis of **LS2** is shown in Figure 4.3.2-5.

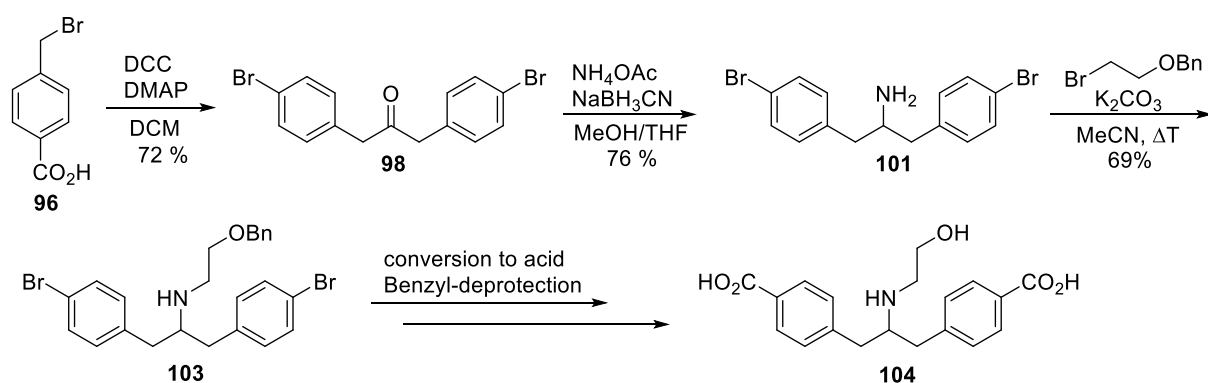


Figure 4.3.2-5. Synthetic pathway to the monosubstituted **LS2**.

The yield of the final carboxylic acid (**104**) was very low due to the harsh reaction conditions that had to be used as well as tedious purification processes and inconvenient solubility properties. Furthermore, only a small amount of residue was processed so no yields are given for that reaction sequence.

In summary, the pathway shown in Figure 4.3.2-5 was identified as a plausible sequence, in which the desired organic residues could be synthesized except for the carboxylic acids. As explained above, this is because the nitrile precursor amine could not be synthesized successfully (see Figure 4.3.2-2), and the final conversion of aryl bromides to aryl carboxylic acids gave mediocre results at best.

To overcome this issue, a different pathway to the carboxylic acids was proposed (Figure 4.3.2-6):

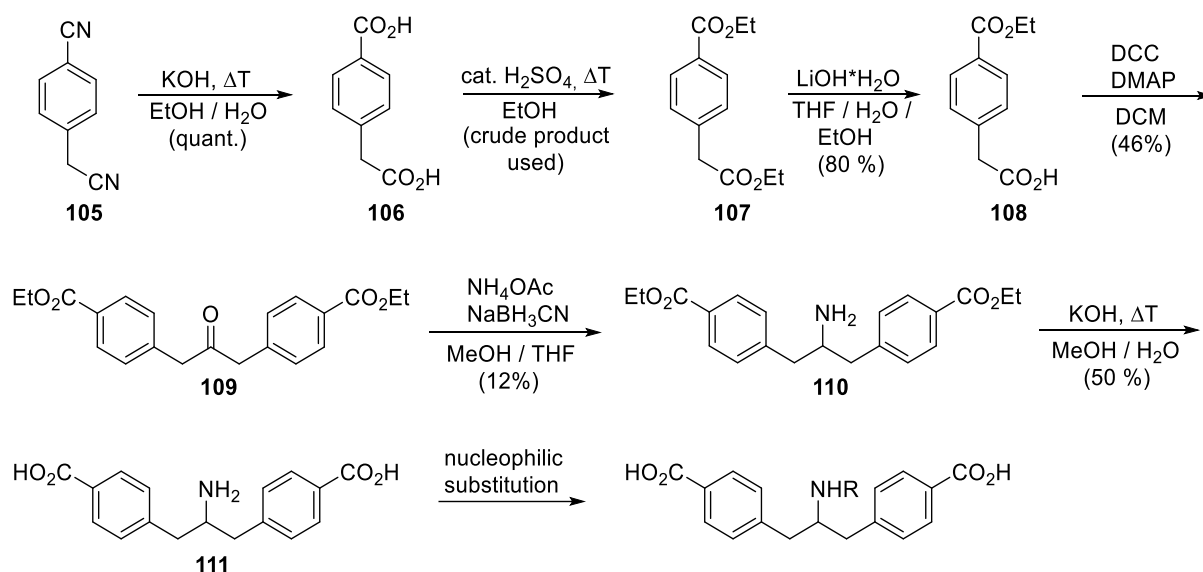


Figure 4.3.2-6. Alternative reaction sequence to the monosubstituted carboxylic acid derivatives of **LS2**.

Starting from the commercially available 4-cyanobenzyl cyanide (**105**), a three-step sequence was necessary to obtain the desired phenylacetic acid derivative (**108**) since a direct esterification of the nitriles (e.g., the Pinner reaction) produced large amounts of oligomers when more than one nitrile is present on the starting material. Consequently, the nitriles were hydrolyzed to carboxylic acids (**106**) in strongly alkaline media in quantitative yield, which subsequently were transformed to the ethyl esters by means of Fischer esterification (**107**). The crude product was directly submitted to saponification under very mild conditions with lithium hydroxide, leading to the selective cleavage of the alkyl ester over the aryl ester in good yield.

This precursor was now subjected to the same reaction sequence that was already described in detail. Noteworthy, the reductive amination to the primary amine proceeded with very poor yield; this is most likely due to unfavorable solubility of the resulting structure **110**. Liquid phase extraction of the amine hydrochloride was not

suitable for the isolation of the pure compound since a large amount of product was soluble in the organic phase (EtOAc) as well as in the aqueous phase and was lost this way.

Prior to the nucleophilic substitution, the esters had to be cleaved to prevent amide formation via intra- or intermolecular mechanisms under the utilized reaction conditions (heat, base, polar aprotic solvents). To achieve this, basic hydrolysis was performed in 50% yield and the final molecule (**111**) was obtained as the hydrochloride salt in high purity. Due to time restrictions and the absence of commercially available reaction partners for nucleophilic substitution, this specific reaction was not performed during the course of this thesis. Still, this reaction route represents a suitable route for the synthesis of the monosubstituted carboxylic acid derivative of **LS2**.

4.3.3 Direct approach for the disubstitution of **LS2**

Since the reductive amination was not successful with secondary amines and nucleophilic substitution only gave secondary amines, it was not possible to obtain the disubstituted **LS2** using these procedures. Instead, a different pathway was envisaged:

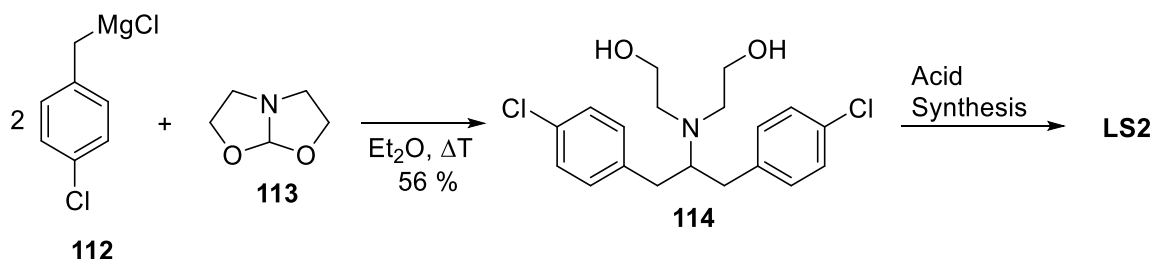


Figure 4.3.3-1. Synthetic pathway to the disubstituted **LS2**.

The commercially available 4-chlorobenzylmagnesium chloride (**112**) was reacted with the also commercially available di-*N,O*-acetale (**113**) in refluxing diethyl ether by means of a Grignard reaction (Figure 4.3.3-1).^[124] This afforded the full core structure (**114**) of the disubstituted **LS2** in one reaction step with 56% yield. Since both reagents were very expensive and very difficult to synthesize, only a very small amount of product could be produced. Furthermore, the purity of the product was only moderate even after column chromatography. Transformation into the hydrochloride salt (or other salts, e.g., sulfate or tartrate salts) and subsequent recrystallization could prove beneficial for the purification. Nevertheless, this method could potentially prove to be a reasonable route to the desired structure.

4.3.4 Synthesis towards a colorimetric assay for binding observation between LS2 and SOD1

Another long-term goal was the functionalization of the mono- or disubstituted structure with a dye that would allow following the binding properties of **LS2** via UV/VIS-spectroscopy. To achieve this goal, the already described covalent approaches needed to be addressed (see Figure 4.3.2-5 and/or 4.3.3-1). In order to render the lead structure cysteine-reactive, the alcohol moieties had to be converted to thiol groups. Afterwards the functionalization with a dye could be carried out, a suitable one being the cysteine-reactive molecule 5,5'-disulfanediybis(2-nitrobenzoic acid), also known as *Ellmanns reagent* or DTNB.^[125] This approach is summarized in Figure 4.3.4-1.

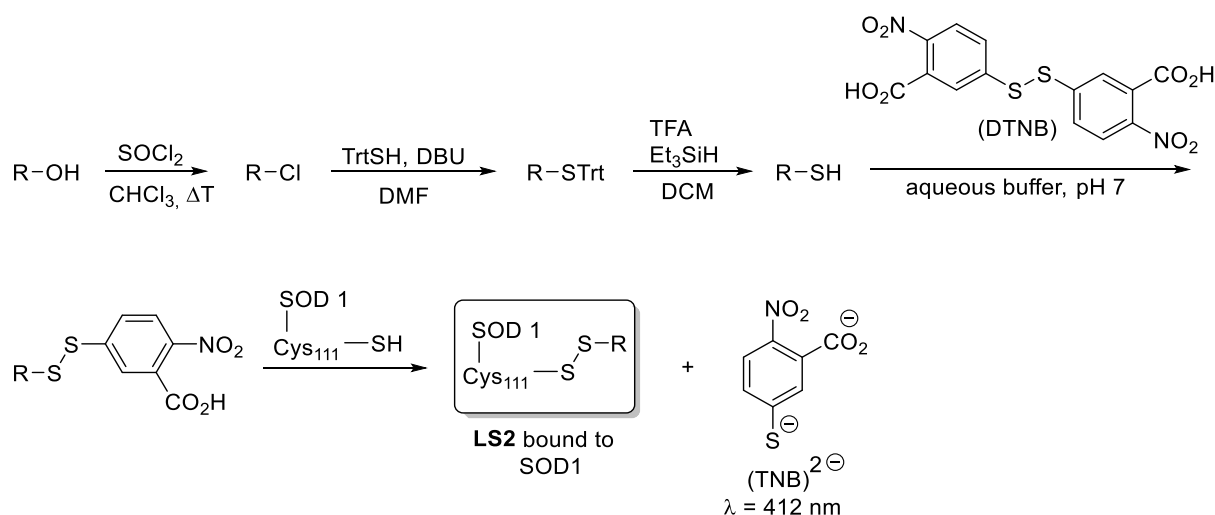


Figure 4.3.4-1. Synthetic scheme for the functionalization of **LS2** with a dye and release of the spectroscopically detectable TNB dye upon binding to SOD1.

As can be seen, the alcohol could be converted to a thiol following a literature known approach by chlorinating said alcohol with thionyl chloride in refluxing chloroform.^[126] The chloride could then be replaced by a protected thiol *via* nucleophilic substitution, which could be cleaved under acidic conditions to afford the free thiol. Formation of a disulfide bridge in aqueous buffer medium with DTNB would then afford the desired functionalized structure. Thiols in biomolecules, such as the free cysteines in SOD1, are able to react with the DTNB-functionalized structure, giving rise to the covalently tethered SOD1 and the TNB dye that is deprotonated twice under moderately alkaline or neutral conditions. Photometrical measurements at 412 nm with known extinction

coefficients would then allow for the quantification of released TNB and consequently of the binding of the lead structure to the protein.

It must be noted that certain requirements need to be fulfilled in order to gain reliable results: Preferably there must be only one possible reaction side for the functionalized molecule in order to ensure that the binding site on the protein remains identical. Furthermore, the functionalized molecule must have a similar affinity to the protein compared to the unfunctionalized molecule; else, no comparison can be made. The binding should be reasonably fast, otherwise photobleaching could diminish the amount of detectable free TNB and lead to false data.

No tests on the core motif of **LS2** were performed. Instead, a model system was used to mimic the reactivity of the dithiol handle and to investigate the reaction conditions (Figure 4.3.4-2).

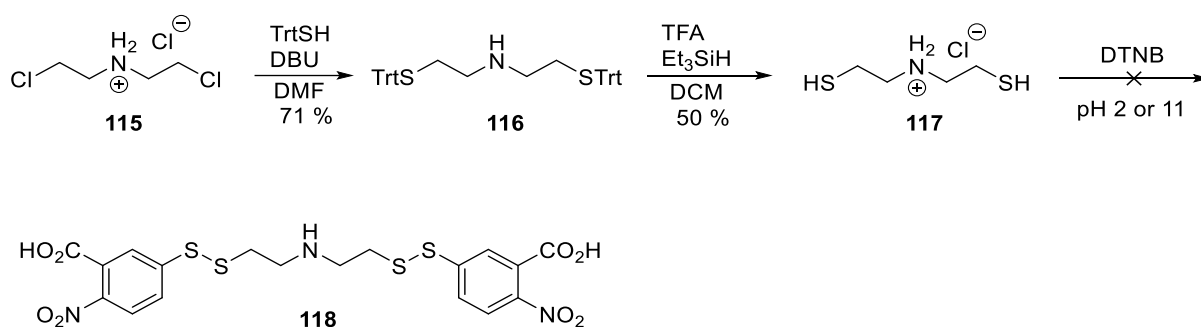


Figure 4.3.4-2. Synthesis of a model system for the DTNB-functionalized **LS2**.

The commercially available bis(2-chloroethyl)ammonium chloride (**115**) was treated with TrtSH in DMF in the presence of DBU to afford the protected dithiol (**116**) in 71% yield. Deprotection with TFA and Et₃SiH in DCM yielded the free dithiol in the form of the hydrochloride salt and small amounts of the disulfide-bridged product (**117**). Functionalization with DTNB under acidic or basic conditions failed to deliver the desired product, therefore, neutral conditions under buffer control seemed to be the most suitable conditions for this test. The optimization of this reaction was not performed during this thesis.

4.3.5 Summary of the advances towards **LS2**

In summary, **LS2** could not be synthesized completely, even though several important advances toward the synthesis could be realized (Figure 4.3.5-1):

For the monosubstituted structure, a reasonable approach was found to deliver the bromide precursor (**103**) in multi-gram quantities, ready for the implementation of the acid groups, in three steps with an overall yield of 13% starting from commercially available compounds.

For the disubstituted structure, a promising although expensive method could be established affording the chloride precursor (**114**) in multi-gram quantities, ready for the implementation of the acid groups.

Reaction conditions for the dye-functionalization of either the mono- or the disubstituted lead structure were investigated and a reliable protocol for the conversion of the primary alcohol to the corresponding thiol could be presented.

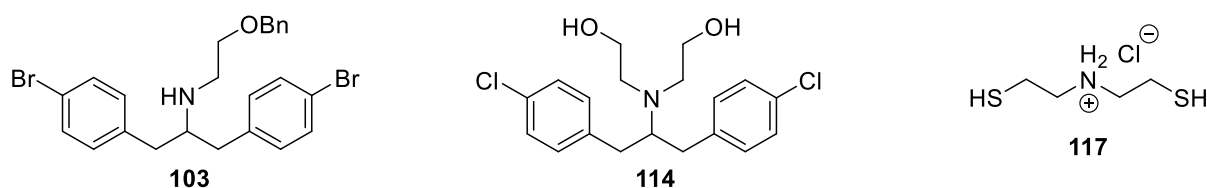


Figure 4.3.5-1. Synthesized precursors and the free thiol as a model reaction.

The synthesis of **LS2** related compounds was very tedious and many different approaches had to be tested. On the contrary, the synthesis of the **LS1** and **LS3** derived structures was more straightforward. Therefore, no optimization of the syntheses mentioned in this chapter were performed during this thesis.

4.4 Synthesis of the molecular library based on **LS3**

LS3 consisted of a biphenyl motif that was symmetrically substituted with methyl groups carrying the respective acid residues. The biphenyl core itself could either be fluorinated or non-fluorinated (Figure 4.4-1).

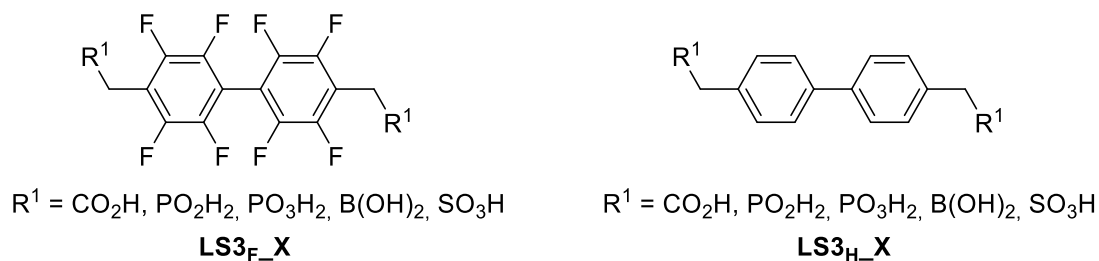


Figure 4.4-1. The two substructures of **LS3**.

The fluorinated structure was chosen as potential candidate to investigate the possibility of a covalent bond with the two Cys₁₁₁ of SOD1 *via* nucleophilic aromatic substitution (Figure 4.4-2) while the protonated structure was used for comparison.

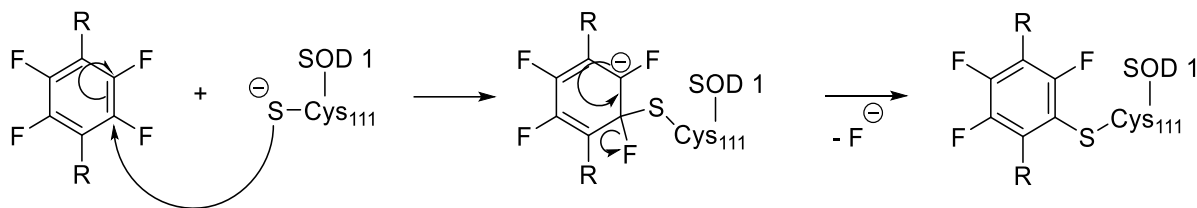


Figure 4.4-2. Mechanism of the intended nucleophilic aromatic substitution.

4.4.1 The fluorinated **LS3**

The retrosynthetic analysis of **LS3** showed a large similarity to the structures mentioned before since the acid groups were to be implemented analogically. The only difference was the fact that for **LS3** one would need to introduce those acid groups starting from alkyl bromides instead of aryl bromides. Other than that, the retrosynthetic sequence was straightforward and is presented in Figure 4.4.1-1.

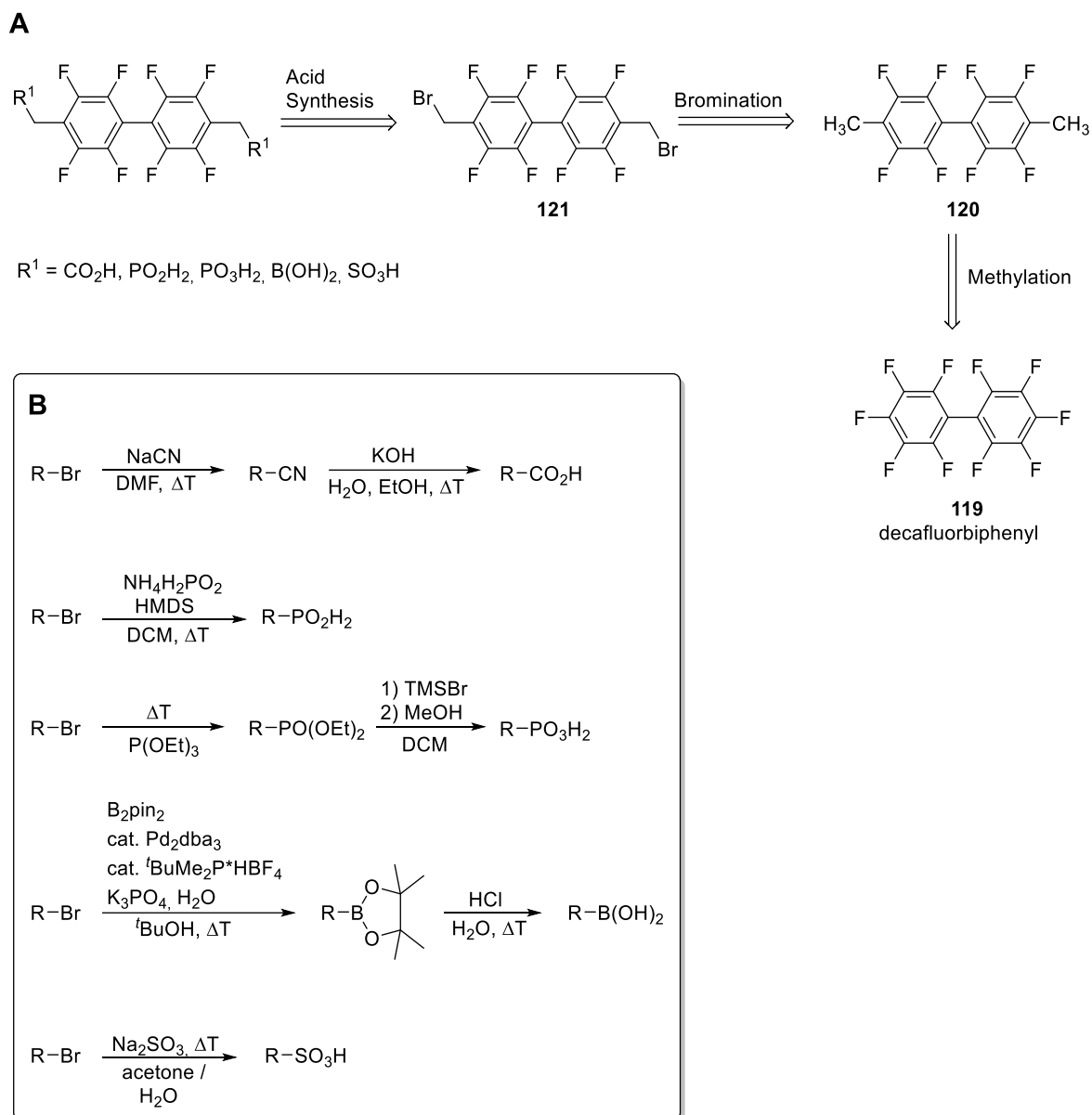


Figure 4.4.1-1. A: Retrosynthetic analysis of **LS3**. **B:** Adjusted synthesis of the different acid moieties.^[113,127,128]

Any acid required can be synthesized from a bromide precursor following the reactions depicted in Figure 4.4.1-1-B. The syntheses are largely similar to the acid syntheses used for **LS1**. The bromide precursor is accessible *via* bromination of the methylated structure, which results from methylation of the penta-fluorinated starting material.

As shown in Figure 4.4.1-1-A, the synthesis started from the commercially available decafluorobiphenyl (**119**). Methylation of this compound would give the required dimethyl compound (**120**) and was achieved by nucleophilic aromatic substitution with methyllithium at low temperatures in Et₂O and THF. This reaction proceeded with a yield of 39%. Bromination was performed according to a literature protocol using NBS in refluxing CCl₄ without the addition of a catalyst or radical starter and yielded the dibromide precursor in 70% yield (**121**).^[129] The syntheses of the acids were performed according to Figure 4.4.1-1.

Reacting the dibromide (**121**) with sodium cyanide in DMSO gave rise to the dinitrile compound (**122**), which was used without further purification. Unfortunately, all efforts to hydrolyze the nitriles to carboxylic acids (**123**) were unsuccessful (see Figure 4.4.1-2). It is assumed that the benzylic position was too reactive under strongly alkaline reaction conditions due to the very strong electron withdrawing effects of the perfluorinated aromatic system, leading to S_NX-like side reactions.

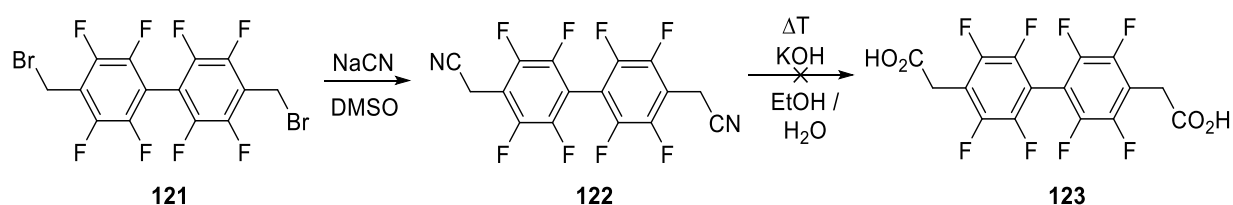


Figure 4.4.1-2. Unsuccessful synthesis of the fluorinated carboxylic acid.

The synthesis of the phosphinic acid was conducted by heating HMDS and ammonium hypophosphite for 2 h in an atmosphere of argon, followed by the addition of the dibromide precursor (**121**) (Figure 4.4.1-3).^[127] The product was obtained after acid-base extraction, but the purity was insufficient for biophysical assays. Unfortunately, all efforts to purify the product *via* HPLC failed, even though the molecule was identified with mass spectrometry and NMR, the synthesis was deemed unsuccessful.

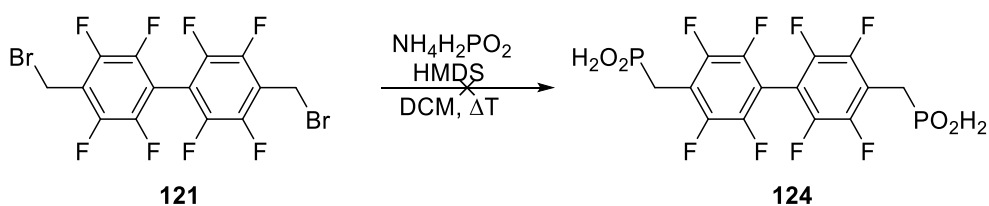


Figure 4.4.1-3. Unsuccessful synthesis of the fluorinated phosphinic acid.

The phosphonic acid was synthesized in a two-step sequence. First, the dibromide precursor (**121**) was subjected to typical Arbusow conditions employing $\text{P}(\text{OEt})_3$ with heating. The resulting diphosphonate ester (**125**) was then cleaved with TMSBr under McKenna conditions.^[110] Precipitation from acidic media gave rise to the desired product (**19**) in 32% combined yield (Figure 4.4.1-4).

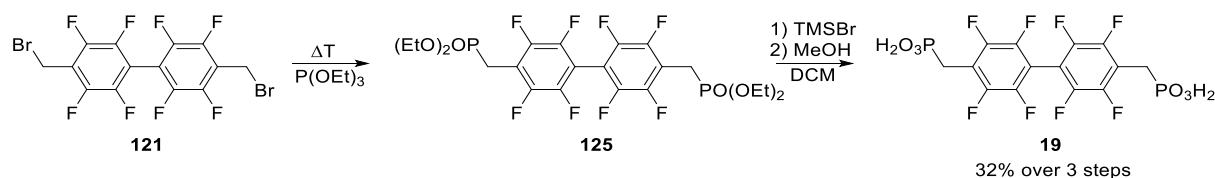


Figure 4.4.1-4. Synthesis of the fluorinated phosphonic acid.

The synthesis of alkyl boronic acids was synthetically challenging and one literature protocol was tested. The dibromide (**121**) was submitted to a palladium-catalyzed cross coupling with B_2pin_2 as the coupling partner in $t\text{BuOH}$ with the addition of several additives, but the starting material was reisolated (Figure 4.4.1-5).^[128] The different solubility properties of the dibromide precursor and the salt-additives could explain the failure of this reaction since neither was soluble enough in the alcoholic reaction medium. Changes to the solvent may prove beneficial to this synthesis, fluorinated solvents may prove to be especially suited to solubilize fluorinated structures.

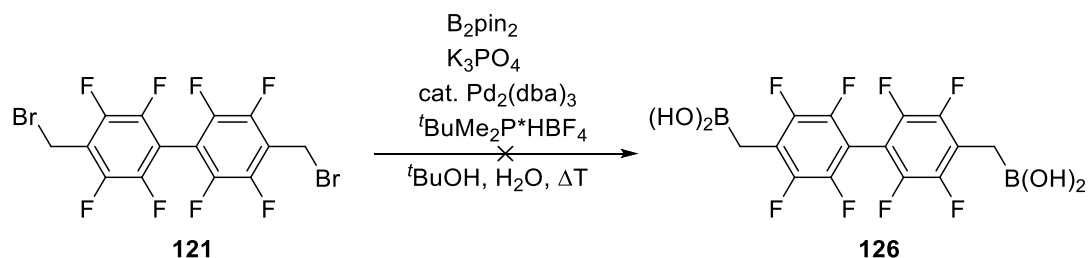


Figure 4.4.1-5. Unsuccessful synthesis of the fluorinated boronic acid.

The sulfonic acid of the fluorinated structure was successfully synthesized by reacting the dibromide (**121**) with sodium sulfite in a solvent mixture of acetone and water with heating. The product (**20**) was obtained after precipitation from strongly acidic water in 29% yield (Figure 4.4.1-6).

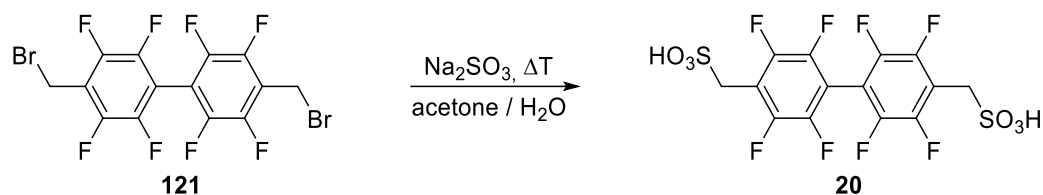


Figure 4.4.1-6. Synthesis of the fluorinated sulfonic acid.

4.4.2 The non-fluorinated **LS3**

The retrosynthetic analysis for the non-fluorinated structure of **LS3** was largely the same as for the fluorinated structure since the synthesis of the acid moieties was untouched by the change in the biphenyl core. The acids were synthesized according to Figure 4.4.1-1-B from the non-fluorinated dibromide precursor. The dibromide was accessible through bromination of the diol starting material (**127**) (Figure 4.4.2-1).

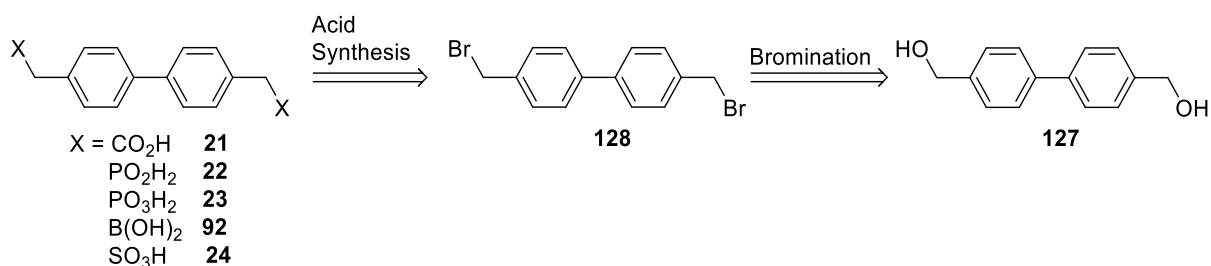


Figure 4.4.2-1. Retrosynthetic analysis of the protonated **LS3**.

The commercially available 4,4'-bis(hydroxymethyl)biphenyl (**127**) was brominated using PBr₃ and a catalytic amount of pyridine in diethyl ether (Figure 4.4.2-2). The product (**128**) was obtained in 85% yield after liquid extraction and recrystallization from a mixture of methanol and diethyl ether.

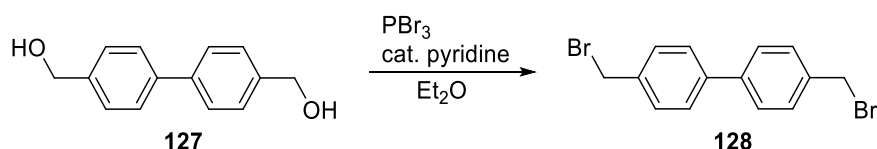


Figure 4.4.2-2. Synthesis of the dibromide precursor (**128**).

Other than that, the reactions were done using the exact same protocols as described. The carboxylic acid (**129**) and the boronic acid (**130**) could not be synthesized during this thesis.

The following **LS3** related molecules were synthesized during this thesis (Figure 4.4.2-3).

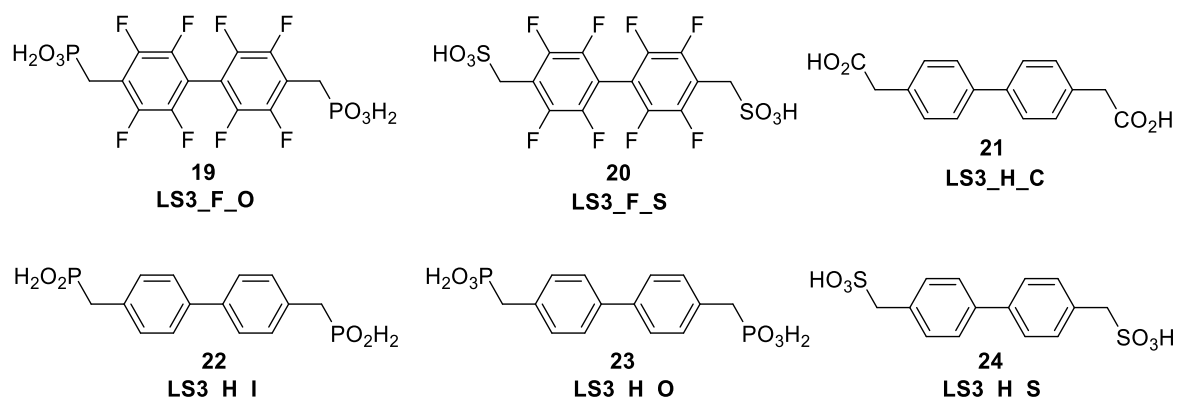


Figure 4.4.2-3. Overview of the synthesized **LS3** related molecules.

The yields of all syntheses related to **LS3** are given in table 4.4.2-1.

Table 4.4.2-1. Overview of the **LS3** related syntheses.

Structure	Conditions	Yield (%)
120	119 , 2.5 MeLi, THF, Et ₂ O, -78 °C	39
121	120 , 2 NBS, CCl ₄ , ΔT	73
123	121 , 3 NaCN, DMF, ΔT then KOH, H ₂ O, EtOH, ΔT	/
124	121 , NH ₄ H ₂ PO ₂ , HMDS, cat. Pd ₂ dba ₃ , cat. XantPhos, DCM, ΔT	/
19	121 , P(OEt) ₃ , ΔT then 10 TMSBr, DCM then MeOH, ΔT	32
126	121 , 2.5 B ₂ pin ₂ , cat. Pd ₂ dba ₃ , cat. ^{DMB} Me ₂ P*HBF ₄ , 4 K ₃ PO ₄ , 20 H ₂ O, ^{DMB} OH, ΔT then 20% HCl, ΔT	/
20	121 , 2.5 Na ₂ SO ₃ , acetone, H ₂ O, ΔT.	29
128	127 , 2.5 PBr ₃ , Et ₂ O, 0.1 pyridine, ΔT	78
129	128 , 3 NaCN, DMF, ΔT then KOH, H ₂ O, EtOH, ΔT	*
22	128 , 3 NH ₄ H ₂ PO ₂ , 3 HMDS, cat. Pd ₂ dba ₃ , cat. XantPhos, DCM, ΔT	17
23	128 , excess P(OEt) ₃ , ΔT then 10 TMSBr, DCM then excess MeOH, ΔT	68
130	128 , 2.5 B ₂ pin ₂ , cat. Pd ₂ dba ₃ , cat. ^{DMB} Me ₂ P*HBF ₄ , 4 K ₃ PO ₄ , 20 H ₂ O, ^{DMB} OH, ΔT then 20% HCl, ΔT	/
24	1 a , 2.5 Na ₂ SO ₃ , acetone, H ₂ O, ΔT	88

* Reaction was not successful. The product was commercially available (BLD Pharm China, Shanghai).

As can be seen from Table 4.4.2-1, the synthesis of some acid moieties varied drastically in terms of yield when comparing the non-fluorinated and the fluorinated structure. The non-fluorinated sulfonic acid (**24**) was synthesized in 88% yield whereas the fluorinated sulfonic acid (**19**) could only be synthesized in 32% yield. This was attributed to different solubilities in water because both acids were precipitated from highly acidic solutions and were not purified further due to their highly polar nature. A similar picture emerges when comparing the phosphinic acids. The non-fluorinated phosphinic acid (**22**) was synthesized in 17% yield while the fluorinated structure (**124**) could not be synthesized at all. This was due to significant amounts of byproducts that could not be removed after the reaction.

4.5 UV/VIS- and fluorescence properties of the Lead Structures

The UV/VIS and fluorescence properties of the lead structures were important because they determined what biophysical assay could be utilized. Fluorescence Anisotropy required a fluorescent molecule and an unlabeled protein. Microscale Thermophoresis did require labeling of the protein and potential fluorescence emissions should not overlap with the emission of the ligand that was used.

Table 4.5-1. UV/Vis and Fluorescence data of the synthesized compounds. Abs = Absorption, Em = Emission. **1-18:** derivatives of **LS1**; **19-24:** derivatives of **LS3**.

Compound	HEPES ^a (absorption/emission, nm)	Compound	PB ^b (absorption/emission, nm)
1	330/440	2	327/445
2	328/440	3	328/440
3	329/440	4	332/445
4	332/444	10	323/409
5	329/439	11	317/409
6	326/432	12	320/409
7	331/437	13	314/407
8	328/432	14	309/403
9	330/440	15	311/400
		16*	327/412
		17*	322/411
		18*	323/409
		19	245/320
		20	241/324
		21	260/321
		22	263/323
		23	264/324
		24	262/318

* 20% DMSO was included in the buffer. a: HEPES (100 mM), NaCl (150 mM), pH 7.4
b: 50 mM sodium phosphate, pH 7.4

As can be seen from Table 4.5-1, **LS1** and **LS3** were fluorescent. In the following chapters the fluorescence properties are explained in more detail:

4.5.1 Optical properties of LS1

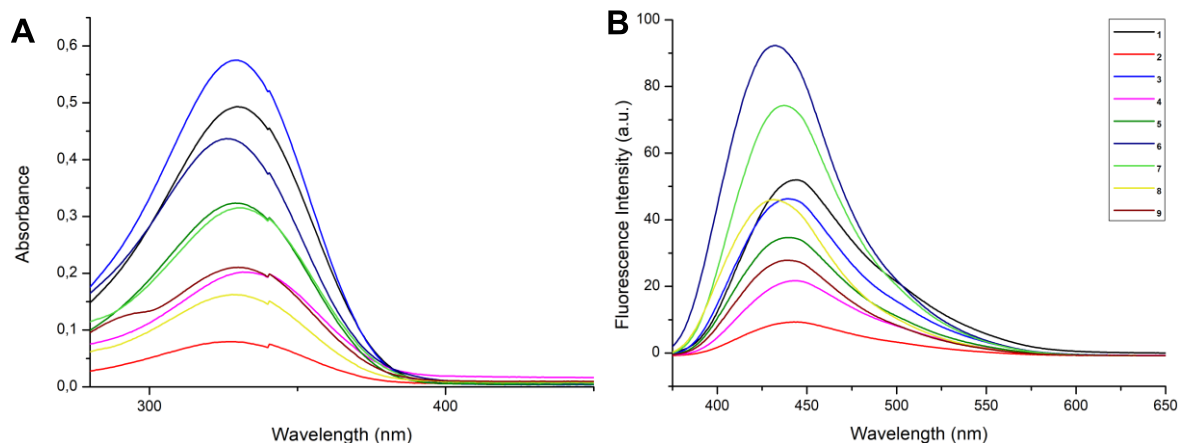


Figure 4.5.1-1. A: Absorption spectra for the synthesized carboxylic acids in HEPES buffer (100 mM HEPES, 150 mM NaCl, pH 7.4). The kink at 340 nm results from a light source switch during the measurement. **B:** Emission spectra for the synthesized carboxylic acids in HEPES buffer (100 mM HEPES, 150 mM NaCl, pH 7.4)

Initially, the carboxylic acids were characterized in terms of their optical properties. As can be seen in Figure 4.5.1-1-A, all synthesized carboxylic acids showed similar absorption maxima which were between 326 nm and 332 nm. However, the observed absorbance varied significantly between the different variants. Meanwhile, no regularity between the *N*-substitution-residues could be observed, which is evident in that both the highest (**3**, TFB) and the lowest (**2**, DMB) absorbance result from alkyl residues. It must be noted that the carboxylic acids could not be easily dissolved in HEPES buffer, which might have resulted in inaccurate stock solutions. The final concentrations might not have been precisely the same for every acid, which could explain some of the drastic differences observed in absorbance intensity.

The emission spectra for **LS1_C** confirmed that the synthesized carboxylic acids were fluorescent (Figure 4.5.1-1-B). The emission maxima were relatively similar and between 432 nm and 444 nm. The emission intensity showed no regularity just as was observed for the absorbance intensity of the investigated carboxylic acids. As most of our studies were carried out in sodium phosphate buffer, the most promising ligand structures were studied again in sodium phosphate buffer.

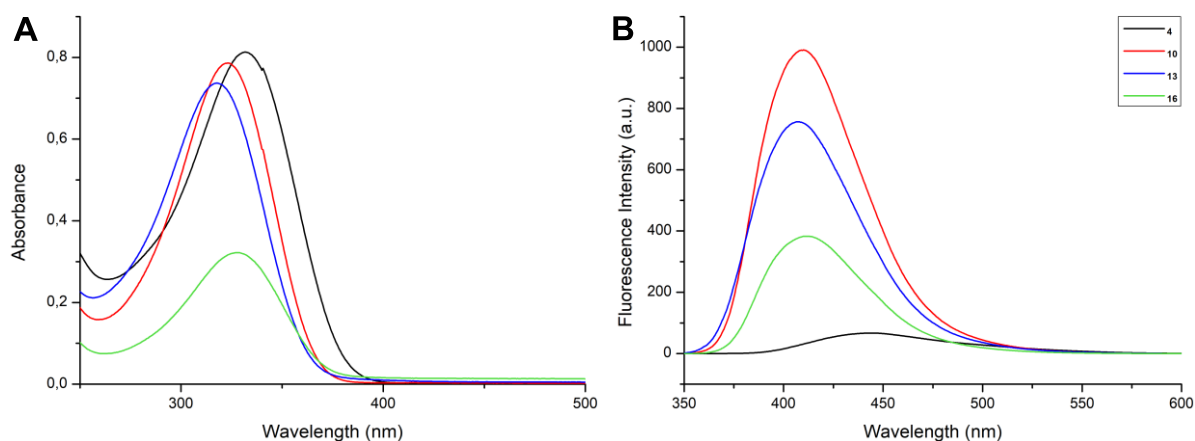


Figure 4.5.1-2. A: Absorption spectra of LS1_MCH in sodium phosphate buffer (50 mM sodium phosphate, pH 7.4). **B:** Emission spectra of LS1_MCH in sodium phosphate buffer (50 mM sodium phosphate, pH 7.4).

As can be seen in Figure 4.5.1-2-A, for MCH-substituted **LS1** variants a similar absorption maximum between 340 and 350 nm could be observed. The boronic acid structure (**16**) showed a significantly smaller absorption peak than the other three acid residues, whose intensities were comparable. This was not reflected in the emission data since the emission intensity of the carboxylic acid structure was noticeably lower compared to the other structures (Figure 4.5.1-2-B, compare with Figure 4.5.1-1-B). The replacement of the carbon atom of the carboxylic acid residue with different heteroatoms (P and B) could possibly influence the electron density in a way that the resulting emission bands were distinctly shifted. The fact that both phosphorous-based acids (**10**) and (**13**) also showed a difference of approximately 30% in terms of intensity confirmed this hypothesis. The emission maxima of the heteroatom-acids were within 10 nm from one another, whereas the emission maximum of the carboxylic acid was shifted by approx. 30 nm to higher wavelengths.

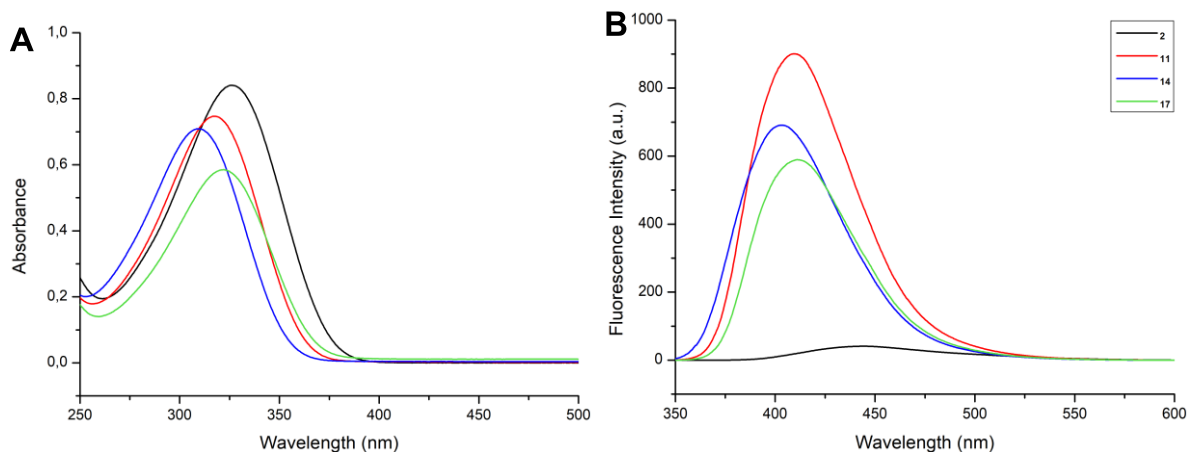


Figure 4.5.1-3. A: Absorption spectra of LS1_DMB in sodium phosphate buffer (50 mM sodium phosphate, pH 7.4). **B:** Emission spectra of LS1_DMB in sodium phosphate buffer (50 mM sodium phosphate, pH 7.4).

The general trend that could be observed for LS1_MCH was also seen for LS1_DMB in that the boronic acid (**17**) showed the lowest absorption maximum (Figure 4.5.1-3-A). However, the intensities of the peaks were much more comparable. Again, all four absorption maxima were similar and in the range of 317 – 323 nm.

The emission spectra for the 3,3'-dimethylbutyl-substituted lead structures confirmed the observed trend: All heteroatom-acids showed intensive emission, whereas the carboxylic acid showed very weak emission while experiencing a shift in maximum of approx. 25 nm (Figure 4.5.1-3-B). This meant that the differences in optical properties due to various alkyl substituents were negligible in comparison to the nature of the acid substituent.

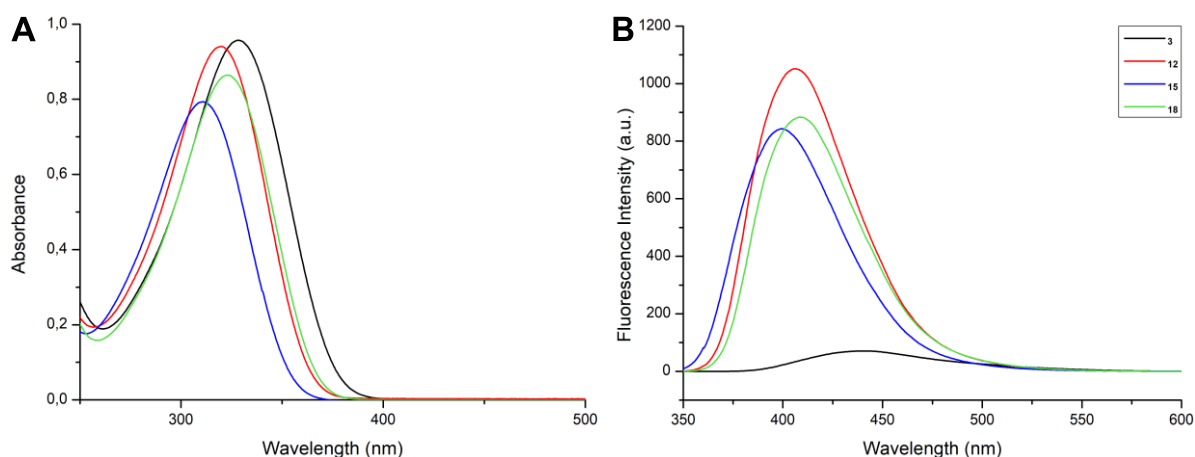


Figure 4.5.1-4. A: Absorption spectra for LS1_TFB in sodium phosphate buffer (50 mM sodium phosphate, pH 7.4). **B:** Emission spectra for LS1_TFB in sodium phosphate buffer (50 mM sodium phosphate, pH 7.4).

The 4,4,4-trifluorobutyl-substituted structure showed similar results compared to the two structures already discussed. The absorption spectra had maxima in the range of 309 to 314 nm, the only noticeable difference was that the boronic acid (**18**) showed a more intensive absorbance than the corresponding phosphonic acid (**15**) (Figure 4.5.1-4-A). The same was observed for the emission, the boronic acid showed a higher intensity than the phosphonic acid, while the carboxylic acid showed a significantly decreased intensity and shift towards higher wavelengths (Figure 4.5.1-4-B).

In summary, **LS1** showed fluorescence for all acid moieties. The carboxylic acids showed the highest absorbances and the lowest emission intensities, resulting in a weak overall fluorescence. All other three acids showed comparable absorbance and emission spectra, with regards to both, the intensity and wavelength of the observed maxima.

4.5.2 Optical properties of **LS3**

LS3 variants were characterized in terms of their optical properties using sodium phosphate buffer. The following curves were obtained:

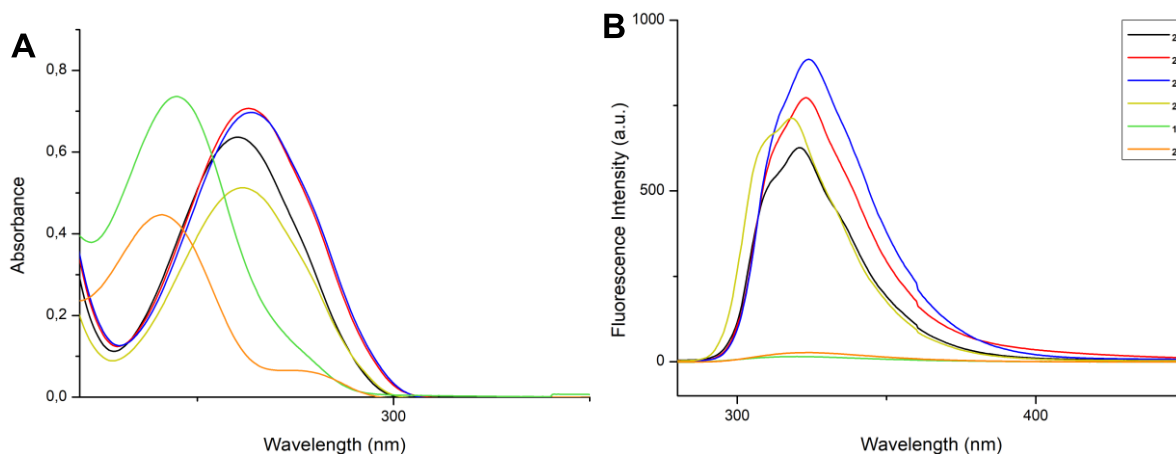


Figure 4.5.2-1. A: Absorption spectra for **LS3** in sodium phosphate buffer (50 mM sodium phosphate, pH 7.4). **B:** Emission spectra for **LS3** in sodium phosphate buffer (50 mM sodium phosphate, pH 7.4).

As can be seen in Figure 4.5.2-1-A, the absorption maxima of all investigated structures were in a rather narrow wavelength range of approx. 23 nm. The fluorination seemed to play a larger role on the absorbance than the nature of the acid moiety. This can clearly be seen when comparing the non-fluorinated sulfonic acid (**24**) and the fluorinated sulfonic acid (**20**): The intensities of the absorbance were roughly similar but the wavelengths were shifted by 21 nm, the fluorinated structure was red-shifted compared to the non-fluorinated structure. The same was true for phosphonic acids (**23**) and (**19**).

The emission spectra of **LS3** revealed a large difference between the non-fluorinated and the fluorinated structures in terms of fluorescence properties (Figure 4.5.2-1-B): The non-fluorinated structures (**21-24**) showed a far greater intensity than the fluorinated structures (**19** and **20**), the difference roughly equaled to a factor of 20. This phenomenon can be explained by the very electron-withdrawing nature of the fluorine atoms that leads to a very low electron density in the aromatic rings. Excitation by light leads to an excited electronic state, this photoexcitation can be quenched almost immediately by delocalisation onto the eight fluorine atoms. None of the four non-fluorinated structures showed the same effect, in fact, their curves were similar in terms of emission maxima and intensities. It is noteworthy that the carboxylic acid showed a

similar spectrum as the other acids. This is a clear difference to all investigated structures from **LS1**, where the carboxylic acid structures showed significantly weaker emission (compare Figures 4.5.1-1-B, 4.5.1-2-B, 4-5.1-3-B and 4.5.1-4-B). This meant that heteroatom-substitution did not seem to play a major role for fluorescence in **LS3**.

In summary, **LS3** showed fluorescence for all presented non-fluorinated acids. The fluorinated structures showed only weak emission while having comparable absorption properties, which meant that their overall fluorescence could be regarded as low. All non-fluorinated structures exhibited strong fluorescence with comparable absorption and emission maxima at similar wavelengths.

4.6 Protein Expression

The protein expression was performed under the supervision of Lisa-Marie Funk in the group of Prof. Kai Tittmann. Using the expression protocol from the group of Prof. Samar Hasnain who generously donated the plasmid vector, hSOD1 wt and the mutant A4V could be acquired. The plasmid vector pET303C-hSOD1wt was replicated in *E. Coli*, subtype BL21 Star™ (DE3). Transcription of the lac-operon was induced by IPTG and the expression of the desired protein was carried out by the T7-RNA-polymerase. In order to determine the optimal harvesting time, samples were drawn each hour and the optical density was determined at 600 nm. The cells were harvested after an incubation time of 20 hours, yielding approximately 32 g of cells from 6 L of culture. SDS-page analysis of the hSOD1 wt expression is shown in Figure 4.6-1.

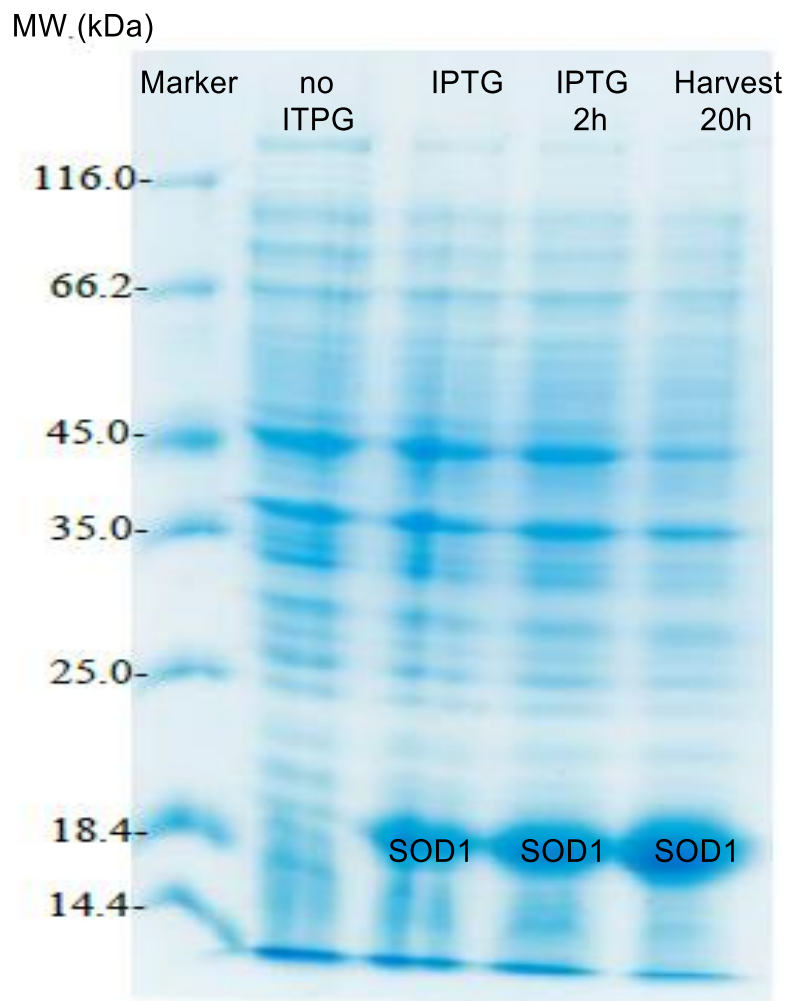


Figure 4.6-1. 15% SDS-page of the hSOD1 wt expression (pET303C-hSOD1wt). IPTG: 0.4 mM.

Afterwards the cells were disrupted and purified; the general procedures are given in the experimental section of this thesis. The resulting SDS-pages showed that the obtained protein was sufficiently pure for its use in later stages. In addition, no great loss of protein in the cell pellets could be observed.

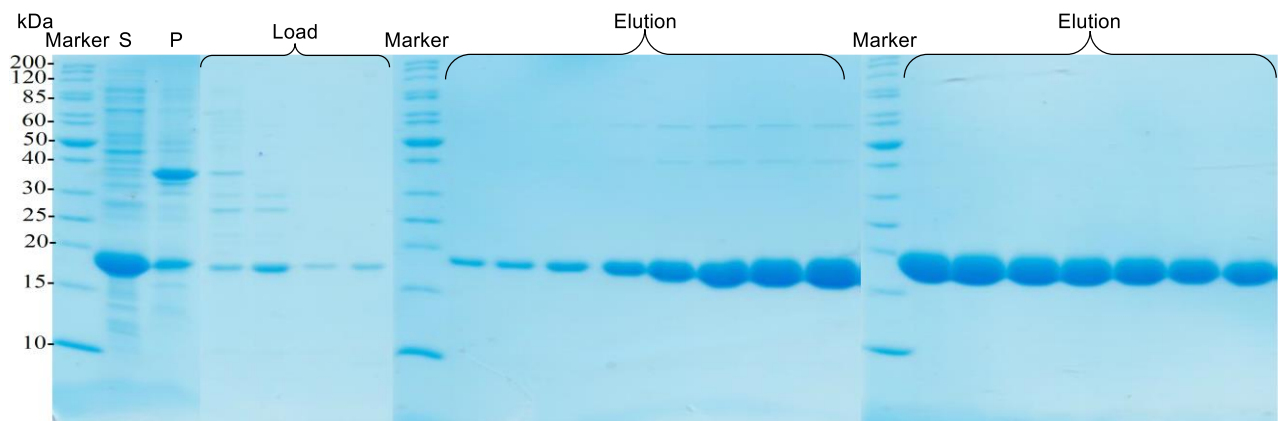


Figure 4.6-2. 15% SDS-page of the hSOD1 wt purification. S: Supernatant. P: Pellets. Load and Elution: TMAE chromatography purification fractions.

As can be seen from Figure 4.6-2, the amount of protein lost during loading steps was negligible. No perfect separation of protein fractions could be achieved, as early elution fractions contained considerable amounts of undesired side products with a molar weight between 40 and 60 kDa. These fractions were discarded and only the pure fractions that were obtained in later stages of the chromatography were used for further purification. The yield of the purification was approximately 60 mg of pure protein from 1 g of cells. Afterwards, both cofactors (Cu, Zn) were reconstituted, yielding 17-20 mg of pure hSOD1 wt from 1 g of cells (the protocol that was used for the reconstitution of both cofactors is given in the experimental section).

Following the outlined expression and purification protocol, the A4V mutant could be obtained in comparable yields after a similar number of steps. As expected, the stability of this mutant was smaller compared to that of the wildtype, especially before both cofactors were introduced. This might have resulted from a literature-known deficiency in the affinity for zinc ions, which could also explain the lower yield (85% of the wt yield).^[130] In summary, hSOD1 wt and its A4V mutant could be expressed, purified and reconstituted in sufficiently high purity and yield for further biophysical experiments.

4.7 Activity analysis

The activity of a protein is usually a good indicator for its successful expression or stability and can be measured by activity assays. Prior to activity analysis, the existence of a stable protein dimer had to be confirmed, since the activity of the dimer was used as a baseline for comparison. Thus, multi angle light scattering was employed to determine the molar mass of the protein in question, and a tight dimer with a mass of approximately 28 kDa could be identified (Figure 4.7-1, left). Afterwards, size exclusion chromatography was used to analyze the protein further; the data was in very good agreement with the MALS-data (Figure 4.7-1, right)

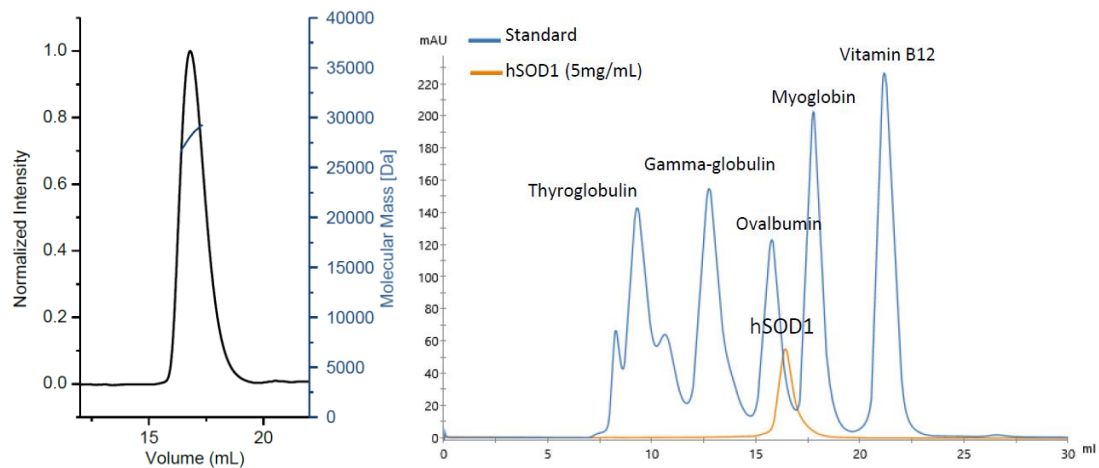


Figure 4.7-1. Left: MALS data for hSOD1 wt. Right: SEC data for hSOD1 wt (orange), Biorad standard (blue). Biorad standard curve is depicted in the appendix. Pictures provided by Viktoria Mrđen Debono.

Additional SEC experiments also confirmed a high tendency to aggregate for the A4V mutant when compared to the hSOD1 wt. As expected, the A4V apo variant in particular showed a high probability for aggregation when compared to the wild type (Figure 4.7-2).

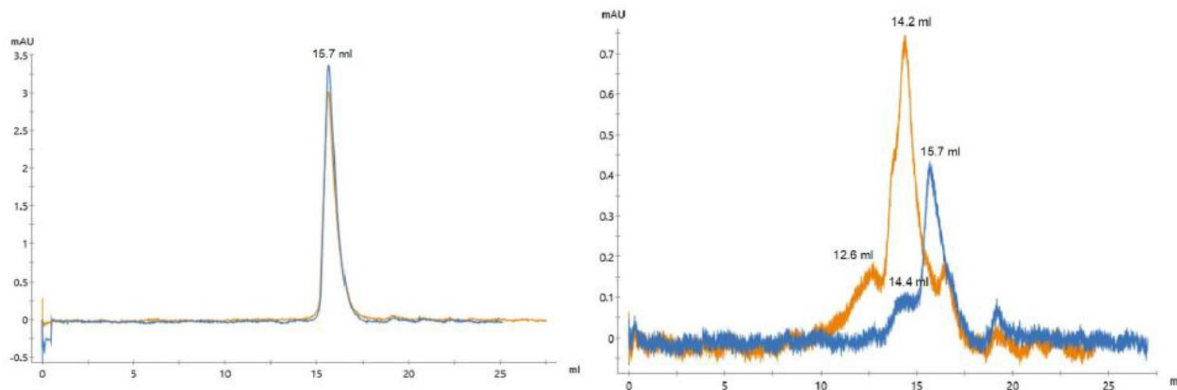


Figure 4.7-2. Left: SEC of hSOD1 wt. Right: SEC of A4V apo (orange) and holo (blue). Pictures provided by Franziska Otto.

In this thesis an indirect assay based on Xanthine Oxidase, commercially available as a SOD test kit, was used to measure the activity of the wild type SOD1 as well as for the A4V mutant. The underlying catalytic cycle is described in Figure 4.7-3.

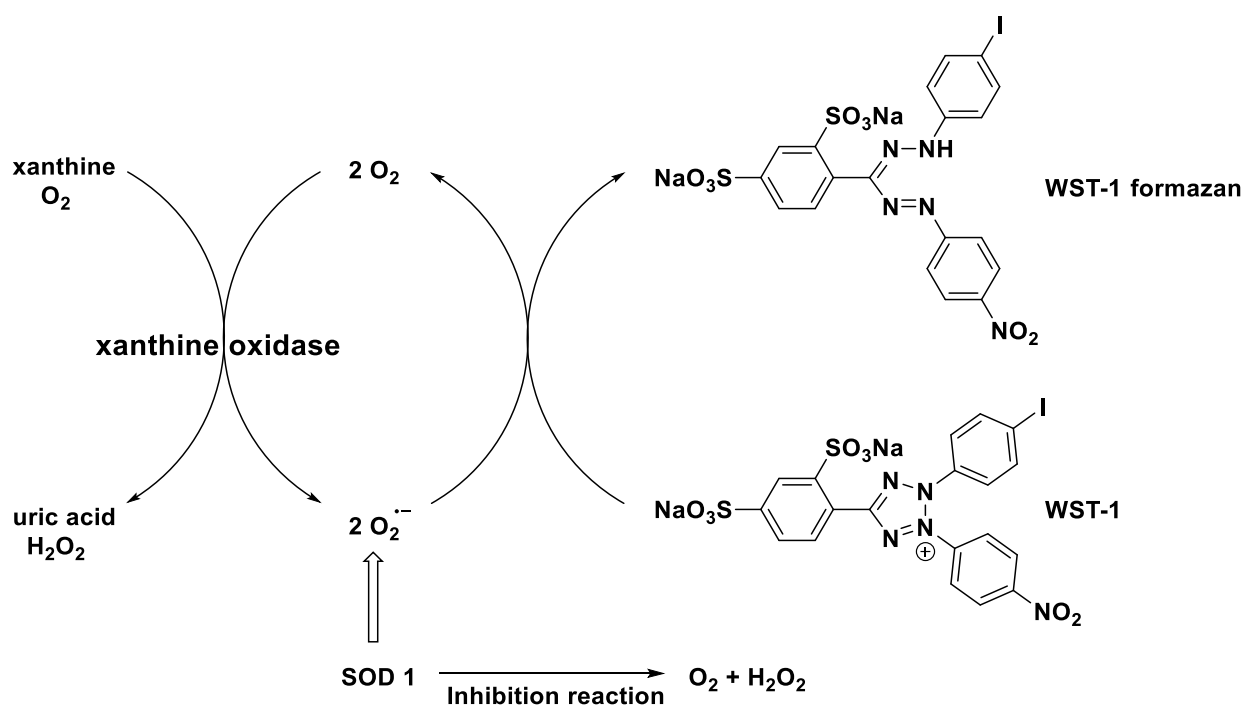


Figure 4.7-3. Catalytic cycle of the commercially available SOD assay kit.

Xanthine Oxidase catalyzes the reaction of xanthine to uric acid in the presence of oxygen, producing hydrogen peroxide as a side product. In a second, connected cycle, superoxide radicals are being produced from free oxygen, which in turn react with a molecule called WST-1. The product of this reaction is a formazan dye whose absorbance can be measured between 420 and 480 nm.^[131] Upon addition of the protein, the catalytic cycle is disturbed and the formation of the formazan dye is

inhibited. This is because SOD1 catalyzes the disproportionation of superoxide radicals into oxygen and hydrogen peroxide; therefore, they cannot participate in the xanthine oxidase cycle. The assay is indirect because instead of measuring the reaction rate of the disproportionation reaction (catalyzed by SOD1) the inhibition of a second reaction is measured. Nevertheless, quantitative values can be obtained in this manner.

The catalytic activity of the fully reconstituted hSOD1 wt could be confirmed by means of this assay (see Figure 4.7-4). Furthermore, copper-deficient hSOD1 showed a significantly lower activity that was comparable to that of bovine SOD1. This again proved the point that copper is essential for the catalytic activity of the protein whereas zinc increases the overall structural integrity of SOD1.^[132,133] Since all target structures were generally well soluble in aqueous buffer solutions, no experiments were performed investigating the effects of co-solvents like DMSO, PEG or glycerol on the activity assay.

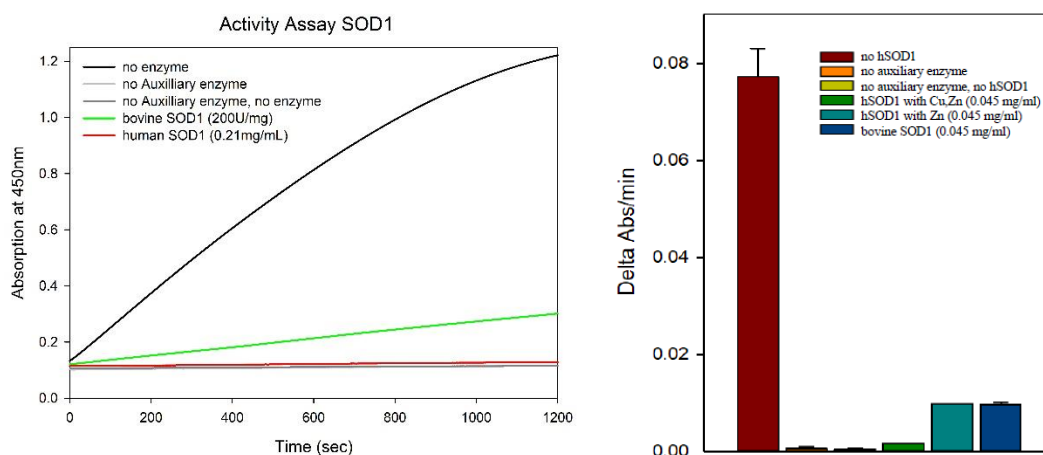


Figure 4.7-4. Activity assay of hSOD1 wt. Left: Time-dependent absorption curve of the assay. Right: Slope diagram of the time-dependent measurement. Pictures provided by Lisa-Marie Funk.

Furthermore, a significantly reduced activity of hSOD1 A4V holo/apo could be confirmed with the activity assay (Figure 4.7-5). The wild type showed a reaction inhibition that was approx. 15 times higher than the reaction inhibition observed for A4V. The differences between apo- and holo-enzyme of the respective types were negligible concerning the large relative errors. Measurements at higher concentrations for hSOD1 A4V confirmed these results (data not included in this thesis).

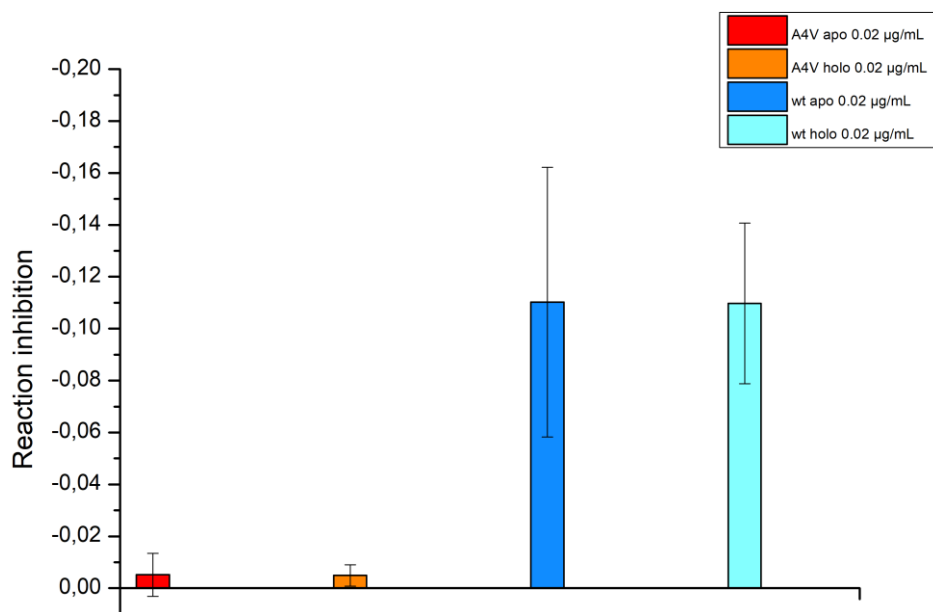


Figure 4.7-5. Acitivity of hSOD1 wt and hSOD1 A4V shown as the reaction inhibition in phosphate buffer (50 mM sodium phosphate, pH 7.4). Raw data was obtained from Viktoria Mrđen Debono and Franziska Otto.

4.8 Binding studies of **LS1** and **LS3** to SOD1

4.8.1 Fluorescence Anisotropy of the **LS1_C** library

The first lead structures that were synthesized were from the library of different *N*-substituted carboxylic acids derived from **LS1**. A fluorescence anisotropy screening of these structures was performed by dissolving the ligand in an appropriate buffer (50 mM sodium phosphate buffer) with a concentration of 40 µM and the protein in a concentration of 250 µM. The resulting mixture was incubated for 2.5 h and afterwards the anisotropy was recorded and compared to the anisotropy of the free ligand (40 µM in the same buffer). The anisotropy was recorded against a “single point”, which was defined through the absorption and emission wavelengths that were obtained before under the same solvent conditions (50 mM sodium phosphate buffer). In this way, the temperature and all other parameters were kept constant throughout the experiments; specific protocols can be found in the experimental section.

The following results were obtained:

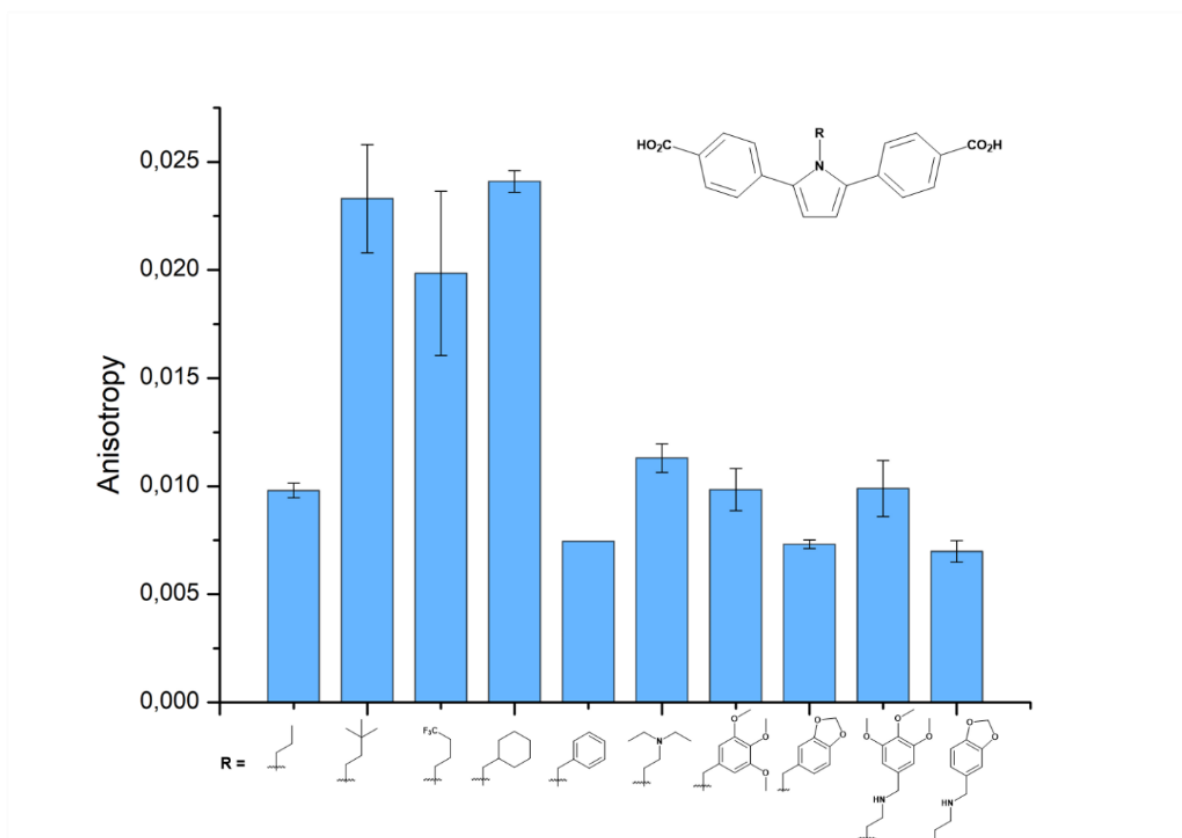


Figure 4.8.1-1. Fluorescence anisotropy of **LS1_C**. The obtained values and the corresponding errors are given. The Benzyl-substituted structure show no error due to two negative results out of three triplicates.

As can be seen from Figure 4.8.1-1, the overall Δ Anisotropy did not have a large value; this can be explained by the following hypotheses:

1. The incubation time might have been too low in order to achieve binding to the protein. After measuring one of the samples on the next day, no significant change could be observed. This meant that the explanation was either wrong or that the binding was weak in general.
2. The concentration of the ligand might have been not high enough in order to achieve binding of any meaningful quantity. Even though this was a plausible hypothesis it would mean that even a 6.25-fold excess of the protein was not enough to show binding of the ligand to the protein which again would justify calling the interaction weak binding.
3. The fluorescence lifetime of the excited state was too short compared to its rotational correlation time as explained above, justifying these findings. In

addition, the overall Δ Anisotropy does not say anything about the strength of the binding on its own.

The results from this assay were utilized in determining the substituents that were best suited for following synthesis. This was because synthesizing each organic acid with all 10 residues would have been beyond the scope of this thesis. The following three residues were chosen: 2,2-dimethylbutane (DMB), 1,1,1-trifluorobutane (TFB) and methylcyclohexane (MCH).

4.8.2 MST binding studies of **LS1** and **LS3**

Microscale Thermophoresis was the most important biophysical assay during this thesis due to several factors: First, the amount of protein necessary is lower compared to other techniques such as Anisotropy or ITC. Second, multiple measurements can be carried out in a short time. Third, the assay requires a labelled protein that was already prepared in our working group and was provided by Viktoria Mrđen Debono. It was used in all MST measurements of all compounds. Furthermore, the results obtained had significantly smaller errors compared to those obtained by other biophysical techniques. The general procedure that was used for MST measurements is depicted in the Experimental Section of this work.

4.8.2.1 MST results for **LS1**

As discussed in chapter 4.5.1, **LS1** variants were fluorescent, and the emission wavelength made us suspect a potential influence on the dye for the protein labelling. It turned out that the highest concentrations in each measurement showed photobleaching, these values were probably the result of an interference of the ligand and the dye. It was concluded that the photobleaching was induced either by the ligand binding to the protein or by fluorescence interference. Therefore, the highest concentrations and the respective MST signals were ignored and taken out of consideration when scanning for a K_d -value, since at lower concentrations no bleaching or quenching could be observed. This procedure ensured that the results were not influenced by either ligand induced photobleaching or fluorescence interference, as was confirmed by the NANOTEMPER software that does not allow determination of a K_d -value when unknown factors signal photobleaching.

The phosphorus-based structures were examined first, since *in silico* studies showed the best docking scores for these structures.

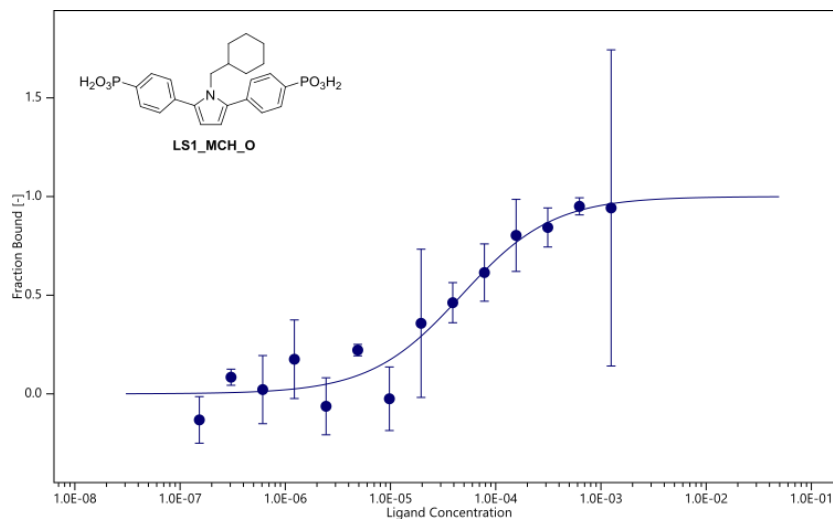


Figure 4.8.2.1-1. MST binding curve for LS1_MCH_O. $K_d = 47 \pm 17 \mu\text{M}$.

LS1_MCH_O gave a K_d -value in the medium μM -range, which was in accordance to the *in silico* screening (Figure 4.8.2.1-1). The S/N ratio was sufficiently high with a value of 10.33 and the response amplitude was 8.03.

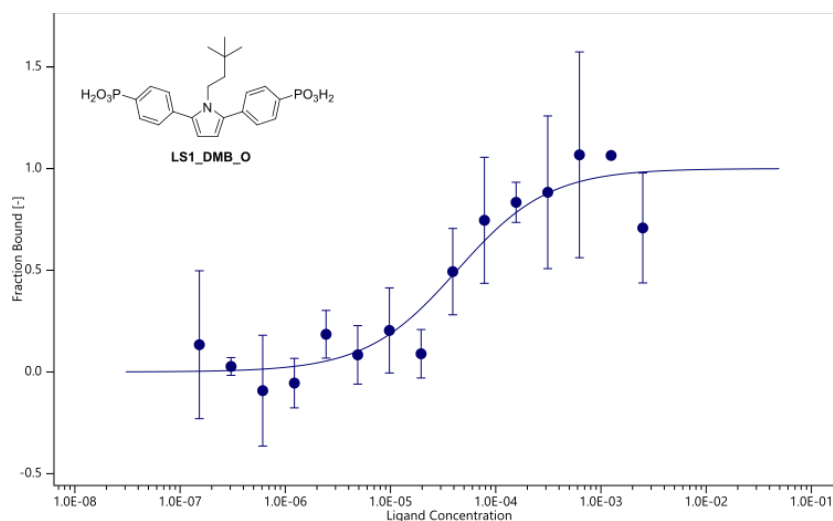


Figure 4.8.2.1-2. MST binding curve for LS1_DMB_O. $K_d = 43 \pm 18 \mu\text{M}$.

Similarly, LS1_DMB_O gave a K_d -value in the medium μM range, which was expected due to the similar chemical structure (Figure 4.8.2.1-2). The S/N ratio of 8.00 was lower as well as the response amplitude of 3.50, but since these values were still well over the threshold, the obtained K_d -value had a high probability of being valid. This ligand also showed the least amount of photobleaching, which resulted in only one full data point being omitted from the measurement. Still, saturation seemed to be achieved for this ligand.

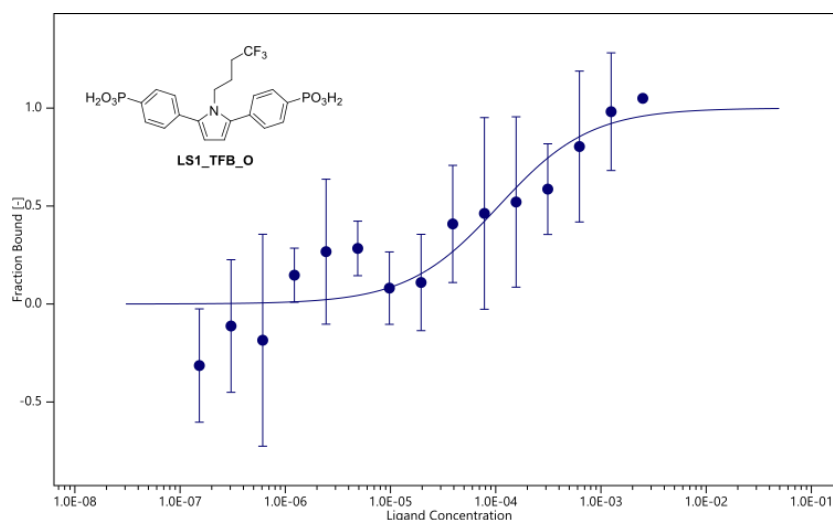


Figure 4.8.2.1-3. MST binding curve for LS1_TFB_O. $K_d = 107 \pm 62 \mu\text{M}$.

LS1_TFB_O also showed moderate binding to the protein, but it had the worst K_d -value of all phosphonic acid derivatives (Figure 4.8.2.1-3). This was explainable considering the trifluoromethyl group could be considered a large deviation from the purely alkyl-substituted structures that were examined before. It also had the largest error relative to the binding strength, the lowest S/N ratio of only 6.29 and the lowest response amplitude of only 1.87. The fluorination did not seem to improve the binding to the protein, even though more hydrogen bonds would be formed compared to the alkyl substitution units discussed before. This could be a hint that hydrophobic interactions play a major role in the binding to the cavity of Cys₁₁₁ as could be expected due to its proximity to the dimer interface, which is largely influenced by those interactions.

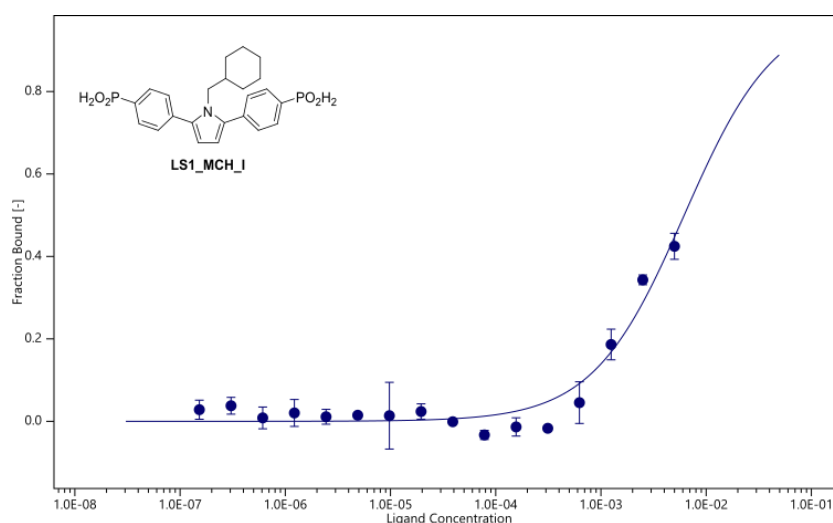


Figure 4.8.2.1-4. MST binding curve for LS1_MCH_I. $K_d = 6.18 \pm 3.90 \text{ mM}$.

The phosphonic acids generally gave higher K_d -values than the phosphonic acids. The first measured phosphonic acid showed very weak binding to the protein and saturation was not achieved (Figure 4.8.2.1-4). Therefore, the response amplitude and the S/N ratio had very high values since the software assumed a very high K_d -value. The S/N ratio was 29.33 and the response amplitude was 24.20. This result was unexpected because the structure of the phosphonic acid moiety is almost identical to that of the phosphonic acid, which gave respectable binding properties. Nevertheless, unknown factors such as binding modes, binding locations or self-clustering of the ligand could have played a role in the results observed.

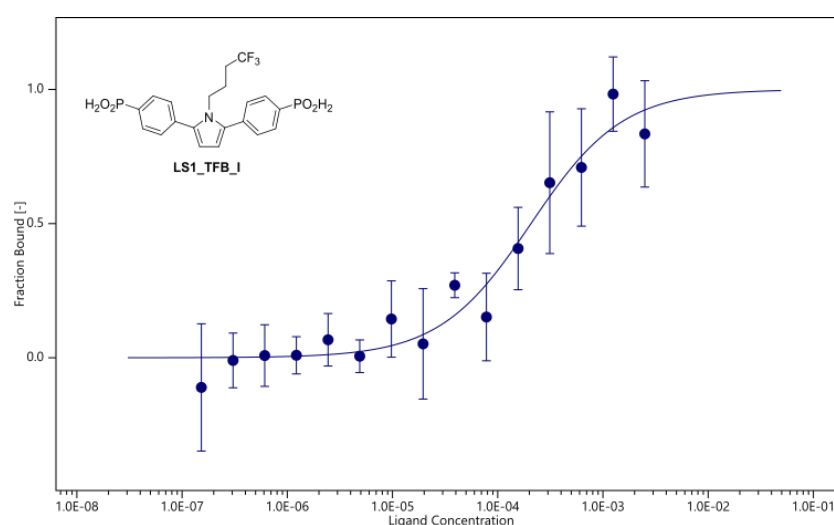


Figure 4.8.2.1-5. MST binding curve for LS1_TFB_I. $K_d = 207 \pm 64 \mu\text{M}$.

In contrast, the 4,4',4''-trifluorobutyl-substituted phosphonic acid showed much stronger binding to the protein than the aforementioned derivative, the S/N ratio was 13.01 and the response amplitude was a low 3.76 (Figure 4.8.2.1-5). This meant that these results were most likely valid and proved that the phosphonic acid moiety can be used in order to enable binding to the protein. The K_d -value was still almost two-fold worse compared to its phosphonic acid counterpart, which again reemphasizes the superiority of the phosphonic acid moiety over the phosphonic acid moiety. This was even more so demonstrated by the fact that the 3,3'-dimethylbutyl-substituted phosphonic acid did not show any binding to the protein and exhibited excessive photobleaching, that rendered evaluation of the obtained data impossible.

The carboxylic acid structures of **LS1** were also measured with MST, but no binding to the protein could be observed. The general handling of the carboxylic acids was rather

tedious compared to the phosphorous-based ligands due to lower solubility and a tendency to aggregate or to show adsorption to the cuvette.

In summary, the phosphorus-based structures of **LS1** were successfully measured by means of MST and showed binding in the middle μM range for all phosphonic acid derivatives regardless of *N*-substitution and weak or no binding for the phosphinic acid derivatives.

4.8.2.2 MST results for **LS2**

The synthesis of a final structure was not successful; therefore, no ligands could be measured. Nevertheless, in order to evaluate the overall fluorescence properties and the suitability of the core structure for MST, LS2_NH₂_C was measured.

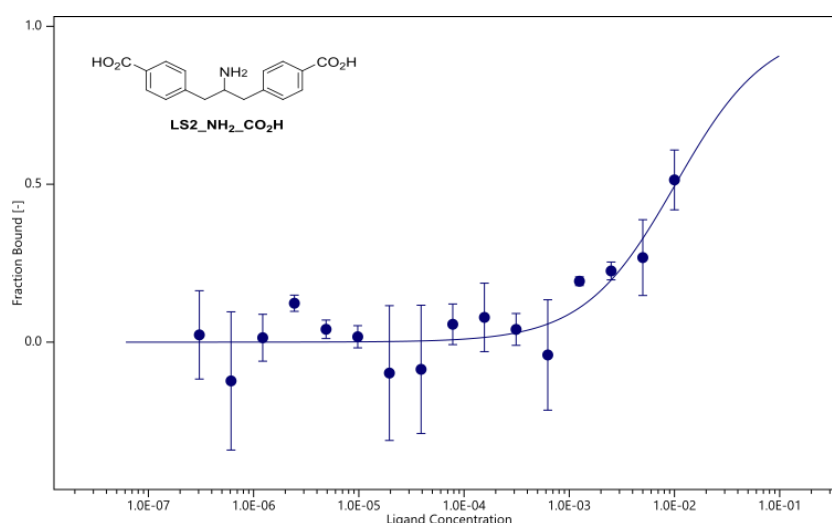


Figure 4.8.2.2-1. MST binding curve for LS2_NH₂_C. $K_d = 10.2 \pm 1.1$ mM.

As can be seen, no saturation of the curve could be achieved (Figure 4.8.2.2-1). This was partly because the solubility of the investigated structure was surprisingly bad in aqueous buffer and low concentrations had to be used. A very weak binding could be observed, the corresponding S/N ratio was 13.8 and the response amplitude was 10.9. It must be emphasized that binding of such magnitude was expected, since the structure was not the final ligand and the free, basic amine could potentially engage in a variety of unwanted binding modes or interferences with the protein. The general suitability of the core structure of **LS2** could be confirmed though, no photobleaching

or quenching upon binding could be observed. This was also expected since no fluorescence of **LS2** could be observed.

4.8.2.3 MST results for **LS3**

As discussed in chapter 4.5.2, **LS3** variants were fluorescent, and the emission wavelength did not overlap with the fluorophore in the relevant wavelength range.

The following binding curves and corresponding K_d – values were obtained:

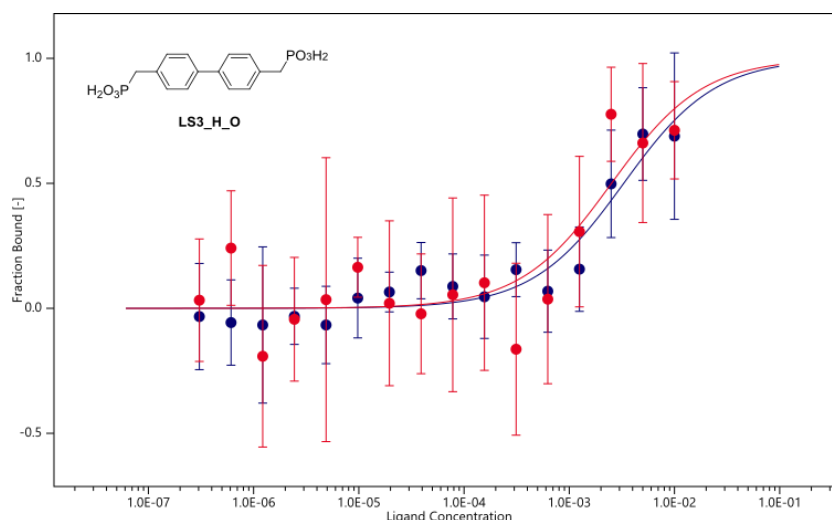


Figure 4.8.2.3-1. MST binding curve for LS3_H_O. Blue: 10% MST power. Red: 40% MST power. $K_d = 3.3 \pm 1.6$ mM (blue), 2.5 ± 2.0 mM (red).

The first ligand that was examined was the phosphonic acid derivative of the non-fluorinated lead structure, because phosphonic acids gave the best docking score, the synthesis was straightforward, and the molecule could be obtained in large quantities (Figure 4.8.2.3-1). In addition, the solubility was the best among all of the acid residues; therefore, the general handling of MST probes was optimized using this ligand. Variation of the incubation time did not show a significant change in the results as was already established in the working group before (data not shown). The same batch of ligand was measured with the same batch of labeled protein at two different days using MST powers of 10% (red curve) and 40% (blue curve) respectively. The corresponding S/N ratios were 13.1 and 6.89, the corresponding response amplitudes were 3.15 and 2.14. It was concluded that using lower MST power led to better results in terms of data significance whilst giving similar K_d -values. Therefore, the MST power was always chosen as low as possible. In general, the error range was very large; this was mainly due to two factors: The curves did not reach a clear saturation even though the ligand

was soluble in the chosen sodium phosphate buffer. Unfortunately, the use of a co-solvent like DMSO or methanol led to a decrease in solubility. In our case, this preliminary result was sufficient, because it proved weak binding between the phosphonic acid residues of the ligand structure and the protein and opened the possibility of observing a general trend between different ligands.

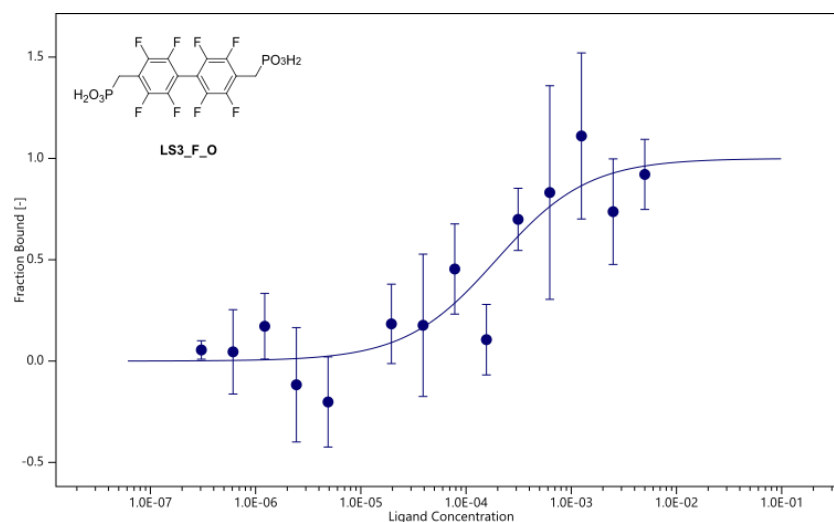


Figure 4.8.2.3-2. MST binding curve for LS3_F_O. $K_d = 1.95 \pm 1.18$ mM.

Comparably, the fluorinated phosphonic acid was shown to bind weakly with a K_d of 1.95 ± 1.18 mM (Figure 4.8.2.3-2). The S/N ratio of 5.99 and the response amplitude of 4.74 did not allow for clean data evaluation and the resulting binding curve was noisy. This was mainly attributed to the lower solubility of the fluorinated structure. The obtained K_d -value was in the mM range, comparable to the non-fluorinated structure.

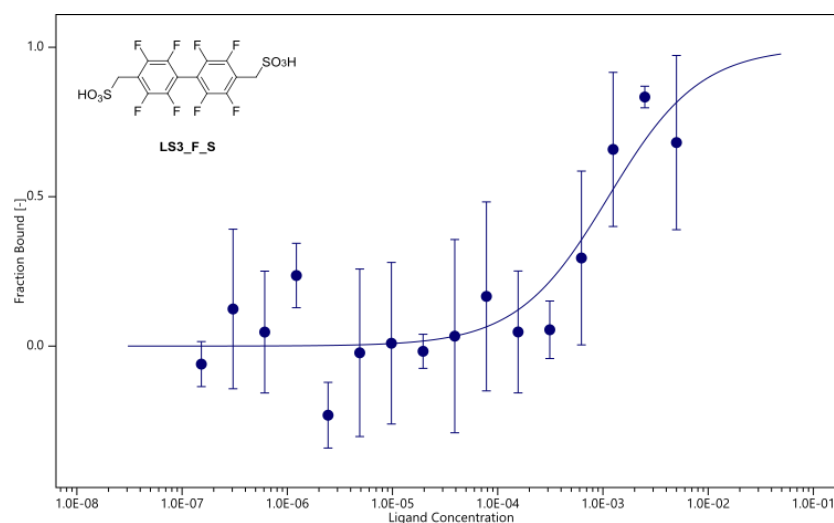


Figure 4.8.2.3-3. MST binding curve for LS3_F_S. $K_d = 1.13 \pm 0.75$ mM.

The fluorinated sulfonic acid did not show stronger binding, and a K_d of 1.13 ± 0.75 mM was recorded (Figure 4.8.2.3-3). The S/N ratio of 7.98 was sufficiently high; unfortunately, the response amplitude of 2.78 was rather low and led to large uncertainties. For the same reasons as mentioned above, this result was considered sufficient to observe a general trend. Interestingly, the non-fluorinated derivative showed no binding at all, even though it was more soluble in the buffer and allowed for a greater spectrum of concentrations in the assay. Up to this point, the reason for the different behavior is unknown.

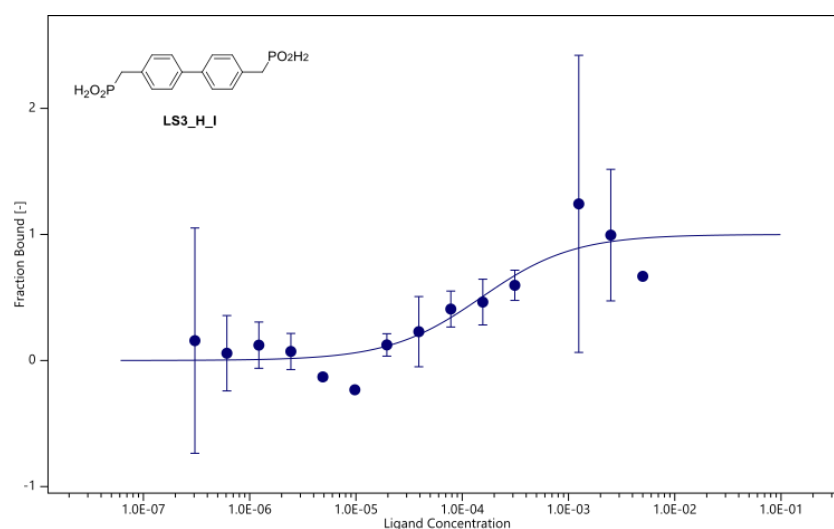


Figure 4.8.2.3-4. MST binding curve for LS3_H_I. $K_d = 151 \pm 93$ μ M.

The best results for **LS3** were achieved for the non-fluorinated phosphinic acid, which showed moderate binding in the μ M range, the S/N ratio was 5.81 and the response amplitude was 5.65 (Figure 4.8.2.3-4). Saturation appeared to be sufficient; unfortunately, no comparison with the fluorinated structure could be made because it was impossible to synthesize it. The phosphinic acids gave the second best docking results next to the phosphonic acids, therefore it was concluded that phosphorous-based structures were most likely the best for an affinity based ligand-protein complex. It also meant that there was a high probability that the *in silico* results were valid

It needs to be noted that aggregation as well as adsorption were major issues during measurements even though precautions were taken to avoid these literature-known mistakes (low binding tips, low binding tubes, premium capillaries).^[134] This unfortunately resulted in somewhat large error bars for some of the MST signals obtained. This could be overcome by measuring more triplicates with subsequent averaging of the values obtained, but that time-consuming process could not be done

in the scope of this thesis. Instead, the general concept of binding to SOD1 with the help of symmetrically aligned acid residues was proven by these measurements. It should be noted that no information about stoichiometry or binding mode, i.e., the location where the binding event occurred, could be obtained with the MST assay.

4.8.3 Results of ITC measurements

As was already described before, ITC was used sparingly in this thesis. LS1_MCH_I was chosen as a model system to answer three different questions:

First, the water solubility of the pyrrole-based **LS1** was expected to vary drastically from the well-soluble library of **LS3**, this could have limited its suitability for ITC. The result of this test was positive; LS1_MCH_I confirmed the general suitability of the core structure for ITC since it was soluble in sufficient amounts in aqueous buffer.

Secondly, the already described MST measurements of this substance needed to be confirmed with a second method. Since Fluorescence Anisotropy failed to deliver a positive result, ITC was the method of choice and it was possible to show potential binding to the protein in a similar magnitude of strength.

Lastly, ITC measurements performed at early stages of the project showed a potential problem for the entirety of the pyrrole based **LS1**, because self-assembling of the aromatic systems was a possibility. This could in turn mask the ITC signal since aromatic interactions tend to be rather strong. In order to test whether this was a general problem, the methylcyclohexyl-substituted pyrrole was chosen as a model system for all alkyl-substituted pyrroles.

Table 4.8.3-1. ITC results for LS1_MCH_I.

LS1_MCH_I	N (sites) (set to 1)	K _d (mM)	ΔH (kcal/mol)	ΔG (kcal/mol)	-TΔS (kcal/mol)
20mM RLS1 300μM hSOD1	1	8.41 ± 0.88	2.79 ± 0.22	2.83	- 0.04
20mM RLS1 175μM hSOD1	1	4.09 ± 0.27	1.31 ± 0.06	3.26	- 1.95
10mM RLS1 175μM hSOD1	1	4.29 ± 0.794	1.34 ± 0.191	3.23	- 1.89

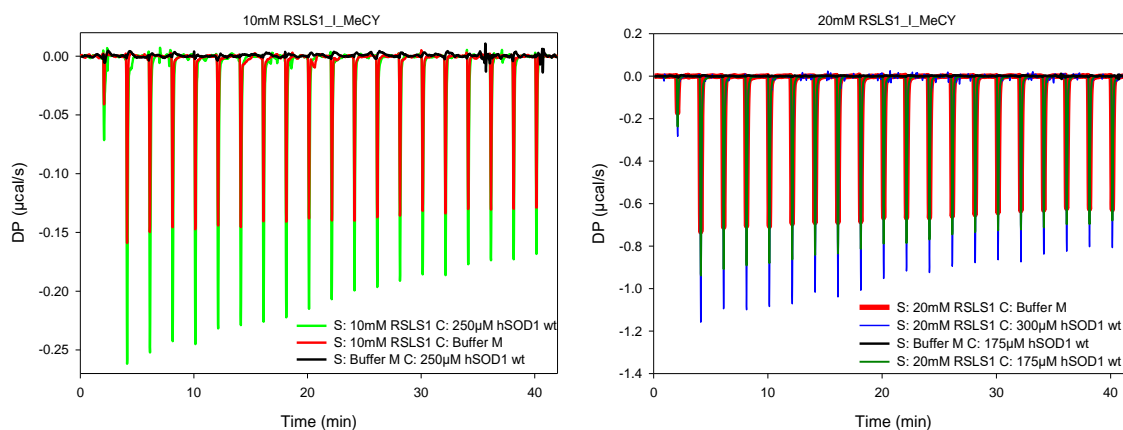


Figure 4.8.3-1 *Left:* Raw data spectrum for 10 mM ligand. *Right:* Raw data spectrum for 20 mM ligand. Spectra were obtained by Lisa-Marie Funk.

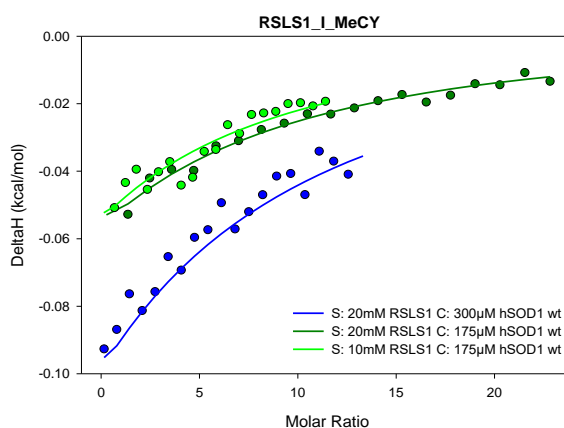


Figure 4.8.3-2. Binding curves (Wiseman plot) for LS1_MCH_I. This spectrum was obtained by Lisa-Marie Funk.

As can be seen from Table 4.8.3-1 and Figure 4.8.3-2, the data obtained could be evaluated and provided significant results. The observed binding strength was in the mM range, therefore the binding between the ligand and the protein was very weak. In addition, no clear saturation of the resulting binding curves could be achieved. This meant that the data was unreliable, and measurements needed to be executed again to obtain more data points. When comparing the K_d -values with the already discussed MST results of LS1_MCH_I (Figure 4.8.2.1-4) it became evident that the data obtained are all in the medium mM range. This means that the ITC measurements confirm the viability of the MST assay for measuring K_d -values. However, since a lot of protein and ligand were needed for ITC measurements, combined with the high time expenditure for this assay, no further ITC measurements were performed.

4.9 Protein crystallization

As was described earlier, the biophysical techniques that were used during this thesis could not be used to identify binding sites or binding modes, instead, X-Ray crystallography is the method of choice for identifying the nature of a protein-ligand complex. Several literature-known procedures for the crystallization of hSOD1 wt were tested, but they could not be reproduced successfully.^[76,135]

Because of that, an automated screen was performed by Elham Paknia from the working group of Prof. Holger Stark (structural dynamics) at the Max Planck Institute for Biophysical Chemistry Göttingen. The exact protocol is given in the experimental section. The best conditions from the automated screen were used to manually perform crystallization with the sitting-drop method and the hanging-drop method, an exemplary result is given in Figure 4.9-1.

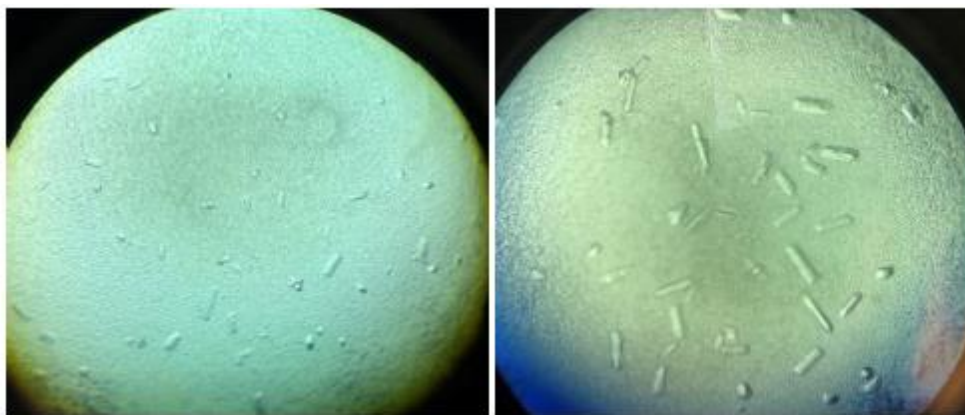


Figure 4.9-1. Crystals of hSOD1 wt. Buffer: 0.1 M MES, 0.2 M ammonium sulfate, pH 6.5, 20% PEG8000. Left: after three days. Right: After 10 days.

Soaking experiments were undertaken with two ligands that were introduced in this thesis (LS1_MCH_I and LS1_DMB_B). Unfortunately, until today, no crystal structure of the protein-ligand complex could be obtained. This could be mainly attributed to three factors:

1. The crystal quality itself was sufficient, but improvements need to be made. The corresponding resolutions were in the range between 2 and 3 Å while typical literature-known crystal structures result from crystals with resolutions around 1 to 1.5 Å.
2. The stability of the crystals needs to be increased. Small environmental changes such as pH, temperature, pressure, local solvent gradients or vibrational stress are able to destroy crystals or seriously damage them within seconds. In addition, the use of co-solvents in the cryoprotectant buffer needs to be optimized in a way that the resolution is not hampered.
3. The soaking itself needs optimization since only very small soaking times could be realized because the soaking solutions quickly damaged the crystals. Published crystal structures of protein-ligand complexes usually have soaking times anywhere between 2 and 24 h. In our case, soaking times of a few minutes were possible, afterwards, the potential harmful effects of the soaking solution were deemed too large to continue the soaking process.

Nevertheless, it was possible to obtain a refined crystal structure of hSOD1 wt by Lisa-Marie Funk, which confirmed the success of the complete expression of hSOD1 wt (Figure 4.9-2).

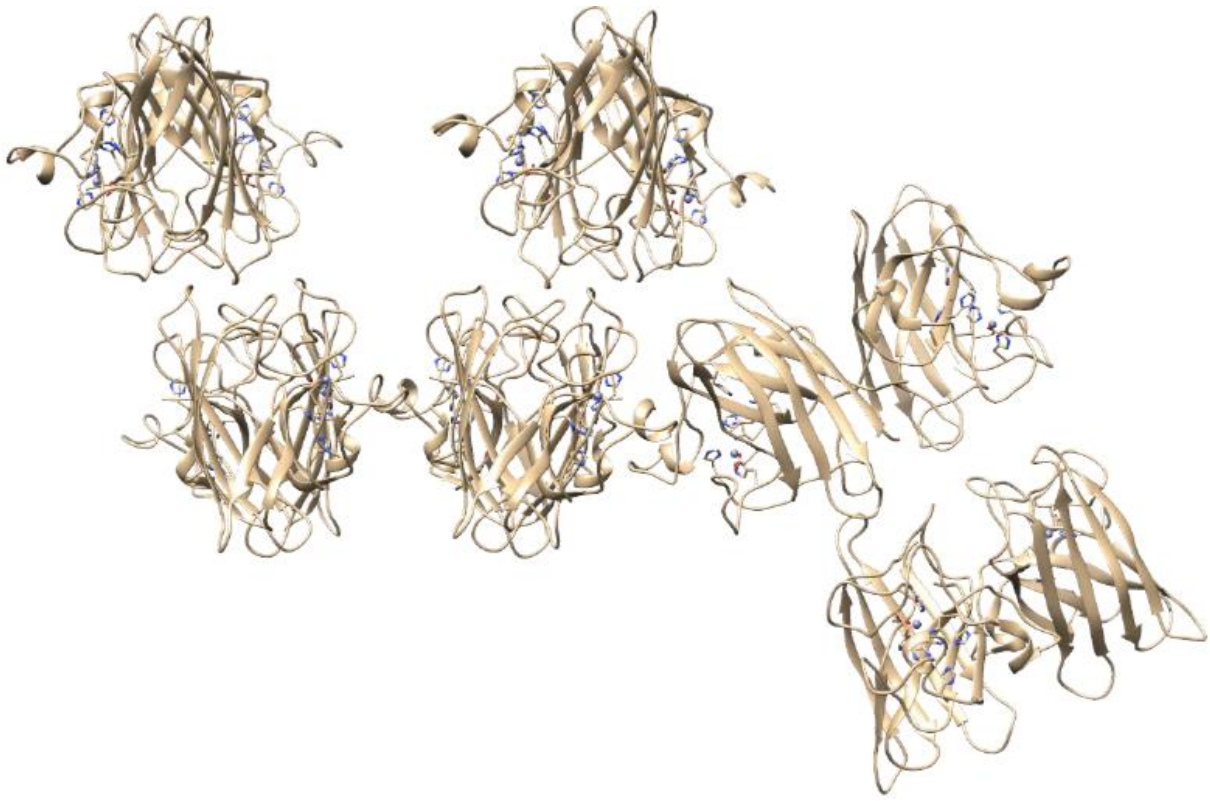


Figure 4.9-2. Refined structure of hSOD1 wt, derived from the crystals obtained by the experiments described above. The picture was obtained by Lisa-Marie Funk.

5 Summary and outlook

ALS is a fatal neurodegenerative disease with limited therapeutic options and no available cure. Mutations in the *sod1* gene are responsible for ca. 10-20 % of all familial ALS cases worldwide. Aggregation of mutated SOD1 protein is a recurring observation and plays a major role in the development of ALS in patients. Several aggregation pathways are discussed in the literature, but the dissociation of the homodimer structure into aggregation prone monomers seems to be one of the critical steps.

The aim of the presented work was to synthesize small organic molecules with an affinity for the SOD1 protein that bear the potential to stabilize the dimer against dissociation or aggregation in ALS. Lead structures were identified through *in silico* screening that followed a structural analysis of the protein cavity around Cys₁₁₁. The resulting structures were then ranked according to their putative binding energy, which was calculated by the open source platform swissdock.ch. Three chemically diverse lead structures were obtained, and their synthesis was envisaged (Figure 5-1).

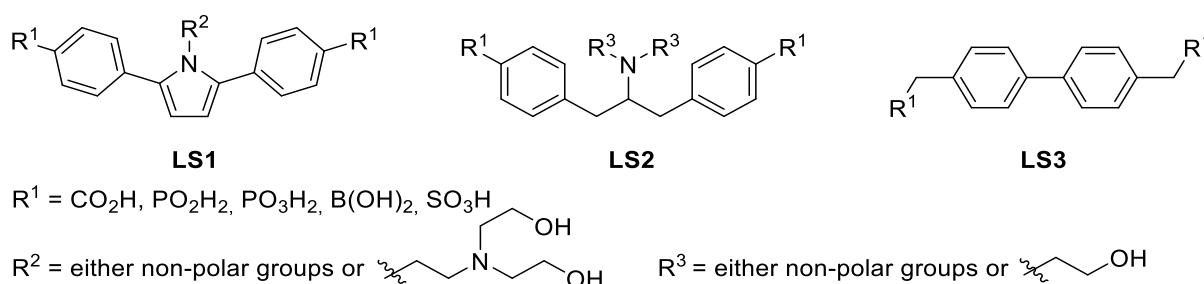


Figure 5-1. Chemical structures of **LS1**, **LS2** and **LS3**.

For **LS1**, a small library of molecules could be obtained that varied by the organic acid residue as well as by the *N*-substitution of the main pyrrole moiety. All desired molecules could be synthesized in amounts necessary for biophysical studies. The overall synthetic scheme for **LS1** is shown in Figure 5-2.

For **LS2**, the library synthesis was not successful, even though a large number of different methods and synthetic pathways were tried. A reasonable one-step procedure towards a possible chlorinated precursor for subsequent acid synthesis was presented, with the drawback of very expensive starting materials. Further optimization of the synthesis is needed, should this ligand scaffold be considered for biophysical assays.

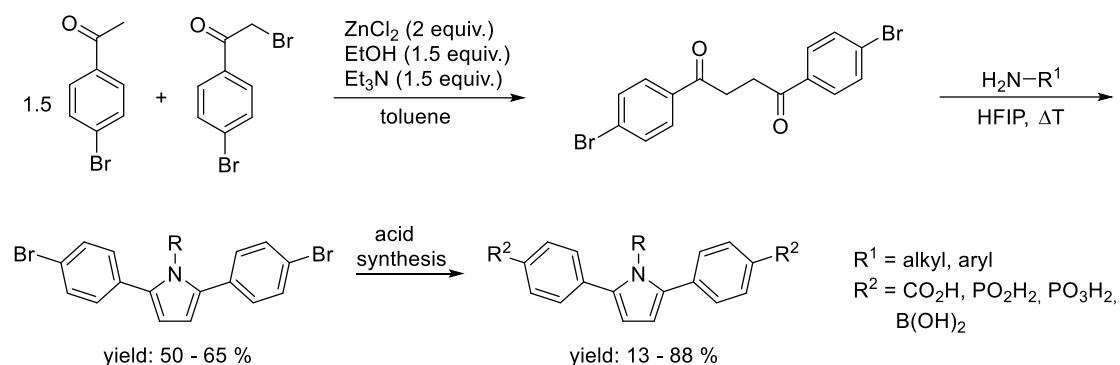


Figure 5-2. Synthetic approach for the library synthesis of **LS1**. 12 different molecules were synthesized.

For **LS3**, another small library of molecules could be obtained that varied by the organic acid residue as well as the substitution of the core biphenyl structure. The fluorinated structures were to be tested in nucleophilic aromatic substitution reactions in order to investigate their potential to engage in covalent binding to the protein *via* the thiol moiety of Cys₁₁₁. Up to this point, no reactivity towards nucleophilic aromatic substitution could be observed. The non-fluorinated structures served as a comparison to the fluorinated structure. The synthesis was performed according to Figure 5-3.

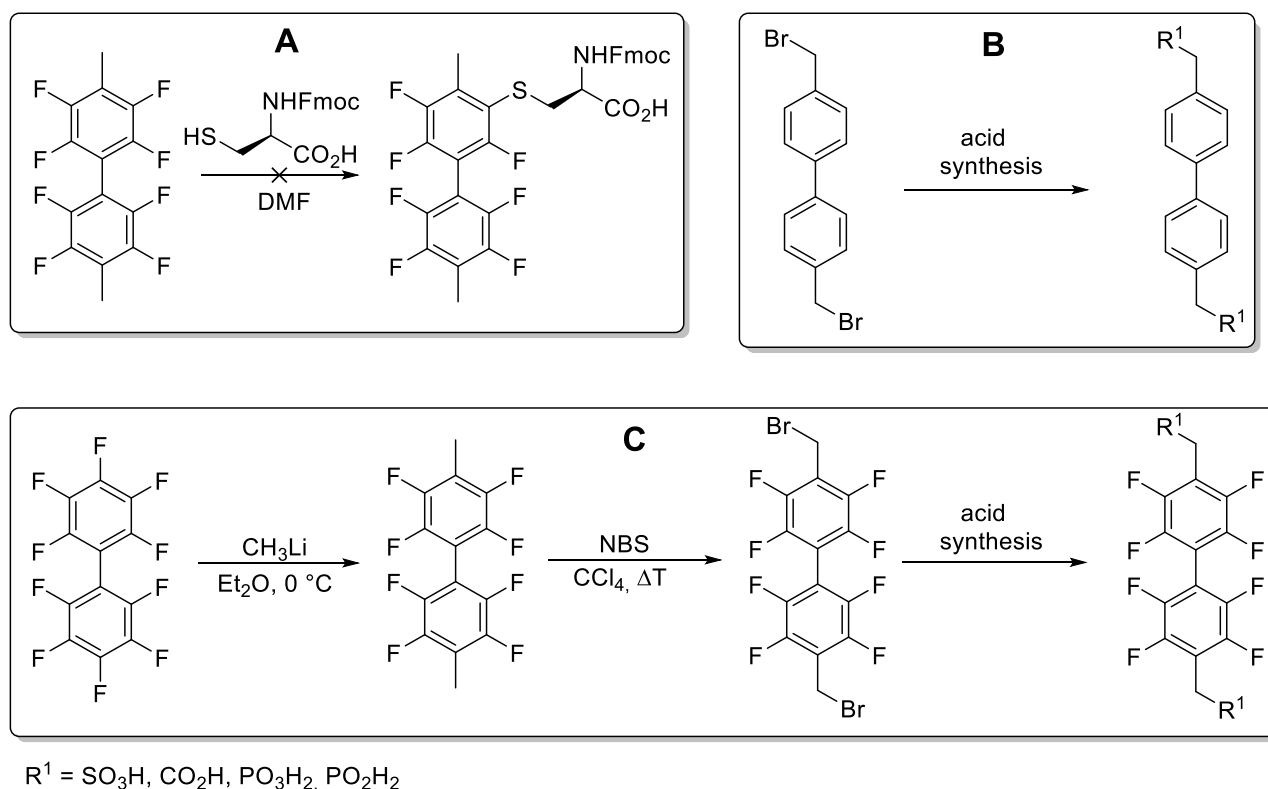


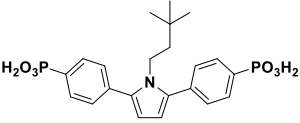
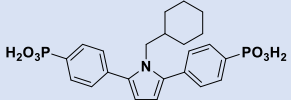
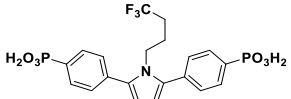
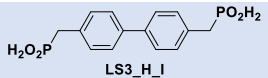

Figure 5-3. A: Reactivity test for nucleophilic aromatic substitution. **B:** Synthesis of the protonated structures of **LS3**. **C:** Synthesis of the fluorinated structures of **LS3**. 5 different molecules were synthesized.

The next step was the expression and purification of hSOD1 wt and hSOD1 A4V proteins using standard protocols (see Experimental section for details). Both variants could be isolated in high purity, the A4V mutant showed significantly lower yields compared to the wild type, as was expected. In addition, the stability of the mutant was lower compared to the stability of the wild type, indicated by high molar mass aggregates after purification via anion exchange chromatography. Activity analysis showed a sharp loss in activity, which is in accordance with the literature. In summary, the wild type and one mutant could be isolated after expression and reconstitution; both showed the expected behavior in terms of activity and stability.

Afterwards, binding studies were conducted using several different assays that were needed to confirm the *in silico* results. All ligands except for the boronic acid derivatives showed a sufficient solubility in water (up to 40 mM). The use of a co-solvent like DMSO or PEG4000 had a negative impact on the overall solubility of the ligands; therefore, the solubility was still the limiting factor for biophysical measurements.

Fluorescence anisotropy was employed to screen the carboxylic acid based library of **LS1** for the *N*-substituents that gave the highest binding (compare Figure 4.8-1). Afterwards, a microscale thermophoresis assay was developed and the resulting libraries of **LS1** and **LS3** were investigated in terms of their binding affinity. Aggregation and adsorption of samples, pipetting errors and the general sensitivity of the method were important factors to consider when the data was analyzed. Substantial errors and varying S/N ratios and/or response amplitudes between measurements of the same substance complicated the evaluation; nevertheless, a general trend could be observed regardless. The resulting structures that showed binding in the μM range are depicted in Table 5-1; all other substances were assessed as insufficient in terms of binding characteristics.

Table 5-1. MST results of selected ligands and their *in silico* binding energy.

ligands	K _d -value (μM)	S/N ratio	response amplitude	binding energy (kJ/mol)
 LS1_DMB_O	43 ± 18	8.00	3.50	53.58
 LS1_MCH_O	47 ± 17	10.33	8.03	54.22
 LS1_TFB_O	107 ± 63	6.29	1.87	53.17
 LS3_H_I	151 ± 93	5.81	5.65	44.35
 LS1_TFB_I	207 ± 64	13.01	3.76	46.09

The obtained results show a correlation between the predicted binding energies from *in silico* studies and the MST assay in that the phosphonic acid residue was the best binding partners for SOD1, followed by phosphinic acid derivatives. The influence of the alkyl residue seemed to be less important than the impact of the acid moiety.

Isothermal Titration Calorimetry was used to confirm already existing biophysical data, since it can be considered the gold standard of protein-ligand complex analysis.^[136] The necessity of using large amounts of protein as well as the complicated procedure involved in measuring K_d-values prevented the use of ITC as a screening assay for the entire library. The K_d-value of LS1_MCH_I that was measured by means of MST could be confirmed by ITC. This meant that both methods could be used as complementary assays for the measurement of K_d-values.

The next steps to improve the binding of potential ligands to the protein need to involve the crystal structure of the protein-ligand complex. Knowledge about binding sites and the exact nature of the interactions between both binding partners is mandatory in order to optimize lead structures. Molecular dynamics simulations could also help to identify and improve ligands for SOD1.

The solubility of the ligands could also be improved by the addition of more polar groups to the aromatic systems of the lead structures. Another possibility would be the synthesis of the furan analogues of the **LS1** derived pyrrole structures since the differences between the different *N*-substituents seemed largely negligible and their impact was impossible to predict with the utilized docking programs. Furthermore, omitting the very hydrophobic substituents would potentially increase the solubility of the resulting ligands. A possible synthetic pathway could make use of the dibromide precursor (**120**) that was already synthesized during the scope of this thesis (see Figure 5-4).

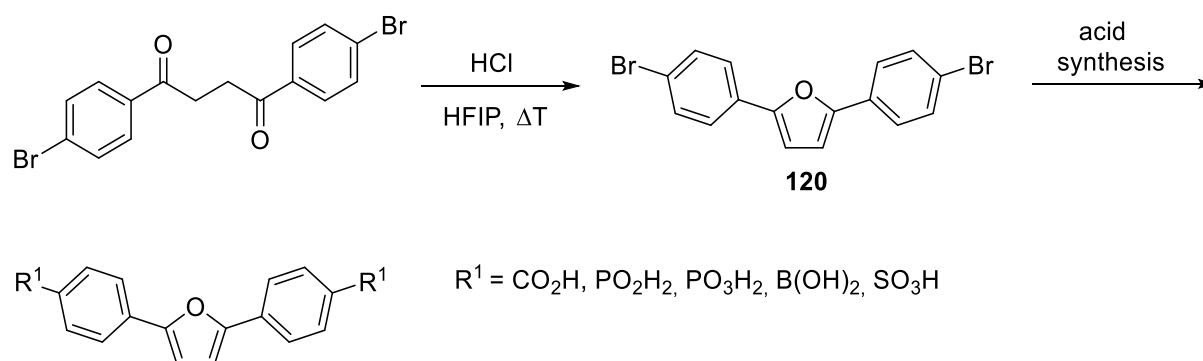
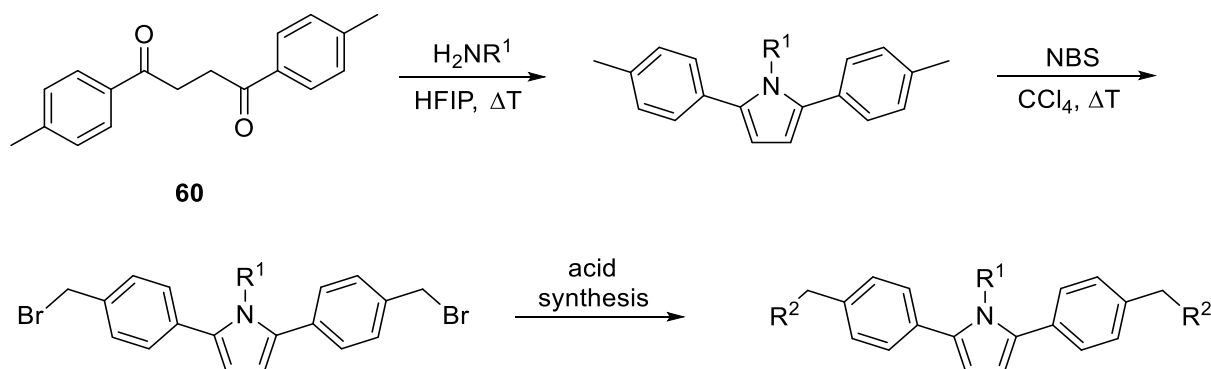


Figure 5-4. Possible synthesis of furan analogues of **LS1**.

In addition, the lead structures could also be extended by a methylene unit that would connect the acid moiety to the benzene ring. Thereby the flexibility of the lead structures would be improved and the steric fit to the binding cavity could be improved. A possible synthesis could start from the already introduced 1,4-diketone **60** (Figure 5-5):



R¹ = alkyl, aryl

R² = CO₂H, PO₂H₂, PO₃H₂, B(OH)₂, SO₃H

Figure 5-5. Possible synthesis of elongated analogues of **LS1**.

On the protein side, more mutants should be expressed with the help of PCR techniques so that the biophysical assays can be expanded on to a broader range of ALS-associated proteins. Mutations that appear far from the dimer interface could potentially be used to gain information about the binding sites of ligands, since their binding modes could vary drastically between different mutants. Thereby it could be proven that the designed ligands show affinity to a variety of mutants instead of showing affinity to the wild type only.

The development of improved conditions for biophysical assays (especially ITC techniques) deserves special attention since more than one assay has to be utilized in order to verify existing binding data.

6. Experimental part

This chapter covers all experiments, measurements and applied methods that were used to obtain the already mentioned results. The first part will depict organic synthesis and the corresponding analytical data. The second part will cover protein expression and all biophysical techniques that were performed in close collaboration with Lisa-Marie Funk from the *Schwann-Schleiden Forschungszentrum für molekulare Enzymologie*, University of Göttingen.

6.1 Ligand synthesis

6.1.1 Analytics

a) NMR spectroscopy

NMR spectra were recorded on a BRUKER Avance III 300 or BRUKER Avance III HD 500 device at the Institute for Organic and Biomolecular Chemistry, University Göttingen. Coupling constants are given in Hertz (Hz). Multiplicities are abbreviated as: singlet (s), broad singlet (br s), doublet (d), triplet (t), quartet (q), quintet (quint), doublet of doublets (dd). The internal standard for ^1H - and ^{13}C -spectroscopy was the solvent residue signal. Used solvents: CDCl_3 (7.26 ppm, 77.16 ppm), MeOD-d_4 (3.33 ppm, 49.00 ppm), DMSO-d_6 (2.50 ppm, 39.52 ppm), CD_2Cl_2 (5.32 ppm, 53.84 ppm), THF-d_8 (3.58 ppm + 1.72 ppm, 67.21 ppm + 25.31 ppm), D_2O (4.79 ppm).

b) Mass spectrometry

Mass spectra were recorded on a *BRUKER microTOF* (ESI) or *JEOL AccuTOF* (EI) device. Applied ionization techniques were Electron Ionization (EI) or Electrospray Ionization (ESI). All shown data is given in m/z.

c) UV/Vis-spectroscopy

UV spectra were recorded on JASCO V-750 spectrometer using the associated software. Black quartz glass cuvettes from HELMA ANALYTICS 104 and a light path length of 10 mm were used. The sample volume was 120 to 150 μL depending on the

substrate. The temperature was set to 25 °C, the scanning speed was typically 200 nm/m, and the associated bandwidth was 2.0 nm.

d) IR-spectroscopy

IR spectra were recorded on a JASCO FT/IR 4100 A spectrometer. The substrates were used as solids or oils without any special treatment or capsuling in a matrix. Wavenumbers are given in cm^{-1} .

e) Melting point

Melting points were measured with a KRÜSS melting point meter (M5000) and the associated capillaries. Note that the standard deviation for all melting points given in this thesis is ± 0.2 °C.

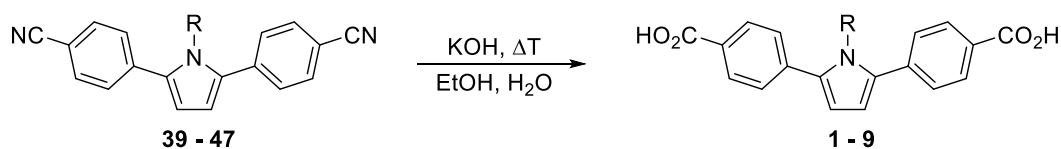
f) Chemicals

All commercially available chemicals for synthesis or analytical purposes were used without further purification if not stated otherwise. Anhydrous solvents were supplied by AcrosOrganics (Thermo Fischer scientific brand) and were stored in the original package over molecular sieves under an atmosphere of argon.

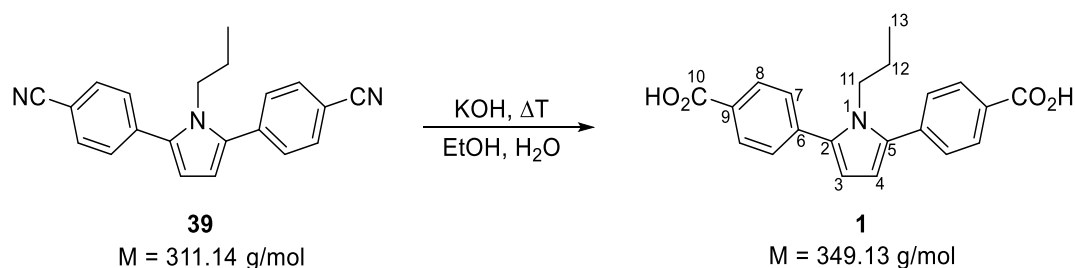
6.1.2 Synthesis procedures

6.1.2.1 Synthesis of the final ligands **1 – 24**

General procedure for the syntheses of the carboxylic acids **1-9**: The N-substituted 2,5-bis(4-cyanophenyl)pyrroles were taken up in a mixture of EtOH and H₂O (1:1) and a large excess of KOH (usually around 15 equiv.) was added. The mixture was stirred and heated to reflux until all solids had dissolved; heating at reflux was then continued for the indicated amount of time. After cooling to room temperature, all volatiles were removed, and the residue was taken up in water. After filtration, the pH was adjusted to 1 with dilute HCl. The resulting precipitate was filtered, washed with water until acid free and dried in air. The crude products were either pure enough to use them directly or were purified via column chromatography or RP-column chromatography.



Synthesis of 4,4'-(1-propyl-1H-pyrrole-2,5-diyl)dibenzoic acid (**1**)



4,4'-(1-propyl-1H-pyrrole-2,5-diyl)dibenzonitrile (**39**) (200 mg, 0.64 mmol, 1 equiv.) was dissolved in a mixture of EtOH and H₂O (1:1, 20 mL) and a large excess of KOH (550 mg) was added to the reaction mixture. The reaction was refluxed for 2 days and was worked-up according to the general procedure. The product was obtained as a yellow solid (95 mg, 0.27 mmol, 42% yield).

m.p.: 295 °C.

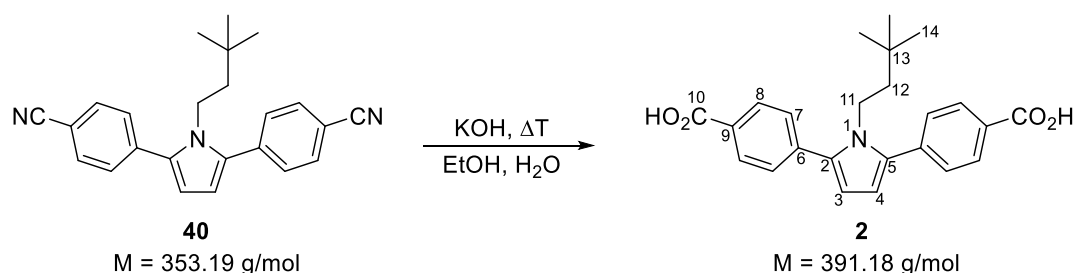
¹H-NMR (300 MHz, CD₃OD): δ (ppm) = 8.11 (d, 4H, J = 7.80 Hz, 8-H, 8'-H), 7.60 (d, 4H, J = 7.80 Hz, 7-H, 7'-H), 6.38 (s, 2H, 3-H, 4'-H), 4.21 (t, 2H, J = 6.9 Hz, 11-H), 1.20 (sex, 2H, J = 6.9 Hz, J = 7.4 Hz, 12-H), 0.41 (t, 3H, J = 7.4 Hz, 13-H).

¹³C-NMR (75 MHz, DMSO-*d*₆): δ (ppm) = 167.55 (C-10), 137.96 (C-2, C-5), 137.07 (C-6, C-6'), 130.21 (C-8, C-8'), 129.36 (C-9, C-9'), 128.46 (C-7, C-7'), 47.38 (C-11), 23.90 (C-12), 10.84 (C-13).

FT-IR (solid): $\tilde{\nu}$ (cm⁻¹) = 2970, 1738, 1672, 1601, 1421, 1365, 1228, 1217, 860, 762.

HR-MS (ESI): m/z calculated for C₂₁H₂₀NO₄ [M+H]⁺ 350.1387; observed 350.1386.

Synthesis of 4,4'-(1-(3,3-dimethylbutyl)-1H-pyrrole-2,5-diyl)dibenzoic acid (**2**)



4,4'-(1-(3,3-dimethylbutyl)-1H-pyrrole-2,5-diyl)dibenzonitrile (**40**) (605 mg, 1.71 mmol, 1 equiv.) was dissolved in a mixture of EtOH and H₂O (1:1, 30 mL) and a large excess of KOH (1.41 g) was added to the reaction mixture. The reaction was refluxed for 2 days and was worked-up according to the general procedure. The product was obtained as yellow crystals (189 mg, 0.48 mmol, 28% yield).

m.p.: 300 °C

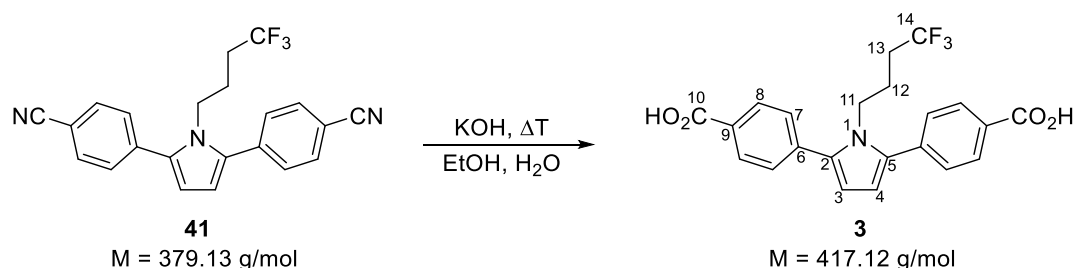
¹H-NMR (300 MHz, CD₃OD): δ (ppm) = 12.99 (s, 2H, CO₂H), 8.02 (d, 4H, *J* = 8.30 Hz, 3-H, 3'-H), 7.63 (d, 4H, *J* = 8.30 Hz, 4-H, 4'-H), 6.39 (s, 2H, 7-H, 7'-H), 4.19 (m, 2H, 8-H), 0.99 (m, 2H, 9-H), 0.52 (s, 9H, 11-H, 11'-H, 11''-H).

¹³C-NMR (75 MHz, CD₃OD): δ (ppm) = 176.56 (C-1, C-1'), 137.87 (C-6, C-6'), 136.34 (C-5, C-5'), 130.10 (C-3, C-3'), 129.43 (C-2, C-2'), 128.68 (C-4, C-4'), 111.58 (C-7, C-7'), 43.98 (C-8), 42.35 (C-9), 29.71 (C-10), 28.96 (C-11, C-11', C-11'').

FT-IR (solid): $\tilde{\nu}$ (cm⁻¹) = 2970, 1739, 1678, 1602, 1419, 1366, 1229, 1217, 861, 763.

HR-MS (ESI): *m/z* calculated for C₂₄H₂₆NO₄ [M+H]⁺ 392.1856; observed 392.1858.

Synthesis of 4,4'-(1-(4,4,4-trifluorobutyl)-1H-pyrrole-2,5-diyl)dibenzoic acid (**3**)



4,4'-(1-(4,4,4-trifluorobutyl)-1H-pyrrole-2,5-diyl)dibenzonitrile (**41**) (133 mg, 0.35 mmol, 1 equiv.) was dissolved in a mixture of EtOH and H₂O (1:1, 20 mL) and a large excess of KOH (290 mg) was added to the reaction mixture. The reaction was refluxed for 2 days and was worked-up according to the general procedure. The product was obtained as an orange solid (90 mg, 0.19 mmol, 54% yield).

m.p.: 292 °C.

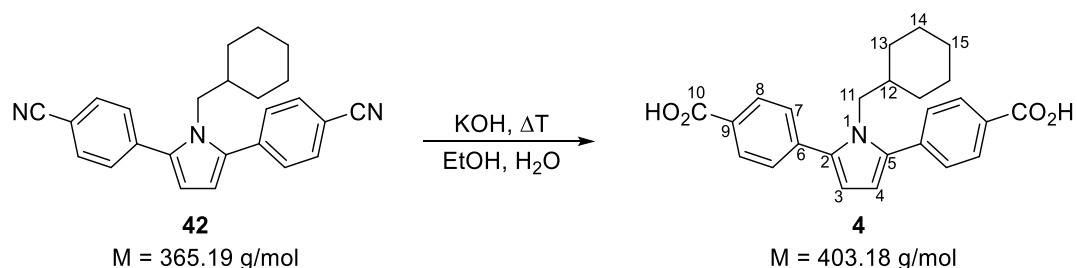
¹H-NMR (300 MHz, CD₃OD): δ (ppm) = 8.13 (d, 4H, *J* = 8.30 Hz, 3-H, 3'-H), 7.63 (d, 4H, *J* = 8.30 Hz, 4-H, 4'-H), 6.44 (s, 2H, 7-H, 7'-H), 4.34 (t, 2H, *J* = 6.6 Hz, 8-H), 1.60-1.29 (m, 6H, 9-H, 10-H).

¹³C-NMR (75 MHz, CD₃OD): δ (ppm) = 168.18 (C-1), 137.85 (C-6, C-6'), 137.38 (C-5, C-5'), 129.90 (C-3, C-3'), 129.05 (C-2, C-2'), 127.91 (C-4, C-4'), 111.40 (C-7, C-7'), 44.21 (C-8), 29.73 (C-9), 29.34 (C-10), 22.80 (C-11).

FT-IR (solid): $\tilde{\nu}$ (cm⁻¹) = 2969, 1740, 1422, 1220.

HR-MS (ESI): *m/z* calculated for C₂₂H₁₉NF₃O₄ [M+H]⁺ 418.1261; observed 418.1257.

Synthesis of 4,4'-(1-(cyclohexylmethyl)-1H-pyrrole-2,5-diyl)dibenzoic acid (**4**)



4,4'-(1-(methylcyclohexyl)-1H-pyrrole-2,5-diyl)dibenzonitrile (**42**) (158 mg, 0.43 mmol, 1 equiv.) was dissolved in a mixture of EtOH and H₂O (1:1, 20 mL) and a large excess of KOH (355 mg) was added to the reaction mixture. The reaction was refluxed for 2 days and was worked-up according to the general procedure. The product was obtained as a slightly yellow powder (155 mg, 0.38 mmol, 88% yield).

m.p.: 183 °C.

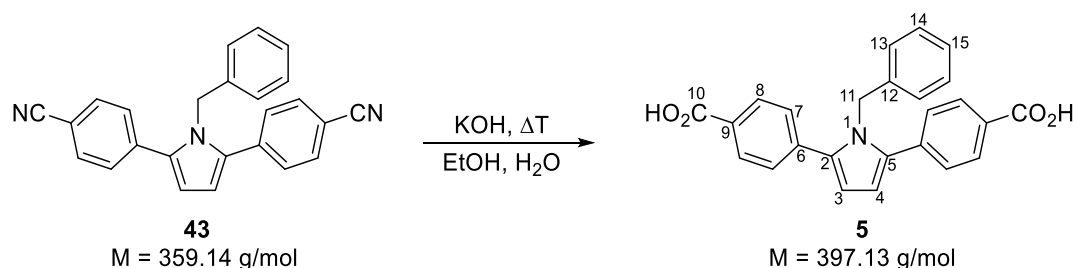
¹H-NMR (300 MHz, CD₃OD): δ (ppm) = 8.11 (d, 4H, J = 8.30 Hz, 8-H, 8'-H), 7.61 (d, 4H, J = 8.30 Hz, 7-H, 7'-H), 6.39 (s, 2H, 3-H, 4-H), 4.10 (d, 2H, J = 7.3 Hz, 11-H), 1.47-1.35 (m, 3H, 12-H, 13-H, 13-H), 1.22-1.01 (m, 3H, 14-H, 14-H, 15-H), 0.94-0.76 (m, 3H, 13'-H, 13'-H, 15-H), 0.53-0.33 (m, 2H, 14'-H, 14'-H).

¹³C-NMR (75 MHz, CD₃OD): δ (ppm) = 168.32 (C-10, C-10'), 138.59 (C-2, C-5), 137.84 (C-6, C-6'), 129.75 (C-8, C-8'), 128.64 (C-9, C-9'), 127.88 (C-7, C-7'), 110.83 (C-3, C-4), 51.88 (C-11), 39.15 (C-12), 29.79 (C-13, C-13'), 25.76 (C-15), 25.06 (C-14, C-14').

FT-IR (solid): $\tilde{\nu}$ (cm⁻¹) = 2970, 1739, 1676, 1604, 1422, 1274, 1230, 1216, 860, 771, 705.

HR-MS (ESI): m/z calculated for C₂₅H₂₆NO₄ [M+H]⁺ 404.1856; observed 404.1864.

Synthesis of 4,4'-(1-benzyl-1H-pyrrole-2,5-diyl)dibenzoic acid (**5**)



4,4'-(1-(benzyl)-1H-pyrrole-2,5-diyl)dibenzonitrile (**43**) (703 mg, 1.96 mmol, 1 equiv.) was dissolved in a mixture of EtOH and H₂O (1:1, 40 mL) and a large excess of KOH (1.62 g) was added to the reaction mixture. The reaction was refluxed for 2 days and was worked-up according to the general procedure. The product was obtained as a slightly yellow solid (746 mg, 1.88 mmol, 96% yield).

m.p.: 273 °C.

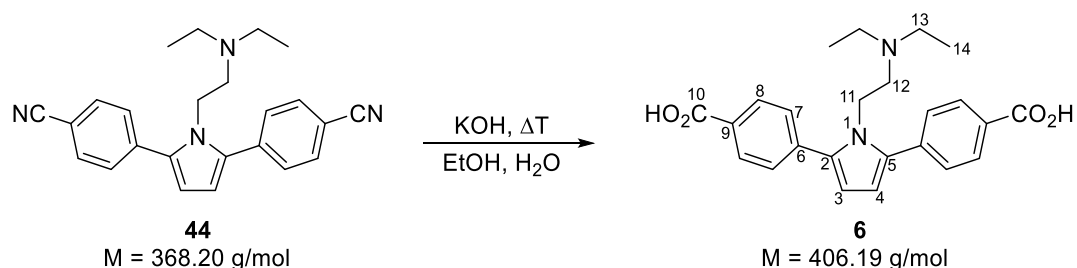
¹H-NMR (300 MHz, DMSO-*d*₆): δ (ppm) = 12.91 (s, 2H, CO₂H), 7.92 (d, 4H, *J* = 8.55 Hz, 8-H, 8'-H), 7.56 (d, 4H *J* = 8.55 Hz, 7-H, 7'-H), 7.13-7.01 (m, 3H, 14-H, 14'-H, 15-H), 6.56-6.47 (m, 4H, 3-H, 4-H, 13-H, 13'-H), 5.38 (s, 2H, 11-H).

¹³C-NMR (75 MHz, DMSO-*d*₆): δ (ppm) = 167.49 (C-10, C-10'), 138.94 (C-13), 137.44 (C-2, C-5), 137.37 (C-6, C-6'), 130.05 (C-8, C-8'), 129.50 (C-9, C-9'), 128.75 (C-14, C-14'), 128.58 (C-7, C-7'), 127.37 (C-15), 125.82 (C-13, C-13'), 112.05 (C-3, C-4), 49.19 (C-11).

FT-IR (solid): $\tilde{\nu}$ (cm⁻¹) = 3130-2020, 2969, 1698, 1604, 1422, 1278, 915, 866, 776, 701.

HR-MS (ESI): *m/z* calculated for C₂₅H₂₀NO₄ [M+H]⁺ 398.1387; observed 398.1385.

Synthesis of 4,4'-(1-(2-(diethylamino)ethyl)-1H-pyrrole-2,5-diyl)dibenzoic acid (**6**)



4,4'-(1-(2-(Diethylamino)ethyl)-1H-pyrrole-2,5-diyl)dibenzonitrile (**44**) (194 mg, 0.53 mmol, 1 equiv.) was dissolved in a mixture of EtOH and H₂O (1:1, 20 mL) and a large excess of KOH (440 mg) was added to the reaction mixture. The reaction was refluxed for 2 days and was worked-up according to the general procedure and with RP-column chromatography (20% MeOH in H₂O). The product was obtained as a light brown, sticky solid (40 mg, 0.1 mmol, 19% yield).

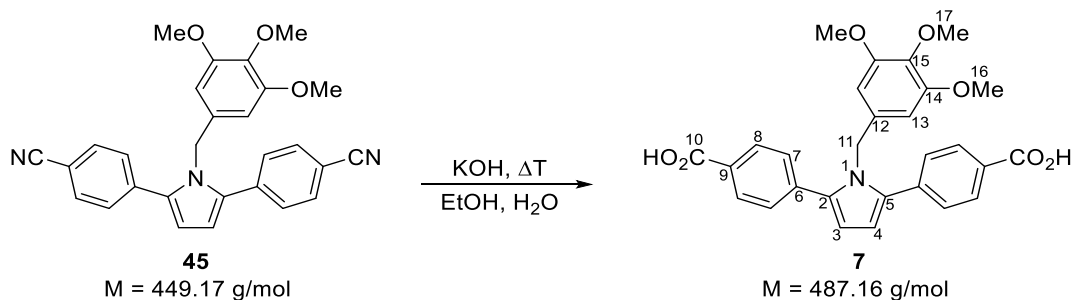
m.p.: 286 (decomp.).

¹H-NMR (300 MHz, DMSO-*d*₆): δ = 7.95 (d, 4H, *J* = 8.17 Hz, 8-H, 8'-H), 7.48 (d, 4H, *J* = 8.17 Hz, 7-H, 4'-H), 6.27 (2, 2H, 3-H, 4-H), 2.05 (m, 6H, 12-H, 13-H, 13'-H), 0.51 (t, 6H, *J* = 7.05 Hz, 11-H, 14-H, 14'-H).

¹³C-NMR could not be measured due to its low solubility in common organic solvents.

HR-MS (ESI): *m/z* calculated for C₂₄H₂₇N₂O₄ [M+H]⁺ 407.1965; observed 407.1963.

Synthesis of 4,4'-(1-(3,4,5-trimethoxybenzyl)-1H-pyrrole-2,5-diyl)dibenzoic acid (7)



4,4'-(1-(3,4,5-trimethoxybenzyl)-1H-pyrrole-2,5-diyl)dibenzonitrile (**45**) (112 mg, 0.25 mmol, 1 equiv.) was dissolved in a mixture of EtOH and H₂O (1:1, 20 mL) and a large excess of KOH (206 mg) was added to the reaction mixture. The reaction was refluxed for 3 days and was worked-up according to the general procedure. The product was obtained as a light yellow solid (23.5 mg, 0.05 mmol, 20% yield).

m.p.: 260 °C (decomp.).

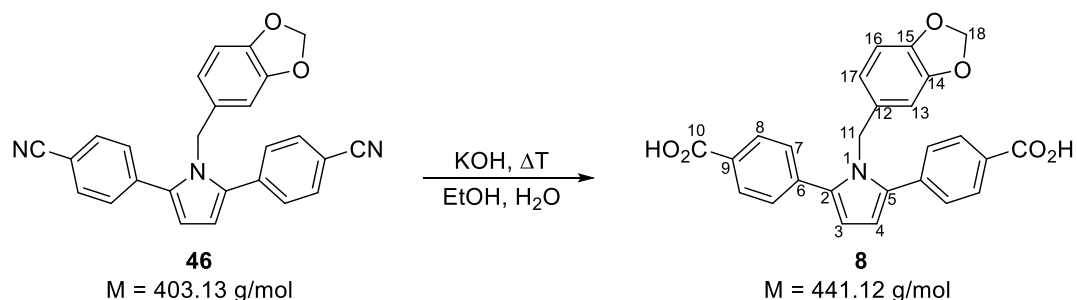
¹H-NMR (300 MHz, DMSO-*d*₆): δ (ppm) = 7.95 (m, 4H, -H, 8'-H), 7.58 (m, 4H, 7-H, 7'-H), 6.49 (m, 2H, 13-H, 13'-H), 5.74 (s, 2H, 3-H, 4-H), 5.28 (2, 2H, 11-H), 3.51 (s, 3H, 17-H), 3.47 (s, 6H, 16-H).

¹³C-NMR (75 MHz, DMSO-*d*₆): δ (ppm) = 167.49 (C-10, C-10'), 153.03 (C-14, C-14'), 137.60 (C-2, C-5), 136.57 (C-15), 134.52 (C-6, C-6'), 130.15 (C-8, C-8'), 129.54 (C-9, C-9'), 128.79 (C-7, C-7'), 112.07 (C-3, C-4), 103.36 (C-13, C-13'), 60.32 (C-17), 55.86 (C-16, C-16'), 49.13 (C-11).

FT-IR (solid): $\tilde{\nu}$ (cm⁻¹) = 1693, 1603, 1421, 1260, 1122, 768.

MS (ESI): *m/z* calculated for C₂₈H₂₆NO₇ [M+H]⁺ 487.1600; observed 487.1900.

Synthesis of 4,4'-(1-(benzo[d][1,3]dioxol-5-ylmethyl)-1H-pyrrole-2,5-diyl)dibenzoic acid (8)



4,4'-(1-(benzo[d][1,3]dioxol-5-ylmethyl)-1H-pyrrole-2,5-diyl)dibenzonitrile (**46**) (68 mg, 0.17 mmol, 1 equiv.) was dissolved in a mixture of EtOH and H₂O (1:1, 20 mL) and a large excess of KOH (141 mg) was added to the reaction mixture. The reaction was refluxed for 3 days and was worked-up according to the general procedure. The product was obtained as a light brown solid (71 mg, 0.16 mmol, 95% yield).

m.p.: 262 °C (decomp.)

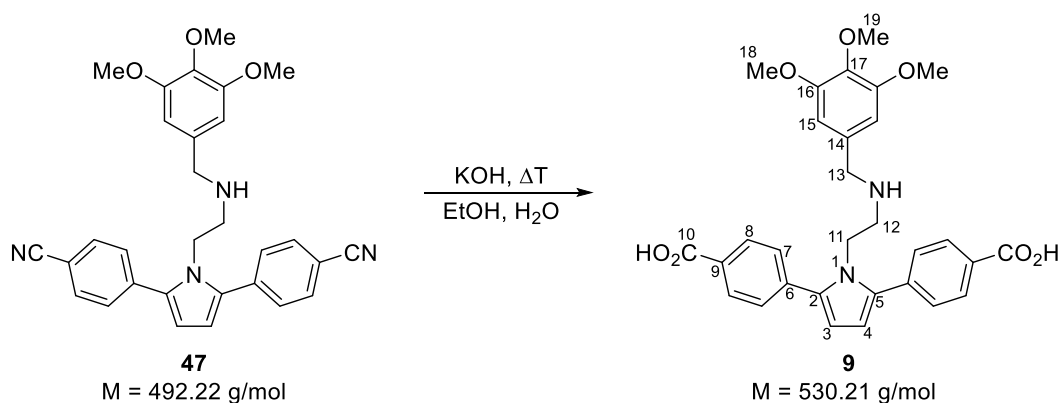
¹H-NMR (300 MHz, DMSO-*d*₆): δ (ppm) = 12.95 (s, 2H, CO₂H), 7.96 (d, 4H, $J = 8.40$ Hz, 8-H, 8'-H), 7.58 (d, 4H, $J = 8.40$ Hz, 7-H, 7'-H), 6.62 (d, 1H, $J = 7.95$ Hz, 13-H), 6.51 (s, 2H, 3-H, 4-H), 6.04-5.95 (m, 2H, 16-H, 17-H), 5.87 (s, 2H, 18-H), 5.29 (s, 2H, 11-H).

¹³C-NMR (75 MHz, DMSO-*d*₆): δ (ppm) = 167.47 (C-10), 147.68 (C-14), 146.47 (C-16), 137.42 (C-2, C-5), 137.32 (C-9, C-9'), 132.70 (C-6, C-6'), 130.10 (C-8, C-8'), 129.46 (C-12), 128.57 (C-7, C-7'), 119.08 (C-13), 112.10 (C-15), 108.46 (C-3, C-4), 106.23 (C-13), 101.30 (C-17), 30.89 (C-11).

FT-IR (solid): $\tilde{\nu}$ (cm⁻¹) = 1679, 1605, 1420, 1245, 1176, 1038, 932, 863, 766, 697.

HR-MS (ESI): m/z calculated for C₂₆H₂₀NO₆ [M+H]⁺ 442.1285; observed 442.1281.

Synthesis of 4,4'-(1-(2-((3,4,5-trimethoxybenzyl)amino)ethyl)-1H-pyrrole-2,5-diyl)dibenzoic acid (**9**)



4,4'-(1-(2-((3,4,5-trimethoxybenzyl)amino)ethyl)-1H-pyrrole-2,5-diyl)dibenzonitrile (**47**) (101 mg, 0.21 mmol, 1 equiv.) was dissolved in a mixture of EtOH and H₂O (1:1, 20 mL) and a large excess of KOH (173 mg) was added to the reaction mixture. The reaction was refluxed for 3 days and was worked-up according to the general procedure and with RP-column chromatography. The product was obtained as an orange semi solid (83 mg, 0.16 mmol, 78% yield).

m.p.: 278 °C (decomp.).

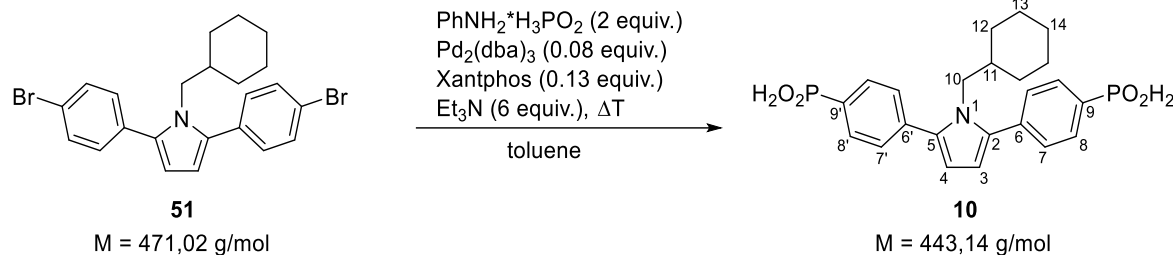
¹H-NMR (300 MHz, DMSO-*d*₆): δ (ppm) = 7.88 (d, 4H, *J* = 8.10 Hz, 8-H, 8'-H), 7.34 (d, 4H, *J* = 8.10 Hz, 7-H, 7'-H), 6.32 (s, 2H, 3-H, 4-H), 6.18 (s, 2H, 15-H, 15'-H), 4.23 (m, 2H, 11-H), 3.67 (s, 6H, 18-H), 3.59 (s, 3H, 19-H), 3.15 (m, 2H, 13-H), 2.24 (m, 2H, 12-H).

¹³C-NMR could not be measured due to its low solubility in common organic solvents.

FT-IR (solid): $\tilde{\nu}$ (cm⁻¹) = 3354, 2969, 1738, 1584, 1541, 1374, 1228, 1216, 994, 767.

HR-MS (ESI): *m/z* calculated for C₃₀H₃₁N₂O₇ [M+H]⁺ 531.2126; observed 531.2123.

Synthesis of ((1-(cyclohexylmethyl)-1H-pyrrole-2,5-diyl)bis(4,1 phenylene))bis(phosphinic acid) (**10**)



2,5-bis(4-bromophenyl)-1-(cyclohexylmethyl)-1H-pyrrole (**51**) (400 mg, 0.85 mmol, 1 equiv.), $\text{Pd}_2(\text{dba})_3$ (61 mg, 0.024 mmol, 8 mol%) and Xantphos (66 mg, 0.11 mmol, 13 mol%) were dissolved in anhydrous toluene (15 mL) under an atmosphere of argon. Triethylamine (0.88 mL, 0.520 g, 5.11 mmol, 6 equiv.) and anilinium hypophosphite (255 mg, 1.69 mmol, 2.2 equiv.) were added to the reaction mixture and it was refluxed for 3 h. After cooling to room temperature, the reaction mixture was diluted with 1 M NaOH (until pH > 12) and MTBE (50 mL). After 20 minutes of stirring the non-soluble solids were removed by filtration through Celite. The resulting organic phase was extracted with 1 M NaOH (2 x 40 mL) and the combined aqueous phases were washed with DCM (2 x 50 mL) and filtered again. The pH value of the aqueous phase was adjusted to pH < 2 with conc. HCl and the resulting precipitate was filtered off. The product was obtained as a pale yellow solid (200 mg, 0.45 mmol, 53% yield).

m.p.: 249.1 °C.

$^1\text{H-NMR}$ (300 MHz, DMSO-d_6): δ (ppm) = 7.84-7.71 (m, 4H, 8-H, 8'-H), 7.66 (dd, 4H, $J = 8.01 \text{ Hz}$, $^4J_{\text{P-H}} = 2.64 \text{ Hz}$, 7-H, 7'-H), 7.54 (d, 2H, $^1J_{\text{P-H}} = 549 \text{ Hz}$, PH), 6.38 (s, 2H, 3-H, 4-H), 4.05 (d, 2H, $J = 6.87 \text{ Hz}$, 10-H), 1.41-1.23 (m, 3H, 13-H, 13-H, 14-H), 1.07-0.89 (m, 3H, 11-H, 12'-H, 12'-H), 0.85-0.62 (m, 3H, 13'-H, 13'-H, 14'-H), 0.44-0.24 (m, 2H, 12-H, 12-H).

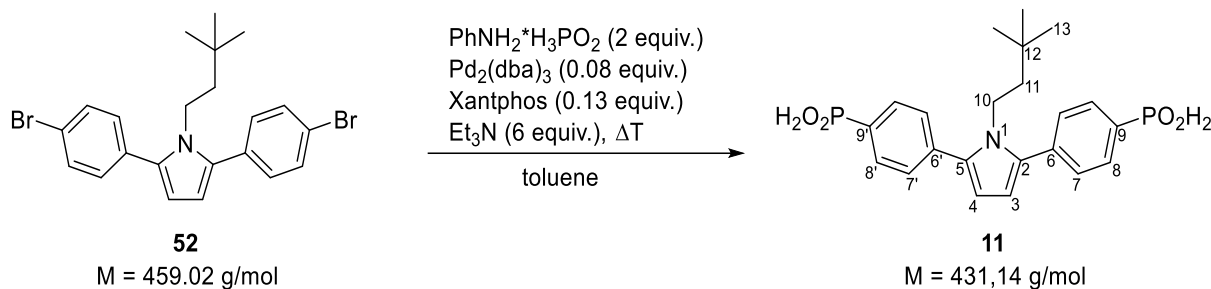
$^{13}\text{C-NMR}$ could not be measured due to its low solubility in common organic solvents.

$^{31}\text{P-NMR}$ (25.8 MHz, DMSO-d_6): δ (ppm) = 16.06 (s, P)

FT-IR (solid): $\tilde{\nu}$ (cm^{-1}) = 2925, 2845, 1598, 1140, 1090, 963, 832, 779, 746.

HR-MS (ESI): m/z calculated for $\text{C}_{23}\text{H}_{27}\text{NO}_4\text{P}_2$ $[\text{M}-2\text{H}]^{2-}$ 220.5635; observed 220.5636.

Synthesis of ((1-(3,3-dimethylbutyl)-1H-pyrrole-2,5-diyl)bis(4,1-phenylene))bis(phosphinic acid) (11)



2,5-bis(4-bromophenyl)-1-(3,3-dimethylbutyl)-1H-pyrrole (**52**) (200 mg, 0.44 mmol, 1 equiv.), Pd₂(dba)₃ (23 mg, 0.01 mmol, 3 mol%) and Xantphos (26 mg, 0.04 mmol, 9 mol%) were dissolved in anhydrous toluene (12 mL) under an atmosphere of argon. Triethylamine (0.31 mL, 0.178 g, 1.74 mmol, 4 equiv.) and anilinium hypophosphite (135 mg, 0.90 mmol, 2.1 equiv.) were added to the reaction mixture and it was refluxed for 3 h. After cooling to room temperature, the reaction mixture was diluted with 1 M NaOH (until pH > 12) and MTBE (50 mL). After 20 minutes of stirring the non-soluble solids were removed by filtration through Celite. The resulting organic phase was extracted with 1 M NaOH (2 x 40 mL) and the combined aqueous phases were washed with DCM (2 x 50 mL) and filtered again. The pH value of the aqueous phase was adjusted to pH < 2 with conc. HCl and the resulting precipitate was filtered off. The product was obtained as a pale brownish solid (120 mg, 0.28 mmol, 64% yield).

m.p.: 193.2 °C.

¹H-NMR (300 MHz, DMSO-d₆): δ (ppm) = 7.78-7.67 (m, 4H, 8-H, 8'-H), 7.66-7.55 (dd, 4H, *J* = 8.01 Hz, ⁴*J*_{P-H} = 2.46 Hz, 7-H, 7'-H), 7.49 (d, 2H, ¹*J*_{P-H} = 537 Hz, PH), 6.34 (s, 2H, 3-H, 4-H), 4.15 (m, 2H, 10-H), 0.99 (m, 2H, 11-H), 0.51 (s, 9H, 13-H).

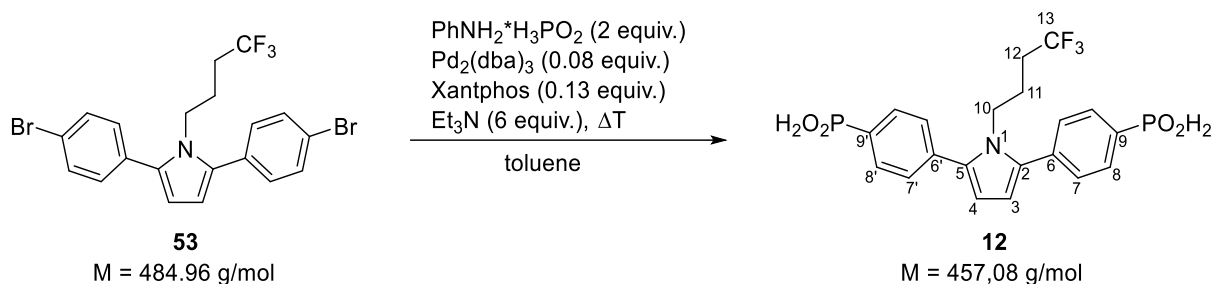
¹³C-NMR (75 MHz, DMSO-d₆): δ (ppm) = 136.82 (C-6, C-6'), 136.28 (C-2, C-5), 133.74 (C-9, C-9'), 130.93 (C-8, C-8'), 128.52 (C-7, C-7'), 111.38 (C-3, C-4), 43.96 (C-11), 42.27 (C-10), 29.71 (C-12), 29.01 (C-13).

³¹P-NMR (25.8 MHz, DMSO-d₆): δ (ppm) = 14.22 (s, P).

FT-IR (solid): $\tilde{\nu}$ (cm⁻¹) = 2951.2362.1596.1131.950.833.782.742.

HR-MS (ESI): m/z calculated for C₂₂H₂₇NO₄P₂ [M-2H]²⁻ 214.5635; observed 214.5642.

Synthesis of ((1-(4,4,4-trifluorobutyl)-1H-pyrrole-2,5-diyl)bis(4,1-phenylene))bis(phosphinic acid) (**12**)



2,5-bis(4-bromophenyl)-1-(4,4,4-trifluorobutyl)-1H-pyrrole (**53**) (200 mg, 0.41 mmol, 1 equiv.), Pd₂(dba)₃ (25 mg, 0.01 mmol, 3 mol%) and Xantphos (32 mg, 0.05 mmol, 10 mol%) were dissolved in anhydrous toluene (12 mL) under an atmosphere of argon. Triethylamine (0.3 mL, 0.172 g, 1.72 mmol, 4.2 equiv.) and anilinium hypophosphite (176 mg, 1.12 mmol, 2.7 equiv.) were added to the reaction mixture and it was refluxed for 3 h. After cooling to room temperature, the reaction mixture was diluted with 1 M NaOH (until pH > 12) and MTBE (50 mL). After 20 minutes of stirring the non-soluble solids were removed by filtration through Celite. The resulting organic phase was extracted with 1 M NaOH (2 x 40 mL) and the combined aqueous phases were washed with DCM (2 x 50 mL) and filtered again. The pH value of the aqueous phase was adjusted to pH < 2 with conc. HCl and the resulting precipitate was filtered off. The product was obtained as a pale brownish solid (100 mg, 0.22 mmol, 53% yield).

m.p.: 215.0 °C.

¹H-NMR (300 MHz, DMSO-d₆): δ (ppm) = 7.85-7.73 (m, 4H, 8-H, 8'-H), 7.72-7.61 (dd, 4H, *J* = 7.82 Hz, ⁴*J*_{P-H} = 2.45 Hz, 7-H, 7'-H), 7.53 (d, 2H, ¹*J*_{P-H} = 546 Hz, PH), 6.43 (s, 2H, 3-H, 4-H), 4.27 (m, 2H, 10-H), 1.71-1.50 (m, 2H, 12-H), 1.37-1.21 (m, 2H, 11-H).

¹³C-NMR (75 MHz, DMSO-d₆): δ (ppm) = 136.99 (C-6, C6'), 133.58 (C-9, C-9'), 131.87 (C-2, C-5), 131.12 (C-8, C-8'), 128.42 (C-7, C-7'), 111.95 (C-3, C-4), 44.50 (C-10), 29.33 (C-13), 25.95 (C-12), 23.08 (C-11).

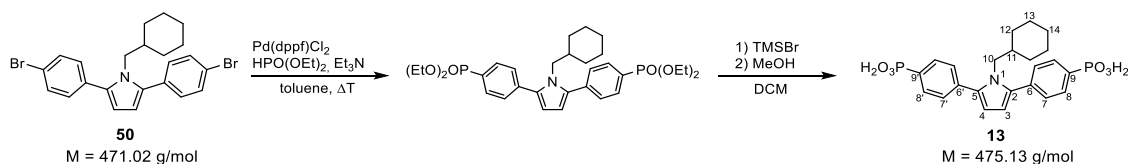
¹⁹F-NMR (400 MHz, DMSO-d₆): δ (ppm) = - 65.04 (s, CF₃).

³¹P-NMR (25.8 MHz, DMSO-d₆): δ (ppm) = 15.89 (s, P).

FT-IR (solid): $\tilde{\nu}$ (cm⁻¹) = 2361, 1597, 1155, 1124, 973, 831, 783.

HR-MS (ESI): m/z calculated for $\text{C}_{20}\text{H}_{20}\text{NO}_4\text{P}_2\text{F}_3$ $[\text{M}-2\text{H}]^{2-}$ 227.5337; observed 227.5340.

Synthesis of ((1-(cyclohexylmethyl)-1H-pyrrole-2,5-diyl)bis(4,1-phenylene))bis(phosphonic acid) (**13**)



2,5-bis(4-bromophenyl)-1-(cyclohexylmethyl)-1H-pyrrole (**50**) (250 mg, 0.53 mmol, 1 equiv.) and Pd(dppf)Cl₂ (41 mg, 0.063 mmol, 12 mol%) were suspended in anhydrous toluene (15 mL) under an atmosphere of argon. Triethylamine (0.25 mL, 0.196 mg, 1.78 mmol, 3.4 equiv.) and diethyl phosphite (180 mg, 1.31 mmol, 2.5 equiv.) were added sequentially and the reaction mixture was refluxed overnight. After cooling to room temperature, the reaction mixture was diluted with toluene (10 mL) and DCM (20 mL) to obtain a clear solution. Silica gel (ca. 10 g) was added, and the solvents were removed under reduced pressure. Purification by column chromatography (2.5% MeOH in DCM, R_f = 0.91) afforded the phosphonate ester as a slightly purple oil that was contaminated with diethyl phosphite. The crude product was dissolved in DCM (20 mL) and TMSBr (2.56 g, > 20 equiv.) was added dropwise to the reaction mixture which was stirred overnight. Afterwards, it was diluted with MeOH (20 mL) and stirred for 1 h, then, the solvents were removed under reduced pressure. The residue was coevaporated with MeOH (20 mL) twice, yielding a brown residue which was dissolved in 1 M NaOH (until no solids were left, pH > 12). The aqueous phase was washed with MTBE (2 x 20 mL) and was then acidified with conc. HCl until pH < 2. The precipitated solid was filtered and washed with water until the washings were acid-free. The solid was dried under reduced pressure and the product was obtained as an off-white solid (110 mg, 0.23 mmol, 43% yield).

m.p.: > 235 °C (decomposition).

¹H-NMR (300 MHz, D₂O): δ (ppm) = 7.60-7.48 (dd, 4H, ³J_{P-H} = 11.34 Hz, J = 8.1 Hz, 8-H, 8'-H), 7.31-7.21 (dd, 4H, J = 8.13 Hz, ⁴J_{P-H} = 2.52 Hz, 7-H, 7'-H), 6.12 (s, 2H, 3-H, 4-H), 3.82 (d, 2H, J = 7.17 Hz, 10-H), 1.19-1.02 (m, 3H, 13-H, 13-H, 14-H), 0.91-0.67 (m, 3H, 11-H, 12'-H, 12'-H), 0.64-0.47 (m, 3H, 13'-H, 13'-H, 14'-H), 0.29-0.05 (m, 2H, 12-H, 12-H).

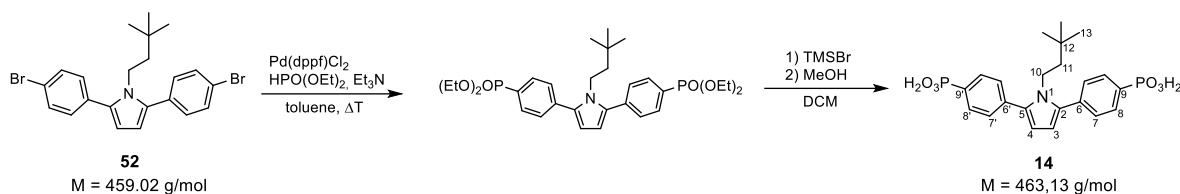
¹³C-NMR (75 MHz, D₂O): δ (ppm) = 139.19 (C-9, C-9'), 137.77 (C-2, C-5), 133.66 (C-6, C-6'), 130.39 (C-8, C-8'), 127.62 (C-7, C-7'), 108.93 (C-3, C-4), 51.51 (C-10), 38.44 (C-11), 29.49 (C-12), 25.56 (C-14), 24.73 (C-13).

³¹P-NMR (25.8 MHz, D₂O): δ (ppm) = 11.15 (s, P).

FT-IR (solid): $\tilde{\nu}$ (cm⁻¹) = 2922, 2362, 2341, 1599, 1136, 920, 833, 776, 746, 730.

HR-MS (ESI): m/z calculated for C₂₃H₂₇NO₆P₂ [M-2H]²⁻ 236.5584; observed 236.5581.

Synthesis of ((1-(3,3-dimethylbutyl)-1H-pyrrole-2,5-diyl)bis(4,1-phenylene))bis(phosphonic acid) (**14**)



2,5-bis(4-bromophenyl)-1-(3,3-dimethylbutyl)-1H-pyrrole (**52**) (250 mg, 0.54 mmol, 1 equiv.) and Pd(dppf)Cl₂ (39 mg, 0.060 mmol, 11 mol%) were suspended in anhydrous toluene (15 mL) under an atmosphere of argon. Triethylamine (0.25 mL, 0.196 mg, 1.78 mmol, 3.4 equiv.) and diethyl phosphite (187 mg, 1.35 mmol, 2.6 equiv.) were added sequentially and the reaction mixture was refluxed overnight. After cooling to room temperature, the reaction mixture was diluted with toluene (20 mL) and DCM (30 mL) to obtain a clear solution. Silica gel (ca. 12 g) was added, and the solvents were removed under reduced pressure. Purification by column chromatography (2.5% MeOH in DCM, R_f = 0.86) afforded the phosphonate ester as a slightly purple oil that was contaminated with diethyl phosphite. The crude product was dissolved in DCM (20 mL) and TMSBr (2.3 g, > 20 equiv.) was added dropwise to the reaction mixture which was stirred overnight. Afterwards, it was diluted with MeOH (20 mL) and stirred for 1 h, then, the solvents were removed under vacuum. The residue was coevaporated with MeOH (20 mL) twice, yielding a brown residue which was dissolved in 1 M NaOH (until no solids were left, pH > 12). The aqueous phase was washed with MTBE (2 x 20 mL) and was then acidified with conc. HCl until pH < 2. The precipitated solid was filtered and washed with water until the washings were acid-free. The solid was dried under vacuum and the product was obtained as a brown solid (130 mg, 0.28 mmol, 52% yield).

m.p.: > 190 °C (decomposition).

¹H-NMR (300 MHz, D₂O): δ (ppm) = 7.65-7.52 (dd, 4H, ³J_{P-H} = 11.34 Hz, J = 8.1 Hz, 8-H, 8'-H), 7.35-7.26 (dd, 4H, J = 8.1 Hz, ⁴J_{P-H} = 2.49 Hz, 7-H, 7'-H), 6.17 (s, 2H, 3-H, 4-H), 4.07-3.89 (m, 2H, 10-H), 0.91-0.77 (m, 2H, 11-H), 0.34 (s, 9H, 13-H).

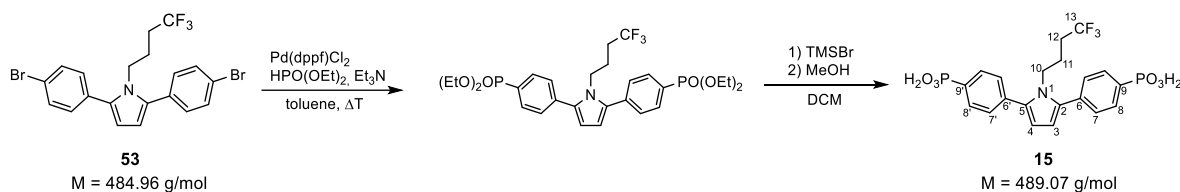
¹³C-NMR could not be measured due to its low solubility in common organic solvents.

³¹P-NMR (25.8 MHz, D₂O): δ (ppm) = 11.11 (s, P).

FT-IR (solid): $\tilde{\nu}$ (cm⁻¹) = 2952, 2359, 2340, 1600, 1139, 990, 932, 836, 780, 743, 732.

HR-MS (ESI): m/z calculated for $C_{22}H_{27}NO_6P_2$ $[M-2H]^{-2}$ 230.5584; observed 230.5584.

Synthesis of ((1-(4,4,4-trifluorobutyl)-1H-pyrrole-2,5-diyl)bis(4,1-phenylene))bis(phosphonic acid) (**15**)



2,5-bis(4-bromophenyl)-1-(4,4,4-trifluorobutyl)-1H-pyrrole (**53**) (250 mg, 0.52 mmol, 1 equiv.) and Pd(dppf)Cl₂ (39 mg, 0.060 mmol, 11 mol%) were suspended in anhydrous toluene (12 mL) under an atmosphere of argon. Triethylamine (0.29 mL, 0.277 mg, 2.1 mmol, 4.0 equiv.) and diethyl phosphite (172 mg, 1.24 mmol, 2.4 equiv.) were added sequentially and the reaction mixture was refluxed overnight. After cooling to room temperature, the reaction mixture was diluted with toluene (10 mL) and DCM (50 mL) to obtain a clear solution. Silica gel (ca. 12 g) was added, and the solvents were removed under reduced pressure. Purification by column chromatography (2.5% MeOH in DCM, R_f = 0.80) afforded the phosphonate ester as a slightly purple oil that was contaminated with diethyl phosphite (yield > 100%). The crude product was dissolved in DCM (40 mL) and TMSBr (2.5 g, > 20 equiv.) was added dropwise to the reaction mixture which was stirred overnight. Afterwards, it was diluted with MeOH (20 mL) and stirred for 1 h, then, the solvents were removed under vacuum. The residue was coevaporated with MeOH (20 mL) twice, yielding a brown residue which was dissolved in 1 M NaOH (until no solids were left, pH > 12). The aqueous phase was washed with EtOAc (2 x 25 mL) and was then acidified with conc. HCl until pH < 2. The precipitated solid was filtered and washed with water until the washings were acid-free. The solid was dried under reduced pressure and the product was obtained as a yellow solid (34 mg, 0.07 mmol, 13% yield).

m.p.: > 190 °C (decomposition).

¹H-NMR (300 MHz, D₂O): δ (ppm) = 7.54-7.43 (dd, 4H, ³J_{P-H} = 11.36 Hz, J = 8.0 Hz, 8-H, 8'-H), 7.26-7.11 (dd, 4H, J = 8.1 Hz, ⁴J_{P-H} = 2.49 Hz, 7-H, 7'-H), 6.11 (s, 2H, 3-H, 4-H), 4.00 (m, 2H, 10-H), 1.38-1.24 (m, 2H, 12-H), 1.15-1.03 (m, 2H, 11-H).

¹³C-NMR could not be measured due to its low solubility in common organic solvents.

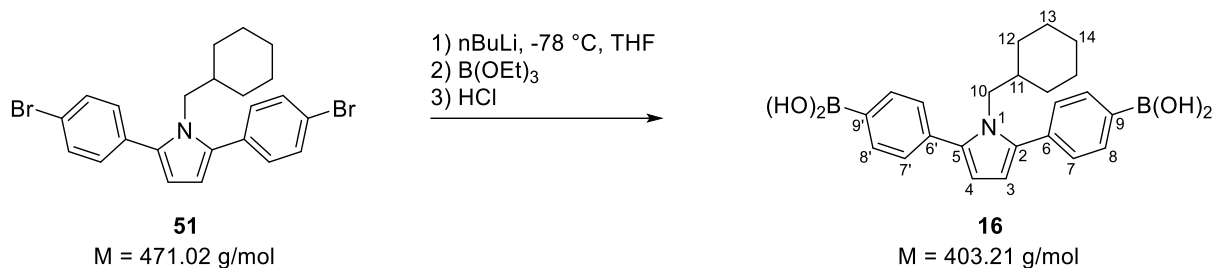
³¹P-NMR (25.8 MHz, D₂O): δ (ppm) = 1.40 (s, P).

¹⁹F-NMR (400 MHz, D₂O): δ (ppm) = -65.02 (s, CF₃).

FT-IR (solid): $\tilde{\nu}$ (cm⁻¹) = 2359, 2340, 1736, 1218, 927, 838, 761, 668.

HR-MS (ESI): m/z calculated for C₂₀H₂₁NF₃O₆P₂ [M+H]⁺ 490.0791; observed 490.0786.

Synthesis of ((1-(cyclohexylmethyl)-1H-pyrrole-2,5-diyl)bis(4,1-phenylene))diboronic acid (**16**)



2,5-bis(4-bromophenyl)-1-(cyclohexylmethyl)-1H-pyrrole (**51**) (270 mg, 0.57 mmol, 1 equiv.) was dissolved in anhydrous THF (12 mL) under an atmosphere of argon. The reaction mixture was cooled to -78 °C and nBuLi (1.6 M in hexane, 1.1 mL, 3 equiv.) was added dropwise to the reaction mixture. Afterwards it was stirred for 45 minutes at -78 °C and then triethyl borate (0.33 g, 2.3 mmol, 4 equiv.) was added at once. The reaction mixture was then allowed to warm to room temperature overnight, after which it was diluted with 4 M HCl until pH < 3. Then, DCM (50 mL) and water (50 mL) were added and the aqueous phase was isolated and washed with DCM (20 mL). The combined organic phases were extracted with 2 M NaOH (2 x 25 mL) and the resulting aqueous phase was washed with DCM (20 mL). The aqueous phase was acidified with conc. HCl until pH < 2. The precipitated solid was filtered and washed with water until the washings were acid-free. The solid was dried under reduced pressure and the product was obtained as an off-white solid (161 mg, 0.4 mmol, 68% yield).

m.p.: > 200 °C (decomposition).

¹H-NMR (300 MHz, DMSO-d₆): δ (ppm) = 8.07 (s, 4H, OH), 7.85 (d, 4H, *J* = 7.88 Hz, 8-H, 8'-H), 7.44 (d, 4H, *J* = 7.88 Hz, 7-H, 7'-H), 6.24 (s, 2H, 3-H, 4-H), 4.02 (m, 2H, 10-H), 1.41-1.22 (m, 3H, 13-H, 13-H, 14-H), 1.09-0.90 (m, 3H, 11-H, 12'-H, 12'-H), 0.82-0.58 (m, 3H, 13'-H, 13'-H, 14-H), 0.41-0.19 (m, 2H, 12-H, 12-H).

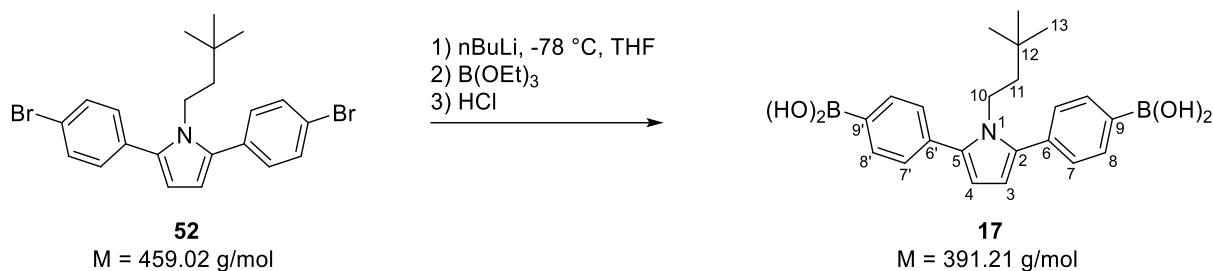
¹¹B-NMR could not be measured due to its low solubility in common organic solvents.

¹³C-NMR (75 MHz, DMSO-d₆): δ (ppm) = 137.89 (C-2, C-5), 135.73 (C-6, C-6'), 134.93 (C-8, C-8'), 127.41 (C-7, C-7'), 110.28 (C-3, C-4), 51.85 (C-10), 30.00 (C-11), 26.03 (C-12), 25.39 (C-13).

FT-IR (solid): $\tilde{\nu}$ (cm⁻¹) = 3374, 2920, 2359, 2341, 1604, 1339, 835, 787, 743.

HR-MS (ESI): m/z calculated for $C_{23}H_{28}B_2O_4N$ $[M+H]^+$ 403.2236; observed 403.2221.

Synthesis of ((1-(3,3-dimethylbutyl)-1H-pyrrole-2,5-diyl)bis(4,1-phenylene))diboronic acid (17)



2,5-bis(4-bromophenyl)-1-(3,3-dimethylbutyl)-1H-pyrrole (**52**) (400 mg, 0.87 mmol, 1 equiv.) was dissolved in anhydrous THF (15 mL) under an atmosphere of argon. The reaction mixture was cooled to -78 °C and nBuLi (1.6 M in hexane, 1.7 mL, 3.1 equiv.) was added dropwise to the reaction mixture. Afterwards it was stirred for 45 minutes at -78 °C and then triethyl borate (0.395 g, 2.3 mmol, 4.1 equiv.) was added at once. The reaction mixture was then allowed to warm to room temperature overnight, after which it was diluted with 4 M HCl until pH < 3. Then, DCM (50 mL) and water (50 mL) were added and the aqueous phase was isolated and washed with DCM (20 mL). The combined organic phases were extracted with 2 M NaOH (2 x 25 mL) and the resulting aqueous phase was washed with DCM (20 mL). The aqueous phase was acidified with conc. HCl until pH < 2. The precipitated solid was filtered and washed with water until the washings were acid-free. The solid was dried under reduced pressure and the product was obtained as an off-white solid (165 mg, 0.42 mmol, 48% yield).

m.p.: 277.5 °C.

¹H-NMR (300 MHz, DMSO-d₆): δ (ppm) = 8.07 (s, 4H, OH), 7.85 (d, 4H, *J* = 7.95 Hz, 8-H, 8'-H), 7.43 (d, 4H, *J* = 7.95 Hz, 7-H, 7'-H), 6.22 (s, 2H, 3-H, 4-H), 4.15 (m, 2H, 10-H), 1.00 (m, 2H, 11-H), 0.51 (s, 9H, 12-H).

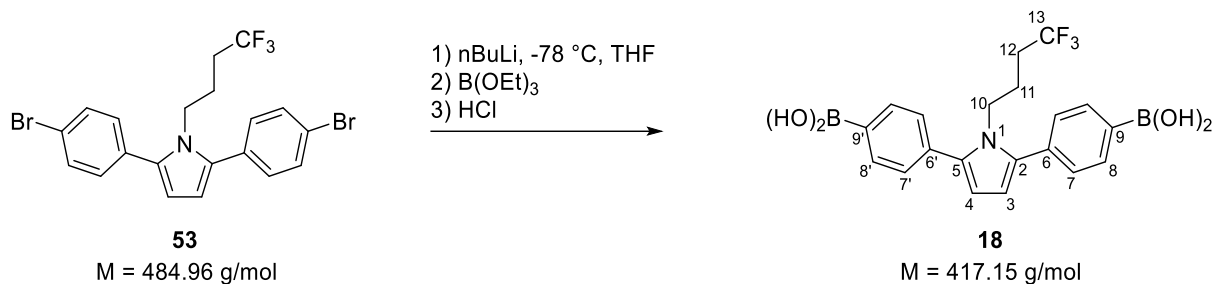
¹¹B-NMR could not be measured due to its low solubility in common organic solvents.

¹³C-NMR (75 MHz, DMSO-d₆): δ (ppm) = 136.41 (C-2, C-5), 135.49 (C-6, C-6'), 134.82 (C-8, C-8'), 127.77 (C-7, C-7'), 110.17 (C-3, C-4), 44.03 (C-11), 41.96 (C-10), 29.69 (C-12), 29.05 (C-13).

FT-IR (solid): $\tilde{\nu}$ (cm⁻¹) = 3349, 2947, 2358, 2341, 1606, 1336, 1107, 1101, 834, 742.

HR-MS (ESI): *m/z* calculated for C₂₂H₂₇B₂O₄N [M+H]⁺ 391.2236; observed 391.2228.

Synthesis of ((1-(4,4,4-trifluorobutyl)-1H-pyrrole-2,5-diyl)bis(4,1-phenylene))diboronic acid (**18**)



2,5-bis(4-bromophenyl)-1-(3,3-dimethylbutyl)-1H-pyrrole (**53**) (157 mg, 0.32 mmol, 1 equiv.) was dissolved in anhydrous THF (6 mL) under an atmosphere of argon. The reaction mixture was cooled to -78 °C and nBuLi (1.6 M in hexane, 0.7 mL, 3.5 equiv.) was added dropwise to the reaction mixture. Afterwards it was stirred for 45 minutes at -78 °C and then triethyl borate (0.200 g, 1.15 mmol, 3.6 equiv.) was added at once. The reaction mixture was then allowed to warm to room temperature overnight, after which it was diluted with 4 M HCl until pH < 3. Then, DCM (50 mL) and water (50 mL) were added and the aqueous phase was isolated and washed with DCM (20 mL). The combined organic phases were extracted with 2 M NaOH (2 x 25 mL) and the resulting aqueous phase was washed with DCM (20 mL). The aqueous phase was acidified with conc. HCl until pH < 2. The precipitated solid was filtered and washed with water until the washings were acid-free. The solid was dried under reduced pressure and the product was obtained as an off-white solid (53 mg, 0.13 mmol, 41% yield).

m.p.: 282 °C.

¹H-NMR (300 MHz, DMSO-*d*₆): δ (ppm) = 7.87 (d, 4H, *J* = 7.79 Hz, 7-H, 7'-H), 7.46 (d, 4H, *J* = 7.79 Hz, 8-H, 8'-H), 6.30 (s, 2H, 3-H, 4-H), 4.24 (m, 2H, 10-H), 1.70-1.47 (m, 2H, 12-H), 1.40-1.18 (m, 2H, 11-H).

¹¹B-NMR could not be measured due to its low solubility in common organic solvents.

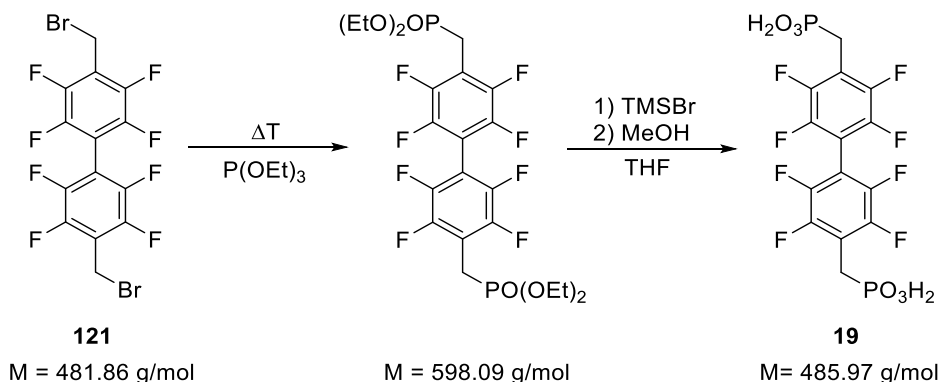
¹³C-NMR (75 MHz, DMSO-*d*₆): δ (ppm) = 137.30 (C-2, C-5), 135.13 (C-6, C-6'), 135.01 (C-8, C-8'), 127.49 (C-7, C-7'), 110.68 (C-3, C-4), 49.19 (C-10), 44.27 (C-12), 27.30 (C-11).

¹⁹F-NMR (400 MHz, DMSO-*d*₆): δ (ppm) = -65.09 (s, CF₃).

FT-IR (solid): $\tilde{\nu}$ (cm⁻¹) = 3363, 2970, 2360, 2341, 1737, 1363, 1216, 1122, 971.

HR-MS (ESI): m/z calculated for $C_{20}H_{21}B_2F_3NO_4$ $[M+H]^+$ 417.1640; observed 417.1629.

Synthesis of ((Perfluoro-[1,1'-biphenyl]-4,4'-diyl)bis(methylene))bis(phosphonic acid) (**19**)



Di-para-bromomethyl-octafluoro-1,1'-biphenyl (**121**) (660 mg, 1.3 mmol, 1 equiv.) and P(OEt)₃ were heated to 156 °C under an atmosphere of argon. Afterwards, excess reagent was removed by distillation under reduced pressure. The residue was purified by column chromatography (hexane/EtOAc 2:1, R_f = 0.55) and the intermediate product was obtained as a slightly yellow oil, contaminated with several phosphorus species. This crude product was directly used for the next step without further purification.

The crude product was dissolved in THF (10 mL) and TMSBr (6.43 g, 42.0 mmol, 30.9 equiv.) was added slowly to the reaction mixture. It was stirred for 3 days at room temperature and then MeOH (10 mL) and water (10 mL) were added to the reaction mixture. After stirring for 1 h, all solvents were removed under reduced pressure. The residue was dissolved in 1 M KOH-solution (15 mL) and the aqueous phase was washed with DCM (2 x 15 mL). Afterwards, it was acidified to pH 1 with conc. HCl and the precipitated solid was isolated by filtration. The product was obtained as a white solid (212 mg, 0.43 mmol, 32% yield).

m.p.: > 250 °C (decomposition).

¹H-NMR (300 MHz, D₂O): δ (ppm) = 2.84 (d, 4H, *J* = 19.05 Hz, 1-H, 1'-H).

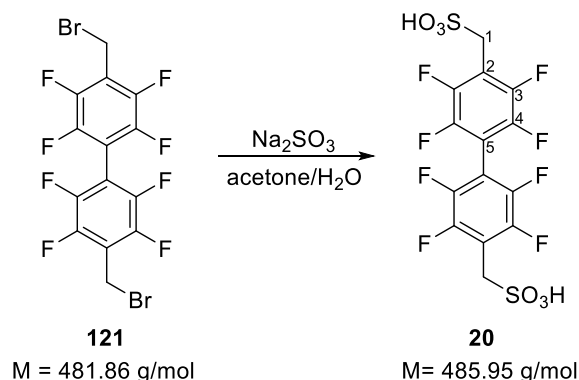
¹⁹F-NMR (282.4 MHz, D₂O): δ (ppm) = -141.74 (m, 4F, 3-F, 3'-F), -142.91 (m, 4F, 4-F, 4'-F).

³¹P-NMR (25.8 MHz, D₂O): δ (ppm) = 14.14 (s, 2P, PO₃H₂).

FT-IR (solid): $\tilde{\nu}$ (cm⁻¹) = 2359, 1458, 1247, 1191, 1010, 952, 930, 728, 716.

HR-MS (ESI): *m/z* calculated for C₁₄H₇F₈O₆P₂ [M-H]⁻ 484.9596; observed 484.9594.

Synthesis of (Perfluoro-[1,1'-biphenyl]-4,4'-diyl)dimethanesulfonic acid (**20**)



Di-para-bibromomethyl-octafluoro-1,1'-biphenyl (**121**) (209 mg, 0.4 mmol, 1 equiv.) was dissolved in a mixture of acetone and water (2:1, 30 mL) and afterwards Na_2SO_3 (140 mg, 1.1 mmol, 2.8 equiv.) was added to the reaction mixture. It was refluxed for 24 h and then acetone was removed under reduced pressure. The resulting aqueous phase was basified to pH 13 with 1 M NaOH, washed with DCM (3 x 15 mL) and acidified to pH 1 with conc. H_2SO_4 . The solvent was removed and the residue was purified by RP-column chromatography. The product was obtained as a white, crystalline solid (61 mg, 0.13 mmol, 29% yield).

m.p.: > 250 °C (decomposition).

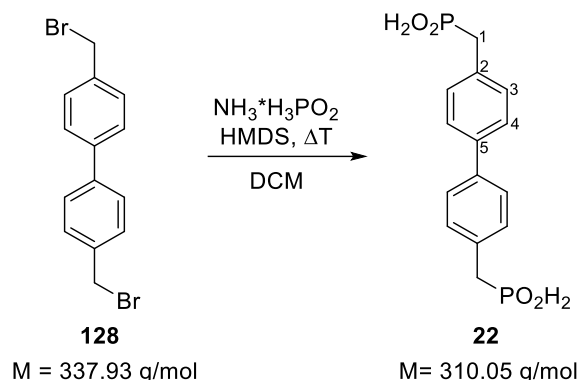
$^1\text{H-NMR}$ (300 MHz, D_2O): δ (ppm) = 4.48 (s, 4H, 1-H, 1'-H).

$^{19}\text{F-NMR}$ (282.4 MHz, D_2O): δ (ppm) = -139.40 (m, 4F, 3-F, 3'-F), -142.33 (m, 4F, 4-F, 4'-F).

FT-IR (solid): $\tilde{\nu}$ (cm^{-1}) = 2359, 1469, 1203, 1175, 1046, 979, 732.

HR-MS (ESI): m/z calculated for $\text{C}_{14}\text{H}_4\text{F}_8\text{O}_6\text{S}_2$ $[\text{M}-2\text{H}]^{2-}$ 241.9666; observed 241.9668.

Synthesis of ([1,1'-biphenyl]-4,4'-diylbis(methylene))bis(phosphinic acid) (**22**)



Ammoniumhypophosphite (0.967 g, 11.9 mmol, 6.1 equiv.) and HMDS (1.83 g, 11.3 mmol, 5.8 equiv.) were heated under an atmosphere of argon at 120 °C for 2 h. Afterwards, anhydrous DCM (30 mL) was added and after all solid particles had dissolved di-para-bromomethyl-octafluoro-1,1'-biphenyl (**128**) (0.67 g, 2.00 mmol, 1 equiv.) was added to the reaction mixture, which was stirred for 1 h. MeOH (5 mL) was added and the resulting mixture was stirred for 1 h, then all solvents were removed under reduced pressure. The residue was taken up in 1 M KOH-solution and the aqueous phase was washed with DCM (2 x 15 mL) and then acidified to pH 1 with conc. HCl. The precipitated solid was isolated by filtration.

This crude product (370 mg) was dissolved in DMSO (10 mL) and adamantan-1-amine (302 mg, 4 mmol, 2 equiv.) were added to the reaction mixture. The precipitated salt was isolated by filtration, washed with Et₂O and dried under vacuum. It was then suspended in 1 M NaOH-solution and the resulting aqueous phase was washed with DCM (2 x 15 mL). Afterwards it was acidified to pH 1 with conc. HCl and the solid was isolated by filtration. The product was obtained as a white solid (0.11 g, 0.34 mmol, 17% yield).

m.p.: > 250 °C (decomposition).

¹H-NMR (300 MHz, D₂O): δ (ppm) = 7.63 (d, 4H, *J* = 8.04 Hz, 4-H, 4'-H), 7.32 (dd, 4H, *J* = 8.04 Hz, *J* = 2.21 Hz, 3-H, 3'-H), 6.91 (d, 2H, *J* = 517 Hz, PHOH), 2.97 (d, 4H, *J* = 17.97 Hz, 1-H, 1'-H).

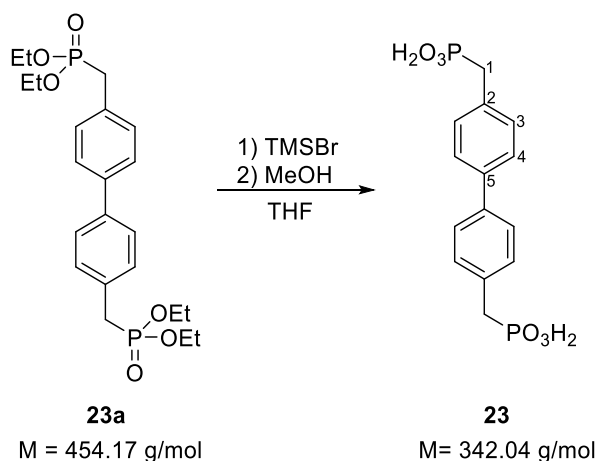
¹³C-NMR (75 MHz, D₂O): δ (ppm) = 137.76 (C-5, C-5'), 132.51 (C-2, C-2'), 129.92 (C-3, C-3'), 126.65 (C-4, C-4'), 39.19 (C-1, C-1').

³¹P-NMR (25.8 MHz, D₂O): δ (ppm) = 28.38 (s, PO₂H₂).

FT-IR (solid): $\tilde{\nu}$ (cm⁻¹) = 2358, 1689, 1496, 1254, 1203, 1091, 974, 827, 709.

HR-MS (ESI): m/z calculated for C₁₄H₁₂O₄P₂ [M-2H]²⁻ 154.0189; observed 154.0189.

Synthesis of ([1,1'-biphenyl]-4,4'-diylbis(methylene))bis(phosphonic acid) (**23**)



Tetraethyl ([1,1'-biphenyl]-4,4'-diylbis(methylene))bis(phosphonate) (**23a**) (504 mg, 1.27 mmol, 1 equiv.) was dissolved in anhydrous THF (10 mL) under an atmosphere of argon. TMSBr (1.72 g, 11.24 mmol, 8.9 equiv.) was added dropwise to the reaction mixture that was stirred at room temperature for three days. Afterwards, MeOH (10 mL) was added and the reaction mixture was stirred for 1 h. The solvents were removed under reduced pressure and the residue was dissolved in 1 M KOH-solution (15 mL). The aqueous phase was washed with DCM (2 x 15 mL) and the pH was adjusted to 1 with conc. HCl. The precipitated solid was isolated by filtration. The product was obtained as a white powder (0.29 g, 0.84 mmol, 68% yield).

m.p.: > 250 °C (decomposition).

¹H-NMR (300 MHz, DMSO-*d*₆): δ (ppm) = 7.55 (d, 4H, *J* = 8.01 Hz, 4-H, 4'-H), 7.32 (dd, 4H, *J* = 8.01 Hz, *J* = 1.92 Hz, 3-H, 3'-H), 2.98 (d, 4H, *J* = 21.42 Hz, 1-H, 1'-H).

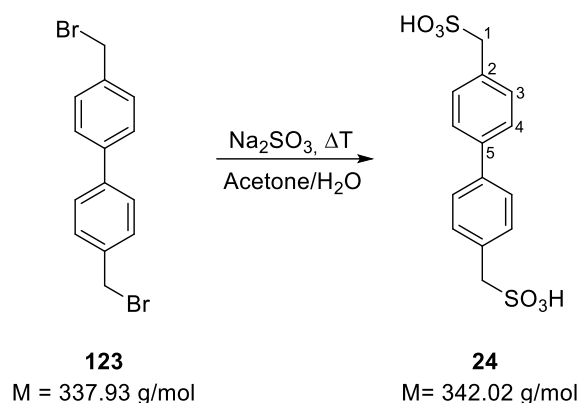
¹³C-NMR (75 MHz, DMSO-*d*₆): δ (ppm) = 138.22 (C-5, C-5'), 133.85 (C-2, C-2'), 130.77 (C-3, C-3'), 126.58 (C-4, C-4'), 35.49 (C-1, C-1').

³¹P-NMR (25.8 MHz, DMSO-*d*₆): δ (ppm) = 21.08 (s, PO₃H₂).

FT-IR (solid): $\tilde{\nu}$ (cm⁻¹) = 2358, 2332, 1090, 1011, 949, 827.

HR-MS (ESI): *m/z* calculated for C₁₄H₁₄O₆P₂ [M-2H]²⁻ 170.0138; observed 170.0140.

Synthesis of [1,1'-biphenyl]-4,4'-diylmethanesulfonic acid (**24**)



4,4'-Bis(bromomethyl)-1,1'-biphenyl (**121**) (0.986 g, 2.90 mmol, 1 equiv.) was dissolved in a mixture of acetone and water (1:1, 20 mL). Na₂SO₃ (1.08 g, 8.7 mmol, 3 equiv.) was added to the reaction mixture and it was refluxed for 30 hours. Afterwards, acetone was removed under reduced pressure and 1 M NaOH-solution was added until the pH was 12. The aqueous phase was washed with DCM (3 x 20 mL) and then it was acidified with conc. H₂SO₄ and cooled to 0 °C. The precipitated solid was isolated by filtration. The product was obtained as a white powder (1.12 g, 2.50 mmol, 88% yield).

m.p.: > 250 °C (decomposition).

¹H-NMR (300 MHz, DMSO-d₆): δ (ppm) = 7.52 (d, 4H, *J* = 8.22 Hz, 3-H, 3'-H), 7.37 (d, 4H, *J* = 8.22 Hz, 4-h, 4'-H), 3.75 (s, 4H, 1-H, 1'-H).

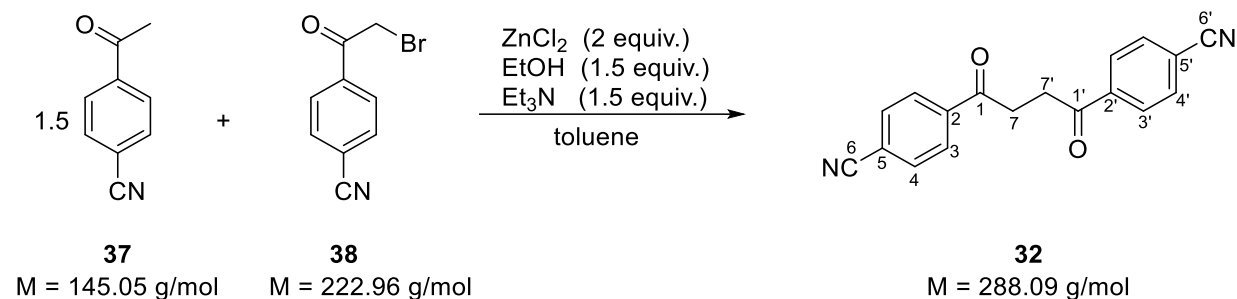
¹³C-NMR (75 MHz, DMSO-d₆): δ (ppm) = 138.71 (C-5, C-5'), 134.86 (C-2, C-2'), 131.19 (C-3, C-3'), 126.19 (C-4, C-4'), 57.64 (C-1, C-1').

FT-IR (solid): $\tilde{\nu}$ (cm⁻¹) =

HR-MS (ESI): *m/z* calculated for C₁₄H₁₃O₆S₂ [M-H]⁻ 341.0159; observed 341.0162.

6.1.2.2 Syntheses for chapter 4.2

Synthesis of 4,4'-Succinyldibenzonitrile (**32**)



ZnCl₂ (5.92 g, 43.4 mmol, 2 equiv.), Et₃N (4.6 mL, 32.6 mmol, 1.5 equiv) and absolute ethanol (2.0 mL, 32.6 mmol, 1.5 equiv.) were suspended in anhydrous toluene (50 mL) under an atmosphere of argon. The reaction mixture was stirred for 60 minutes. Then, 4-acetylbenzonitrile (**37**) (4.73 g, 32.6 mmol, 1.5 equiv.) and 4-(2-bromoacetyl)benzonitrile (**38**) (4.84 g, 21.7 mmol, 1 equiv.) were added and the suspension was stirred at room temperature for 7 days. The resulting yellow precipitate was filtered off, dissolved in hot DMF (150 mL, 80 °C) and crystallized by slow addition of methanol (20 mL). After storing at 0 °C for 12 hours, the crystals were filtered off and dried in air. The product was obtained as a slightly yellow, microcrystalline powder (3.75 g, 13.0 mmol, 70% yield).

m.p.: 261 °C.

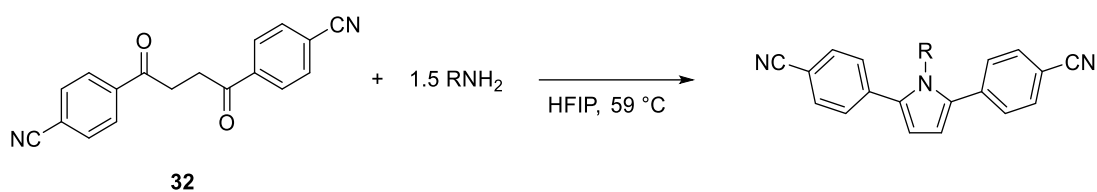
¹H-NMR (300 MHz, DMSO-*d*₆): δ (ppm) = 8.16 (d, 4 H, *J* = 8.61 Hz, 3-H, 3'-H), 8.02 (d, 4 H, *J* = 8.61 Hz, 4-H, 4'-H), 3.47 (s, 4 H, 7-H, 7'-H).

¹³C-NMR could not be measured due to its low solubility in common organic solvents.

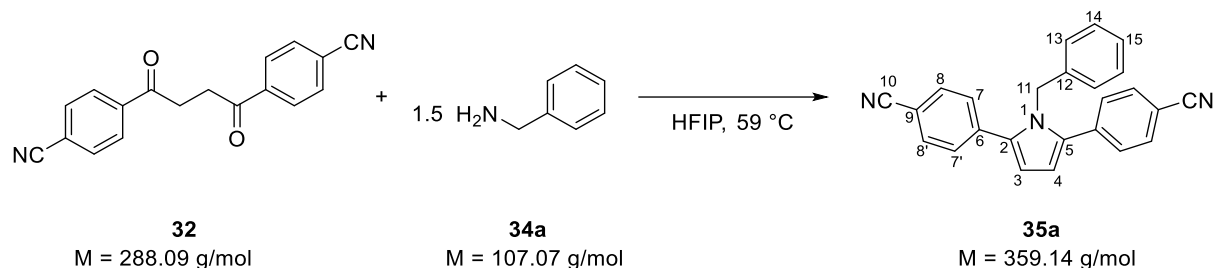
FT-IR (solid): $\tilde{\nu}$ (cm⁻¹) = 2225, 1680, 1402, 1319, 1304, 1381, 1191, 1172, 1010, 860, 840, 783, 713, 694.

HR-MS (ESI): *m/z* calculated for C₁₈H₁₁N₂O₂Na [M+Na]⁺ 311.0791; observed 311.0786.

General procedure for the synthesis of 1,2,5-substituted Pyrroles: The respective 1,4-diketone (1 equiv.) was dissolved in hexafluoroisopropanol (4-10 mL) at ambient temperature. The respective amine (1.5 equiv.) was added slowly, and the mixture was stirred for the indicated time either at room temperature or under reflux conditions. The reaction mixture was allowed to cool to room temperature and the solvent was removed under reduced pressure. The residue was dissolved in dichloromethane and washed with 4 M HCl to remove excess amine. The organic phase was dried over MgSO₄ and the solvent was removed under reduced pressure. The products were mostly pure; however, in some cases column chromatography was necessary using hexane/EtOAc as eluents.



Synthesis of 4,4'-(1-benzyl-1H-pyrrole-2,5-diyl)dibenzonitrile (35a) (43)



The reaction mixture was refluxed for 2 days and worked-up according to the general procedure. For purification, column chromatography (n-hexane/EtOAc 4:1, $R_f = 0.40$) was performed. The product was obtained as yellow crystals (338 mg, 0.94 mmol, 74% yield).

m.p.: 168 °C.

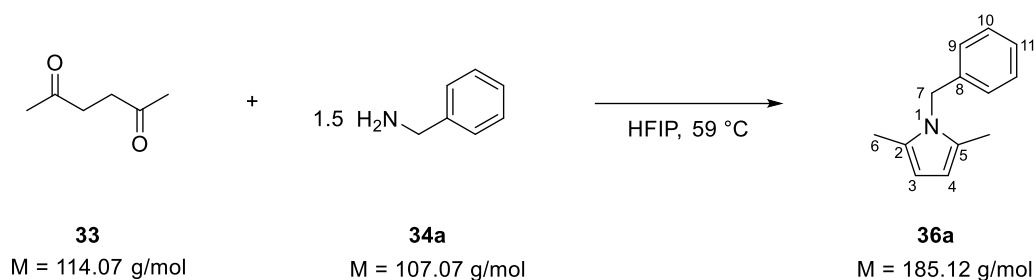
$^1\text{H-NMR}$ (300 MHz, CDCl_3): $\delta = 7.58$ (d, 4H, $J = 6.2$ Hz, 8-H, 8'-H), 7.42 (d, 4H, $J = 6.2$ Hz, 7-H, 7'-H), 7.17-7.12 (m, 3H, 13-H, 13'-H, 15-H), 6.66-6.60 (m, 2H, 14-H, 14'-H), 6.47 (s, 2H, 3-H, 4-H), 5.21 (s, 2H, 11-H).

$^{13}\text{C-NMR}$ (75 MHz, CD_2Cl_2): $\delta = 137.9$ (C-2, C-5), 137.3 (C-6, C-6'), 136.6 (C-12), 132.2 (C-8, C-8'), 128.8 (C-7, C-7'), 128.7 (C-14, C-14'), 127.5 (C-15), 125.5 (C-13, C-13'), 118.7 (C-10, C-10'), 112.1 (C-9, C-9'), 110.6 (C-3, C-4), 49.4 (C-11).

FT-IR (solid): $\tilde{\nu}$ (cm^{-1}) = 2922, 2221, 1599, 1178, 796, 706.

HR-MS (ESI): m/z calculated for $\text{C}_{25}\text{H}_{17}\text{N}_3+\text{Na}^+$ 382.1315 $[\text{M}+\text{Na}]^+$; observed 382.1314.

Synthesis of 1-benzyl-2,5-dimethyl-1H-pyrrole (36a)



The reaction mixture was stirred at room temperature for 5 minutes and worked-up according to the general procedure. The product was obtained as a slightly brown solid (363 mg, 1.97 mmol, 99% yield).

m.p.: 48 °C.

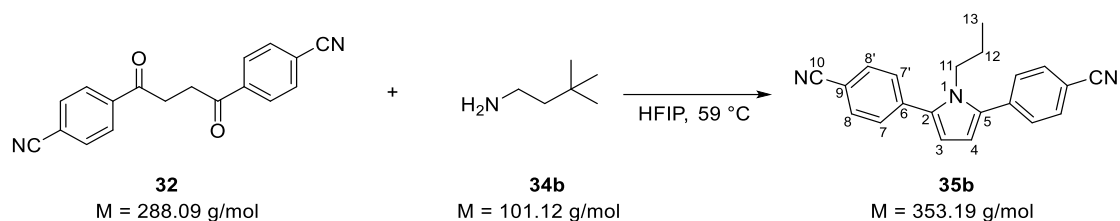
¹H-NMR (300 MHz, CD₂Cl₂): δ [ppm] = 7.35-7.19 (m, 3H, 10-H, 10'-H, 11-H), 6.91 (d, 2H, J = 8.43 Hz, 9-H, 9'-H), 5.81 (s, 2H, 3-H, 4-H), 5.03 (2, 2H, 7-H), 2.14 (s, 6H, 6-H, 6'-H).

¹³C-NMR (75 MHz, CD₂Cl₂): δ [ppm] = 138.9 (C-8), 128.6 (C-11), 127.7 (C-2, C-5), 126.9 (C-10, C-10'), 125.7 (C-9, C-9'), 105.4 (C-3, C-4), 46.6 (C-7), 12.2 (C-6, C-6').

FT-IR (solid): $\tilde{\nu}$ (cm⁻¹): 2918, 1652, 1493, 1408, 1355, 1303, 754, 725, 701, 689.

HR-MS (ESI): m/z calculated for C₁₃H₁₅N+H⁺: 186.1277 [M+H]⁺; observed 186.1275.

Synthesis of 4,4'-(1-propyl-1H-pyrrole-2,5-diyl)dibenzonitrile (35b) (39)



The reaction mixture was refluxed for 2 days and worked-up according to the general procedure. For purification column chromatography (hexane/EtOAc 4:1, $R_f = 0.57$) was performed. The product was obtained as yellow crystals (432 mg, 1.31 mmol, 76% yield).

m.p.: 144 °C.

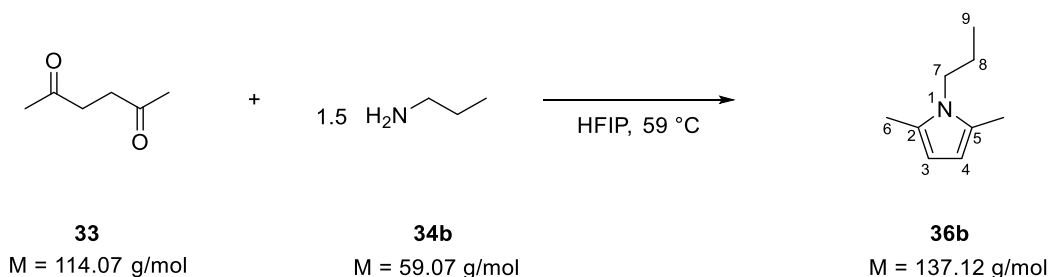
$^1\text{H-NMR}$ (300 MHz, CDCl_3): δ (ppm) = 7.72 (d, 4H, $J = 6.2$ Hz, 8-H, 8'-H), 7.55 (d, 4H, $J = 6.2$ Hz, 7-H, 7'-H), 6.38 (s, 2H, 3-H, 4-H), 4.06 (7, 2H, $J = 7.1$ Hz, 11-H), 1.18 (sex, 2H, $J = 7.2$ Hz, 12-H), 0.43 (t, 3H, $J = 7.4$ Hz, 13-H).

$^{13}\text{C-NMR}$ (75 MHz, CDCl_3): δ (ppm) = 137.97 (C-2, C-5), 136.73 (C-6, C-6'), 132.50 (C-8, C-8'), 128.84 (C-7, C-7'), 118.84 (C-10, C-10'), 112.11 (C-9, C-9'), 110.54 (C-3, C-4), 47.51 (C-11), 24.07 (C-12), 10.60 (C-13).

FT-IR (solid): $\tilde{\nu}$ (cm^{-1}) = 2922, 2358, 2341, 2220, 1600, 834, 777.

HR-MS (ESI): m/z calculated for $\text{C}_{21}\text{H}_{18}\text{N}_3$ $[\text{M}+\text{H}]^+$ 312.1495; observed 312.1492.

Synthesis of 2,5-dimethyl-1-propyl-1H-pyrrole (36b)



The reaction mixture was stirred at room temperature for 5 minutes and worked-up according to the general procedure. The product was obtained as a brown oil (269 mg, 1.97 mmol, 99% yield).

m.p.: 192 °C.

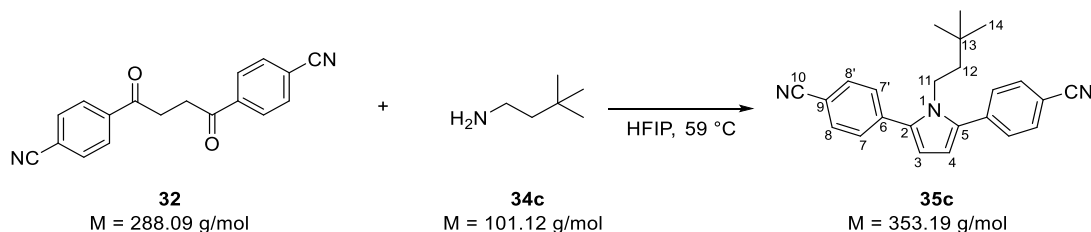
¹H-NMR (300 MHz, CD₂Cl₂): δ [ppm] = 5.68 (s, 2H, 3-H, 4-H), 3.69 (t, 2H, *J* = 7.5 Hz, 7-H), 2.20 (s, 6 H, 6-H, 6'-H), 1.63 (m, 2 H, *J* = 7.5 Hz, 8-H), 0.94 (t, 3H, *J* = 7.5 Hz, 9-H).

¹³C-NMR (75 MHz, CD₂Cl₂): δ [ppm] = 127.0 (C-2, C-5), 104.9 (C-3, C-4), 45.1 (C-7), 24.3 (C-8), 12.2 (C-6, C-6'), 11.0 (C-9).

FT-IR (solid): $\tilde{\nu}$ (cm⁻¹) = 2962, 1660, 1518, 1406, 1298, 1018, 892, 742.

HR-MS (ESI): *m/z* calculated for C₉H₁₅N+H⁺ 138.1277 [M+H]⁺; observed 138.1273.

Synthesis of 4,4'-(1-(3,3-dimethylbutyl)-1H-pyrrole-2,5-diyl)dibenzonitrile (35c) (40)



The reaction mixture was refluxed for 2 days and worked-up according to the general procedure. For purification column chromatography (hexane/EtOAc 4:1, $R_f = 0.73$) was performed. The product was obtained as yellow crystals (378 mg, 1.07 mmol, 56% yield).

m.p.: 192 °C.

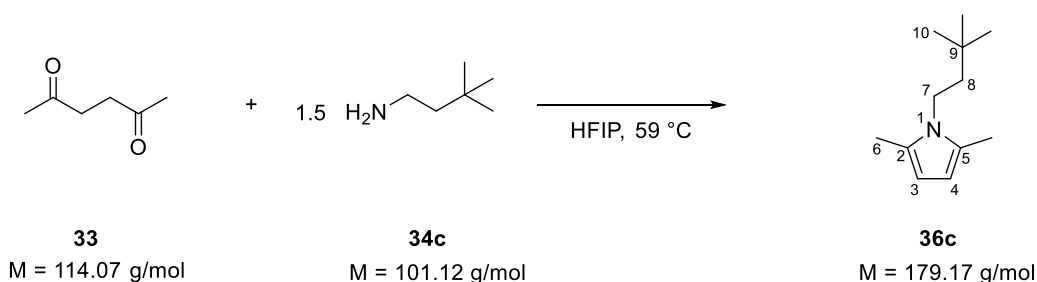
$^1\text{H-NMR}$ (300 MHz, CDCl_3): δ (ppm) = 7.73 (d, 4H, $J = 6.2$ Hz, 8-H, 8'-H), 7.56 (d, 4H, $J = 6.2$ Hz, 7-H, 7'-H), 6.38 (s, 2H, 3-H, 4-H), 4.07 (t, 2H, $J = 7.0$ Hz, 11-H), 1.02 (t, 2H, $J = 7.0$ Hz, 12-H), 0.56 (s, 9H, 14-H, 14'-H, 14''-H).

$^{13}\text{C-NMR}$ (75 MHz, CDCl_3): δ (ppm) = 137.87 (C-2, C-5), 136.10 (C-6, C-6'), 132.40 (C-8, C-8'), 129.02 (C-7, C-7'), 118.82 (C-10, C-10'), 112.06 (C-9, C-9'), 110.65 (C-3, C-4), 43.98 (C-12), 42.46 (C-11), 29.56 (C-13), 28.73 (C-14).

FT-IR (solid): $\tilde{\nu}$ (cm^{-1}) = 2959, 2222, 1602, 1491, 1476, 1332, 1268, 1249, 1234, 1178, 1113, 1062, 850, 839, 769, 677.

HR-MS (ESI): m/z calculated for $\text{C}_{24}\text{H}_{22}\text{N}_3\text{Na}$ $[\text{M}+\text{Na}]^+$ 376.1784; observed 376.1785.

Synthesis of 1-(3,3-dimethylbutyl)-2,5-dimethyl-1H-pyrrole (36c)



The reaction mixture was stirred at room temperature for 5 minutes and worked-up according to the general procedure. The product was obtained as a red-brown solid, (341 mg, 1.91 mmol, 97% yield).

m.p.: 49 °C.

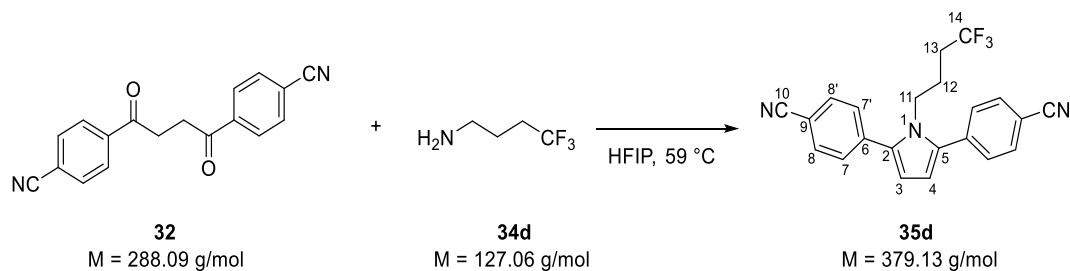
¹H-NMR (300 MHz, CD₂Cl₂): δ [ppm] = 5.67 (s, 2H, 3-H, 4-H), 3.74 (m, 2H, *J* = 4.56 Hz, 7-H), 2.19 (s, 6H, 6-H, 6'-H), 1.46 (m, 2H, *J* = 4.56 Hz, 8-H), 1.01 (s, 9H, 10-H, 10'-H, 10''-H).

¹³C-NMR (75 MHz, CD₂Cl₂): δ [ppm] = 126.7 (C-2, C-5), 104.9 (C-3, C-4), 44.5 (C-8), 39.8 (C-7), 29.7 (C-9), 28.9 (C-10, C-10', C-10''), 12.0 (C-6, C-6').

FT-IR (solid): $\tilde{\nu}$ (cm⁻¹) = 2954, 1515, 1464, 1442, 1410, 1636, 1296, 1247, 1216, 1179, 1015, 975, 740.

HR-MS (ESI): *m/z* calculated for C₁₂H₂₁N+H⁺: 180.1747 [M+H]⁺; observed 180.1747.

Synthesis of 4,4'-(1-(4,4,4-trifluorobutyl)-1H-pyrrole-2,5-diyl)dibenzonitrile (35d) (41)



The reaction mixture was refluxed for 2 days and worked-up according to the general procedure. For purification column chromatography (hexane/EtOAc 2:1, $R_f = 0.79$) was performed. The product was obtained as yellow crystals (338 mg, 0.89 mmol, 50% yield).

m.p.: 136 °C.

$^1\text{H-NMR}$ (300 MHz, CD_2Cl_2): δ (ppm) = 7.75 (d, 4H, $J = 6.2$ Hz, 8-H, 8'-H), 7.58 (d, 4H, $J = 6.2$ Hz, 7-H, 7'-H), 6.44 (s, 2H, 3-H, 4-H), 4.20 (m, 2H, 11-H), 1.56-1.29 (m, 4H, 12-H, 13-H).

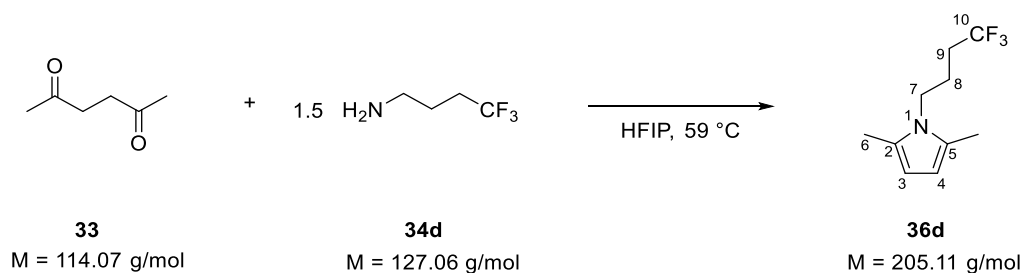
$^{13}\text{C-NMR}$ (75 MHz, CD_2Cl_2): δ (ppm) = 137.33 (C-2, C-5), 136.97 (C-6, C-6'), 132.67 (C-8, C-8'), 128.72 (C-7, C-7'), 118.67 (C-10, C-10'), 112.58 (C-9, C-9'), 110.81 (C-3, C-4), 44.53 (C-11), 29.95 (q, C-13), 23.03 (d, C-12).

$^{19}\text{F-NMR}$ (282 MHz): $\delta = -66.90$.

FT-IR (solid): $\tilde{\nu}$ (cm^{-1}) = 2224, 1599, 1492, 1250, 1244, 1151, 1019, 1010, 841, 774, 677.

HR-MS (ESI): m/z calculated for $\text{C}_{22}\text{H}_{17}\text{F}_3\text{N}_3$ $[\text{M}+\text{H}]^+$ 380.1369; observed 380.1364.

Synthesis of 2,5-dimethyl-1-(4,4,4-trifluorobutyl)-1H-pyrrole (36d)



The reaction mixture was stirred at room temperature for 5 minutes and worked-up according to the general procedure. The product was obtained as a red solid (386 mg, 1.88 mmol, 94% yield).

m.p.: 51 °C.

¹H-NMR (300 MHz, CD₂Cl₂): δ [ppm] = 5.71 (s, 2H, 3-H, 4-H), 3.81 (t, 2H, *J* = 5.22 Hz, 7-H), 2.20 (s, 6H, 6-H, 6'-H), 2.18-2.03 (m, 2H, 8-H), 1.93-1.81 (m, 2H, 9-H).

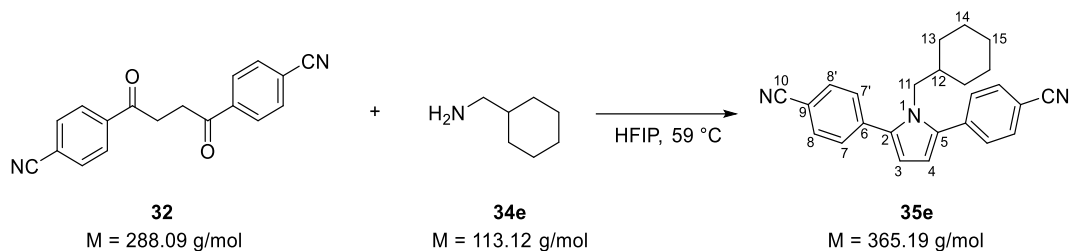
¹³C-NMR (75 MHz, CD₂Cl₂): δ [ppm] = 127.2 (q, C-10), 127.0 (C-2, C-5), 105.5 (C-3, C-4), 42.0 (C-7), 30.9 (q, C-8), 23.4 (C-8), 12.1 (C-6, C-6').

¹⁹F-NMR (282 MHz): δ = -66.52.

FT-IR (solid): $\tilde{\nu}$ (cm⁻¹) = 2939, 1402, 1380, 1290, 1251, 1135, 1032, 751;

HR-MS (ESI):. *m/z* calculated for C₁₀H₁₄F₃N+H⁺ 206.1151 [M+H]⁺; observed 206.1151.

Synthesis of 4,4'-(1-(cyclohexylmethyl)-1H-pyrrole-2,5-diyl)dibenzonitrile (35e) (42)



The reaction mixture was refluxed for 2 days and worked-up according to the general procedure. For purification column chromatography (hexane/EtOAc 4:1, $R_f = 0.75$) was performed. The product was obtained as yellow crystals (436 mg, 1.19 mmol, 65% yield).

m.p.: 161 °C.

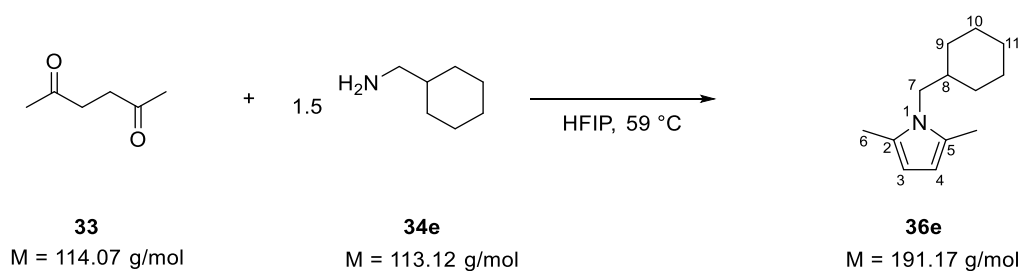
$^1\text{H-NMR}$ (300 MHz, CD_2Cl_2): δ (ppm) = 7.70 (d, 4H, $J = 6.2$ Hz, 8-H, 8'-H), 7.53 (d, 4H, $J = 6.2$ Hz, 7-H, 7'-H), 6.35 (s, 2H, 3-H, 4-H), 3.92 (d, 2H, 11-H), 1.55 (s, 1H, 12-H), 1.41 (m, 2H, 13-H, 13'-H), 1.09-0.73 (m, 6H, 14-H, 14'-H, 15-H), 0.37 (m, 2H, 13-H, 13'-H).

$^{13}\text{C-NMR}$ (75 MHz, CD_2Cl_2): δ (ppm) = 138.01 (C-2, C-5), 137.32 (C-6, C-6'), 132.41 (C-8, C-8'), 128.62 (C-7, C-7'), 118.78 (C-10, C-10'), 112.00 (C-9, C-9'), 110.36 (C-3, C-4), 52.38 (C-11), 39.42 (C-12), 30.09 (C-13, C-13'), 25.94 (C-15), 25.39 (C-14, C-14').

FT-IR (solid): $\tilde{\nu}$ (cm^{-1}) = 2922, 2226, 1604, 1490, 1179, 836, 771.

HR-MS (EI): m/z calculated for $\text{C}_{25}\text{H}_{23}\text{N}_3\text{Na}$ $[\text{M}+\text{Na}]^+$ 388.1784; observed 388.1783.

Synthesis of 1-(cyclohexylmethyl)-2,5-dimethyl-1H-pyrrole (36e)



The reaction mixture was stirred at room temperature for 10 minutes and worked-up according to the general procedure. The product was obtained as a brown oil (375 mg, 1.97 mmol, 98% yield).

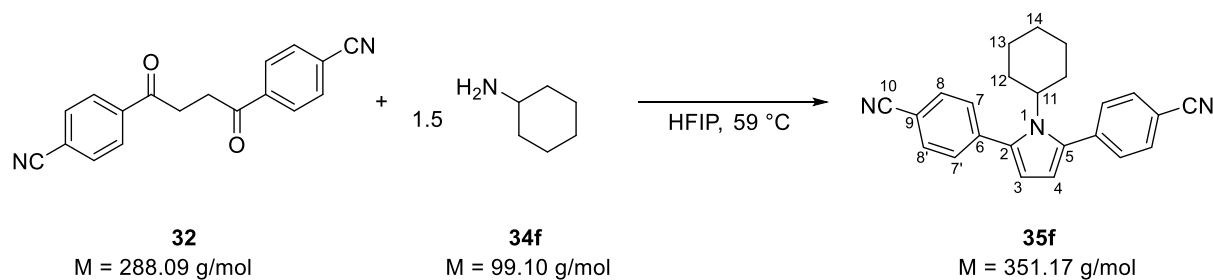
¹H-NMR (300 MHz, CD₂Cl₂): δ [ppm] = 5.68 (s, 2H, 3-H, 4-H), 3.54 (d, 2H, *J* = 7.14 Hz, 7-H), 2.18 (s, 6H, 6-H, 6'-H), 1.80-1.55 (m, 6H, C-8, C-9, C-9', C-10, C-10', C-11), 1.30-1.11 (m, 3H, C-10, C-10', C-11), 1.06-0.88 (m, 2H, C-9, C-9').

¹³C-NMR (75 MHz, CD₂Cl₂): δ [ppm] = 127.6 (C-2, C-5), 104.9 (C-3, C-4), 49.8 (C-7), 39.5 (C-8), 31.0 (C-9, C-9'), 26.5 (C-11), 26.0 (C-10, C-10'), 12.6 (C-6, C-6').

FT-IR (solid): $\tilde{\nu}$ (cm⁻¹) = 2919, 2848, 1511, 1446, 1403, 1353, 1291, 1018, 966, 738.

HR-MS (ESI): *m/z* calculated for C₁₃H₂₁N+H⁺ 192.1747 [M+H]⁺; observed 192.1747.

Synthesis of 4,4'-(1-cyclohexyl-1H-pyrrole-2,5-diyl)dibenzonitrile (35f)



The reaction mixture was refluxed for 2 days and worked-up according to the general procedure. For purification column chromatography (n-hexane/EtOAc 4:1, $R_f = 0.61$) was performed. The product was obtained as a light yellow solid (537 mg, 1.53 mmol, 76% yield).

m.p.: 189 °C;

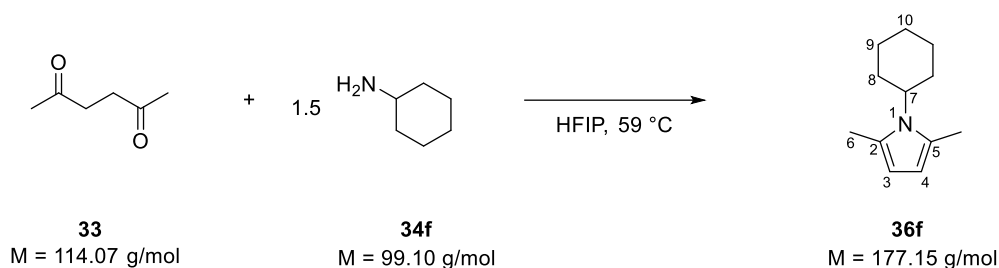
$^1\text{H-NMR}$ (300 MHz, CD_2Cl_2): δ [ppm] = 7.72 (d, $J = 8.43$ Hz, 4H, 8-H, 8'-H), 7.55 (d, 2H $J = 8.43$ Hz, 7-H, 7'-H), 6.24 (s, 2H, 3-H, 4-H), 3.93 (tt, 1H, $J = 3.33$ Hz, $J = 12.15$ Hz, 11-H), 1.85 (d, 2H, $J = 12.27$ Hz, 12-H, 12'-H), 1.70-1.41 (m, 5H, 12-H, 12'-H, 13-H, 13'-H, 14-H), 1.17-0.99 (m, 2H, (13-H, 13'-H)), 0.89-0.69 (m, 1H, 14-H).

$^{13}\text{C-NMR}$ (75 MHz, CD_2Cl_2): δ [ppm] = 139.3 (C-2, C-5), 136.3 (C-6, C-6'), 131.9 (C-8, C-8'), 130.4 (C-7, C-7'), 118.8 (C-10), 111.9 (C-3, C-4), 110.8 (C-9, C-9'), 59.5 (C-11), 34.6 (C-12, C-12'), 26.4 (C-13, C-13'), 25.1 (C-14).

FT-IR (solid): $\tilde{\nu}$ (cm^{-1}) = 2923, 2857, 2222, 1603, 1489, 1451, 1410, 1397, 1376, 1320, 1265, 1225, 1198, 1177, 1110, 1017, 843, 833, 770, 692.

HR-MS (EI): m/z calculated for $\text{C}_{24}\text{H}_{21}\text{N}_3$ 351.1730 $[\text{M}]^+$; observed 351.1730.

Synthesis of 1-cyclohexyl-2,5-dimethyl-1H-pyrrole (36f)



The reaction mixture was stirred at room temperature for 10 minutes and worked-up according to the general procedure. The product was obtained as a yellow solid (340 mg, 1.92 mmol, 96% yield).

m.p.: 56 °C.

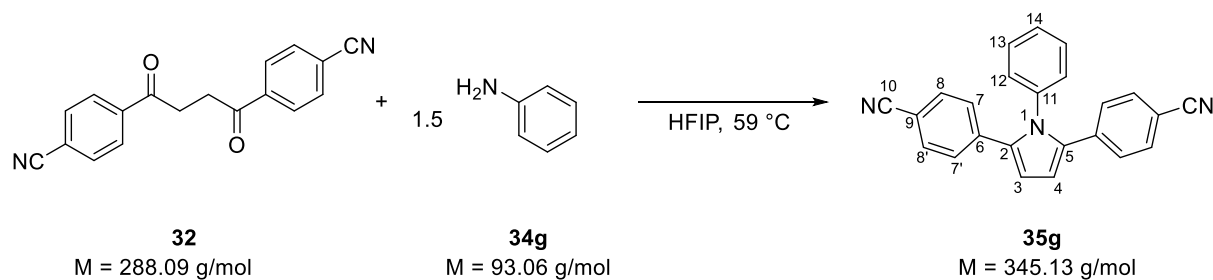
¹H-NMR (300 MHz, CD₂Cl₂): δ [ppm] = 5.64 (s, 2H, 3-H, 4-H), 3.99-3.79 (m, 1H, 7-H), 2.26 (s, 6H, 6-H, 6'-H), 1.98-1.67 (m, 7H, 8-H, 8'-H, 9-H, 9'-H, 10-H), 1.49-1.14 (m, 3H, 9-H, 9'-H, 10-H).

¹³C-NMR (75 MHz, CD₂Cl₂): δ [ppm] = 127.5 (C-2, C-5), 106.0 (C-3, C-4), 56.3 (C-7), 32.5 (C-8, C-8'), 26.6 (C-9, C-9'), 25.6 (C-10), 14.1 (C-6, C-6').

FT-IR (solid): $\tilde{\nu}$ (cm⁻¹) = 2927, 2852, 1654, 1446, 1396, 1344, 1293, 1260, 1215, 1188, 1145, 1057, 1019, 994, 891, 777, 744.

HR-MS (ESI): *m/z* calculated for C₁₂H₁₉N+H⁺ 178.1590 [M+H]⁺; observed 178.1594.

Synthesis of 4,4'-(1-phenyl-1H-pyrrole-2,5-diyl)dibenzonitrile (35g)



The reaction mixture was refluxed for 2 days and worked-up according to the general procedure. For purification column chromatography (n-hexane/EtOAc 6:1, $R_f = 0.43$) was performed. The product was obtained as a yellow solid (421 mg, 1.22 mmol, 61% yield).

m.p.: 192 °C.

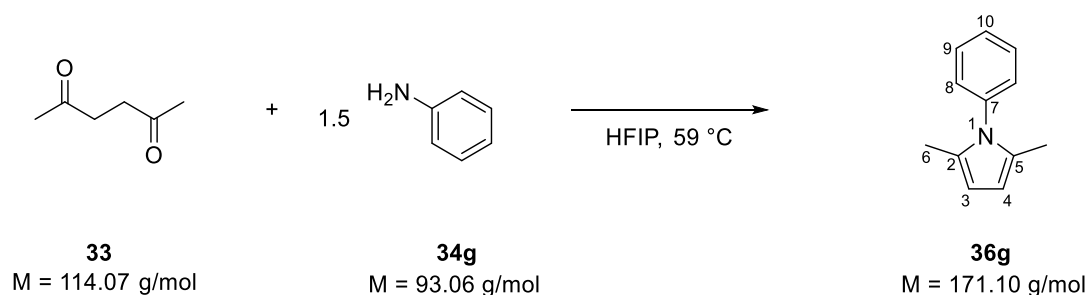
$^1\text{H-NMR}$ (300 MHz, CD_2Cl_2): δ [ppm] = 7.46 (d, 4H, $J = 8.52$ Hz, 8-H, 8'-H), 7.41-7.30 (m, 3H, 13-H, 13'-H, 14-H), 7.14 (d, 2H, $J = 8.52$ Hz, 7-H, 7'-H), 7.06 (d, 2H, $J = 7.86$ Hz, 12-H, 12'-H), 6.63 (s, 2H, 3-H, 4-H).

$^{13}\text{C-NMR}$ (75 MHz, CD_2Cl_2): δ [ppm] = 138.0 (C-2, C-5), 137.1 (C-6, C-6'), 135.3 (C-11), 131.8 (C-8, C-8'), 129.4 (C-13, C-13'), 128.7 (C-12, C-12'), 128.6 (C-7, C-7'), 128.4 (C-14), 118.8 (C-10, C-10'), 112.2 (C-3, C-4), 109.7 (C-9, C-9').

FT-IR (solid): $\tilde{\nu}$ (cm^{-1}) = 2361, 2222, 1599, 1491, 1428, 1346, 1179, 842, 778, 698.

HR-MS (ESI): m/z calculated for $\text{C}_{24}\text{H}_{15}\text{N}_3 + \text{Na}^+$ 368.1158 $[\text{M} + \text{Na}]^+$; observed 368.1153.

Synthesis of 2,5-dimethyl-1-phenyl-1H-pyrrole (36g)



The reaction mixture was stirred at room temperature for 15 minutes and worked-up according to the general procedure. The product was obtained as a yellow solid (308 mg, 1.80 mmol, 90% yield).

m.p.: 51 °C.

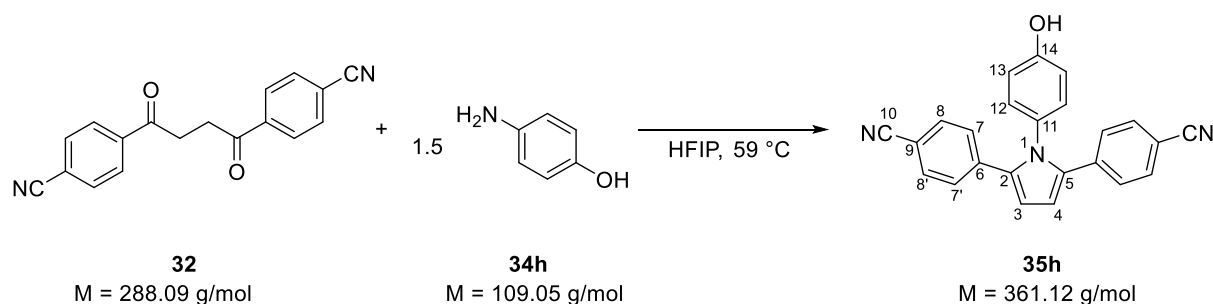
¹H-NMR (300 MHz, CD₂Cl₂): δ [ppm] = 7.51-7.36 (m, 3H, 9-H, 9'-H, 10-H), 7.25-7.16 (m, 2H, 8-H, 8'-H), 5.83 (s, 2H, 3-H, 4-H), 2.00 (s, 6H, 6-H, 6'-H).

¹³C-NMR (75 MHz, CD₂Cl₂): δ [ppm] = 139.1 (C-7), 128.9 (C-9, C-9'), 128.4 (C-2, C-5), 128.3 (C-10), 127.51 (C-8, C-8'), 105.7 (C-3, C-4), 12.7 (C-6, C-6').

FT-IR (solid): $\tilde{\nu}$ (cm⁻¹) = 2920, 1596, 1495, 1401, 1318, 1067, 1037, 1006, 772, 746, 716, 684.

HR-MS (ESI): *m/z* calculated for C₁₂H₁₃N+H⁺ 172.1121 [M+H]⁺; observed 172.1123.

Synthesis of 4,4'-(1-(4-hydroxyphenyl)-1H-pyrrole-2,5-diyl)dibenzonitrile (35h)



The reaction mixture was refluxed for 2 days in an atmosphere of argon, was protected from sunlight and was worked-up according to the general procedure. For purification column chromatography (n-hexane/EtOAc 3:1, $R_f = 0.54$) was performed. The product was obtained as a yellow solid (296 mg, 0.82 mmol, 41% yield).

m.p.: 195 °C.

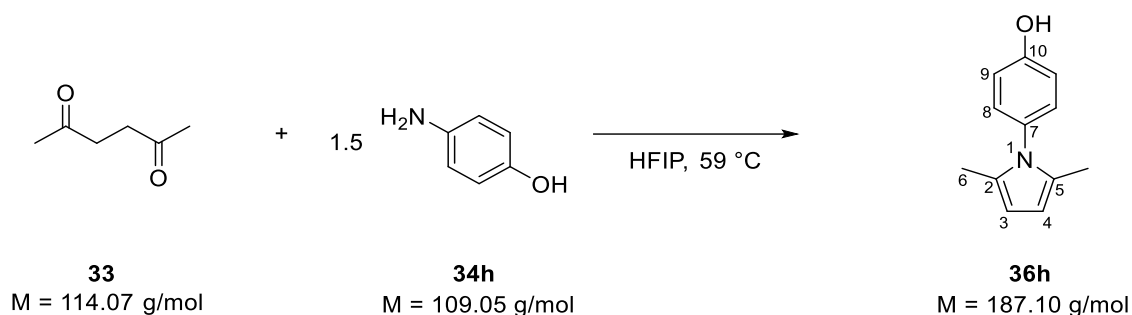
$^1\text{H-NMR}$ (300 MHz, DMSO- d_6): δ [ppm] = 9.86 (2, 1H, OH), 7.68 (d, 2H, $J = 8.58$ Hz, 8-H, 8'-H), 7.23 (d, 2H, $J = 8.58$ Hz, 7-H, 7'-H), 6.99 (d, 2H, $J = 8.70$ Hz, 12-H, 12'-H), 6.75-6.73 (m, 4H, 3-H, 4-H, 13-H, 13'-H).

$^{13}\text{C-NMR}$ (75 MHz, DMSO- d_6): δ [ppm] = 157.8 (C-14), 137.4 (C-2, C-5), 135.7 (C-6, C-6'), 132.5 (C-8, C-8'), 130.3 (C-12, C-12'), 129.3 (C-11), 128.7 (C-7, C-7'), 119.3 (C-10, C-10'), 116.5 (C-13, C-13'), 112.6 (C-3, C-4), 109.1 (C-9, C-9').

FT-IR (solid): $\tilde{\nu}$ (cm^{-1}) = 3335, 2922, 2237, 2222, 1596, 1515, 1259, 1220, 1014, 836, 797, 781, 656.

HR-MS (ESI): m/z calculated for $\text{C}_{24}\text{H}_{14}\text{N}_3\text{O}^-$ 360.1142 [M-H] $^-$; observed 360.1133.

Synthesis of 4-(2,5-dimethyl-1H-pyrrol-1-yl)phenol (36h)



The reaction mixture was refluxed for 15 minutes and worked-up according to the general procedure. The product was obtained as a yellow solid (329 mg, 1.76 mmol, 88% yield).

m.p.: 103 °C.

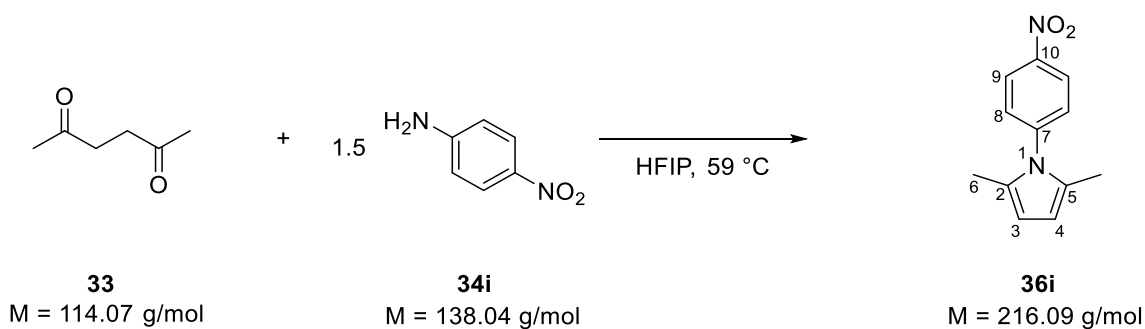
¹H-NMR (300 MHz, CD₂Cl₂): δ [ppm] = 7.07 (d, 2H, *J* = 8.7 Hz, 8-H, 8'-H), 6.91 (d, 2H, *J* = 8.7 Hz, 9-H, 9'-H), 5.81 (s, 2H, 3-H, 4-H), 5.16 (s, 1H, OH), 1.99 (s, 6H, 6-H, 6'-H).

¹³C-NMR (75 MHz, CD₂Cl₂): δ [ppm] = 155.1 (C-10), 131.9 (C-7), 129.5 (C-8, C-8'), 128.7 (C-2, C-5), 115.6 (C-9, C-9'), 105.3 (C-3, C-4), 12.6 (C-6, C-6').

FT-IR (solid): $\tilde{\nu}$ (cm⁻¹) = 3242, 1512, 1440, 1408, 1217, 1095, 999, 838, 820, 751.

HR-MS (ESI): *m/z* calculated for C₁₂H₁₃NO+H⁺ 188.1070 [M+H]⁺; observed 188.1070.

Synthesis of 2,5-dimethyl-1-(4-nitrophenyl)-1H-pyrrole (36i)



The reaction mixture was refluxed for 15 minutes and worked-up according to the general procedure. The product was obtained as a brown solid (389 mg, 1.80 mmol, 90% yield).

m.p.: 143 °C.

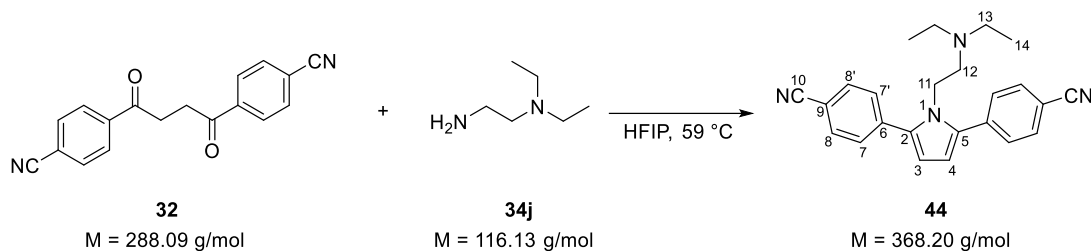
¹H-NMR (300 MHz, CD₂Cl₂): δ [ppm] = 8.33 (d, 2H, *J* = 6 Hz, 9-H, 9'-H), 7.39 (d, 2H, *J* = 6 Hz, 8-H, 8'-H), 5.91 (s, 2h; 3-H, 4-H), 2.06 (s, 6H, 6'-H).

¹³C-NMR (75 MHz, CD₂Cl₂): δ [ppm] = 128.9 (C-9, C-9'), 128.4 (C-2, C-5), 124.4 (C-8, C-8'), 107.3 (C-3, C-4), 12.8 (C-6, C-6').

FT-IR (solid): $\tilde{\nu}$ (cm⁻¹) = 1594, 1516, 1490, 1396, 1335, 1223, 1094, 1000, 853, 776, 764, 718, 689.

HR-MS (ESI): *m/z* calculated for C₁₂H₁₂N₂O₂+H⁺ 217.0972 [M+H]⁺; observed 217.0977.

Synthesis of 4,4'-(1-(2-(diethylamino)ethyl)-1H-pyrrole-2,5-diyl)dibenzonitrile (44)



The reaction mixture was refluxed for 2 days and worked-up according to the general procedure. For purification column chromatography (DCM/MeOH 99:1, $R_f = 0.38$) was performed. The product was obtained as yellow crystals (370 mg, 1.00 mmol, 54% yield).

m.p.: 135 °C.

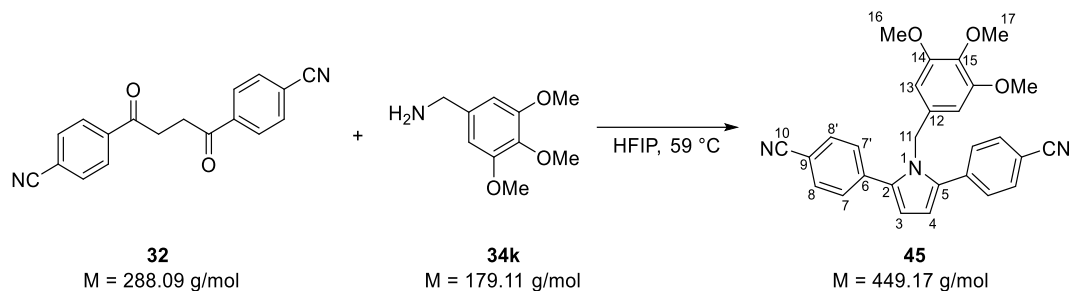
$^1\text{H-NMR}$ (300 MHz, CDCl_3): δ (ppm) = 7.73 (d, 4H, $J = 8.25$ Hz, 8-H, 8'-H), 7.60 (d, 4H, $J = 8.25$ Hz, 7-H, 7'-H), 6.39 (s, 2H, 3-H, 4-H), 4.14 (t, 2H, $J = 7.05$ Hz, 11-H), 2.13-1.99 (m, 6H, 12-H, 13-H, 13'-H), 6.05 (t, 6H, $J = 7.13$ Hz, 14-H, 14'-H).

$^{13}\text{C-NMR}$ (75 MHz, CD_2Cl_2): δ (ppm) = 137.93 (C-2, C-5), 136.65 (C-6, C-6'), 132.42 (C-8, C-8'), 129.01 (C-7, C-7'), 118.82 (C-10, C-10'), 111.91 (C-9, C-9'), 110.41 (C-3, C-4), 52.40 (C-12), 47.29 (C-13, C-13'), 44.57 (C-11), 11.43 (C-14, C-14').

FT-IR (solid): $\tilde{\nu}$ (cm^{-1}) = 2970, 2956, 2225, 1738, 1603, 1382, 1215, 838, 779.

HR-MS (ESI): m/z calculated for $\text{C}_{24}\text{H}_{25}\text{N}_4$ $[\text{M}+\text{H}]^+$ 369.2074; observed 369.2069.

Synthesis of 4,4'-(1-(3,4,5-trimethoxybenzyl)-1H-pyrrole-2,5-diyl)dibenzonitrile (45)



The reaction mixture was refluxed for 2 days and worked-up according to the general procedure. For purification column chromatography (hexane/EtOAc 2:1, $R_f = 0.34$) was performed. The product was obtained as an orange solid (227.1 mg, 0.51 mmol 40% yield).

m.p.: 163 °C.

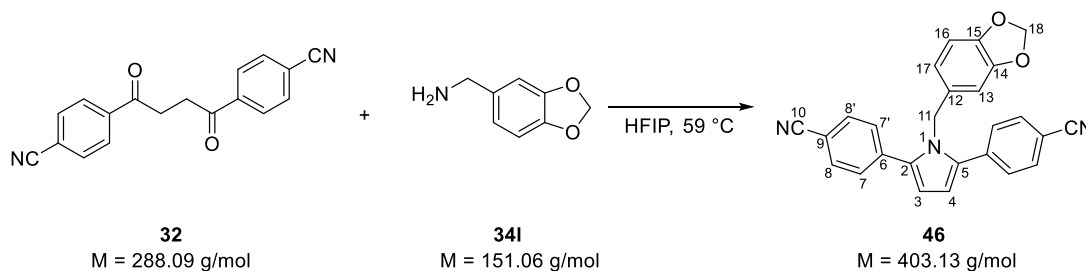
$^1\text{H-NMR}$ (300 MHz, CDCl_3): δ (ppm) = 7.65 (d, 4H, $J = 8.5$ Hz, 8-H, 8'-H), 7.47 (d, 4H, $J = 8.5$ Hz, 7-H, 7'-H), 6.49 (s, 2H, C-3, C-4), 5.82 (s, 2H, C-13, C-13'), 5.15 (2, 2H, C-11), 3.77 (s, 3H, 17-H), 3.63 (s, 6H, 16-H).

$^{13}\text{C-NMR}$ (75 MHz, CDCl_3): δ (ppm) = 153.48 (C-14), 137.46 (C-2, C-5), 136.88 (C-6, C-6'), 133.57 (C-15), 132.42 (C-8, C-8'), 128.93 (C-7, C-7'), 118.66 (C-10, C-10'), 112.40 (C-9, C-9'), 110.74 (C-3, C-4), 106.73 (C-12), 102.62 (C-13, C-13'), 60.86 (C-16), 55.94 (C-17), 49.29 (C-11).

FT-IR (solid): $\tilde{\nu}$ (cm^{-1}) = 2969, 2358, 2228, 1739, 1597, 1455, 1328, 1232, 1123, 1016, 845, 787.

HR-MS (ESI): m/z calculated for $\text{C}_{28}\text{H}_{23}\text{N}_3\text{O}_3\text{Na}$ $[\text{M}+\text{Na}]^+$ 472.1632; observed 472.1637.

Synthesis of 4,4'-(1-(benzo[d][1,3]dioxol-5-ylmethyl)-1H-pyrrole-2,5-diyl)dibenzonitrile (46)



The reaction mixture was refluxed for 3 days and worked-up according to the general procedure. For purification column chromatography (hexane/EtOAc 2:1, $R_f = 0.56$) was performed. The product was obtained as an orange solid (100.4 mg, 0.25 mmol, 36% yield, heavily contaminated with grease).

m.p.: 168 °C.

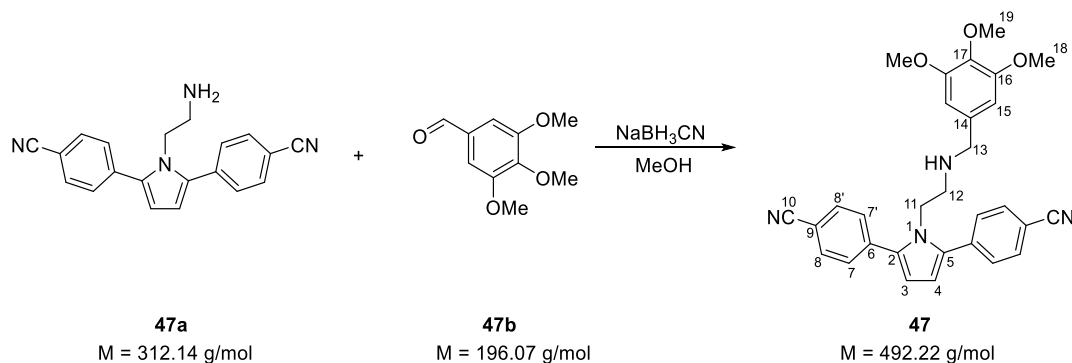
$^1\text{H-NMR}$ (300 MHz, CDCl_3): δ (ppm) = 7.62 (d, 4H, $J = 8.40$ Hz, 8-H, 8'-H), 7.46 (d, 4H, $J = 8.40$ Hz, 7-H, 7'-H), 6.58 (d, 1H, $J = 8.43$ Hz, 13-H), 6.48 (s, 2H, 3H, 4-H), 6.11-6.09 (m, 2H, 16-H, 17-H), 5.90 (s, 2H, 18-H), 5.13 (s, 2H, 11-H).

$^{13}\text{C-NMR}$ (300 MHz, CDCl_3): δ (ppm) = 148.16 (C-14), 146.92 (C-15), 137.40 (C-2, C-5), 136.64 (C-6, C-6'), 132.37 (C-8, C-8'), 131.82 (C-12), 128.89 (C-7, C-7'), 118.87 (C-9, C-9'), 118.77 (C-16), 112.29 (C-10, C-10'), 110.67 (C-17), 108.32 (C-13), 105.95 (C-3, C-4), 101.17 (C-18), 49.03 (C-11).

FT-IR (solid): $\tilde{\nu}$ (cm^{-1}) = 2963, 1738, 1258, 1085, 1012, 786.

HR-MS (ESI): m/z calculated for $\text{C}_{26}\text{H}_{18}\text{N}_3\text{O}_2$ $[\text{M}+\text{H}]^+$ 404.1394; observed 404.1394.

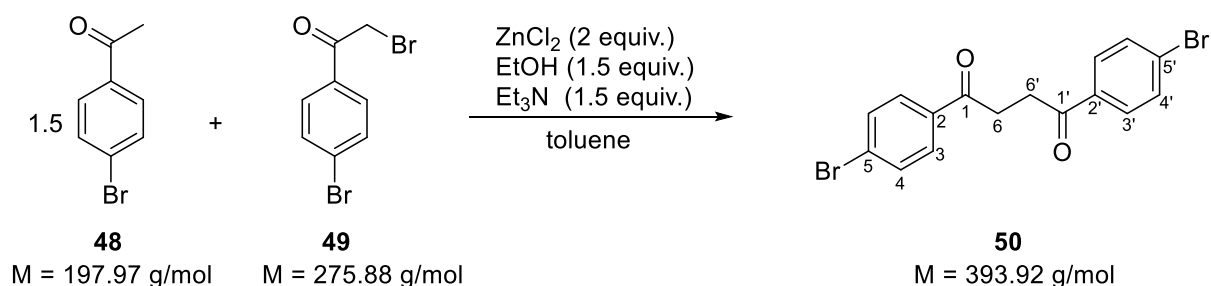
Synthesis of 4,4'-(1-(2-((3,4,5-trimethoxybenzyl)amino)ethyl)-1H-pyrrole-2,5-diyl)dibenzonitrile (**47**)



4,4'-(1-(2-Aminoethyl)-1H-pyrrole-2,5-diyl)dibenzonitrile (**47a**) (197 mg, 0.63 mmol, 1 equiv.) and 3,4,5-trimethoxybenzaldehyde (**47b**) (155 mg, 0.79 mmol, 1.25 equiv.) were dissolved in methanol (40 mL) and NaBH₃CN (80 mg, 1.27 mmol, 2 equiv.) was slowly added to the reaction mixture. It was stirred for 3 days and then conc. HCl was added until pH 2 was reached. The resulting solution was basified to pH 12 with NaOH and the solvents were removed under reduced pressure. The resulting orange residue was purified by column chromatography (DCM, R_f = 0.20). The product was obtained as a yellow, viscous oil that was heavily contaminated with both educts. The product was used for the next reaction step without further purification.

HR-MS (ESI): m/z calculated for C₃₀H₂₉N₄O₃ [M+H]⁺ 493.2234; observed 493.2235

Synthesis of 1,4-bis(4-Bromophenyl)butane-1,4-dione (**50**)



ZnCl₂ (5.11 g, 37.5 mmol, 2 equiv.), Et₃N (4.0 mL, 28.1 mmol, 1.5 equiv.) and absolute ethanol (1.72 mL, 28.1 mmol, 1.5 equiv.) were suspended in anhydrous toluene (50 mL) under an atmosphere of argon. The reaction mixture was stirred for 60 minutes. Then, 1-(4-bromophenyl)ethan-1-one (**48**) (5.56 g, 28.1 mmol, 1.5 equiv.) and 2-bromo-1-(4-bromophenyl)ethan-1-one (**49**) (5.17 g, 17.8 mmol, 1 equiv.) was added and the resulting suspension was stirred for 7 days at room temperature. The reaction mixture was washed with 10% H₂SO₄ (50 mL) and a saturated solution of NaHCO₃ (50 mL). The aqueous phase was extracted with EtOAc (2 x 50 mL) and the combined organic phases were dried over Na₂SO₄. The solvent was evaporated under reduced pressure. The residue was recrystallized from EtOAc (ca. 100 mL) and the product was obtained as a colorless crystalline solid (4.98 g, 12.7 mmol, 71% yield).

m.p.: 289 °C.

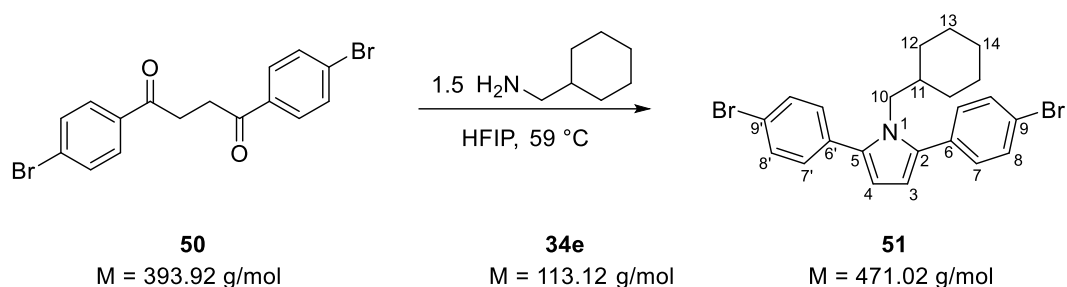
¹H-NMR (300 MHz, DMSO-*d*₆): δ (ppm) = 7.95 (d, 4H, *J* = 8.85 Hz, 3-H, 3'-H, 7-H, 7'-H), 7.76 (d, 4H, *J* = 8.85 Hz, 4-H, 4'-H, 6-H, 6'-H), 3.39 (2, 4H, 8-H, 8'-H).

¹³C-NMR could not be measured due to its low solubility in common organic solvents.

FT-IR (solid): $\tilde{\nu}$ (cm⁻¹) = 2896, 1667, 1583, 1568, 1482, 1406, 1389, 1279, 1189, 1104, 1071, 977, 742, 783, 760, 658.

HR-MS (ESI): *m/z* calculated for C₁₆H₁₃Br₂O₂ [M+H]⁺ 394.9277; observed 394.9289.

Synthesis of 2,5-bis(4-bromophenyl)-1-(cyclohexylmethyl)-1H-pyrrole (**51**)



1,4-Bis(4-bromophenyl)butane-1,4-dione (**50**) (3 g, 7.62 mmol, 1 equiv.) was dissolved in HFIP (20 mL) and methylcyclohexylamine (**34e**) (1.29 g, 11.43 mmol, 1.5 equiv.) was added slowly. The resulting mixture was refluxed for 3 days after which the solvents were evaporated. The residue was dissolved in DCM (50 mL) and was washed with water and brine (20 mL each), dried over anhydrous MgSO_4 and the solvent was evaporated. The residue was purified with column chromatography (Hexane/Ethyl acetate 8:1, $R_f = 0.82$). The product was obtained as an off-white solid (2.80 g, 5.95 mmol, 78% yield).

m.p.: 153 °C.

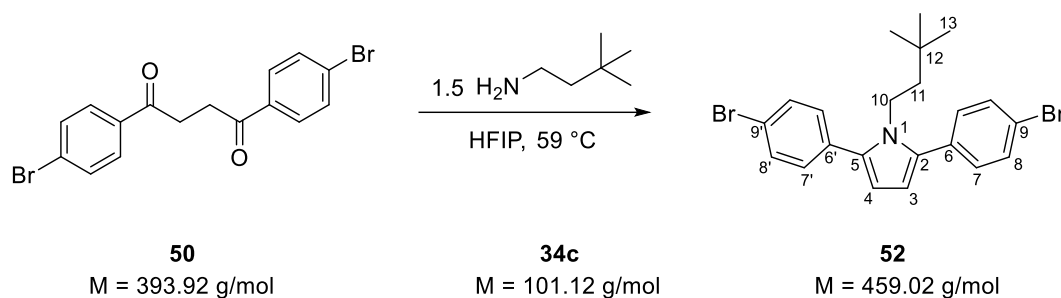
$^1\text{H-NMR}$ (300 MHz, DCM-d_2): δ (ppm) = 7.55 (d, 4H, $J = 8.43$ Hz, 7-H, 7'-H), 7.33 (d, 4H, $J = 8.43$ Hz, 8-H, 8'-H), 6.23 (s, 2H, 3-H, 4-H), 3.89 (d, 2H, $J = 7.32$ Hz, 10-H), 1.41 (m, 3H, 13-H, 13-H, 14-H), 1.1-0.96 (m, 3H, 11-H, 12'-H, 12'-H), 0.93-0.75 (m, 3H, 13'-H, 13'-H, 14-H), 0.50-0.30 (m, 2H, 12-H, 12-H).

$^{13}\text{C-NMR}$ (75 MHz, DCM-d_2): δ (ppm) = 136.62 (C-2, C-5), 133.19 (C-6, C-6'), 131.62 (C-8, C-8'), 130.18 (C-7, C-7'), 120.63 (C-9, C-9'), 109.98 (C-3, C-4), 51.81 (C-10), 39.05 (C-11), 30.03 (C-12), 26.07 (C-14), 25.44 (C-13).

FT-IR (solid): $\tilde{\nu}$ (cm^{-1}) = 2970, 1738, 1365, 1228, 1217.

HR-MS (ESI): m/z calculated for $\text{C}_{23}\text{H}_{24}\text{Br}_2\text{N}$ $[\text{M}+\text{H}]^+$ 472.0270; observed 472.0262.

Synthesis of 2,5-bis(4-bromophenyl)-1-(3,3-dimethylbutyl)-1H-pyrrole (**52**)



1,4-Bis(4-bromophenyl)butane-1,4-dione (**50**) (3 g, 7.62 mmol, 1 equiv.) was dissolved in HFIP (20 mL) and 3,3-dimethylbutan-1-amine (**34c**) (1.16 g, 11.43 mmol, 1.5 equiv.) was added slowly. The resulting mixture was refluxed for 3 days after which the solvents were evaporated. The residue was dissolved in DCM (50 mL) and was washed with water and brine (20 mL each), dried over anhydrous MgSO_4 and the solvent was evaporated. The residue was purified with column chromatography (Hexane/Ethyl acetate 8:1, $R_f = 0.86$). The product was obtained as a white solid (1.52 g, 3.31 mmol, 43% yield).

m.p.: 175 – 186 $^\circ\text{C}$.

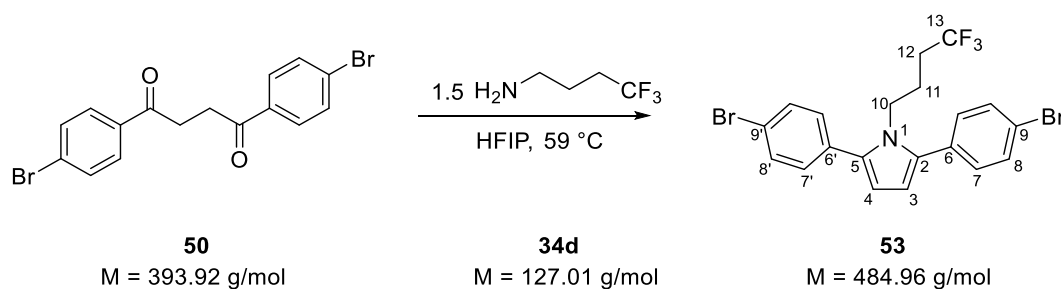
$^1\text{H-NMR}$ (300 MHz, DCM-d_2): δ (ppm) = 7.56 (d, 4H, $J = 8.37 \text{ Hz}$, 7-H, 7'-H), 7.33 (d, 4H, $J = 8.37 \text{ Hz}$, 8-H, 8'-H), 6.23 (s, 2H, 3-H, 4-H), 4.07-3.97 (m, 2H, 10-H), 1.12-1.02 (m, 2H, 11-H), 0.58 (s, 9H, 13-H).

$^{13}\text{C-NMR}$ (75 MHz, DCM-d_2): δ (ppm) = 135.24 (C-2, C-5), 132.88 (C-6, C-6'), 131.53 (C-8, C-8'), 130.47 (C-7, C-7'), 120.92 (C-9, C-9'), 109.95 (C-3, C-4), 43.87 (C-11), 41.89 (C-10), 29.37 (C-12), 28.48 (C-13).

FT-IR (solid): $\tilde{\nu}$ (cm^{-1}) = 2957, 1666, 1477, 1120, 1007, 822, 769.

HR-MS (EI): m/z calculated for $\text{C}_{22}\text{H}_{23}\text{Br}_2\text{N}$ [M] 459.0197; observed 459.0196.

Synthesis of 2,5-bis(4-bromophenyl)-1-(4,4,4-trifluorobutyl)-1H-pyrrole (**53**)



1,4-Bis(4-bromophenyl)butane-1,4-dione (**50**) (3 g, 7.62 mmol, 1 equiv.) was dissolved in HFIP (20 mL) and 4,4,4-trifluorobutan-1-amine (**34d**) (1.45 g, 11.43 mmol, 1.5 equiv.) was added slowly. The resulting mixture was refluxed for 3 days after which the solvents were evaporated. The residue was dissolved in DCM (50 mL) and was washed with water and brine (20 mL each), dried over anhydrous MgSO₄ and the solvent was evaporated. The residue was purified with column chromatography (Hexane/Ethyl acetate 8:1, R_f = 0.75). The product was obtained as an off-white solid (2.25 g, 4.64 mmol, 61% yield).

m.p.: 184 °C.

¹H-NMR (300 MHz, DCM-d₂): δ (ppm) = 7.58 (d, 2H, *J* = 8.34 Hz, 7-H, 7'-H), 7.33 (d, 2H, *J* = 8.34 MHz, 8-H, 8'-H), 6.29 (s, 2H, 3-H, 4-H), 4.13 (t, 2H, *J* = 6.48 Hz, 10-H), 1.56-1.32 (m, 4H, 11-H, 12-H).

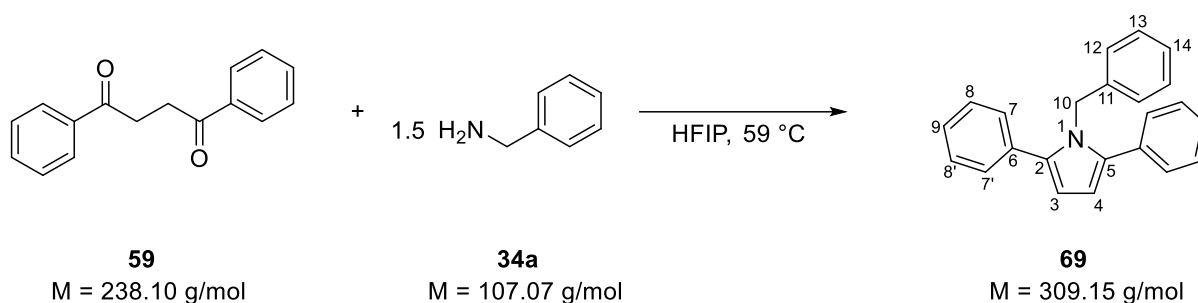
¹³C-NMR (75 MHz, DCM-d₂): δ (ppm) = 136.10 (C-2, C-5), 132.43 (C-6, C-6'), 131.85 (C-8, C-8'), 130.18 (C-7, C-7'), 126.61 (C-13), 121.19 (C-9, C-9'), 110.61 (C-3, C-4), 44.00 (C-10), 30.06 (C-12), 22.98 (C-11).

¹⁹F-NMR (262 MHz, DCM-d₂): δ (ppm) = -66.90 (s, CF₃).

FT-IR (solid): $\tilde{\nu}$ (cm⁻¹) = 2969, 1738, 1366, 1229, 1217, 1126, 1010, 830, 781.

HR-MS (EI): *m/z* calculated for C₂₀H₁₆Br₂NF₃ [M] 484.9602; observed 484.9610.

Synthesis of 1-benzyl-2,5-diphenyl-1H-pyrrole (69)



The reaction mixture was refluxed for 2 days and worked-up according to the general procedure. For purification column chromatography (n-hexane/EtOAc 9:1, $R_f = 0.76$) was performed. The product was obtained as colorless crystals (381 mg, 1.23 mmol, 62% yield).

m.p.: 131 °C.

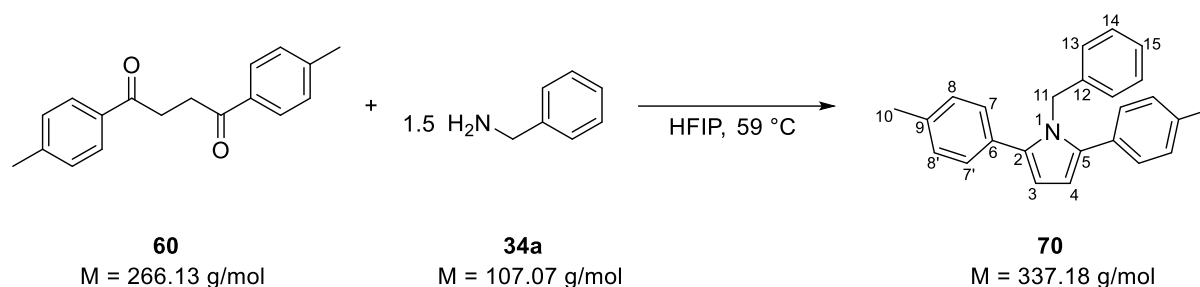
¹H-NMR (300 MHz, CD₂Cl₂): δ [ppm] = 7.42-7.23 (m, 10H, 7-H, 7'-H, 8-H, 8'-H, 9-H, 9'-H), 7.14-7.05 (m, 3H, 13-H, 13'-H, 14-H), 6.63-6.58 (m, 2H, 12-H, 12'-H), 6.35 (s, 2H, 3-H, 4-H), 5.28 (s, 2H, 10-H).

¹³C-NMR (75 MHz, CD₂Cl₂): δ [ppm] = 139.2 (C-11), 136.9 (C-2, C-5), 133.7 (C-6, C-6'), 128.9 (C-8, C-8'), 128.3 (C-7, C-7'), 128.2 (C-13, C-13'), 127.0 (C-9, C-9'), 126.7 (C-14), 125.8 (C-12, C-12'), 109.8 (C-3, C-4), 48.6 (C-10).

FT-IR (solid): $\tilde{\nu}$ (cm⁻¹) = 2357, 1599, 1480, 1448, 1360, 1321, 1024, 752, 731, 699, 663.

HR-MS (ESI): m/z calculated for C₂₃H₁₉N+H⁺ 310.1590 [M+H]⁺; observed 310.1595.

Synthesis of 1-benzyl-2,5-di-p-tolyl-1H-pyrrole (70)



The reaction mixture was refluxed for 2 days and worked-up according to the general procedure. For purification column chromatography (n-hexane/EtOAc 19:1, $R_f = 0.72$) was performed. The product was obtained as colorless crystals (550 mg, 1.64 mmol, 82% yield).

m.p.: 144 °C.

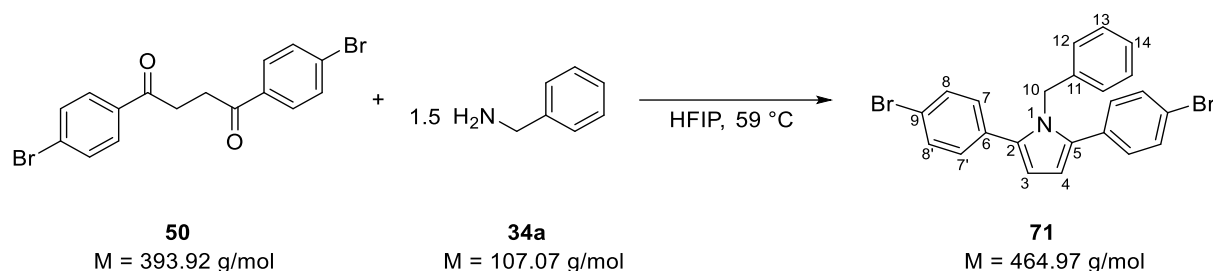
$^1\text{H-NMR}$ (300 MHz, CD_2Cl_2): δ [ppm] = 7.25 (d, 4H, $J = 8.1$ Hz, 7-H, 7'-H), 7.17-7.07 (m, 7H, 8-H, 8'-H, 14-H, 14'-H, 15-H), 6.64-6.60 (m, 2H, 13-H, 13'-H), 6.28 (2, 2H, 3-H, 4-H), 5.24 (s, 2H, 11-H), 2.34 (s, 6H, 10-H, 10'-H).

$^{13}\text{C-NMR}$ (75 MHz, CD_2Cl_2): δ [ppm] = 139.5 (C-11), 136.8 (C-2, C-5), 136.5 (C-9, C-9'), 130.8 (C-6, C-6'), 129.0 (C-7, C-7'), 128.8 (C-8, C-8'), 128.2 (C-14, C-14'), 126.7 (C-15), 125.7 (C-13, C-13'), 109.4 (C-3, C-4), 48.4 (C-11), 20.8 (C-10, C-10').

FT-IR (solid): $\tilde{\nu}$ (cm^{-1}) = 2967, 2357, 2340, 1736, 1436, 1365, 1216.

HR-MS (ESI): m/z calculated for $\text{C}_{25}\text{H}_{23}\text{N}+\text{H}^+$ 338.1903 $[\text{M}+\text{H}]^+$; observed 338.1902.

Synthesis of 1-benzyl-2,5-bis(4-bromophenyl)-1H-pyrrole (71)



The reaction mixture was refluxed for 2 days and worked-up according to the general procedure. For purification column chromatography (n-hexane/EtOAc 8:1, $R_f = 0.56$) was performed. The product was obtained as colorless crystals (735 mg, 1.58 mmol, 79% yield).

m.p.: 174 °C.

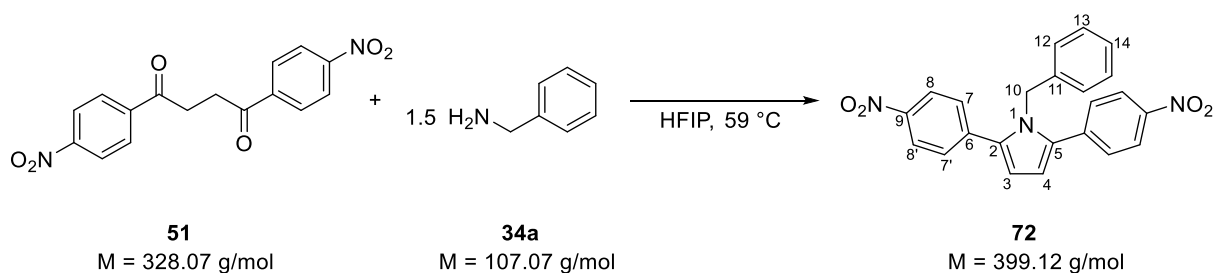
$^1\text{H-NMR}$ (300 MHz, CD_2Cl_2): δ [ppm] = 7.46 (d, 4H, $J = 8.46$ Hz, 7-H, 7'-H), 7.24 (d, 4H, $J = 8.46$ Hz, 8-H, 8'-H), 7.17-7.08 (m, 3H, 13-H, 13'-H, 14-H), 6.64-6.57 (m, 2H, 12-H, 12'-H), 6.35 (s, 2H, 3-H, 4-H), 5.20 (s, 2H, 10-H).

$^{13}\text{C-NMR}$ (75 MHz, CD_2Cl_2): δ [ppm] = 138.8 (C-11), 136.0 (C-2, C-5), 132.5 (C-6, C-6'), 131.5 (C-7, C-7'), 130.4 (C-8, C-8'), 128.4 (C-13, C-13'), 127.0 (C-14), 125.7 (C-12, C-12'), 121.0 (C-9, C-9'), 110.3 (C-3, C-4), 48.7 (C-10).

FT-IR (solid): $\tilde{\nu}$ (cm^{-1}) = 2962, 2031, 1477, 1409, 1358, 1322, 1259, 1097, 1068, 1008, 820, 776, 762, 715.

HR-MS (ESI): m/z calculated for $\text{C}_{23}\text{H}_{17}\text{Br}_2\text{N}+\text{H}^+$ 465.9801 $[\text{M}+\text{H}]^+$; observed 465.9800.

Synthesis of 1-benzyl-2,5-bis(4-nitrophenyl)-1H-pyrrole (72)



The reaction mixture was refluxed for 2 days and worked-up according to the general procedure. For purification column chromatography (n-hexane/EtOAc 6:1, $R_f = 0.43$) was performed. The product was obtained as a brown solid (528 mg, 1.32 mmol, 66% yield).

m.p.: 139 °C.

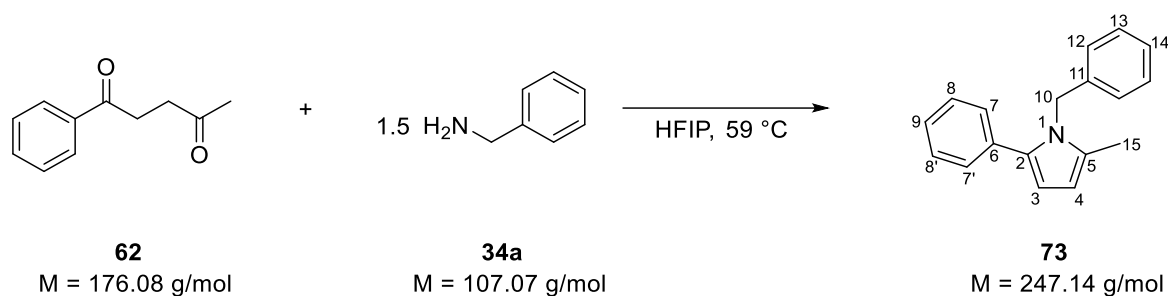
¹H-NMR (300 MHz, CD₂Cl₂): δ [ppm] = 8.20 (d, 4H, $J = 8.88$ Hz, 8-H, 8'-H), 7.56 (d, 4H, $J = 8.88$ Hz, 7-H, 7'-H), 7.17-7.10 (m, 3H, 13-H, 13'-H, 14-H), 6.67-6.61 (m, 2H, 12-H, 12'-H), 6.59 (s, 2H, 3-H, 4-H), 5.32 (s, 2H, 10-H, the signal overlaps with the solvent residue proton signal).

¹³C-NMR (75 MHz, CD₂Cl₂): δ [ppm] = 146.6 (C-9), 139.3 (C-11), 137.9 (C-6, C-6'), 137.0 (C-2, C-5), 128.9 (C-7, C-7'), 128.6 (C-13, C-13'), 127.4 (C-14), 125.7 (C-10), 123.8 (C-8, C-8'), 112.9 (C-3, C-4), 49.5 (C-10).

FT-IR (solid): $\tilde{\nu}$ (cm⁻¹) = 2960, 2921, 2851, 1590, 1508, 1337, 1258, 1012, 792, 750, 697, 678.

HR-MS (EI): m/z calculated for C₂₃H₁₇N₃O₄ 399.1214 [M]⁺; observed 399.1212.

Synthesis of 1-benzyl-2-methyl-5-phenyl-1H-pyrrole (73)



The reaction was refluxed for 2 days and worked-up according to the general procedure. For purification column chromatography (Hexane/EtOAc, 20:1, $R_f = 0.46$) was performed. The product was obtained as a slightly yellow oil (175 mg, 1.42 mmol, 71% yield).

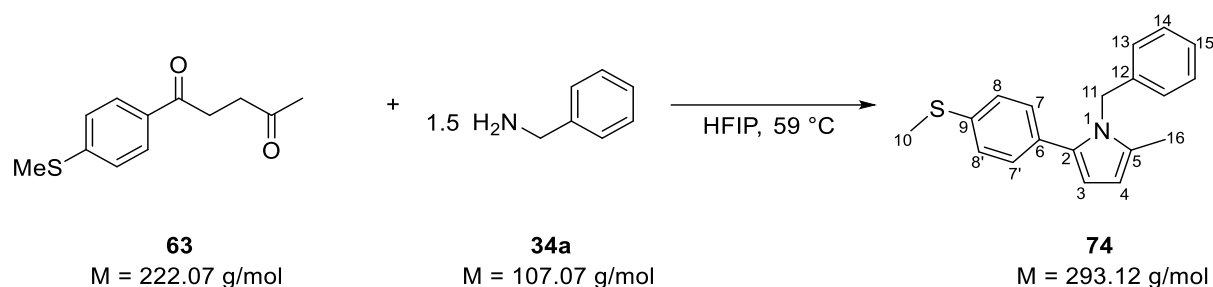
$^1\text{H-NMR}$ (300 MHz, CD_2Cl_2): δ [ppm] = 7.35-7.19 (m, 9H, 7-H, 7'-H, 8-H, 8'-H, 9-H, 13-H, 13'-H, 14-H), 6.89 (d, 2H, $J = 8.19$ Hz, 12-H, 12'-H), 6.18 (d, 1H, $J = 3.45$ Hz, 3-H), 6.01 (dd, 1H, $J = 3.45$ Hz, $J = 0.84$ Hz, 4-H), 5.15 (s, 2H, 10-H), 2.14 (s, 3H, 15-H).

$^{13}\text{C-NMR}$ (75 MHz, CD_2Cl_2): δ [ppm] = 139.1 (C-2), 134.4 (C-11), 133.9 (C-6), 130.5 (C-5), 128.6 (C-8), 128.5 (C-9), 128.3 (C-7), 126.9 (C-14), 126.5 (C-12), 125.6 (C-13), 108.0 (C-3), 107.2 (C-4), 47.5 (C-10), 12.3 (C-15).

FT-IR (solid): $\tilde{\nu}$ (cm^{-1}) = 2914, 1601, 1512, 1495, 1474, 1452, 1444, 1406, 1354, 1310, 1073, 1026, 748, 726, 695, 574, 536, 458.

HR-MS (ESI): m/z calculated for $\text{C}_{18}\text{H}_{17}\text{N}+\text{H}^+$ 248.1434 $[\text{M}+\text{H}]^+$; observed 248.1437.

Synthesis of 1-benzyl-2-methyl-5-(4-(methylthio)phenyl)-1H-pyrrole (74)



The reaction was refluxed for 2 days and worked-up according to the general procedure. For purification column chromatography (n-hexane/EtOAc, 20:1, $R_f = 0.64$) was performed. The product was obtained as an off-white solid (232 mg, 1.58 mmol, 79% yield).

m.p.: 87.9 °C.

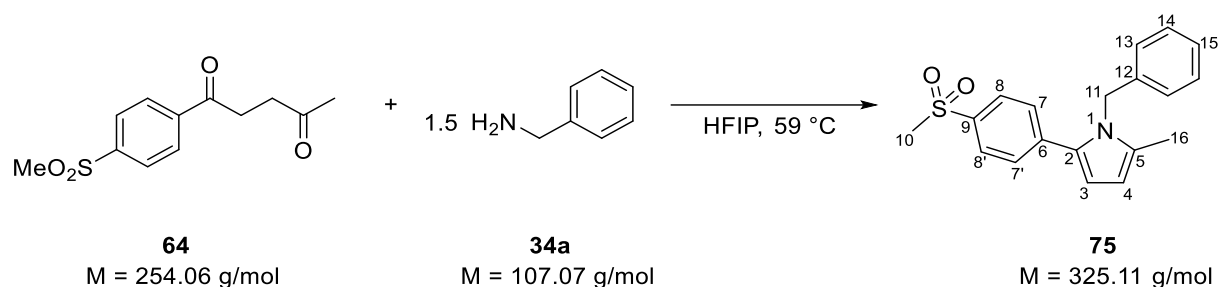
$^1\text{H-NMR}$ (300 MHz, CD_2Cl_2): δ [ppm] = 7.33-7.14 (m, 7H, C-8, C-13, C-13', C-14, C-14', C-15), 6.89 (d, 2H, $J = 6.84$ Hz, 7-H, 7'-H), 6.16 (d, 1H, $J = 3.45$ Hz, 3-H), 6.00 (dd, 1H, $J = 3.45$ Hz, $J = 0.78$ Hz, 4-H), 5.12 (s, 2H, 11-H), 2.45 (s, 3H, 10-H), 2.13 (s, 3H, 16-H).

$^{13}\text{C-NMR}$ (75 MHz, CD_2Cl_2): δ [ppm] = 139.1 (C-2), 130.7 (C-5), 130.3 (C-12), 128.8 (C-14), 128.6 (C-7), 126.9 (C-15), 126.4 (C-13), 125.8 (C-8), 125.4 (C-6), 107.9 (C-3), 107.2 (C-4), 47.5 (C-11), 15.5 (C-10), 12.3 (C-16).

FT-IR (solid): $\tilde{\nu}$ (cm^{-1}) = 2917, 1510, 1496, 1434, 1414, 1356, 1311, 1105, 1029, 818, 760, 727, 694.

HR-MS (ESI): m/z calculated for $\text{C}_{19}\text{H}_{19}\text{NS}+\text{H}^+$ 294.1311 $[\text{M}+\text{H}]^+$; observed 294.1314.

Synthesis of 1-benzyl-2-methyl-5-(4-(methylsulfonyl)phenyl)-1H-pyrrole (75)



The reaction was refluxed for 2 days and worked-up according to the general procedure. For purification column chromatography (n-hexane/EtOAc, 2:1, $R_f = 0.55$) was performed. The product was obtained as a yellow solid (254 mg, 1.56 mmol, 78% yield).

m.p.: 140.4 °C.

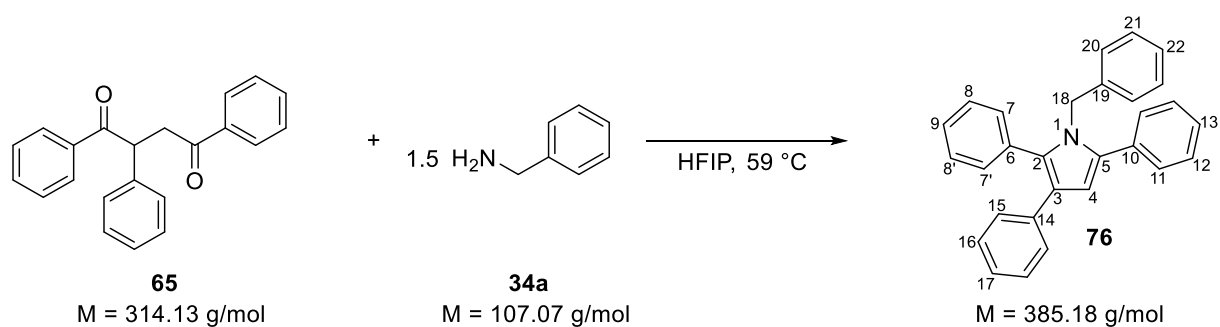
$^1\text{H-NMR}$ (300 MHz, CD_2Cl_2): δ [ppm] = 7.80 (d, 2H, $J = 8.31$ Hz, 7-H, 7'-H), 7.46 (d, 2H, $J = 8.31$ Hz, 8-H, 8'-H), 7.35-7.21 (m, 3H, 14-H, 14'-H, 15-H), 6.91 (d, 2H, $J = 7.29$ Hz, 13-H, 13'-H), 6.36 (d, 1H, $J = 3.57$ Hz, 3-H), 6.08 (d, 1H, $J = 3.57$ Hz, 4-H), 5.19 (s, 2H, 11-H), 3.00 (s, 3H, 10-H), 2.17 (s, 3H, 16-H).

$^{13}\text{C-NMR}$ (75 MHz, CD_2Cl_2): δ [ppm] = 139.1 (C-2), 138.5 (C-9), 137.9 (C-6), 132.9 (C-12), 132.5 (C-5), 128.8 (C-14, C-14'), 128.3 (C-8, C-8'), 127.5 (C-7, C-7'), 127.2 (C-15), 125.5 (C-13, C-13'), 110.3 (C-3), 108.1 (C-4), 47.8 (C-11), 44.4 (C-10), 12.3 (C-16).

FT-IR (solid): $\tilde{\nu}$ (cm^{-1}) = 2922, 1593, 1316, 1302, 1147, 964, 776, 761, 738, 726, 697.

HR-MS (ESI): m/z calculated for $\text{C}_{19}\text{H}_{19}\text{NO}_2\text{S}+\text{H}^+$ 326.1209 $[\text{M}+\text{H}]^+$; observed 326.1211.

Synthesis of 1-benzyl-2,3,5-triphenyl-1H-pyrrole (76)



The reaction was refluxed for 3 days and worked-up according to the general procedure. For purification column chromatography (n-hexane/EtOAc, 10:1, $R_f = 0.63$) was performed. The product was obtained as a white solid (285 mg, 1.48 mmol, 74% yield).

m.p.: 167.5 °C.

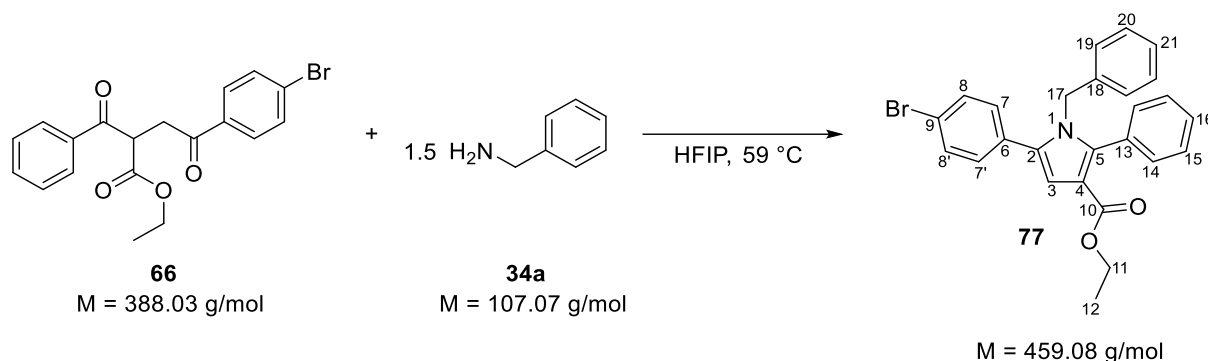
¹H-NMR (300 MHz, CD₂Cl₂): δ [ppm] 7.55-7.00 (m, 18H, 7-H, 7'-H, 8-H, 8'-H, 9-H, 11-H, 11'-H, 12-H, 12'-H, 13-H, 15-H, 15'-H, 16-H, 16'-H, 17-H, 21-H, 21'-H, 22-H), 6.66-6.61 (m, 2H, 20-H, 20'-H), 6.57 (s, 1H, 4-H), 5.13 (s, 2H, 18-H).

¹³C-NMR (75 MHz, CD₂Cl₂): δ [ppm] = 139.1 (C-2), 136.3 (C-10), 135.6 (C-19), 133.5 (C-6), 133.1 (C-14), 132.4 (C-5), 131.3 (C-8, C-8'), 129.0 (C-12, C-12'), 128.4 (C-16, C-16'), 128.4 (C-7, C-7'), 128.1 (C-15, C-15'), 128.0 (C-21, C-21'), 127.7 (C-9), 127.6 (C-11, C-11'), 127.1 (C-13), 126.7 (C-17), 125.9 (C-20, C-20'), 125.2 (C-22), 123.3 (C-3), 109.6 (C-4), 48.3 (C-18).

FT-IR (solid): $\tilde{\nu}$ (cm⁻¹) = 1600, 1450, 1341, 805, 766, 750, 740, 695.

HR-MS (EI): m/z calculated for C₂₉H₂₃N 385.1830 [M]⁺; observed 385.1835.

Synthesis of ethyl 1-benzyl-5-(4-bromophenyl)-2-phenyl-1H-pyrrole-3-carboxylate (77)



The reaction was refluxed for 3 days and worked-up according to the general procedure. For purification column chromatography (n-hexane/EtOAc, 10:1, $R_f = 0.30$) was performed. The product was obtained as a colorless oil (377 mg, 1.64 mmol, 82% yield).

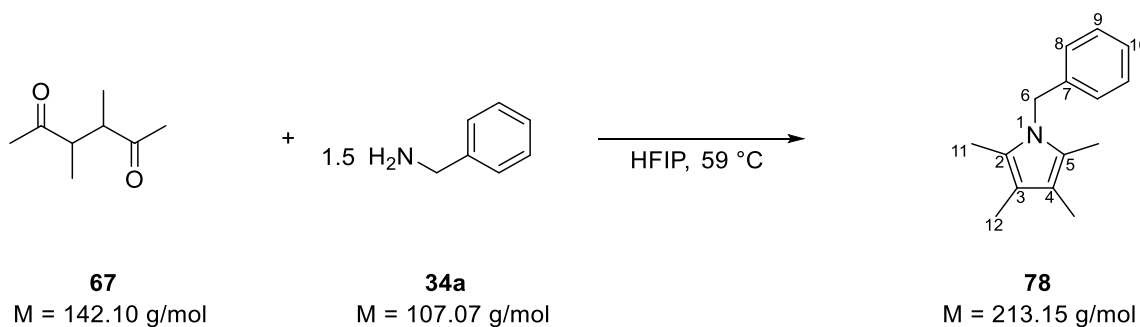
$^1\text{H-NMR}$ (300 MHz, CD_2Cl_2): δ [ppm] = 7.47 (d, 2H, $J = 8.55$ Hz, 14-H, 14'-H), 7.40-7.20 (m, 7H, 7-H, 7'-H, 8-H, 8'-H, 9-H, 15-H, 15'-H), 7.19-7.07 (m, 3H, 20-H, 20'-H, 21-H), 6.79 (s, 1H, 4-H), 6.66-6.57 (m, 2H, 19-H, 19'-H), 5.05 (s, 2H, 17-H), 4.10 (q, 2H, $J = 7.12$ Hz, 11-H), 1.12 (t, 3H, $J = 7.12$ Hz, 12-H).

$^{13}\text{C-NMR}$ (75 MHz, CD_2Cl_2): δ [ppm] = 164.2 (C-10), 140.2 (C-13), 138.0 (C-18), 133.8 (C-6), 132.0 (C-2), 131.7 (C-5), 131.6 (C-14, C-14'), 130.8 (C-7, C-7', C-8, C-8'), 128.3 (C-20, C-20'), 128.3 (C-9), 127.7 (C-15, C-15'), 127.1 (C-21), 125.7 (C-19, C-19'), 121.7 (C-3), 114.4 (C-4), 111.2 (C-16), 59.4 (C-11), 48.5 (C-17), 13.9 (C-12).

FT-IR (solid): $\tilde{\nu}$ (cm^{-1}) = 1712, 1474, 1454, 1413, 1267, 1176, 1100, 1073, 1035, 984, 836, 823, 778, 759, 736, 720, 706, 696.

HR-MS (EI): m/z calculated for $\text{C}_{26}\text{H}_{22}\text{BrNO}_2$ 459.0834 $[\text{M}]^+$; observed 459.0830.

Synthesis of 1-benzyl-2,3,4,5-tetramethyl-1H-pyrrole (78)



The reaction was stirred for 5 minutes and worked-up according to the general procedure. For purification column chromatography (n-hexane/EtOAc, 10:1, $R_f = 0.85$) was performed. The product was obtained as a reddish oil (175 mg, 1.64 mmol, 82% yield).

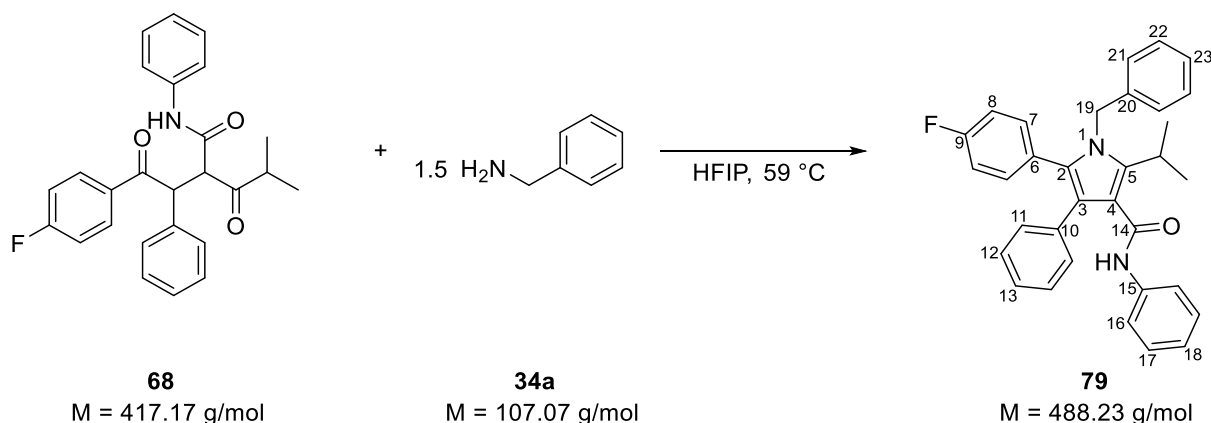
$^1\text{H-NMR}$ (300 MHz, CD_2Cl_2): δ [ppm] = 7.32-7.19 (m, 3H, 9-H, 9'-H, 10-H), 6.88 (d, 2H, $J = 6.9$ Hz, 8-H, 8'-H), 4.96 (s, 2H, 6-H), 2.03 (s, 6H, 11-H, 11'-H), 1.94 (s, 6H, 12-H, 12'-H).

$^{13}\text{C-NMR}$ (75 MHz, CD_2Cl_2): δ [ppm] = 139.6 (C-7), 128.5 (C-9, C-9'), 126.7 (C-2, C-5), 125.8 (C-8, C-8'), 122.3 (C-10), 113.0 (C-3, C-4), 46.7 (C-6), 9.5 (C-11, C-11'), 9.2 (C-12, C-12').

FT-IR (solid): $\tilde{\nu}$ (cm^{-1}) = 2916, 2857, 1643, 1495, 1453, 1393, 1351, 1215, 1190, 1101, 1029, 729, 695.

HR-MS (ESI): m/z calculated for $\text{C}_{15}\text{H}_{19}\text{N}+\text{H}^+$ 214.1590 $[\text{M}+\text{H}]^+$; observed 214.1589.

Synthesis of 1-benzyl-5-(4-fluorophenyl)-2-isopropyl-N,4-diphenyl-1H-pyrrole-3-carboxamide (79)



The reaction mixture was heated for 3 days in a pressure tube at 95 °C. Afterwards, the reaction mixture was diluted with ⁱPrOH and acetone (1:1, ca. 15 mL) and cooled to 0 °C. The precipitated solid was isolated by filtration, washed with cold water to remove trace solvents, and dried under vacuum to afford the desired product. The product was obtained as a yellow crystalline solid (344 mg, 0.68 mmol, 34% yield).

m.p.: 219 °C.

¹H-NMR (300 MHz, CD₂Cl₂): δ [ppm] = 7.37-6.84 (m, 19, H, 6-H, 6'-H, 7-H, 7'-H, 10-H, 10'-H, 11-H, 11'-H, 12-H, 15-H, 15'-H, 16-H, 16'-H, 17-H, 22-H, 22'-H, 23-H, 23'-H, 24-H), 5.09 (s, 2H, 20-H), 3.24 (sept, 1H, 18-H), 1.36 (d, 6H, *J* = 6.81 Hz, 19-H, 19'-H).

¹³C-NMR (75 MHz, CD₂Cl₂): δ [ppm] = 160.68 (C-14), 141.31 (C-4), 138.53 (C-9), 138.47 (C-14), 134.83 (C-21), 133.17 (C-7, C-7'), 130.46 (C-11, C-11'), 129.34 (C-1), 128.63 (C-6, C-6'), 128.29 (C-10, C-10'), 128.04 (C-5), 127.20 (C-12), 126.54 (C-17), 125.52 (C-23, C-23'), 123.47 (C-22, C-22'), 121.80 (C-2), 119.46 (C-16, C-16'), 116.12 (C-3), 115.16 (C-24), 114.87 (C-15, C-15'), 47.91 (C-20), 26.63 (C-18), 21.13 (C-19, C-19').

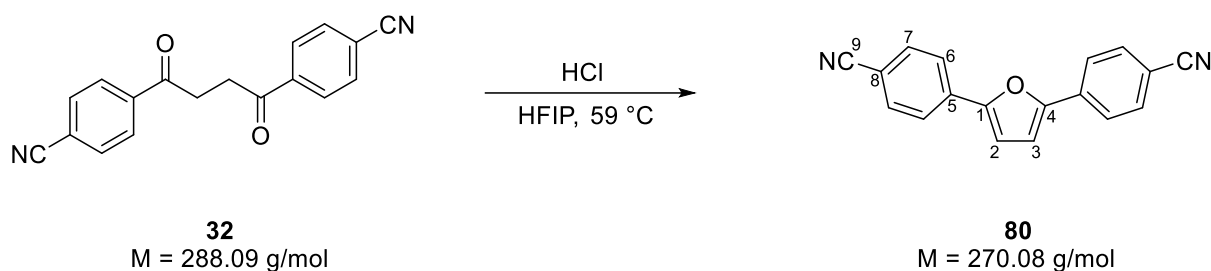
¹⁹F-NMR (282 MHz, CD₂Cl₂): δ [ppm] = -114.44.

FT-IR (solid): $\tilde{\nu}$ (cm⁻¹) = 3403, 2962, 1661, 1595, 1563, 1525, 1496, 1437, 1309, 1242, 1217, 1154, 845, 752, 736, 693.

HR-MS (ESI): *m/z* calculated for C₃₃H₂₉FN₂O+H⁺ 489.2337 [M+H]⁺; observed 489.2338.

General procedure for the synthesis of 2,5-substituted Furans or Thiophenes: The 1,4-diketone (2 mmol) was dissolved in 4-10 mL 1,1,1,3,3,3-hexafluoroisopropanol at ambient temperature. Hydrochloric acid (catalytic amounts) for furans or Lawesson's reagent (3.5 mmol) for thiophenes was added slowly and the mixture was stirred for the indicated time under reflux conditions. The reaction mixture was allowed to cool to room temperature and the solvent was removed. The residue was dissolved in an appropriate solvent and the insoluble solids were removed by filtration. The organic phase was dried over MgSO_4 and the solvent was removed under reduced pressure. The residue was purified with an appropriate method (column chromatography or recrystallization).

Synthesis of 4,4'-(furan-2,5-diyl)dibenzonitrile (**80**)



The reaction was refluxed for 2 h and worked-up according to the general procedure. For purification, the crude product was recrystallized from THF. The product was obtained as a yellow solid (238 mg, 0.88 mmol, 88% yield).

m.p.: 292.1 °C.

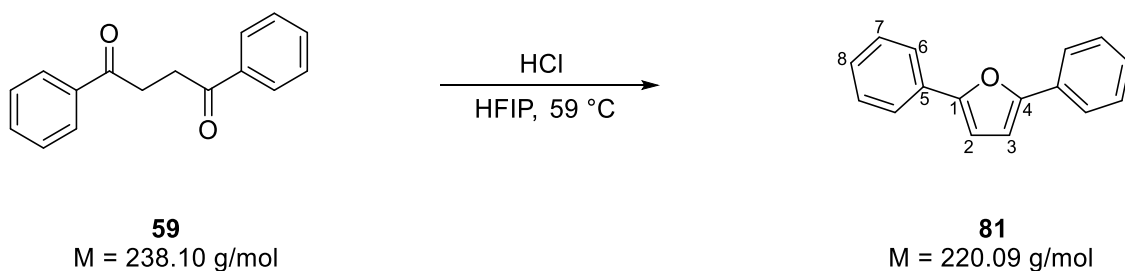
¹H-NMR (300 MHz, CD₂Cl₂): δ [ppm] = 7.86 (d, 4H, *J* = 8.7 Hz, 6-H, 6-H, 6'-H, 6'-H), 7.72 (d, 4H, *J* = 8.7 Hz, 7-H, 7-H, 7'-H, 7'-H), 6.99 (s, 2H, 2-H, 3-H).

¹³C-NMR (75 MHz, CD₂Cl₂): δ [ppm] = 152.8 (C-1, C-4), 133.8 (C-5, C-5'), 132.7 (7-C, 7-C, 7'-C, 7'-C), 124.1 (6-C, 6-C, 6'-C, 6'-C), 118.7 (9-C, 9'-C), 110.9 (8-C, 8'-C), 110.7 (2-C, 3-C).

FT-IR (solid): $\tilde{\nu}$ (cm⁻¹) = 3352, 2222, 1605, 842, 792, 664.

HR-MS (ESI): *m/z* calculated for C₁₈H₁₀N₂O+Na⁺ 293.0685 [M+Na]⁺; observed 293.0678.

Synthesis of 2,5-diphenylfuran (81)



The reaction was refluxed for 3 h and worked-up according to the general procedure. For purification column chromatography (n-hexane/EtOAc, 10:1, $R_f = 0.85$) was performed. The product was obtained as a white solid (176 mg, 0.80 mmol, 80% yield).

m.p.: 91 °C.

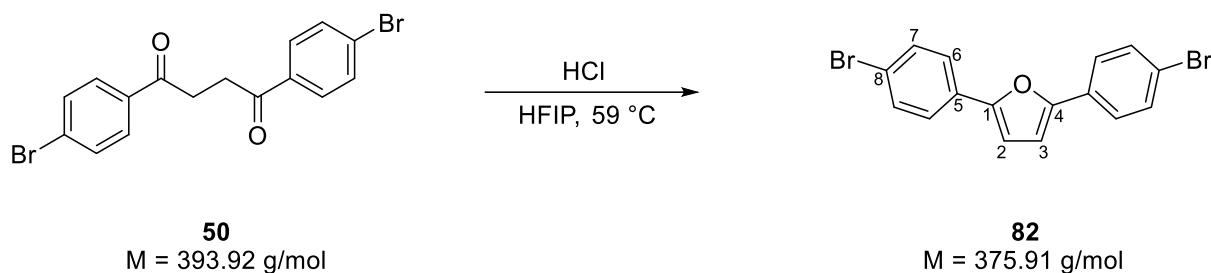
$^1\text{H-NMR}$ (300 MHz, CD_2Cl_2): δ [ppm] = 7.79 (d, 4H, $J = 7.29$ Hz, 6-H, 6'-H), 7.45 (t, 4H, $J = 7.29$ Hz, 7-H, 7'-H), 7.31 (7, 2H, $J = 7.29$ Hz, 8-H, 8'-H), 6.80 (s, 2H, 2-H, 3-H).

$^{13}\text{C-NMR}$ (75 MHz, CD_2Cl_2): δ [ppm] = 155.3 (C-1, C-4), 130.7 (C-5, C-5'), 128.7 (C-7, C-7'), 127.4 (C-8, C-8'), 123.6 (C-6, C-6'), 107.3 (C-2, C-3).

FT-IR (solid): $\tilde{\nu}$ (cm^{-1}) = 3039, 1610, 1488, 1480, 1260, 1021, 928, 794, 754, 689, 671.

HR-MS (EI): m/z calculated for $\text{C}_{16}\text{H}_{12}\text{O}$: 220.0888 $[\text{M}]^+$; observed 220.0890.

Synthesis of 2,5-bis(4-bromophenyl)furan (82)



The reaction was refluxed for 2 h and worked-up according to the general procedure. For purification, the crude product was recrystallized from THF. The product was obtained as colorless needles (342 mg, 0.91 mmol, 91% yield).

m.p.: 205.9 °C.

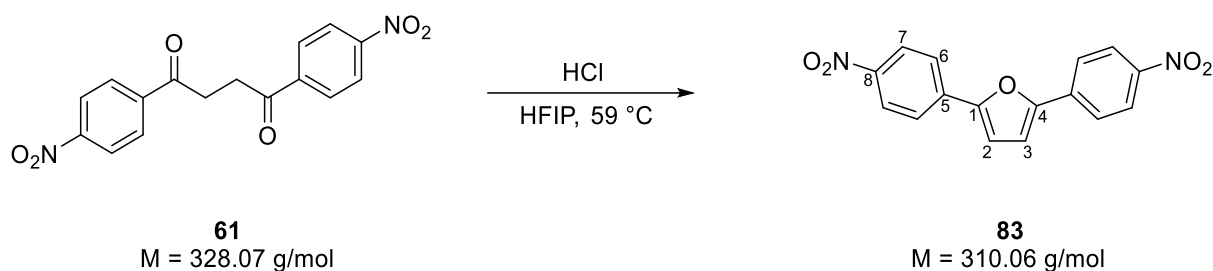
¹H-NMR (300 MHz, DMSO-*d*₆): δ [ppm] = 7.79 (d, 4H, *J* = 8.58 Hz, 7-H, 7-H, 7'-H, 7'-H), 7.65 (d, 4H, *J* = 8.58 Hz, 6-H, 6-H, 6'-H, 6'-H), 7.17 (s, 2H, 2-H, 3-H).

¹³C-NMR (75 MHz, DMSO-*d*₆): δ [ppm] = 152.4 (C-1, C-4), 132.3 (C-6, C-6, C-6', C-6'), 129.6 (C-5, C-5'), 126.0 (C-7, C-7, C-7', C-7'), 121.1 (C-8, C-8'), 109.7 (C-2, C-3).

FT-IR (solid): $\tilde{\nu}$ (cm⁻¹) = 1471, 1406, 1106, 1072, 1020, 1004, 924, 824, 790, 715, 669.

HR-MS (EI): *m/z* calculated for C₁₆H₁₀Br₂O: 375.9098 [M]⁺; observed 375.9104.

Synthesis of 2,5-bis(4-nitrophenyl)furan (83)



The reaction was refluxed for 2 h and worked-up according to the general procedure. For purification the crude product was recrystallized from THF. The product was obtained as an orange solid (264 mg, 0.85 mmol, 85% yield).

m.p.: 270.4 °C.

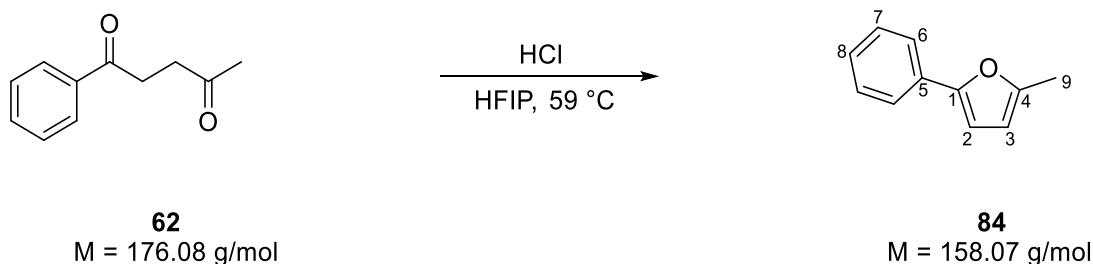
¹H-NMR (300 MHz, DMSO-*d*₆): δ [ppm] = 8.35 (d, 4H, *J* = 8.85 Hz, 7-H, 7-H, 7'-H, 7'-H), 8.15 (d, 4H, *J* = 8.85 Hz, 6-H, 6-H, 6'-H, 6'-H), 7.56 (s, 2H, 2-H, 3-H).

¹³C-NMR (75 MHz, DMSO-*d*₆): δ [ppm] = 153.0 (C-1, C-4), 135.7 (C-8, C-8'), 125.1 (C-7, C-7, C-7', C-7'), 125.0 (C-6, C-6, C-6', C-6'), 113.6 (C-5, C-5'), 100.0 (C-2, C-3).

FT-IR (solid): $\tilde{\nu}$ (cm⁻¹) = 3117, 1594, 1504, 1485, 1327, 1287, 1105, 1035, 930, 851, 792, 750, 690.

HR-MS (EI): *m/z* calculated for C₁₆H₁₀N₂O₅: 310.0584 [M]⁺; observed 310.0582.

Synthesis of 2-methyl-5-phenylfuran (84)



The reaction was refluxed for 6 h and worked-up according to the general procedure. For purification column chromatography (n-pentane, $R_f = 0.82$) was performed. The product was obtained as a slightly yellow oil (128 mg, 0.81 mmol, 81% yield).

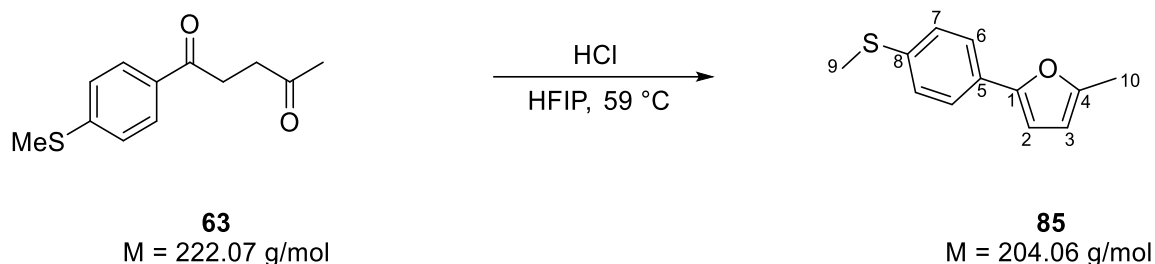
$^1\text{H-NMR}$ (300 MHz, CD_2Cl_2): δ [ppm] = 7.62 (d, 2H, $J = 7.38$ Hz, 7-H, 7'-H), 7.36 (t, 2H, $J = 7.77$ Hz, 8-H, 8'-H), 7.22 (t, 1H, $J = 7.95$ Hz, 9-H), 6.57 (d, 1H, $J = 3.20$ Hz, 3-H), 6.08 (d, 1H, $J = 3.20$ Hz, 2-H), 2.37 (s, 3H, 5-H).

$^{13}\text{C-NMR}$ (75 MHz, CD_2Cl_2): δ [ppm] = 152.1 (C-6), 131.1 (C-4), 128.6 (C-8, C-8'), 126.7 (C-9), 123.1 (C-7, C-7'), 107.6 (C-2), 105.9 (C-3), 100.0 (C-1), 13.4 (C-5).

FT-IR (solid): $\tilde{\nu}$ (cm^{-1}) = 2918, 1667, 1595, 1546, 1488, 1446, 1205, 1065, 1021, 784, 756, 589, 661.

HR-MS (EI): m/z calculated for $\text{C}_{11}\text{H}_{10}\text{O}$: 158.0732 $[\text{M}]^+$; observed 158.0728.

Synthesis of 2-methyl-5-(4-(methylthio)phenyl)furan (85)



The reaction was refluxed for 2 h and worked-up according to the general procedure. For purification column chromatography (n-hexane/EtOAc, 10:1, $R_f = 0.74$) was performed. The product was obtained as a yellow solid (177 mg, 0.87 mmol, 87% yield).

m.p.: 81.8 °C.

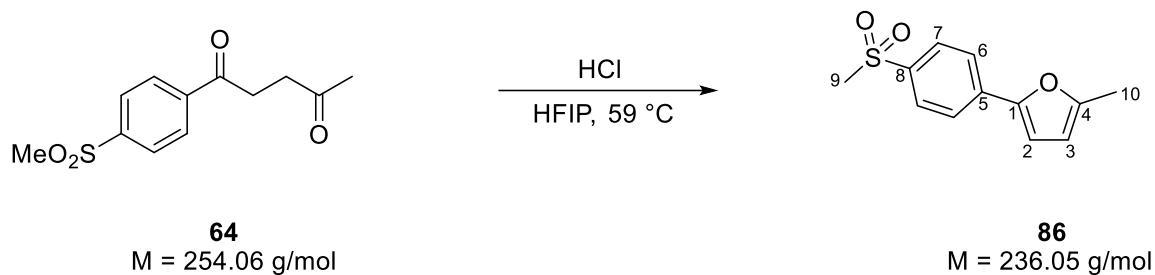
$^1\text{H-NMR}$ (300 MHz, CD_2Cl_2): δ [ppm] = 7.55 (d, 2H, $J = 8.55$ Hz, 6-H, 6'-H), 7.24 (d, 2H, $J = 8.55$ Hz, 5-H, 5'-H), 6.52 (d, 1H, $J = 3.18$ Hz, 2-H), 6.07 (d, 1H, $J = 3.18$ Hz, 3-H), 2.49 (s, 3H, 10-H), 2.35 (s, 3H, 9-H).

$^{13}\text{C-NMR}$ (75 MHz, CD_2Cl_2): δ [ppm] = 152.0 (C-1), 151.8 (C-4), 136.9 (C-8), 128.1 (C-5), 126.6 (C-6, C-6'), 123.6 (C-7, C-7'), 107.7 (C-3), 105.6 (C-2), 15.6 (C-9), 13.4 (C-10).

FT-IR (solid): $\tilde{\nu}$ (cm^{-1}) = 2912, 2402, 1689, 1553, 1492, 1433, 1073, 1020, 974, 793, 771.

HR-MS (EI): m/z calculated for $\text{C}_{12}\text{H}_{12}\text{OS}$: 204.0609 $[\text{M}]^+$; observed 204.0599.

Synthesis of 2-methyl-5-(4-(methylsulfonyl)phenyl)furan (86)



The reaction was refluxed for 4 h and worked-up according to the general procedure. For purification column chromatography (n-hexane/EtOAc, 4:1, $R_f = 0.74$) was performed. The product was obtained as a white solid (194 mg, 0.82 mmol, 82% yield).

m.p. (decomposition): 140 °C;

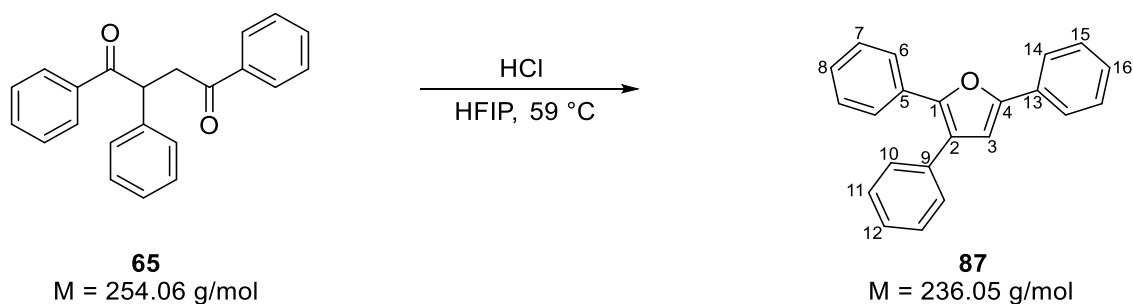
$^1\text{H-NMR}$ (300 MHz, CD_2Cl_2): δ [ppm] = 7.89 (d, 2H, $J = 8.61$ Hz, 6-H, 6'-H), 7.79 (d, 2H, $J = 8.61$ Hz, 7-H, 7'-H), 6.78 (d, 1H, $J = 3.29$ Hz, 2-H), 6.15 (dd, 1H, $J = 3.29$ Hz, $J = 0.87$ Hz, 3-H), 3.04 (s, 3H, 9-H), 2.39 (s, 3H, 10-H).

$^{13}\text{C-NMR}$ (75 MHz, CD_2Cl_2): δ [ppm] = 154.2 (C-5), 150.3 (C-4), 138.0 (C-8), 135.8 (C-1), 127.9 (C-6, C-6'), 123.4 (C-7, C-7'), 109.4 (C-2), 108.4 (C-3), 44.5 (C-9), 13.5 (C-10).

FT-IR (solid): $\tilde{\nu}$ (cm^{-1}) = 2919, 1590, 1300, 1279, 1143, 1089, 1026, 835, 796, 775.

HR-MS (ESI): m/z calculated for $\text{C}_{12}\text{H}_{12}\text{O}_3\text{S}+\text{H}^+$ 237.0580 $[\text{M}+\text{H}]^+$; observed 237.0582.

Synthesis of 2,3,5-triphenylfuran (87)



The reaction was refluxed for 4 h and worked-up according to the general procedure. For purification column chromatography (n-hexane/EtOAc, 20:1, $R_f = 0.79$) was performed. The product was obtained as colorless crystals (207 mg, 0.70 mmol, 70% yield).

m.p.: 95 °C.

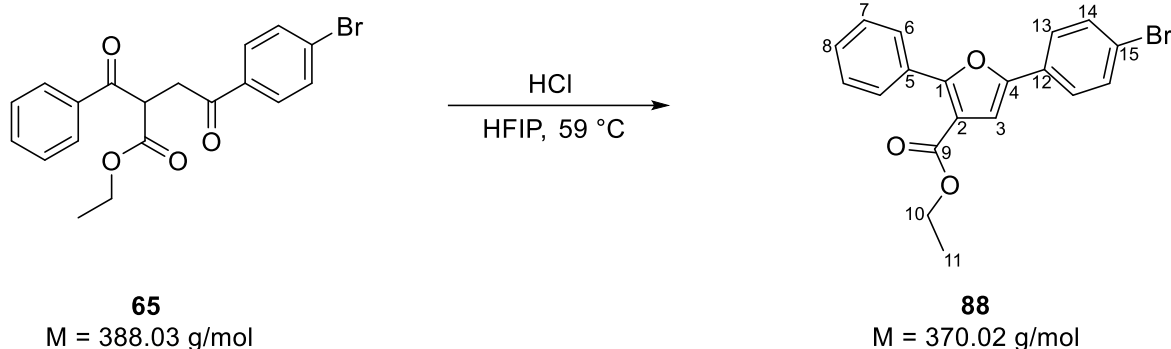
$^1\text{H-NMR}$ (300 MHz, CD_2Cl_2): δ [ppm] = 7.79 (d, 2H, $J = 7.71$ Hz, 14-H, 14'-H), 7.62 (d, 2H, $J = 7.17$ Hz, 6-H, 6'-H), 7.51-7.23 (m, 11H, 7-H, 7'-H, 8-H, 10-H, 10'-H, 11-H, 11'-H, 12-H, 15-H, 15'-H, 16-H), 6.87 (s, 1H, 2-H).

$^{13}\text{C-NMR}$ (75 MHz, CD_2Cl_2): δ [ppm] = 152.5 (C-13), 147.9 (C-1), 134.2 (C-9), 131.1 (C-13), 130.4 (C-5), 128.8 (C-10, C-10'), 128.7 (C-15, C-15'), 128.6 (C-7, C-7'), 127.4 (C-11, C-11'), 127.6 (C-16), 127.6 (C-8), 127.3 (C-12), 126.1 (C-6, C-6'), 124.6 (C-3), 123.7 (C-14, C-14'), 109.5 (C-2).

FT-IR (solid): $\tilde{\nu}$ (cm^{-1}) = 2922, 2360, 1487, 1143, 950, 804, 766, 753, 687, 568.

HR-MS (EI): m/z calculated for $\text{C}_{22}\text{H}_{16}\text{O}$ 296.1201 $[\text{M}]^+$; observed 296.1202.

Synthesis of ethyl 5-(4-bromophenyl)-2-phenylfuran-3-carboxylate (**88**)



The reaction was refluxed for 4 h and worked-up according to the general procedure. For purification column chromatography (n-hexane/EtOAc, 3:1, $R_f = 0.88$) was performed. The product was obtained as a colorless liquid (315 mg, 0.85 mmol, 85% yield).

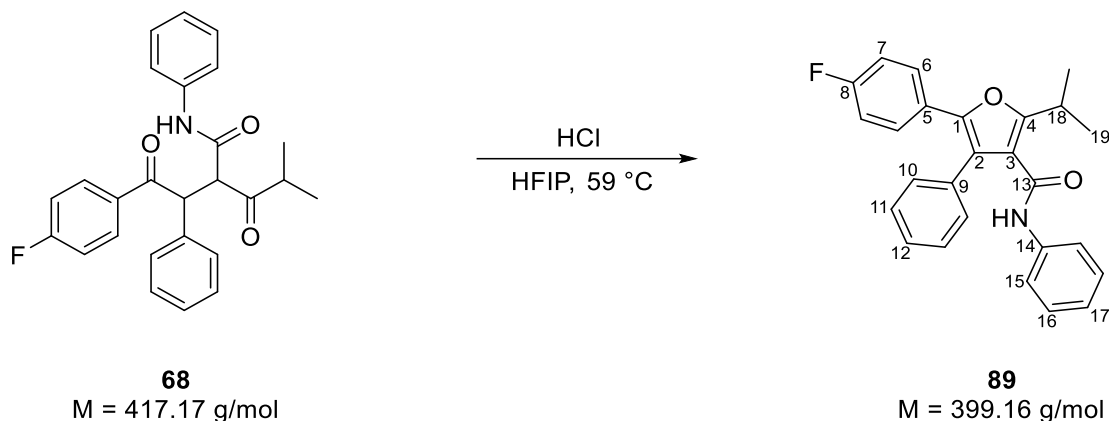
$^1\text{H-NMR}$ (300 MHz, CD_2Cl_2): δ [ppm] = 8.06 (d, 2H, $J = 8.34$ Hz, 13-H, 13'-H), 7.64 (d, 2H, $J = 8.58$ Hz, 6-H, 6'-H), 7.57 (d, 2H, $J = 8.58$ Hz, 7-H, 7'-H), 7.52-7.39 (m, 3H, 14-H, 14'-H, 15-H), 7.13 (s, 1H, 2-H), 4.31 (q, 2H, $J = 7.11$ Hz, 10-H), 1.35 (t, 3H, $J = 7.11$ Hz, 11-H).

$^{13}\text{C-NMR}$ (75 MHz, CD_2Cl_2): δ [ppm] = 163.1 (C-9), 156.5 (C-12), 151.3 (C-5), 132.0 (C-7, C-7'), 129.6 (C-1), 129.4 (C-15), 128.8 (C-4), 128.3 (C-13, C-13'), 128.1 (C-14, C-14'), 125.4 (C-6, C-6'), 121.8 (C-8), 116.1 (C-3), 108.5 (C-2), 60.7 (C-10), 14.0 (C-11).

FT-IR (solid): $\tilde{\nu}$ (cm^{-1}) = 2973, 2360, 1271, 1479, 1267, 1238, 1157, 1094, 1071, 825, 813, 776, 753, 683.

HR-MS (EI): m/z calculated for $\text{C}_{19}\text{H}_{16}\text{BrO}_3$ 371.0277 $[\text{M}]^+$; observed 371.0280.

Synthesis of 5-(4-fluorophenyl)-2-isopropyl-N,4-diphenylfuran-3-carboxamide (89)



The reaction was refluxed for 14 h and worked-up according to the general procedure. For purification column chromatography (n-hexane/EtOAc, 4:1, $R_f = 0.62$) was performed. The product was obtained as a brown solid (219 mg, 0.55 mmol, 55% yield).

m.p.: 160 °C.

$^1\text{H-NMR}$ (300 MHz, CD_2Cl_2): δ [ppm] = 7.38-7.21 (m, 8H, 11-H, 11'-H, 12-H, 15-H, 15'-H, 16-H, 16'-H, 17-H), 7.21-7.12 (m, 2H, 10-H, 10'-H), 6.89 (m, 2H, 6-H, 6'-H), 6.72 (m, 2H, 7-H, 7'-H), 2.43 (sept, 1H, $J = 6.78$ Hz, 18-H), 1.01 (d, 6H, $J = 6.78$ Hz, 19-H, 19'-H).

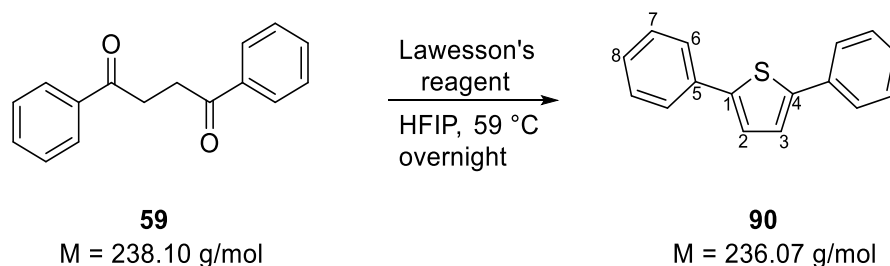
$^{13}\text{C-NMR}$ (75 MHz, CD_2Cl_2): δ [ppm] = 186.04 (C-4), 168.82 (C-13), 163.38 (C-8), 160.10 (C-1), 135.09 (C-14), 134.79 (C-9), 132.06 (C-6, C-6'), 130.77 (C-11, C-11'), 130.02 (C-15), 128.65 (C-16, C-16'), 128.10 (C-10, C-10'), 127.40 (C-15, C-15'), 127.33 (C-12), 127.10 (C-17), 116.55 (C-2), 114.60 (C-7, C-7'), 105.05 (C-3), 30.88 (C-18), 18.95 (C-19, C-19').

$^{19}\text{F-NMR}$ (282 MHz, CD_2Cl_2): δ [ppm] = -114.49.

FT-IR (solid): $\tilde{\nu}$ (cm^{-1}) = 2965, 1592, 1504, 1489, 1222, 1156, 1074, 845, 740, 704, 687.

HR-MS (ESI): m/z calculated for $\text{C}_{26}\text{H}_{22}\text{FNO}_2 + \text{H}^+$ 400.1707 $[\text{M} + \text{H}]^+$; observed 400.1699.

Synthesis of 2,5-diphenylthiophene (90)



1,4-Diphenylbutane-1,4-dione (**59**) (200.2 mg, 0.84 mmol, 1 equiv.) and Lawesson's Reagent (564.5 mg, 1.26 mmol, 3 equiv.) were dissolved in 1,1,1,3,3,3-hexafluoroisopropanol (6 mL) in an atmosphere of argon. The reaction mixture was refluxed for 18 hours. The solvent was evaporated and the yellow residue was purified with column chromatography (n-hexane/EtOAc 25:1, $R_f = 0.6$). The $^1\text{H-NMR}$ spectrum revealed a mixture of the product and the corresponding furan in a ratio of 4:1. 139.0 mg, 70% yield. After recrystallization from hexane the product was obtained as white crystals. 29.5 mg, 15% yield. A furan impurification of 2 % was detected by $^1\text{H-NMR}$ spectroscopy.

m.p.: 151.7 °C.

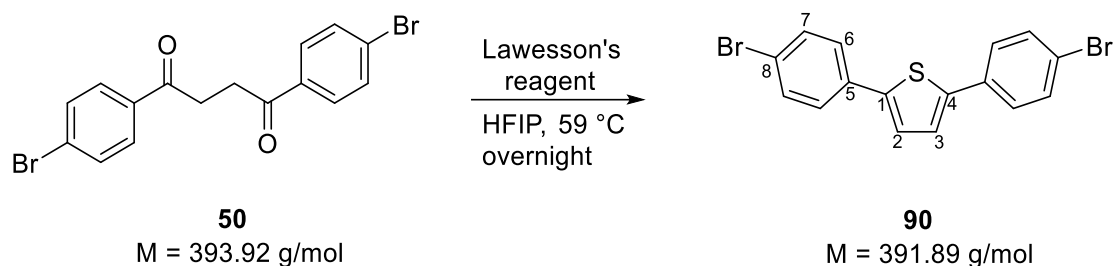
$^1\text{H-NMR}$ (300 MHz, CD_2Cl_2): δ [ppm] = 7.66 (d, 4H, $J = 7.26$ Hz, 7-H, 7'-H), 7.41 (t, 4H, $J = 7.26$ Hz, 8-H, 8'-H), 7.37-7.25 (m, 4H, 3-H, 4-H, 9-H, 9'-H).

$^{13}\text{C-NMR}$ (75 MHz, CD_2Cl_2): δ [ppm] = 143.5 (C-2, C-5), 134.2 (C-6, C-6'), 128.9 (C-8, C-8'), 127.6 (C-9, C-9'), 125.5 (C-7, C-7'), 124.1 (C-3, C-4).

FT-IR (solid): $\tilde{\nu}$ (cm^{-1}) = 2158, 1453, 939, 902, 803, 746, 682.

HR-MS (EI): m/z calculated for $\text{C}_{16}\text{H}_{12}\text{S}$ 236.0660 $[\text{M}]^+$; observed 236.0660.

Synthesis of 2,5-bis(4-Bromophenyl)thiophene (91)



1,4-bis(4-Bromo-phenyl)butane-1,4-dione (**50**) (402.3 mg, 1.0 mmol, 1 equiv.) and Lawesson's Reagent (636.2 mg, 1.5 mmol, 3 equiv.) were dissolved in 1,1,1,3,3,3-hexafluoroisopropanol (6 mL) in an atmosphere of argon. The reaction mixture was refluxed for 18 hours. The solvent was evaporated and the yellow residue was purified with column chromatography (n-hexane/EtOAc 25:1, $R_f = 0.55$). The product was obtained as a white white solid (328.5 mg, 0.83 mmol, 83 % yield).

m.p.: 206.5 °C;

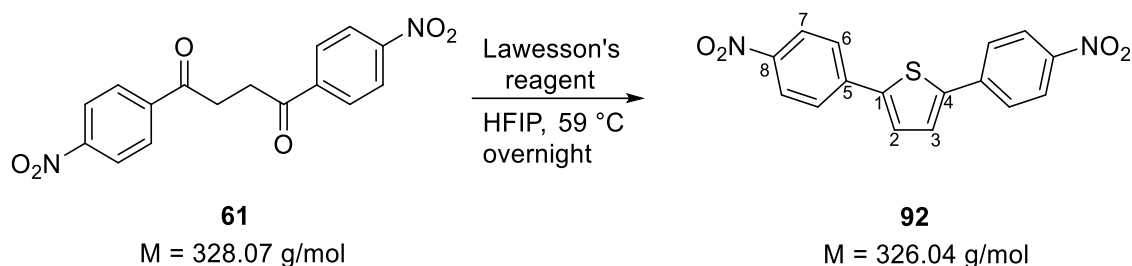
$^1\text{H-NMR}$ (300 MHz, CD_2Cl_2): δ [ppm] = 7.52 (s, 8H, 7-H, 7'-H, 8-H, 8'-H), 7.32 (s, 2H, 3-H, 4-H).

$^{13}\text{C-NMR}$ (75 MHz, CD_2Cl_2): δ [ppm] = 142.59 (C-2, C-5), 133.1 (C-6, C-6'), 132.0 (C-8, C-8'), 127.0 (C-7, C-7'), 124.6 (C-3, C-4), 121.4 (C-9, C-9').

FT-IR (solid): $\tilde{\nu}$ (cm^{-1}) = 3076, 1446, 1400, 1118, 934, 825, 794.

HR-MS (EI): m/z calculated for $\text{C}_{16}\text{H}_{10}\text{Br}_2\text{S}$ 391.8870 $[\text{M}]^+$; observed 391.8867.

Synthesis of 2,5-bis(4-Nitrophenyl)thiophene (**92**)



1,4-bis(4-Nitrophenyl)-butane-1,4-dione (**61**) (330 mg, 1.0 mmol, 1 equiv.) and Lawesson's Reagent (622.6 mg, 1.5 mmol, 3 equiv.) were dissolved in 1,1,1,3,3,3-hexafluoroisopropanol (6 mL) in an atmosphere of argon. The reaction mixture was refluxed for 8 hours. The solvent was evaporated and the yellow residue was refluxed in saturated sodium carbonate solution (20 mL) for 14 h. The suspension was then extracted with dichloromethane (3 × 30 mL). The combined organic layers were washed with saturated sodium carbonate solution (30 mL) and brine (30 mL). After drying over magnesium sulfate and evaporation of the solvent the product was obtained as a highly hygroscopic orange solid (270 mg, 0.82 mmol, 82% yield).

m.p. (decomposition): 257.0 °C.

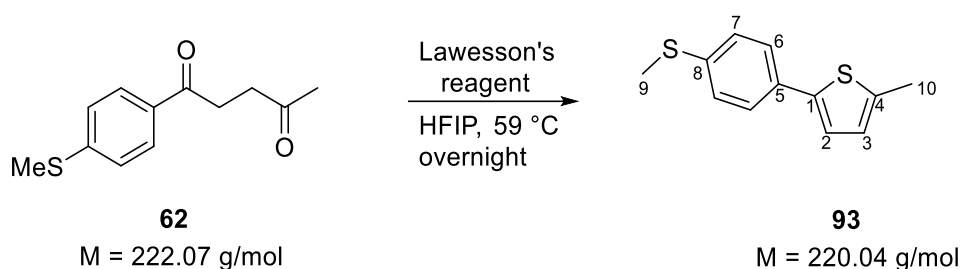
¹H-NMR (300 MHz, CD₂Cl₂): δ [ppm] = 8.28 (d, 4H, *J* = 8.89 Hz, 8-H, 8'-H), 7.83 (d, 4H, *J* = 8.91 Hz, 7-H, 7'-H), 7.57 (s, 2H, 3-H, 4-H).

¹³C-NMR could not be measured due to its low solubility in common organic solvents.

FT-IR (solid): $\tilde{\nu}$ (cm⁻¹) = 1587, 1506, 1335, 1278, 1107, 846, 796, 746, 682.

HR-MS (EI): *m/z* calculated for C₁₆H₁₀N₂O₄S 326.0361 [M]⁺; observed 326.0358.

Synthesis of 2-Methyl-5-(4-(methylthio)phenyl)thiophene (93)



1-(4-(Methylthio)phenyl)pentane-1,4-dione (**62**) (223.7 mg, 1.0 mmol, 1 equiv.) and Lawesson's Reagent (638.2 mg, 1.5 mmol, 3 equiv.) were dissolved in 1,1,1,3,3,3-hexafluoroisopropanol (6 mL) in an atmosphere of argon. The reaction mixture was refluxed for 20 hours. The solvent was evaporated and the yellow residue was purified with column chromatography (n-hexane/EtOAc 25:1, $R_f = 0.65$). The product was obtained as a light yellow solid (161.0 mg, 0.73 mmol, 73 % yield).

m.p.: 117.7 °C.

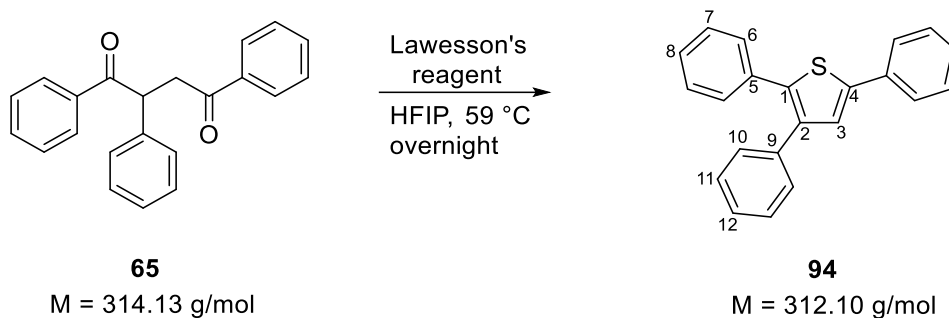
$^1\text{H-NMR}$ (300 MHz, CD_2Cl_2): δ [ppm] = 7.47 (d, 2 H, $J = 8.37$, 7-H, 7'-H), 7.23 (d, 2 H, $J = 8.34$ Hz, 8-H, 8'-H), 7.09 (d, 2H, $J = 3.51$ Hz, 4-H), 6.73 (d, 2 H, $J = 3.48$ Hz, 3-H), 2.49 (s, 6 H, 11-H, 12-H).

$^{13}\text{C-NMR}$ (75 MHz, CD_2Cl_2): δ [ppm] = 141.9 (C-9), 140.0 (C-5), 137.9 (C-2), 132.1 (C-6), 127.3 (C8), 126.8 (C-4), 126.2 (C-7), 123.2 (C-3), 16.2 (C-11), 15.7 (C-12).

FT-IR (solid): $\tilde{\nu}$ (cm^{-1}) = 2915, 1497, 1404, 1095, 944, 815, 796.

HR-MS (EI): m/z calculated for $\text{C}_{12}\text{H}_{12}\text{S}_2$ 220.0380 $[\text{M}]^+$; observed 220.0379.

Synthesis of 2,3,5-Triphenylthiophene (**94**)

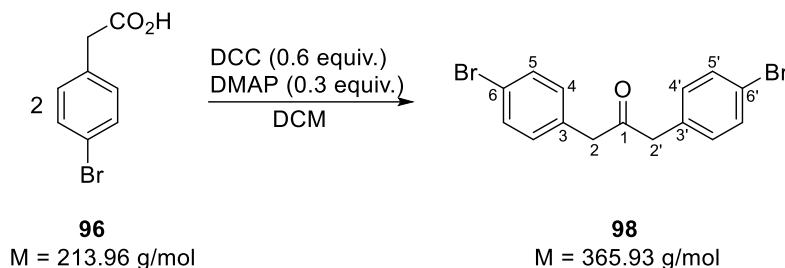


1,2,4-Triphenylbutane-1,4-dione (**65**) (317.2 mg, 1.0 mmol, 1 equiv.) and Lawesson's Reagent (609.4 mg, 1.5 mmol, 3 equiv.) were dissolved in 1,1,1,3,3,3-hexafluoroisopropanol (9 mL) in an atmosphere of argon. The reaction mixture was refluxed for 14 hours. The solvent was evaporated and the yellow residue purified with column chromatography (n-hexane/EtOAc 25:1, $R_f = 0.7$). The $^1\text{H-NMR}$ spectrum showed a mixture of the product and the corresponding furan in a ratio of 1:1. Recrystallization from n-hexane had no effect on the purity. The mixture was obtained as slightly yellow crystals (300.1 mg, 0.91 mmol, 91% yield).

HR-MS (EI): m/z calculated for $\text{C}_{22}\text{H}_{16}\text{S}$ 312.0973 $[\text{M}]^+$; observed 312.0974.

6.1.2.3 Syntheses for chapter 4.3

Synthesis of 1,3-bis(4-bromophenyl)propan-2-one (**98**)



DCC (0.5 g, 2.42 mmol, 0.6 equiv.) and DMAP (148 mg, 1.21 mmol, 0.3 equiv.) were dissolved in anhydrous DCM (20 mL) under an atmosphere of argon. 4-Bromophenylacetic acid (**96**) (1.73 g, 8.07 mmol, 2 equiv.) dissolved in anhydrous DCM (25 mL) was added slowly to the reaction mixture which turned orange and gas evolution was observed. The reaction mixture was stirred overnight. The precipitated DCU was removed by filtration through Celite, the filter cake was washed with MeCN (50 mL), and afterwards the solvents were removed from the combined organic phases. The yellow residue was dissolved in EtOAc (50 mL) and it was washed with 1 M HCl (50 mL) to remove DMAP, then with a saturated solution of NaHCO₃ (50 mL) to remove 4-Bromophenylacetic acid, then with a saturated solution of NaCl (50 mL) and the solvents were removed. The yellow residue was recrystallized from EtOH to give the desired product as slightly yellow needles (1.07 g, 2.92 mmol, 72% yield).

m.p.: 115 °C.

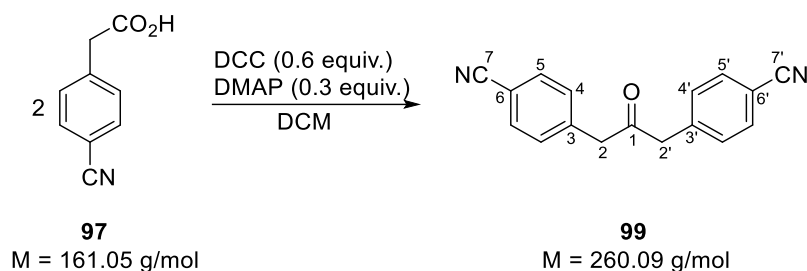
¹H-NMR (300 MHz, CDCl₃): δ (ppm) = 7.44 (d, 4H, *J* = 8.36 Hz, 5-H, 5'-H), 7.01 (d, 4H, *J* = 8.36 Hz, 4-H, 4'-H), 3.68 (s, 4H, 2-H, 2'-H).

¹³C-NMR (300 MHz, CDCl₃): δ (ppm) = 204.23 (C-1), 132.59 (C-3, C-3'), 131.86 (C-5, C-5'), 131.17 (C-4, C-4'), 121.27 (C-6, C-6'), 48.47 (C-2, C-2').

FT-IR (solid): $\tilde{\nu}$ (cm⁻¹) = 2970, 2359, 1738, 1712, 1506, 1471, 1413, 1365, 1336, 1216, 1052, 768, 688.

HR-MS (EI): *m/z* calculated for C₁₅H₁₂Br₂ONa [M+Na]⁺ 388.9147; observed 388.9145.

Synthesis of 1,3-bis(4-bromophenyl)propan-2-one (**99**)



DCC (1.57 g, 2.42 mmol, 0.6 equiv.) and DMAP (466 mg, 1.21 mmol, 0.3 equiv.) were dissolved in anhydrous DCM (40 mL) under an atmosphere of argon. 4-Bromophenylacetic acid (**96**) (2.05 g, 12.7 mmol, 2 equiv.) dissolved in anhydrous DCM (30 mL) was added slowly to the reaction mixture which turned orange and gas evolution was observed. The reaction mixture was stirred overnight. The precipitated DCU was removed by filtration through Celite, the filter cake was washed with MeCN (80 mL), and afterwards the solvents were removed from the combined organic phases. The yellow residue was dissolved in EtOAc (80 mL) and it was washed with 1 M HCl (60 mL) to remove DMAP, then with a saturated solution of NaHCO₃ (60 mL) to remove 4-Bromophenylacetic acid, then with a saturated solution of NaCl (60 mL) and the solvents were removed. The yellow residue was recrystallized from EtOH to give the desired product as slightly yellow needles (1.51 g, 9.4 mmol, 74% yield).

m.p.: 148 °C.

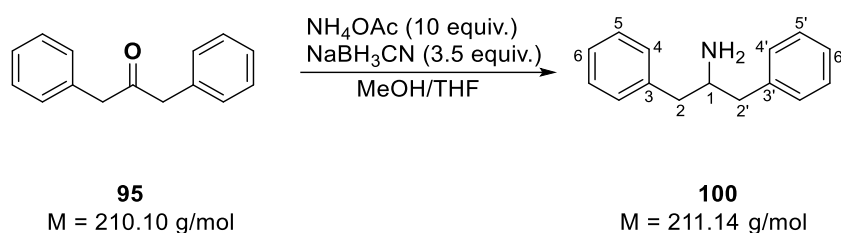
¹H-NMR (300 MHz, CDCl₃): δ (ppm) = 7.64 (d, 4H, *J* = 8.13 Hz, 5-H, 5'-H), 7.29 (d, 4H, *J* = 8.13 Hz, 4-H, 4'-H), 3.87 (s, 4H, 2-H, 2'-H).

¹³C-NMR (300 MHz, CDCl₃): δ (ppm) = 202.30 (C-1), 138.57 (C-3, C-3'), 132.48 (C-5, C-5'), 130.36 (C-4, C-4'), 118.53 (C-7, C-7'), 111.44 (C-6, C-6'), 49.21 (C-2, C-2').

FT-IR (solid): $\tilde{\nu}$ (cm⁻¹) = 2927, 2357, 2223, 1712, 1605, 1338, 1057, 848, 807.

HR-MS (EI): *m/z* calculated for C₁₇H₁₂N₂O [M-H]⁻ 259.0877; observed 259.0877.

Synthesis of 1,3-diphenylpropan-2-amine (100)



1,3-Diphenylacetone (**95**) (1 g, 4.76 mmol, 1 equiv.) was dissolved in a mixture of MeOH and THF (5:1, 45 mL) and NH_4OAc (6.70 g, 48 mmol, 10 equiv.) was added at once. The reaction mixture was stirred until all solids were dissolved, then NaBH_3CN (1.04 g, 16.7 mmol, 3.5 equiv.) was added in small portions over the course of 3 days. Afterwards, concentrated HCl was added to the reaction mixture until the vigorous evolution of HCN and H_2 ceased (HCN gas was bubbled through a solution of 13% NaOCl to convert it to the non-toxic NaOCN), the pH of the suspension was 1-2. All solvents were removed under reduced pressure and the off-white residue was suspended in a mixture of DCM and water (both 60 mL). The white precipitate was filtered off, this was the insoluble hydrochloride salt of the product. The solid was recrystallized from a mixture of *i*PrOH and EtOAc (1:1, ca. 25 mL). The product was obtained as a white solid (613 mg, 2.90 mmol, 61% yield).

m.p.: 197 °C (as the hydrochloride salt).

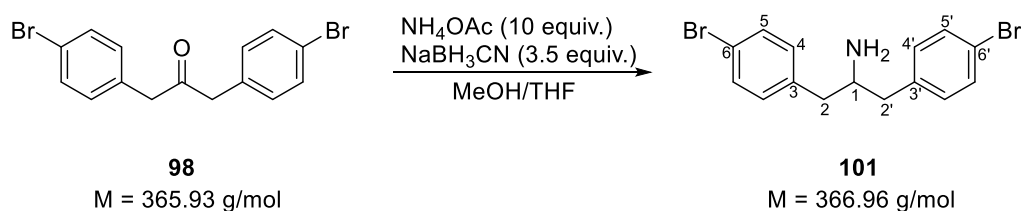
$^1\text{H-NMR}$ (300 MHz, DCM-d_2): δ (ppm) = 7.38-7.18 (m, 10H, 4-H, 5-H, 6-H), 3.32 (m, 1H, 1-H), 2.92-2.83 (m, 2H, 2-H, 2'-H), 2.64-2.54 (m, 2H, 2-H, 2'-H), 1.27 (br s, 2H, NH_2).

$^{13}\text{C-NMR}$ (300 MHz, DCM-d_2): δ (ppm) = 139.42 (C-3), 129.25 (C-5), 128.46 (C-4), 126.27 (C-6), 54.17 (C-1), 44.20 (C-2).

FT-IR (solid): $\tilde{\nu}$ (cm^{-1}) = 3409, 2962, 2359, 1738, 1453, 1366, 1217, 1054, 1032, 754, 701.

HR-MS (EI): m/z calculated for $\text{C}_{15}\text{H}_{18}\text{N}$ $[\text{M}+\text{H}]^+$ 212.1434; observed 212.1434.

Synthesis of 1,3-bis(4-bromophenyl)propan-2-amine (101)



1,3-Bis(4-bromophenyl)propan-2-one (**98**) (3 g, 8.20 mmol, 1 equiv.) was dissolved in a mixture of MeOH and THF (5:1, 200 mL) and NH_4OAc (6.32 g, 82 mmol, 10 equiv.) was added at once. The reaction mixture was stirred until all solids were dissolved, then NaBH_3CN (1.8 g, 28.7 mmol, 3.5 equiv.) was added in small portions over the course of 3 days. Afterwards, concentrated HCl was added to the reaction mixture until the vigorous evolution of HCN and H_2 ceased (HCN gas was bubbled through a solution of 13% NaOCl to convert it to the non-toxic NaOCN), the pH of the suspension was 1-2. All solvents were removed under reduced pressure and the off-white residue was suspended in a mixture of DCM and water (both 150 mL). The white precipitate was filtered off, this was the insoluble hydrochloride salt of the product. In order to produce the free base, the dried powder was suspended in a mixture of DCM and a saturated aqueous solution of K_2CO_3 (both 50 mL) and the mixture was stirred until all solids dissolved in the organic phase. The aqueous phase was extracted with DCM (2 x 20 mL) and the combined organic phases were dried over Na_2SO_4 . Removal of the solvent gave the product as a colorless oil (2.29 g, 6.24 mmol, 76% yield).

The transformation of the hydrochloride salt into the free base is critical for the success of the following reaction because the *in situ* formation of the free base gives rise to chloride-bromide exchange prior to a nucleophilic substitution.

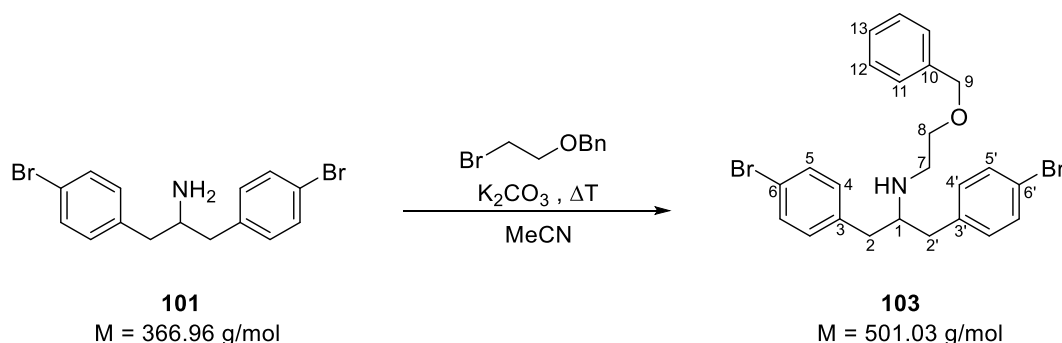
$^1\text{H-NMR}$ (300 MHz, DCM-d_2): δ (ppm) = 7.45 (d, 4H, $J = 8.36$ Hz, 5-H, 5'-H), 7.10 (d, 4H, $J = 8.36$ Hz, 4-H, 4'-H), 3.26 (m, 1H, 1-H), 2.86-2.72 (m, 2H, 2-H, 2'-H), 2.62-2.47 (m, 2H, 2-H, 2'-H), 1.64 (s, 2H, NH_2).

$^{13}\text{C-NMR}$ (75 MHz, DCM-d_2): δ (ppm) = 137.93 (C-3, C-3'), 131.63 (C-5, C-5'), 130.97 (C-4, C-4'), 120.33 (C-6, C-6'), 53.94 (C-1), 43.26 (C-2, C-2').

FT-IR (solid): $\tilde{\nu}$ (cm^{-1}) = 2970, 2359, 1735, 1365, 1215, 786, 668.

HR-MS (ESI): m/z calculated for $\text{C}_{15}\text{H}_{15}\text{Br}_2\text{N}$ $[\text{M}+\text{H}]^+$ 367.9644; observed 367.9647.

Synthesis of N-(2-(benzyloxy)ethyl)-1,3-bis(4-bromophenyl)propan-2-amine (103)



1,3-Bis(4-bromophenyl)propan-2-amine (**101**) (203 mg, 0.55 mmol, 1 equiv.) was dissolved in 15 mL MeCN. To this solution were added K_2CO_3 (190 mg, 1.38 mmol, 2.5 equiv.) and ((2-bromoethoxy)methyl)benzene (296 mg, 1.38 mmol, 2.5 equiv.). The reaction mixture was refluxed for 48 h and was then cooled to room temperature. The solids were removed by filtration and the reaction mixture was diluted with toluene (20 mL). The organic phase was washed with water (20 mL), brine (20 mL) and was dried over $MgSO_4$ and then the solvents were evaporated. The residue was purified by column chromatography (hexane/EtOAc 10:1 \rightarrow EtOAc, $R_f = 0.47$). The product was obtained as a yellow oil (192 mg, 0.38 mmol, 69%).

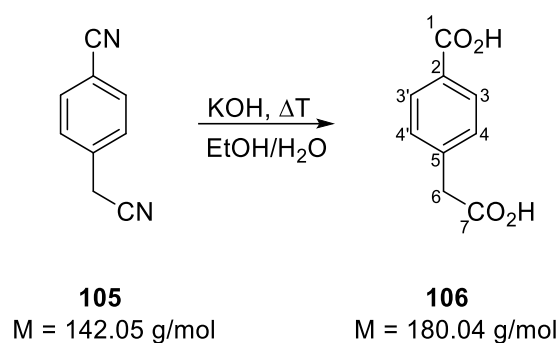
1H -NMR (300 MHz, CD_2Cl_2): δ (ppm) = 7.43 – 7.24 (7H, m, 5-H, 5'-H, 12-H, 13-H), 7.24-7.16 (m, 2H, 11-H), 7.07 (4H, d, $J = 8.4$ Hz, 4-H, 4'-H), 4.38 (s, 2H, 9-H), 3.49 (t, 2H, $J = 5.2$ Hz, 8-H), 3.02 (m, 1H, 1-H), 2.78 (t, 2H, $J = 5.2$ Hz, 7-H), 2.62 (t, 4H, $J = 6.48$ Hz, 2-H, 2'-H).

^{13}C -NMR (75 MHz, CD_2Cl_2): δ (ppm) = 139.01 (C-3, C-3'), 138.96 (C-10), 131.68 (C-4, C-4'), 131.60 (C-5, C-5'), 128.68 (C-12), 127.87 (C-11), 127.85 (C-13), 120.20 (C-6, C-6'), 73.21 (C-9), 70.29 (C-8), 60.59 (C-1), 47.12 (C-7), 40.24 (C-2, C-2').

FT-IR (solid): $\tilde{\nu}$ (cm^{-1}) = 3032, 2926, 2843, 1647, 1491, 1401, 1114, 1043, 1008, 745, 696, 458.

HR-MS (ESI): m/z calculated for $C_{24}H_{25}Br_2N$ $[M+H]^+$ 502.0376; observed 502.0373.

Synthesis of 4-(Carboxymethyl)benzoic acid (**106**)



4-(Cyanomethyl)benzonitrile (**105**) (20 g, 140.8 mmol, 1 equiv.) was dissolved in ethanol (150 mL) and a solution of KOH (36 g, 642.9 mmol, 4.6 equiv.) in water (150 mL) was added. The reaction mixture was refluxed overnight and afterwards ethanol was removed under reduced pressure. The aqueous phase was washed with DCM (2 x 50 mL) and was then acidified to pH 1 with concentrated HCl. The precipitated solid was filtered and dried. The product was obtained as an off-white solid (27 g, quant.) that was slightly contaminated with organic salts originating from neutralization of the alkaline aqueous phase.

m.p.: 230 °C.

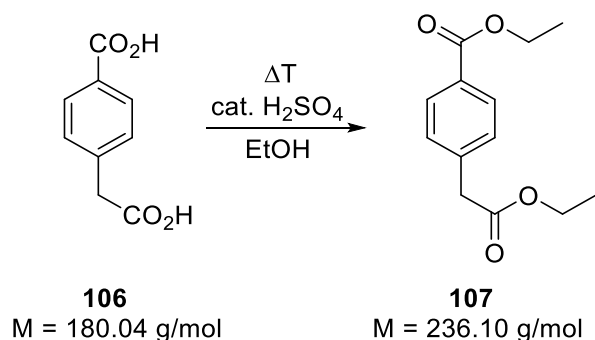
¹H-NMR (300 MHz, D₂O + NaOD): δ (ppm) = 7.65 (d, 2H, $J = 8.22$ Hz, 3-H, 3'-H), 7.16 (d, 2H, $J = 8.22$ Hz, 4-H, 4'-H), 4.31 (s, 2H, 6-H).

¹³C-NMR (75 MHz, D₂O + NaOD): δ (ppm) = 180.51 (C-7), 175.54 (C-1), 140.41 (C-5), 134.08 (C-2), 128.98 (C-3, C-3'), 128.84 (C-4, C-4').

FT-IR (solid): $\tilde{\nu}$ (cm⁻¹) = 2980, 1677, 1427, 1256, 1100, 1016, 934, 881, 730.

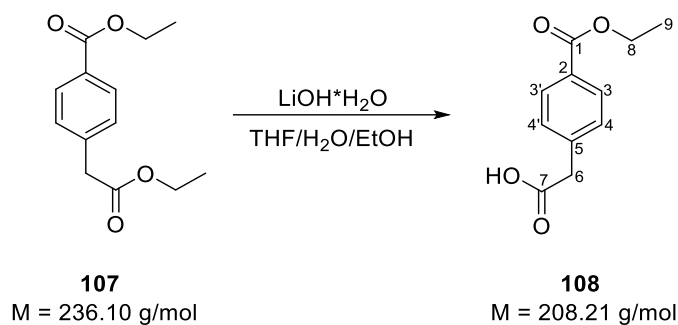
HR-MS (ESI): m/z calculated for C₉H₇O₄ [M-H]⁻ 179.0350; observed 179.0340.

Synthesis of Ethyl 4-(2-ethoxy-2-oxoethyl)benzoate (107)



4-(Carboxymethyl)benzoic acid (**106**) (27 g, contaminated with a small amount of inorganic salts) was suspended in EtOH (300 mL) and 10 mL of conc. H₂SO₄ was added slowly. The reaction mixture was refluxed overnight and afterwards ethanol was removed under reduced pressure. The oily residue was dissolved in a mixture of sat. NaHCO₃ solution (200 mL) and DCM (100 mL), the organic phase was separated. The aqueous phase was extracted with DCM (3 x 30 mL) and the combined organic phases were washed with water (100 mL) and dried over MgSO₄. The solvent was removed, and the oily residue was analyzed by means of TLC. Product formation was confirmed, alongside the formation of both mono-esterificated products and educt. Separation of this large amount of material (21.1 g) by column chromatography was deemed impossible and the crude product was used for the next reaction step without further purification.

Synthesis of 2-(4-(Ethoxycarbonyl)phenyl)acetic acid (**108**)



Ethyl 4-(2-ethoxy-2-oxoethyl)benzoate (**107**) (21.1 g, crude product) was dissolved in a mixture of THF/H₂O/EtOH (150 mL / 150 mL / 50 mL) and LiOH·H₂O (4.01 g, approx. 1.2 equiv.) was added. The resulting solution was stirred at room temperature overnight, after which THF and EtOH were removed under reduced pressure. The aqueous phase was washed with EtOAc (2 x 100 mL) and afterwards it was acidified to pH 1 with conc. HCl. The precipitated solid was isolated by filtration and dried under reduced pressure. The product was obtained as an off-white solid (17.05 g, 81.94 mmol).

m.p.: 100 °C.

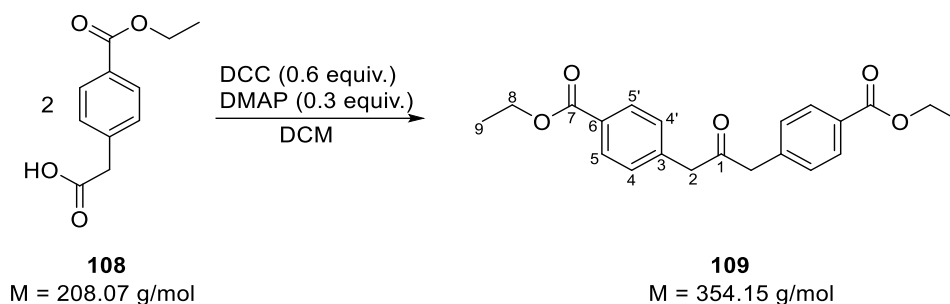
¹H-NMR (300 MHz, CD₂Cl₂): δ (ppm) = 8.00 (d, 2H, *J* = 8.15 Hz, 3-H, 3'-H), 7.37 (d, 2H, *J* = 8.15 Hz, 4-H, 4'-H), 4.35 (q, 2H, *J* = 7.09 Hz, 8-H), 3.74 (s, 2H, 6-H), 1.37 (t, 3H, *J* = 7.09 Hz, 9-H).

¹³C-NMR (75 MHz, CD₂Cl₂): δ (ppm) = 176.33 (C-7), 166.10 (C-1), 138.43 (C-5), 129.68 (C-2), 129.61 (C-3, C-3'), 129.47 (C-4, C-4'), 60.98 (C-8), 40.65 (C-6), 14.06 (C-9).

FT-IR (solid): $\tilde{\nu}$ (cm⁻¹) = 2980, 1691, 1408, 1270, 1170, 1099, 762, 712.

HR-MS (ESI): *m/z* calculated for C₁₁H₁₃O₄ [M+H]⁺ 209.0808; observed 209.0810.

Synthesis of Diethyl 4,4'-(2-oxopropane-1,3-diyl)dibenzoate (**109**)



2-(4-(Ethoxycarbonyl)phenyl)acetic acid (**108**) (11.55 g, 55.5 mmol, 2 equiv.) and DMAP (2.03 g, 16.7 mmol, 0.3 equiv.) were dissolved in anhydrous DCM (70 mL) under an atmosphere of argon. DCC (6.89 g, 33.3 mmol, 0.6 equiv.) dissolved in anhydrous DCM (100 mL) was added to the reaction mixture and the resulting suspension was stirred overnight. The precipitated DCU was removed by filtration over Celite, the filter cake was washed with MeCN (200 mL). The solvents were removed, and the residue was dissolved in a mixture of hexane/EtOAc (100 mL / 100 mL). The organic phase was washed with 1 M HCl to remove DMAP (80 mL), saturated aqueous NaHCO₃-solution (80 mL) and brine (100 mL) and was dried over MgSO₄. The solvents were removed under reduced pressure and the residue was recrystallized from EtOH. The product was obtained as slightly yellow crystals (4.5 g, 12.7 mmol, 46% yield).

m.p.: > 200 °C (decomposition).

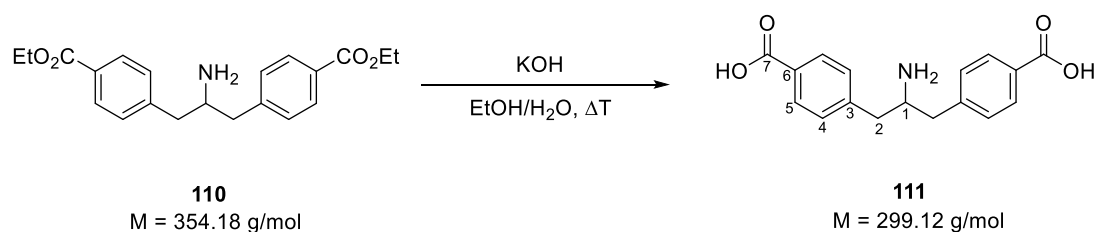
¹H-NMR (300 MHz, CD₂Cl₂): δ (ppm) = 7.98 (d, 4H, *J* = 8.16 Hz, 5-H, 5'-H), 7.24 (d, 4H, *J* = 8.16 Hz, 4-H, 4'-H), 4.34 (q, 4H, *J* = 7.11 Hz, 8-H, 8'-H), 3.83 (s, 4H, 2-H), 1.37 (t, 6H, *J* = 7.11 Hz, 9-H).

¹³C-NMR (75 MHz, CD₂Cl₂): δ (ppm) = 204.09 (C-1), 166.50 (C-7, C-7'), 139.39 (C-3, C-3'), 130.06 (C-5, C-5'), 130.03 (C-4, C-4'), 129.91 (C-6, C-6'), 61.34 (C-8, C-8'), 49.54 (C-2, C-2'), 14.50 (C-9, C-9').

FT-IR (solid): $\tilde{\nu}$ (cm⁻¹) = 2991, 1704, 1610, 1276, 1178, 1102, 1051, 1021, 859, 746, 714.

HR-MS (ESI): *m/z* calculated for C₂₁H₂₂O₅ [M+H]⁺ 355.1540; observed 355.1547.

Synthesis of 4,4'-(2-Aminopropane-1,3-diyl)dibenzoic acid (**111**)



Diethyl 4,4'-(2-aminopropane-1,3-diyl)dibenzoate (**110**) (0.25 g, 0.71 mmol, 1 equiv.) was dissolved in a mixture of EtOH/H₂O (1:1, 10 mL). KOH (142 mg, 3.55 mmol, 5 equiv.) was added and the reaction mixture was heated to reflux overnight. After cooling to room temperature, the solvents were removed *in vacuo*. The residue was taken up in H₂O (10 mL) and the solution was acidified to pH 1 with conc. HCl. The precipitated solid was filtered, washed with water until acid-free and dried *in vacuo*. The product was obtained as a white solid (106 mg, 0.36 mmol, 50 % yield).

m.p.: > 290 °C (decomposition).

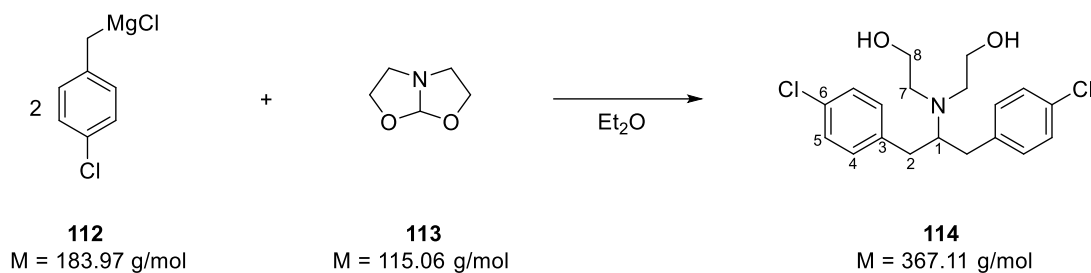
¹H-NMR (300 MHz, CD₂Cl₂): δ (ppm) = 8.27 (br s, 3H, NH₃⁺), 7.87 (d, 4H, *J* = 8.1 Hz, 5-H, 5'-H), 7.38 (d, 4H, *J* = 8.1 Hz, 4-H, 4'-H), 3.73 (m, 1H, 1-H, overlaps with residual water), 3.14-2.81 (m, 4H, 2-H, 2'-H, overlaps with residual water).

¹³C-NMR (75 MHz, CD₂Cl₂): δ (ppm) = 167.63 (C-7), 141.93 (C-3), 130.10 (C-5), 130.03 (C-4), 129.83 (C-6), 52.99 (C-1), 39.28 (C-2).

FT-IR (solid): $\tilde{\nu}$ (cm⁻¹) = 2913, 1695, 1604, 1382, 1230, 1184, 1119, 750, 694.

HR-MS (ESI): *m/z* calculated for C₁₇H₁₈NO₄ [M+H]⁺ 300.1230; observed 300.1225.

Synthesis of 2,2'-((1,3-bis(4-chlorophenyl)propan-2-yl)azanediyl)bis(ethan-1-ol) (114)



Tetrahydro-7aH-oxazolo[2,3-b]oxazole (**113**) (691 mg, 6.00 mmol, 1 equiv.) was dissolved in anhydrous Et₂O (50 mL) under an atmosphere of argon. With vigorous stirring a solution of (4-chlorobenzyl)magnesium chloride (**112**) (50 mL, 0.25 M in Et₂O, 12.5 mmol, 2.1 equiv.) was added dropwise to the reaction mixture, which was stirred for 12 h at room temperature. Afterwards it was diluted with sat. NH₄Cl-solution (50 mL) and the organic phase was isolated. The aqueous phase was extracted with Et₂O (2 x 30 mL), the combined organic phases were washed with water (30 mL), brine (30 mL) and were dried over MgSO₄. The solvent was removed under reduced pressure and the residue was purified with column chromatography (hexane/EtOAc 1:1, R_f = 0.1). The product was obtained as a yellow solid (757 mg, 2.06 mmol, 34% yield).

m.p.: 120 °C.

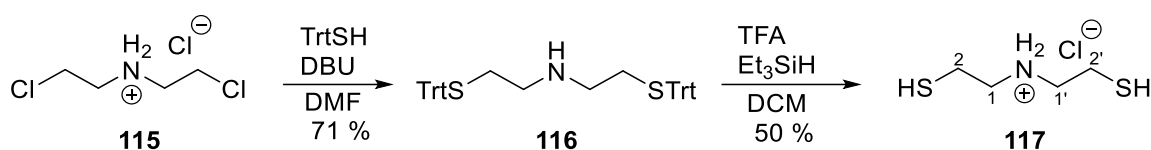
¹H-NMR (300 MHz, CDCl₃): δ (ppm) = 7.27 (d, 4H, *J* = 8.42 Hz, 5-H, 5'-H), 7.11 (d, 4H, *J* = 8.42 Hz, 4-H, 4'-H), 3.40 (t, 4H, *J* = 5.36 Hz, 8-H, 8'-H), 3.01 (quint, 1H, *J* = 7.2 Hz, 1-H), 2.90-2.52 (m, 8H, 2-H, 2'-H, 7-H, 7'-H), 1.77 (s, 2H, NH₂).

¹³C-NMR (75 MHz, CDCl₃): δ (ppm) = 138.92 (C-3), 131.71 (C-6), 130.49 (C-4), 128.47 (C-5), 65.58 (C-1), 59.97 (C-8), 51.51 (C-7), 35.80 (C-2).

FT-IR (solid): $\tilde{\nu}$ (cm⁻¹) = 3447, 2925, 23410, 1734, 1489, 1407, 1086, 1066, 1012, 837, 802, 738, 510, 438.

HR-MS (ESI): *m/z* calculated for C₁₉H₂₄Cl₂NO₂ [M+H]⁺ 368.1179; observed 368.1182.

Synthesis of bis(2-mercaptoethyl)ammonium chloride (117)



Bis(2-chloroethyl)ammonium chloride (2.0 g, 11.3 mmol, 1 equiv.) and triphenylmethanethiol (6.79 g, 24.6 mmol, 2.18 equiv.) were dissolved in anhydrous DMF (10 mL) under an atmosphere of argon. DBU (6 mL, 38.7 mmol, 3.4 equiv.) was dissolved in anhydrous DMF (6 mL) and the solution was added to the reaction mixture. Afterwards it was heated at 100 °C for 1 h. After cooling to room temperature the reaction mixture was poured into water (500 mL). The resulting solid was filtered off and dissolved in EtOAc (100 mL). The organic phase was washed with water (2 x 50 mL) and dried over MgSO₄. The solvent was removed *in vacuo* and the resulting yellow solid was washed with boiling EtOH. The product was obtained as a white solid (4.98 g, 8.02 mmol, 71% yield) and was used directly for the next reaction step.

Bis(2-(tritylthio)ethyl)amine (1.01 g, 1.63 mmol, 1 equiv.) was dissolved in DCM (5 mL). The reaction mixture was cooled to 0 °C and TFA (5 mL) was added dropwise. Afterwards, Et₃SiH (0.54 mL, 3.38 mmol, 2 equiv.) was added and the reaction mixture was stirred for 24 h at room temperature. The solvent was removed *in vacuo* and the residue was coevaporated with toluene (2 x 10 mL). The residue was dissolved in water (25 mL) and the aqueous phase was washed with toluene (20 mL). The organic phase was reextracted with water (10 mL) and the combined aqueous phases were acidified to pH 1 with conc. HCl. The solvent was removed *in vacuo* and the hydrochloride salt of the product was obtained as a white solid (141 mg, 0.82 mmol, 50% yield).

m.p.: 155 °C.

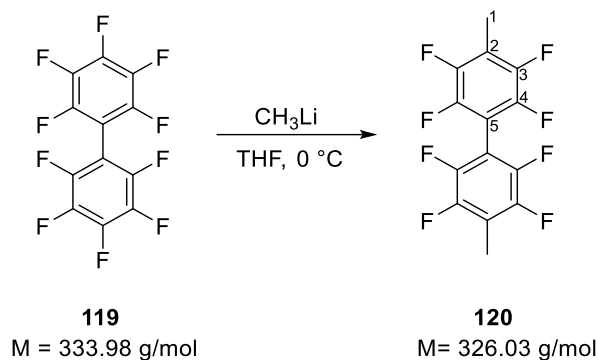
¹H-NMR (300 MHz, DMSO-d₆): δ (ppm) = 8.98 (br s, 2H, NH₂⁺), 3.19-3.03 (m, 4H, 1-H, 1'-H), 2.95 (t, 2H, *J* = 8.30 Hz, SH), 2.83-2.70 (m, 4H, 2-H, 2'-H).

¹³C-NMR (75 MHz, DMSO-d₆): δ (ppm) = 49.77 (C-1, C-1'), 20.14 (C-2, C-2').

HR-MS (ESI): *m/z* calculated for C₄H₁₀NS₂ [M+H]⁺ 136.0249; observed 136.0250 (note that under ESI conditions the disulfide compound was observed).

6.1.2.4 Syntheses for chapter 4.4

Synthesis of Di-para-bimethyl-octafluoro-1,1'-biphenyl (**120**)



Perfluoro-1,1'-biphenyl (**119**) (2.95 g, 8.8 mmol, 1 equiv.) was dissolved in anhydrous THF (12 mL) under an atmosphere of argon. The reaction mixture was cooled to 0 °C and a solution of methyllithium (6.2 mL, 3.3 M in DEM, 19.2 mmol, 2.2 equiv.) was added dropwise in a fashion that the vigorous reaction was kept minimal. The resulting purple solution was stirred at room temperature for 2 h and then diluted with EtOAc (15 mL). The organic phase was washed with water (2 x 15 mL) and brine (15 mL) and was dried over MgSO₄. The solvent was removed under reduced pressure and the residue was purified by column chromatography (7:1 hexane/EtOAc, R_f = 0.69). The product was obtained as a white solid (1.14 g, 3.5 mmol, 39% yield).

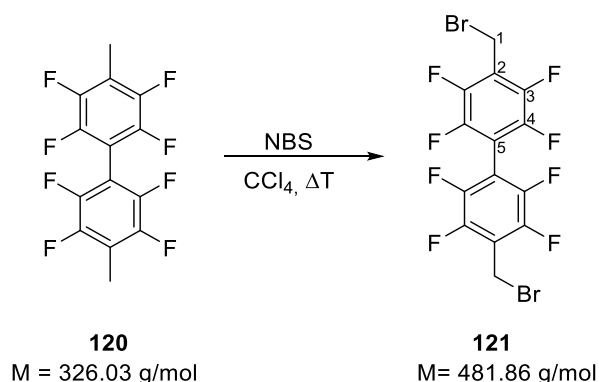
m.p.: 141 °C.

¹H-NMR (300 MHz, CDCl₃): δ (ppm) = 2.36 (t, 6H, *J* = 2.16 Hz, 1-H, 1'-H).

¹⁹F-NMR (282.4 MHz, CDCl₃): δ (ppm) = -140.27 (m, 4F, 3-F, 3'-F), -142.89 (m, 4F, 4-F, 4'-F).

HR-MS (EI): *m/z* calculated for C₁₄H₆F₈ [M] 326.0336; observed 326.0333.

Synthesis of Di-para-bibromomethyl-octafluoro-1,1'-biphenyl (**121**)



Di-para-bimethyl-octafluoro-1,1'-biphenyl (**120**) (1.14 g, 3.5 mmol, 1 equiv.) was dissolved in CCl₄ (10 mL) and NBS (1.32 g, 7.4 mmol, 2.1 equiv.) was added at once. The resulting reaction mixture was refluxed for 24 h. Afterwards, it was diluted with EtOAc (50 mL) and the organic phase was washed with water (2 x 20 mL) and brine (20 mL) and dried over MgSO₄. The solvents were removed under reduced pressure and the residue was purified by column chromatography (hexane, R_f = 0.46). The product was obtained as a white, crystalline solid (1.24 g, 2.56 mmol, 73% yield).

m.p.: 148 °C.

¹H-NMR (300 MHz, CDCl₃): δ (ppm) = 4.58 (s, 4H, 1-H, 1'-H).

¹⁹F-NMR (282.4 MHz, CDCl₃): δ (ppm) = -137.44 (m, 4F, 3-F, 3'-F), -141.56 (m, 4F, 4-F, 4'-F).

6.2 Biological methods

6.2.1 Materials

a) Chemicals

All commercially available chemicals for biological or analytical purposes were used without further purification if not stated otherwise. Anhydrous solvents were supplied by AcrosOrganics (Thermo Fischer scientific brand) and were stored in the original package over molecular sieves under an atmosphere of argon.

b) Enzymes

DNase I	AppliChem GmbH
Lysozyme	AppliChem GmbH
Phusion polymerase	Thermo Fischer scientific

c) Plasmids

pET303C-hSOD1wt	donated by Prof. Samar Hasnain, University of Liverpool
-----------------	---

d) Bacterial strains

<i>E. coli</i> BL21 (DE3)	Invitrogen TM
<i>E. coli</i> BL21 Star™	Invitrogen TM
<i>E. coli</i> XL1 blue	Stratagene

e) Kits and associated solutions

dNTP mix (10 mM)	Thermo Fischer scientific
NucleoSpin™ Plasmid Kit	Macherey Nagel
NucleoSpin™ Gel/PCR clean up	Macherey Nagel
Bradford reagent (conc. x5)	SERVA electrophoresis GmbH

Gel Filtration standard	BioRad laboratories GmbH
Pierce™ unstained protein	Thermo Fischer scientific
Molecular weight marker	
Gene Rule DNA ladder mix	Thermo Fischer scientific
DNA loading dye (x6)	Thermo Fischer scientific
SOD assay kit (19160 -1kt - f)	Sigma Aldrich Chemie GmbH

f) Crystallization screens

AdditiveScreen™ HR-418	Hampton Reasearch Corp.
The AmSO ₄ suite	QIAGEN
Classic Lite	QIAGEN
Classics	QIAGEN
Classic II	QIAGEN
Compass	QIAGEN
Index	Hampton Research
MBclass	QIAGEN
MBclass II	QIAGEN
PACT	QIAGEN
PEGs	QIAGEN
pHCLear	QIAGEN
Protein Complex	QIAGEN
Wizard Classic 1+2	Rigaku

g) Media

LB medium – yeast extract (0.5% w/v), tryptone (1% w/v), NaCl (0.5% w/v)

LB agar plates – yeast extract (0.5% w/v), tryptone (1% w/v), NaCl (0.5% w/v),
Agar (2% w/v)

h) Mutagenesis primers

hSOD1A4V Fwd	5`-GCGACGAAGGTCGTGTGCGTG-3`
hSOD1A4V Rew	CACGCACACGACCTTCGTCGC
hSOD1C6F Fwd	GACGAAGGCCGTGTTCGTGCTGAAGG
hSOD1C6F Rew	CCTTCAGCACGAACACGGCCTTCGTC
hSOD1D90A Fwd	CAATGTGACTGCTGCCAAAGATGGTGTGG
hSOD1D90A Rew	CCACACCATCTTTGGCAGCAGTCACATTG
hSOD1G93C Fwd	CTGACAAAGATTGCGTGGCCGATGTGT
hSOD1G93C Rew	ACACATCGGCCACGCAATCTTTGTCAG

i) Sequencing primers

T7 promotor 5'-TAATACGACTCACTATAGGG-3'

5' – GCGACGAAGGTCGTGTGCGTG– 3'

T7 terminator 5'-AGCTAGTTATTGCTCAGCGG-3'

6.2.2 Devices

a) Analytics

Fluoromax 4 spectrofluorometer	BRUKER
NanoDropOne	Thermo Fischer scientific
Spectrofluorometer FP-8500	JASCO GmbH
UV-Vis spectrophotometer V-750	JASCO GmbH

X-Ray BeamLine P14	EMBL Hamburg
Arium®proVF	Sartorius AG
C1000 thermal cycler	BioRad Laboratories GmbH
CFX96™ Optical Reaction Module	BioRad Laboratories GmbH
Thermocycler TProfessional	Biometra
pH-electrode Minitrode Hamilton	Mettler Toledo GmbH
pH-electrode	Mettler Toledo GmbH
Monolith NT.115Pico	NanoTemper Technologies GmbH
Melting point meter (M5000)	A. KRÜSS Optronic GmbH

b) Cell culture and cell disruption

Biofermenter, Biostat	C Sartorius AG
Incubation shaker, Unitron	Infors AG
Microfluidizer, M-110S	Microfluidics
Multifuge 1S-R	Thermo Fischer scientific

c) Centrifuges and lab rotors

Avanti™ HP-30I	Beckman Coulter GmbH
Rotor JA-10	Beckman Coulter GmbH
Rotor JA-30.50 Ti	Beckman Coulter GmbH
Avanti™ J-20XPI	Beckman Coulter GmbH
Rotor JLA-8.1000	Beckman Coulter GmbH
Rotor SW40 Ti	Beckman Coulter GmbH
Rotor SW60 class GH	Beckman Coulter GmbH
Optima™ L-90K Ultracentrifuge	Beckman Coulter GmbH
Eppendorf 5810R	Eppendorf AG
Rotor A-4-81	Eppendorf AG
Mikro 200	Hettich GmbH & Co. KG
Rotor 2424 B	Hettich GmbH & Co. KG
Universal 320R	Hettich GmbH & Co. KG
Rotor 1420 A/B	Hettich GmbH & Co. KG

Rotor 1617 A	Hettich GmbH & Co. KG
Rotor 1620 A	Hettich GmbH & Co. KG

d) Liquid chromatography

Fractogel® EMD TMAE 650 (S)	Merck KGaA
ÄKTAprime plus	GE Healthcare Europe
ÄKTApurifier	GE Healthcare Europe
HiPrep™ 26/10 desalting (50 mL)	GE Healthcare Europe
HiTrap™ 26/10 desalting (5 mL)	GE Healthcare Europe
Superdex™ 200 HiLoad™ 16/60	GE Healthcare Europe
Superdex™ 75 10/300 GL	GE Healthcare Europe
Superdex™ 200 10/300 GL	GE Healthcare Europe
Superdex® 200 Increase 10/300 GL	GE Healthcare Europe
Superloop (10 mL, 50 mL, 150 mL)	GE Healthcare Europe

6.2.3 Molecular biology protocols

6.2.3.1 Plasmid transformation

The plasmid pET303C-hSOD1wt was donated by Prof. Samar Hasnain from the University of Liverpool. This plasmid was introduced into competent cells of different strains: the multiplication of the plasmid was performed with the XL1-Blue strain, recombinant protein expression was done with BL21 (DE3) and BL21 Star™ (DE3) strains.

The commercially available competent cells (50 µg) were thawed on ice for 15 min and 1 ng of plasmid was added. The components were mixed by flicking. The obtained cells were incubated on ice for 25 minutes. Afterwards, the cells were exposed to a heat shock (42 °C, 20 s), followed by subsequent incubation on ice for 5 min.^[137] To the cells was then added 1 mL SOC medium preheated to 37 °C. The obtained cell suspension was incubated at 37 °C, 800 rpm for 70 min to induce cell growth.

After that, the cells were placed onto LB-agar plates that were pretreated with carbenicillin (100 µg/mL) and incubated overnight at 37 °C.

6.2.3.2 Plasmid DNA isolation

Single colonies of the aforementioned transformed cells were manually picked and incubated with LB medium (6 x 10 mL) pretreated with carbenicillin (100 µg/mL) overnight at 37 °C, 200 rpm. The optical density (OD₆₀₀) was followed throughout the growing process. When OD₆₀₀ = 3 – 3.5 could be observed, cells were harvested by centrifugation at 4 °C, 9000 rpm, 5 min. The obtained pellet was used for subsequent plasmid isolation following a protocol from MachereyNagel using the NucleoSpin™ Plasmid kit.

6.2.3.3 Determination of DNA concentration

The concentration of the processed DNA c was calculated using the Beer-Lambert law according to the following equation

$$A_{260} = c * d * \varepsilon$$

With A_{260} : absorbance measured at 260 nm using a NanoDrop One™ device, ε : 50 ng/µl*cm, d : 1cm.

6.2.3.4 DNA sequencing

The sequencing of the obtained plasmids was performed by GATC Biotech AG using the primers mentioned in section 6.2.1 i.

6.2.3.5 PCR (Polymerase Chain Reaction)

The employed PCR conditions consisted of the QuickChange protocol (Stratagene), which was adapted for the Phusion® DNA-polymerase. The used mutagenesis primers are listed in section 6.2.1 h. The template DNA with the unmodified sequence was then digested by the addition of 5 equivalents of restriction enzyme (DpnI), followed by incubation at 37 °C overnight. The digestion suspension was then inactivated by heating it at 80 °C for 20 min.

6.2.3.6 Horizontal agarose gel electrophoresis

The obtained DNA samples were mixed with DNA loading dye (6x) and loaded onto agarose gels (1% agarose containing 1x TAE buffer [40 mM Tris, 20 mM acetic acid, 1 mM EDTA, pH 7.0]). Gel staining was performed with ethidium bromide (2 µg/mL) for 15 min, followed by visualization with UV-light. The separated DNA fragments were compared with a 1kb DNA ladder dye to visualize the size of the purified fractions.

6.2.4 Protein expression

6.2.4.1 hSOD1 wt and mutant expression

The following protocol was used for the expression of the wild type as well as of all mentioned mutants:

200 mL of sterilized LB medium (10 g/L tryptone, 5 g/L yeast extract, 5 g/L NaCl) containing 100 µg/mL carbenicillin was inoculated with two to three colonies of *E. coli* BL21 Star™ (DE3), holding the desired plasmid. This preculture was incubated overnight at 37 °C, 200 rpm. The preculture was then aliquoted and centrifuged at 10 °C, 9000 rpm for 15 min. The supernatant was discarded and the pellet was resuspended in 4 mL of fresh LB medium per 50 mL preculture. The obtained main cultures were incubated at 37 °C, 200 rpm. The protein expression was induced by addition of IPTG (200 mM, 2 mL) and ZnSO₄ (500 mM, 1 mL) after OD₆₀₀ was 0.6 – 0.8. Afterwards the cells were incubated overnight at 25 °C, 200 rpm. Successful expression of the desired protein was verified with SDS-page analysis. The obtained cells were harvested by centrifugation at 4 °C, 4800 rpm, 20 min. The cell pellets were suspended in approx. 5 – 10 mL buffer A per aliquot, transferred to 50 mL falcon tubes and centrifuged at 4 °C, 400 rpm, 20 min. The resulting cell pellets were frozen at -78 °C for long-term storage and at -20 °C for short-term storage.

6.2.4.2 hSOD1 Purification

The used purification protocol was obtained by Dr. Michael Capper from the University of Liverpool and was optimized by Lisa-Marie Funk. The cell pellets (each approx. 10 g) were suspended in 4 mL/g loading buffer A (20 mM Tris, pH 8.0) and the suspension was cooled on ice. Then, 0.5 mM PMSF, 5 µg/mL DNase I, 5 mM MgCl₂ and a small

amount of lysozyme were added subsequently. The resulting suspension was stirred at 0 °C for 45 min. A microfluidizer device was used to achieve lysis of the cells in 3 to 5 cycles at 1034 bar each. Afterwards the cell suspension was centrifuged at 10 °C, 75.000 x g, 30 min. The supernatant was dialyzed against buffer A (2 L, 20 mM Tris, pH 8.0) for 16 h at 4 °C. The resulting solution was centrifuged at 10 °C, 75.000 g, 20 min. The supernatant was loaded onto a TMAE column equilibrated with buffer A. The loaded column was washed with buffer A until no traces of unbound protein were visible in the flow-through. Elution was performed using buffer B (20 mM Tris, 500 mM NaCl, pH 8.0) with a gradient of 20% in 150 mL. After elution if the desired protein the column was washed with 100% buffer B to remove any traces of bound proteins from the column. The success of the purification was verified by SDS-page analysis. The resulting fractions containing pure protein were combined and concentrated using a Corning-Spin-X UF micro concentrator. The resulting protein was stored at – 78 °C for long-term storage or used immediately.

6.2.4.3 SDS-page analysis

Stacking gel: 5% acrylamide, 125 mM Tris, 0.1% (w/v) SDS, pH 6.8.

Separating gel: 15% acrylamide, 375 mM Tris, 0.1% (w/v) SDS, pH 8.0.

Samples were mixed with sample buffer (0.1 M Tris, 25% (v/v) glycerol, 2% (w/v) SDS, 0.02% (w/v) bromophenol blue, 2.5% β-mercaptoethanol, pH 6.8) and incubated at 95 °C for 5 min. SDS-page analysis was conducted at 35 mA, 150 W, 300 V for 30 min or until no further elution could be observed. Afterwards, the gels were stained with staining solution (0.25% (w/v) Coomassie Brilliant Blue G250, 30% (v/v) ethanol, 6% acetic acid) for 5 min at room temperature. Excess dye was removed by washing the stained gels with destaining solution (30% (v/v) ethanol, 10% (v/v) acetic acid).

6.2.4.4 Determination of protein concentration

The Beer-Lambert law was used to measure the absorbance of tryptophan at 280 nm on a NanoDrop One™ device. The molecular weight of hSOD1 was approx. 15936 kDa and the used molecular extinction coefficient was $\epsilon_{280} = 5500 \text{ M}^{-1} \text{ cm}^{-1}$. An

alternative method using a standard Bradford-protocol gave the same results during the course of this work.^[138] Since the Bradford approach was more time consuming the spectroscopic method was primarily used.

6.2.4.5 Cofactor reconstitution

The purified protein (see 6.2.4.2) was dialyzed against 2 L buffer D1 (100 mM sodium acetate, 5 mM EDTA, pH 3.8) at 4 °C for 16 h to remove zinc ions that were added during the purification process. Afterwards, the protein was dialyzed against 2 L buffer D2 (100 mM sodium acetate, 150 mM NaCl, pH 3.8) at 4 °C for 4 h. The protein was then incubated with 10 mM CuSO₄ for 15 min, followed by incubation with 10 mM ZnSO₄ for 15 min. The resulting holo-enzyme was desalted using a HiPrep 26/10 desalting column. Used buffers included Tris buffer (20 mM Tris, pH 8.0) for crystallization, SP buffer (50 mM sodium phosphate, pH 7.4) and HEPES buffer (100 mM HEPES, 150 mM NaCl, pH 7.4) for biophysical analysis and assays.

6.2.4.6 Activity assays

A SOD1 activity assay kit from Sigma Aldrich was used to measure the catalytic activity in this thesis. 220 µL of sample mixture were prepared by mixing 200 µL of WST working solution with 20 µL of buffer containing the desired sample (protein, ligands or nothing for blank measurements). The resulting sample mixture was incubated for 2 min at 25 °C. Afterwards, 40 µL of xanthine oxidase were added and the initiated reaction was analyzed spectroscopically over the course of 2 minutes. The absorbance of the sample was recorded at 440 nm in triplicates and the measured value were plotted against time. The slope of the resulting curve was calculated in the 0-50 s period and the inhibition of SOD1 samples was calculated in % following the equation

$$\text{Inhibition (\%)} = \frac{\text{slope (control)} - \text{slope (sample)}}{\text{slope (control)}}$$

6.2.4.7 Size exclusion chromatography (SEC)

A Superdex Increase 200 10/300 GL column was used to run size exclusion chromatography experiments. Prior to use, it was equilibrated with sodium phosphate

buffer (50 mM, pH 7.4), afterwards, the sample was loaded onto the column (150 μ L hSOD1 solution, 0.1 – 0.5 mg/mL). The used flow rate was 0.5 mL/min and the purification was performed at 4 °C. A commercially available gel-filtration standard (BioRad laboratories) was used to acquire a calibration curve for the molecular weight of the fractions obtained from the experiment. The partition coefficient K_{av} was calculated using the following equation

$$K_{av} = \frac{V_e - V_0}{V_c - V_0}$$

With V_e as the elution volume, V_c as the geometric column volume and V_0 as the empty column volume. The obtained values for the partition coefficient were plotted against the molecular weight that resulted from the standard, using a logarithmic scale for the abscissa.

6.2.4.8 X-ray crystallography

The used protein was thawed on ice and centrifuged for at 4 °C, 13.000 x g for 15 min. afterwards, protein stock solutions were prepared using a concentration range of 5-20 mg/mL in Tris buffer (20 mM Tris, pH 8). After that, 500 μ L of well solution was prepared (18-22 % (w/v) PEG-8000, 0.2 M ammonium sulfate, 0.1 M HEPES, pH 6.5). The hanging-drop diffusion method was chosen for screening the optimal conditions for crystal growth, two drops were used per well, filled with a mixture of 2 μ L protein stock solution and 2 μ L well solution. The resulting crystal plate was stored at -20 °C for 3-10 days, after which crystal growth could be observed. Crystals that were suitable for X-Ray analysis were picked and incubated with 50% (w/v) PEG-8000 in cryo-protecting solution (20% DMSO, 0.2 M ammonium sulfate, 0.1 M MES, 1 mM ZnSO₄, 1 mM CuSO₄), increasing the amount of PEG-8000 in steps of 5% over the course of 1-4 min depending on the quality of the crystal. The resulting crystals were then soaked with solutions of the desired ligands for a short period of time (1 – 10 min).

Diffraction data of all obtained crystals were measured at the P14 BeamLine at DESY Hamburg at 100 K. All data processing was carried out by Lisa-Marie Funk.^[139]

6.3 Biophysical assays

6.3.1 UV/VIS and fluorescence measurements

Absorption and Emission spectra were recorded on a JASCO V-750 UV/VIS-Spectrophotometer and a JASCO FP-8500 Fluorescence Spectrometer using the following device settings:

Table 6.3-1. General device setting for absorption and emission measurements.

	Absorption measurement	Emission measurement
Measurement range	750 – 190 nm	650 – 200 nm
Data interval	0.5 nm	0.5 nm
Scan speed	200 nm/s	200 nm/s
Bandwidth	2.0 nm	5 nm
Response	0.24 s	0.2 s
Sensitivity	N/A	Very low
Temperature	25 °C	25 °C

The concentration of the ligands was kept at a consistent value of 40 μM to ensure the possibility of a rational comparison between them. Before each UV/VIS measurement, a baseline was recorded using the same buffer and/or solvent mixture as for the upcoming measurement.

6.3.2 Fluorescence Anisotropy

Anisotropy measurements were performed using a FluoroMax[®] (Horiba) device and the corresponding software FluorEssence[™] (Horiba). The measurements were done using the following protocol:

1. Samples were prepared in the following way: The final concentration of the respective ligand was set to 40 μM by dilution of the stock solution with phosphate buffer (50 mM sodium phosphate, pH 7.4). The final concentration of the protein was either 250 or 0 μM and was achieved by dilution of the protein

stock solution with phosphate buffer (50 mM sodium phosphate, pH 7.4). The necessary amounts of protein stock solution, ligand stock solution and buffer were pipetted and mixed by pipetting

2. The samples were incubated for 2.5 h at room temperature.
3. The samples were centrifuged at room temperature, 10.000 x g, 2 min
4. The samples were loaded into a cuvette and the anisotropy was measured against a “single point” at 20 °C. The “single point” was defined by the absorption and emission maxima of the respective ligand.
5. Each data point consisted of up to ten individual measurements that were performed until the relative error was smaller than 5% or all 10 measurements were done. The mean value of all performed measurements was given as the result of each data point.
6. A series of triplicates of data points was measured for each sample.
7. The sample with 0 µM protein was used as a blank.
8. Analysis of the data was done with Origin.

6.3.3 Microscale thermophoresis (MST)

The chosen labelling strategy ensured that the protein was fluorescent to allow fluorescence analysis of the protein-ligand complex under MST conditions. The labelling was based on the reaction of an active NHS-ester group from the dye with primary amines from the protein at neutral pH, resulting in an amide bond. SOD1 offers 11 lysine residues for the reaction with the NHS-ester in each monomer compared to only one N terminus of the AA chain that would also be able to react with said ester. In turn, it was concluded that the majority of the dye was bound away from the dimer interface and from the binding cavity of interest, so no interactions between dye and ligands were assumed.

The fully reconstituted protein was prepared according to section 6.2.4.5 and was diluted with phosphate buffer to a concentration of 200 µM. The used NHS-dye (2nd generation red NHS dye from the Monolith labelling kit by NanoTemper) was dissolved in DMSO, the final concentration was 600 µM. The protein and the dye were mixed by pipetting in a 1:1 molar ratio, the resulting solution was incubated for 1.5 h in absence

of light. Afterwards, unreacted dye was removed with SEC (according to section 6.2.4.7), employing a Superdex 200 10/300 GL column.

The degree of labelling (DOL) was calculated using the following equation

$$DOL = \frac{c(dye)}{c(protein)}$$

The concentration of the dye was calculated using the Beer-Lambert equation similar to section 6.2.3.3 with $\epsilon_{dye} = 195.000 \text{ M}^{-1}\text{cm}^{-1}$. The concentration of the protein was calculated using the following equation

$$c(protein) = \frac{A_{280} - (A_{650} * cf_{650})}{\epsilon(protein) * d}$$

A_{280} : absorbance at 280 nm, A_{650} : absorbance at 650 nm, cf_{650} : 0.04 (dye-dependent correction factor), $\epsilon(protein)$: extinction factor of the protein ($10.800 \text{ M}^{-1}\text{cm}^{-1}$), d : path length of the instrument (1 cm). The calculated DOL ranged from 0.3 to 1.1 in different labelling implementations.

The labelling was performed by Viktoria Mrđen Debono.

MST measurements were performed using the following protocol:

1. The labelled protein concentration was adjusted to 10 nM with assay buffer (50 mM phosphate buffer, 0.05% Tween-20).
2. The ligand was used with the highest possible concentration, ranging from 10 to 40 mM in phosphate buffer (50 mM sodium phosphate, pH 7.4) depending on the substrate. A dilution series was prepared in a way that the concentration was halved after each iteration, starting with 20 μL of ligand and diluting with 10 μL of buffer each time. A total number of 16 samples were prepared.
3. 10 μL of the protein stock were added to each of the 16 ligand solutions and were mixed by pipetting.
4. The samples were incubated for 2.5 h at room temperature in the absence of light.
5. The samples were centrifuged at room temperature, $10.000 \times g$, 2 min.
6. Samples were loaded onto Monolith NT.115 Premium Capillaries (NanoTemper).

7. The measurements were done using a Monolith NT.115 Pico instrument using varying LED power and MST power at 22 °C.
8. Analysis of the MST data was done using the provided MO. Affinity Analysis Software version 2.3 (NanoTemper).

6.3.4 Isothermal Titration Calorimetry (ITC)

ITC measurements were done using the following protocol on a MicroCal PEAQ-ITC instrument (Malvern):

1. The protein was reconstituted in HEPES buffer (100 mM HEPES, 150 mM NaCl, pH 7.4) or phosphate buffer (50 mM sodium phosphate, pH 7.4) depending on the substrate. The ligands were dissolved in the appropriate buffer at the highest concentration possible, ranging from 10 to 40 mM. Protein and ligand stocks were degassed prior to use for 2 min using a stream of nitrogen.
2. The measurement cell was flushed with ligand stock (50 – 200 μ L).
3. The sample was loaded onto a syringe with a concentration of 10 nM in the respective buffer.
4. The sample was titrated against hSOD1 wt (175 μ M) with a rate of 1 μ L/min.
5. Analysis of the obtained data was done using the provided software.

All ITC measurements and analyses were done by Lisa-Marie Funk.

6.4 Protein structure and ligand structure preparation for *in silico* screening

The crystal structure that was used in this thesis was obtained from the RCSB Protein Data Bank with the ID 2C9U. The file was opened with Pymol and prepared for *in silico* studies by removing water molecules, phosphate anions and by adding charges wherever necessary. Moreover, the amino acid chain was investigated in order to validate its integrity. The file was opened with Chimera and saved as either a PDB or a PDBQT file, depending on the used docking program.

The corresponding ligand structures were prepared in ChemDraw3D (v 15.1) and saved as either a PDB or mol2 file, depending on the used docking program.

Molecular docking was performed with two different programs: AutoDockVina and the open source platform swissdock.ch. In AutoDockVina, the whole protein was chosen as the receptor, the ligand was assumed rigid with non-rotatable bonds except for those of functional groups. All other parameters were set to default. Docking with swissdock.ch was performed by following the instructions on the respective website and required no special treatment of files or other parameters. Instead, all necessary files had to be uploaded onto the website or could be directly connected via the RCSB Protein Data Bank in case for proteins.

The obtained ligands were then ranked according to their docking score (typically given in negative Gibbs free energy, kcal/mol or kJ/mol) that resulted from the used scoring functions. Since the resulting docking poses from both approaches were largely indistinguishable, swissdock.ch was chosen as the main platform for screening large amounts of ligands since it was more suitable for this approach. It is assumed that predicting docking poses is far more reliable than predicting binding affinities of protein-ligand complexes. Therefore, docking poses were treated as the decisive criteria for choosing suitable ligands for synthesis and biophysical assays over docking scores.

7 Bibliography

- [1] J.S. Salameh, R.H. Brown, J.D. Berry, Amyotrophic Lateral Sclerosis: Review, *Semin. Neurol.* **2015**, *35*, 469–476.
- [2] D.R. Kumar, F. Aslinia, S.H. Yale, J.J. Mazza, Jean-martin charcot: The father of neurology, *Clin. Med. Res.* **2011**, *9*, 46–49.
- [3] J.J. Alappat, Ethnic variation in the incidence of ALS: A systematic review, *Neurology.* **2007**, *69*, 711.
- [4] S. Zarei, K. Carr, L. Reiley, K. Diaz, O. Guerra, P.F. Altamirano, W. Pagani, D. Lodin, G. Orozco, A. China, A comprehensive review of amyotrophic lateral sclerosis, *Surg. Neurol. Int.* **2015**, *6*.
- [5] Z.R. Manjaly, K.M. Scott, K. Abhinav, L. Wijesekera, J. Ganesalingam, L.H. Goldstein, A. Janssen, A. Dougherty, E. Willey, B.R. Stanton, M.R. Turner, M.A. Ampong, M. Sakel, R.W. Orrell, R. Howard, C.E. Shaw, P.N. Leigh, A. Al-Chalabi, The sex ratio in amyotrophic lateral sclerosis: A population based study, *Amyotroph. Lateral Scler.* **2010**, *11*, 439–442.
- [6] M.C. Kiernan, S. Vucic, B.C. Cheah, M.R. Turner, A. Eisen, O. Hardiman, J.R. Burrell, M.C. Zoing, Amyotrophic lateral sclerosis, *Lancet.* **2011**, *377*, 942–955.
- [7] J.M. Statland, R.J. Barohn, A.L. McVey, J.S. Katz, M.M. Dimachkie, Patterns of Weakness, Classification of Motor Neuron Disease, and Clinical Diagnosis of Sporadic Amyotrophic Lateral Sclerosis, *Neurol. Clin.* **2015**, *33*, 735–748.
- [8] R. Tandan, W.G. Bradley, Amyotrophic lateral sclerosis: Part 1. Clinical features, pathology, and ethical issues in management, *Ann. Neurol.* **1985**, *18*
- [9] A. Chiò, G. Logroscino, O. Hardiman, R. Swingler, D. Mitchell, E. Beghi, B.G. Traynor, Prognostic factors in ALS: A critical review, *Amyotroph. Lateral Scler.* **2009**, *10(5-6)*, 310-323.
- [10] E. Longinetti, F. Fang, Epidemiology of amyotrophic lateral sclerosis: An update of recent literature, *Curr. Opin. Neurol.* **2019**, *32*, 771–776.
- [11] P.F. Chance, B.A. Rabin, S.G. Ryan, Y. Ding, M. Scavina, D. Conway, B. Crain, J.W. Griffin, D.R. Cornblath, Erratum: Linkage of the gene for an autosomal dominant form of juvenile amyotrophic lateral sclerosis to chromosome 9q34 (American Journal of Human Genetics (March) 62 (633-640)), *Am. J. Hum. Genet.* **1998**, *63*, 295.
- [12] R. Mezzini, L.L. Flynn, I.L. Pitout, S. Fletcher, S.D. Wilton, P.A. Akkari, ALS Genetics, Mechanisms, and Therapeutics: Where Are We Now?, *Front. Neurosci.* **2019**, *13*, 1–27.
- [13] F. Laferrière, M. Polymenidou PhD, Advances and challenges in understanding the multifaceted pathogenesis of amyotrophic lateral sclerosis, *Swiss Med. Wkly.* **2015**, *145*, 1–13.
- [14] B. Oskarsson, D.K. Horton, H. Mitsumoto, Potential Environmental Factors in Amyotrophic Lateral Sclerosis, *Neurol. Clin.* **2015**, *33*, 877–888.
- [15] J.M. Morahan, B. Yu, R.J. Trent, R. Pamphlett, A genome-wide analysis of brain DNA methylation identifies new candidate genes for sporadic amyotrophic lateral sclerosis, *Amyotroph. Lateral Scler.* **2009**, *10*, 418–429.
- [16] I.R.A. Mackenzie, R. Rademakers, The role of transactive response DNA-binding protein-43 in amyotrophic lateral sclerosis and frontotemporal dementia, *Curr. Opin. Neurol.* **2008**, *21*, 693–700.
- [17] N. Ticozzi, V. Silani, A.L. Leclerc, P. Keagle, C. Gellera, A. Ratti, F. Taroni, T.J. Kwiatkowski, D.M. McKenna-Yasek, P.C. Sapp, R.H. Brown, J.E. Landers, Analysis of FUS gene mutation in familial amyotrophic lateral sclerosis within an Italian cohort, *Neurology.* **2009**, *73*, 1180–1185.
- [18] D. Sau, S. De Biasi, L. Vitellaro-Zuccarello, P. Riso, S. Guarnieri, M. Porrini, S. Simeoni, V. Crippa, E. Onesto, I. Palazzolo, P. Rusmini, E. Bolzoni, C. Bendotti, A. Poletti, Mutation of SOD1 in ALS: A gain of a loss of function, *Hum. Mol. Genet.* **2007**, *16*, 1604–1618.

- [19] D.B. Medinas, V. Valenzuela, C. Hetz, Proteostasis disturbance in amyotrophic lateral sclerosis, *Hum. Mol. Genet.* **2017**, *26*, R91–R104.
- [20] R. Balendra, A.M. Isaacs, C9orf72-mediated ALS and FTD: multiple pathways to disease, *Nat. Rev. Neurol.* **2018**, *14*, 544–558.
- [21] Aditi, L. Glass, T.R. Dawson, S.R. Wenthe, An amyotrophic lateral sclerosis-linked mutation in GLE1 alters the cellular pool of human Gle1 functional isoforms, *Adv. Biol. Regul.* **2016**, *62*, 25–36.
- [22] Z. Butti, S.A. Patten, RNA dysregulation in amyotrophic lateral sclerosis, *Front. Genet.* **2019**, *10* 1–18.
- [23] L. Renaud, V. Picher-Martel, P. Codron, J.P. Julien, Key role of UBQLN2 in pathogenesis of amyotrophic lateral sclerosis and frontotemporal dementia, *Acta Neuropathol. Commun.* **2019**, *7*, 1–11.
- [24] H. Muyderman, T. Chen, Mitochondrial dysfunction in amyotrophic lateral sclerosis - A valid pharmacological target?, *Br. J. Pharmacol.* **2014**, *171*, 2191–2205.
- [25] H. Blasco, S. Mavel, P. Corcia, P.H. Gordon, The Glutamate Hypothesis in ALS: Pathophysiology and Drug Development, *Curr. Med. Chem.* **2014**, *21*, 3551–3575.
- [26] N. Geevasinga, P. Menon, P.H. Özdinler, M.C. Kiernan, S. Vucic, Pathophysiological and diagnostic implications of cortical dysfunction in ALS, *Nat. Rev. Neurol.* **2016**, *12*, 651–661.
- [27] J. Cady, E.D. Koval, B.A. Benitez, C. Zaidman, J. Jockel-Balsarotti, P. Allred, R.H. Baloh, J. Ravits, E. Simpson, S.H. Appel, A. Pestronk, A.M. Goate, T.M. Miller, C. Cruchaga, M.B. Harms, TREM2 variant p.R47H as a risk factor for sporadic amyotrophic lateral sclerosis, *JAMA Neurol.* **2014**, *71*, 449–453.
- [28] D. Petrov, C. Mansfield, A. Moussy, O. Hermine, ALS clinical trials review: 20 years of failure. Are we any closer to registering a new treatment?, *Front. Aging Neurosci.* **2017**, *9*, 1–11.
- [29] T. Dharmadasa, M.C. Kiernan, Riluzole, disease stage and survival in ALS, *Lancet Neurol.* **2018**, *17*, 385–386.
- [30] C. Jackson, T. Heiman-Patterson, P. Kittrell, T. Baranovsky, G. McAnanama, L. Bower, W. Agnese, M. Martin, Radicava (edaravone) for amyotrophic lateral sclerosis: US experience at 1 year after launch, *Amyotroph. Lateral Scler. Front. Degener.* **2019**, *20*, 605–610.
- [31] D.J. Sanger, H. Depoortere, The pharmacology and mechanism of action of zolpidem, *CNS Drug Rev.* **1998**, *4*, 323–340.
- [32] S. Paganoni, E.A. Macklin, S. Hendrix, J.D. Berry, M.A. Elliott, S. Maiser, C. Karam, J.B. Caress, M.A. Owegi, A. Quick, J. Wymer, S.A. Goutman, D. Heitzman, T. Heiman-Patterson, C.E. Jackson, C. Quinn, J.D. Rothstein, E.J. Kasarskis, J. Katz, L. Jenkins, S. Ladha, T.M. Miller, S.N. Scelsa, T.H. Vu, C.N. Fournier, J.D. Glass, K.M. Johnson, A. Swenson, N.A. Goyal, G.L. Pattee, P.L. Andres, S. Babu, M. Chase, D. Dagostino, S.P. Dickson, N. Ellison, M. Hall, K. Hendrix, G. Kittle, M. McGovern, J. Ostrow, L. Pothier, R. Randall, J.M. Shefner, A. V. Sherman, E. Tustison, P. Vigneswaran, J. Walker, H. Yu, J. Chan, J. Wittes, J. Cohen, J. Klee, K. Leslie, R.E. Tanzi, W. Gilbert, P.D. Yeramian, D. Schoenfeld, M.E. Cudkowicz, Trial of Sodium Phenylbutyrate–Tauroursodiol for Amyotrophic Lateral Sclerosis, *N. Engl. J. Med.* **2020**, *383*, 919–930.
- [33] T. Iannitti, B. Palmieri, Clinical and experimental applications of sodium phenylbutyrate, *Drugs R D.* **2011**, *11*, 227–249.
- [34] A.E. Elia, S. Lalli, M.R. Monsurrò, A. Sagnelli, A.C. Taiello, B. Reggiori, V. La Bella, G. Tedeschi, A. Albanese, Tauroursodeoxycholic acid in the treatment of patients with amyotrophic lateral sclerosis, *Eur. J. Neurol.* **2016**, *23*, 45–52.
- [35] Masitinib trial, (n.d.) <https://clinicaltrials.gov/ct2/show/NCT03127267>.
- [36] S.A. Al-Zaidy, J.R. Mendell, From Clinical Trials to Clinical Practice: Practical Considerations for Gene Replacement Therapy in SMA Type 1, *Pediatr. Neurol.* **2019**, *100*, 3–11.

- [37] E. Schönfelder, A. Osmanovic, L.H. Müschen, S. Petri, O. Schreiber-Katz, Costs of illness in amyotrophic lateral sclerosis (ALS): A cross-sectional survey in Germany, *Orphanet J. Rare Dis.* **2020**, *15*, 1–12.
- [38] D. Candas, J.J. Li, MnSOD in Oxidative Stress Response-Potential Regulation via Mitochondrial Protein Influx, *Antioxidants & Redox Signaling*, *20(10)*, **2014**, 1–60.
- [39] C. Biology, P. Division, Review Article, **2002**, *33*, 337–349.
- [40] I. Fridovich, *Historical Perspective*, **1988**, *5*, 363–369.
- [41] I.A. Abreu, D.E. Cabelli, Biochimica et Biophysica Acta Superoxide dismutases — a review of the metal-associated mechanistic variations, *BBA - Proteins Proteomics*. **2010**, *1804*, 263–274.
- [42] B.F. Lavelle, M.E. Mcadam, E.M. Fielden, P.B. Robertst, A Pulse-Radiolysis Study of the Catalytic Mechanism of the Iron-Containing Superoxide Dismutase from Photobacterium leiognathi, *Biochemical Journal* **1977**, *161*, 3–11.
- [43] J. Richardson, K.A. Thomas, B.H. Rubin, D.C. Richardson, Crystal structure of bovine Cu,Zn superoxide dismutase at 3 Å resolution: chain tracing and metal ligands, *Proc. Natl. Acad. Sci. U. S. A.* **1975**, *72*, 1349–1353.
- [44] R.W. Strange, S. V. Antonyuk, M.A. Hough, P.A. Doucette, J.S. Valentine, S.S. Hasnain, Variable metallation of human superoxide dismutase: Atomic resolution crystal structures of Cu-Zn, Zn-Zn and as-isolated wild-type enzymes, *J. Mol. Biol.* **2006**, *356*, 1152–1162.
- [45] P.A. Doucette, L.J. Whitson, X. Cao, V. Schirf, B. Demeler, J.S. Valentine, J.C. Hansen, P.J. Hart, Dissociation of human copper-zinc superoxide dismutase dimers using chaotrope and reductant: Insights into the molecular basis for dimer stability, *J. Biol. Chem.* **2004**, *279*, 54558–54566.
- [46] R. Rakhit, A. Chakrabarty, Structure, folding, and misfolding of Cu,Zn superoxide dismutase in amyotrophic lateral sclerosis, *Biochim. Biophys. Acta - Mol. Basis Dis.* **2006**, *1762*, 1025–1037.
- [47] M.A. Liebert, Y. Furukawa, T.V.O. Halloran, Posttranslational Modifications in Cu,Zn-Superoxide Dismutase and Mutations Associated with Amyotrophic Lateral Sclerosis, *Antioxidants & Redox Signaling*, **2006**, *8(5-6)*, 847-867.
- [48] R. Wroe, A. Wai-Ling Butler, P.M. Andersen, J.F. Powell, A. Al-Chalabi, ALSOD: The amyotrophic lateral sclerosis online database, *Amyotroph. Lateral Scler.* **2008**, *9*, 249–250.
- [49] G.S.A. Wright, S. V. Antonyuk, S.S. Hasnain, The biophysics of superoxide dismutase-1 and amyotrophic lateral sclerosis, *Q. Rev. Biophys.* **2019**, *52*, e12.
- [50] A.G. Reaume, J.L. Elliott, E.K. Hoffman, N.W. Kowall, R.J. Ferrante, D.F. Siwek, H.M. Wilcox, D.G. Flood, M.F. Beal, R.H. Brown, R.W. Scott, W.D. Snider, Motor neurons in Cu/Zn superoxide dismutase-deficient mice develop normally but exhibit enhanced cell death after axonal injury, *Nat. Genet.* **1996**, *13*, 43–47.
- [51] J.B. Sampson, J.S. Beckman, Hydrogen peroxide damages the zinc-binding site of zinc-deficient Cu,Zn superoxide dismutase, *Arch. Biochem. Biophys.* **2001**, *392*, 8–13.
- [52] C. Gill, J.P. Phelan, T. Hatzipetros, J.D. Kidd, V.R. Tassinari, B. Levine, M.Z. Wang, A. Moreno, K. Thompson, M. Maier, J. Grimm, A. Gill, F.G. Vieira, SOD1-positive aggregate accumulation in the CNS predicts slower disease progression and increased longevity in a mutant SOD1 mouse model of ALS, *Sci. Rep.* **2019**, *9*, 1–13.
- [53] L. McAlary, S.S. Plotkin, J.J. Yerbury, N.R. Cashman, Prion-Like Propagation of Protein Misfolding and Aggregation in Amyotrophic Lateral Sclerosis, *Front. Mol. Neurosci.* **2019**, *12*, 262.
- [54] L.I. Buijn, M.W. Becher, M.K. Lee, K.L. Anderson, N.A. Jenkins, N.G. Copeland, S.S. Sisodia, J.D. Rothstein, D.R. Borchelt, D.L. Price, D.W. Cleveland, ALS-linked SOD1 mutant G85R mediates damage to astrocytes and promotes rapidly progressive disease with SOD1-containing inclusions, *Neuron*. **1997**, *18*, 327–338.

- [55] B.F. Shaw, A. Durazo, A.M. Nersissian, J.P. Whitelegge, K.F. Faull, J.S. Valentine, Local Unfolding in a Destabilized, Pathogenic Variant of Superoxide Dismutase 1 Observed with H / D Exchange and Mass Spectrometry, *Journal of B. Chemistry* **2006**, *281*, 18167–18176.
- [56] M.A. Hough, J.G. Grossmann, S. V Antonyuk, R.W. Strange, P.A. Doucette, J.A. Rodriguez, L.J. Whitson, P.J. Hart, L.J. Hayward, J.S. Valentine, S.S. Hasnain, Dimer destabilization in superoxide dismutase may result in disease-causing properties: Structures of motor neuron disease mutants, *Proc. Natl. Acad. Sci. U. S. A.* **2004**, *101*, 5976–5981.
- [57] A. Kerman, H.L. Sidney, J. Robertson, A. Chakrabartty, Amyotrophic lateral sclerosis is a non-amyloid disease in which extensive misfolding of SOD1 is unique to the familial form, *Acta Neuropathol.* **2010**, *119*(3), 335–344.
- [58] L. Banci, I. Bertini, M. Boca, V. Calderone, F. Cantini, S. Girotto, M. Vieru, Structural and dynamic aspects related to oligomerization of apo SOD1 and its mutants, *Proc. Natl. Acad. Sci. U. S. A.* **2009**, *106*, 6980–6985.
- [59] L. Banci, I. Bertini, A. Durazo, S. Girotto, E.B. Gralla, M. Martinelli, J.S. Valentine, M. Vieru, J.P. Whitelegge, Metal-free superoxide dismutase forms soluble oligomers under physiological conditions: A possible general mechanism for familial ALS, *Prot- Nat. Acad. Sci. USA* **2007**, *104*(27), 11263-7.
- [60] H.R. Broom, J.A.O. Rumfeldt, K.A. Vassall, E.M. Meiering, Destabilization of the dimer interface is a common consequence of diverse ALS- associated mutations in metal free SOD1, *Protein Science* **2015**, *24*, 2081–2089.
- [61] M. Chattopadhyay, E. Nwadiibia, C.A. Strong, E.B. Gralla, S. Valentine, J.P. Whitelegge, The Disulfide Bond, but not Zinc or Dimerization, Controls Initiation and Seeded Growth in Amotrophic Lateral Sclerosis-linked Cu-Zn Superoxide Dismutase (SOD1) Fibrillation, *J. Biol. Chem.* **2015**, *290*, 30624–36.
- [62] K. Sea, S.H. Sohn, A. Durazo, Y. Sheng, B.F. Shaw, X. Cao, A.B. Taylor, L.J. Whitson, S.P. Holloway, P.J. Hart, D.E. Cabelli, E.B. Gralla, J. Selverstone, Insights into the Role of the Unusual Disulfide Bond in Copper-Zinc Superoxide Dismutase, *J Bio Chem* **290** (2015) 2405–2418.
- [63] S.S. Ray, R.J. Nowak, K. Strokovich, R.H. Brown, T. Walz, P.T. Lansbury, An Intersubunit Disulfide Bond Prevents in Vitro Aggregation of a Superoxide Dismutase-1 Mutant Linked to Familial Amyotrophic Lateral Sclerosis, *Biochemistry.* **2004**, *43*, 4899–4905.
- [64] T.E. Brotherton, Y. Li, J.D. Glass, Neurobiology of Disease Cellular toxicity of mutant SOD1 protein is linked to an easily soluble, non-aggregated form in vitro, *Neurobiol. Dis.* **2013**, *49*, 49–56.
- [65] M. Watanabe, M. Dykes-hoberg, V.C. Culotta, D.L. Price, P.C. Wong, J.D. Rothstein, Histological Evidence of Protein Aggregation in Mutant SOD1 Transgenic Mice and in Amyotrophic Lateral Sclerosis Neural Tissues, *Neurobiol. Dis.* **2001**, *941*, 933–941.
- [66] W.G. Ganesan S, Rohde G, Mutant SOD1 detoxification mechanisms in intact single cells, *Cell Death Differ.* **2008**, *15*, 312–321.
- [67] M.T. Carri, M. Cozzolino, SOD1 and mitochondria in ALS: a dangerous liaison, *J. Bioenerg. Biomembr.* **2011**, *43*(6), 593–599.
- [68] C.P.W. Soon, P.S. Donnelly, B.J. Turner, L.W. Hung, P.J. Crouch, N.A. Sherratt, J. Tan, N.K. Lim, L. Lam, L. Bica, S. Lim, J.L. Hickey, J. Morizzi, A. Powell, D.I. Finkelstein, J.G. Culvenor, C.L. Masters, J. Duce, A.R. White, K.J. Barnham, Q. Li, Diacetylbis (N (4) - methylthiosemicarbazonato) Copper (II) (Cu II (atsm)) Protects against Peroxynitrite-induced Nitrosative Damage and Prolongs Survival in Amyotrophic Lateral Sclerosis Mouse Model, *J. Biol. Chem.* **2011**, *286*, 44035–44044.
- [69] J.R. Williams, E. Trias, P.R. Beilby, N.I. Lopez, E.M. Labut, C.S. Bradford, B.R. Roberts, E.J. Mcallum, P.J. Crouch, T.W. Rhoads, C. Pereira, M. Son, L. Elliott, M.C. Franco, A.G. Est, L. Barbeito, S. Joseph, I. Nathan, M. Edwin, S. Bradford, R. Blaine, J. Erin, J. Peter, W. Timothy, L. Jeffrey, M. Clara, Copper delivery to the CNS by CuATSMeffectively treats motor neuron

- disease in SODG93Amice co-expressing the Copper-Chaperone-for-SOD, *Neurobiol. Dis.* **2016**, *89*, 1-9.
- [70] F.G. Vieira, T. Hatzipetros, K. Thompson, A.J. Moreno, J.D. Kidd, V.R. Tassinari, B. Levine, S. Perrin, A. Gill, CuATSM efficacy is independently replicated in a SOD1 mouse model of ALS while unmetallated ATSM therapy fails to reveal benefits, *IBRO Reports.* **2017**, *2*, 47–53.
- [71] L. Banci, I. Bertini, O. Blaževič, V. Calderone, F. Cantini, J. Mao, A. Trapananti, M. Vieru, I. Amori, M. Cozzolino, M.T. Carri, Interaction of cisplatin with human superoxide dismutase, *J. Am. Chem. Soc.* **2012**, *134*, 7009–7014.
- [72] G.S.A. Wright, S. V. Antonyuk, S.S. Hasnain, A faulty interaction between SOD1 and hCCS in neurodegenerative disease, *Sci. Rep.* **2016**, *6*, 1–9.
- [73] S.S. Ray, R.J. Nowak, R.H. Brown, P.T. Lansbury, Small-molecule-mediated stabilization of familial amyotrophic lateral sclerosis-linked superoxide dismutase mutants against unfolding and aggregation, *Proc. Natl. Acad. Sci. U. S. A.* **2005**, *102*, 3639–3644.
- [74] R.J. Nowak, G.D. Cuny, S. Choi, P.T. Lansbury, S.S. Ray, Improving Binding Specificity of Pharmacological Chaperones That Target Mutant Superoxide Dismutase-1 Linked to Familial Amyotrophic Lateral Sclerosis Using Computational Methods, *J. Med. Chem.* **2010**, *53*, 2709–2718.
- [75] S. Antonyuk, R.W. Strange, S.S. Hasnain, Structural Discovery of Small Molecule Binding Sites in Cu - Zn Human Superoxide Dismutase Familial Amyotrophic Lateral Sclerosis Mutants Provides Insights for Lead Optimization, *J. Med. Chem.* **2010** 1402–1406.
- [76] G.S.A. Wright, S. V Antonyuk, N.M. Kershaw, R.W. Strange, S.S. Hasnain, Ligand binding and aggregation of pathogenic SOD1, *Nat. Commun.* **2013**, *4*, 1710–1758.
- [77] E. Pokrishevsky, L. Mcalary, N.E. Farrowell, B. Zhao, M. Sher, J.J. Yerbury, N.R. Cashman, Tryptophan 32-mediated SOD1 aggregation is attenuated by pyrimidine-like compounds in living cells, *Sci. Rep.* **2018**, 1–12.
- [78] E. Pokrishevsky, R.H. Hong, I.R. Mackenzie, N.R. Cashman, Spinal cord homogenates from SOD1 familial amyotrophic lateral sclerosis induce SOD1 aggregation in living cells, *PLoS One* **2017**, 1–10.
- [79] J.R. Auclair, K.J. Boggio, G.A. Petsko, D. Ringe, J.N. Agar, Strategies for stabilizing superoxide dismutase (SOD1), the protein destabilized in the most common form of familial amyotrophic lateral sclerosis, *Proc. Natl. Acad. Sci. U. S. A.* **2010**, *107*, 21394–21399.
- [80] M.J. Capper, G.S.A. Wright, L. Barbieri, E. Luchinat, E. Mercatelli, L. Mcalary, J.J. Yerbury, P.M.O. Neill, S. V Antonyuk, L. Banci, S.S. Hasnain, The cysteine-reactive small molecule ebselen facilitates effective SOD1 maturation, *Nat. Commun.* **2018**, *9*, 1–9.
- [81] V. Chantadol, G.S.A. Wright, K. Ampornnanai, M. Shahid, S. V Antonyuk, G. Washbourn, M. Rogers, N. Roberts, M. Pye, P.M.O. Neill, S.S. Hasnain, Ebselen as template for stabilization of A4V mutant dimer for motor neuron disease therapy, *Commun. Biol.* **2020**, *3(1)*, 2–11.
- [82] N.J. Moerke, Fluorescence Polarization (FP) Assays for Monitoring Peptide-Protein or Nucleic Acid-Protein Binding, *Curr. Protoc. Chem. Biol.* **2009**, *1*, 1–15.
- [83] M.R. Arkin, M.A. Glicksman, H. Fu, J.J. Havel, Y. Du, Inhibition of Protein-Protein Interactions: Non-Cellular Assay Formats, *Assay Guid. Man.* **2004**, 1–23.
- [84] E. Feinstein, G. Deikus, E. Rusinova, E.L. Rachofsky, J.B.A. Ross, W.R. Laws, Constrained analysis of fluorescence anisotropy decay: Application to experimental protein dynamics, *Biophys. J.* **2003**, *84*, 599–611.
- [85] E. Gratton, M. Limkeman, A continuously variable frequency cross-correlation phase fluorometer with picosecond resolution, *Biophys. J.* **1983**, *44*, 315–324.
- [86] W. Becker, A. Bergmann, M.A. Hink, K. König, K. Benndorf, C. Biskup, Fluorescence Lifetime Imaging by Time-Correlated Single-Photon Counting, *Microsc. Res. Tech.* **2004**, *63*, 58–66.

- [87] R. Magnez, B. Thiroux, S. Taront, Z. Segoula, B. Quesnel, X. Thuru, PD-1/PD-L1 binding studies using microscale thermophoresis, *Sci. Rep.* **2017**, *7*, 1–8.
- [88] C.J. Wienken, P. Baaske, U. Rothbauer, D. Braun, S. Duhr, Protein-binding assays in biological liquids using microscale thermophoresis, *Nat. Commun.* **2010**, *1*(100).
- [89] M. Jerabek-Willemsen, C.J. Wienken, D. Braun, P. Baaske, S. Duhr, Molecular interaction studies using microscale thermophoresis, *Assay Drug Dev. Technol.* **2011**, *9*, 342–353.
- [90] S. Duhr, D. Braun, Why molecules move along a temperature gradient, *Proc. Natl. Acad. Sci. U. S. A.* **2006**, *103*, 19678–19682.
- [91] M. Jerabek-Willemsen, T. André, R. Wanner, H.M. Roth, S. Duhr, P. Baaske, D. Breitsprecher, MicroScale Thermophoresis: Interaction analysis and beyond, *J. Mol. Struct.* **2014**, *1077*, 101–113.
- [92] M.W. Freyer, E.A. Lewis, Isothermal Titration Calorimetry: Experimental Design, Data Analysis, and Probing Macromolecule/Ligand Binding and Kinetic Interactions, *Methods Cell Biol.* **2008**, *84*, 79–113.
- [93] I. Jelesarov, H.R. Bosshard, Isothermal titration calorimetry and differential scanning calorimetry as complementary tools to investigate the energetics of biomolecular recognition, *J. Mol. Recognit.* **1999**, *12*, 3–18.
- [94] C. Song, S. Zhang, H. Huang, Choosing a suitable method for the identification of replication origins in microbial genomes, *Front. Microbiol.* **2015**, *6*, 1–18.
- [95] A. Rickli, O.D. Moning, M.C. Hoener, M.E. Liechti, Receptor interaction profiles of novel psychoactive tryptamines compared with classic hallucinogens, *Eur. Neuropsychopharmacol.* **2016**, *26*, 1327–1337.
- [96] et al. Etrup A, Hansen M, Santini MA, Radiosynthesis and in vivo evaluation of a series of substituted ¹¹C-phenethylamines as 5-HT_{2A} agonist PET tracers, *Eur. J. Nucl. Med. Mol. Imaging.* **2011**, *38*, 681–693.
- [97] V. Estévez, M. Villacampa, J. Carlos Menéndez, Recent advances in the synthesis of pyrroles by multicomponent reactions, *Chem. Soc. Rev.* **2014**, *43*, 4633–4657.
- [98] L. Zhao, C. Bruneau, H. Doucet, Palladium-Catalysed Direct Polyarylation of Pyrrole Derivatives, *ChemCatChem.* **2013**, *5*, 255–262.
- [99] L. He, P.W.H. Chan, W.M. Tsui, W.Y. Yu, C.M. Che, Ruthenium(II) porphyrin-catalyzed amidation of aromatic heterocycles, *Org. Lett.* **2004**, *6*, 2405–2408.
- [100] J. Hofmann, E. Gans, T. Clark, M.R. Heinrich, Radical Arylation of Anilines and Pyrroles via Aryldiazotates, *Chem. - A Eur. J.* **2017**, *23*, 9647–9656.
- [101] H. Cho, R. Madden, B. Nisanci, B. Török, The Paal-Knorr reaction revisited. A catalyst and solvent-free synthesis of underivatized and N-substituted pyrroles, *Green Chem.* **2015**, *17*, 1088–1099.
- [102] A. Devi, Shallu, M.L. Sharma, J. Singh, Paal-Knorr pyrrole synthesis using recyclable amberlite IR 120 acidic resin: A green approach, *Synth. Commun.* **2012**, *42*, 1480–1488.
- [103] B. Wang, Y. Gu, C. Luo, T. Yang, L. Yang, J. Suo, Pyrrole synthesis in ionic liquids by Paal-Knorr condensation under mild conditions, *Tetrahedron Lett.* **2004**, *45*, 3417–3419.
- [104] S. Handy, K. Lavender, Organic synthesis in deep eutectic solvents: Paal-Knorr reactions, *Tetrahedron Lett.* **2013**, *54*, 4377–4379.
- [105] I. Colomer, A.E.R.R. Chamberlain, M.B. Haughey, T.J. Donohoe, Hexafluoroisopropanol as a highly versatile solvent, *Nat. Rev. Chem.* **2017**, *1*, 0088.
- [106] D. Akbaşlar, O. Demirkol, S. Giray, Paal-knorr pyrrole synthesis in water, *Synth. Commun.* **2014**, *44*, 1323–1332.

- [107] S.K. De, Simple synthesis of pyrroles under solvent-free conditions, *Synth. Commun.* **2008**, *38*, 2768–2774.
- [108] N.M. Nevar, A. V. Kel'in, O.G. Kulinkovich, One step preparation of 1,4-diketones from methyl ketones and α -bromomethyl ketones in the presence of $ZnCl_2 \cdot t\text{-BuOH} \cdot Et_2NR$ as a condensation agent, *Synthesis (Stuttg)*. **2000**, *9*, 1259–1262.
- [109] M. Kalek, J. Stawinski, Efficient synthesis of mono- and diarylphosphinic acids: a microwave-assisted palladium-catalyzed cross-coupling of aryl halides with phosphinate, *Tetrahedron*. **2009**, *65*, 10406–10412.
- [110] C.M. Sevrain, M. Berchel, H. Couthon, P.A. Jaffrès, Phosphonic acid: Preparation and applications, *Beilstein J. Org. Chem.* **2017**, *13*, 2186–2213.
- [111] A. Hafner, M. Meisenbach, J. Sedelmeier, Flow Chemistry on Multigram Scale: Continuous Synthesis of Boronic Acids within 1 s, *Org. Lett.* **2016**, *18*, 3630–3633.
- [112] M.A. Fernández-Rodríguez, Q. Shen, J.F. Hartwig, A general and long-lived catalyst for the palladium-catalyzed coupling of aryl halides with thiols, *J. Am. Chem. Soc.* **2006**, *128*, 2180–2181.
- [113] C. Kahrs, M. Schmidtman, M.S. Wickleder, J. Christoffers, Pyridine and Pyrimidine Functionalized Benzene Sulfonic and Disulfonic Acids as New Linker Compounds for Coordination Polymers, *European J. Org. Chem.* **2018**, *2018*, 6499–6506.
- [114] X. Huang, X. Li, M. Zou, S. Song, C. Tang, Y. Yuan, N. Jiao, From ketones to esters by a Cu-catalyzed highly selective C(CO)-C(alkyl) bond cleavage: Aerobic oxidation and oxygenation with air, *J. Am. Chem. Soc.* **2014**, *136*, 14858–14865.
- [115] L. Hong woo, K. Young min, L. Yoo, Choong, K. Kang, Sung, A. Soon kil, An efficient method for the large-scale synthesis of Atorvastatin Calcium. biomolecules & therapeutics, *Biomol. Ther. (Seoul)*. **2008**, *16*, 28–33.
- [116] F. Stauffer, R. Neier, Synthesis of tri- and tetrasubstituted furans catalyzed by trifluoroacetic acid, *Org. Lett.* **2000**, *2*, 3535–3537.
- [117] Hexafluoroisopropanol as a Solvent for Halogenation of (Het)aromatics, *Synfacts*. **2018**, *14* 0244.
- [118] M. Tajbakhsh, R. Hosseinzadeh, H. Alinezhad, S. Ghahari, A. Heydari, S. Khaksar, Catalyst-free one-pot reductive alkylation of primary and secondary amines and N,N-dimethylation of amino acids using sodium borohydride in 2,2,2-trifluoroethanol, *Synthesis (Stuttg)*. **2011**, 490–496.
- [119] A.F. Abdel-Magid, C.A. Maryanoff, Reductive amination of aldehydes and ketones with weakly basic anilines using sodium triacetoxyborohydride, *Synlett*. **1990**, *9*, 537–539.
- [120] Akerlof, Preparation of Dibenzyl Ketone and Phenylacetone, *J. Chem. Inf. Model.* **1970**, *53*, 1689–1699.
- [121] D.R. Romer, Convenient laboratory method for the synthesis of symmetrical 1,3-diphenylacetone derivatives, *Synthesis (Stuttg)*. **2011**, *17*, 2721–2723.
- [122] M.L. Keshtov, E.I. Mal'tsev, D. V. Marochkin, A. V. Muranov, A.R. Khokhlov, New photo- and electroluminescent conjugated copolyfluorenes with 7,8,10-triarylfluoranthene units in the backbone, *Polym. Sci. - Ser. B*. **2012**, *54*, 289–296.
- [123] W.K. An, M.Y. Han, C.A. Wang, S.M. Yu, Y. Zhang, S. Bai, W. Wang, Insights into the asymmetric heterogeneous catalysis in porous organic polymers: Constructing A TADDOL-Embedded chiral catalyst for studying the structure-activity relationship, *Chem. - A Eur. J.* **2014**, *20*, 11019–11028.
- [124] H. Walther, L. Haase, H. Gross, B. Costisella, I. Keitel, Aldehyde, tert. Amine bzw. Acetale aus Amidacetalen und Grignardverbindungen, *J. Furr Prakt. Chemie.* **1980**, *322*, 902–908.
- [125] P.W. Riddles, R.L. Blakeley, B. Zerner, Ellman's reagent: 5,5'-Dithiobis(2-nitrobenzoic Acid) - a Reexamination, *Anal. Biochem.* **1979**, *94*, 75–81.

- [126] Y. Kuang, K. Balakrishnan, V. Gandhi, X. Peng, Hydrogen Peroxide Inducible DNA Cross-Linking Agents: targeted Anticancer Prodrugs, *J. Am. Chem. Soc.* **2011**, *133*(48), 19278–19281.
- [127] E.A. Boyd, A.C. Regan, K. James, Synthesis of alkyl phosphinic acids from silyl phosphonites and alkyl halides, *Tetrahedron Lett.* **1994**, *35*, 4223–4226.
- [128] A. Joshi-Pangu, X. Ma, M. Diane, S. Iqbal, R.J. Kribs, R. Huang, C.Y. Wang, M.R. Biscoe, Palladium-catalyzed borylation of primary alkyl bromides, *J. Org. Chem.* **2012**, *77*, 6629–6633.
- [129] H. Yi, M. Albrecht, A. Valkonen, K. Rissanen, Perfluoro-1,1'-biphenyl and perfluoronaphthalene and their derivatives as π -acceptors for anions, *New J. Chem.* **2015**, *39*, 746–749.
- [130] J.P. Crow, J.B. Sampson, Y. Zhuang, J.A. Thompson, J.S. Beckman, Decreased zinc affinity of amyotrophic lateral sclerosis, associated superoxide dismutase mutants leads to enhanced catalysis of tyrosine nitration by peroxyxynitrite, *J. Neurochem.* **1997**, *69*, 1936–1944.
- [131] A.S. Tan, M. V. Berridge, Superoxide produced by activated neutrophils efficiently reduces the tetrazolium salt, WST-1 to produce a soluble formazan: A simple colorimetric assay for measuring respiratory burst activation and for screening anti-inflammatory agents, *J. Immunol. Methods.* **2000**, *238*, 59–68.
- [132] H.J. Forman, I. Fridovich, On the stability of bovine superoxide dismutase. The effects of metals., *J. Biol. Chem.* **1973**, *248*, 2645–2649.
- [133] H.T. Li, M. Jiao, J. Chen, Y. Liang, Roles of zinc and copper in modulating the oxidative refolding of bovine copper, zinc superoxide dismutase, *Acta Biochim. Biophys. Sin. (Shanghai)*. **2010**, *42*, 183–194.
- [134] E. Fisher, Y. Zhao, R. Richardson, M. Janik, A.K. Buell, F.I. Aigbirhio, G. Tóth, Detection and Characterization of Small Molecule Interactions with Fibrillar Protein Aggregates Using Microscale Thermophoresis, *ACS Chem. Neurosci.* **2017**, *8*, 2088–2095.
- [135] R. Manjula, G.S.A. Wright, R.W. Strange, B. Padmanabhan, Assessment of ligand binding at a site relevant to SOD1 oxidation and aggregation, *FEBS Lett.* **2018**, *592*, 1725–1737.
- [136] S. Vega, O. Abian, A. Velazquez-Campoy, A unified framework based on the binding polynomial for characterizing biological systems by isothermal titration calorimetry, *Methods.* **2015**, *76*, 99–115.
- [137] H. Inoue, H. Nojima, H. Okayama, High efficiency transformation of *Escherichia coli* with plasmids, *Gene.* **1990**, *96*, 23–28.
- [138] M M Bradford, A rapid and sensitive method for the quantitation of microgram quantities of protein utilizing the principle of protein-dye binding, *Anal Biochem.* **1976**, *72*, 248–54.
- [139] W. Kabsch, Xds., *Acta Crystallogr. D. Biol. Crystallogr.* **2010**, *66*, 125–32.

8 Appendix

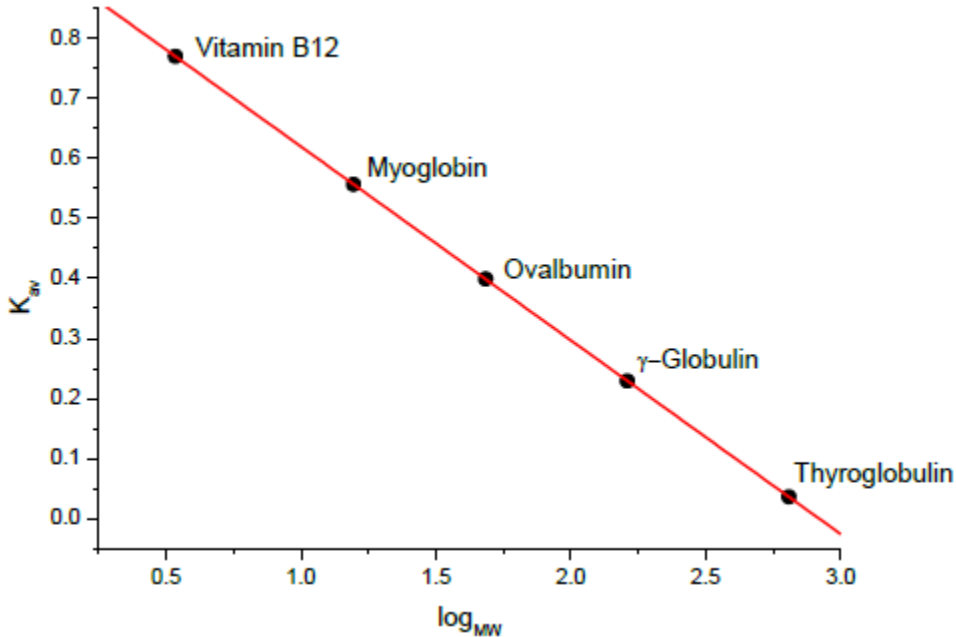


Figure 8-1. Biorad standard curve for SEC.

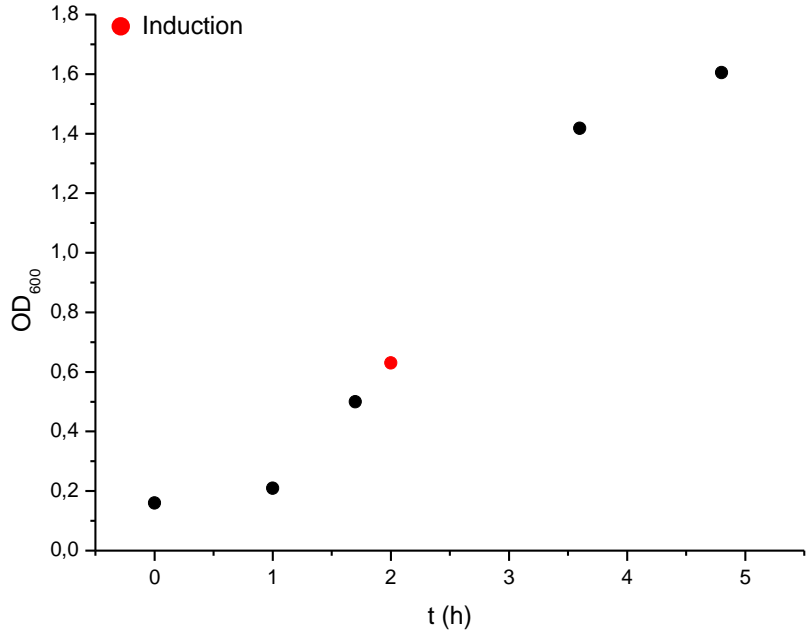


Figure 8-2. Growth curve for hSOD1 wt with indicated induction.

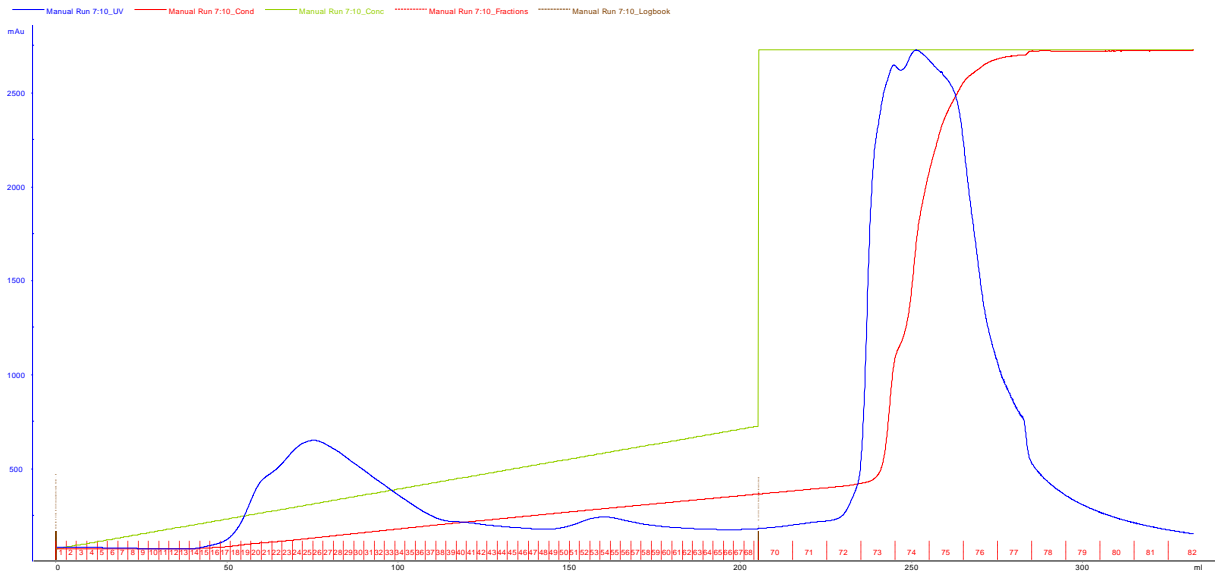


Figure 8-3. Purification of hSOD1 wt on a TMAE column.

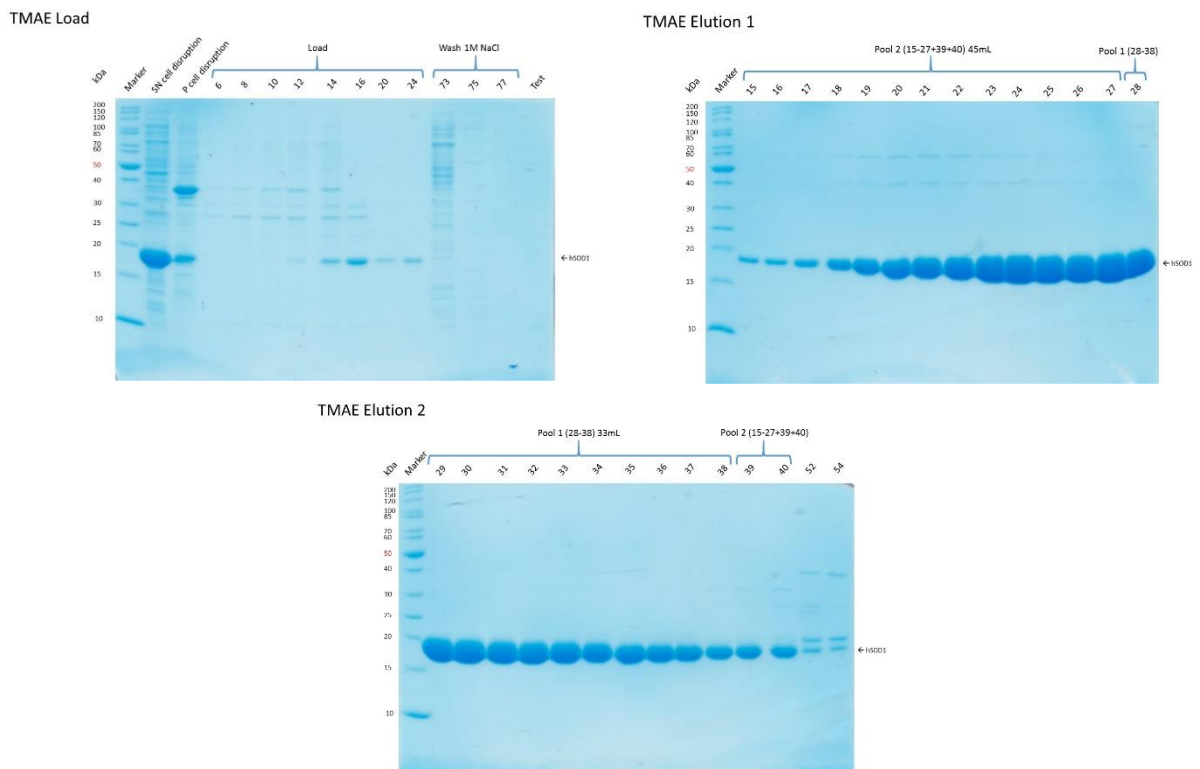
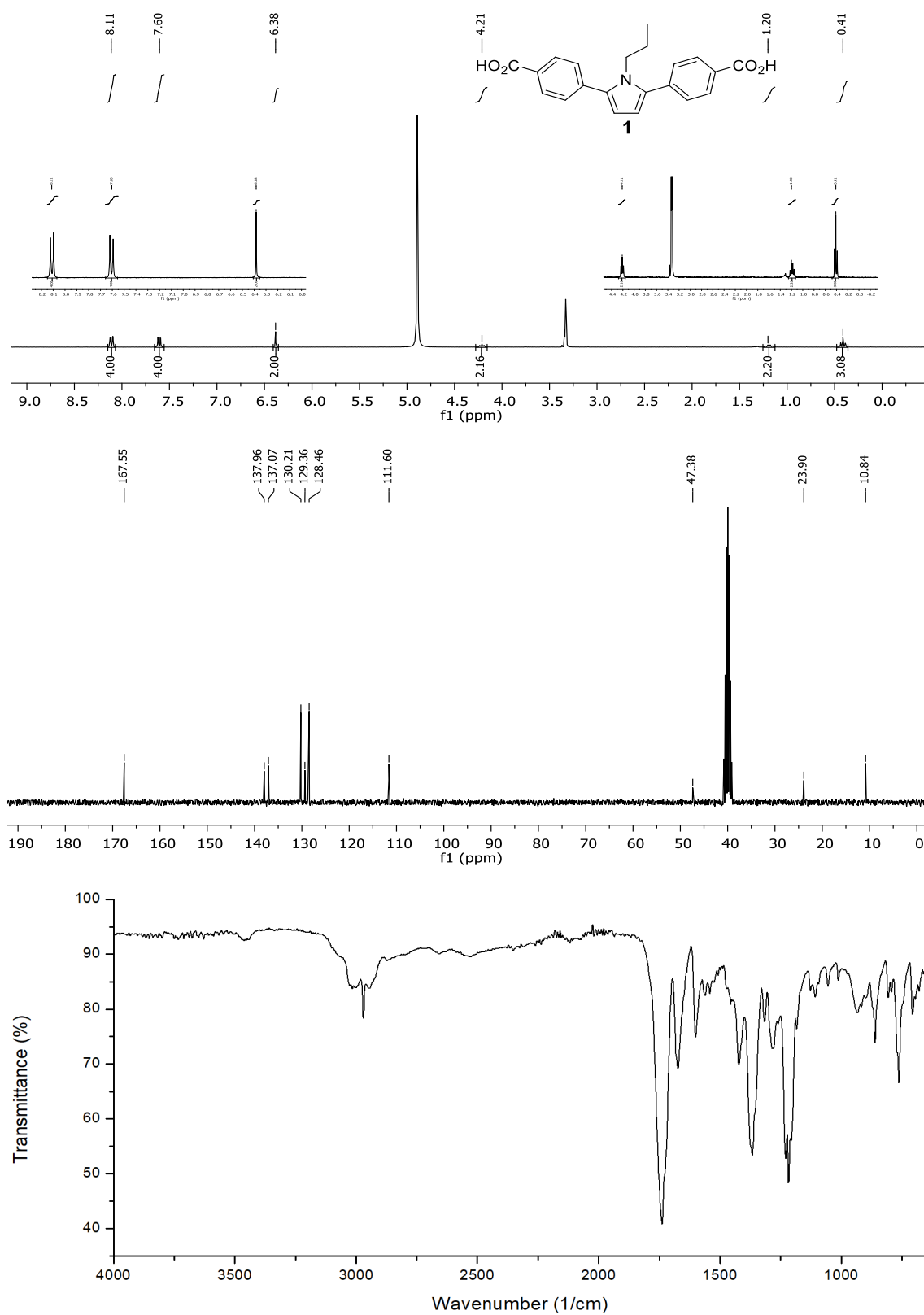
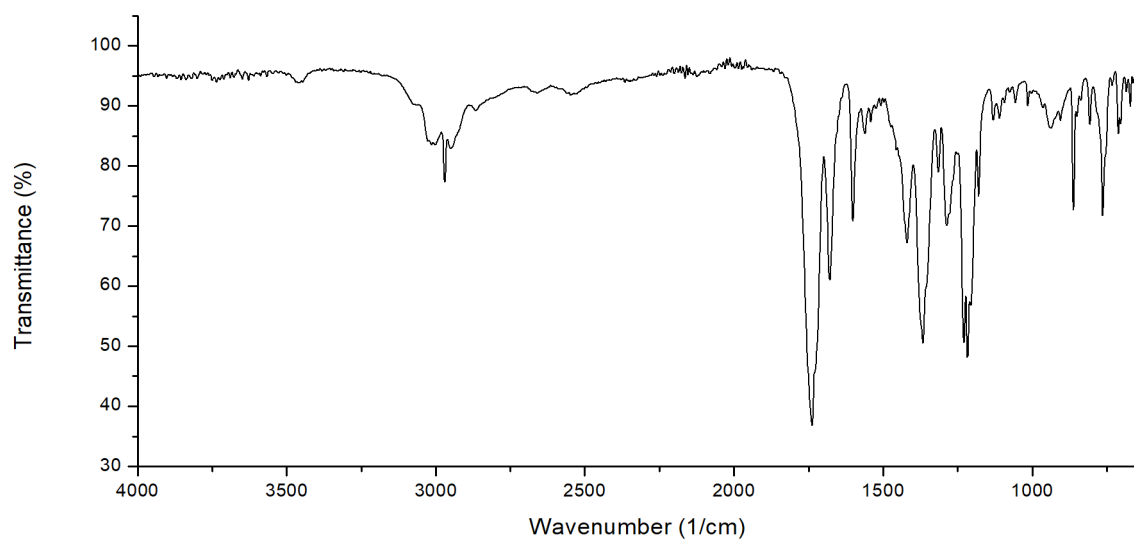
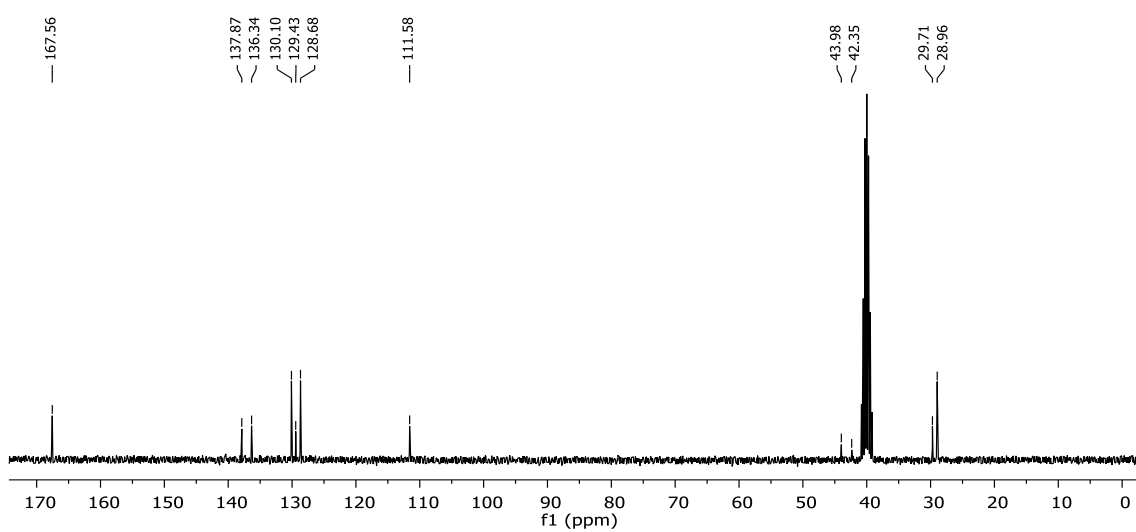
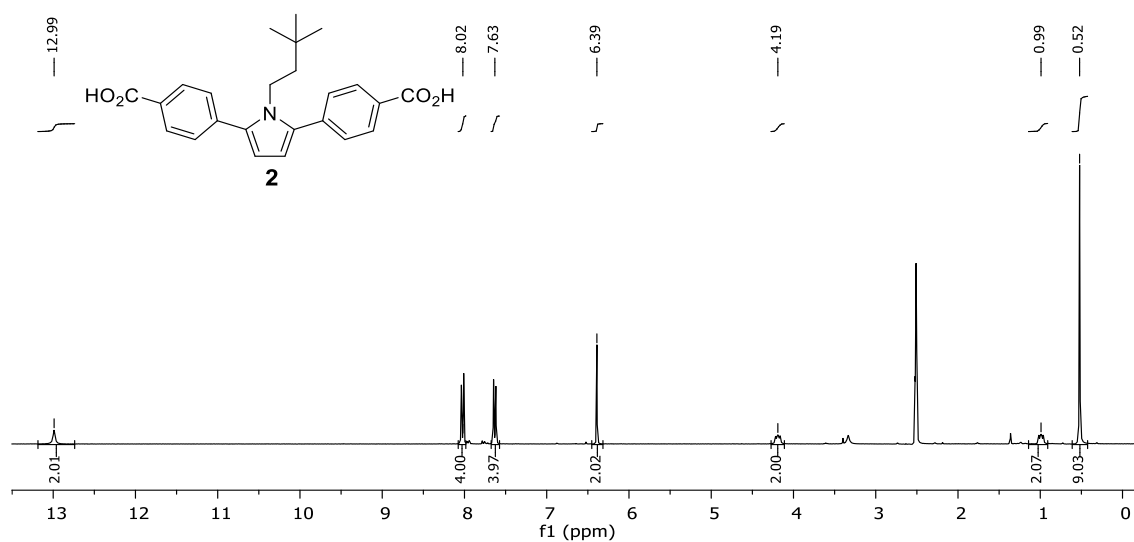


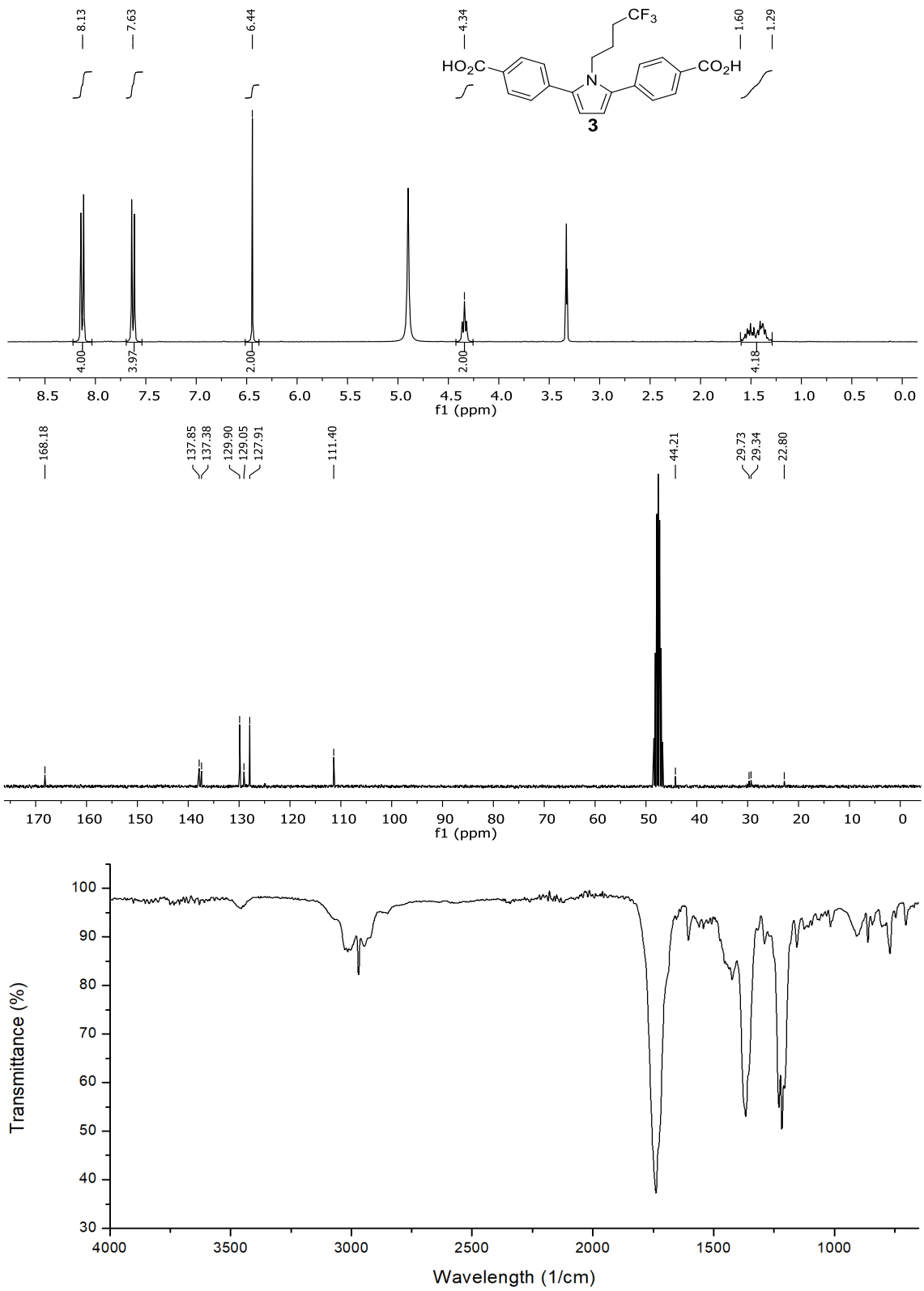
Figure 8-4. SDS-page gels of the second purification of hSOD1 wt.

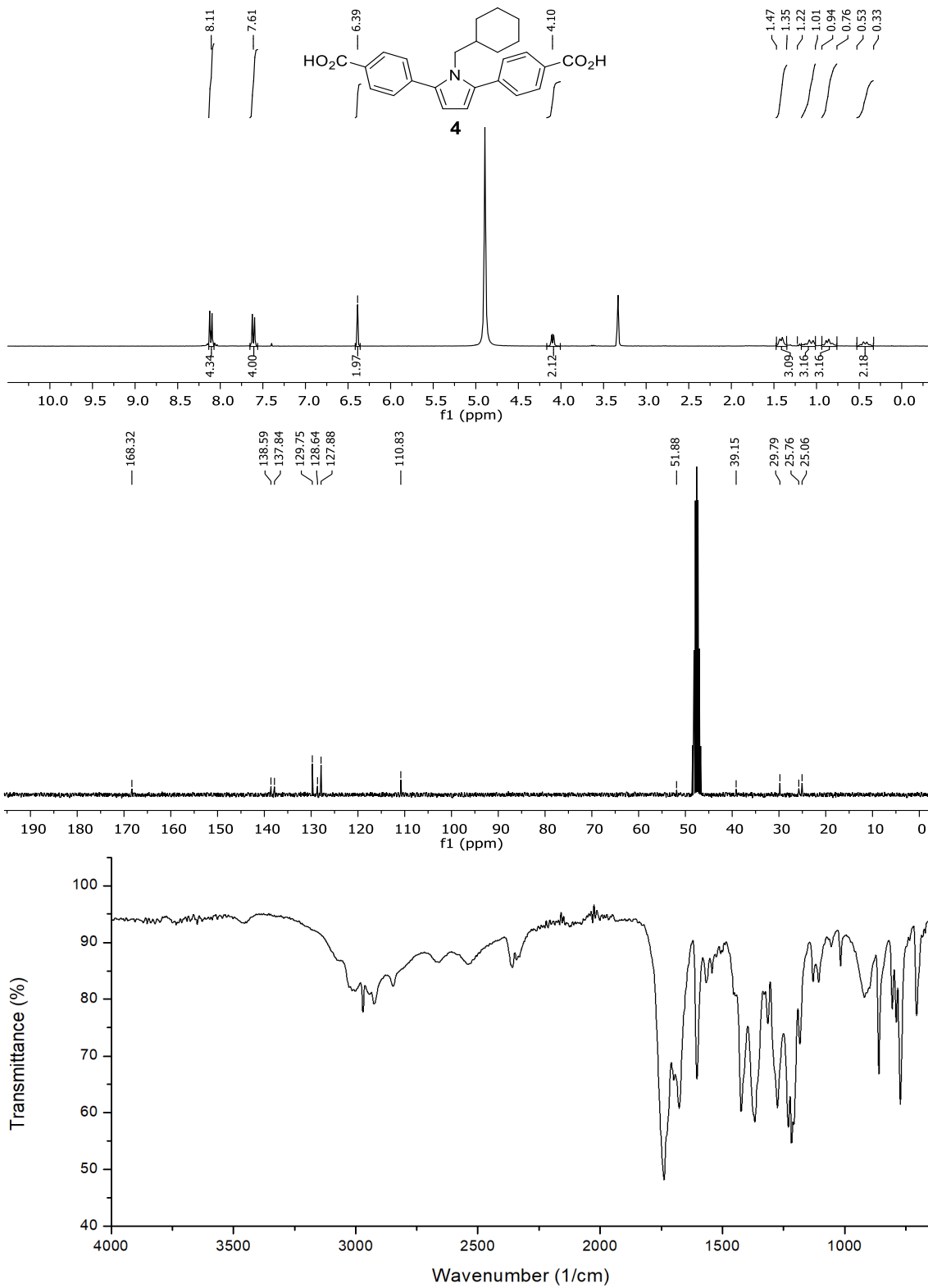
8.1 Analytics

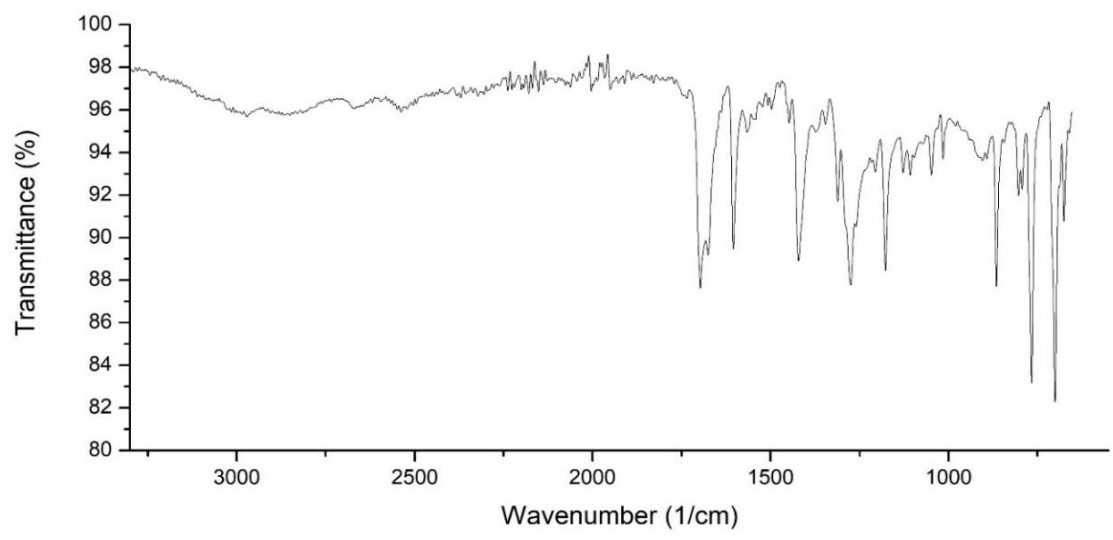
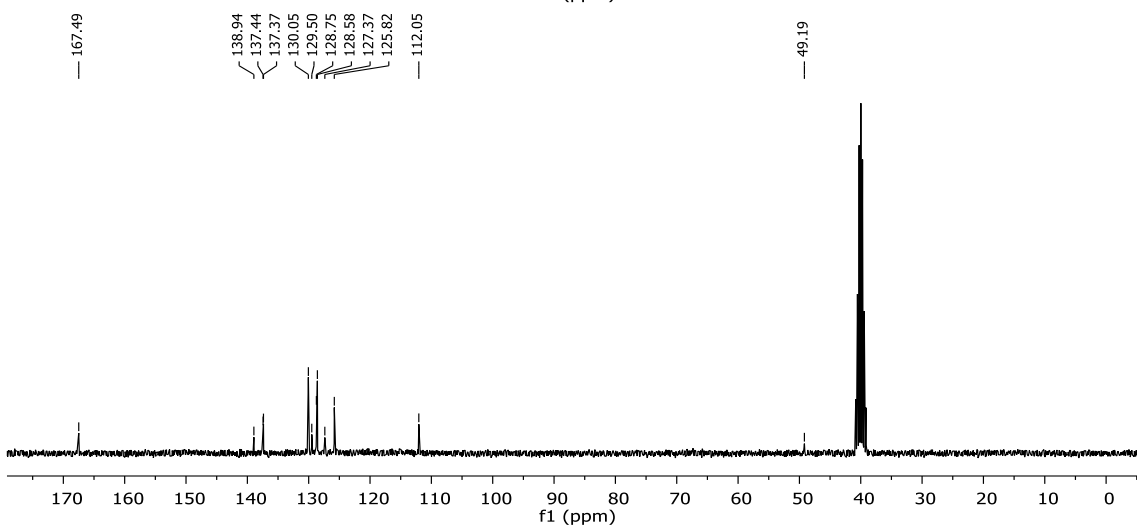
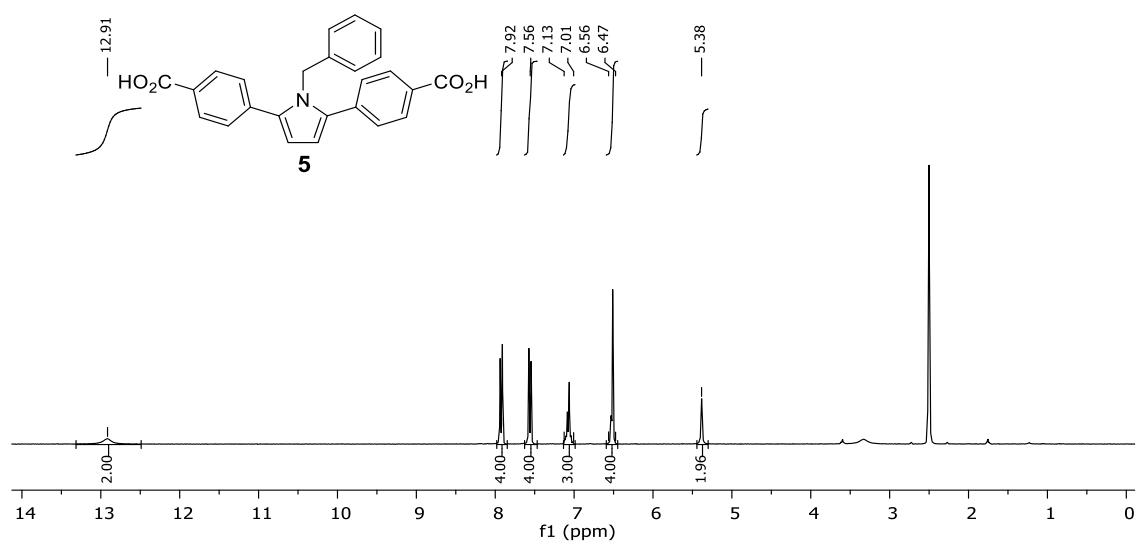
8.1.1 NMR and IR spectra

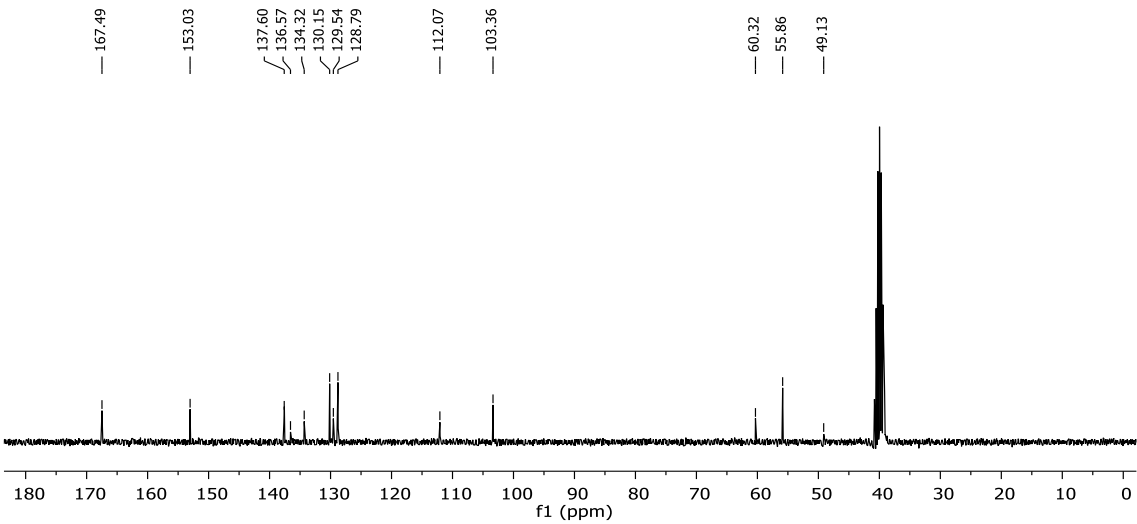
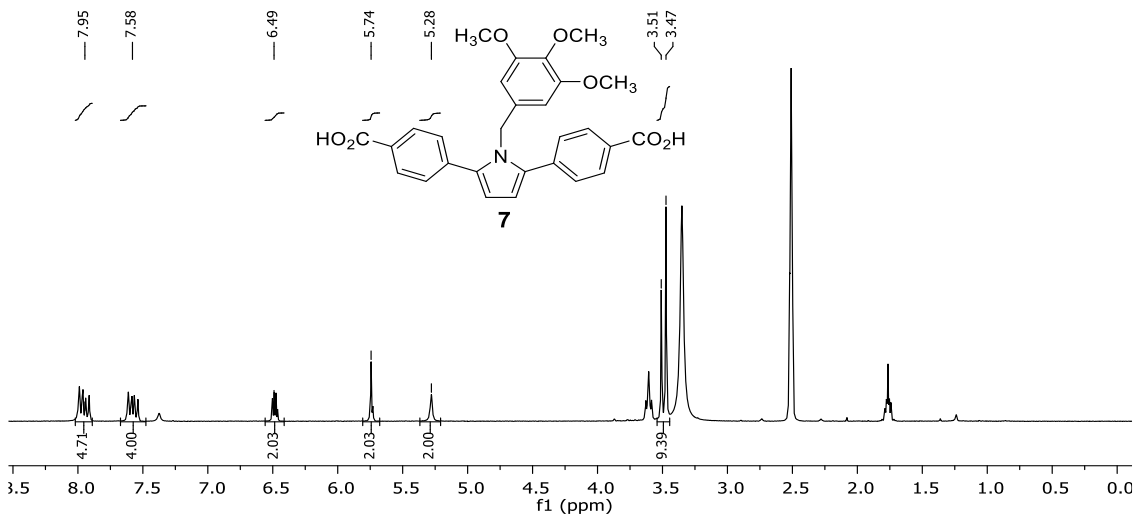
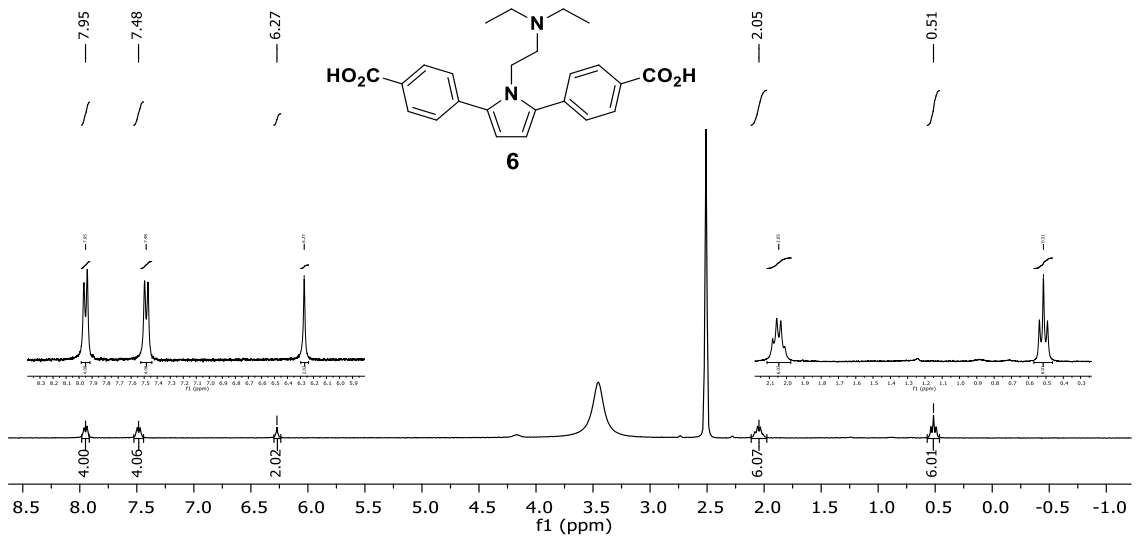


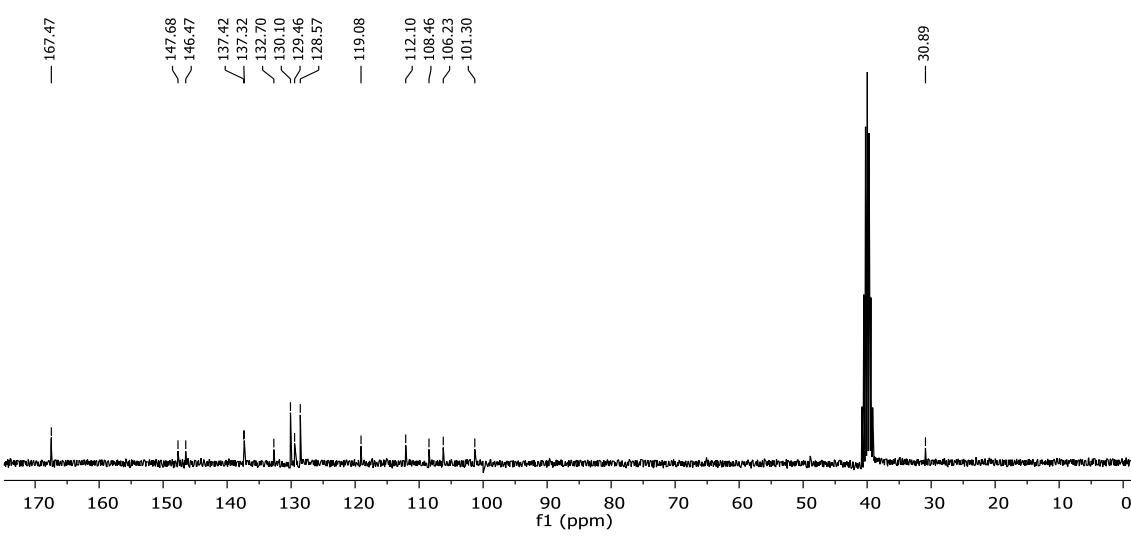
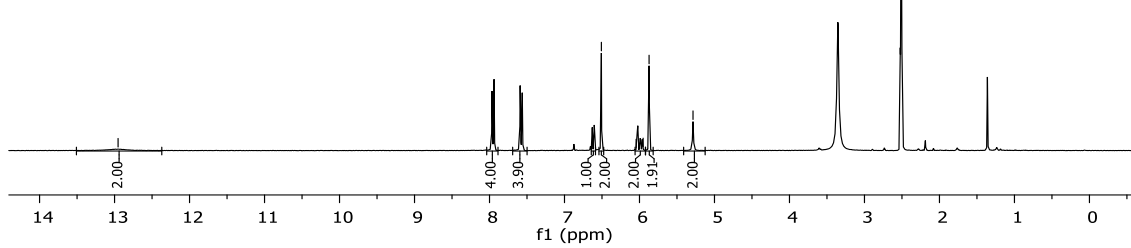
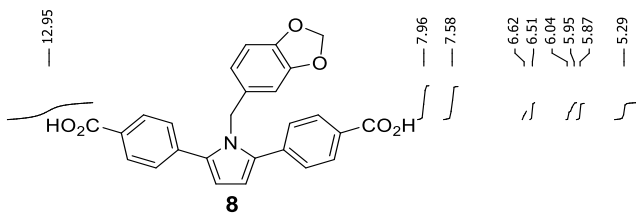
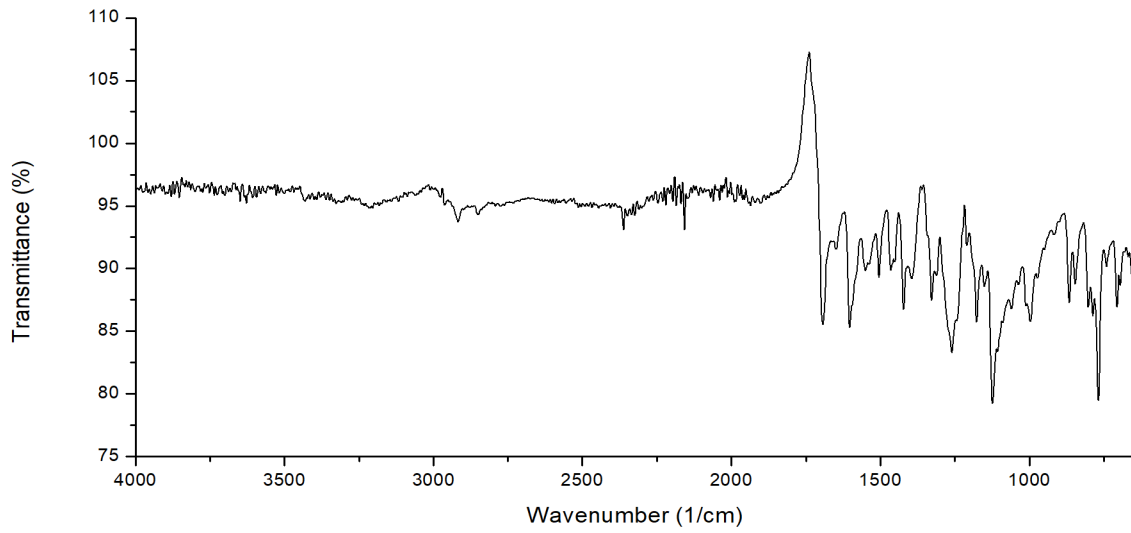


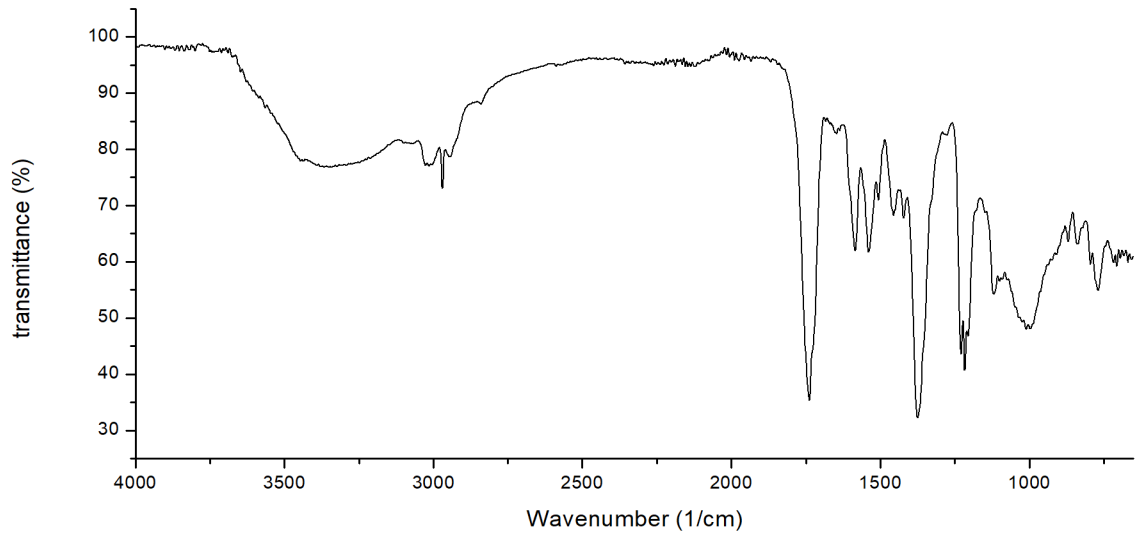
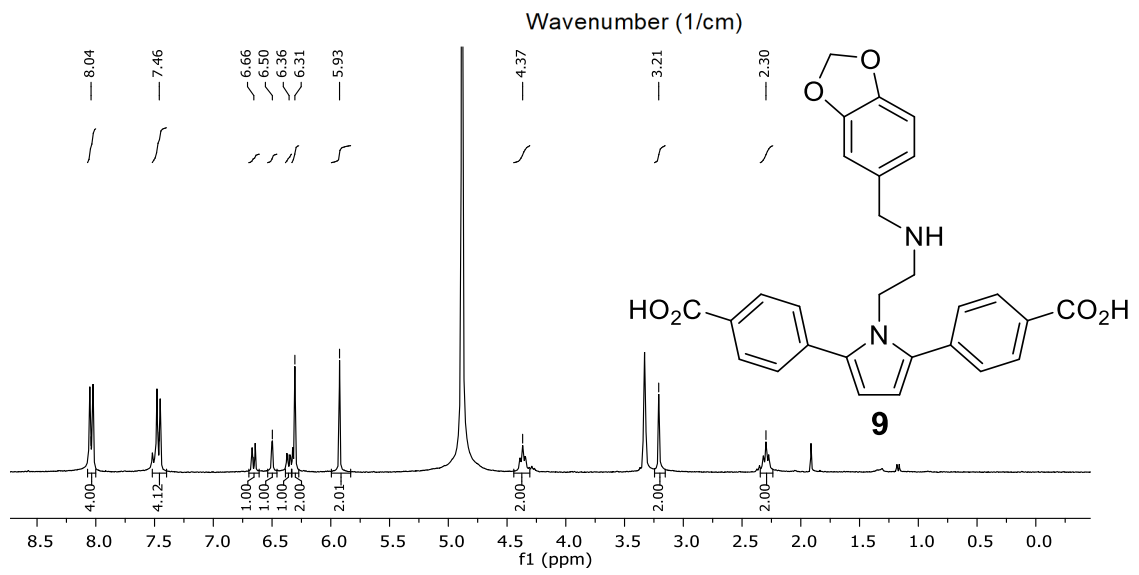
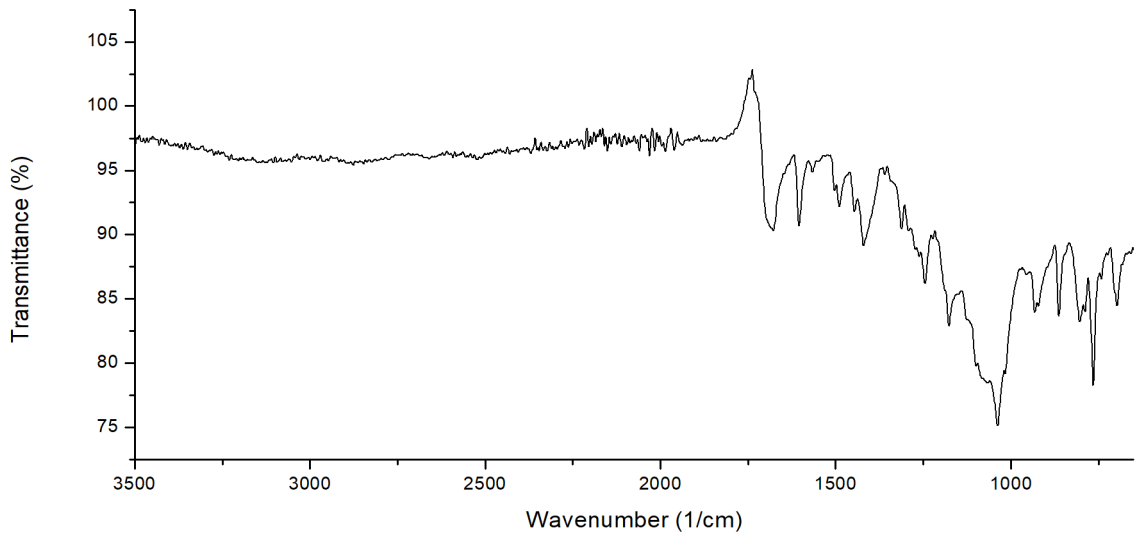


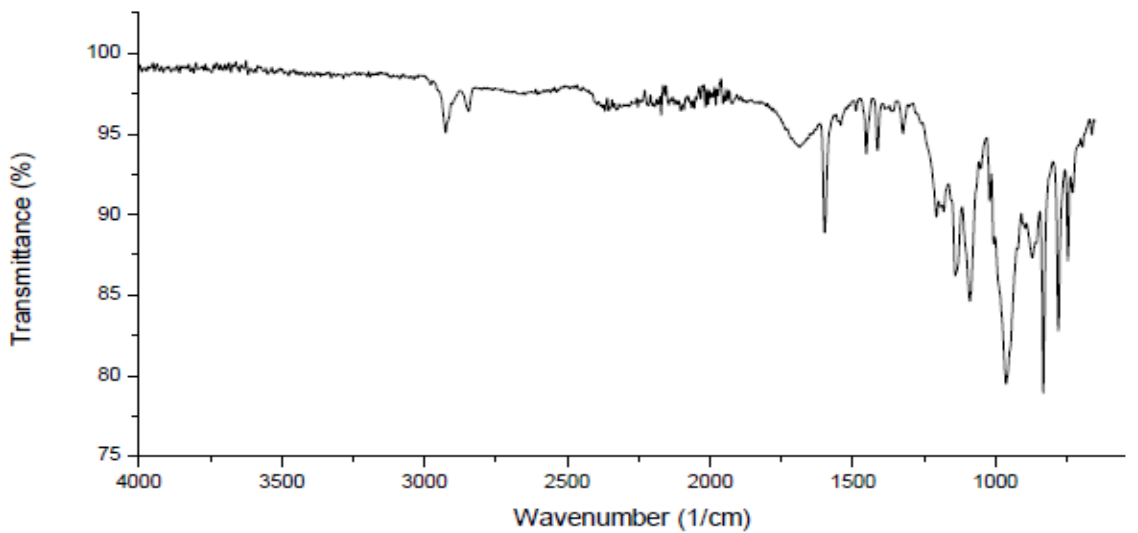
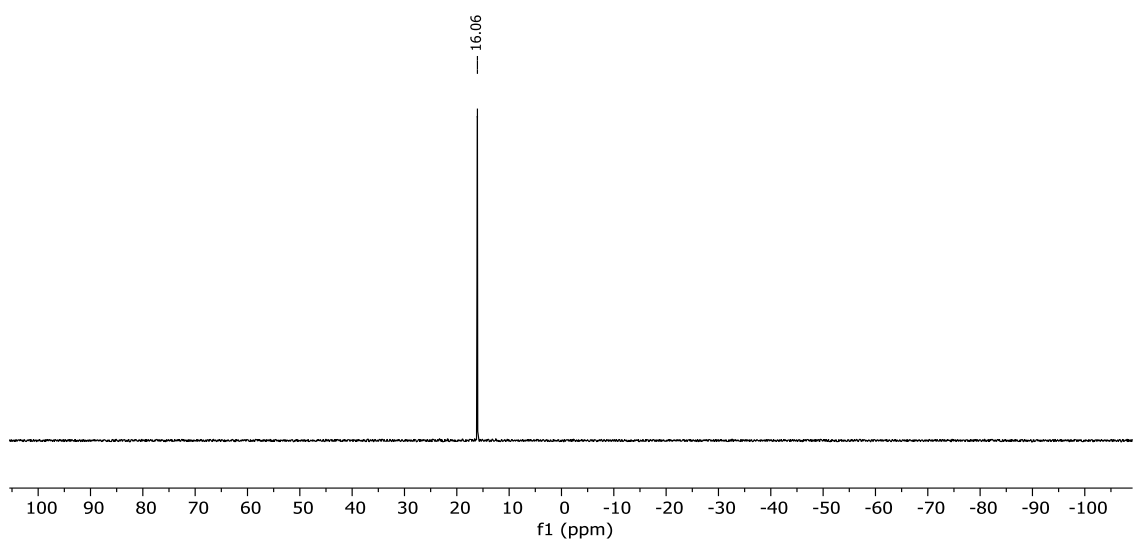
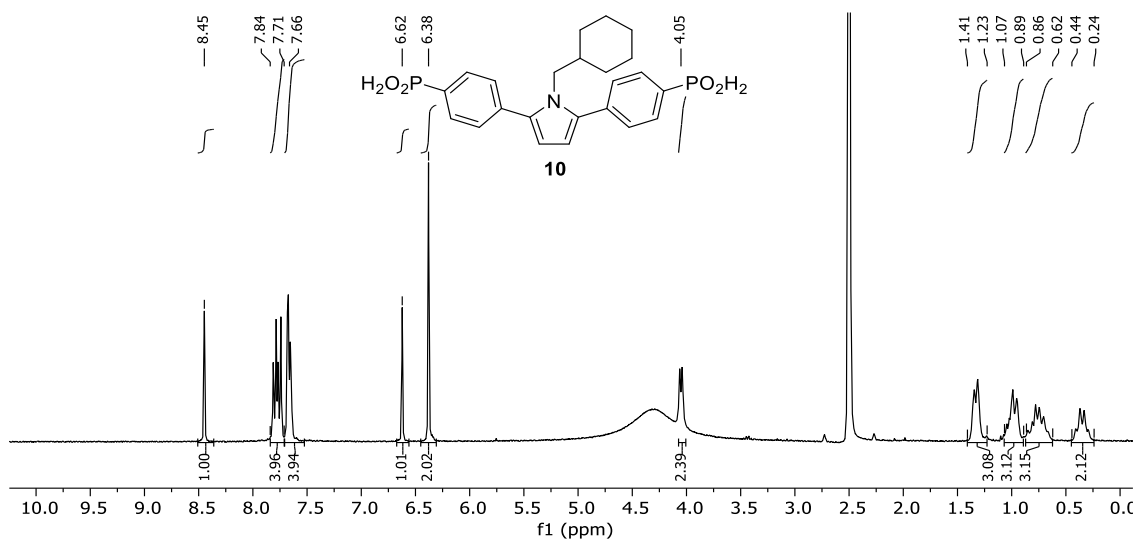


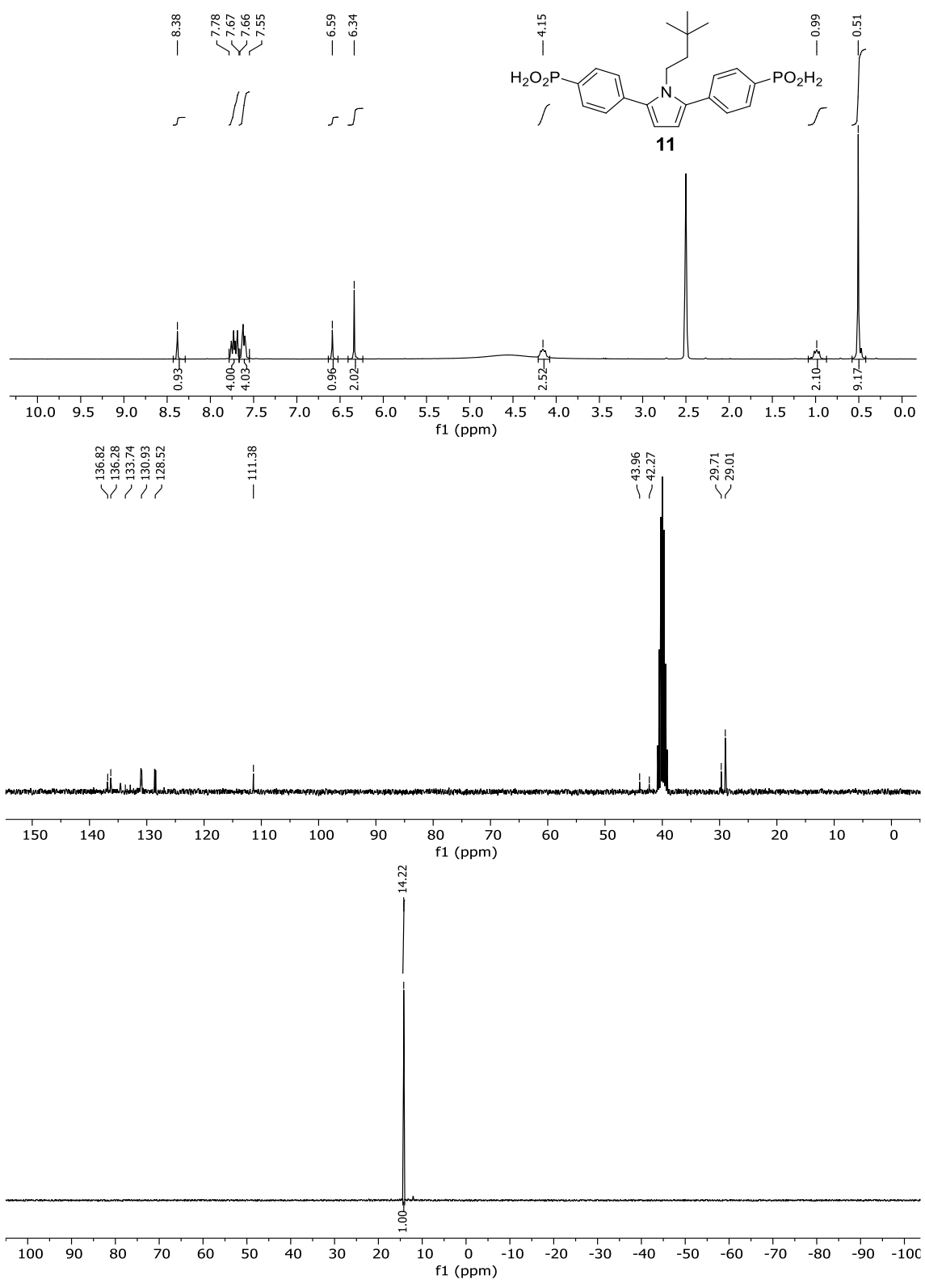


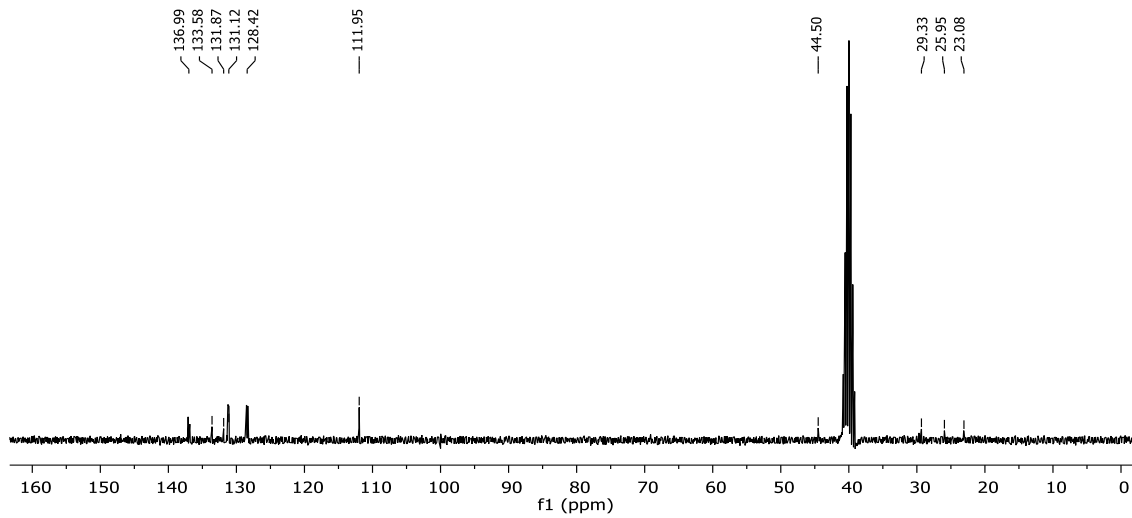
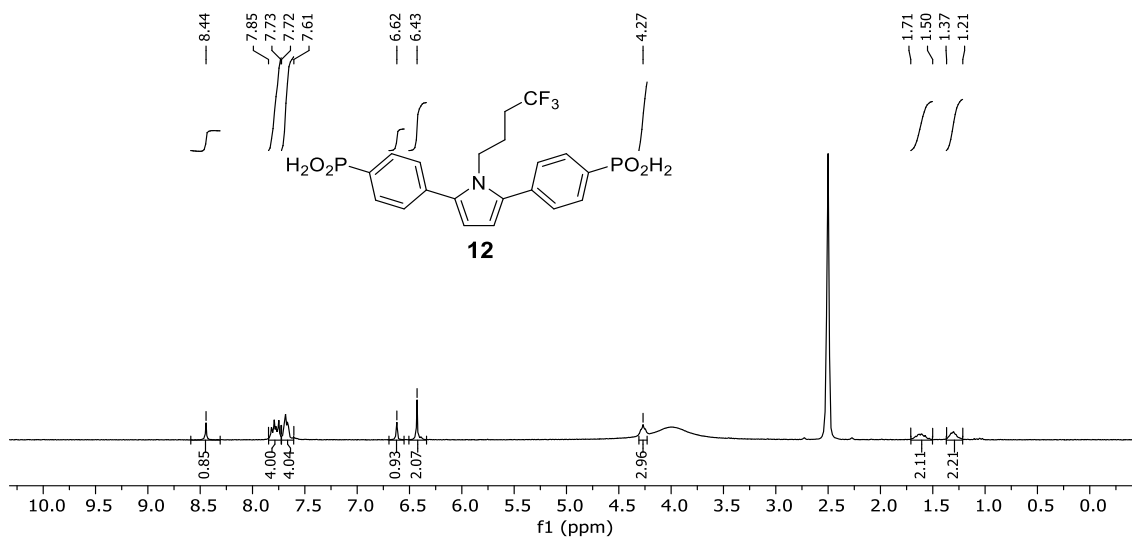
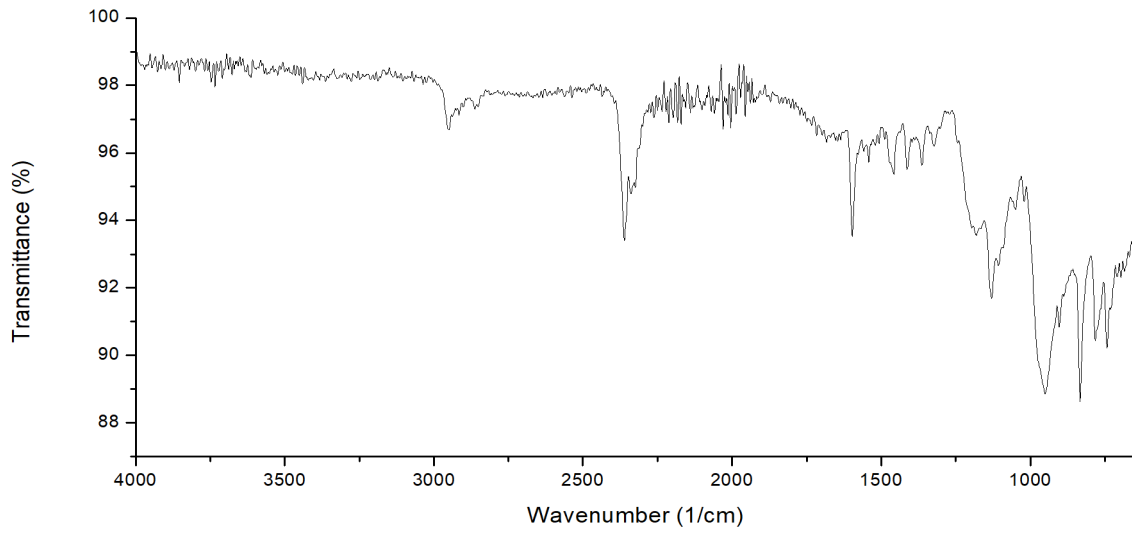


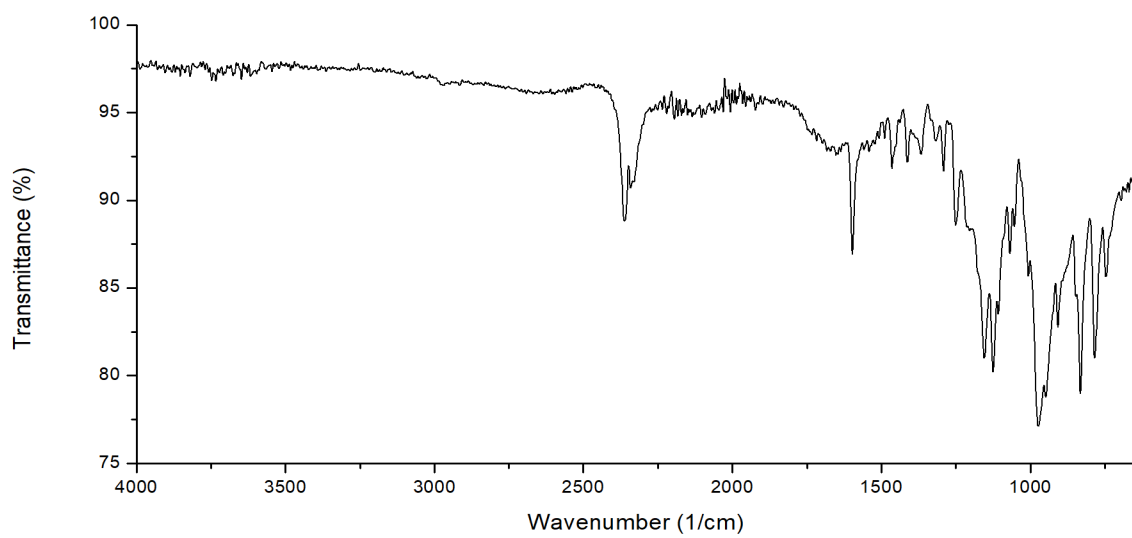
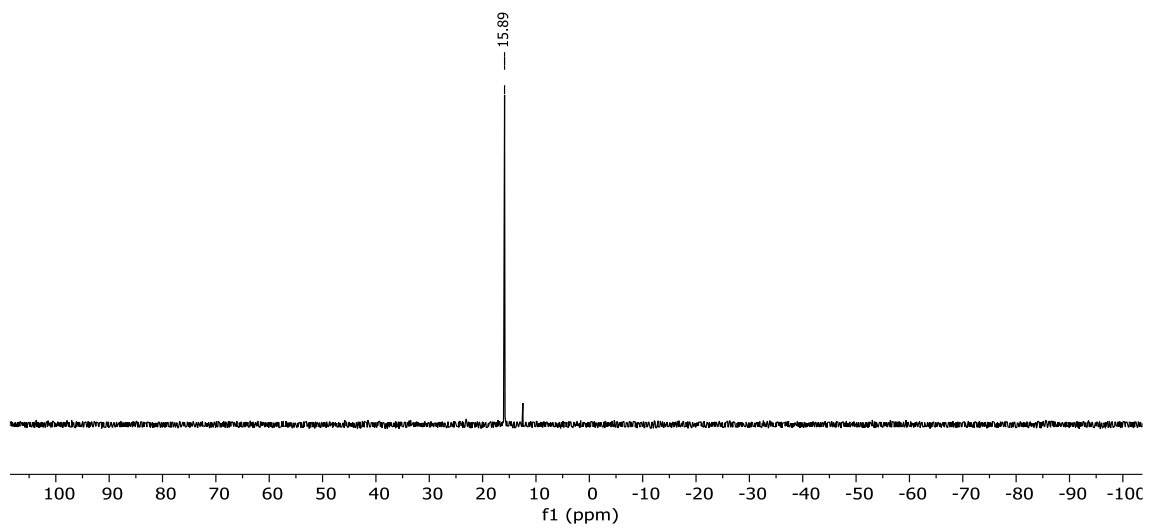
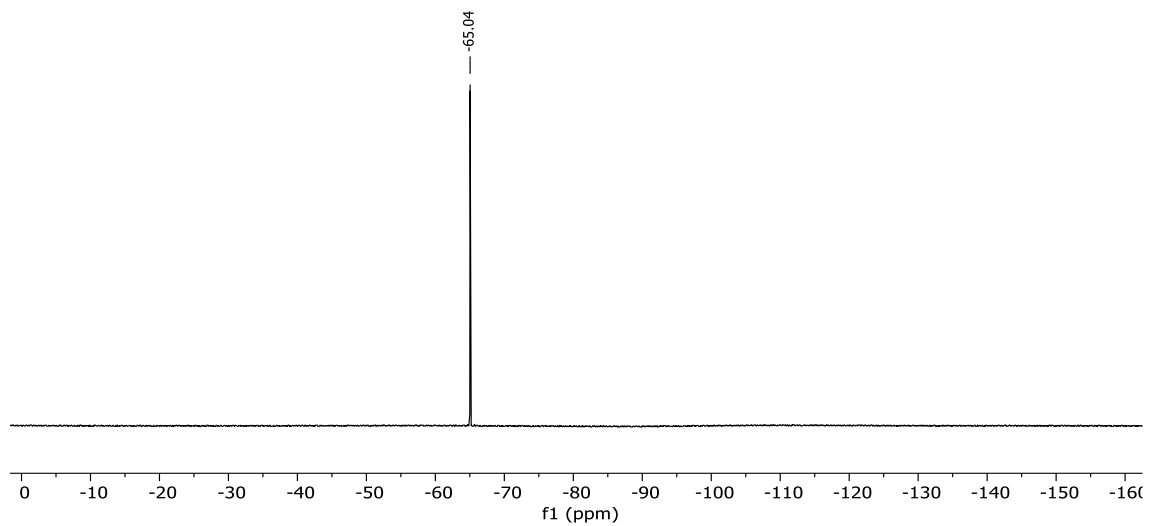


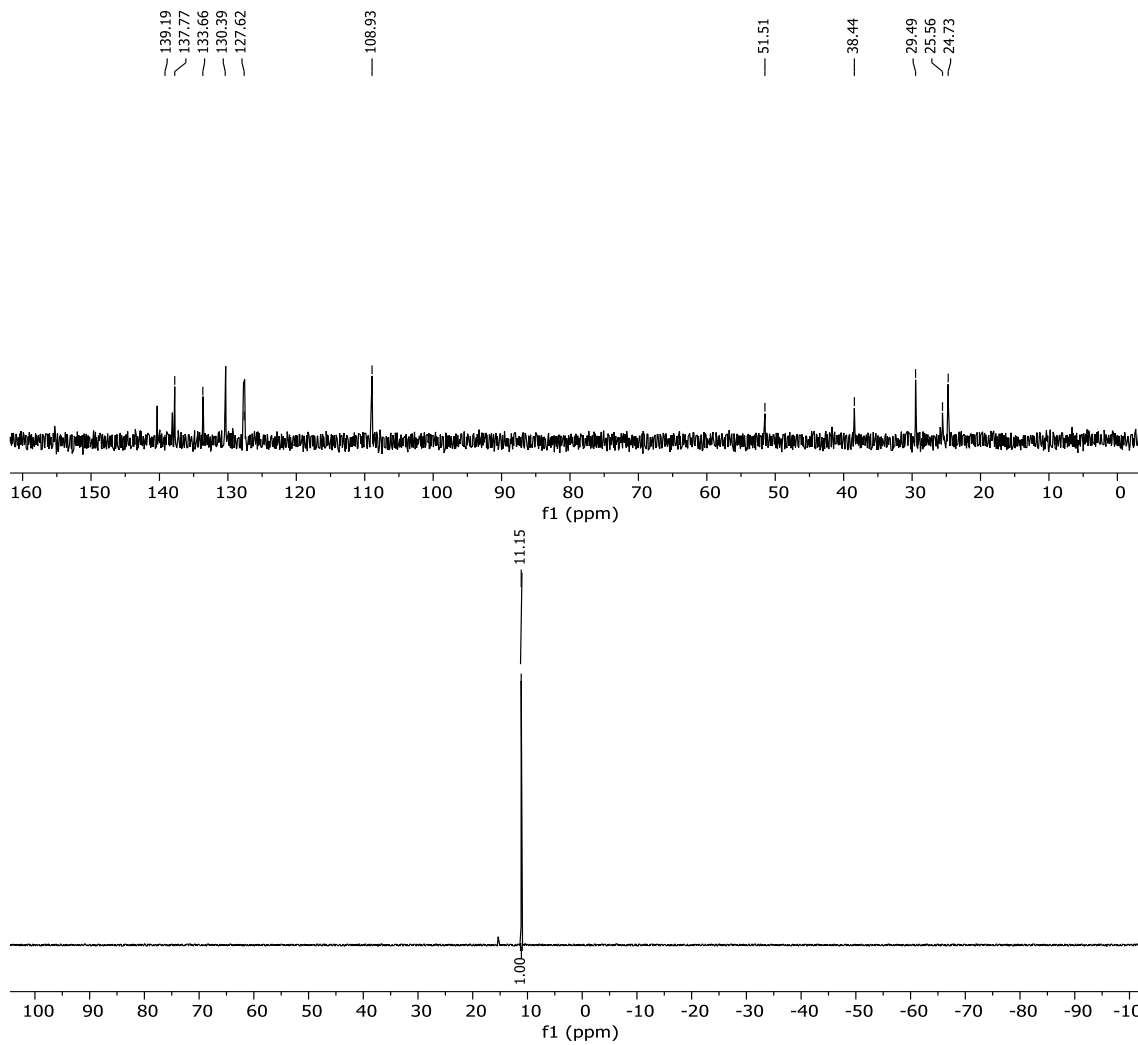
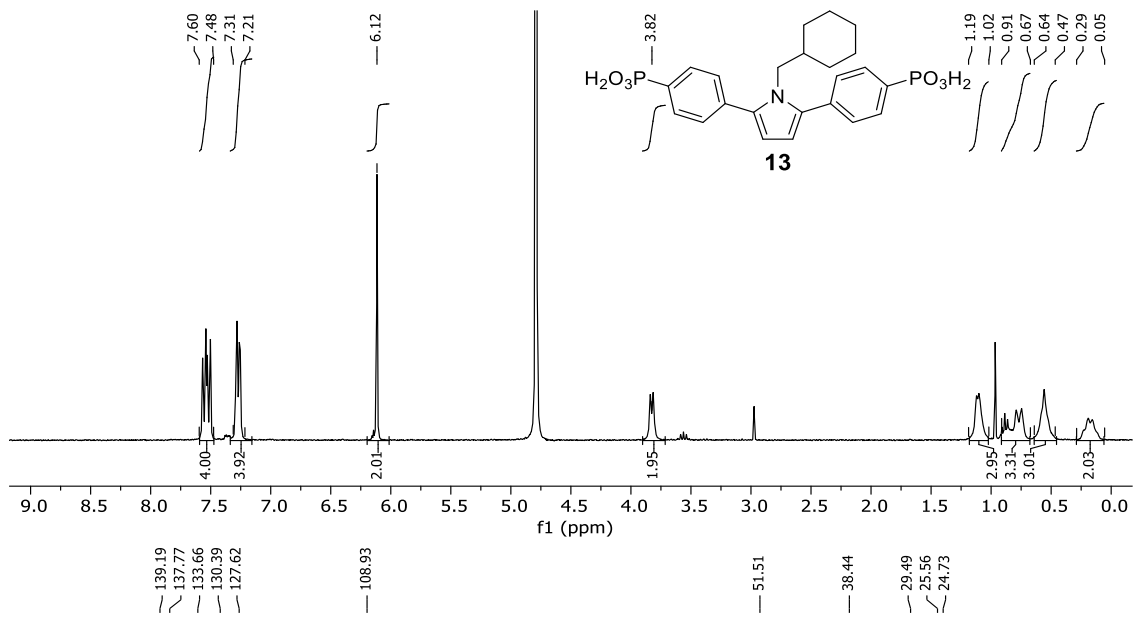


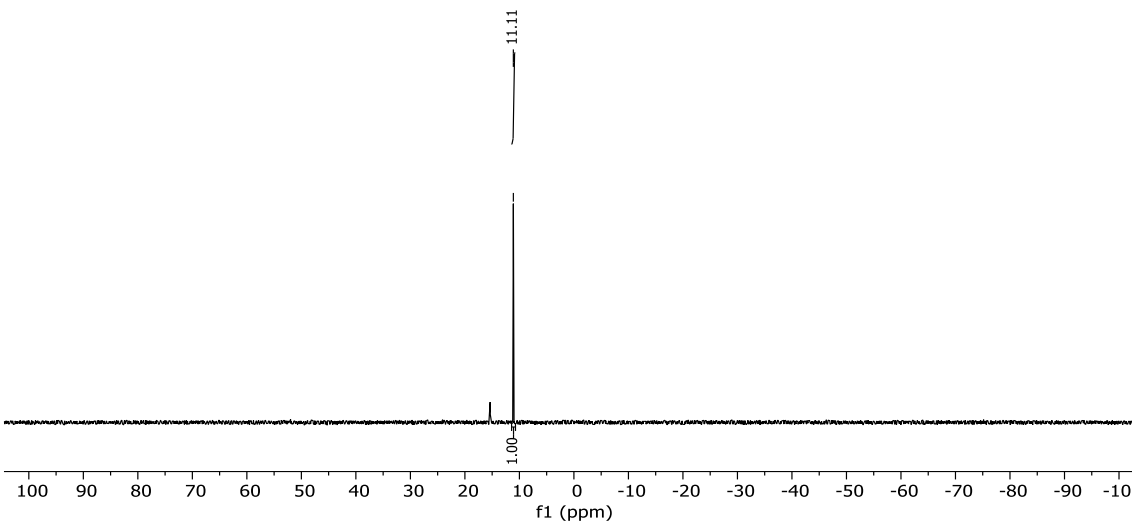
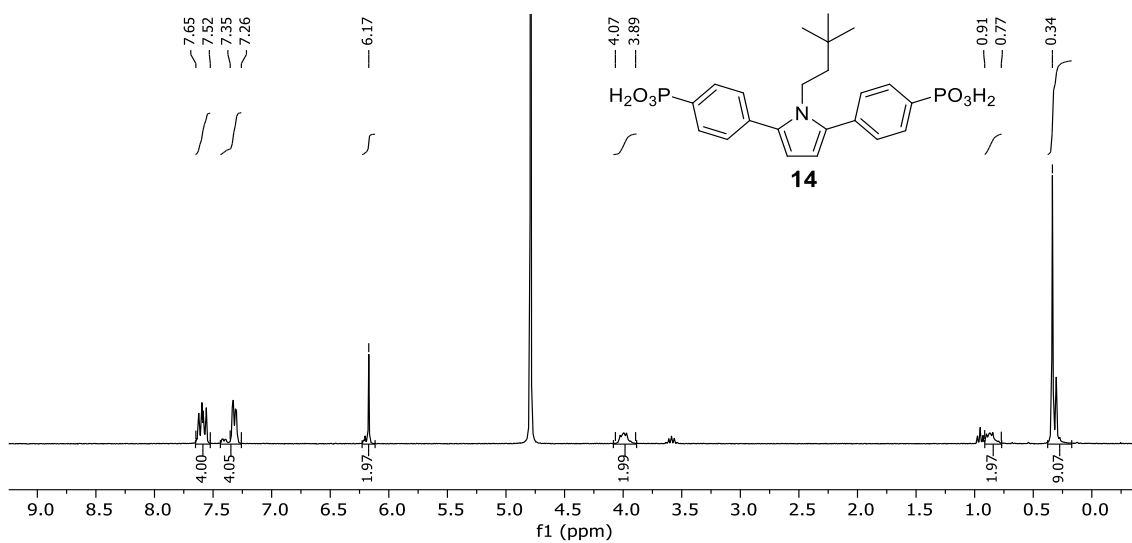
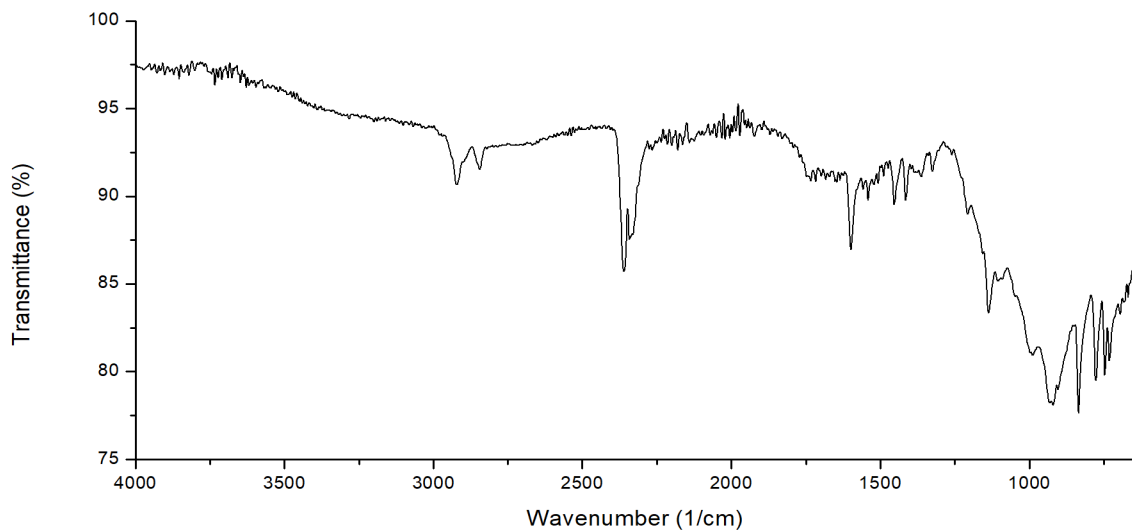


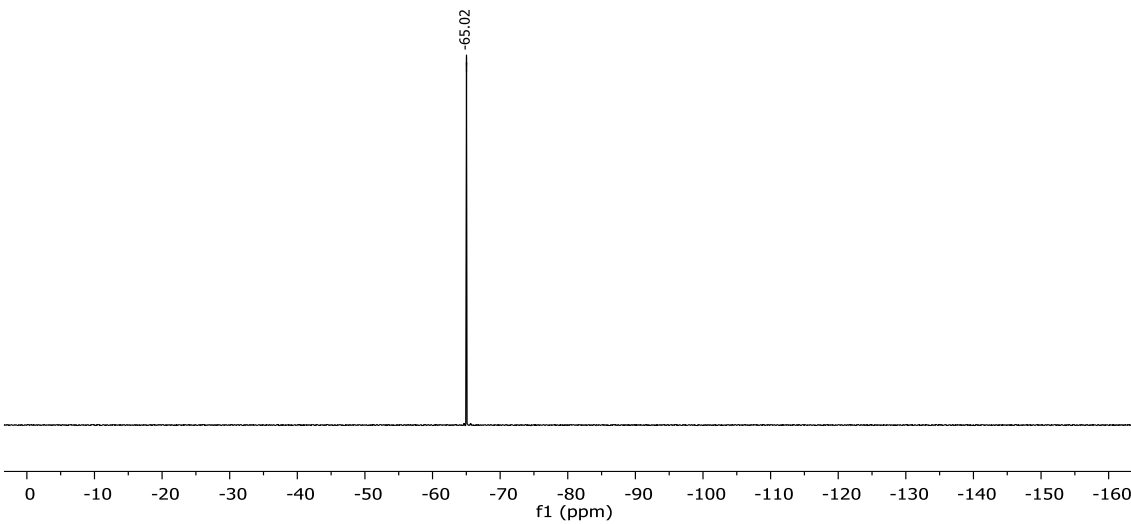
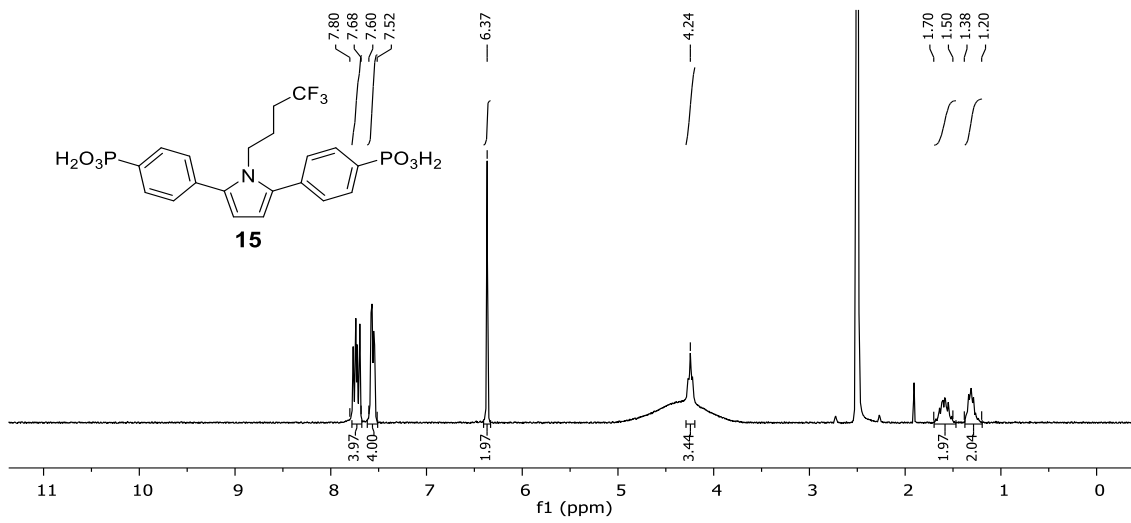
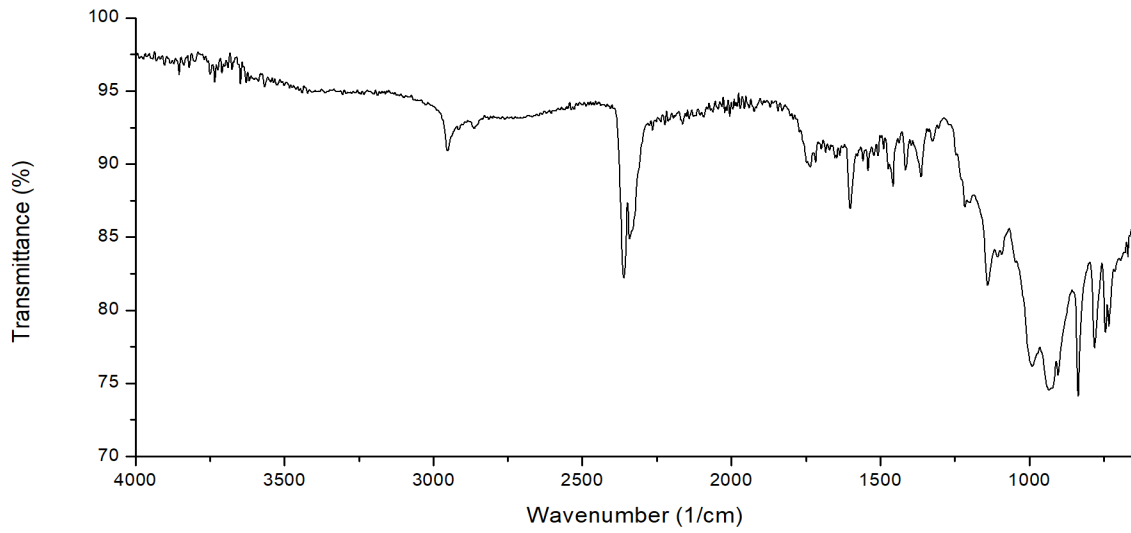


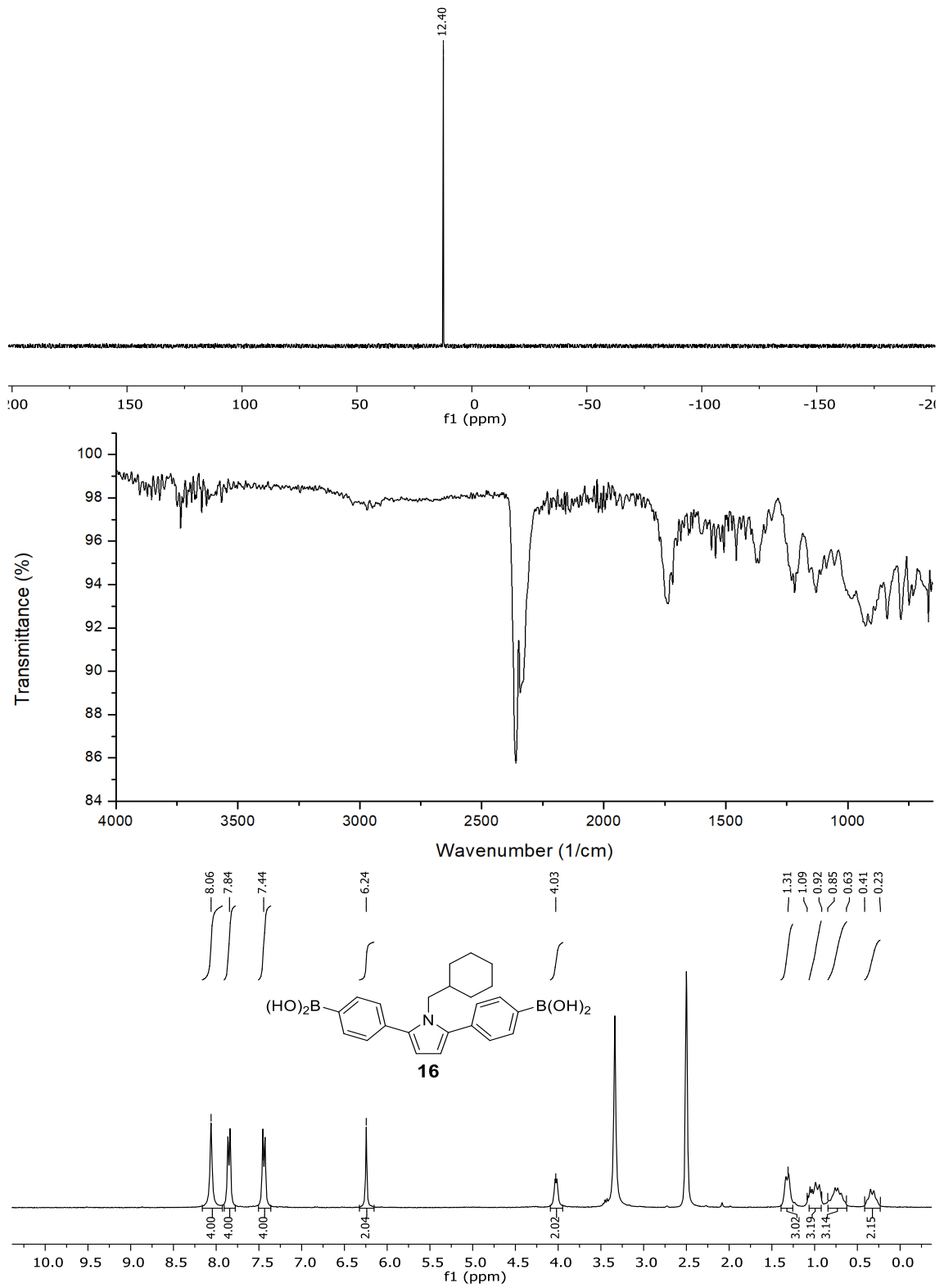


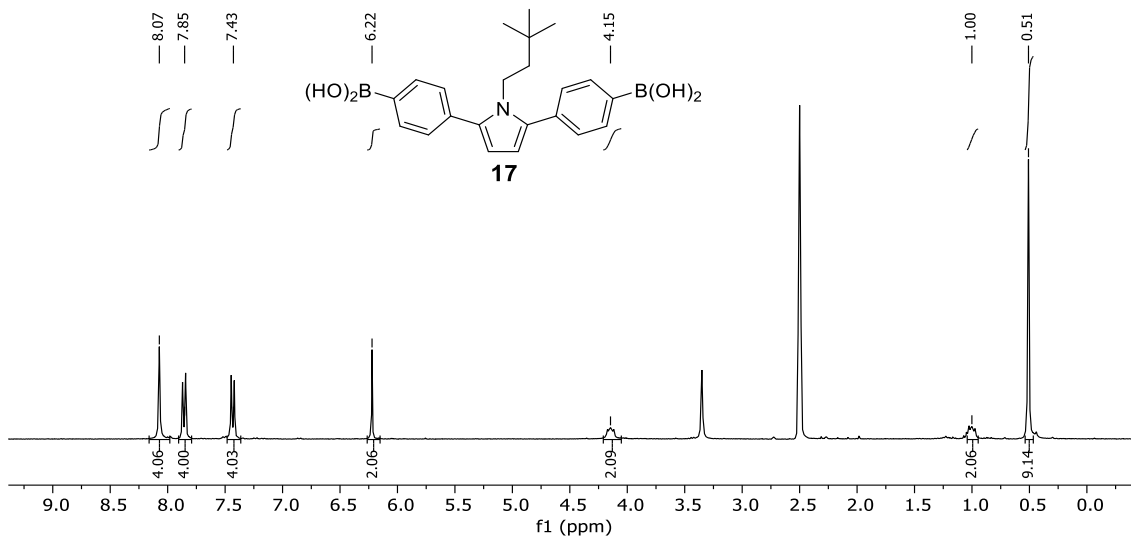
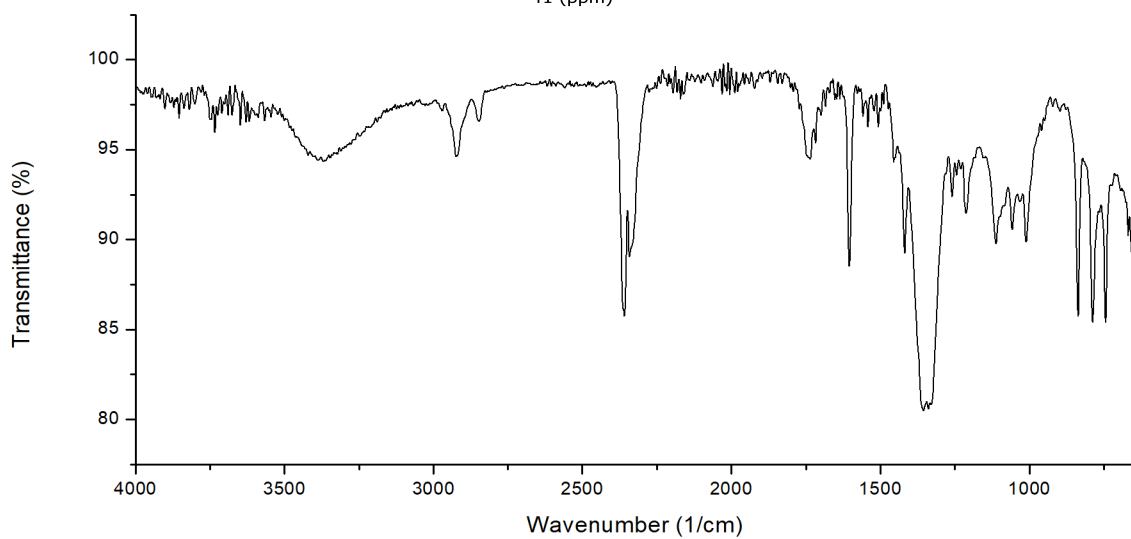
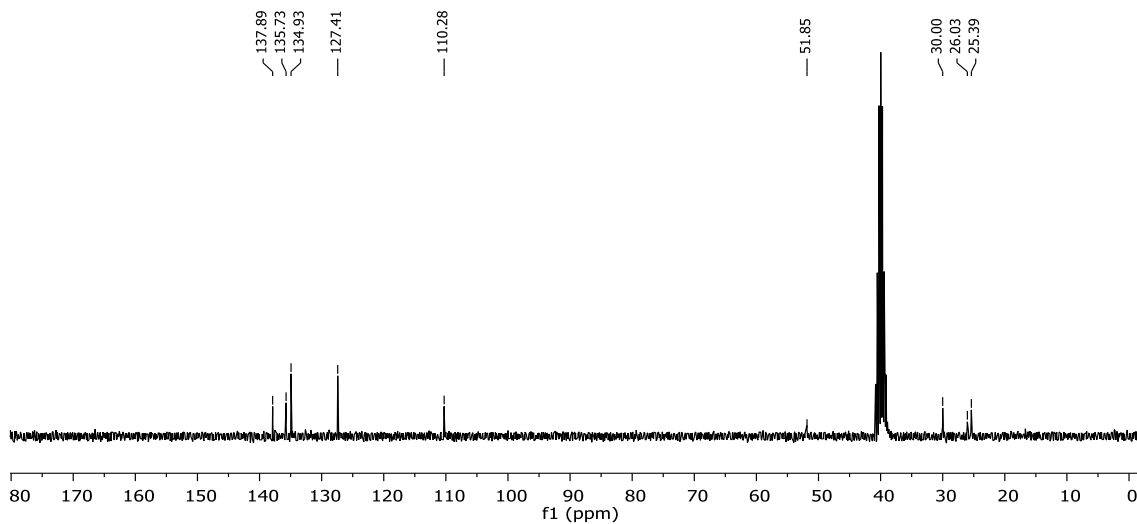


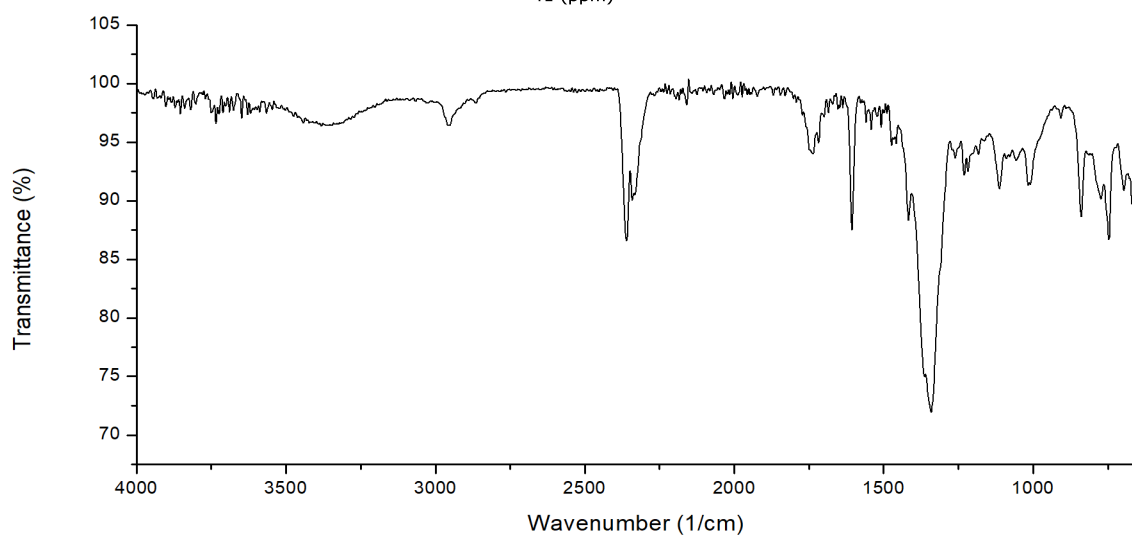
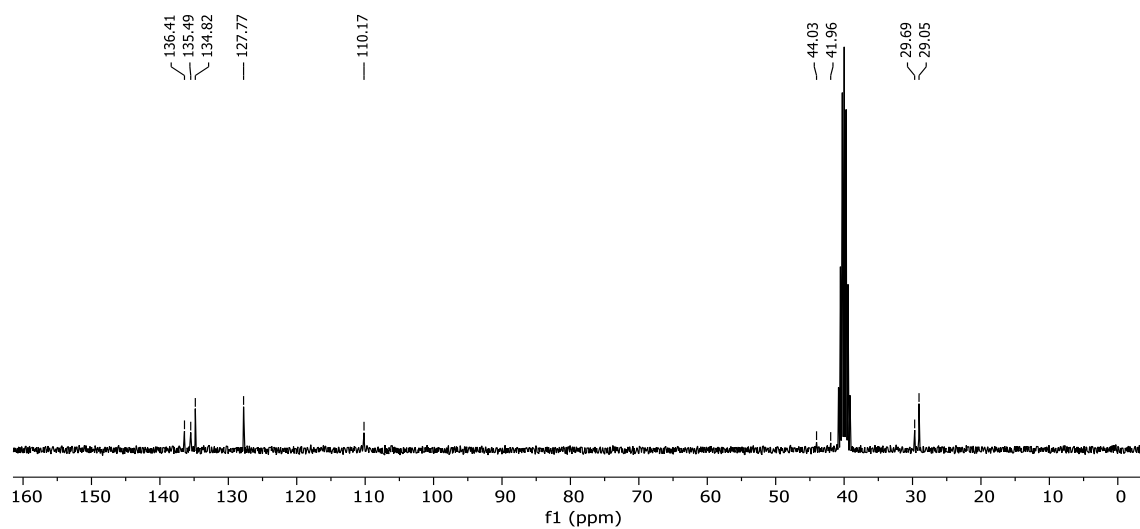


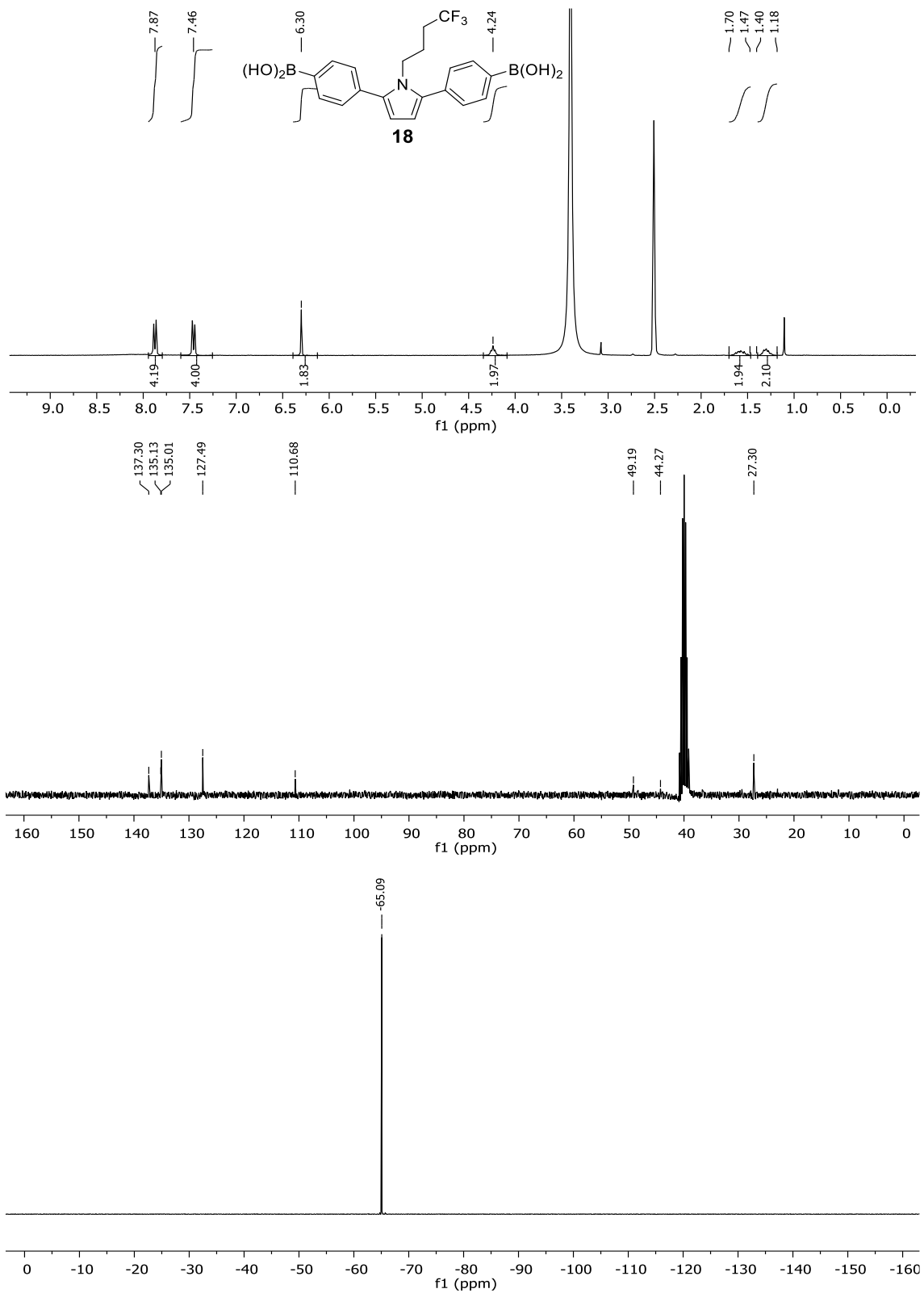


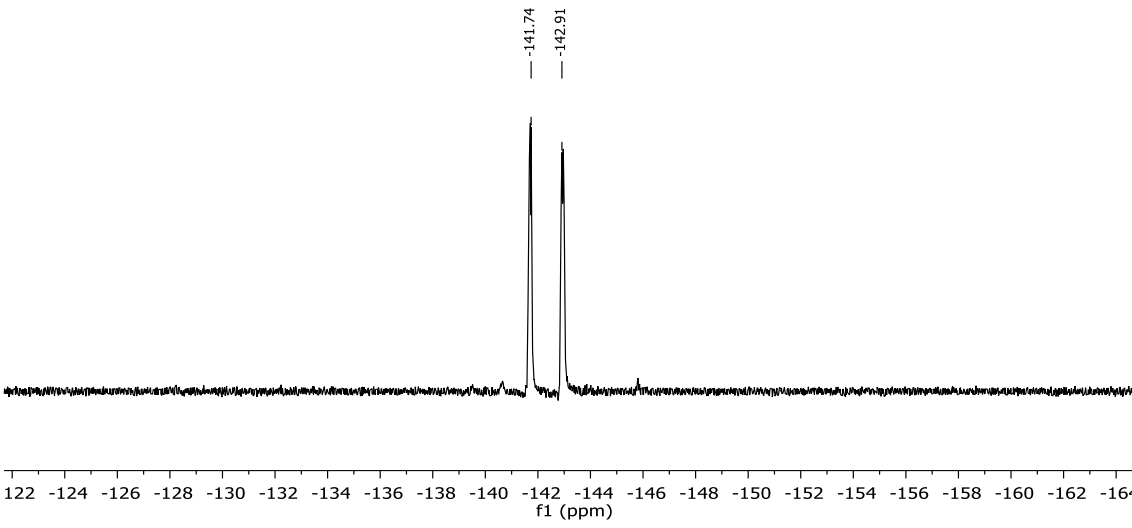
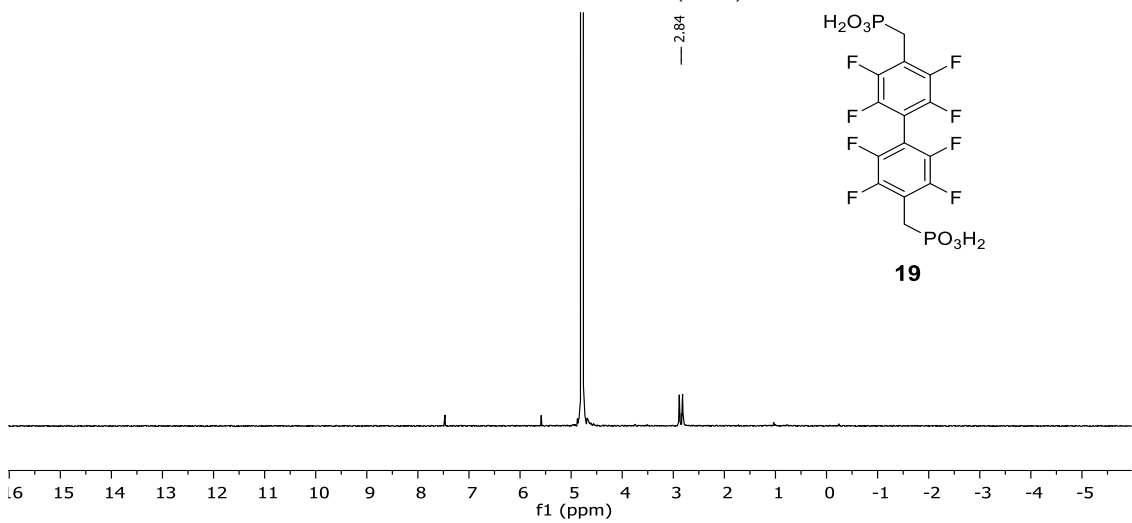
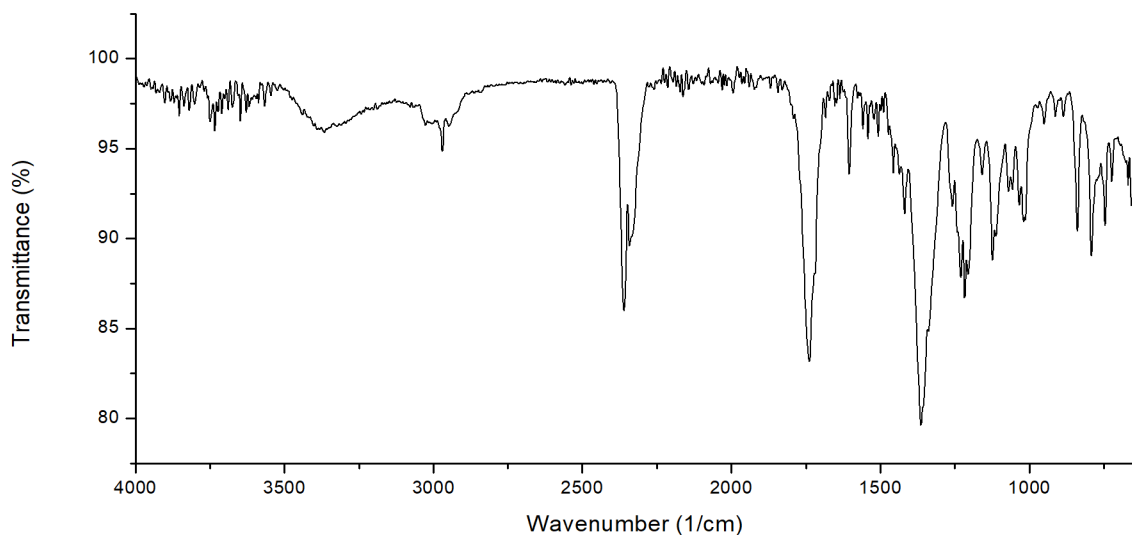


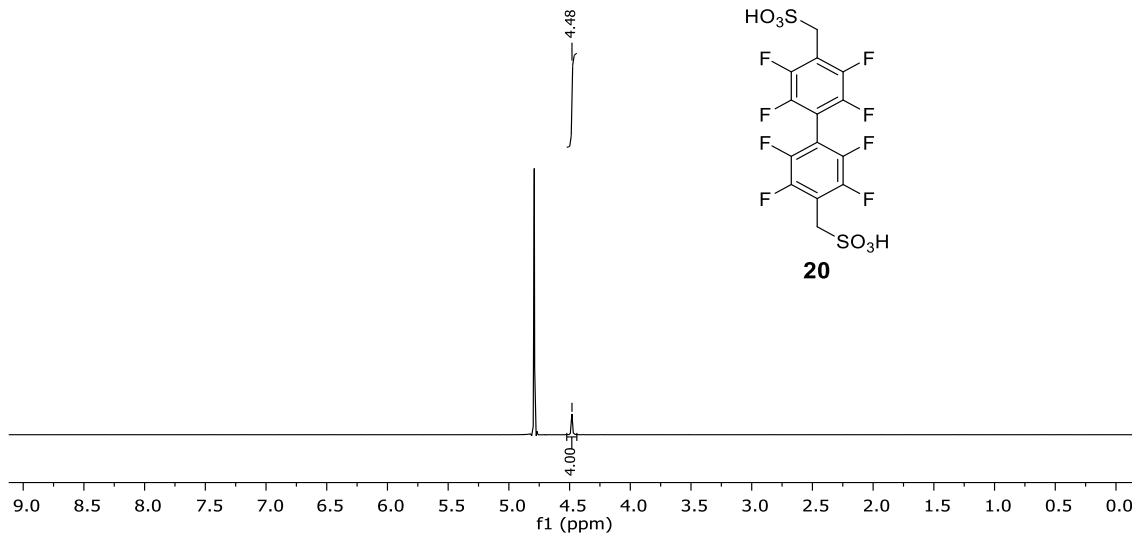
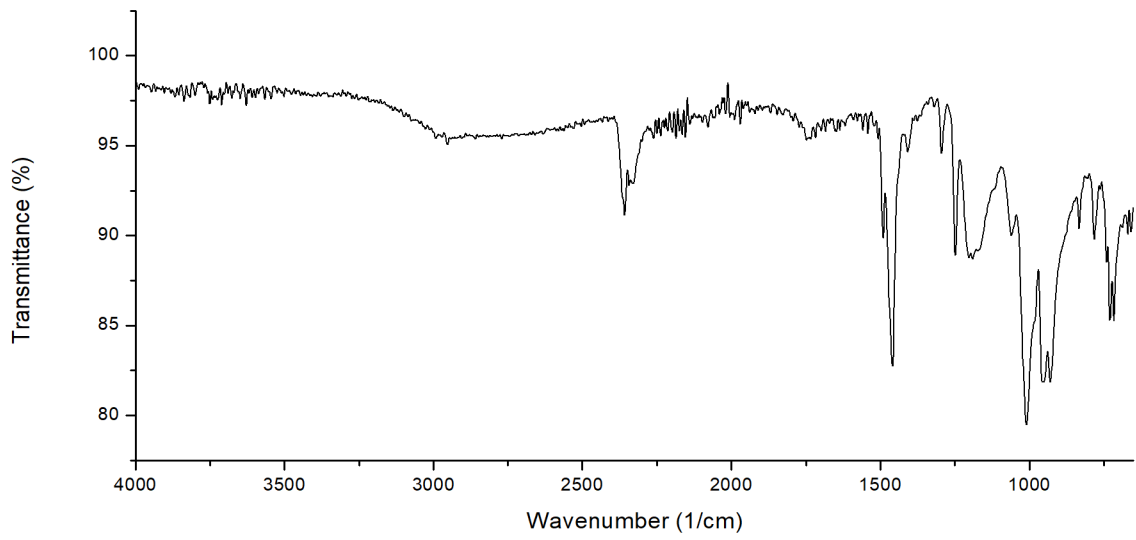
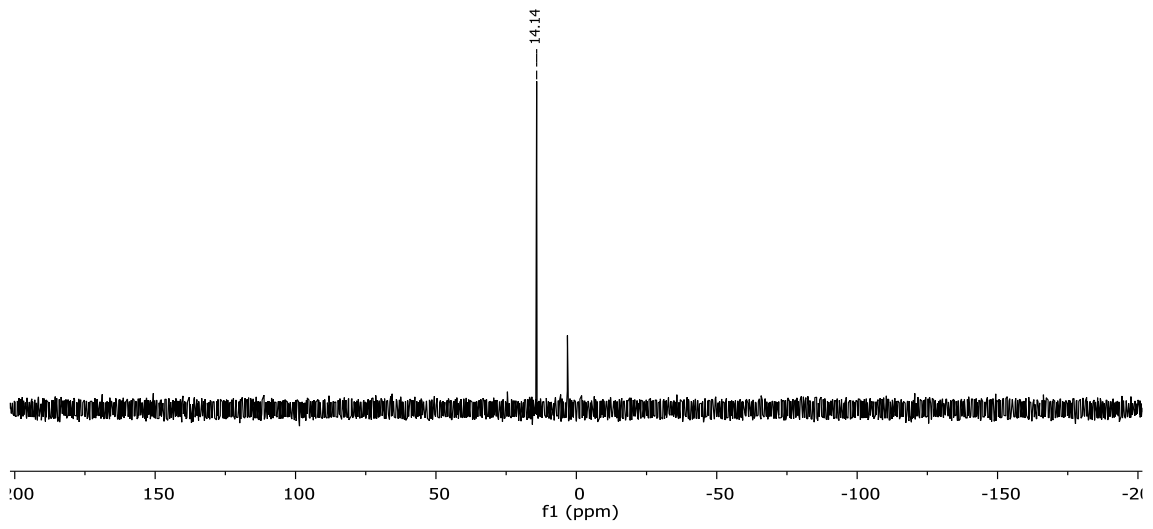


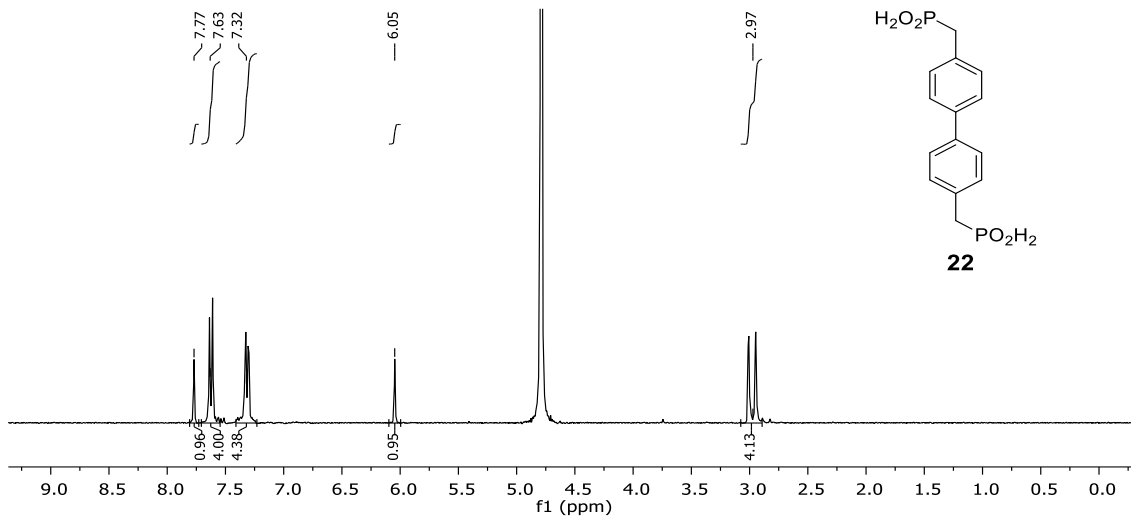
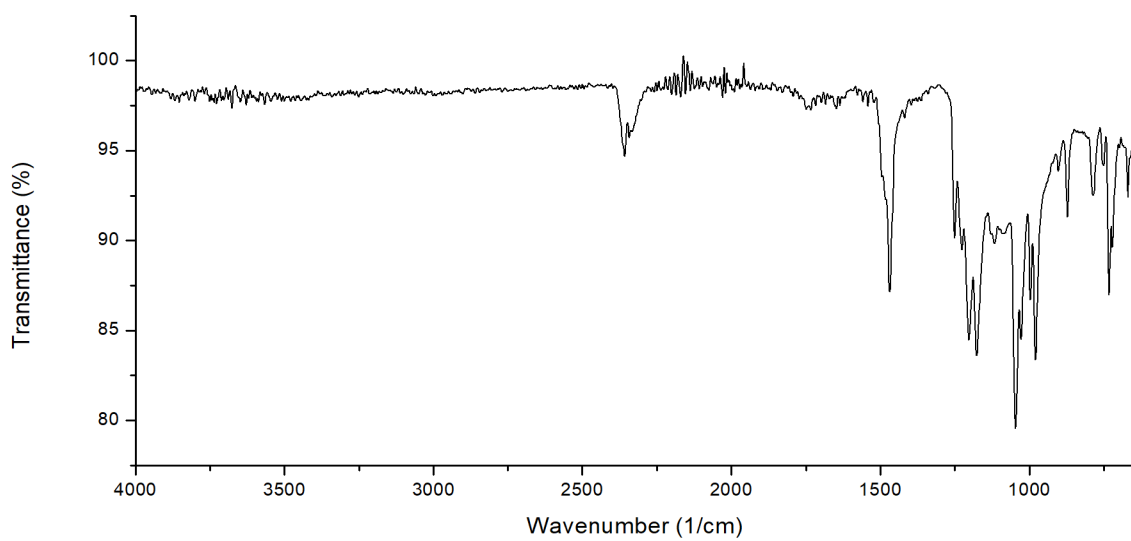
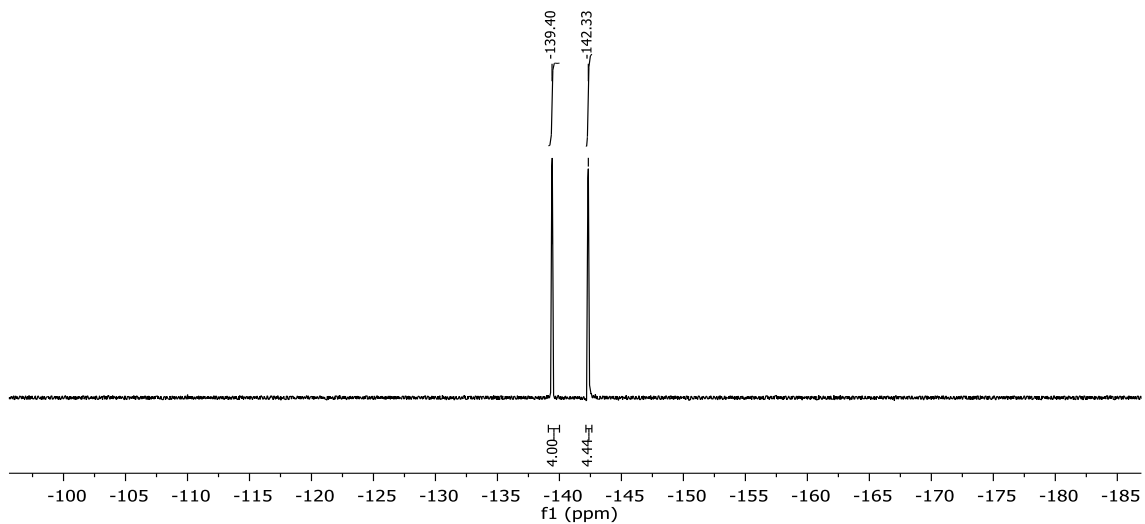


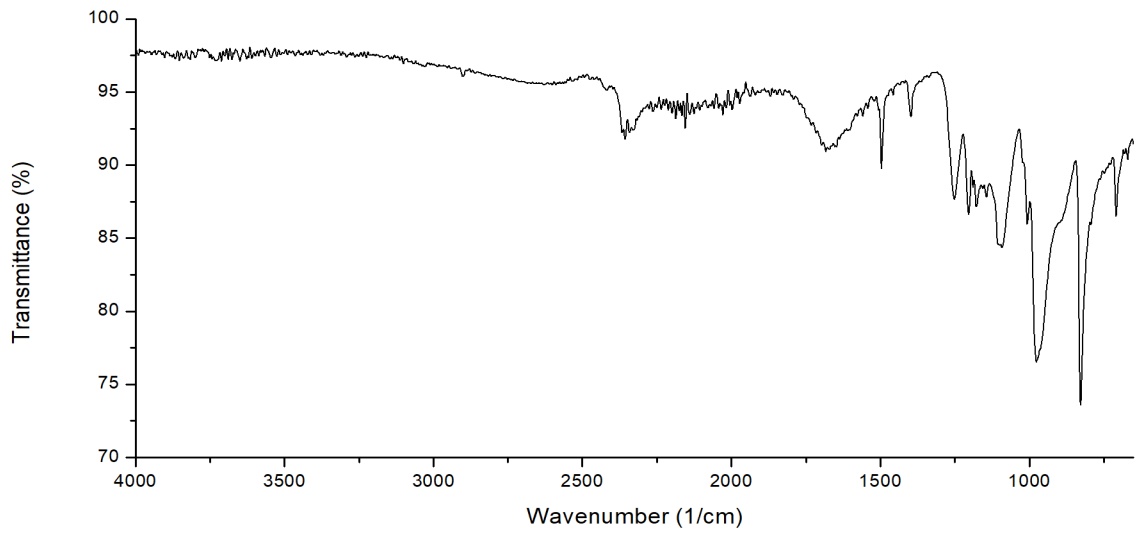
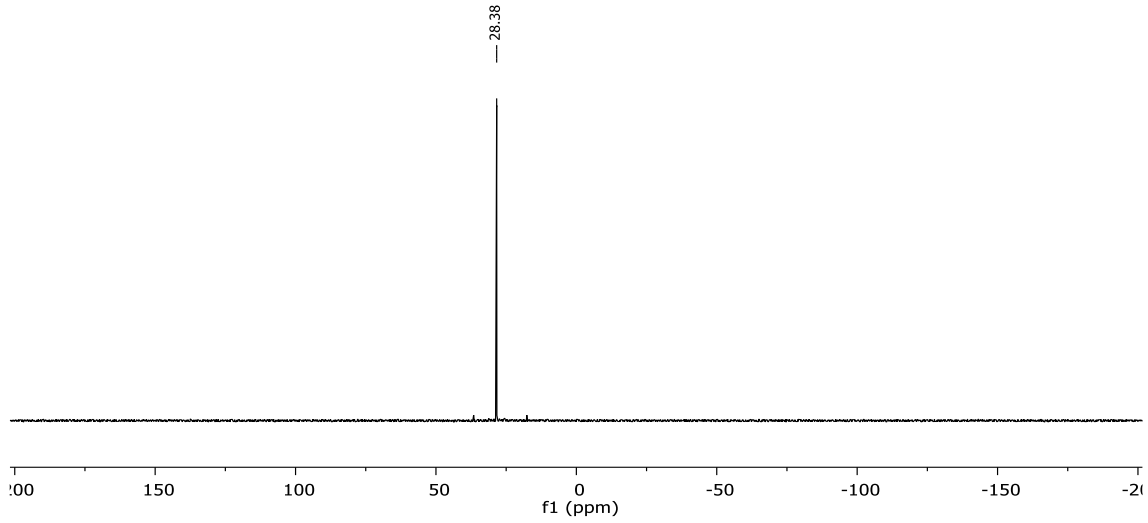
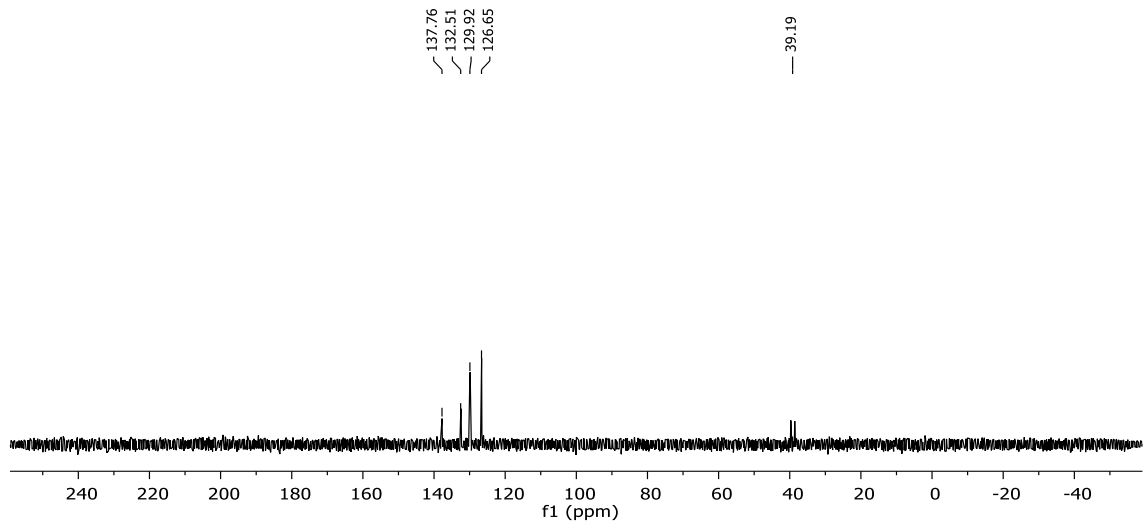


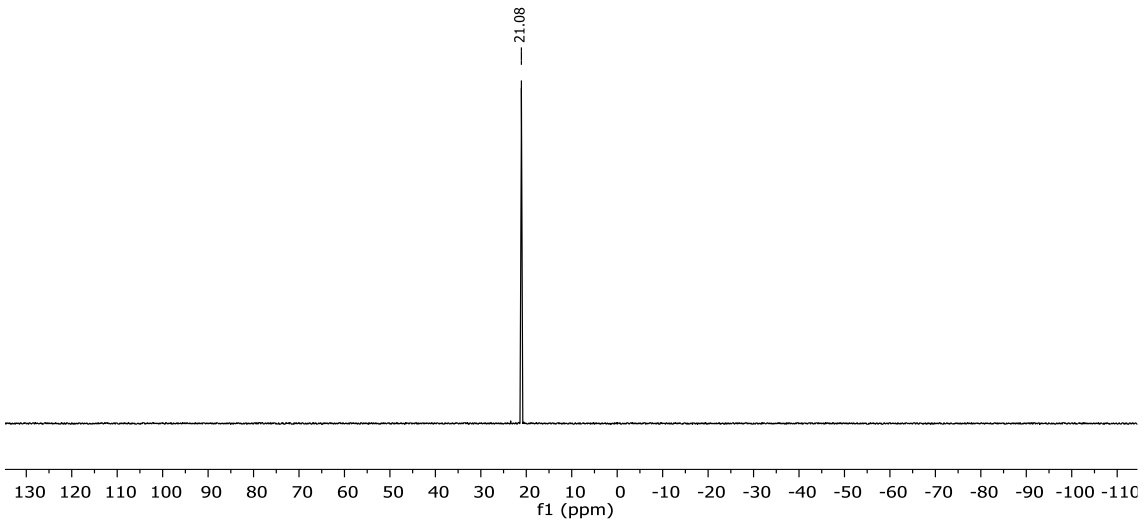
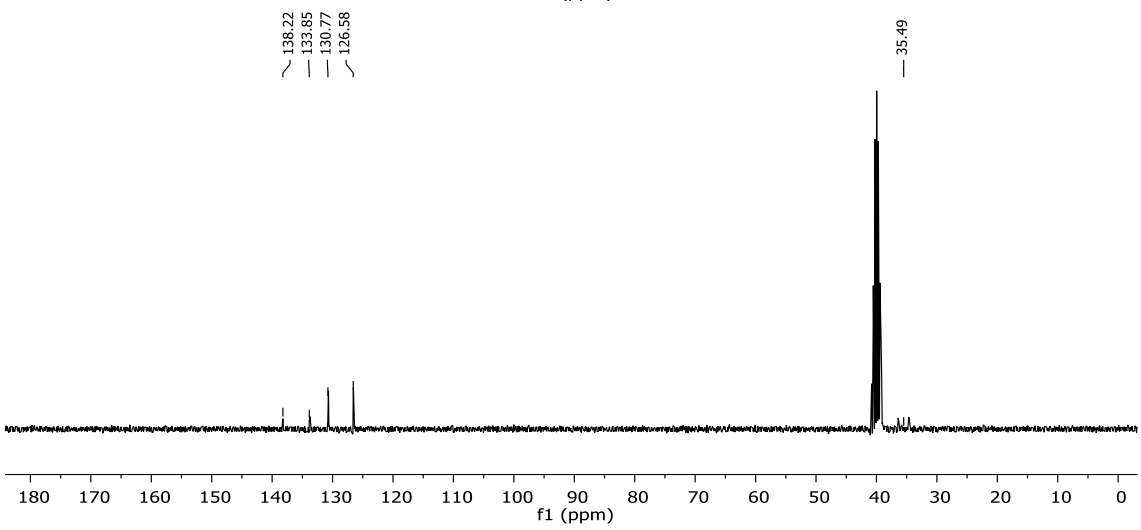
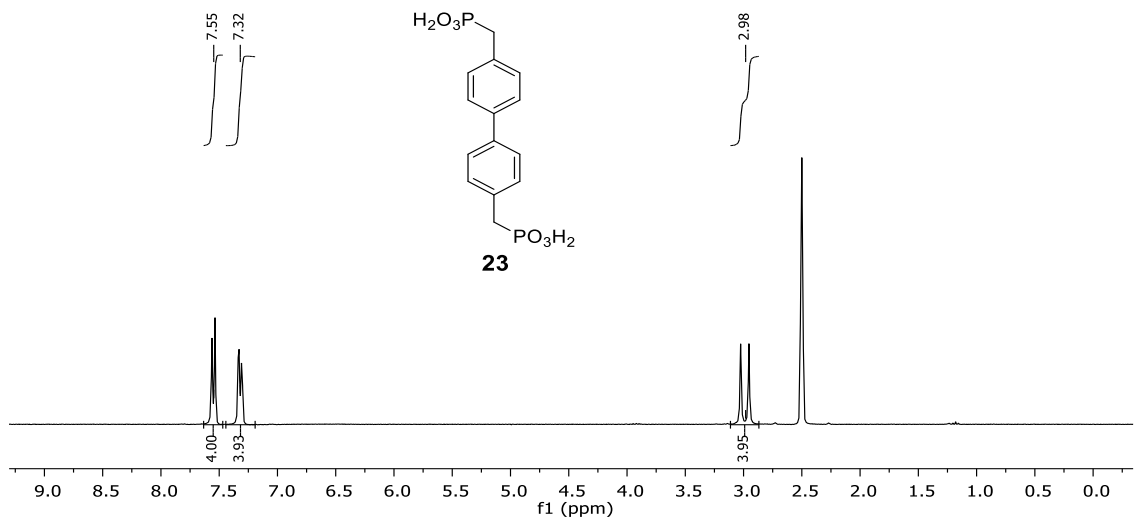


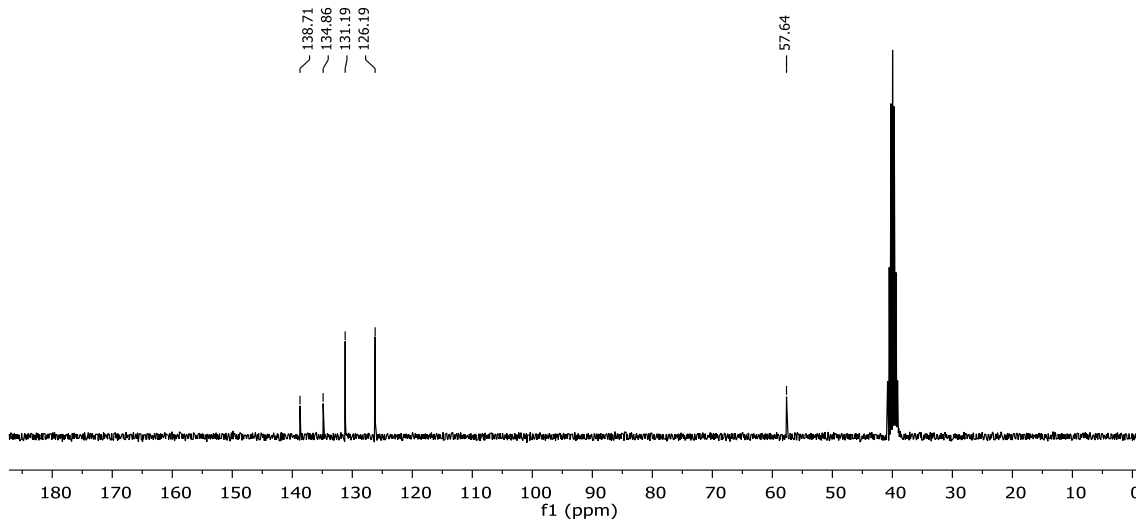
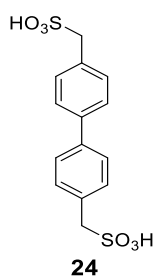
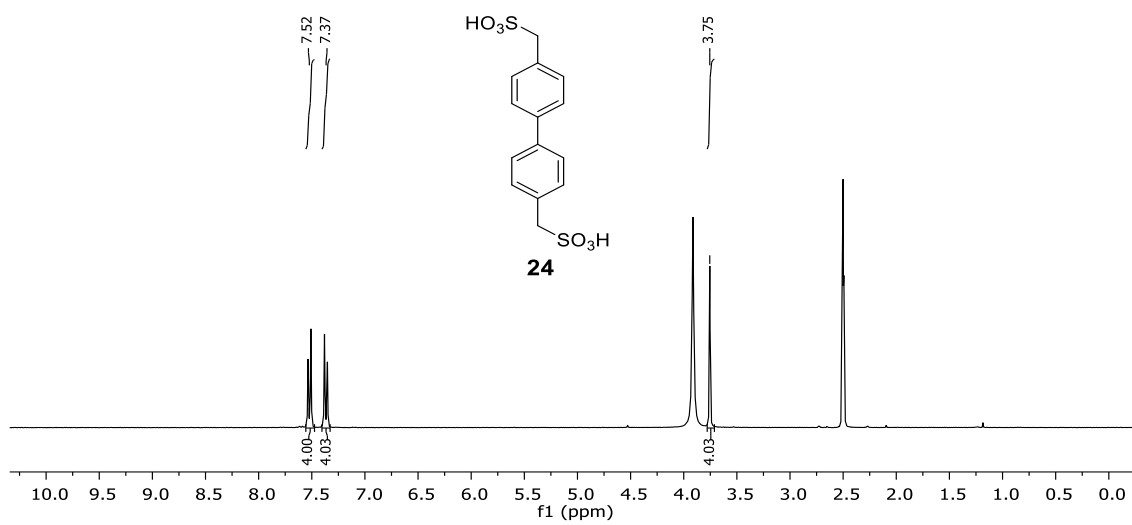
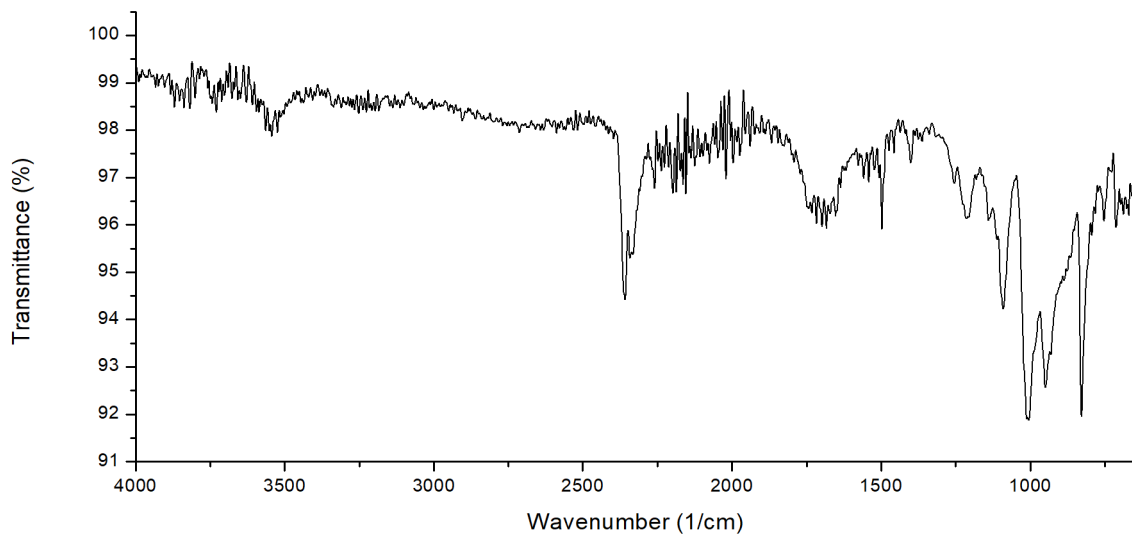


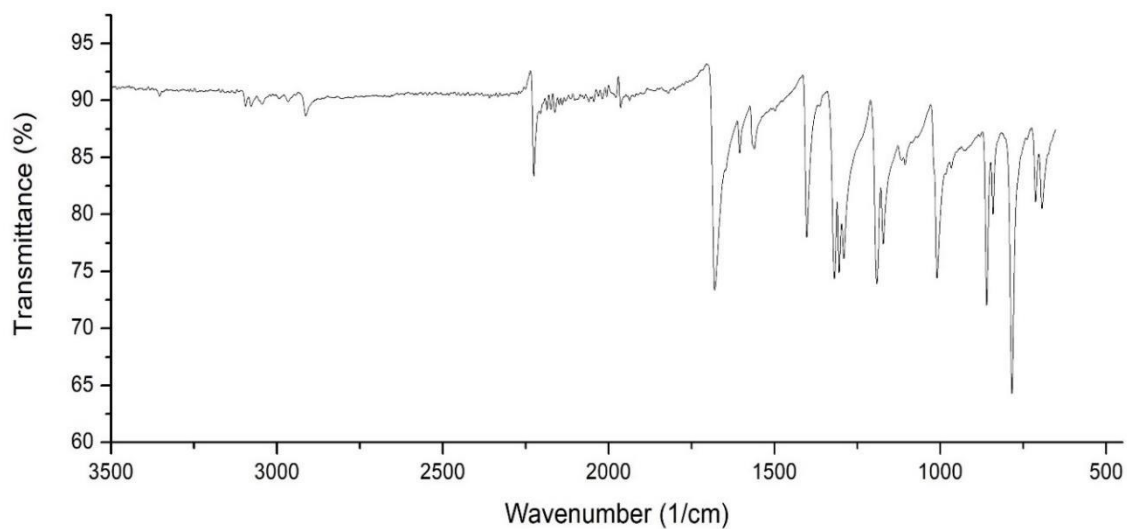
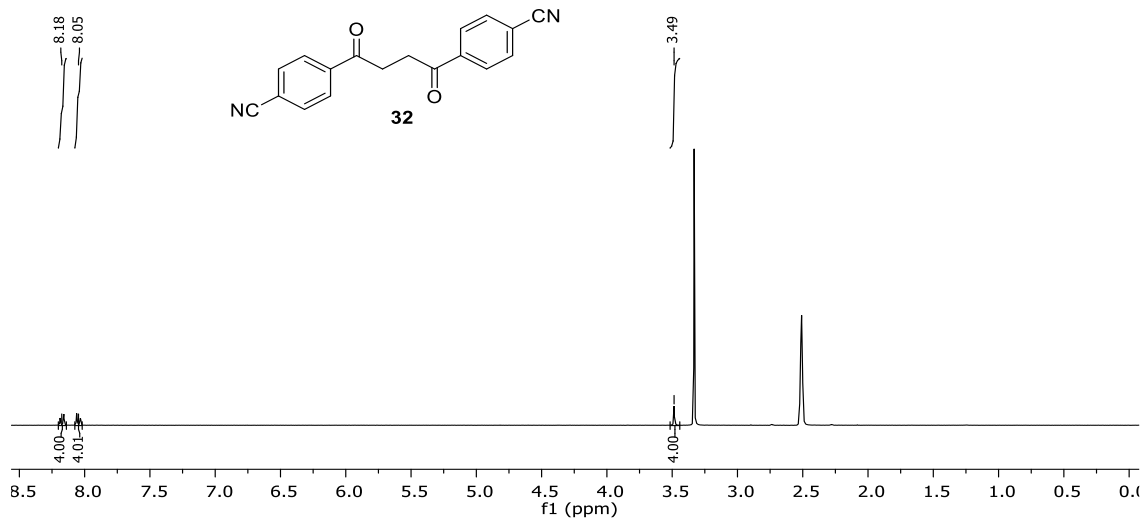
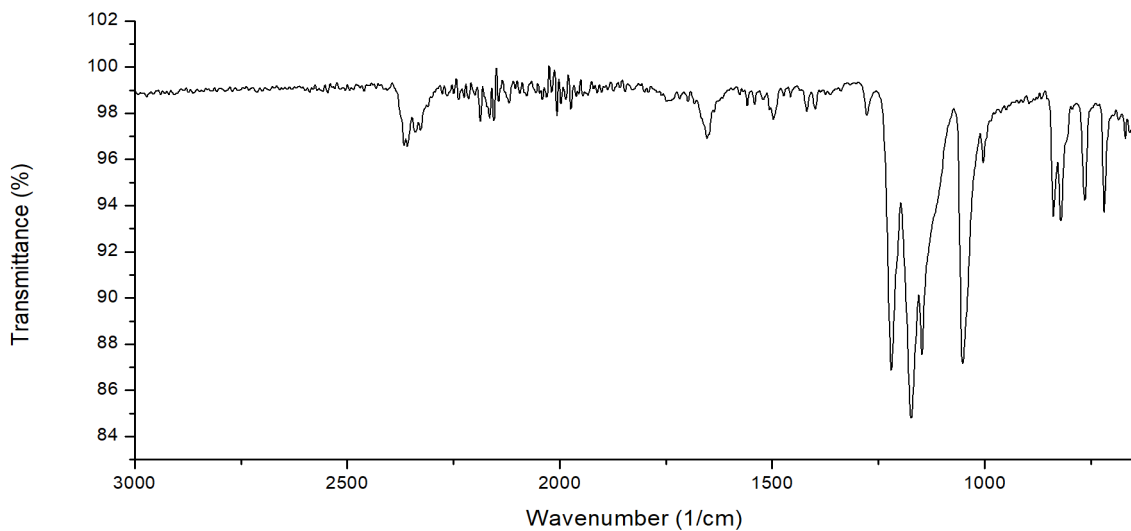


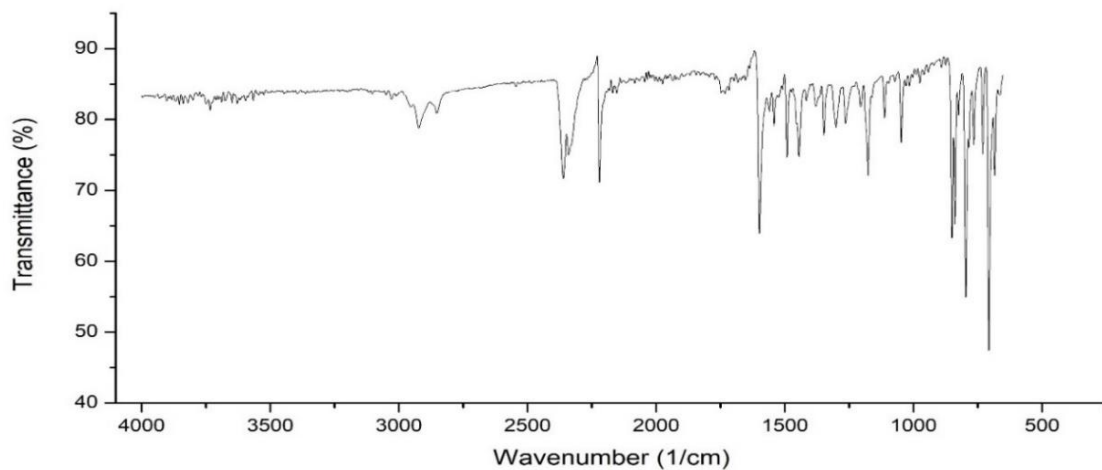
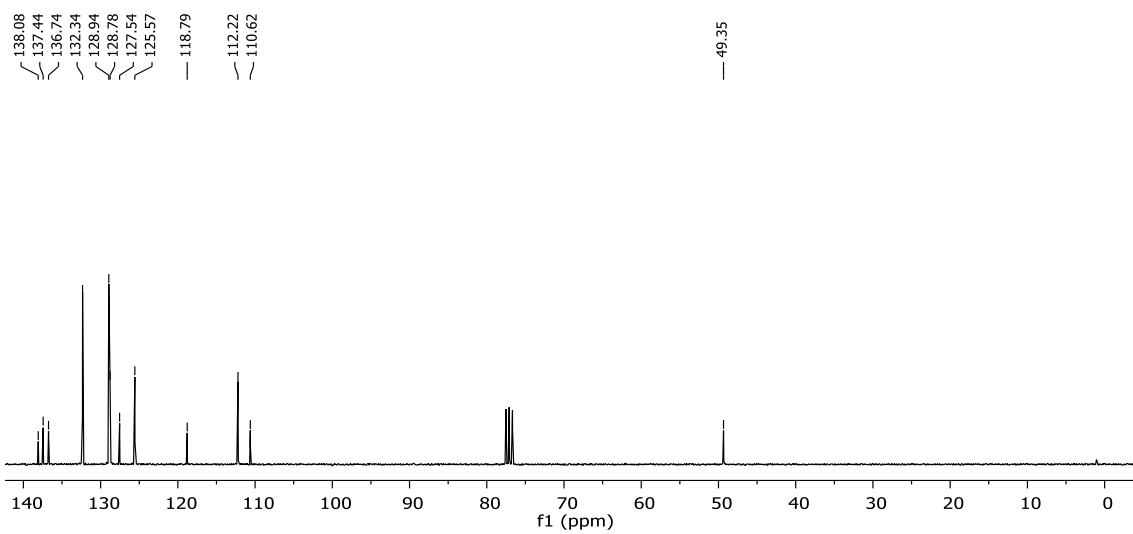
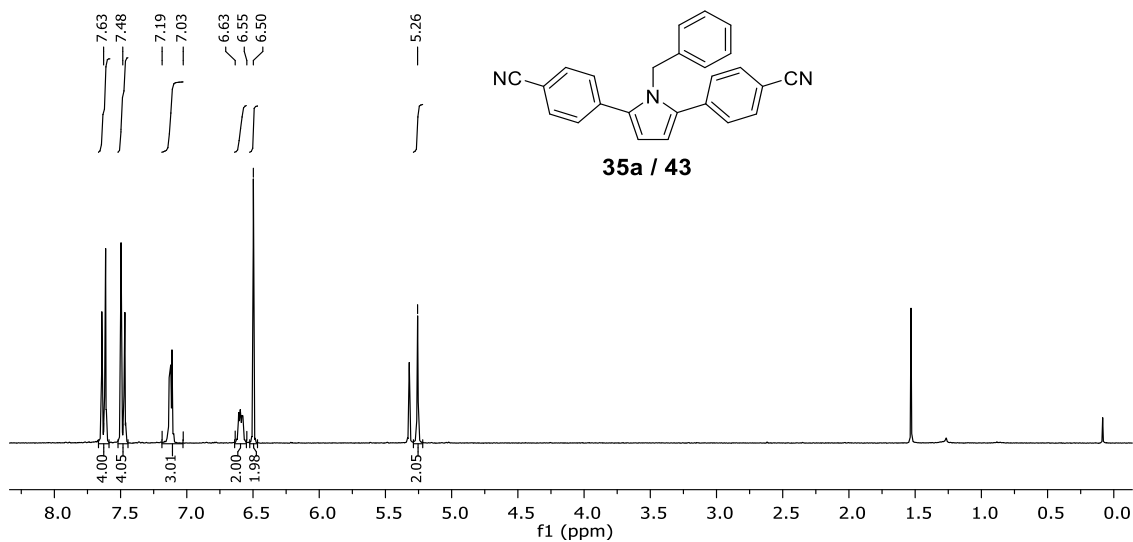


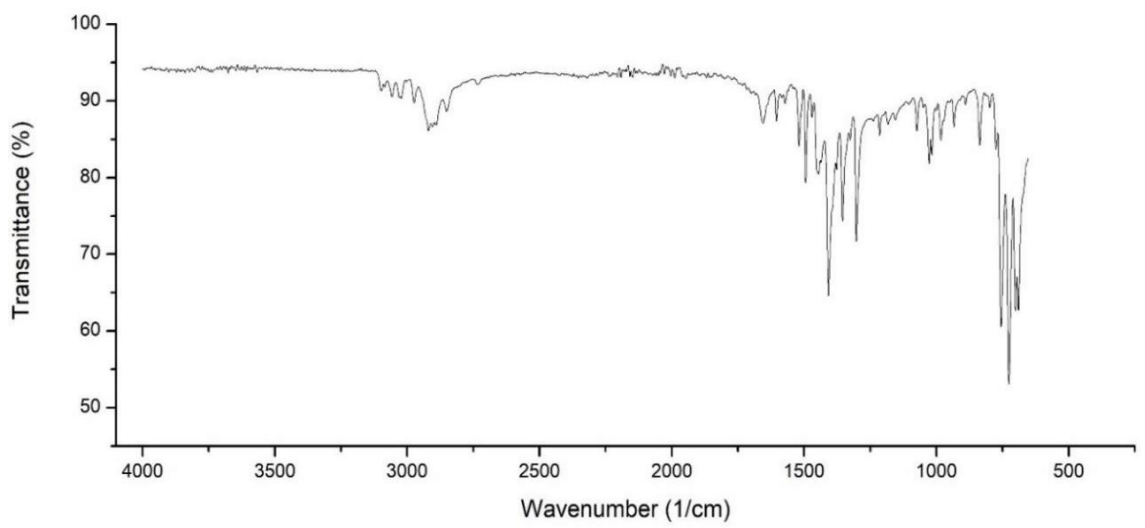
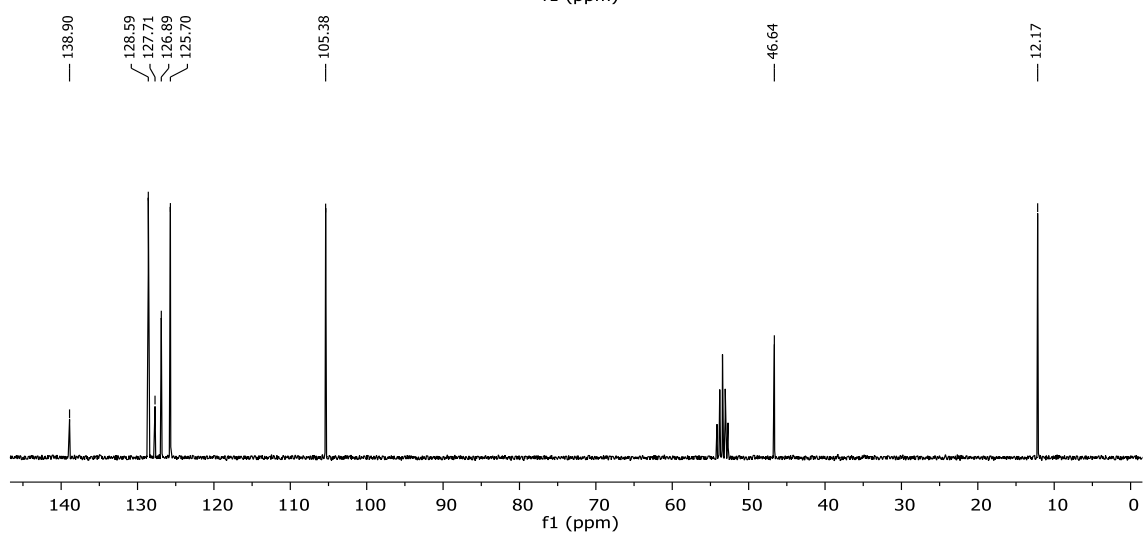
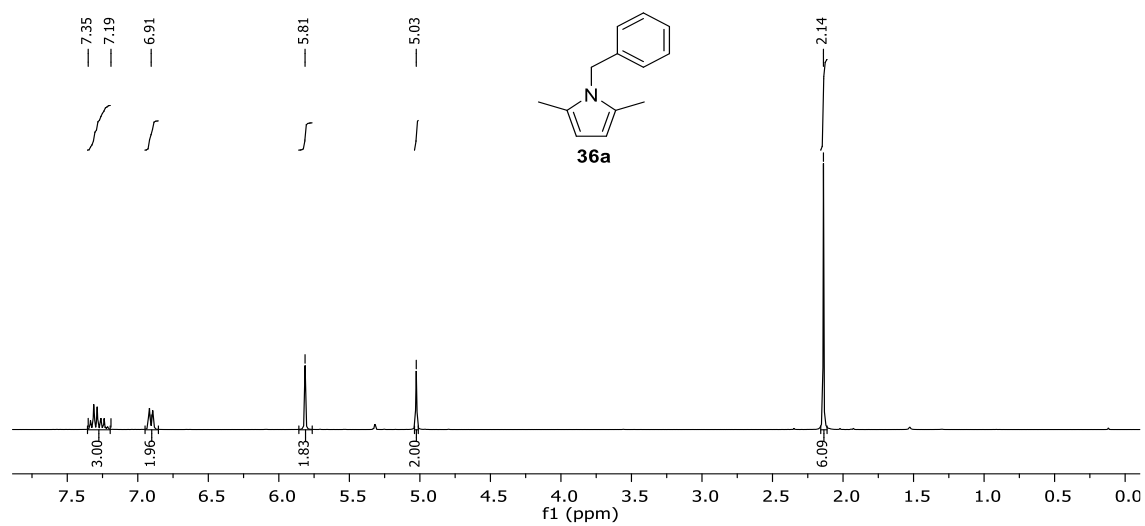


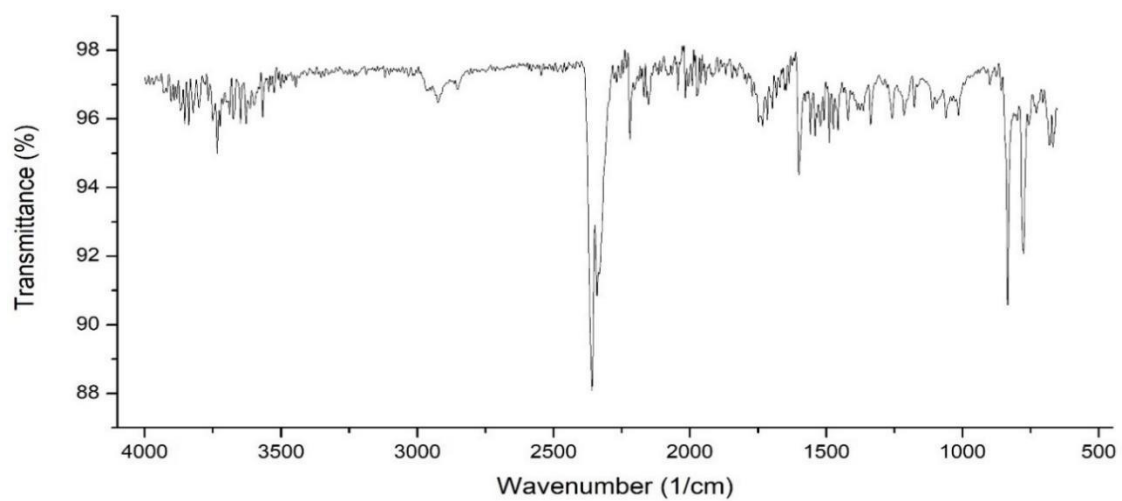
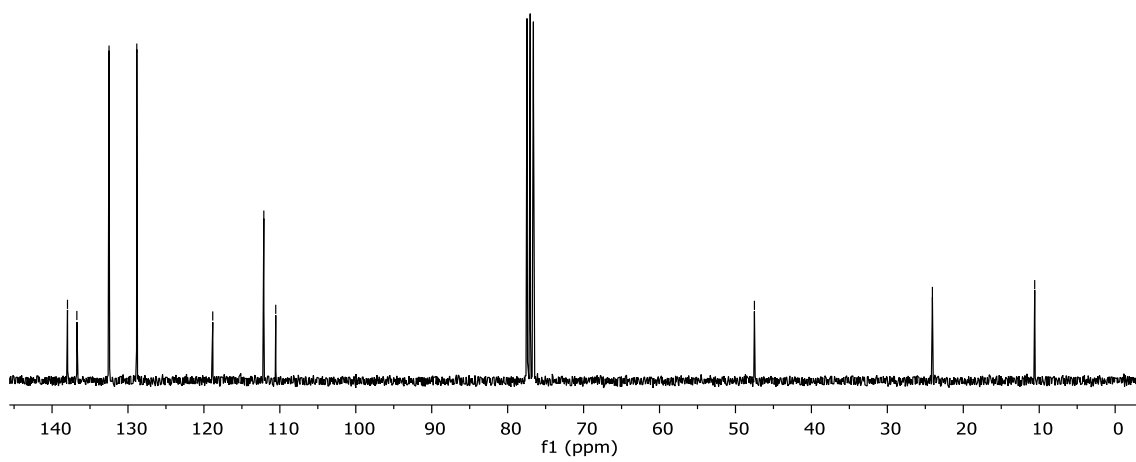
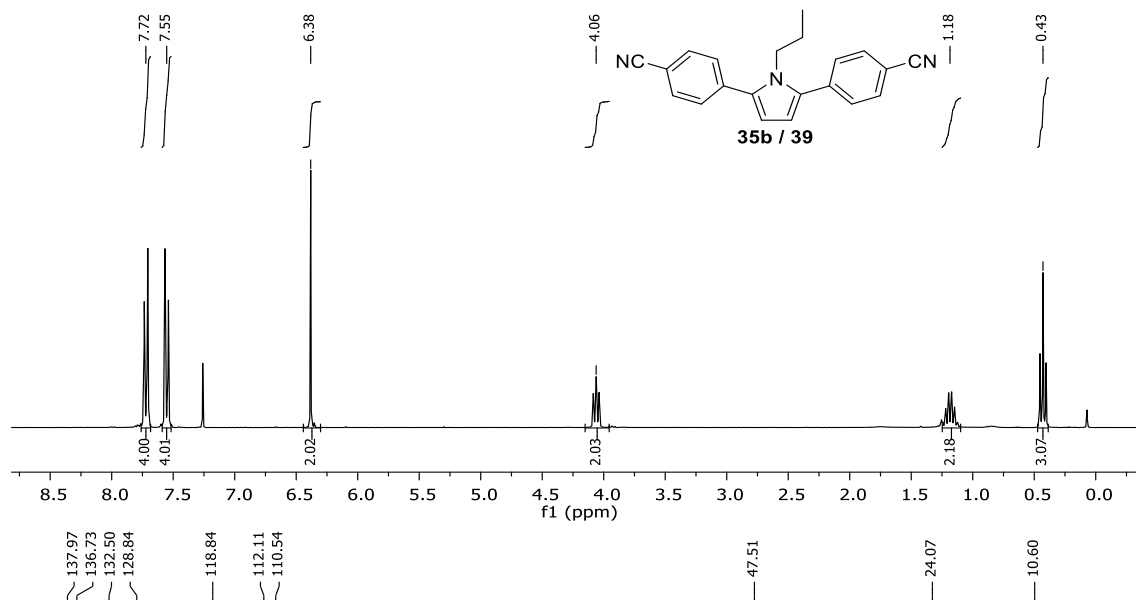


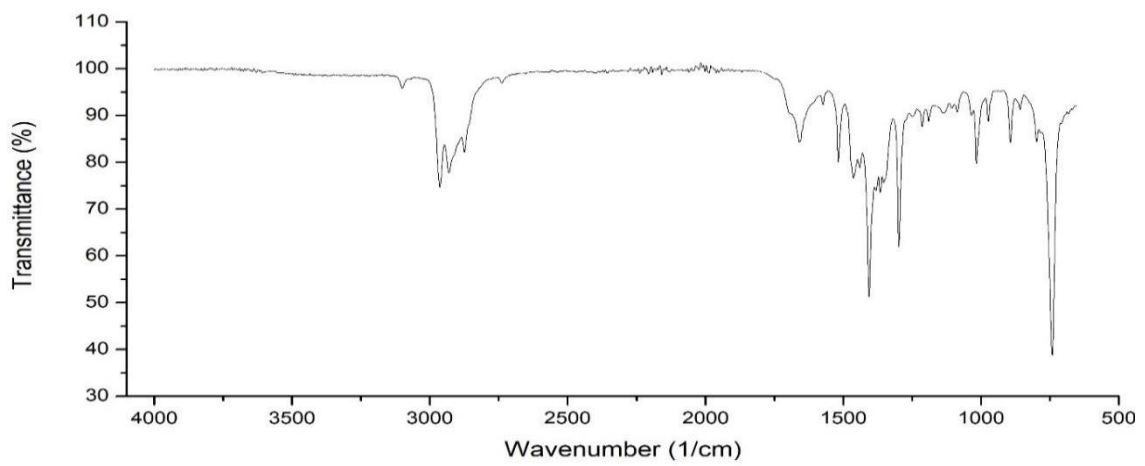
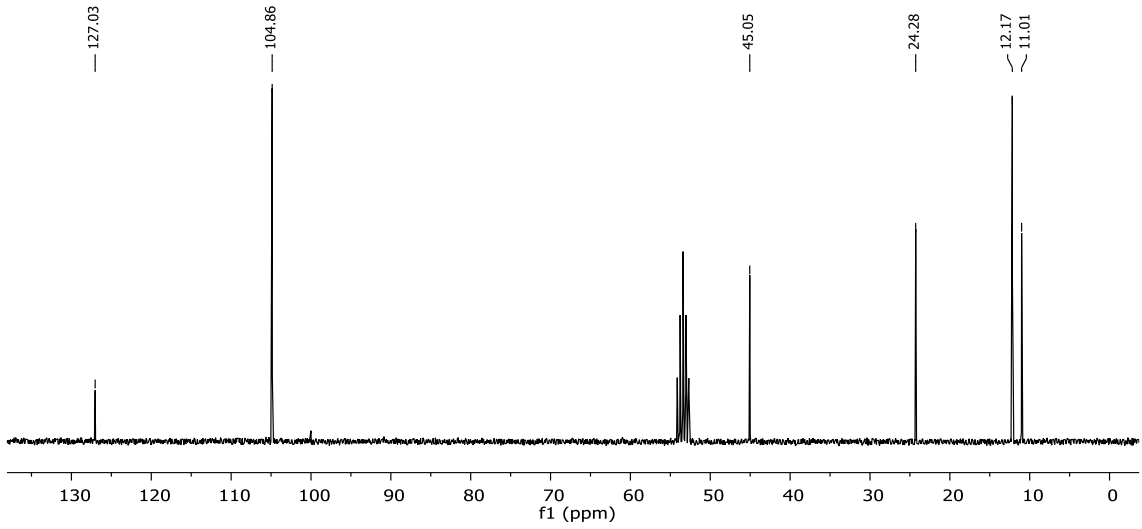
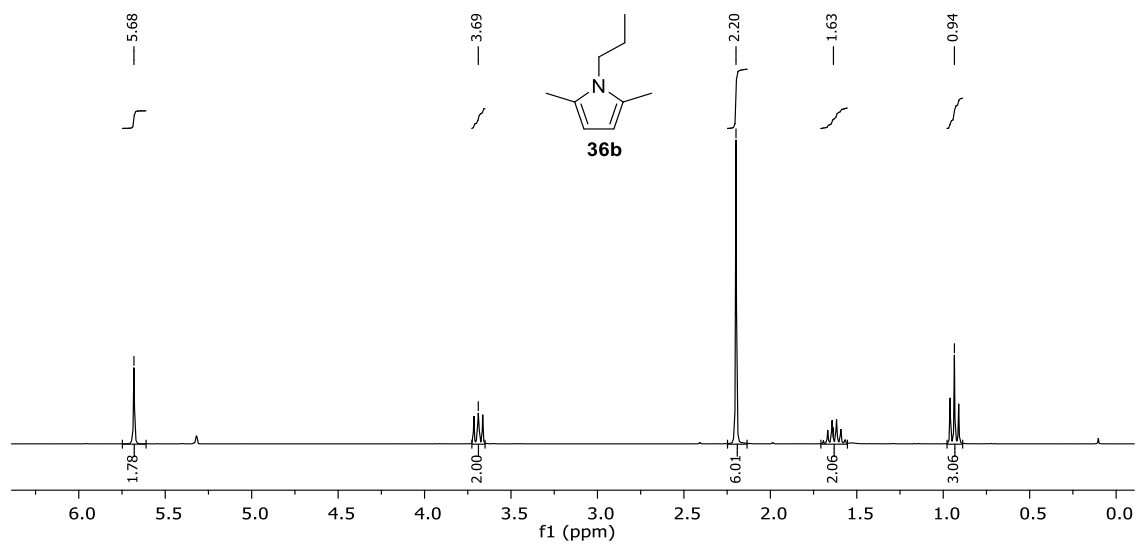


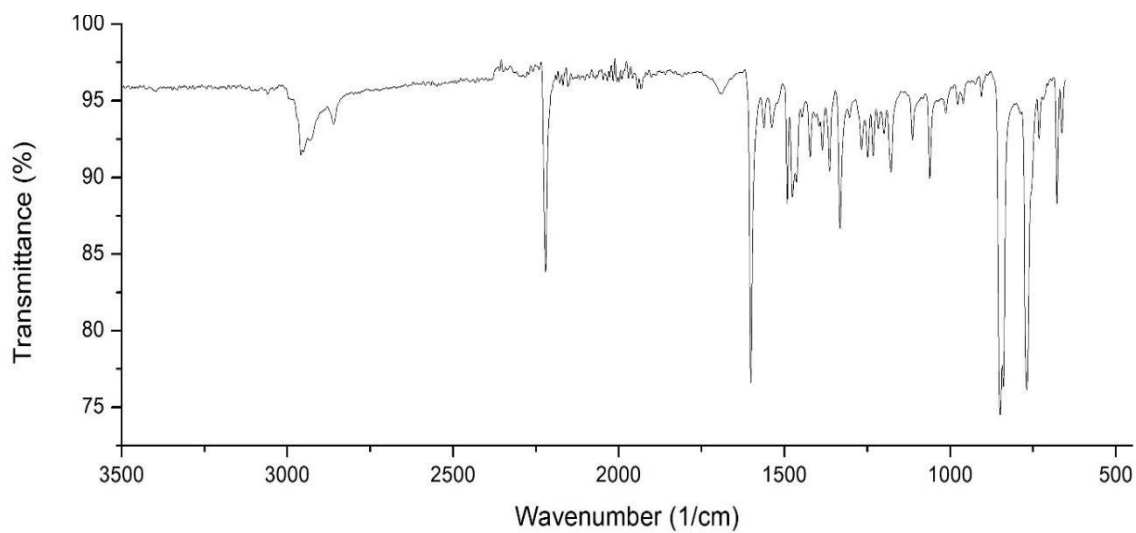
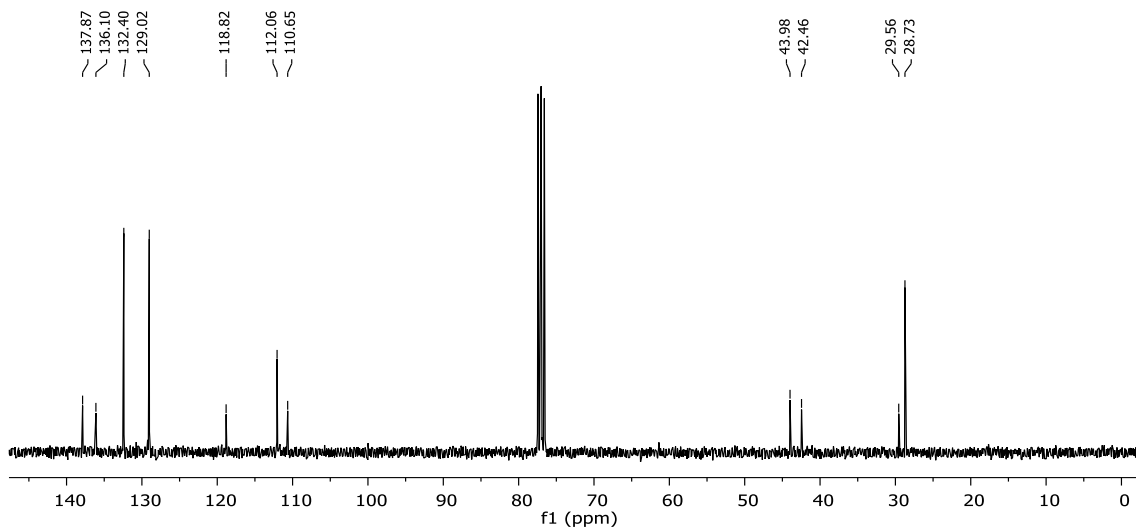
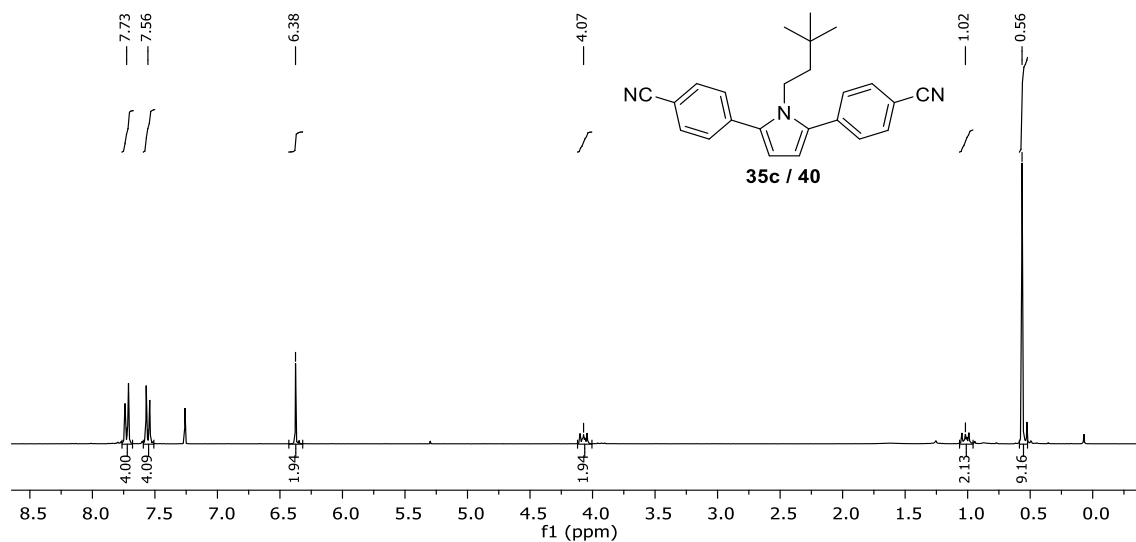


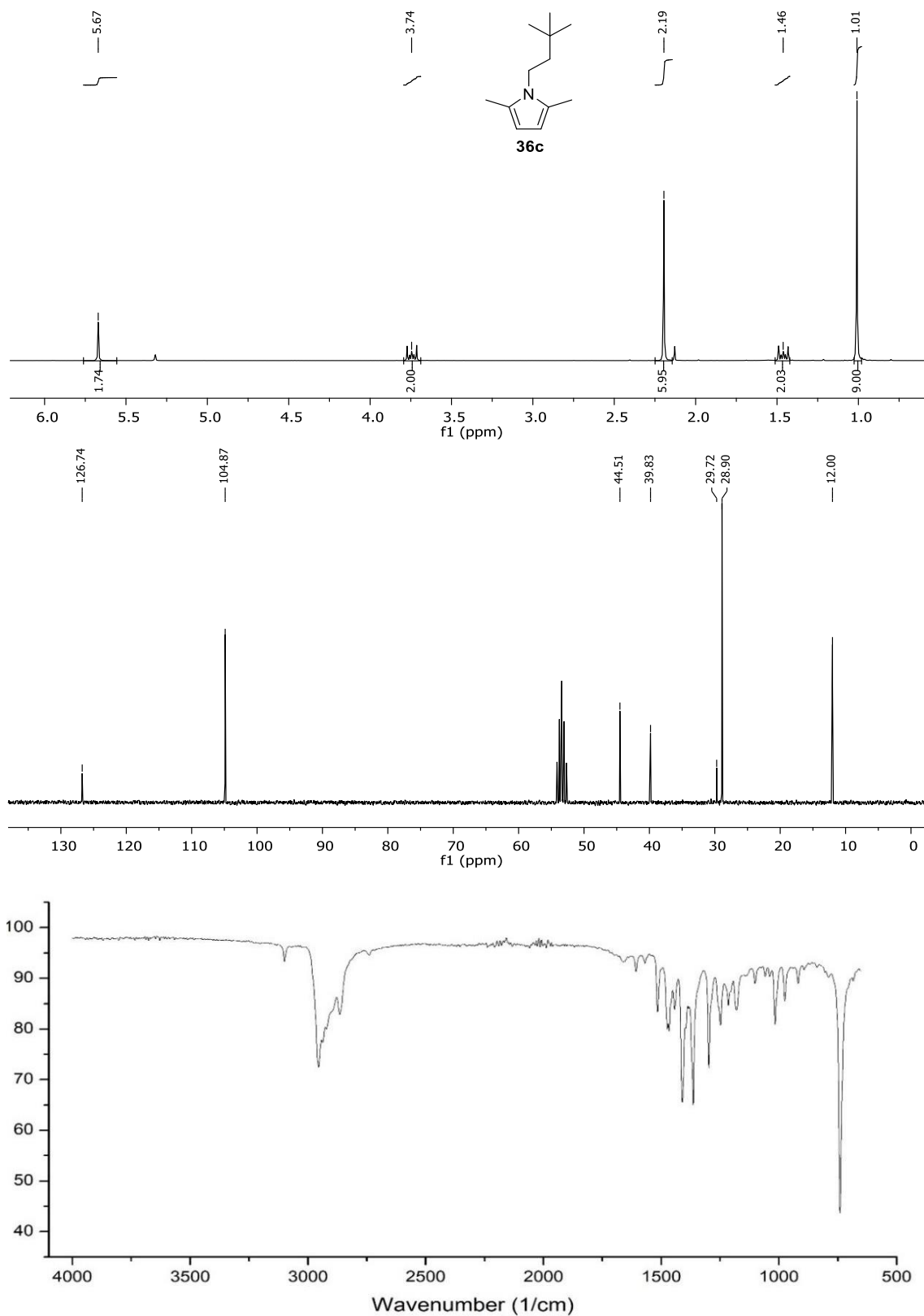


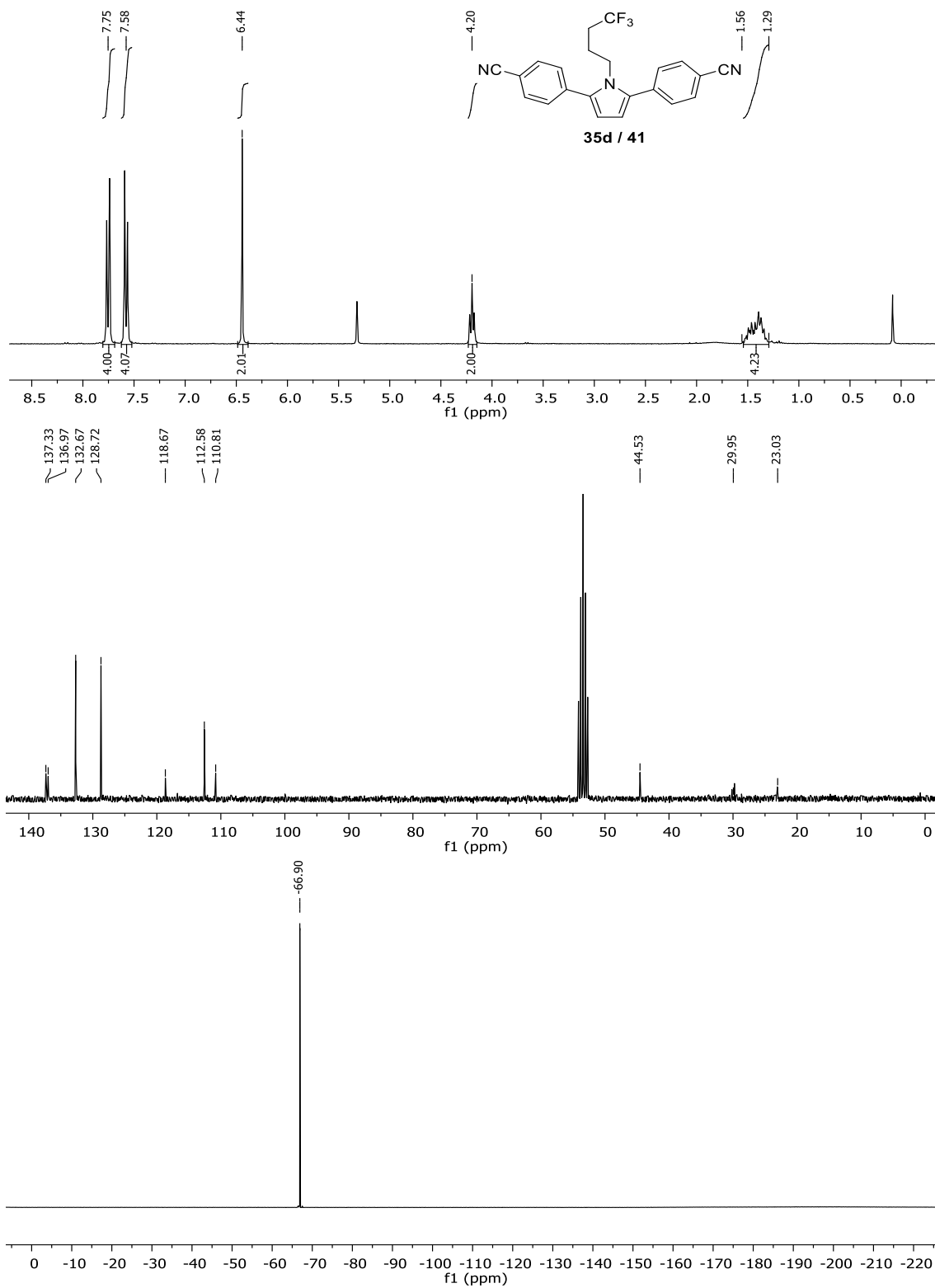


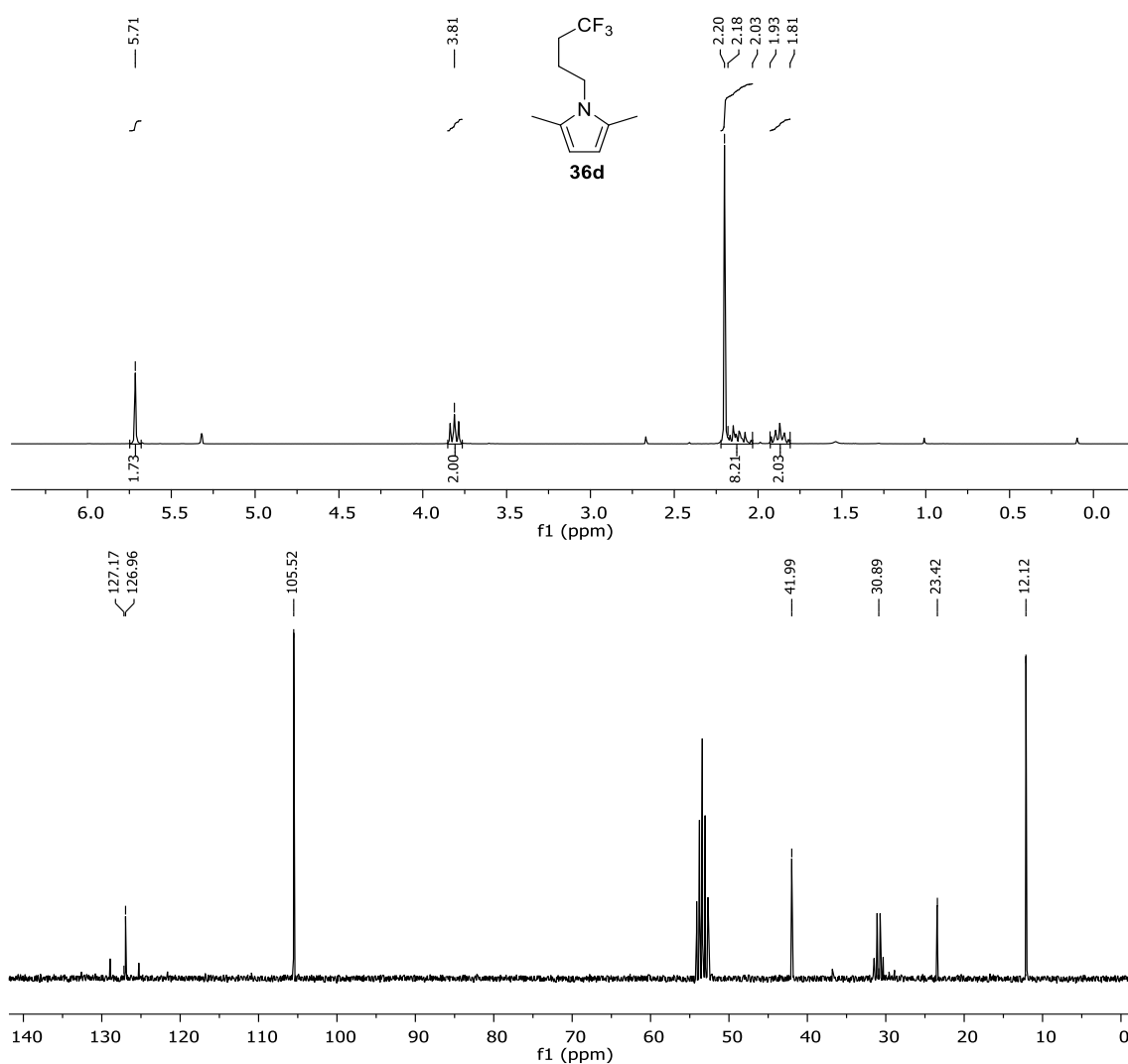
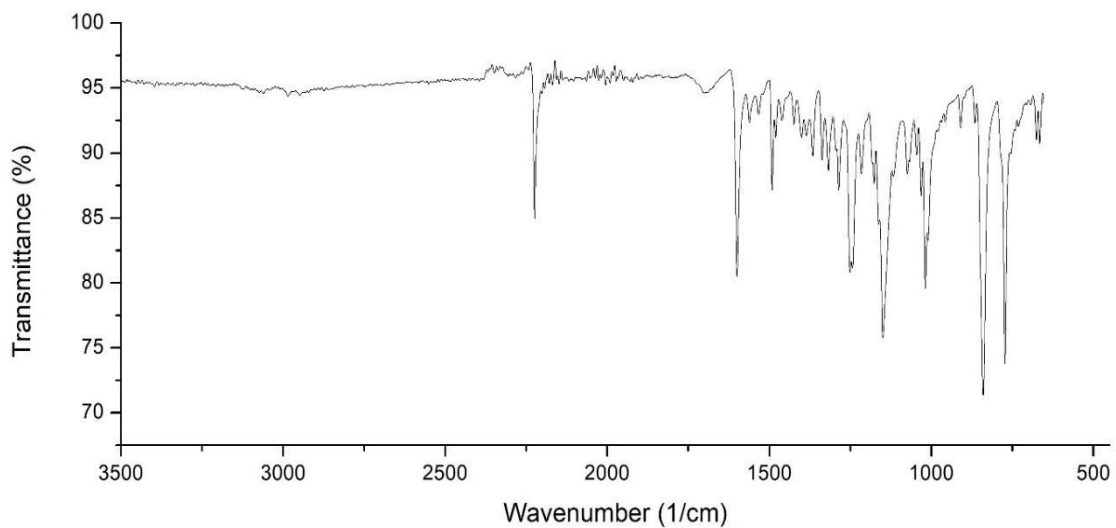


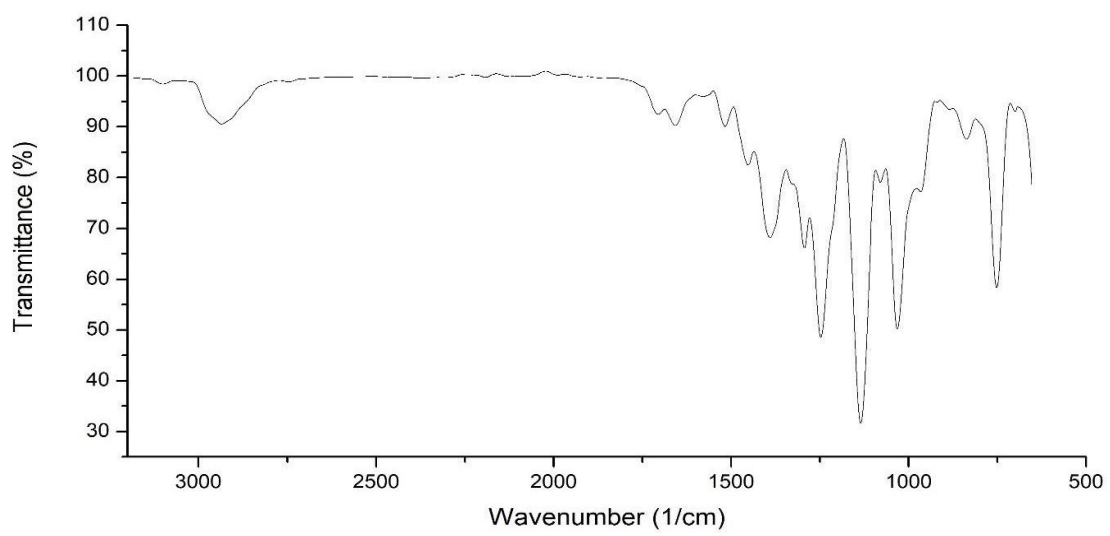
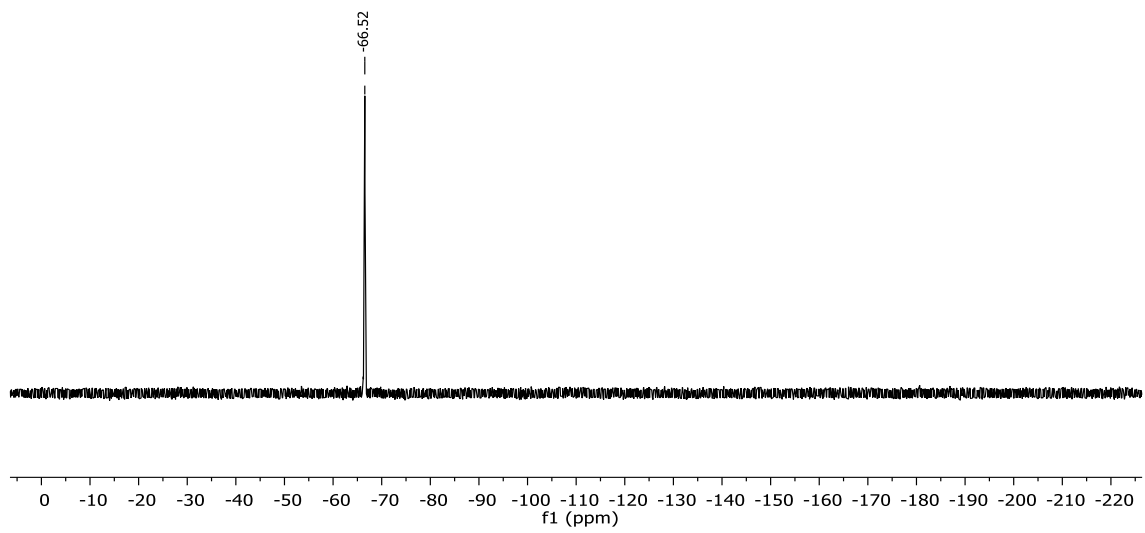


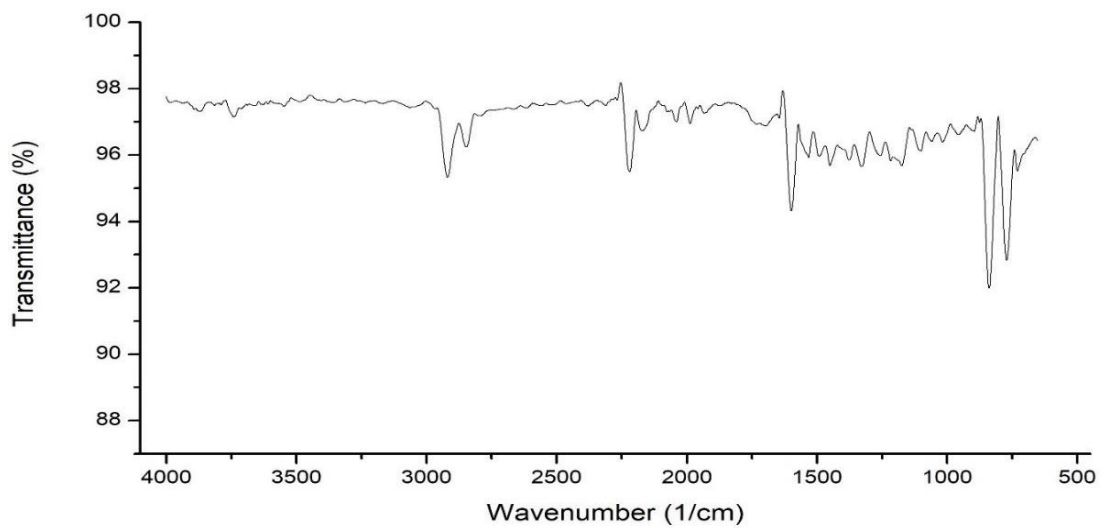
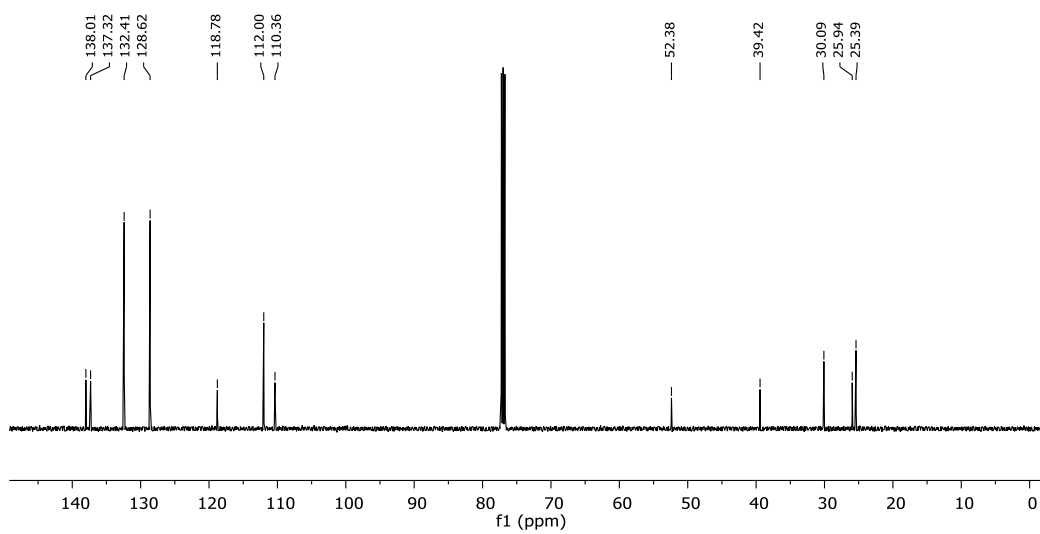
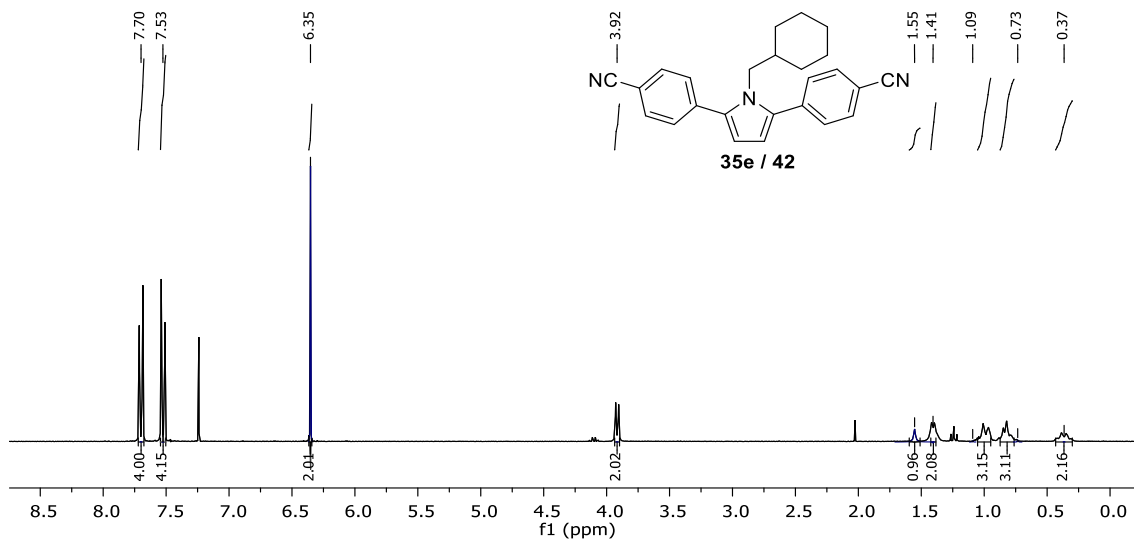


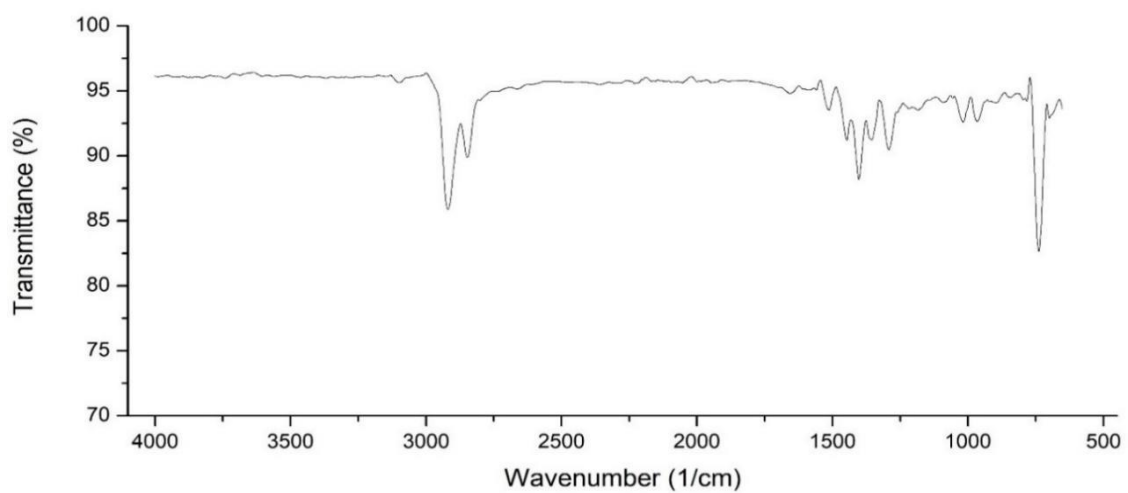
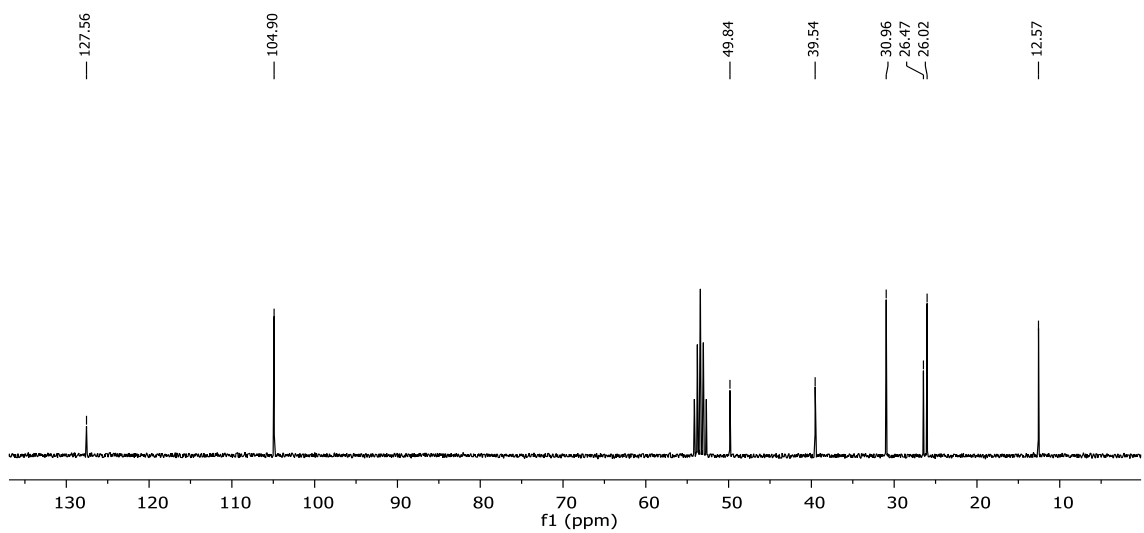
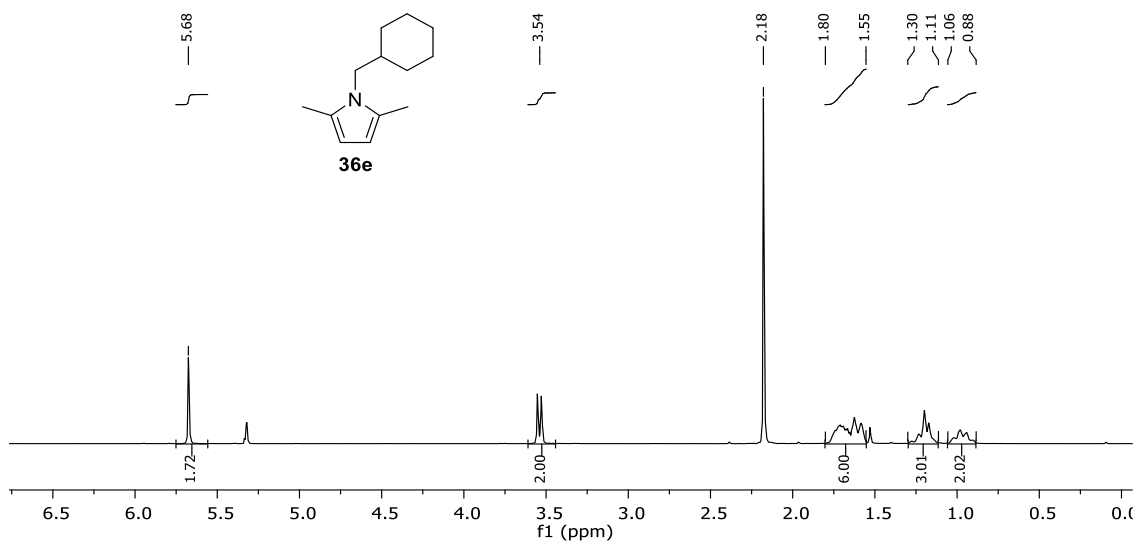


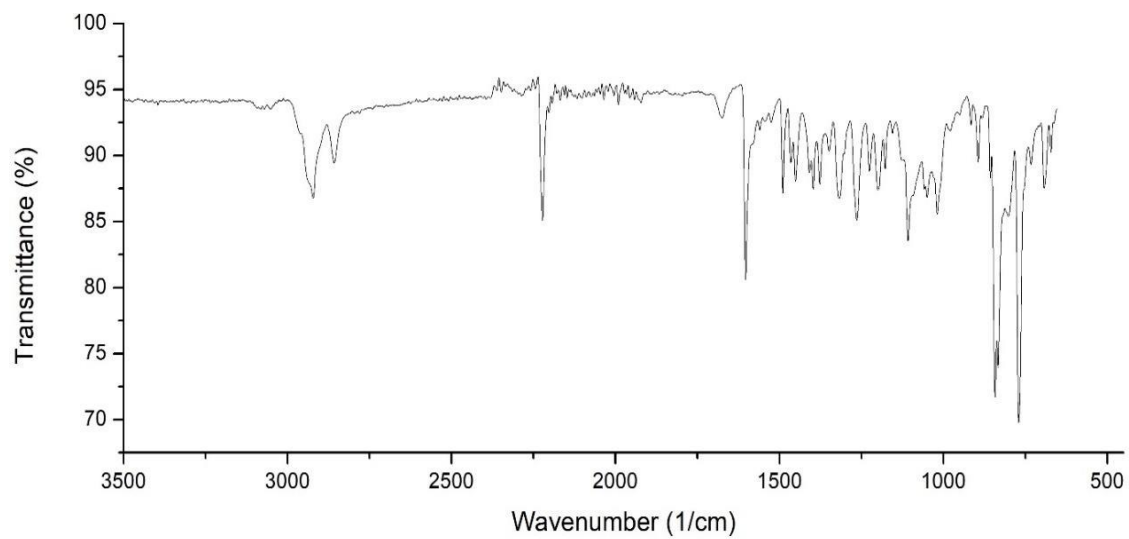
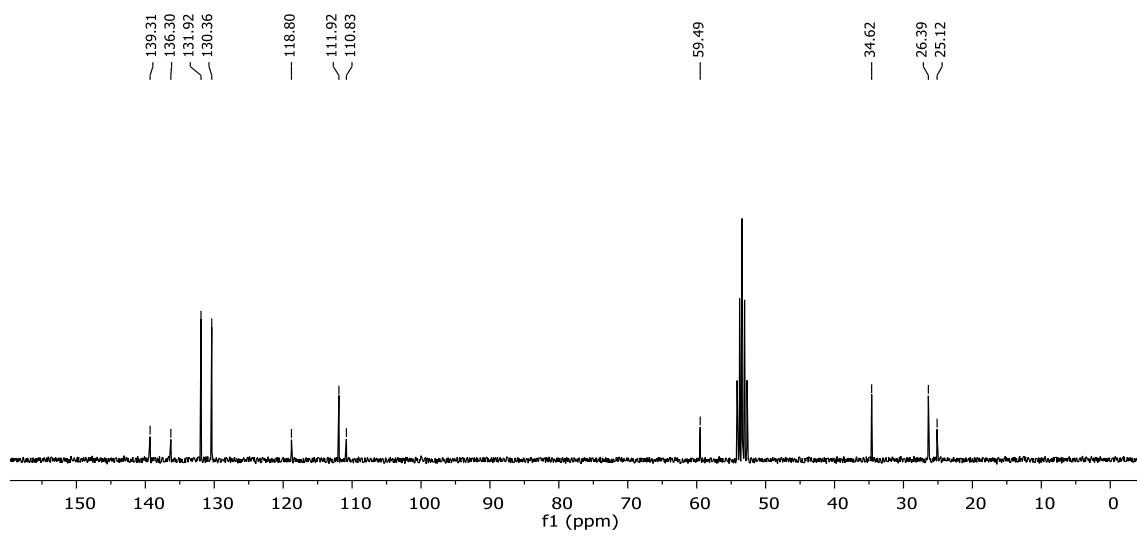
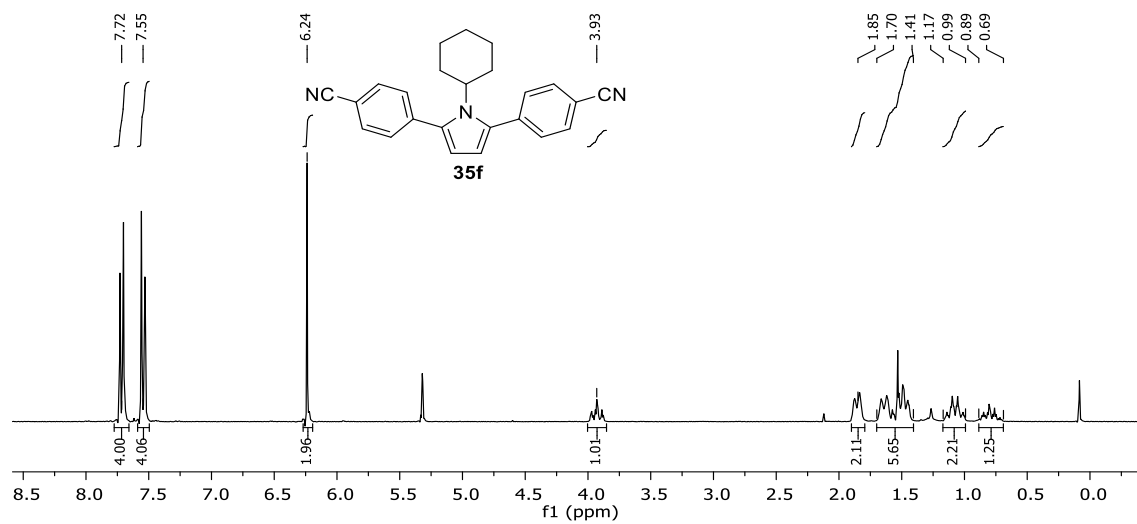


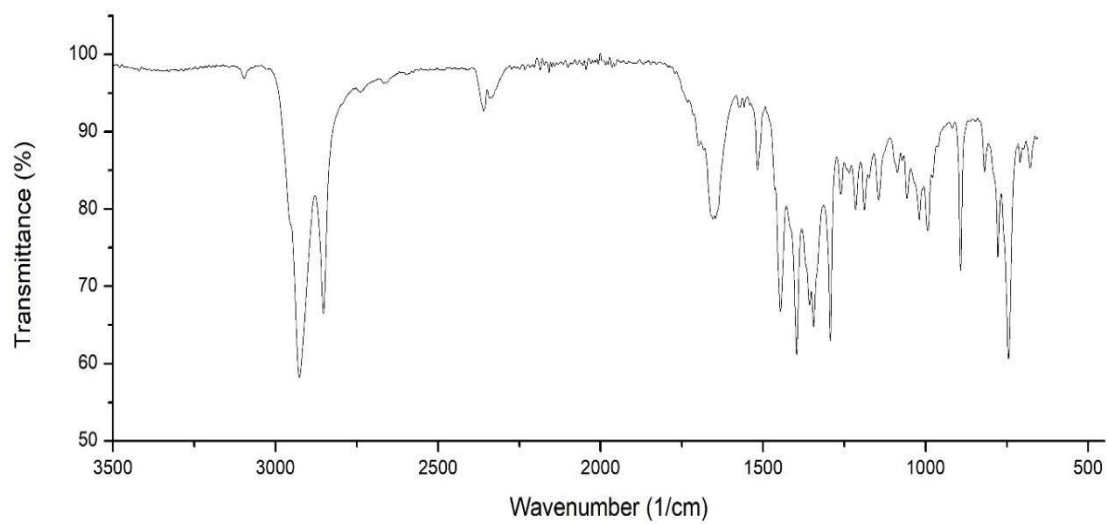
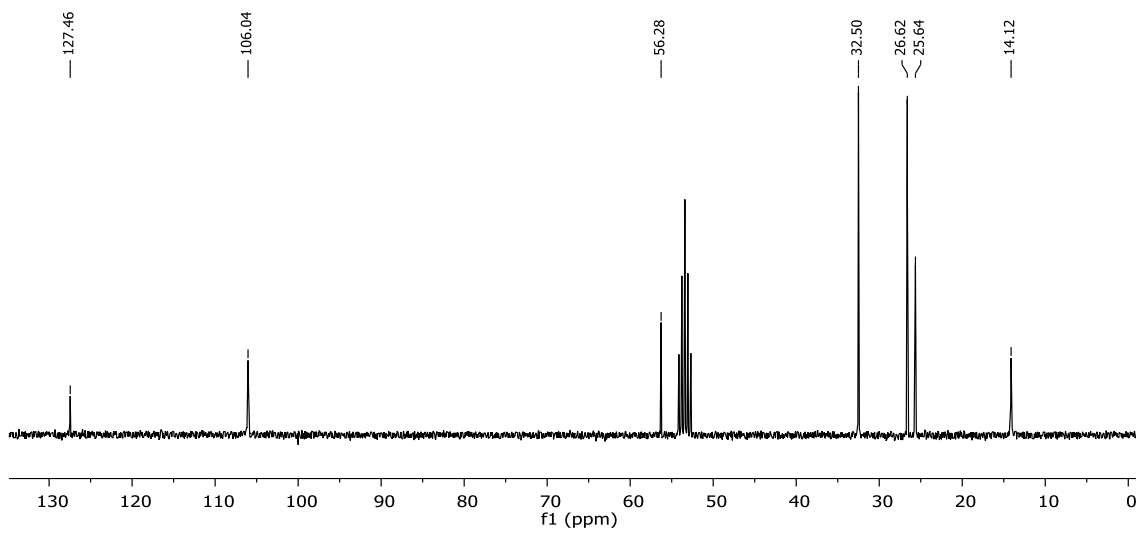
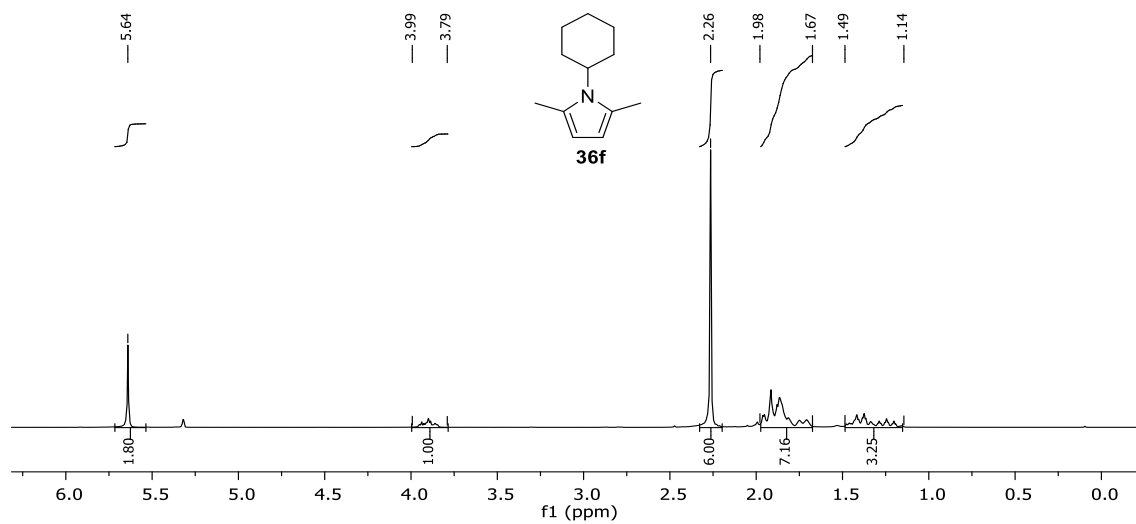


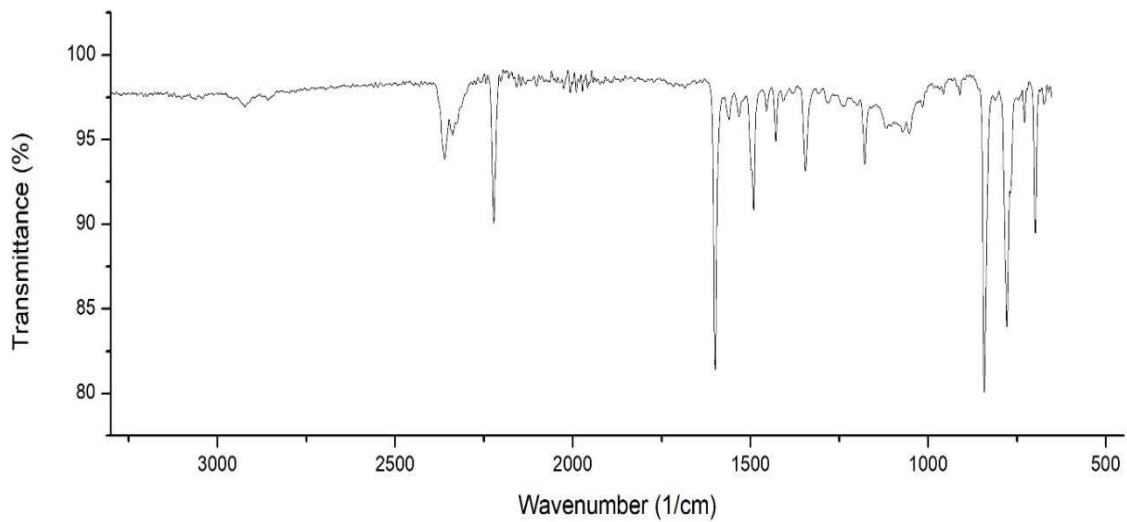
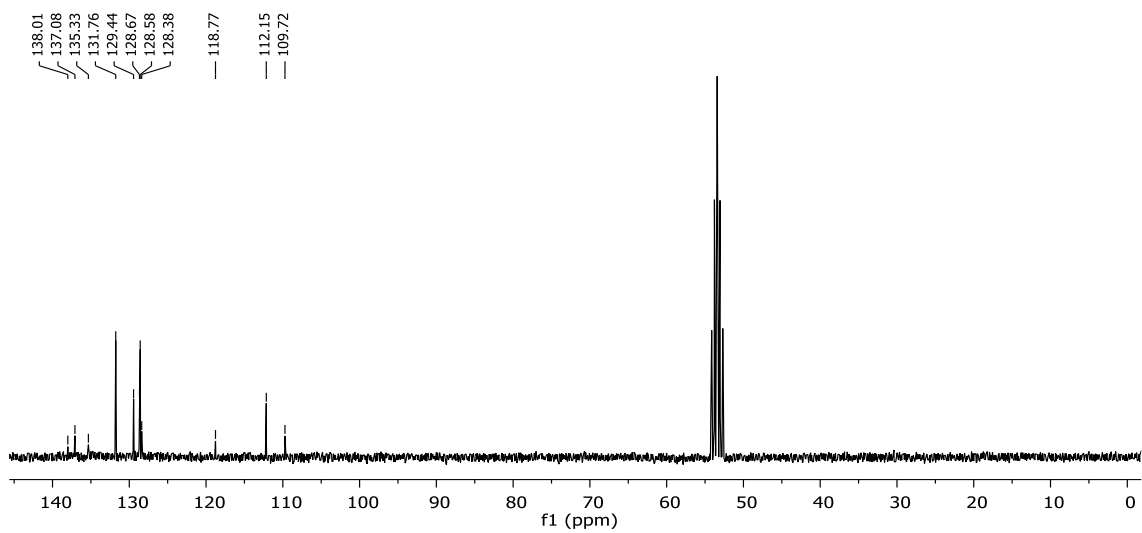
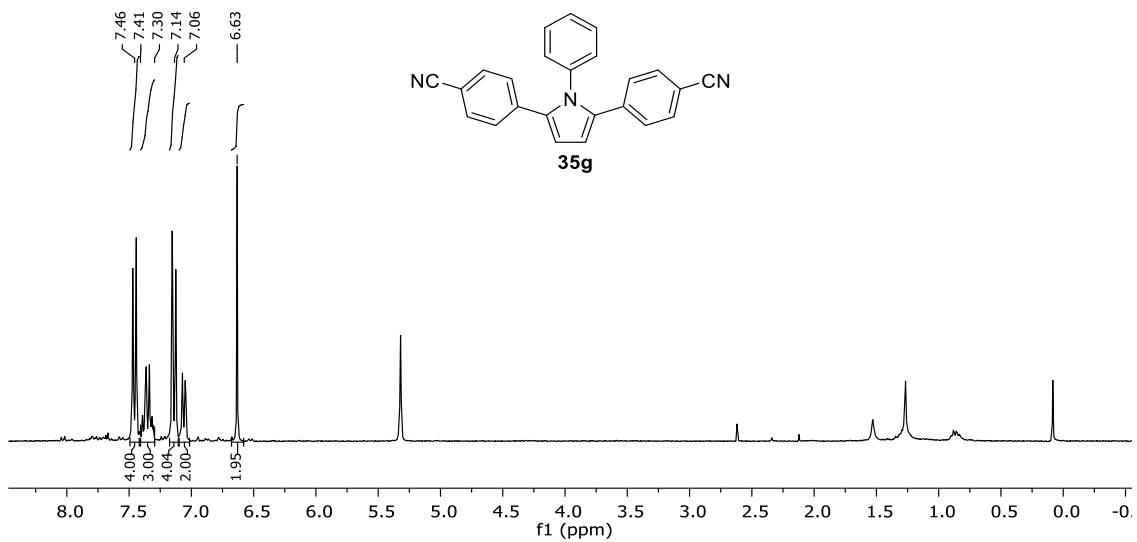


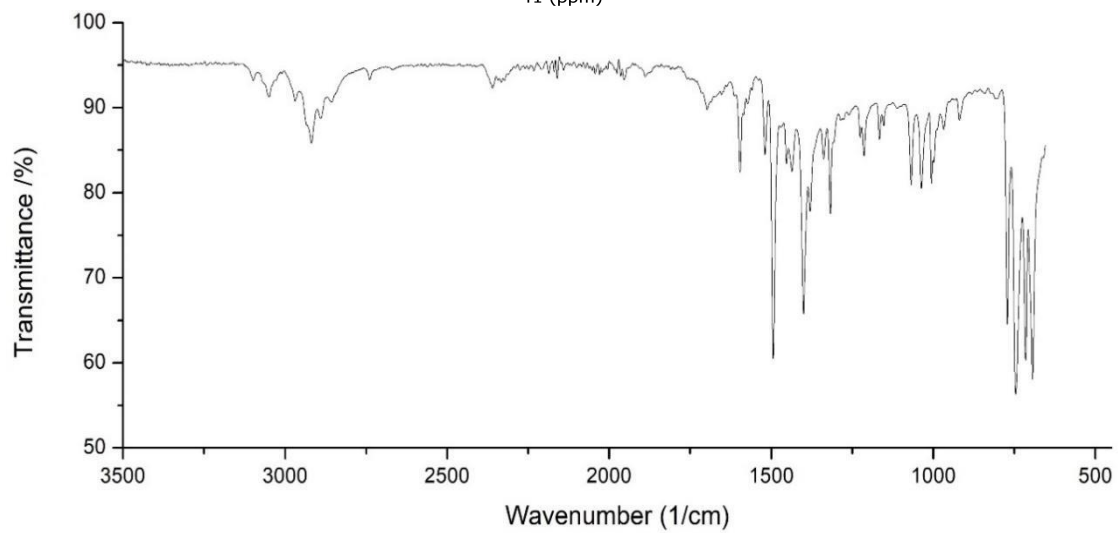
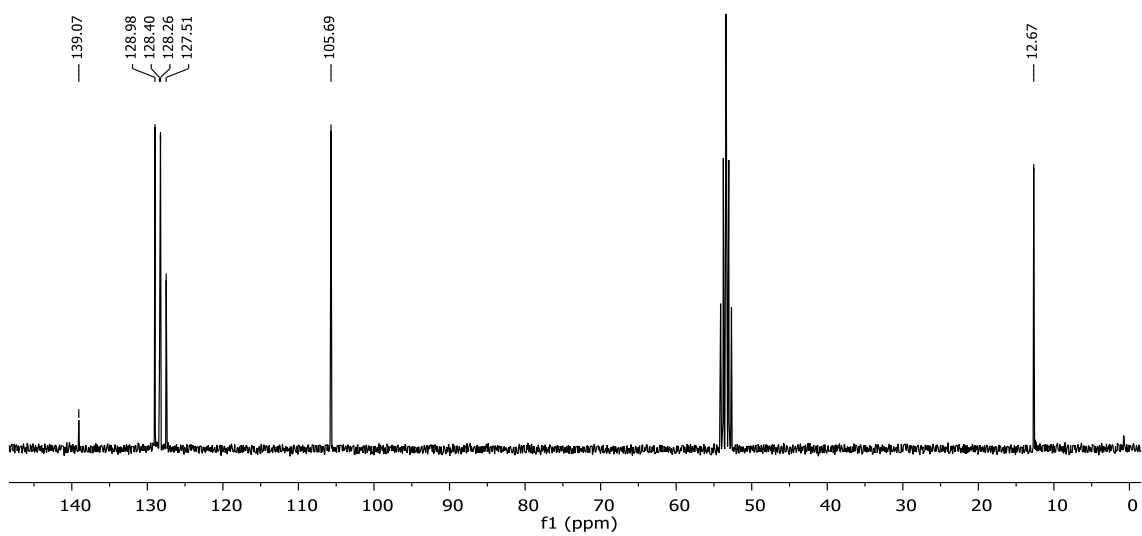
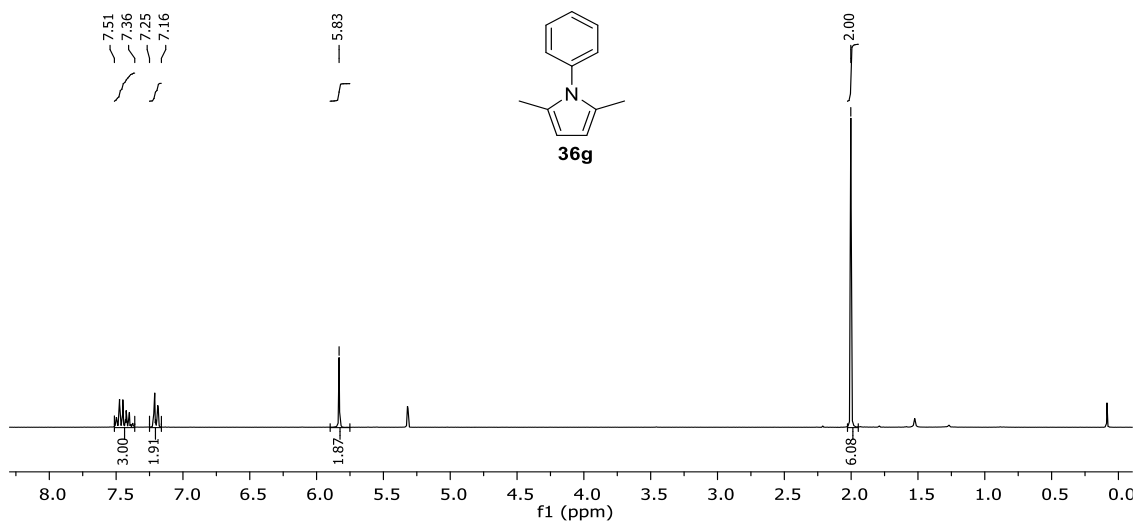


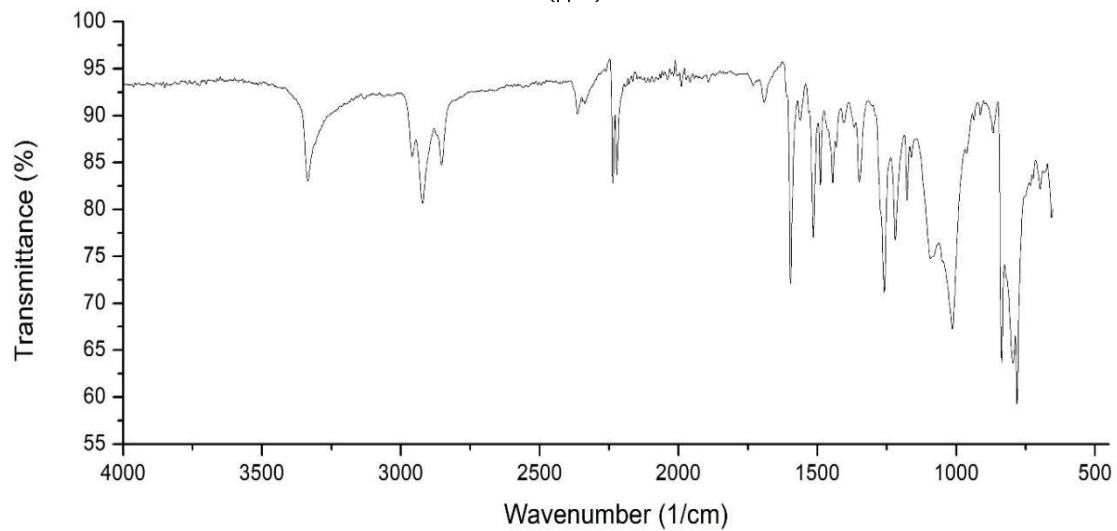
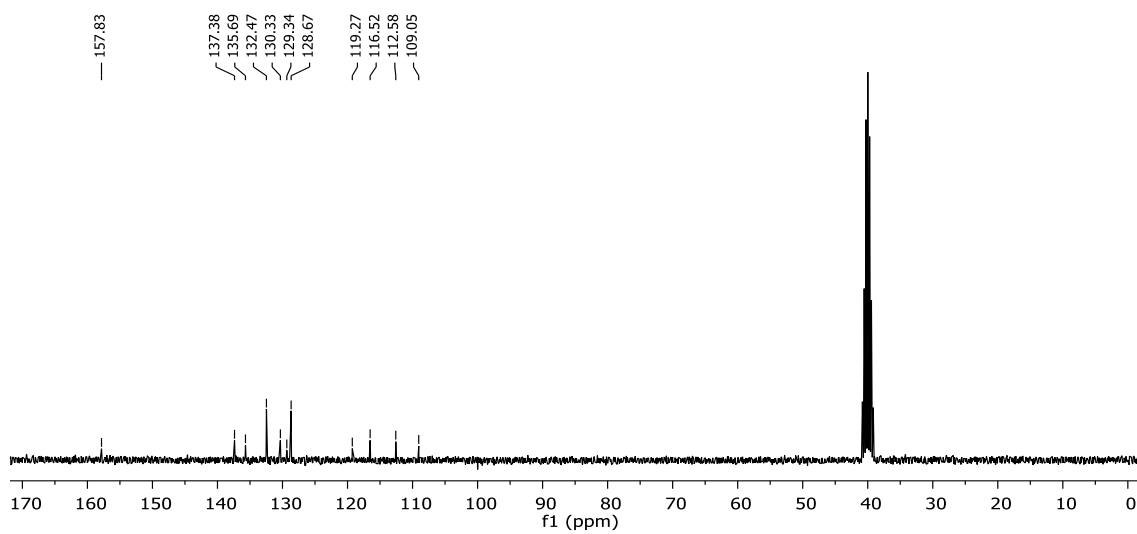
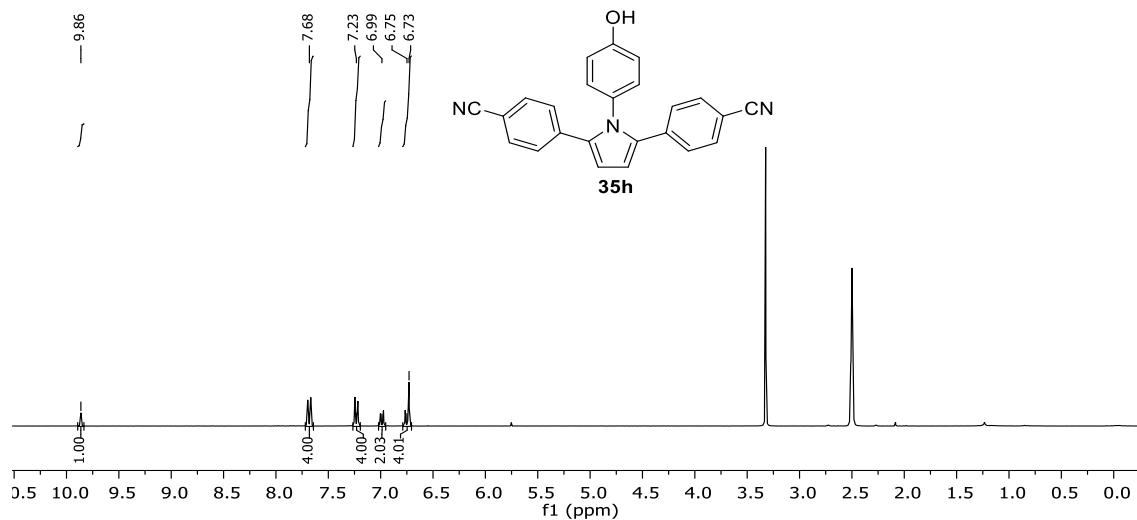


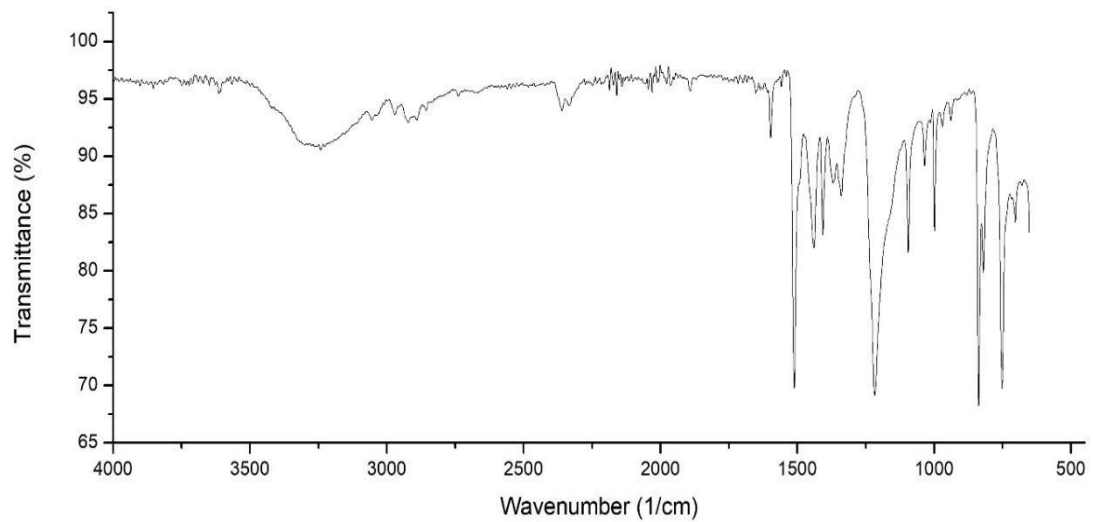
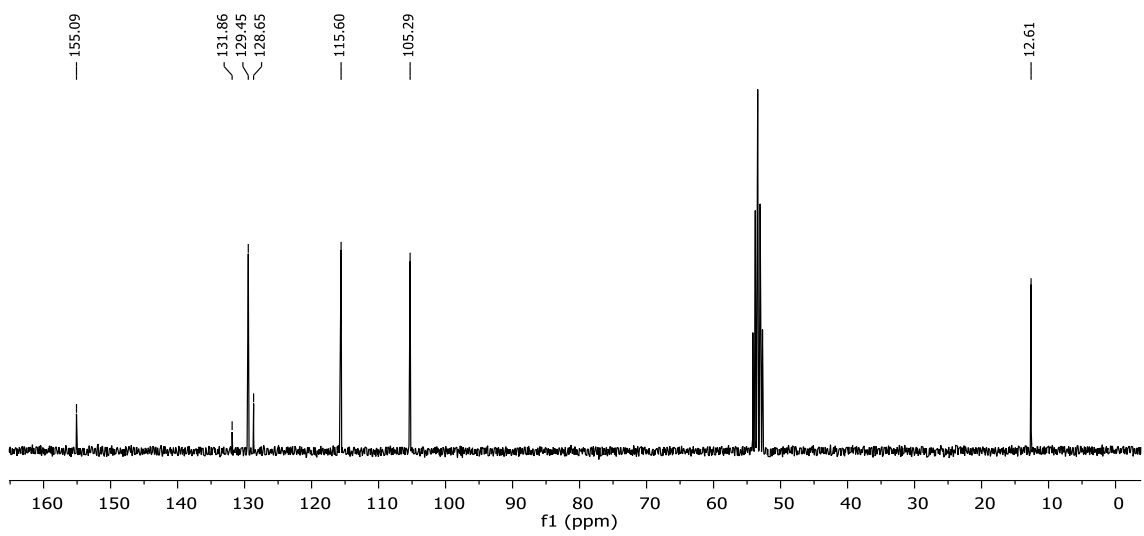
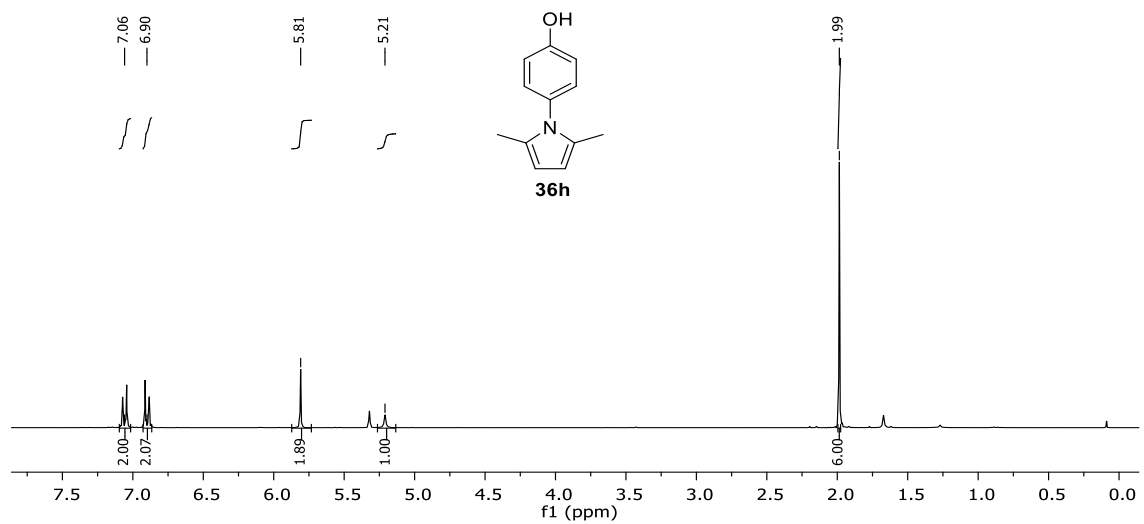


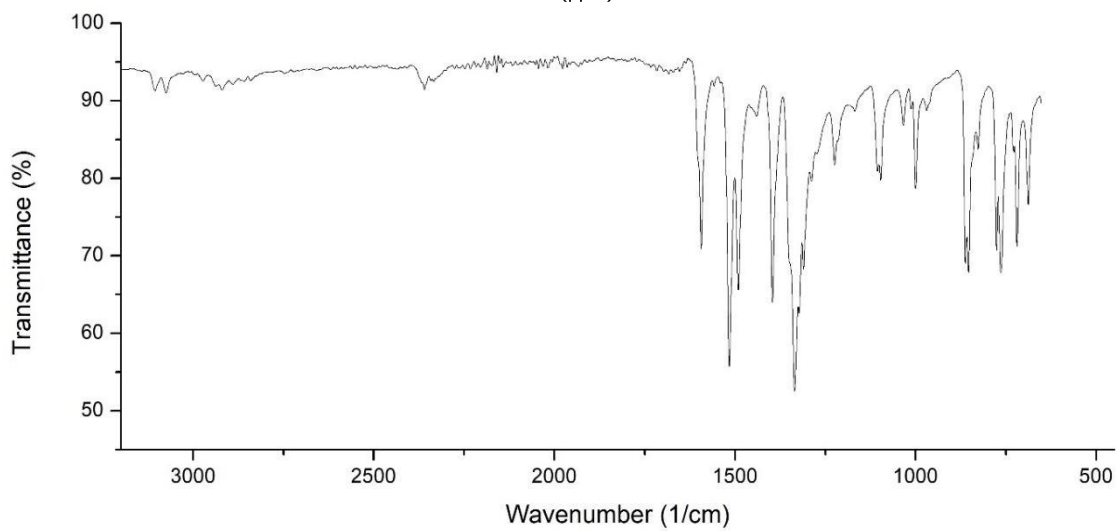
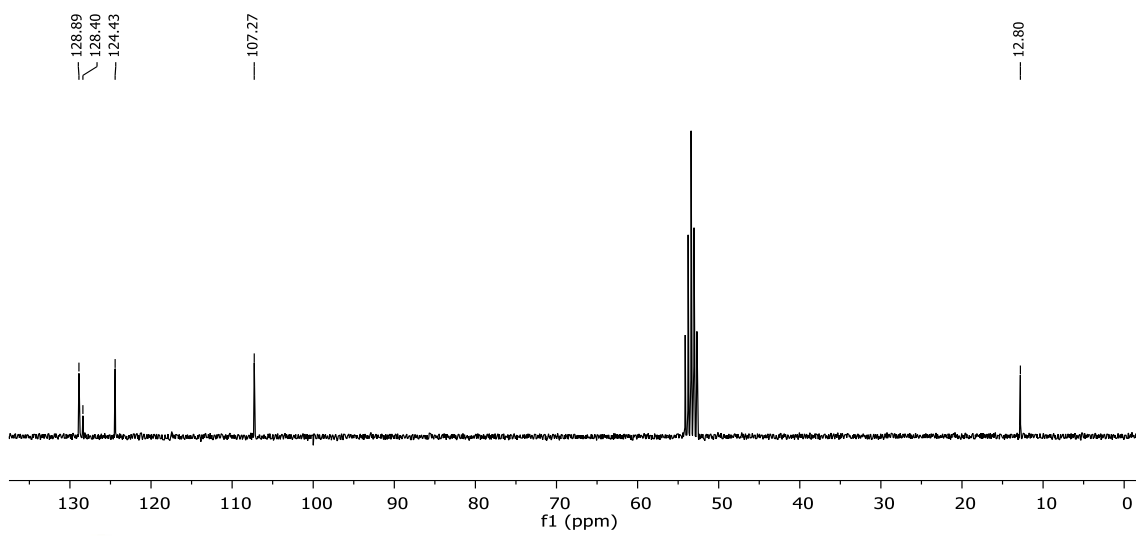
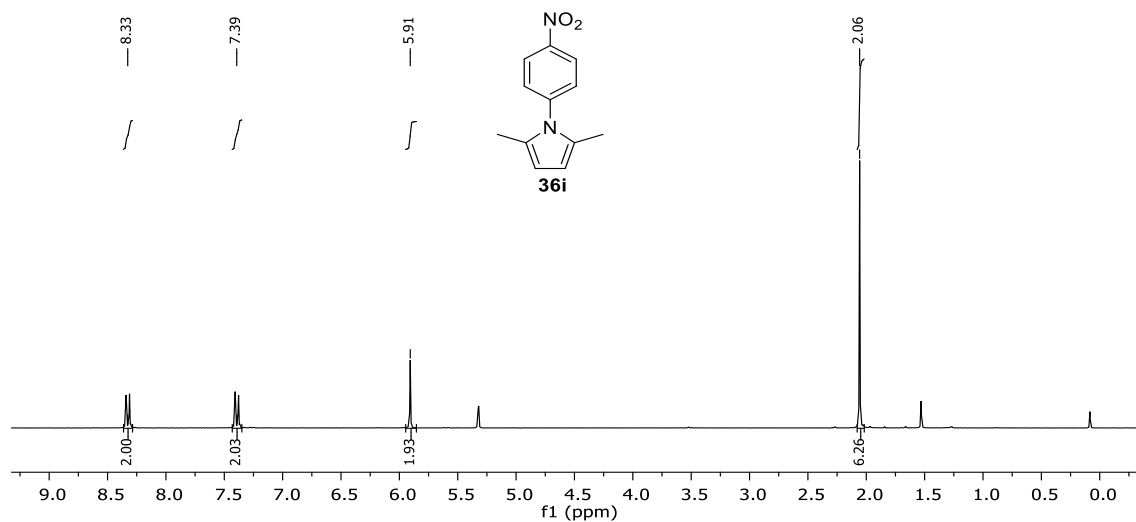


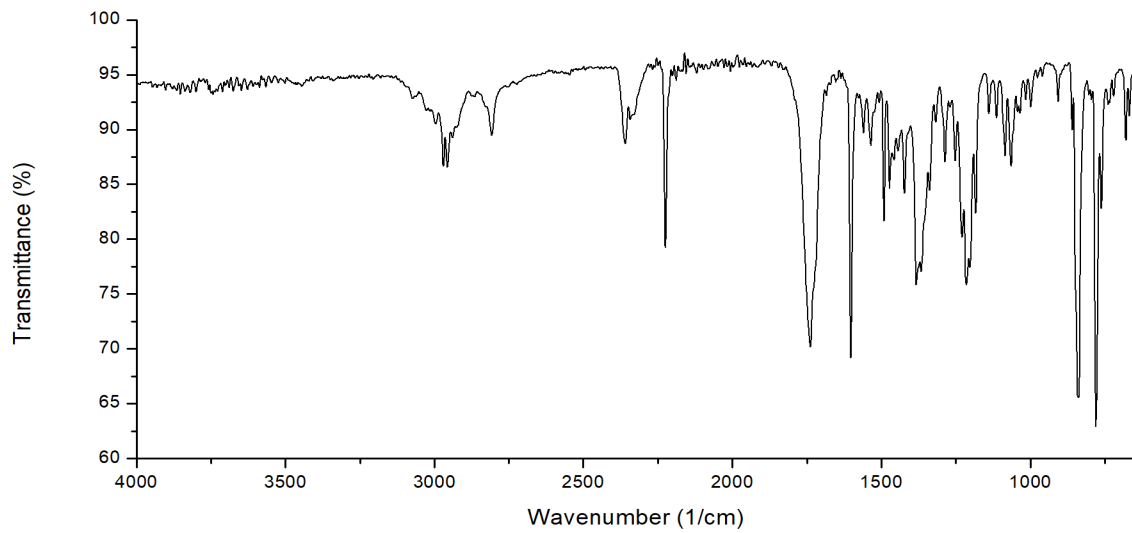
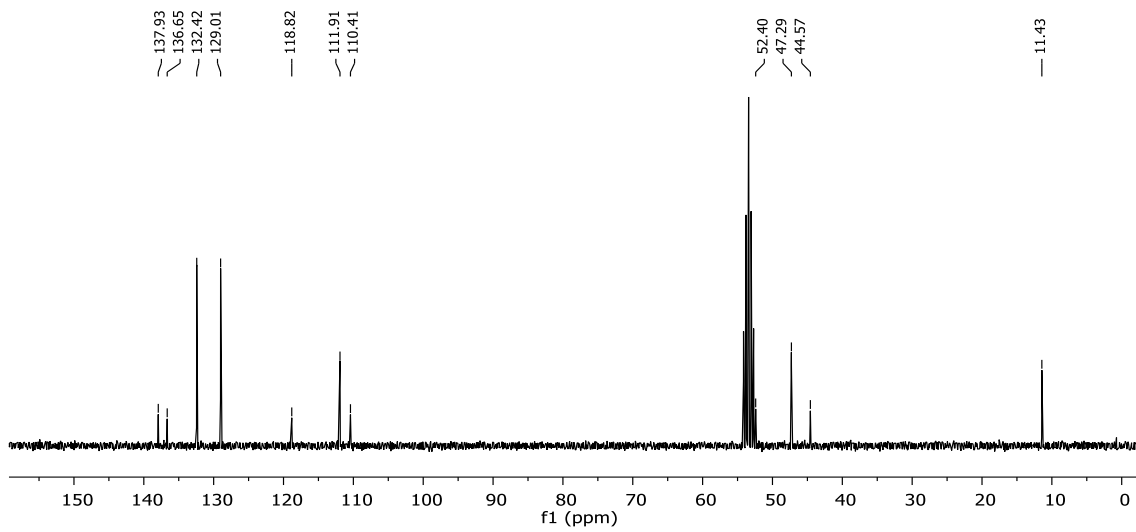
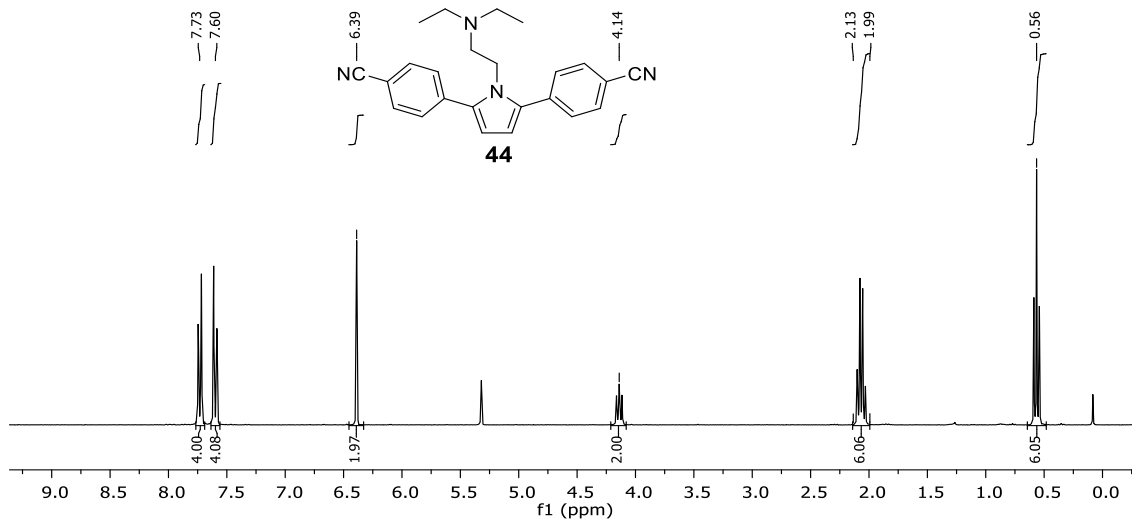


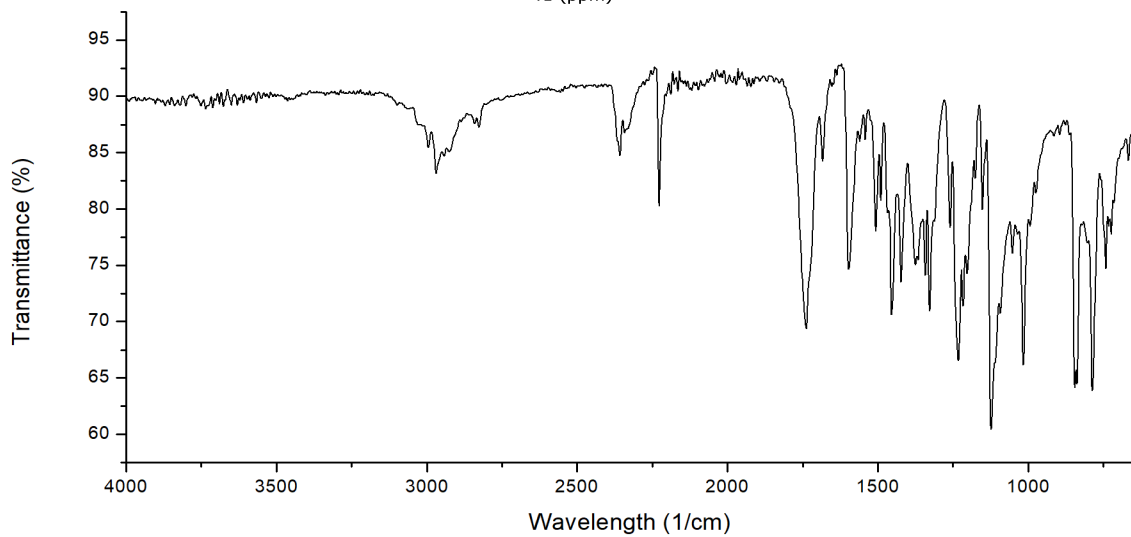
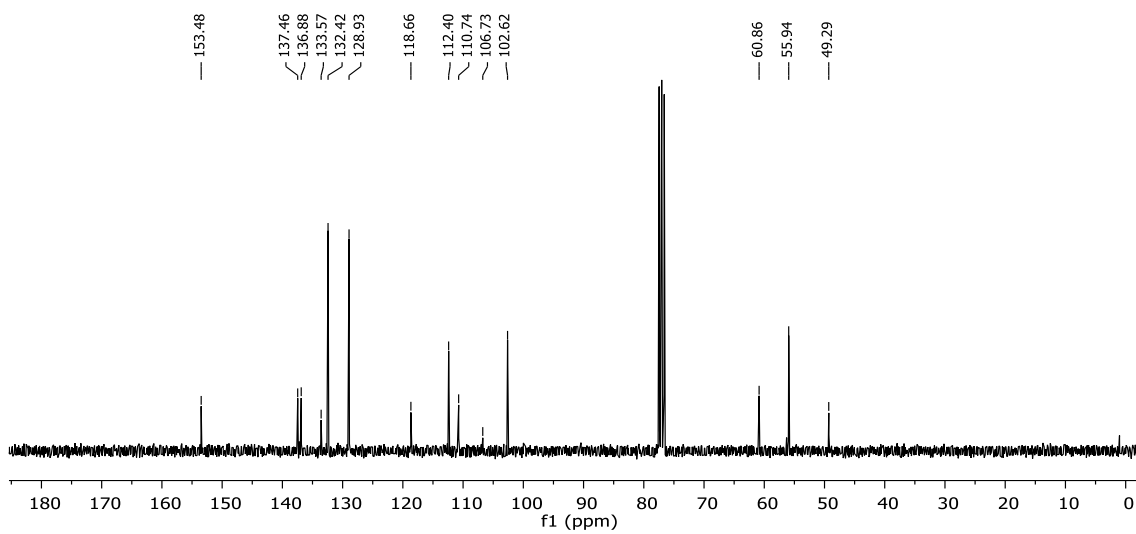
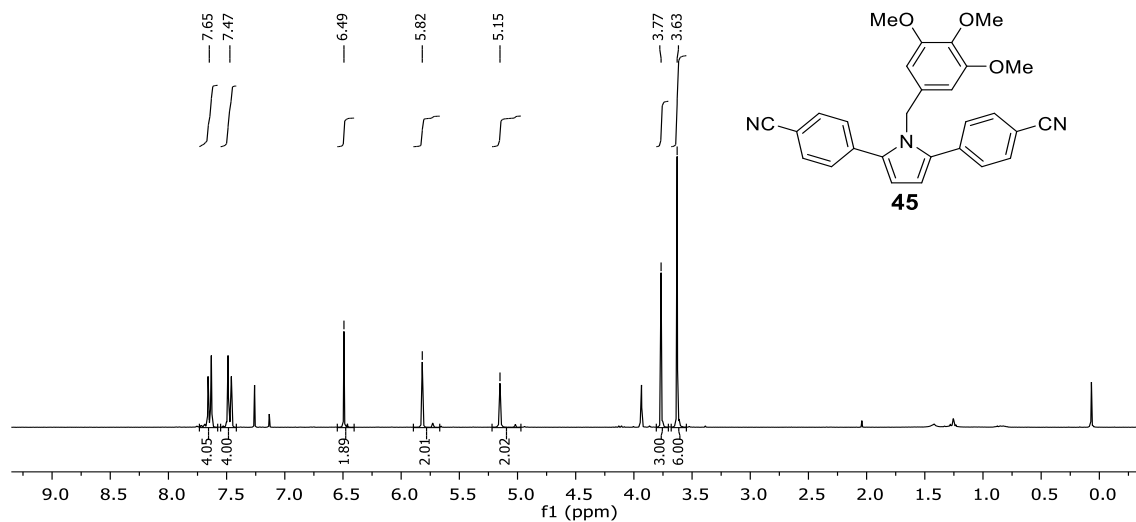


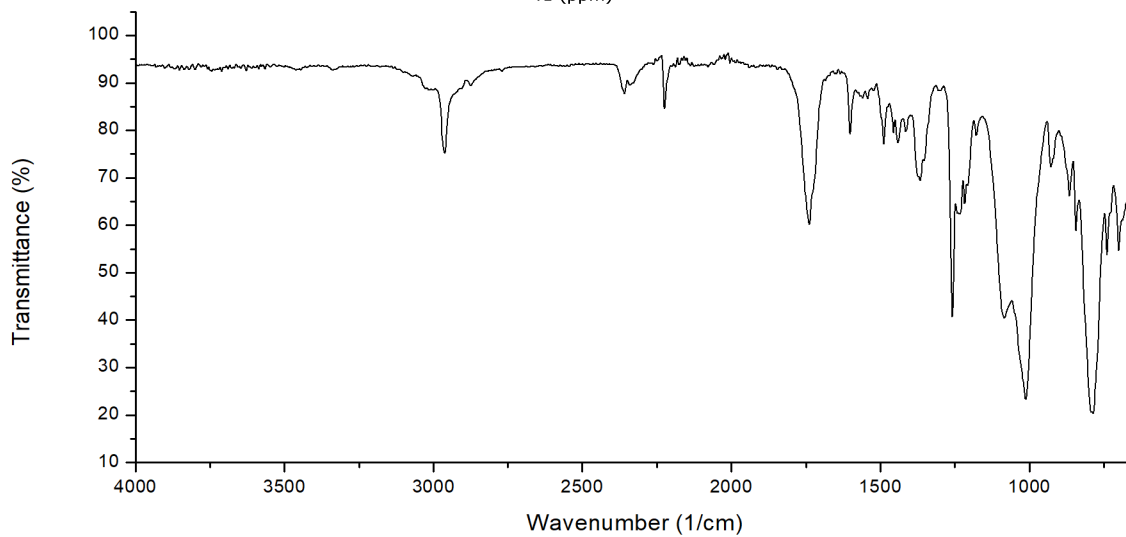
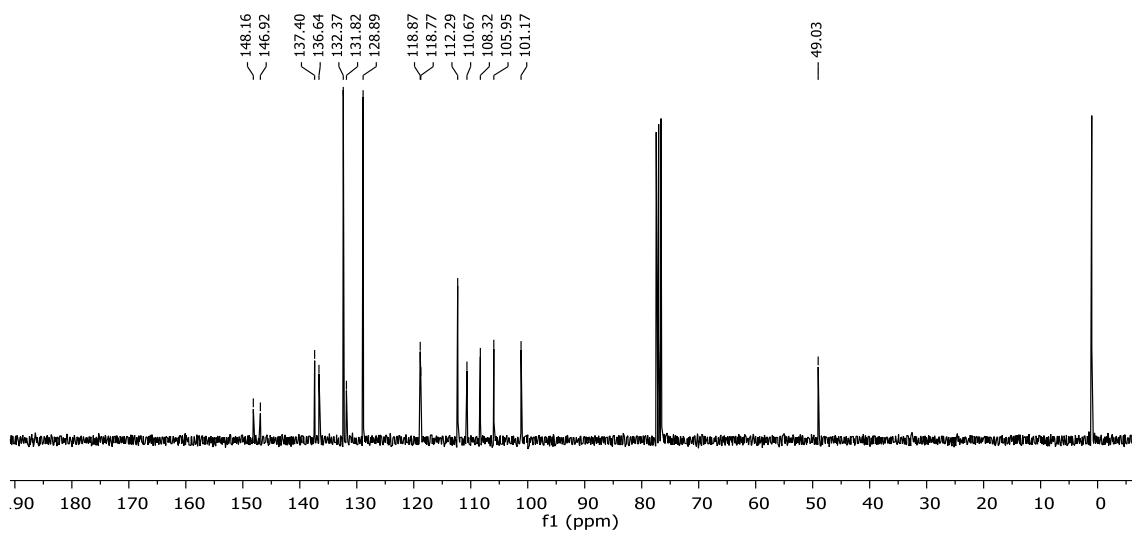
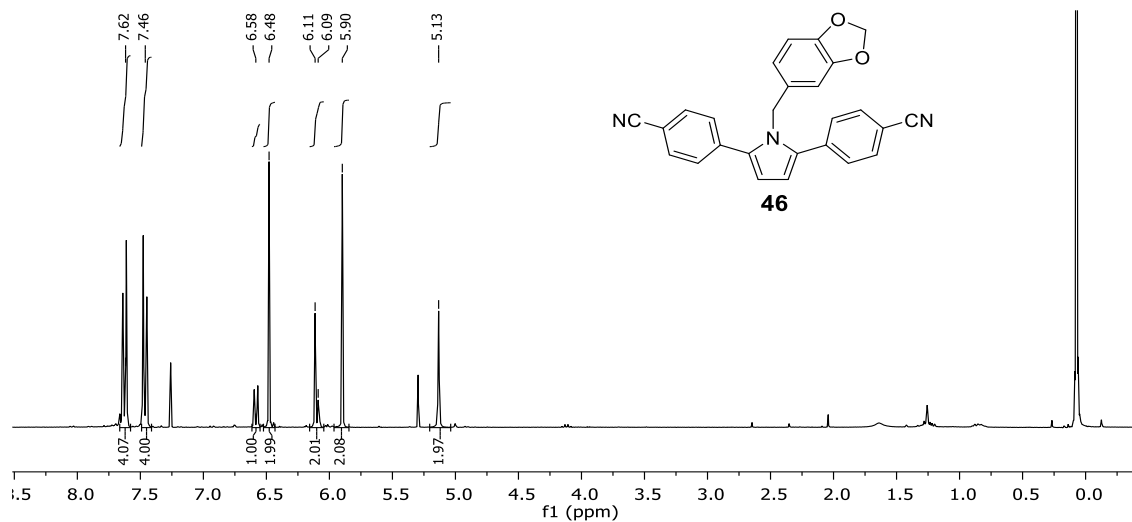


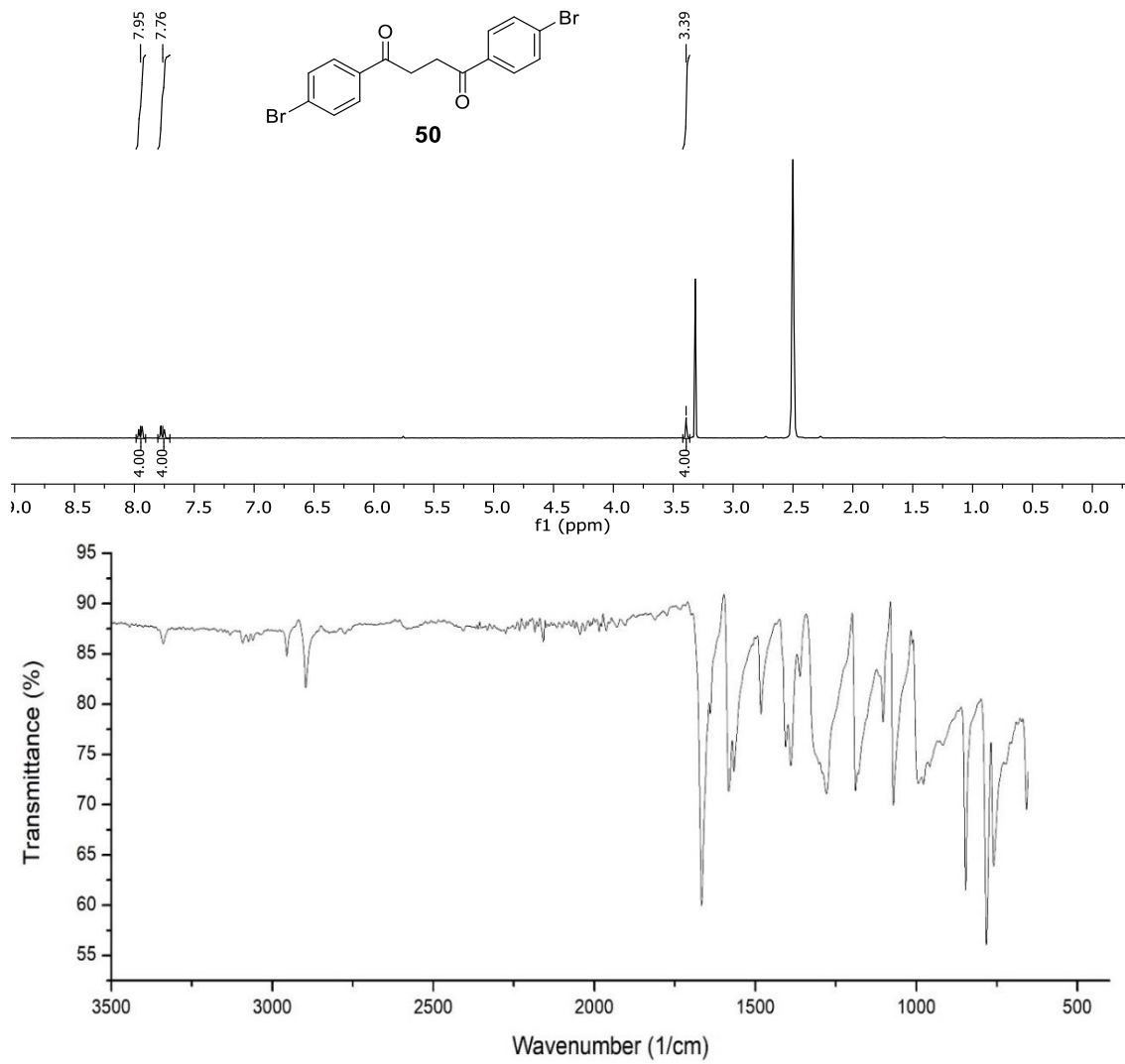


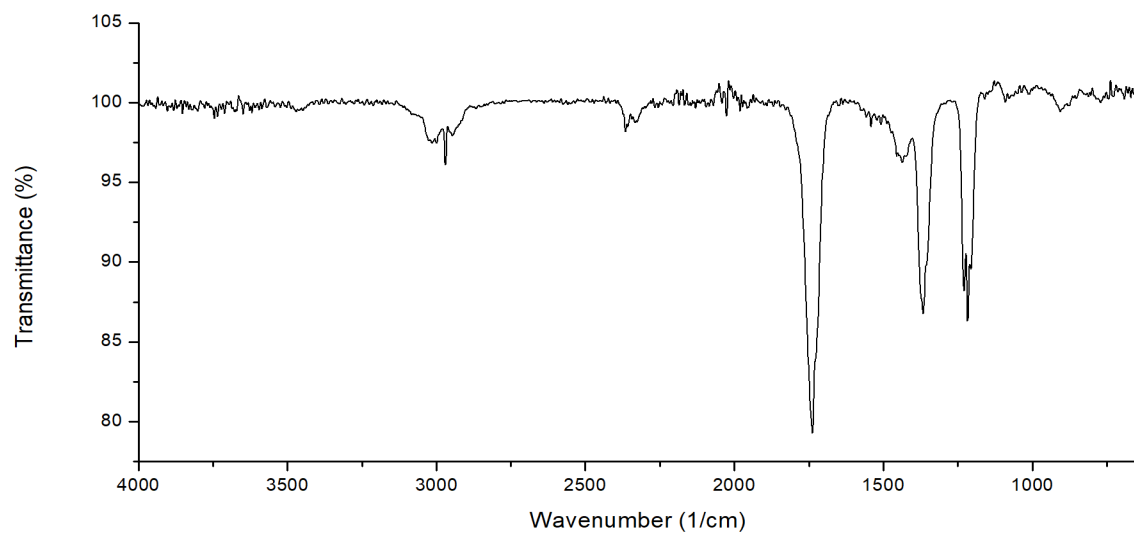
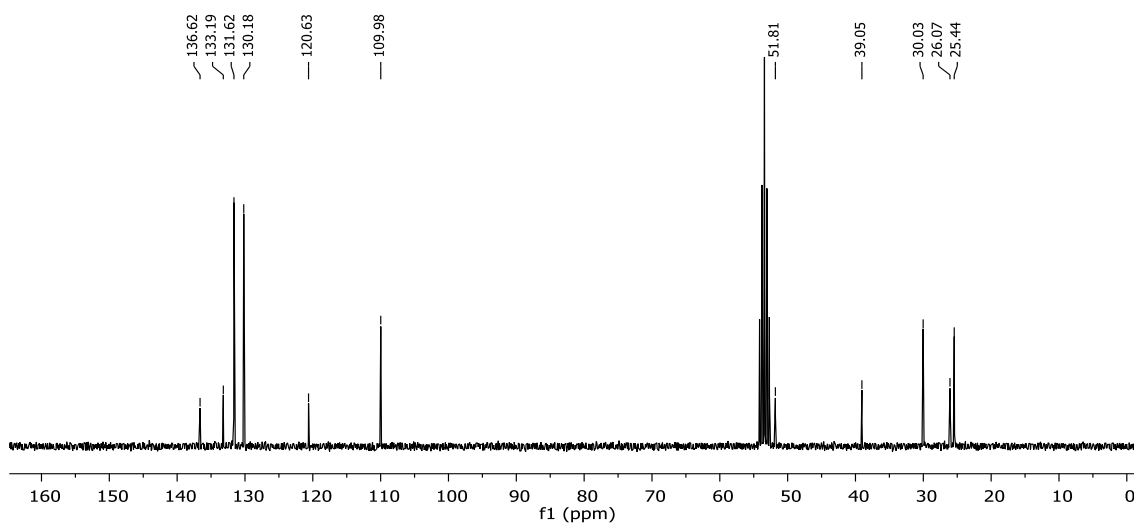
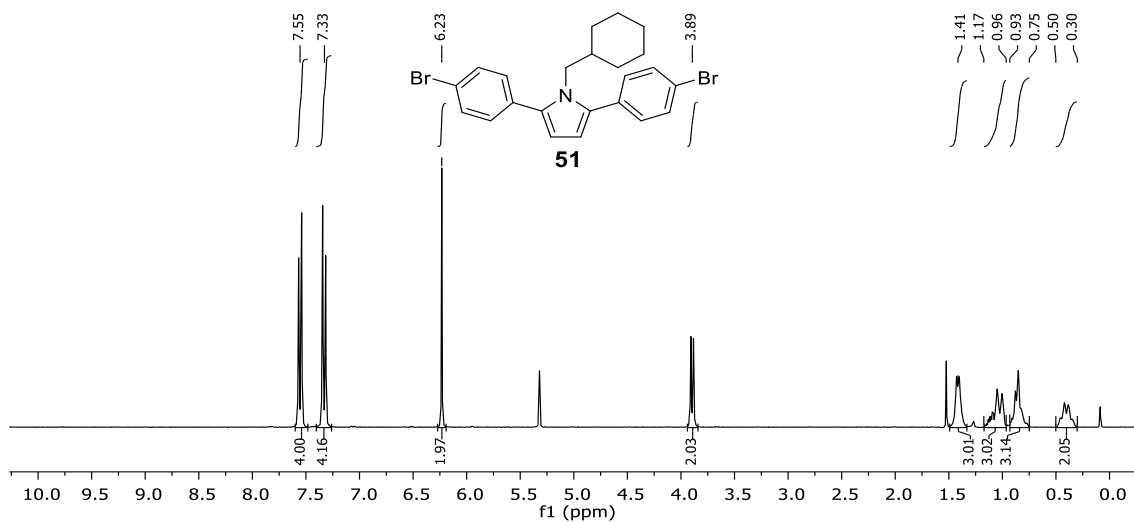


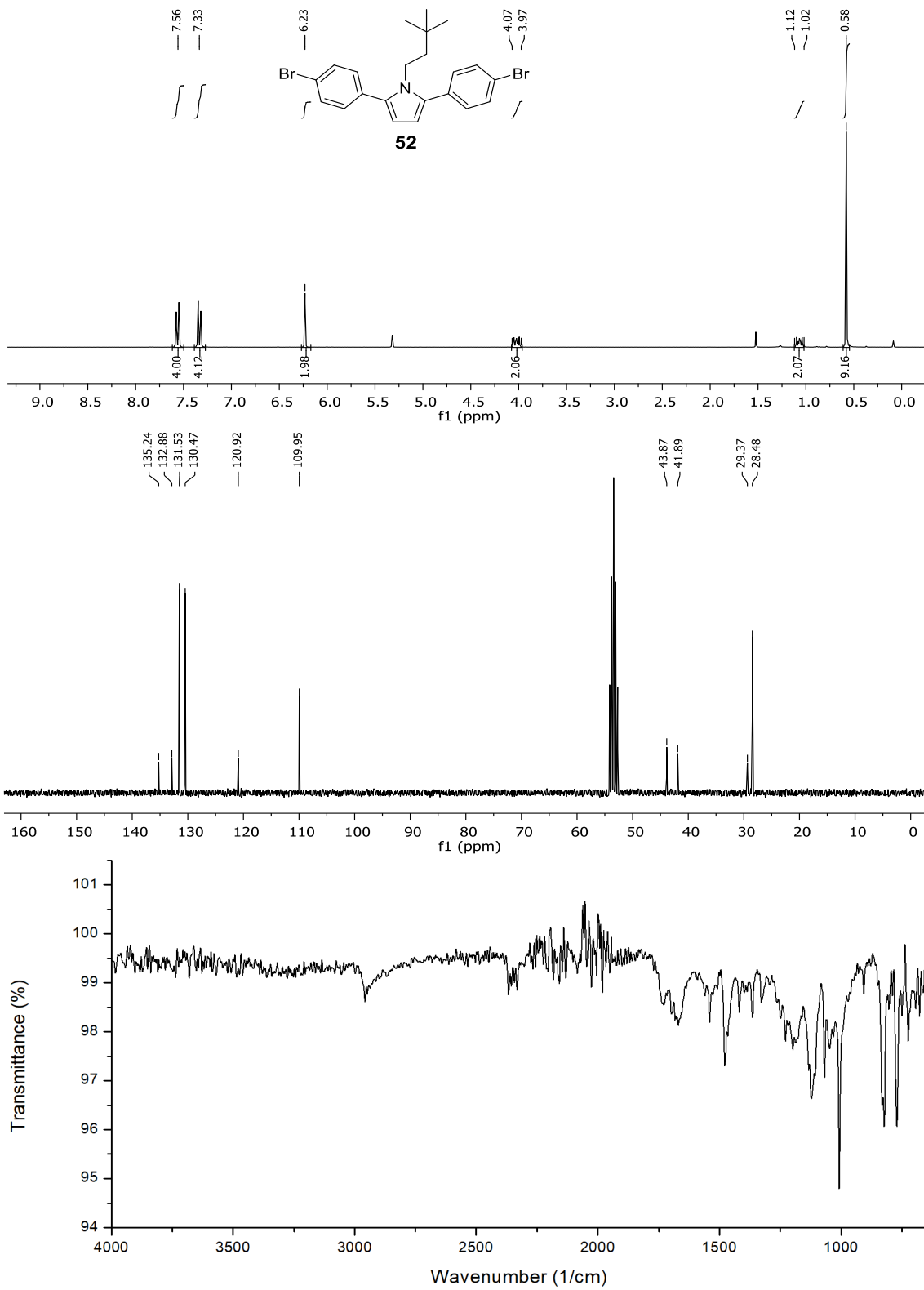


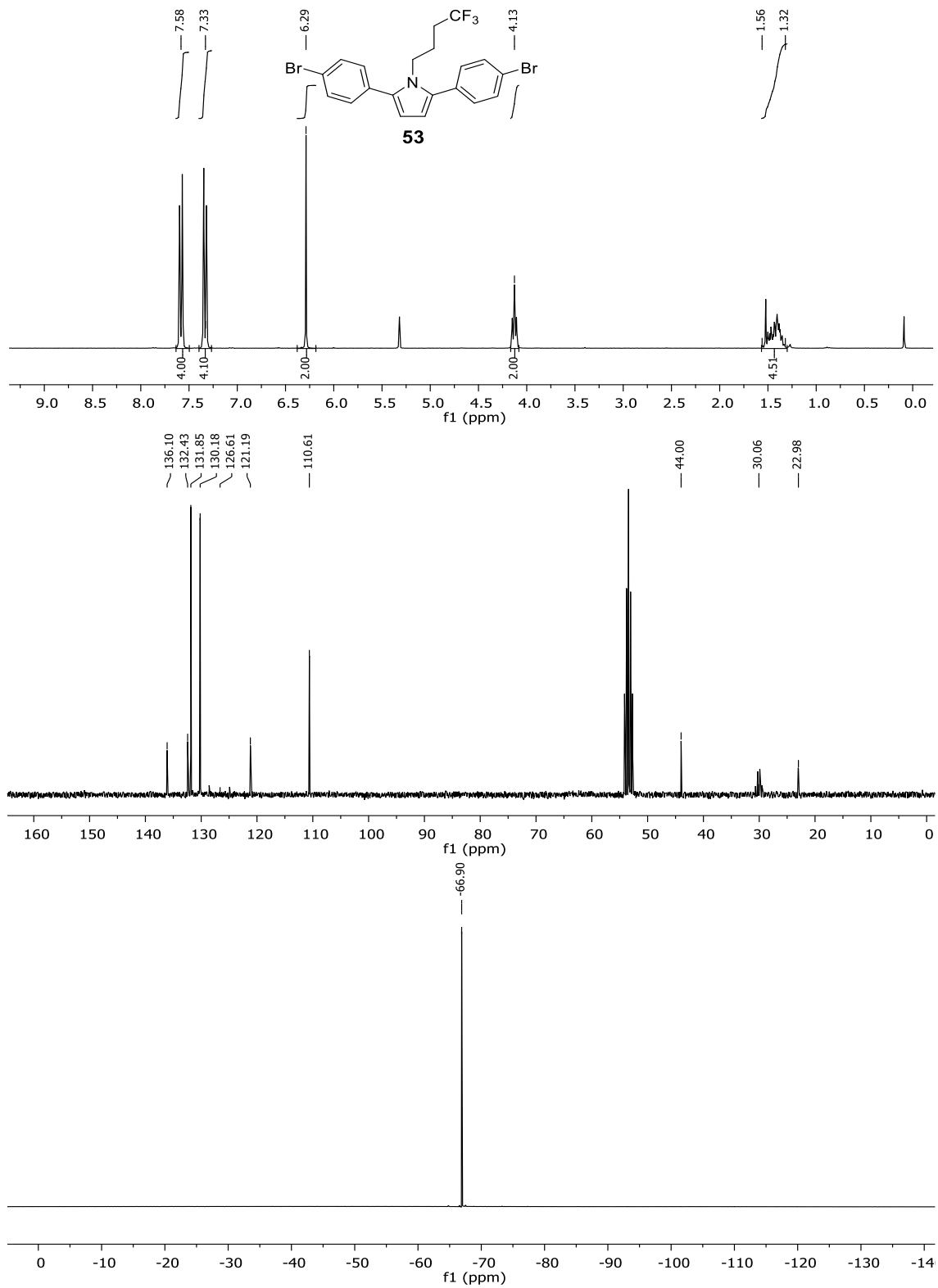


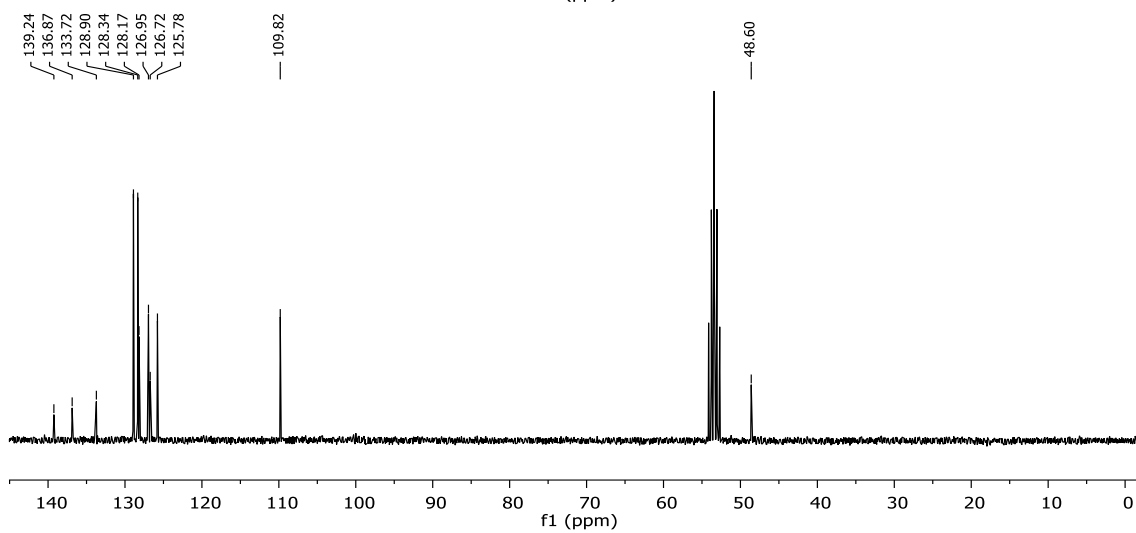
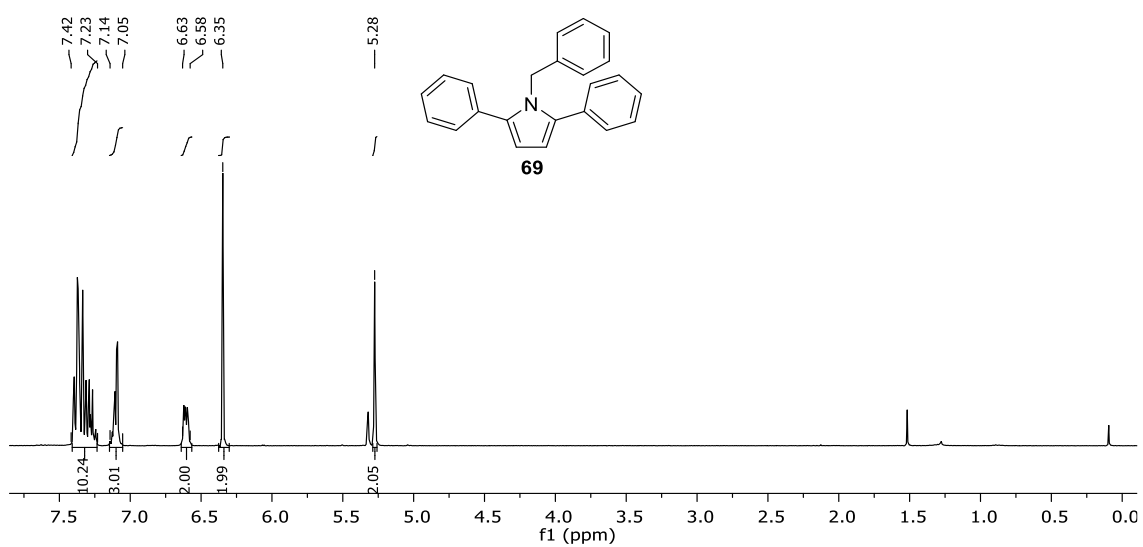
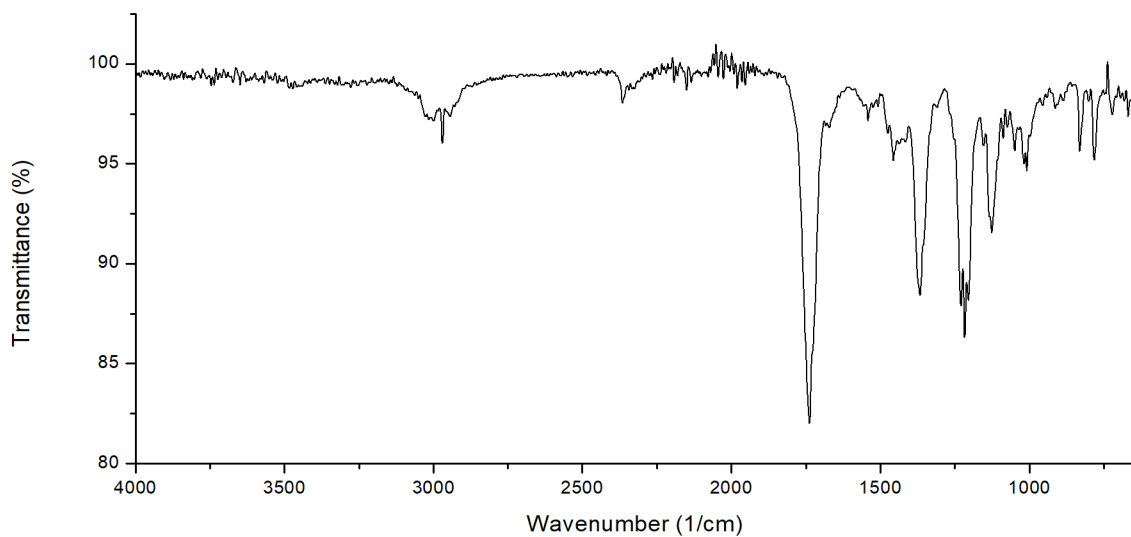


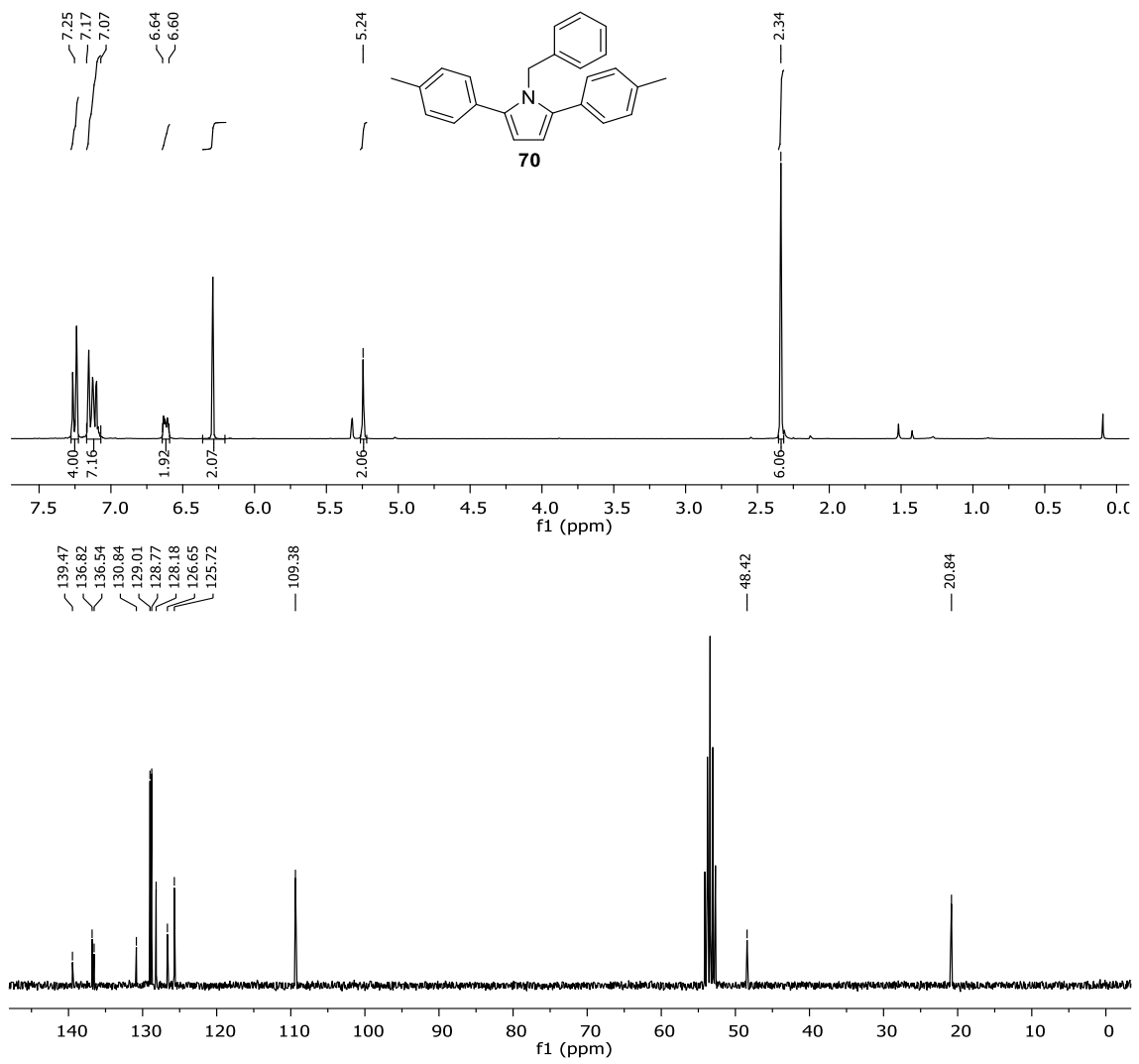
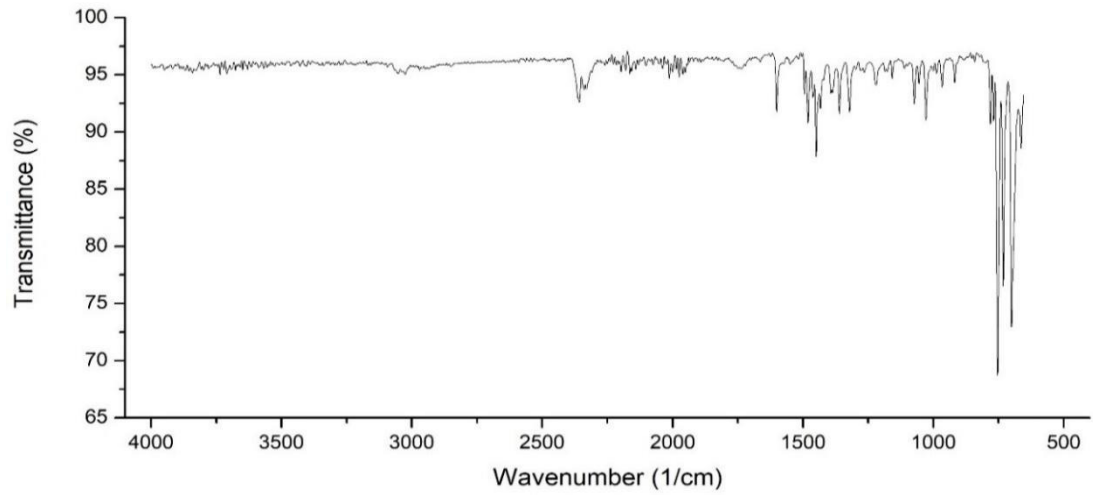


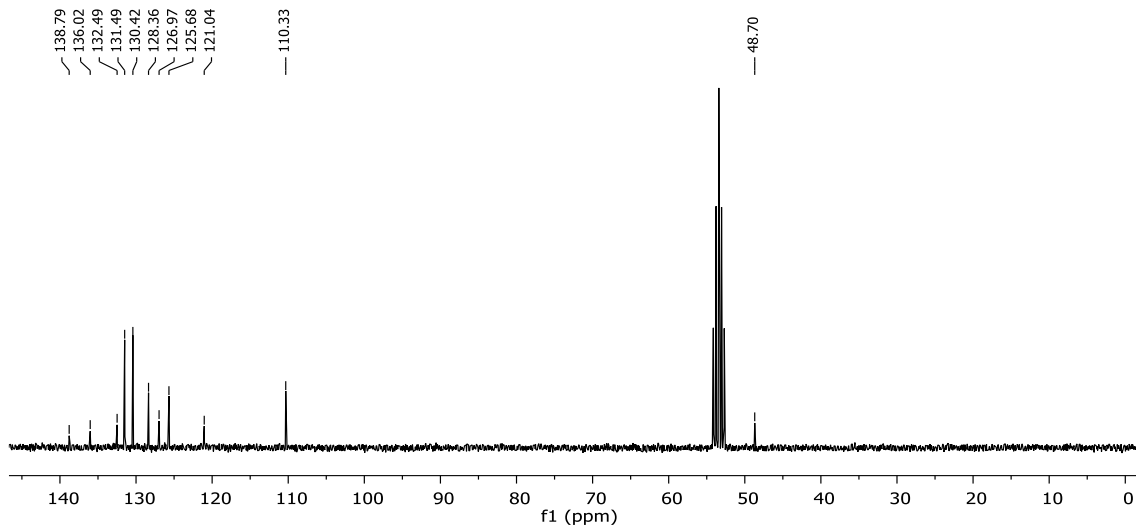
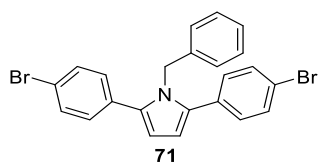
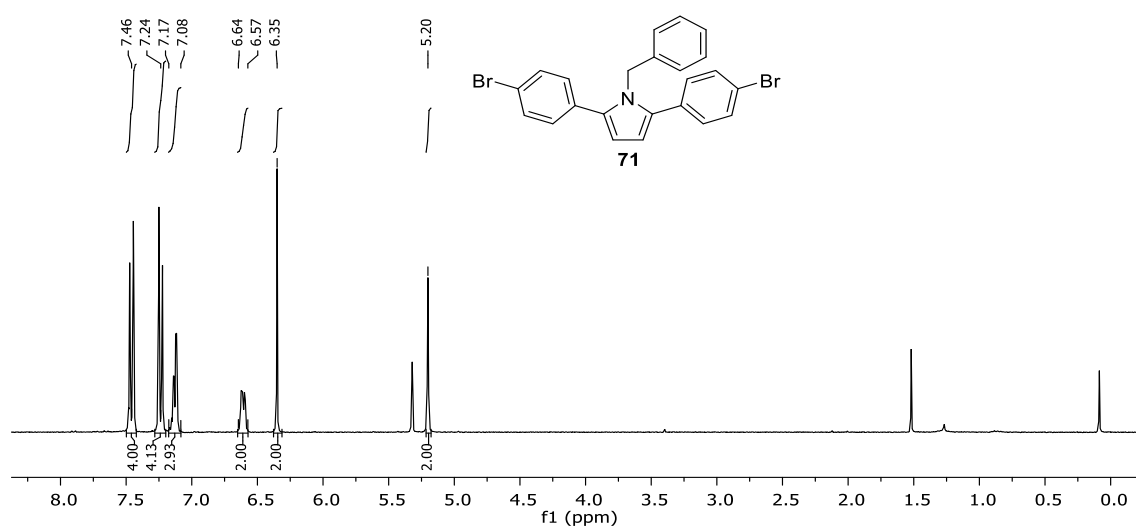
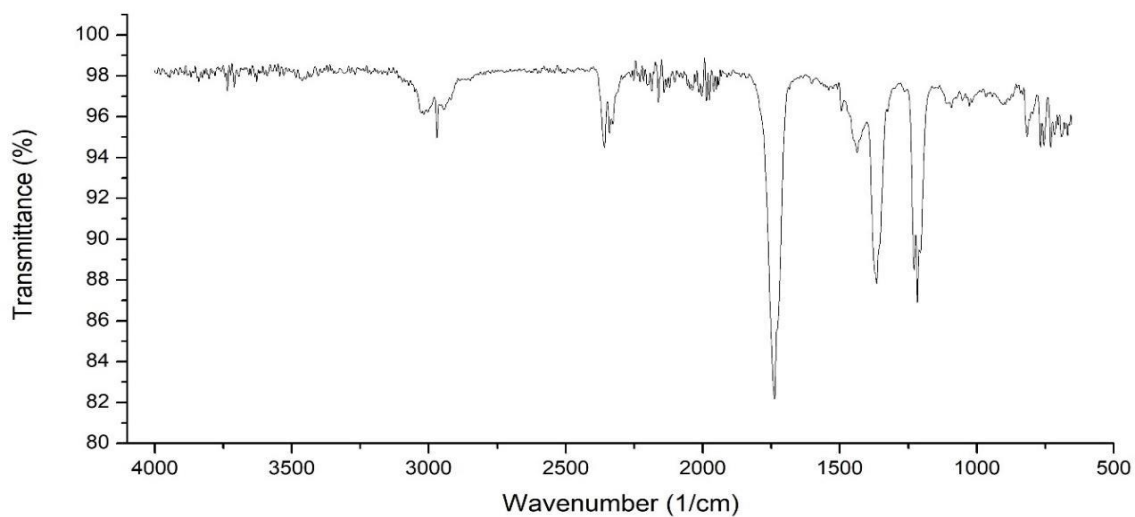


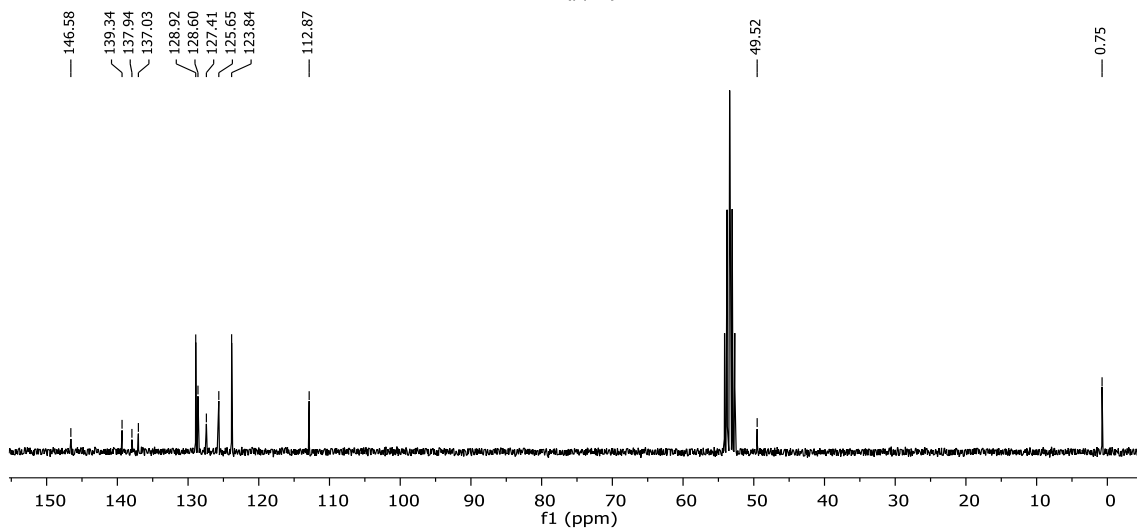
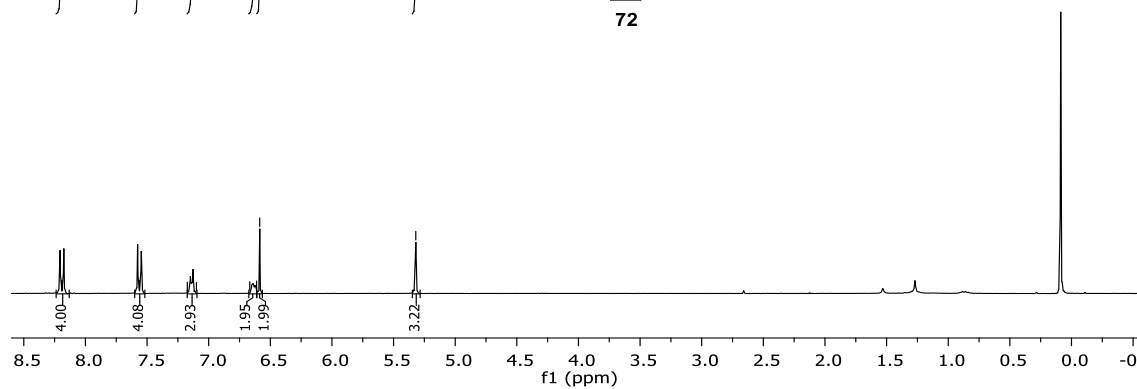
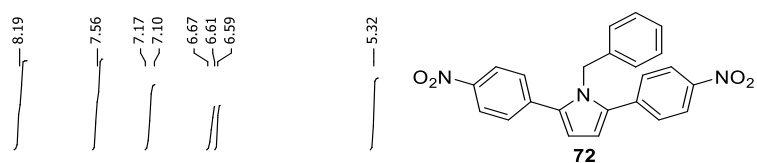
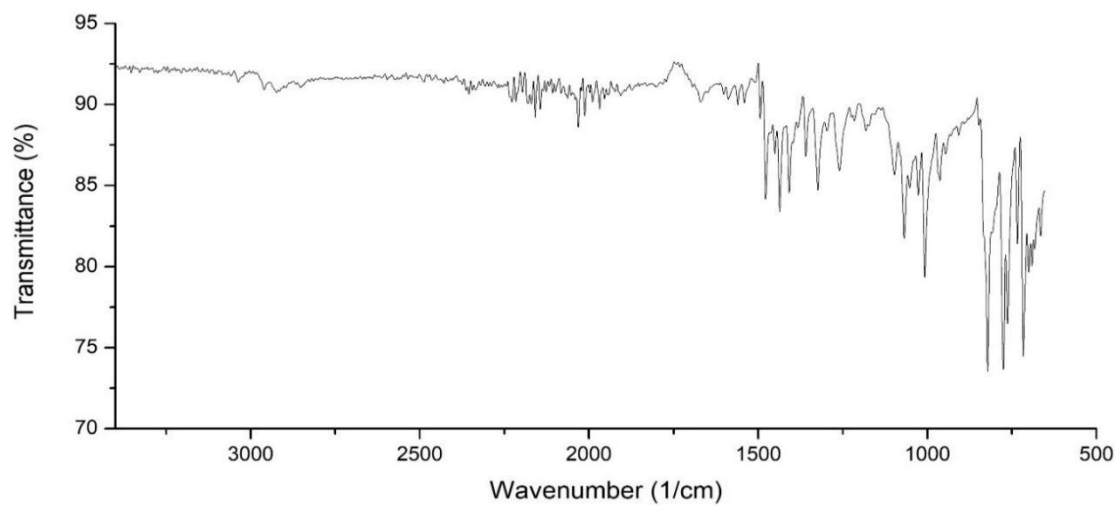


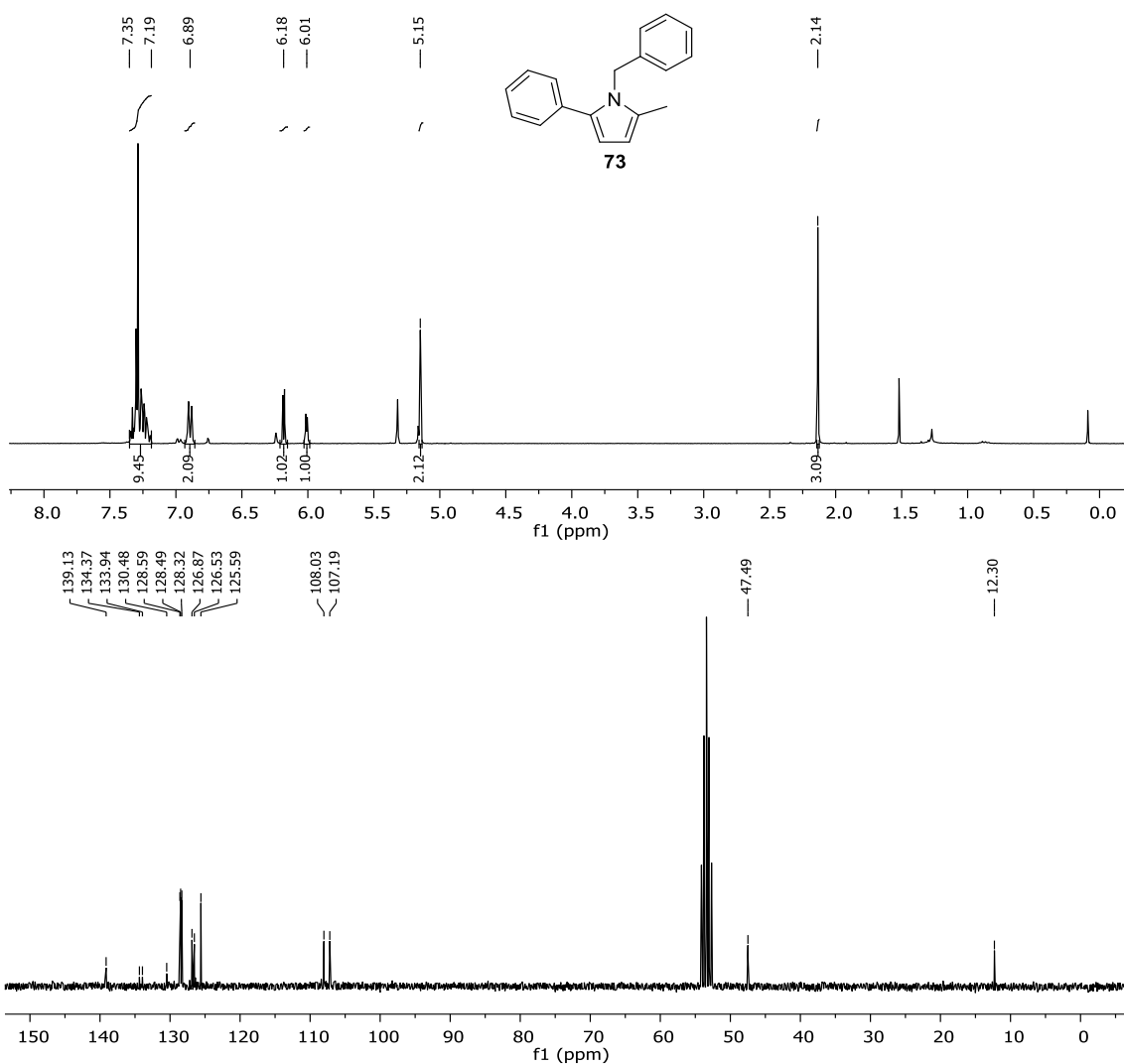
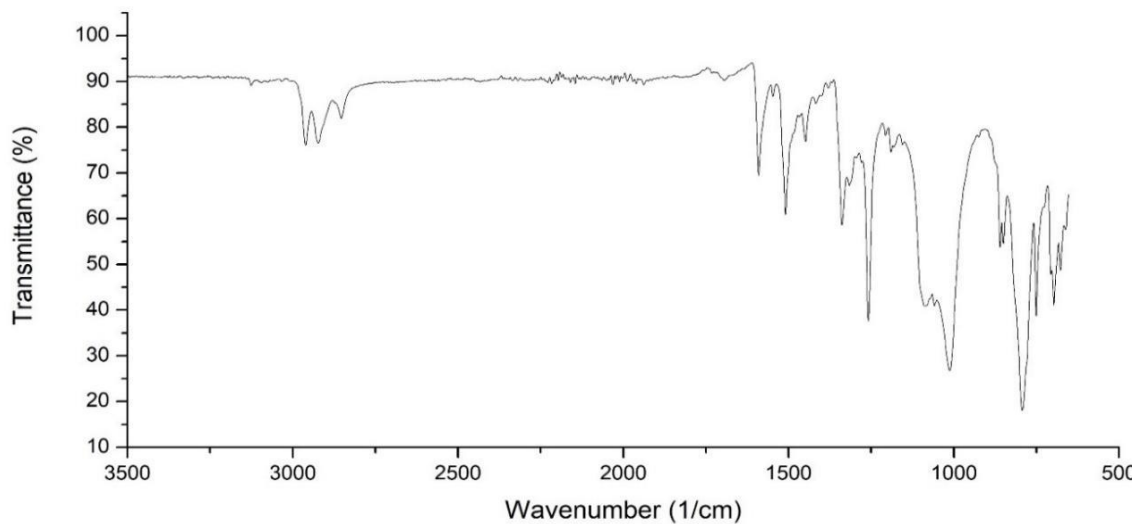


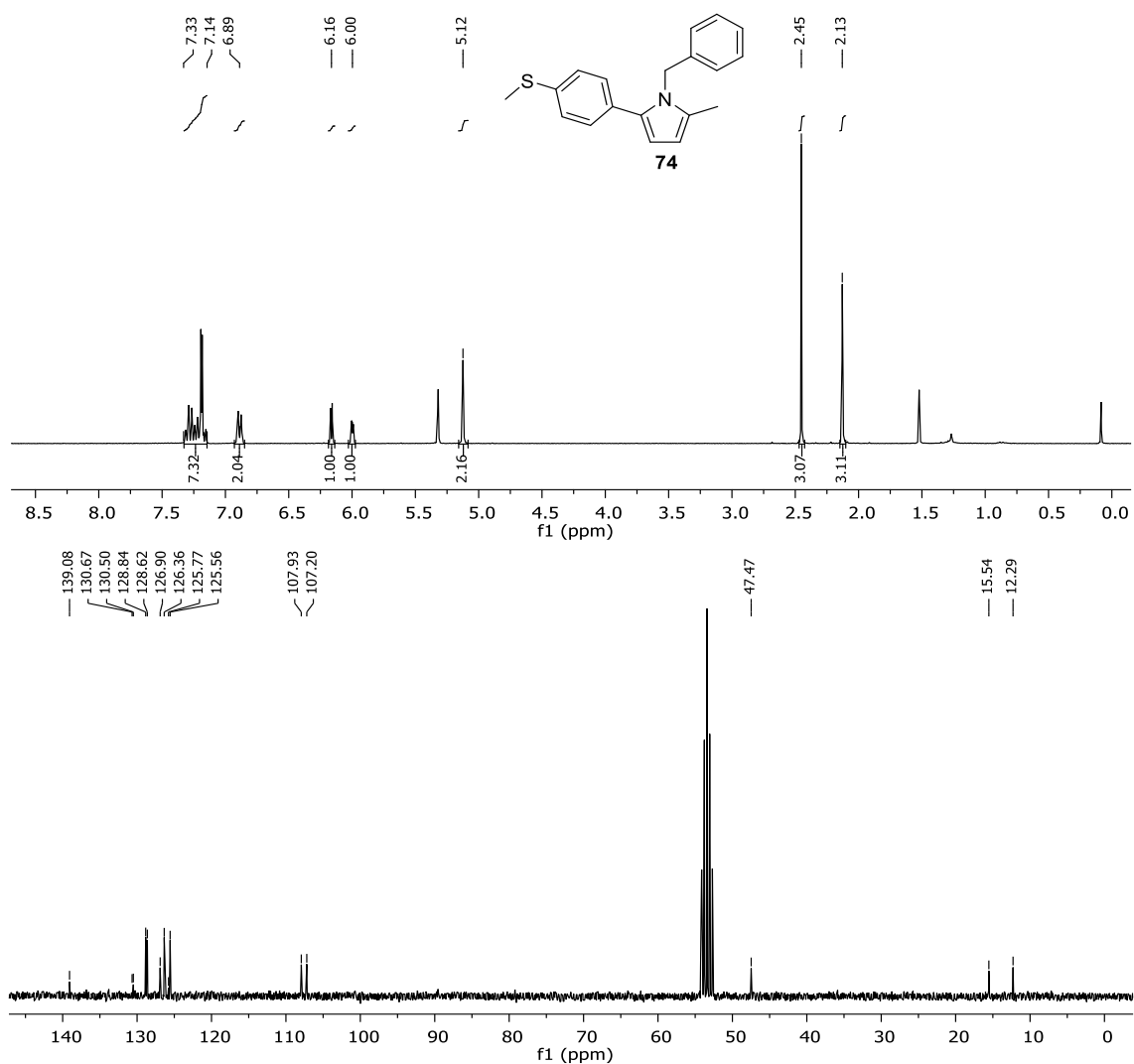
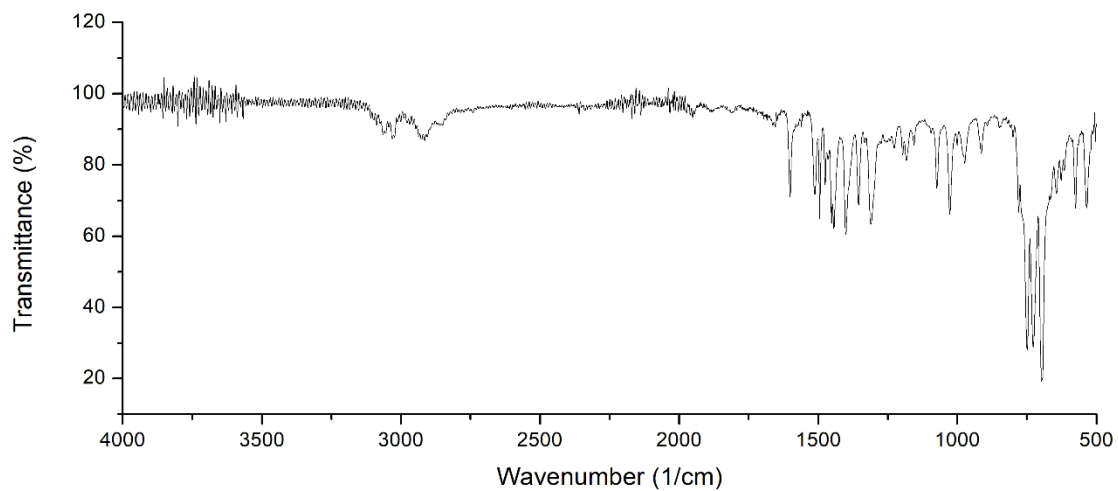


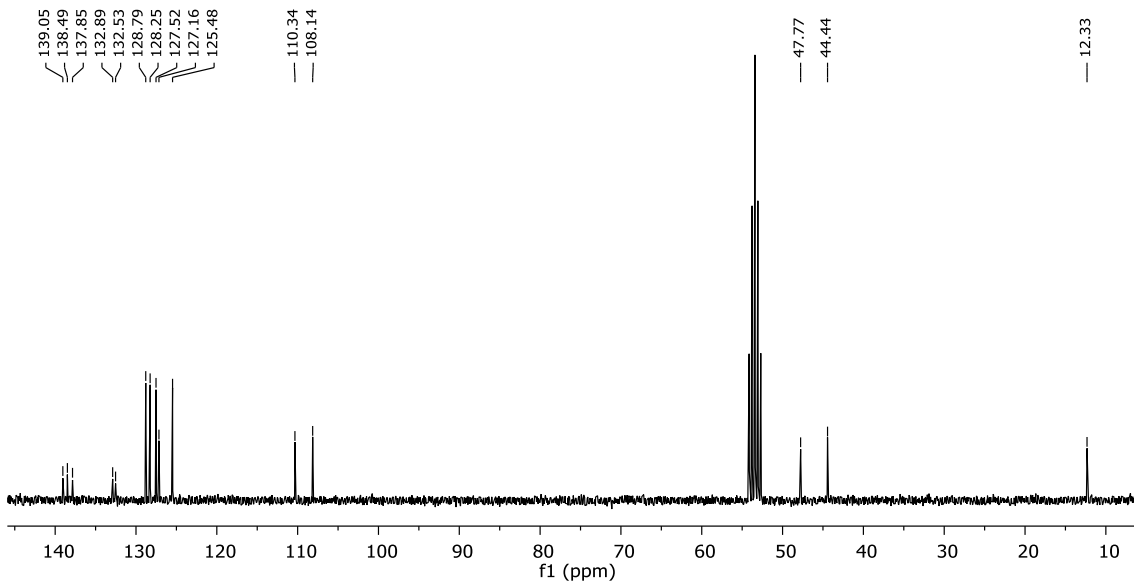
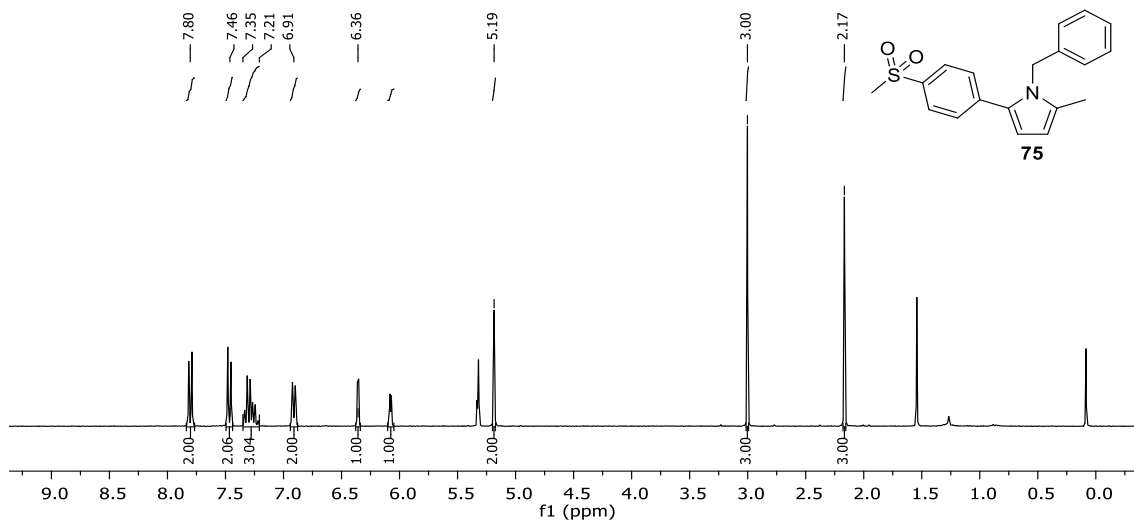
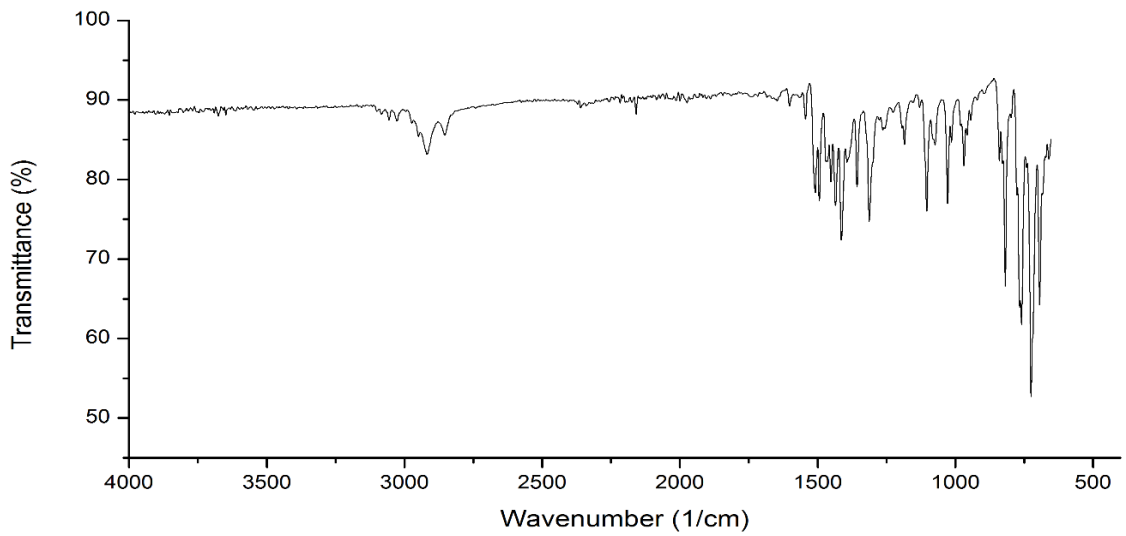


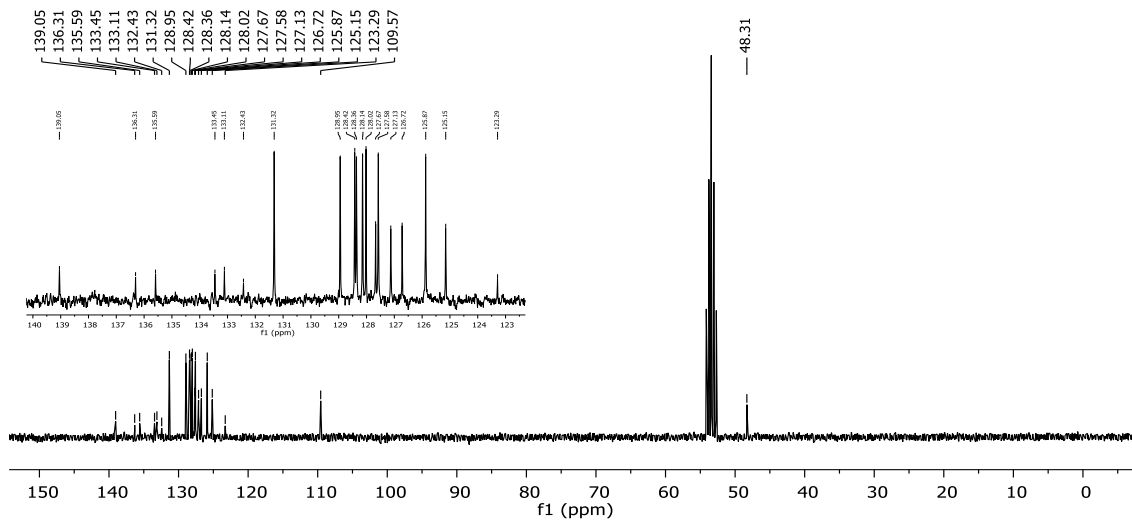
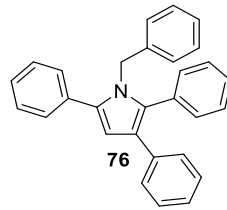
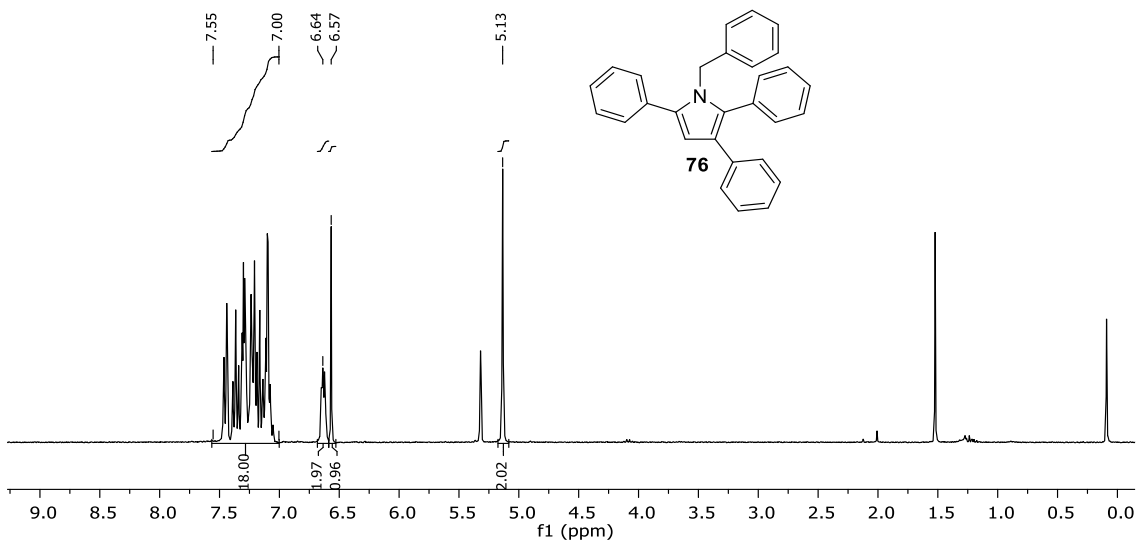
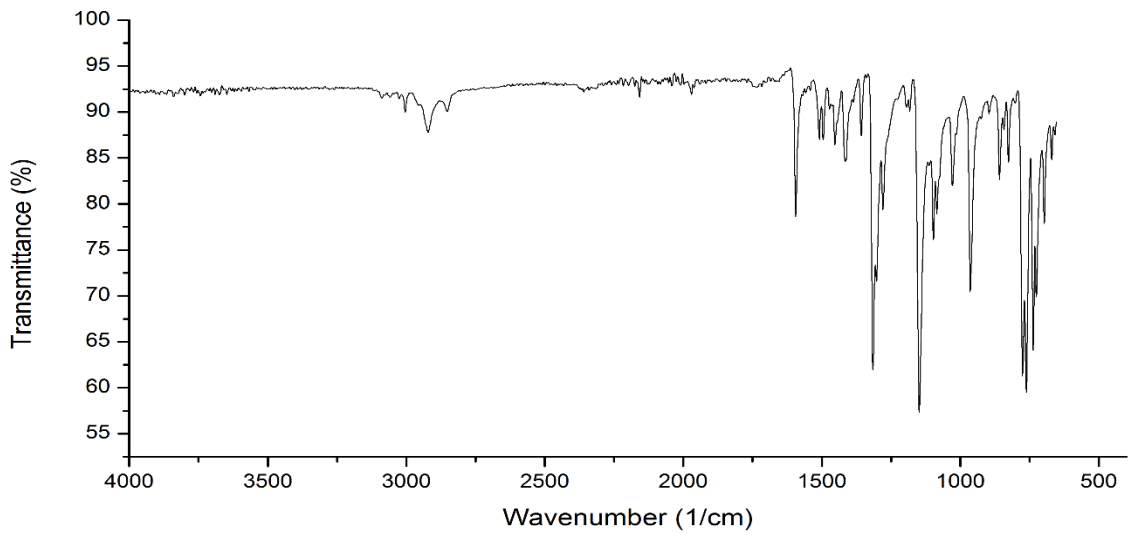


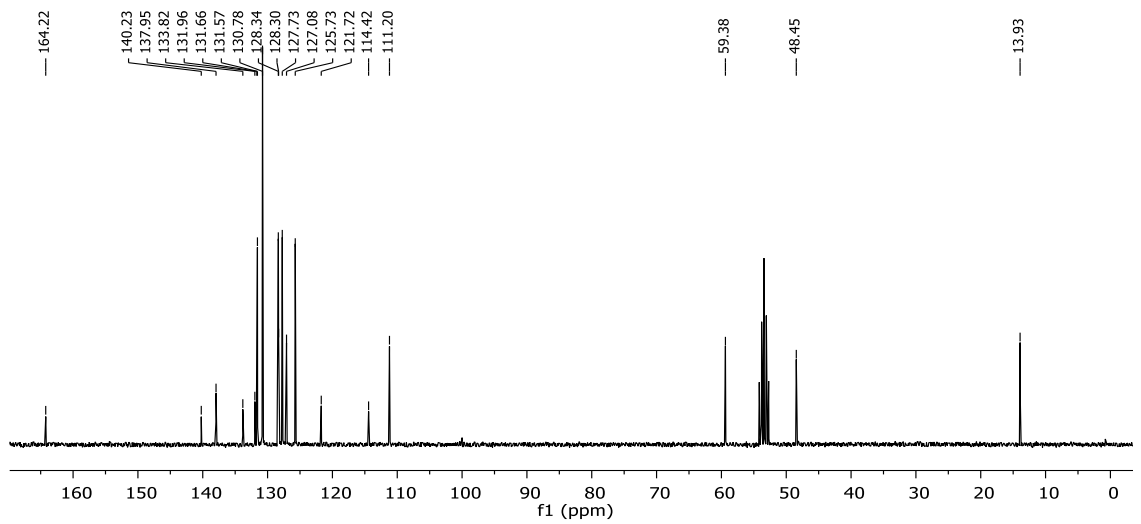
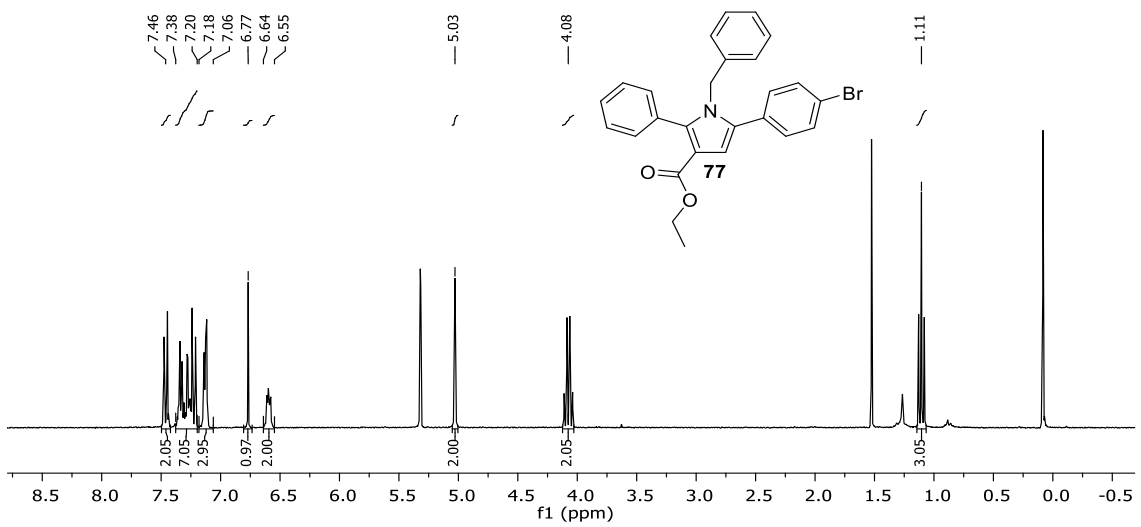
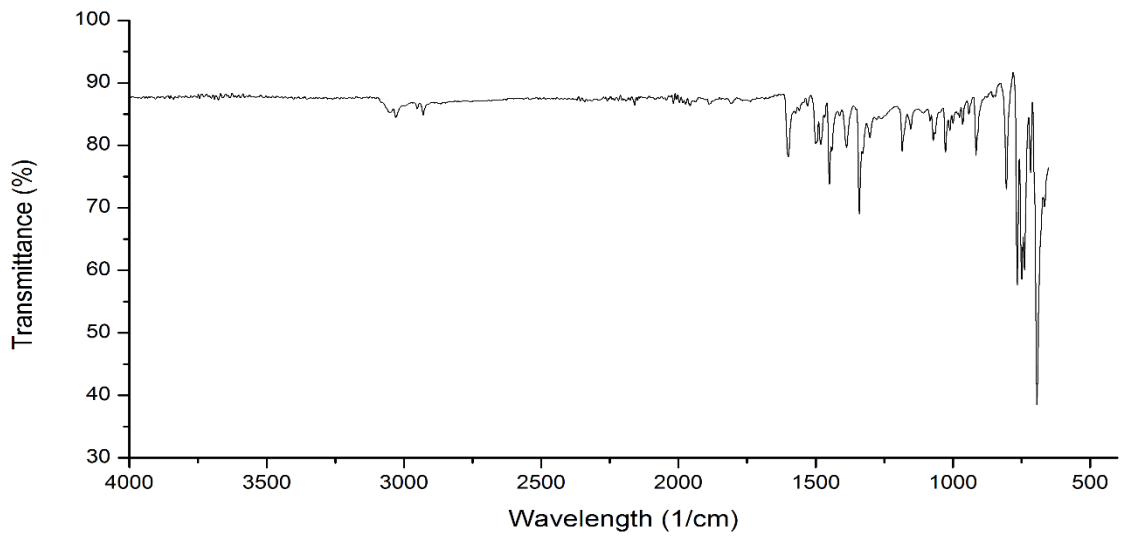


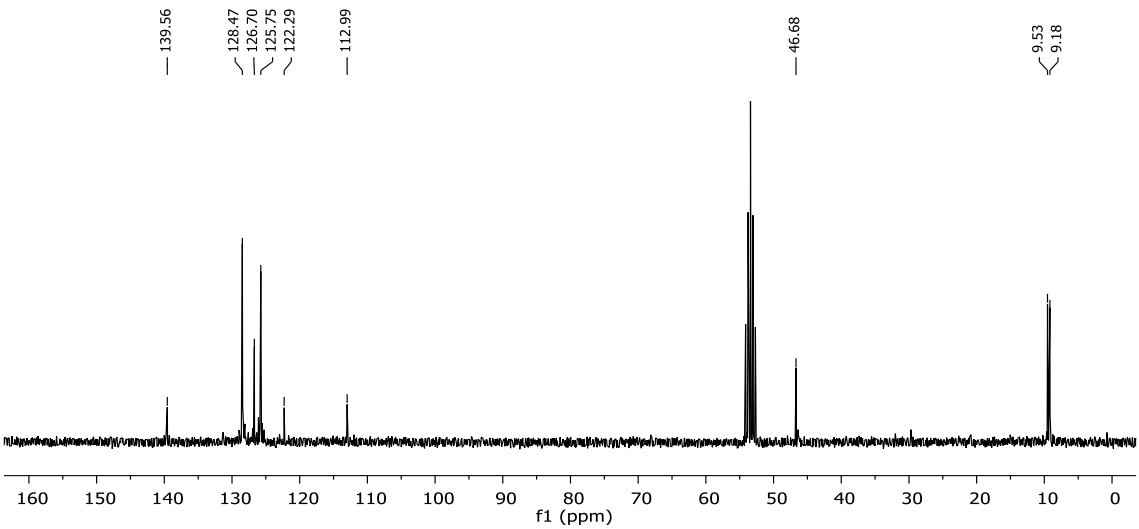
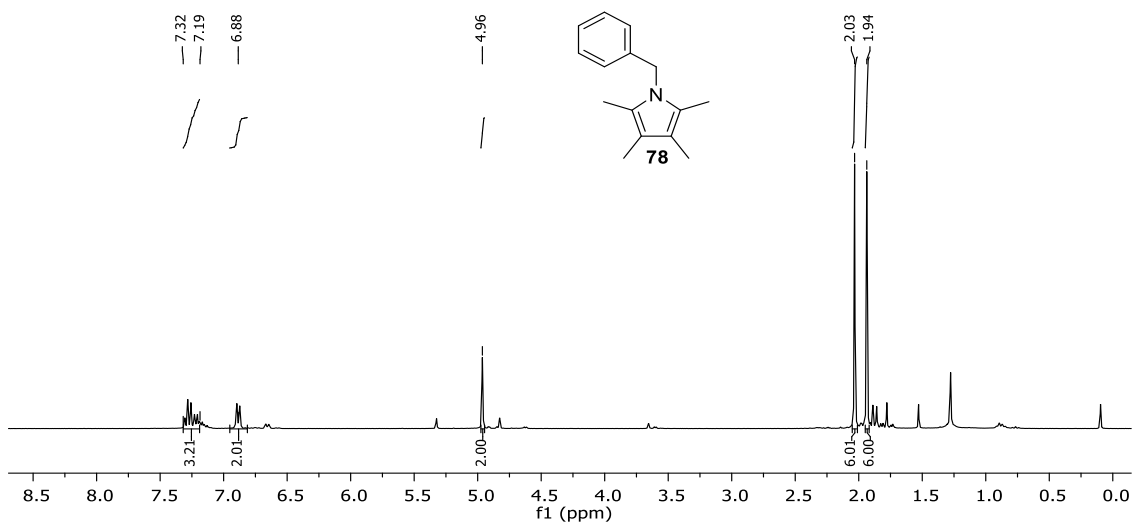
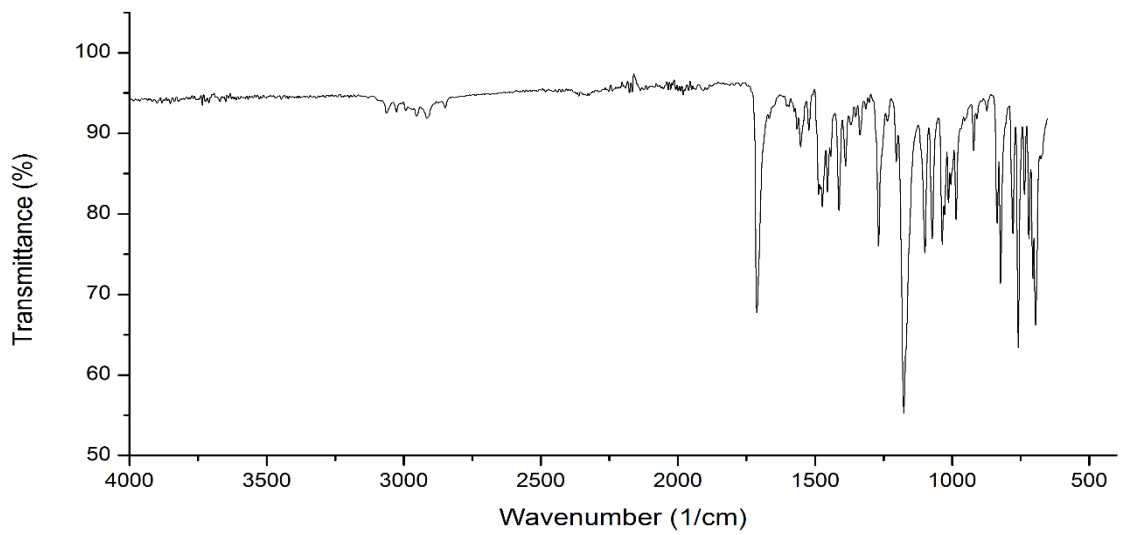


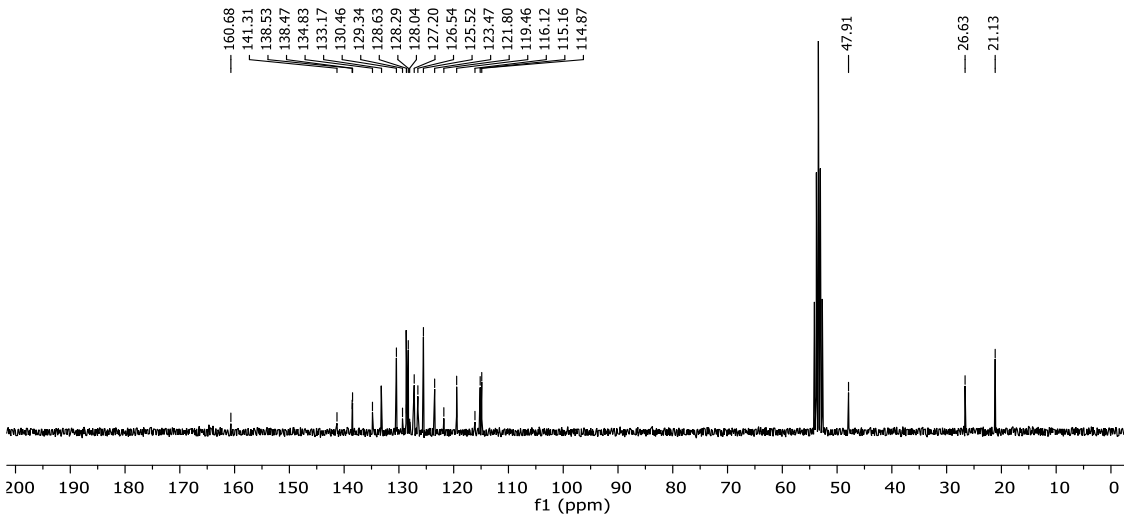
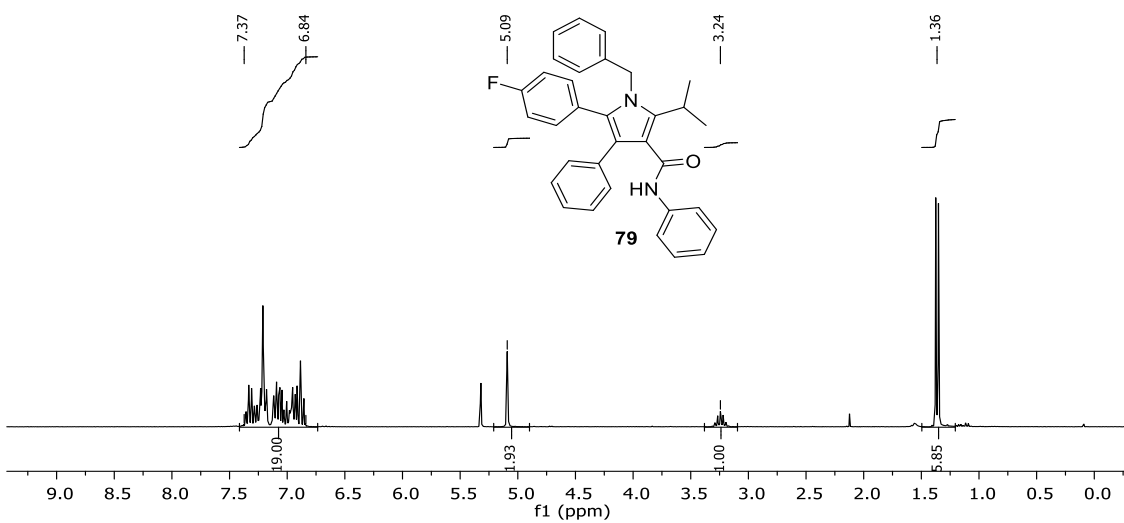
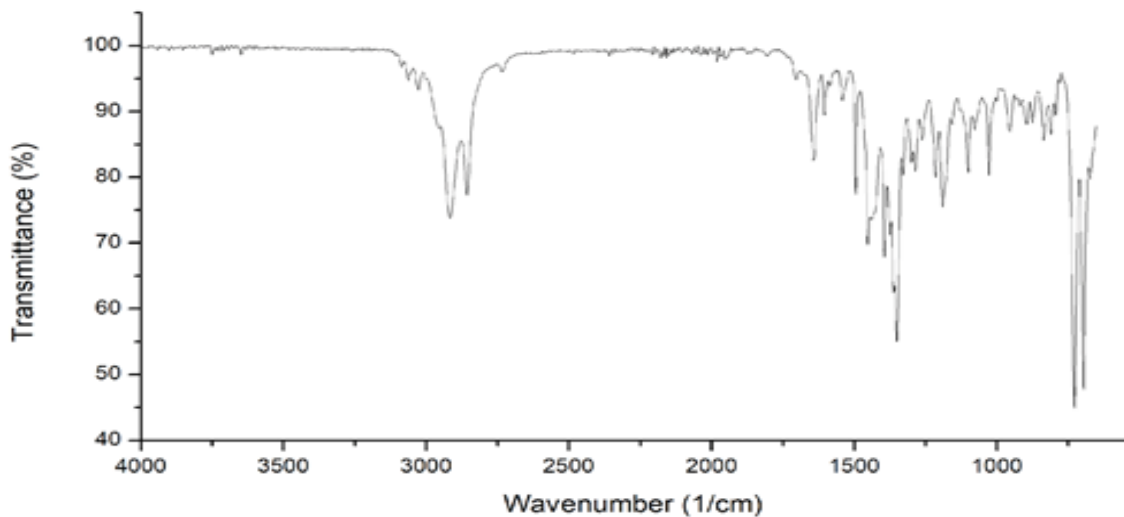


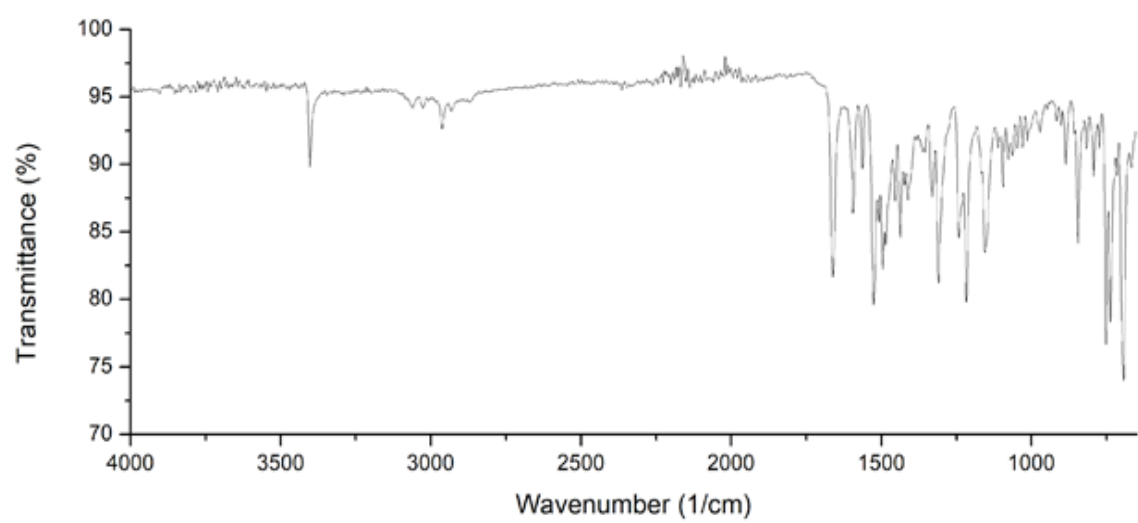
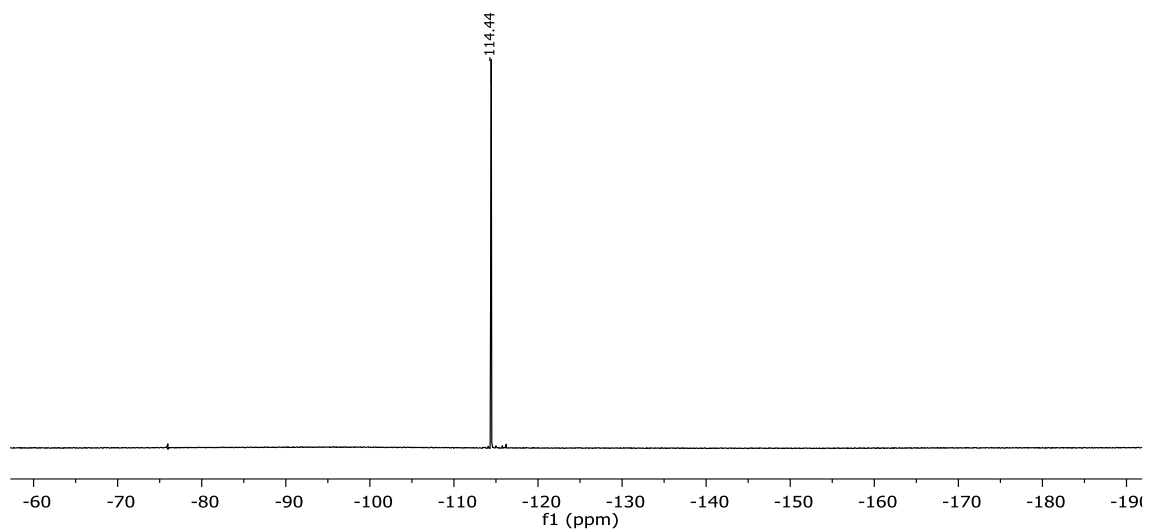


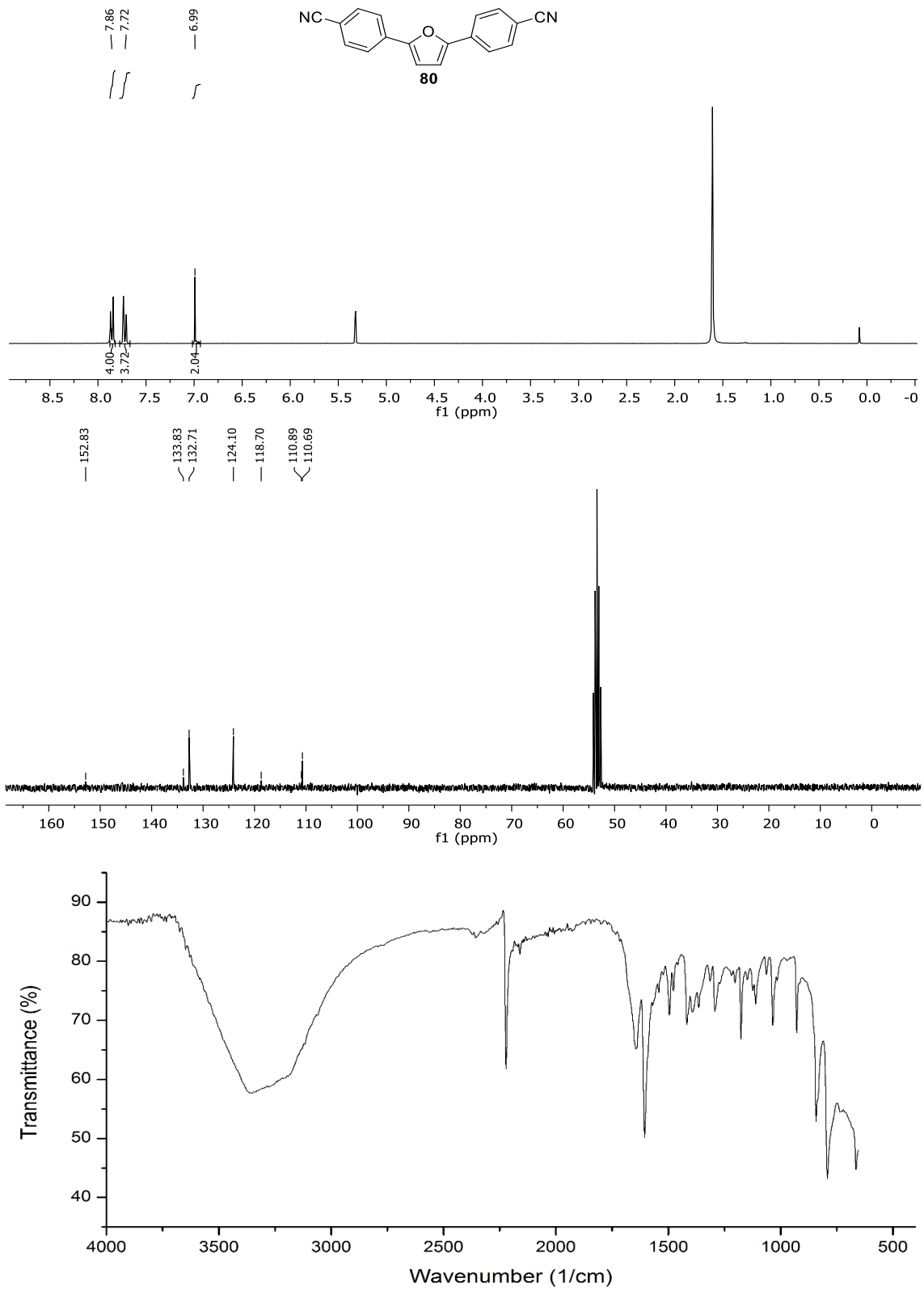


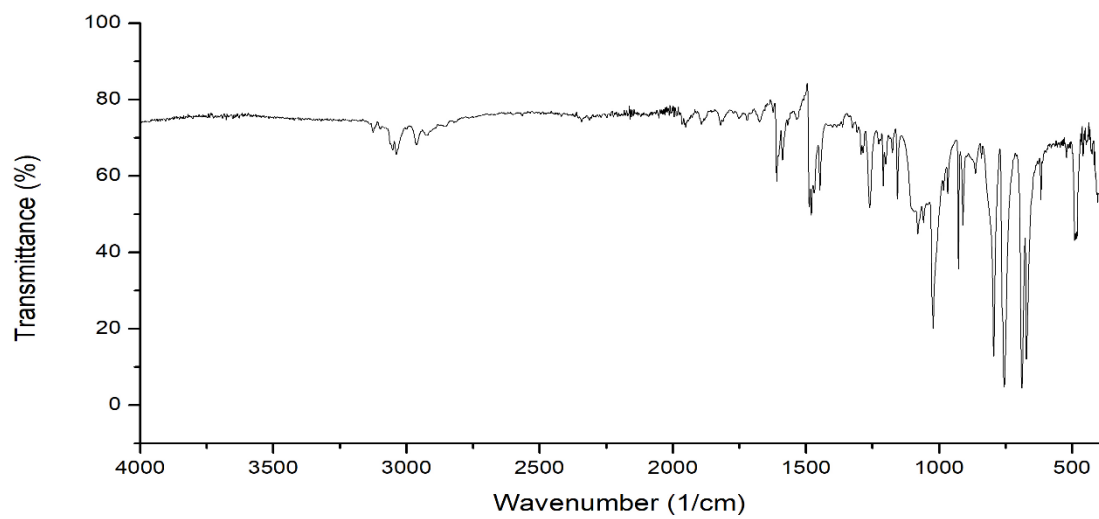
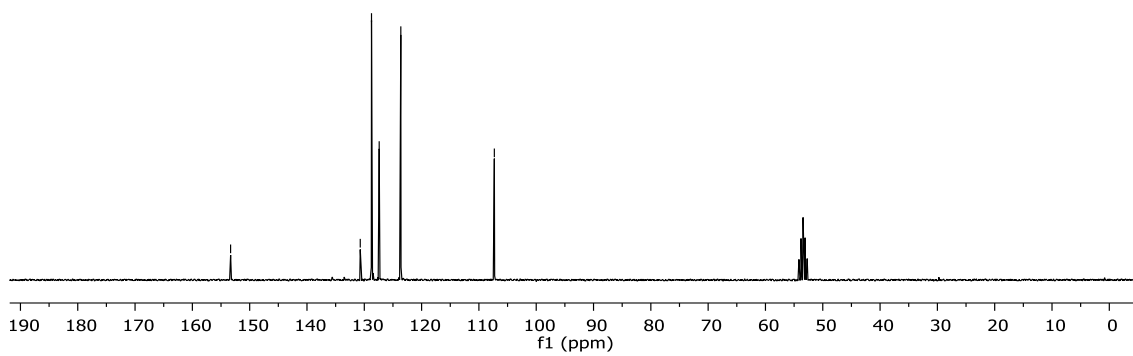
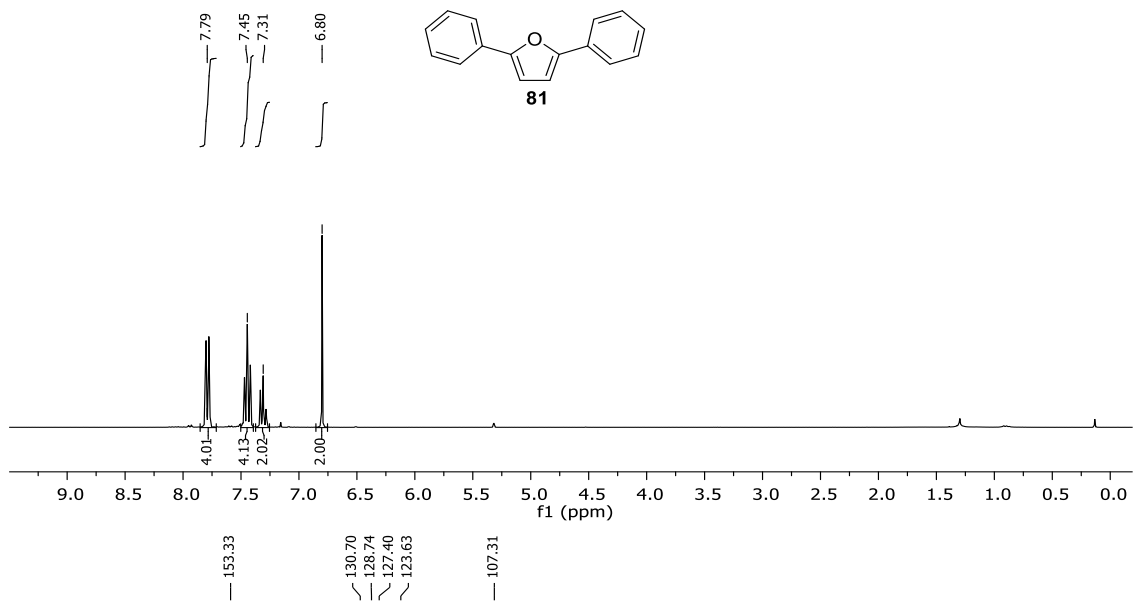


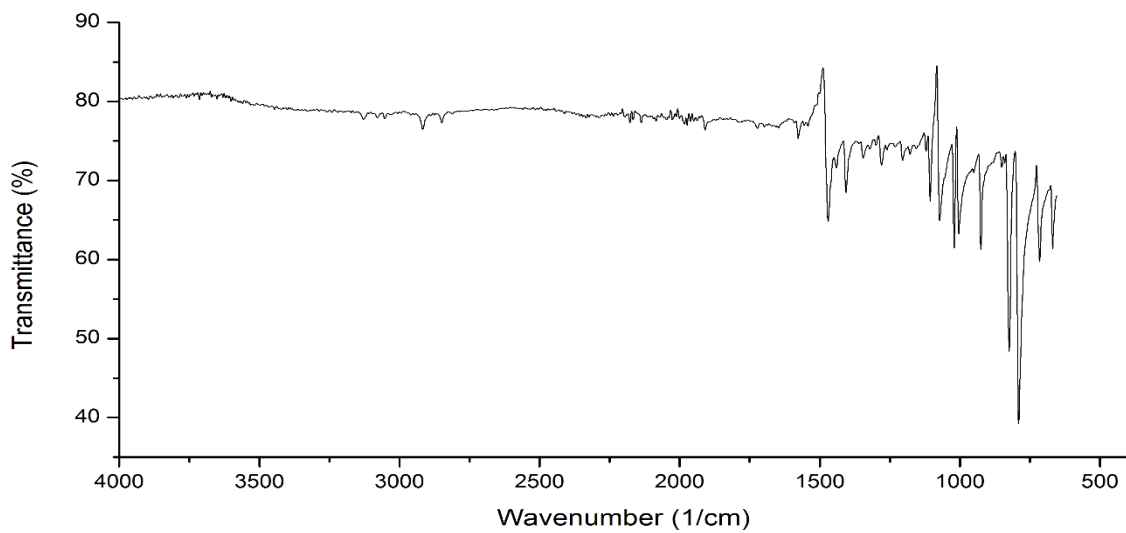
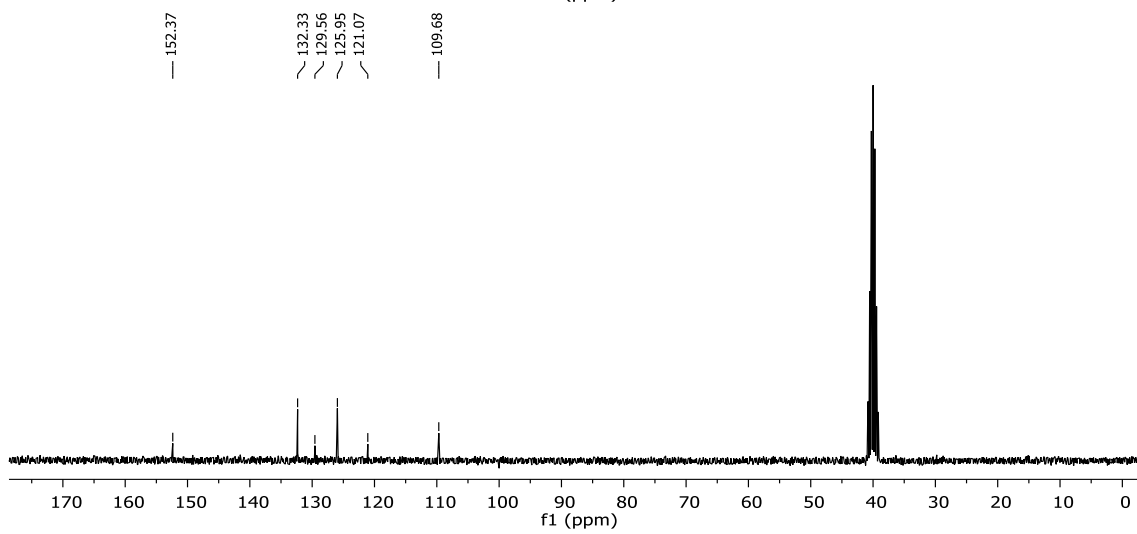
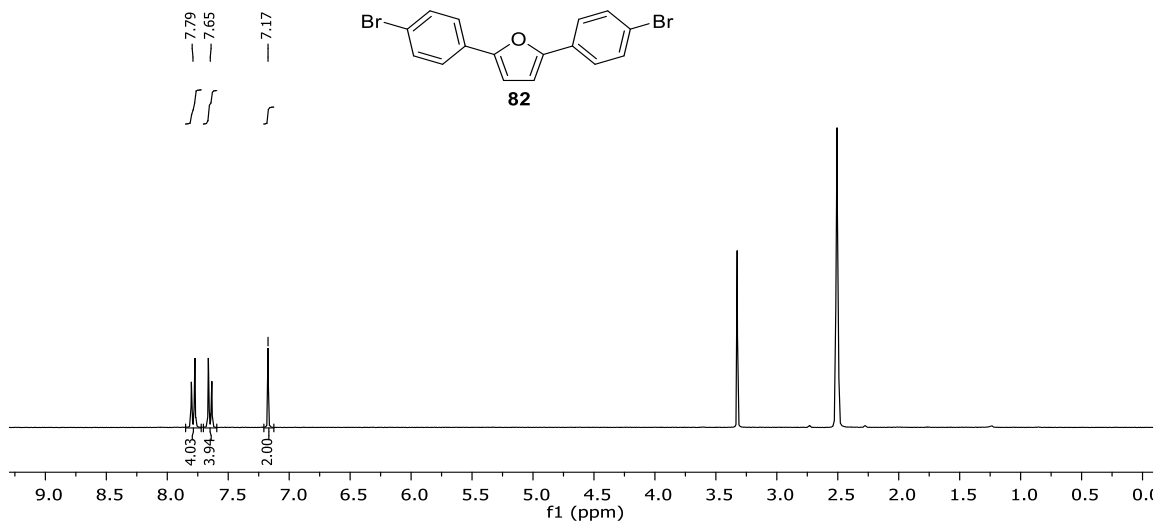


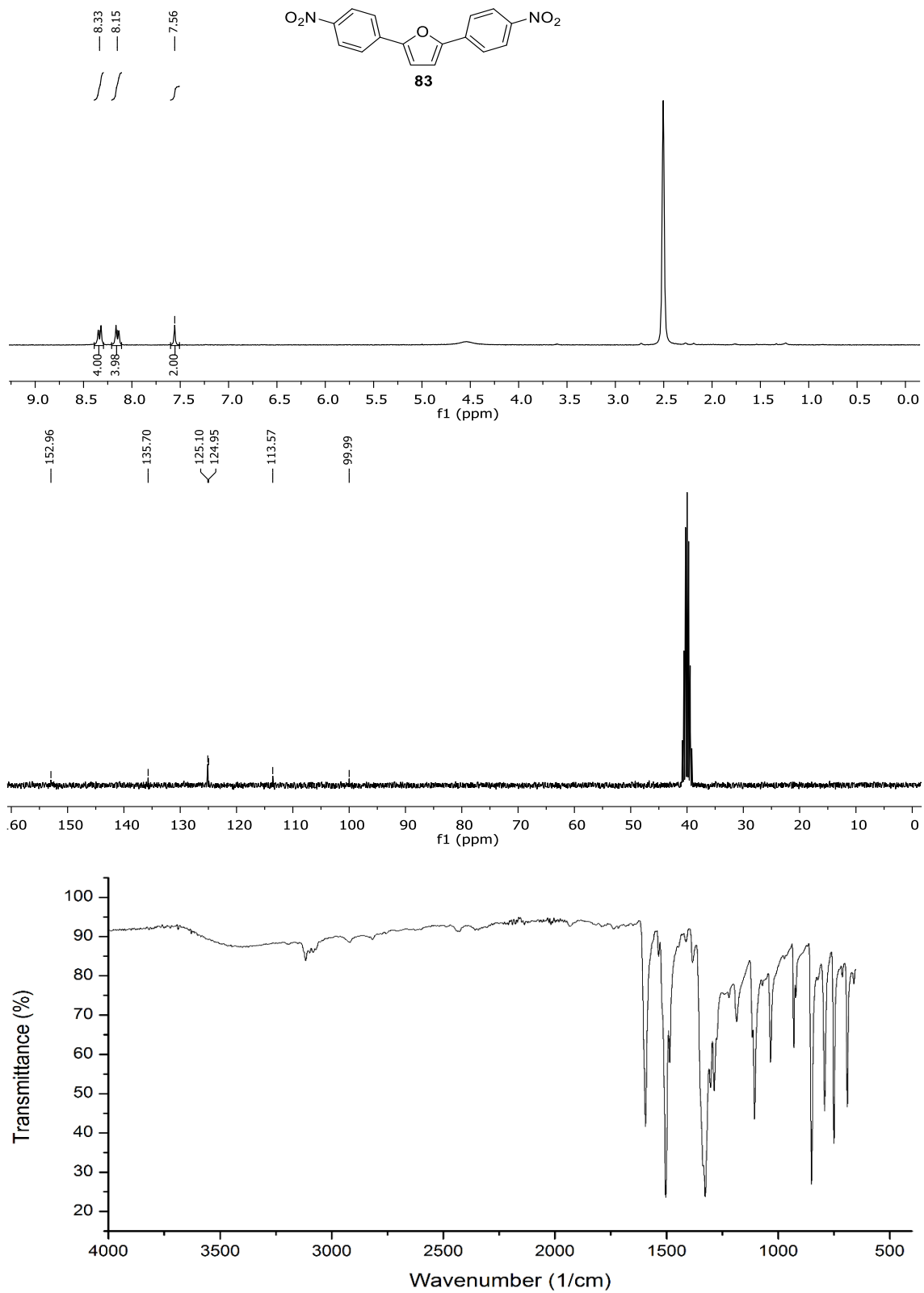


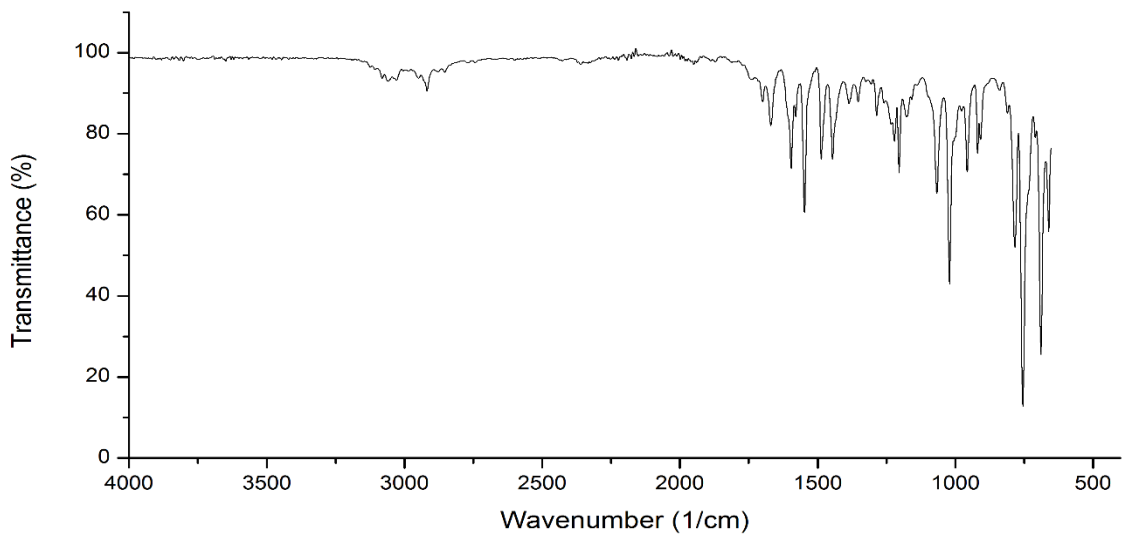
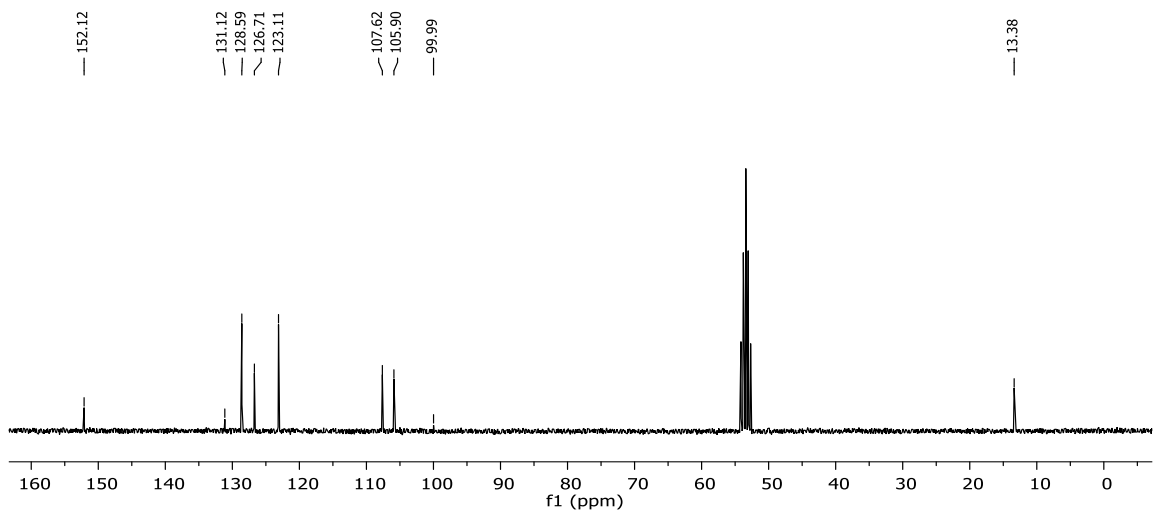
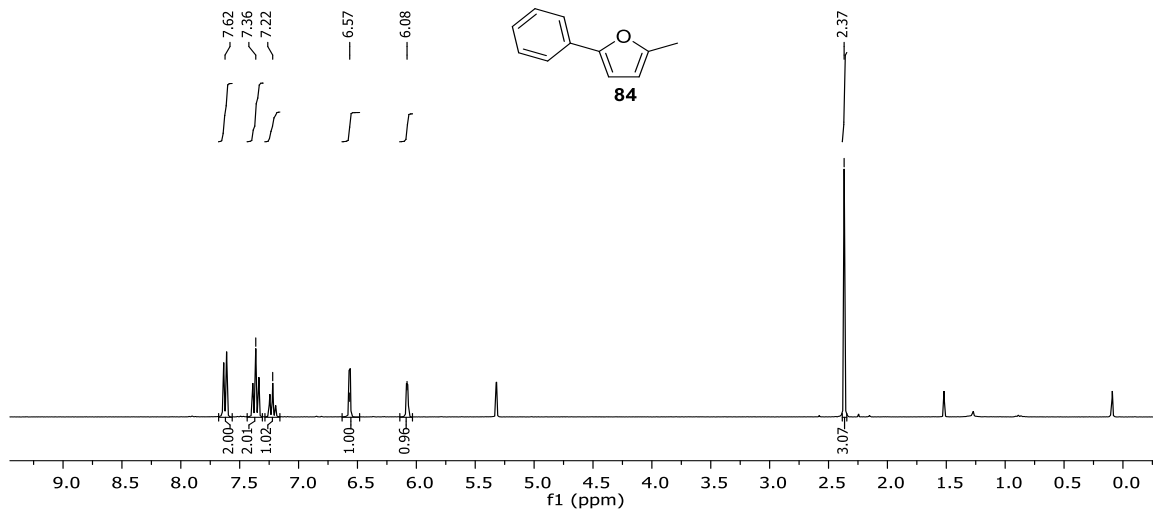


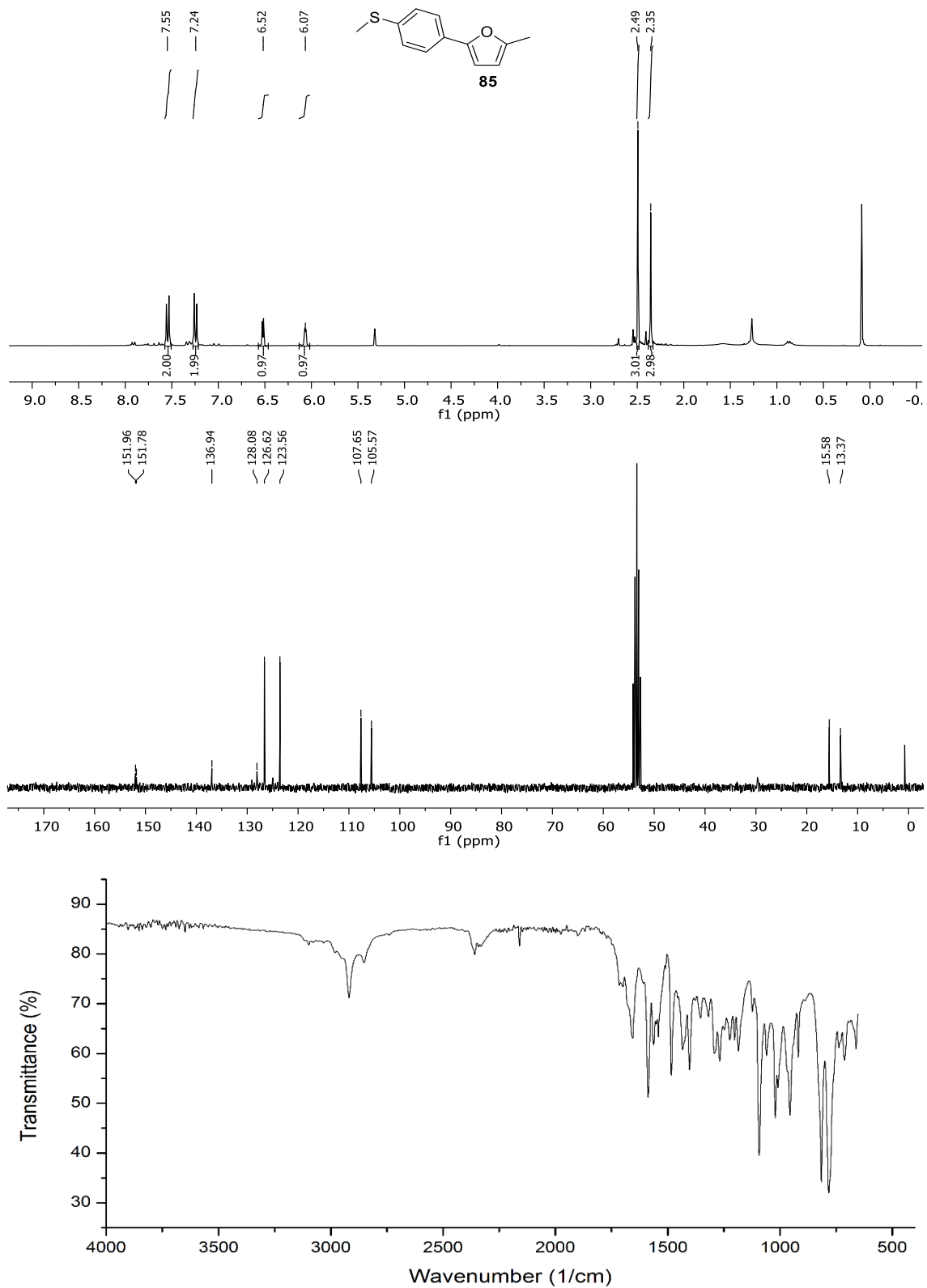


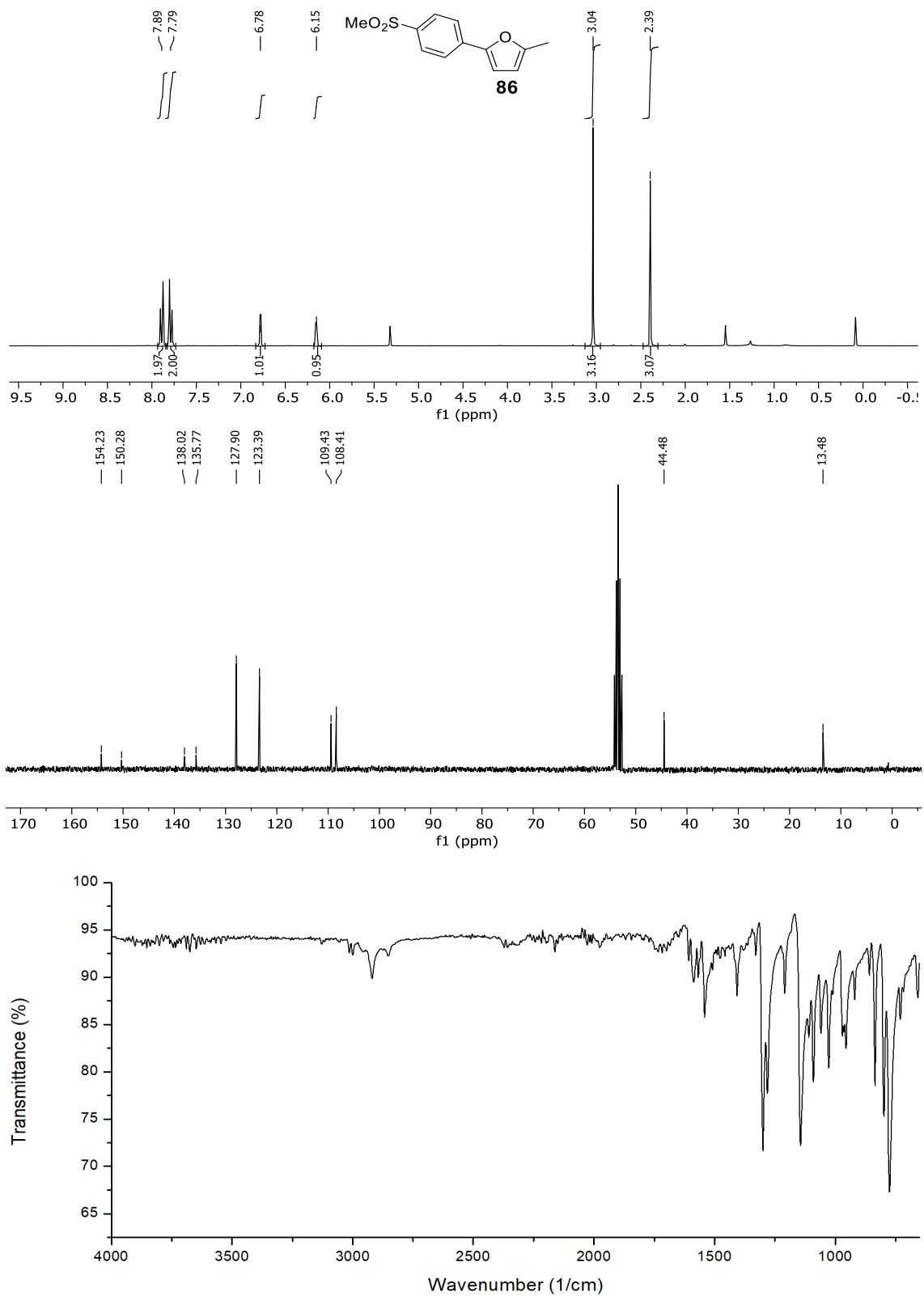


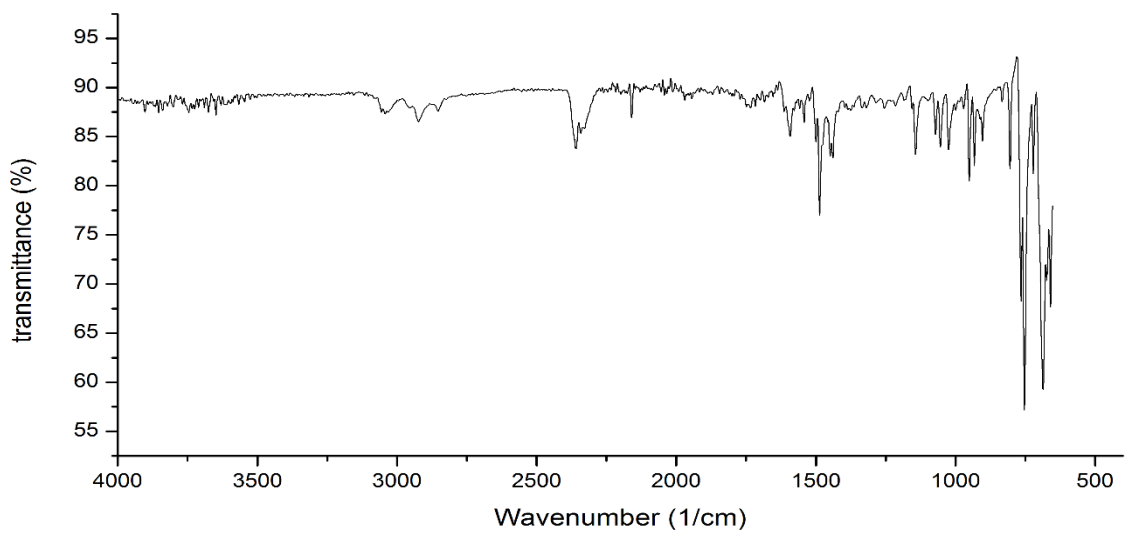
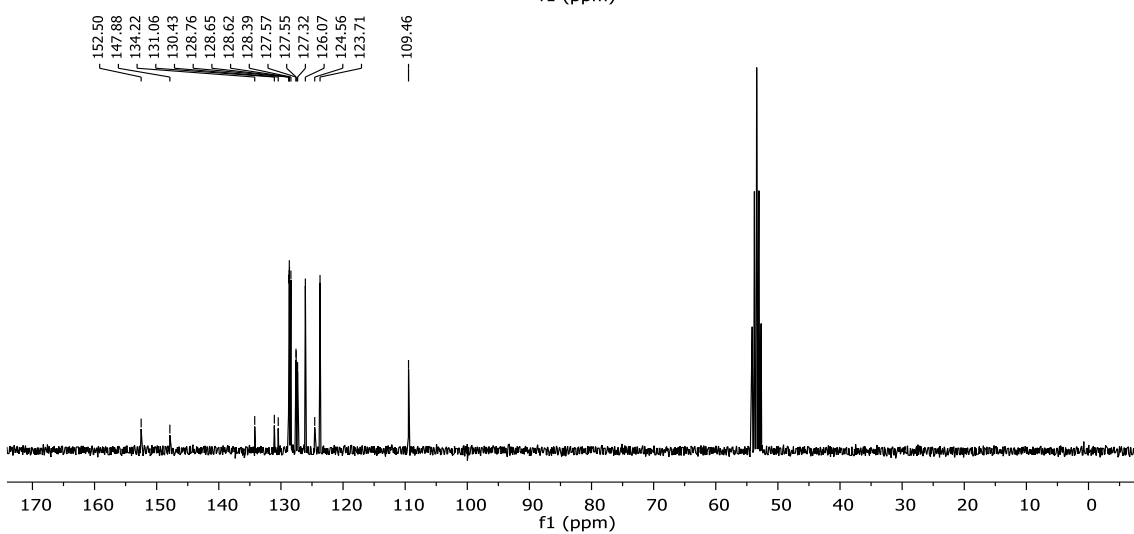
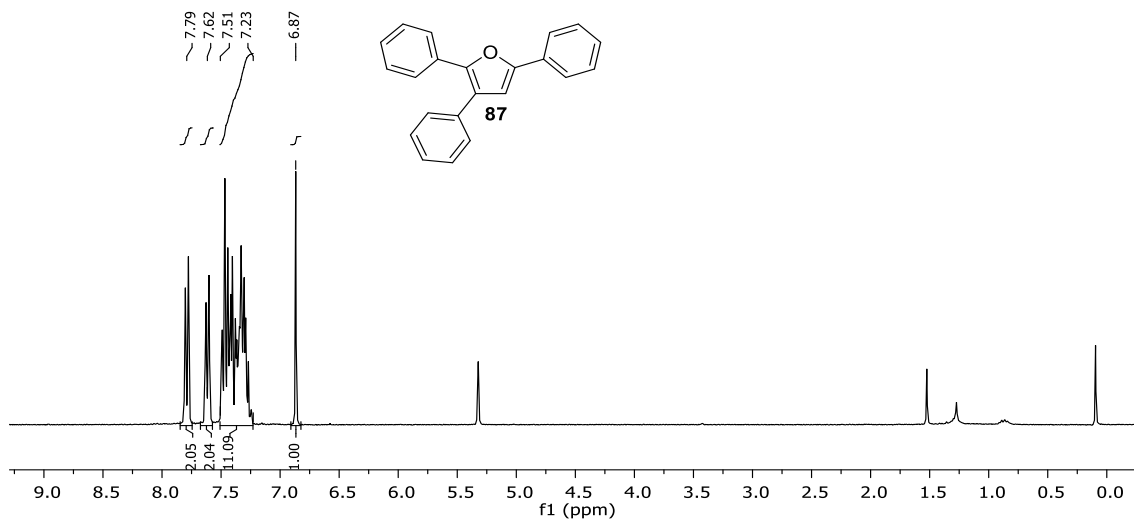


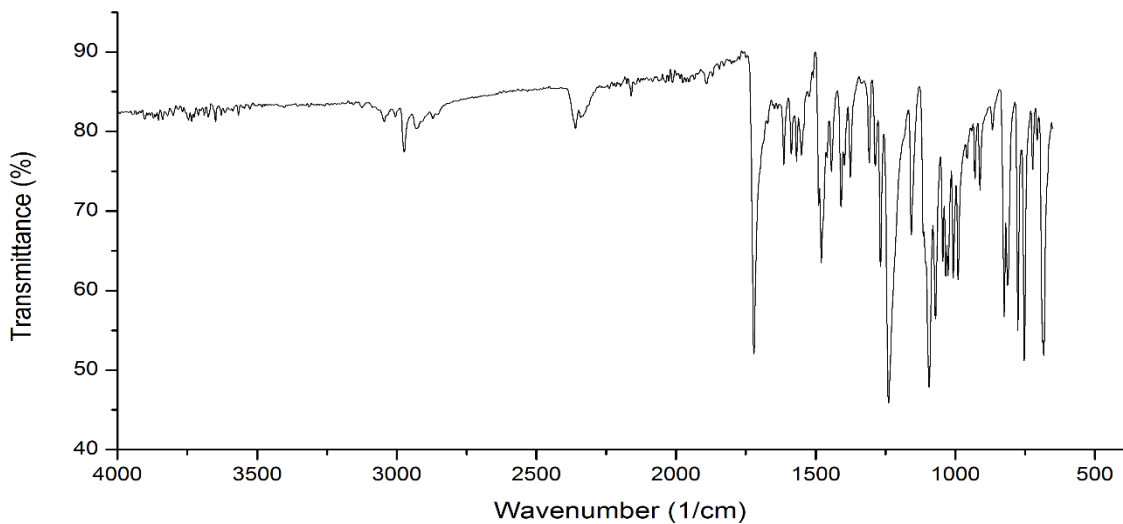
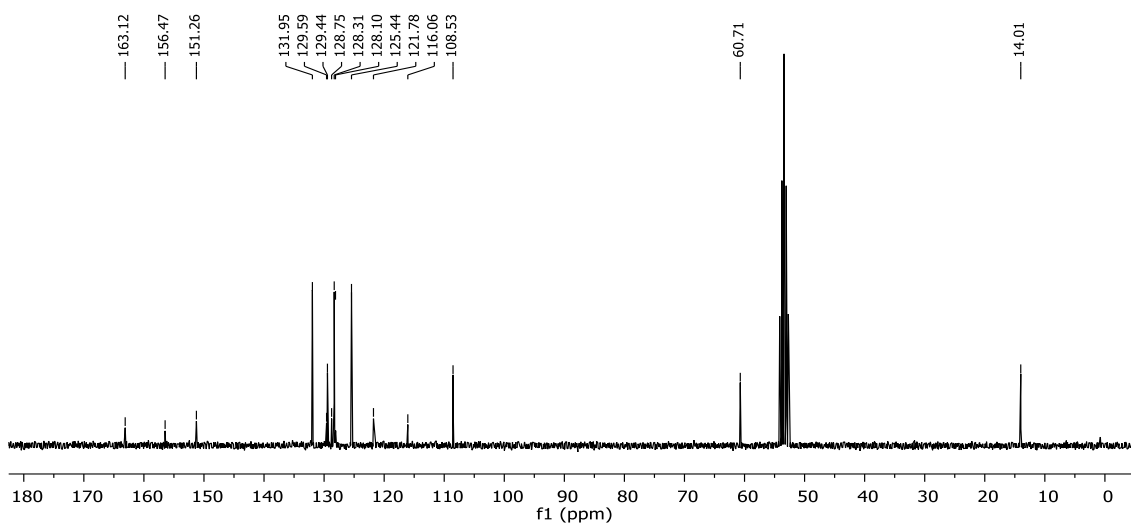
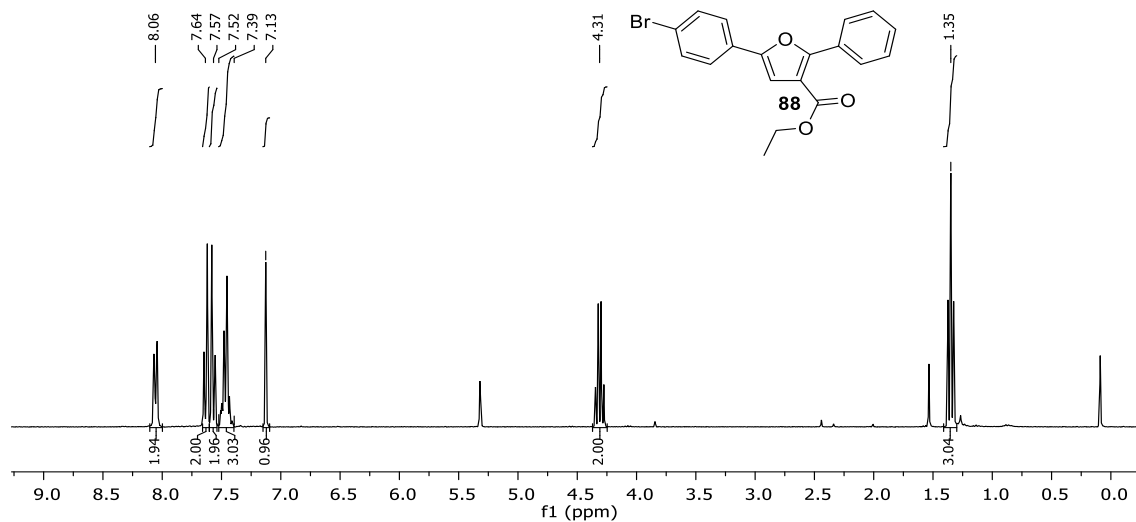


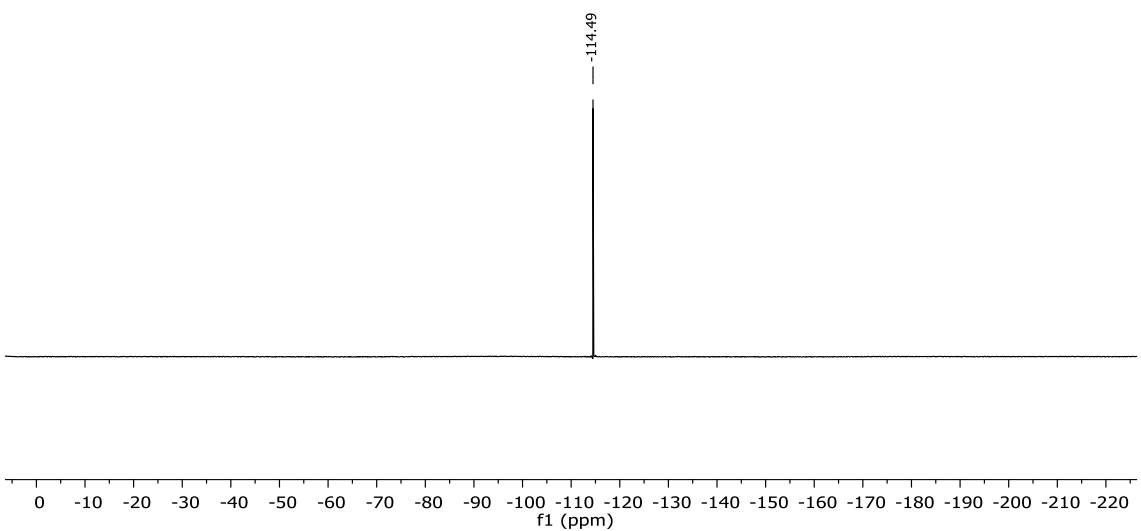
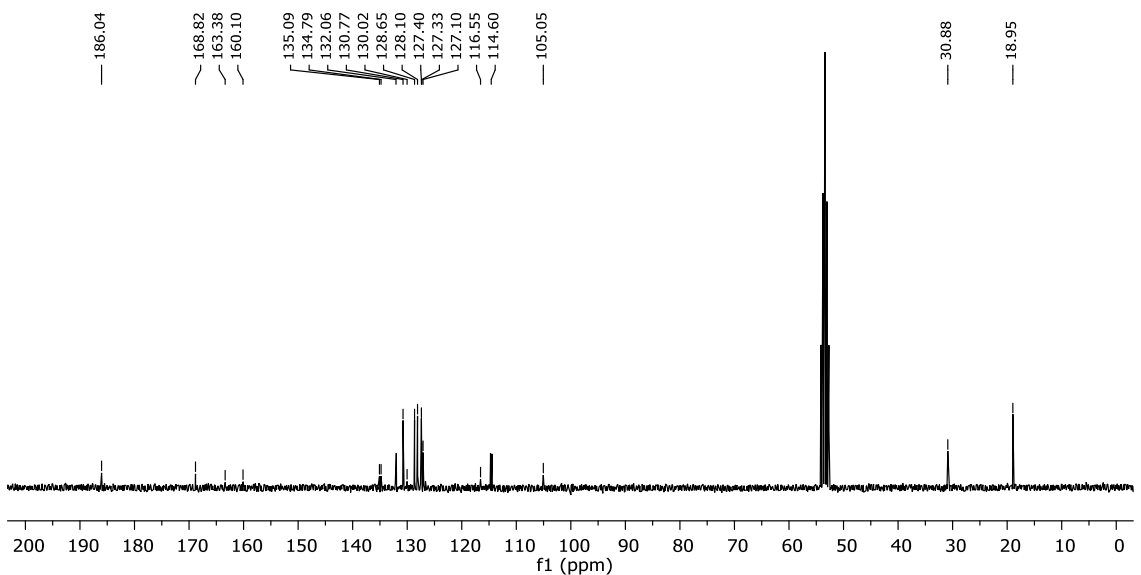
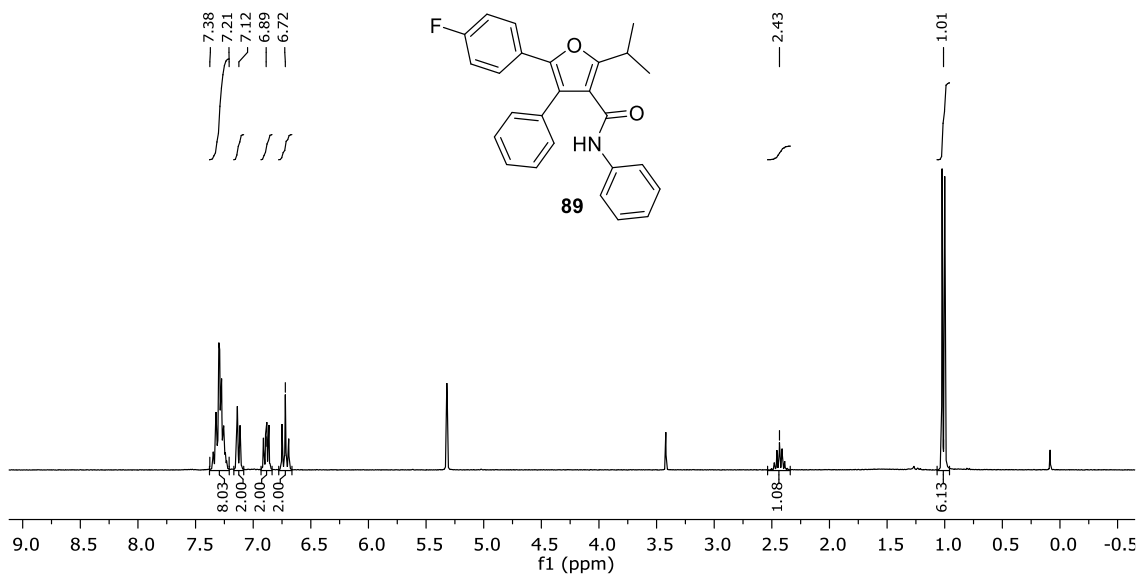


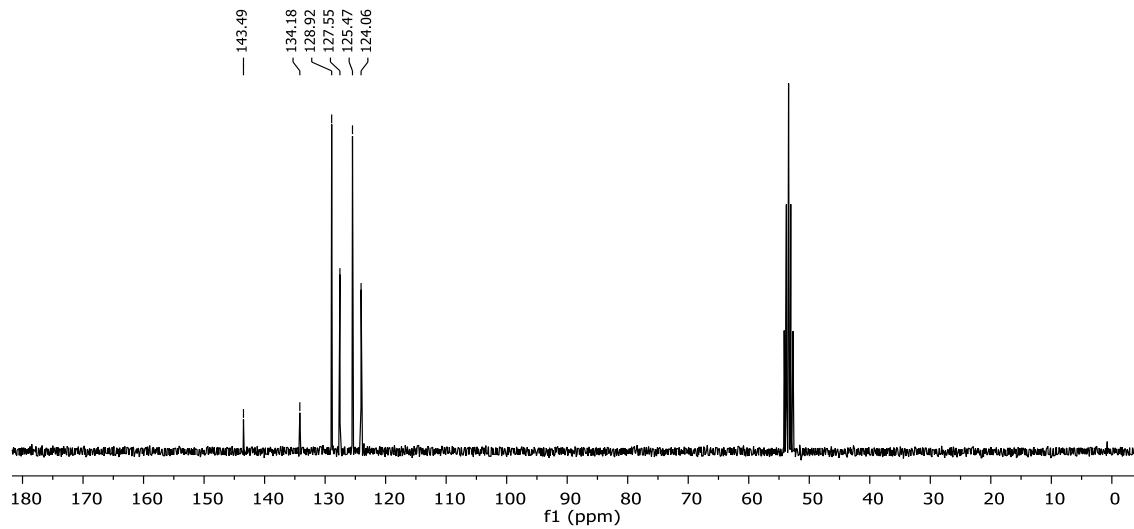
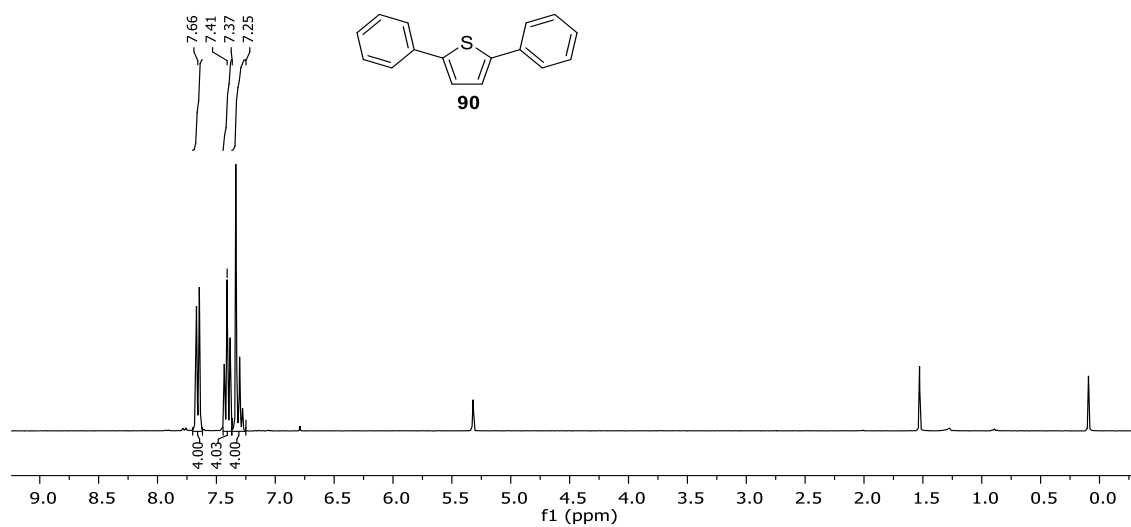
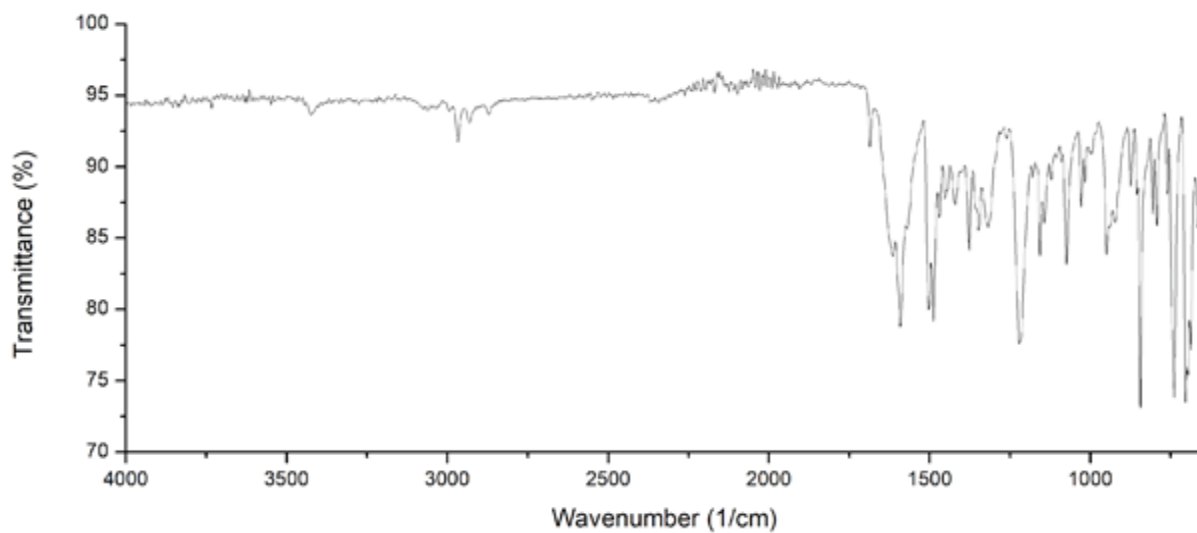


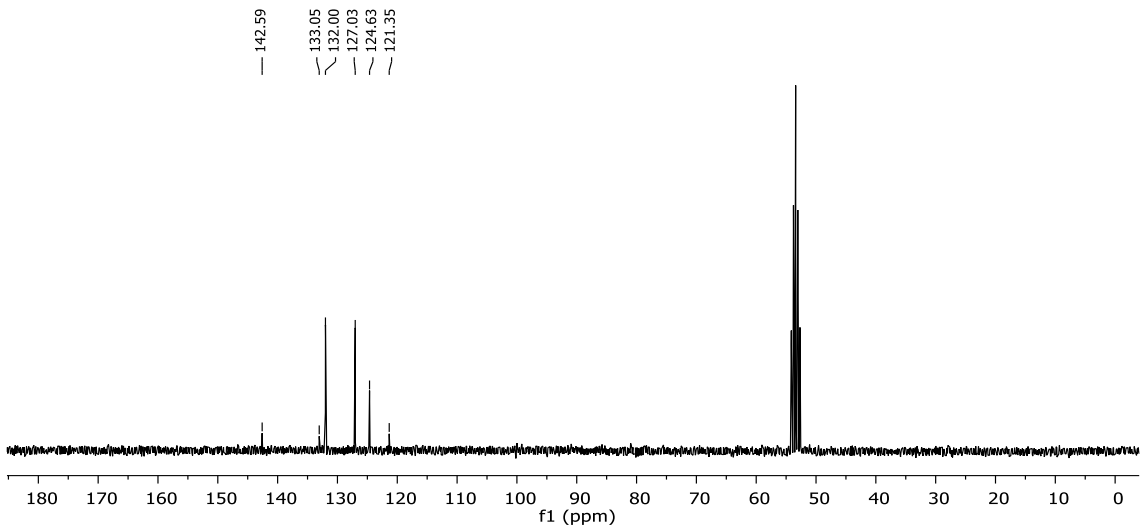
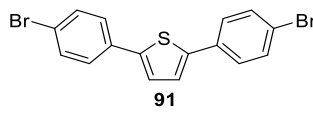
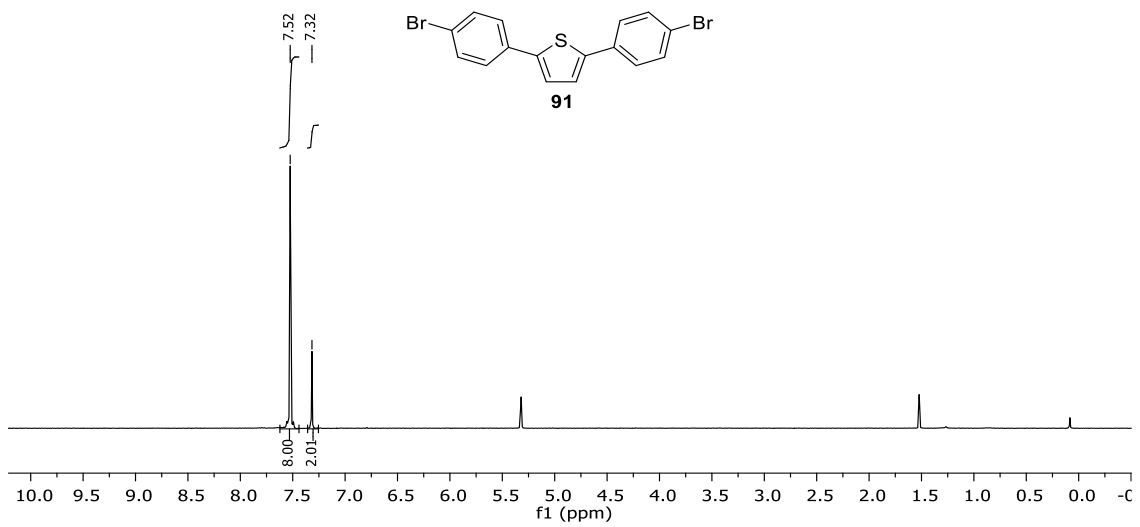
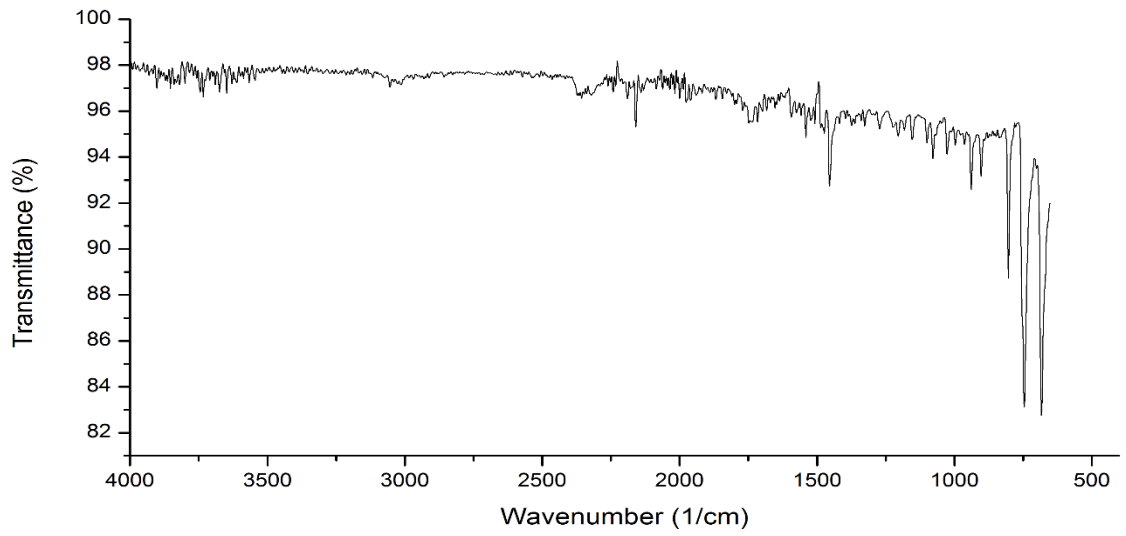


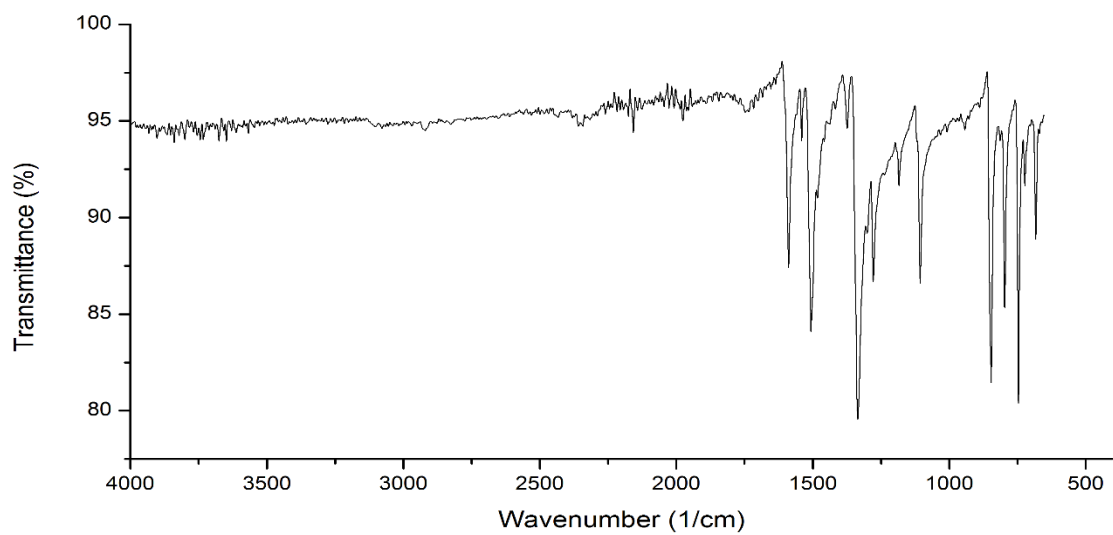
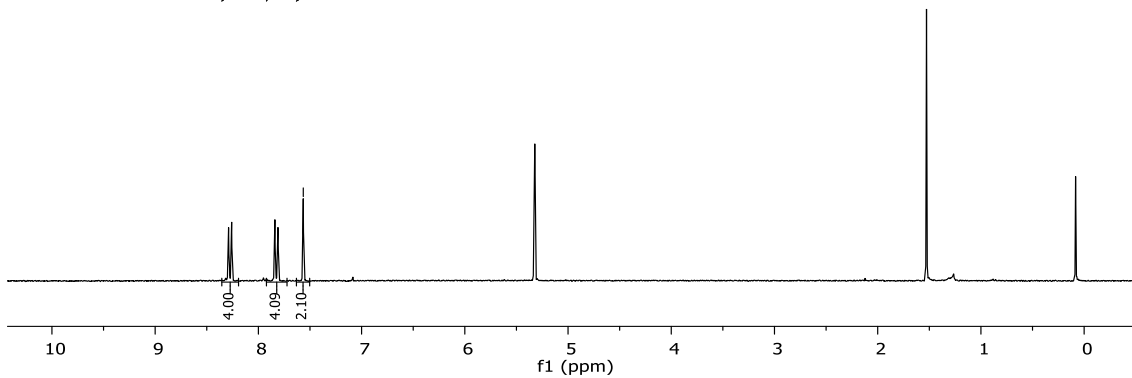
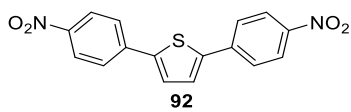
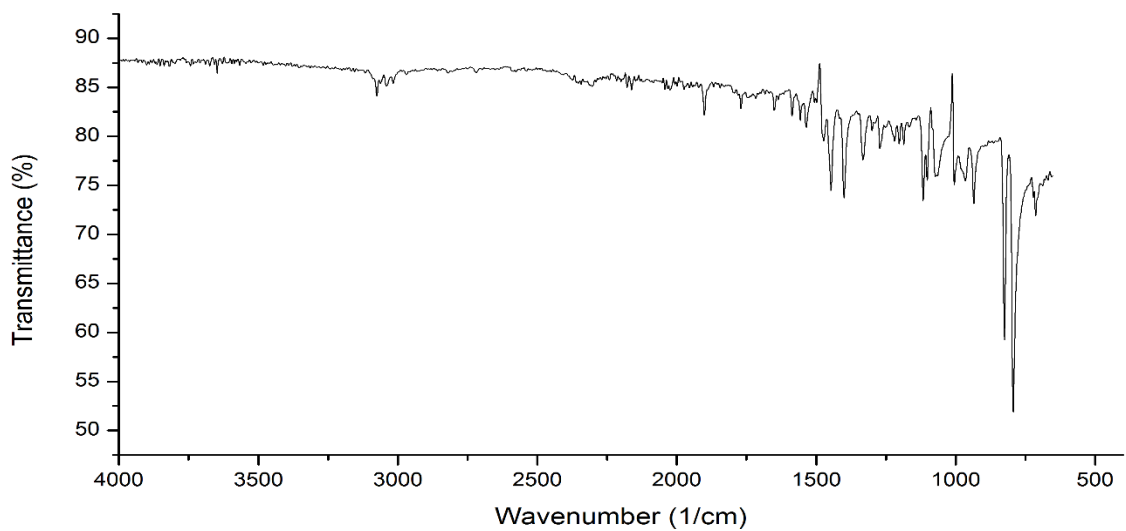


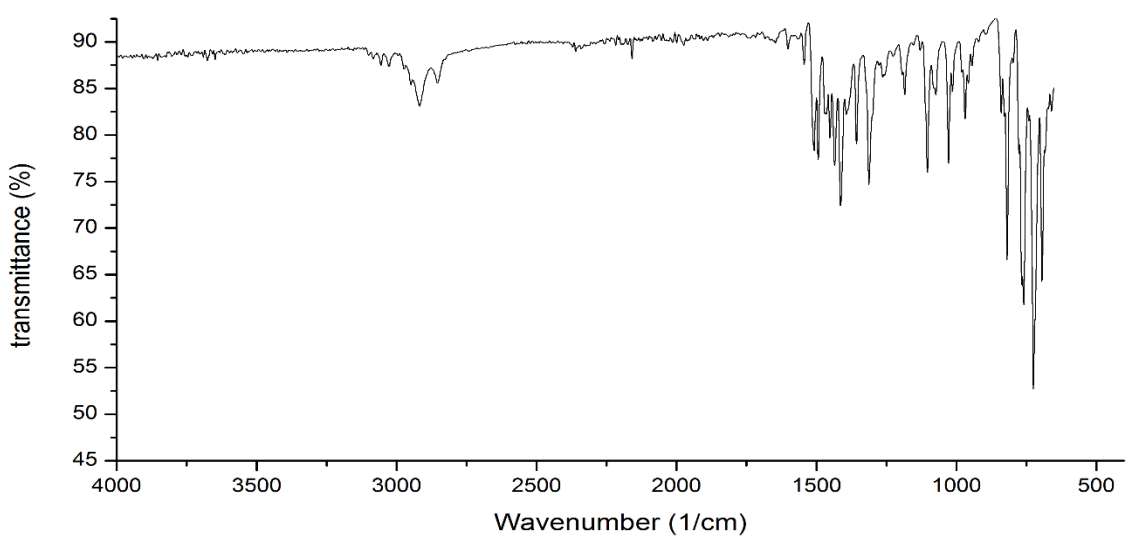
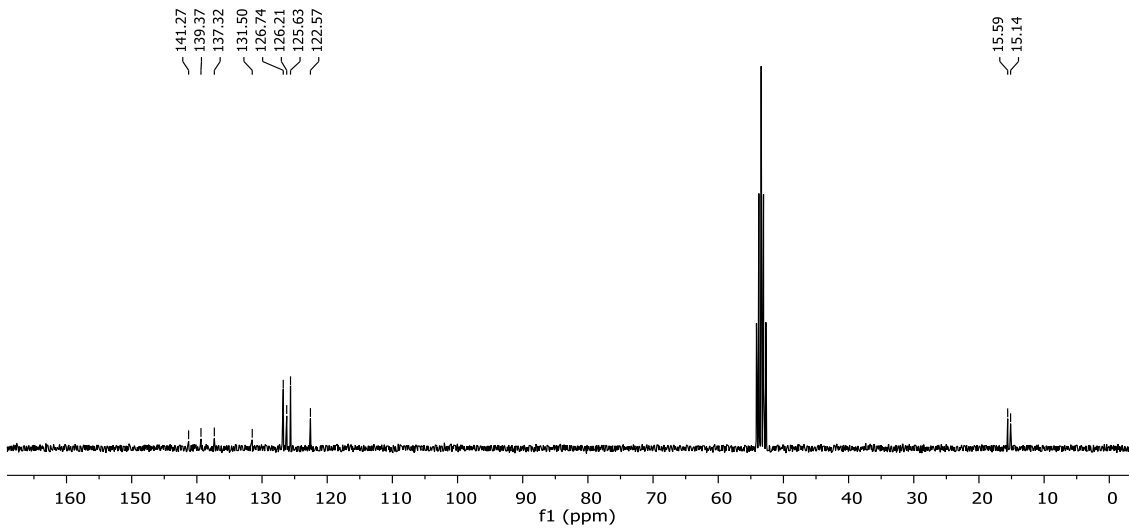
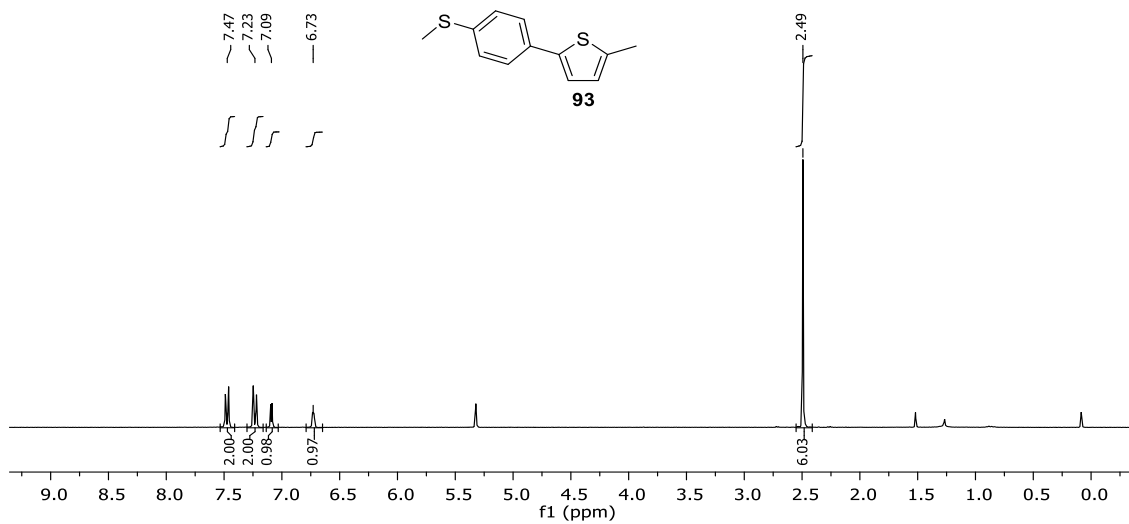


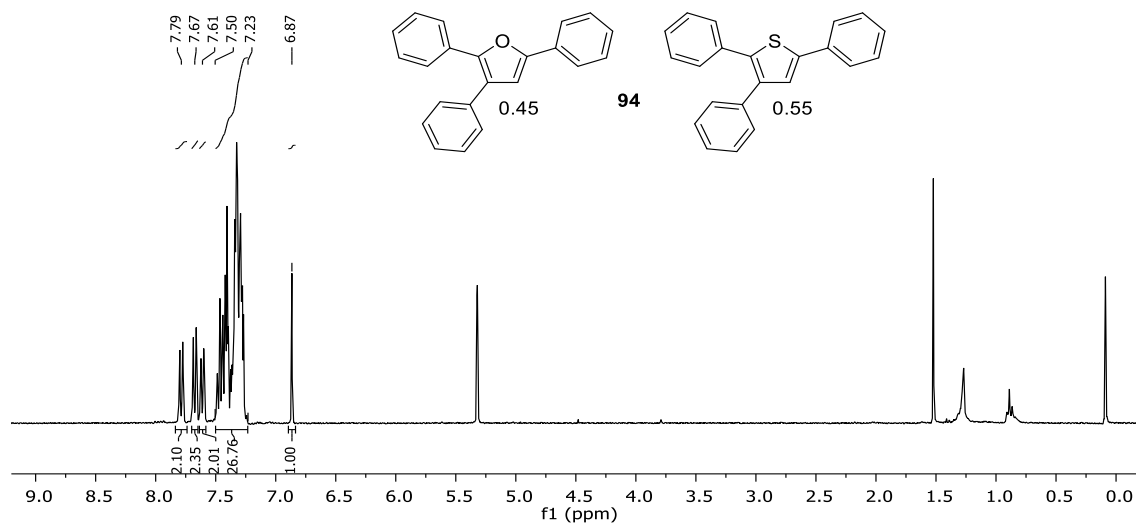




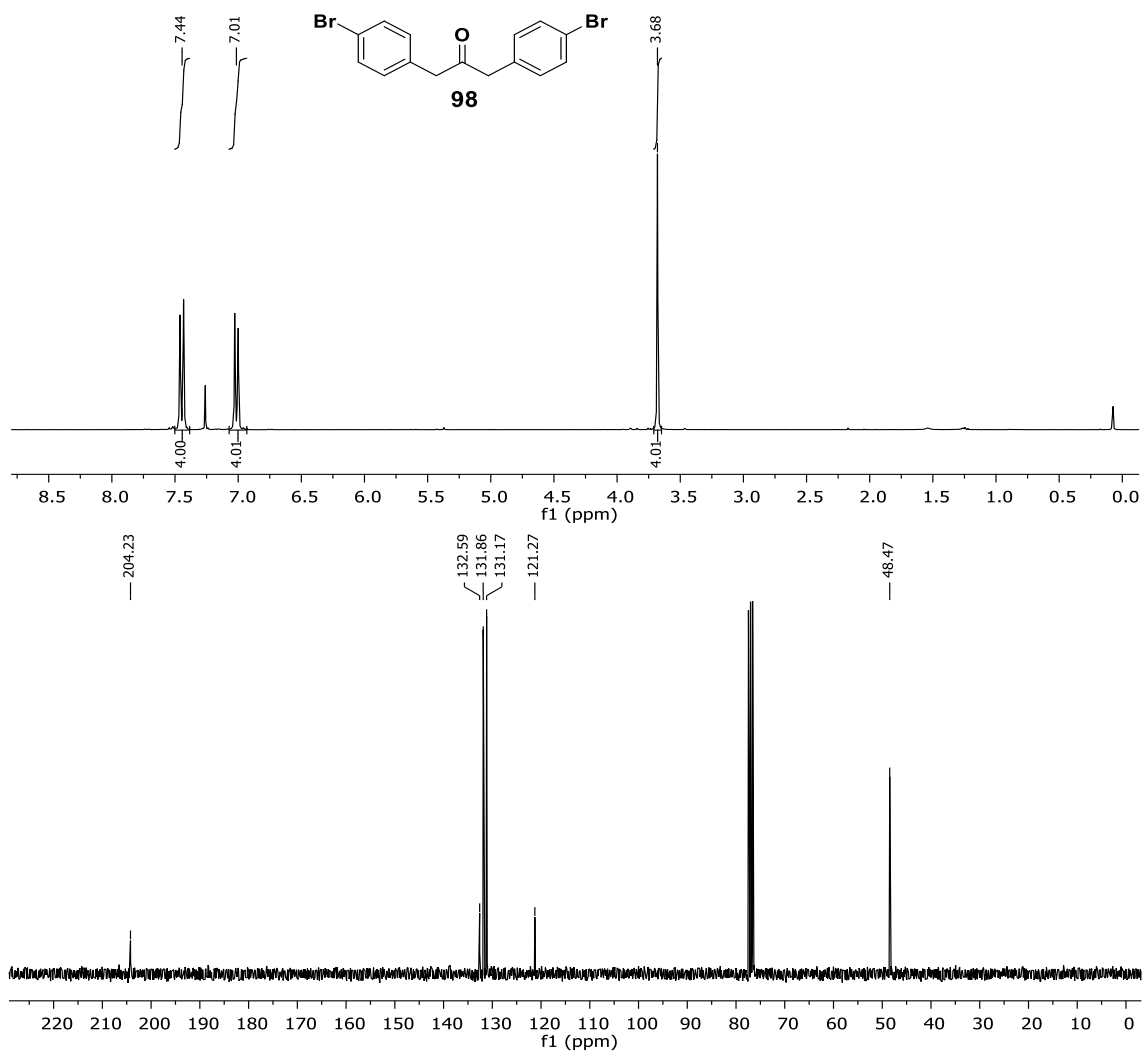


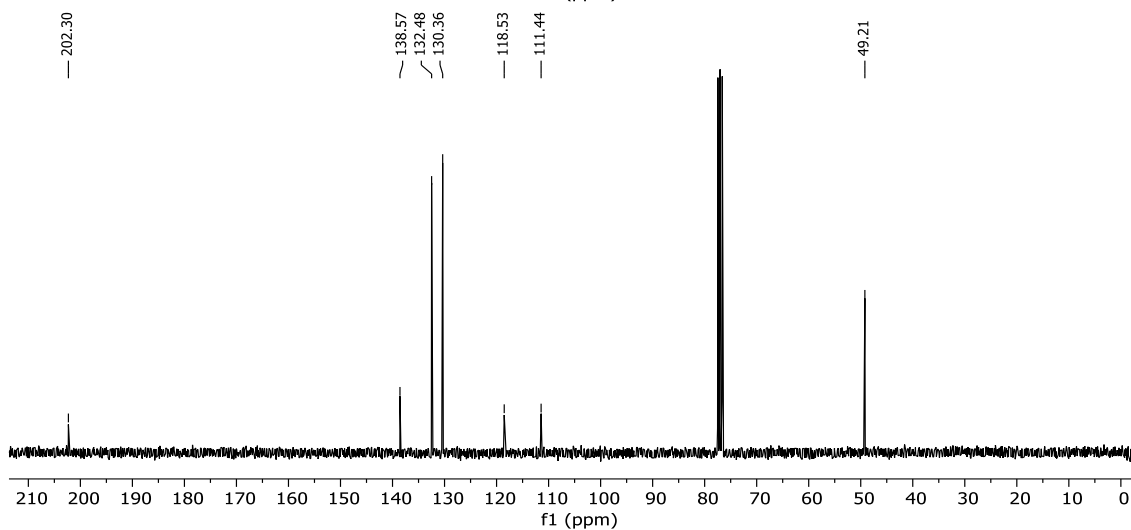
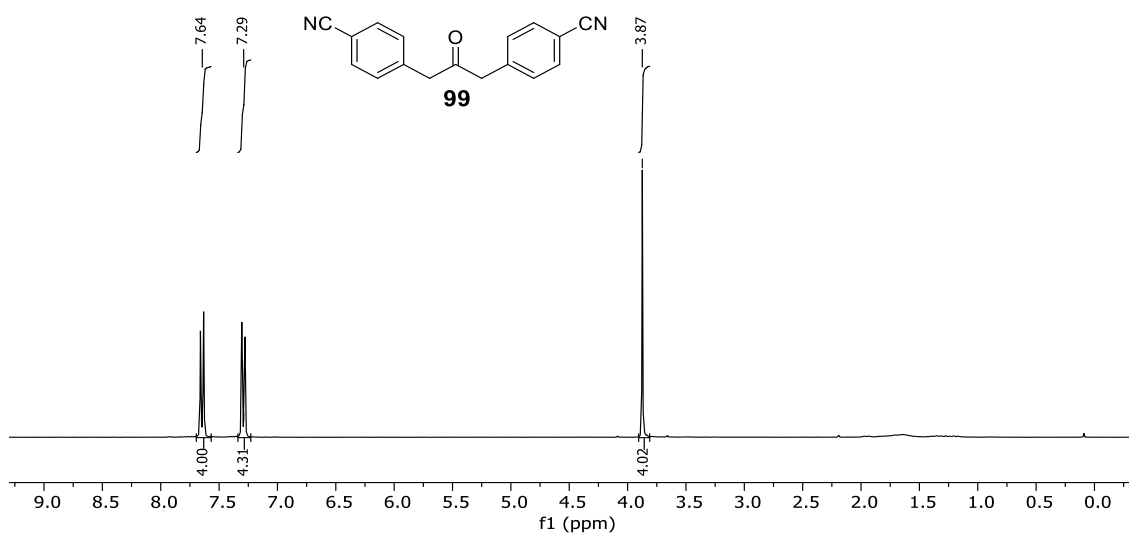
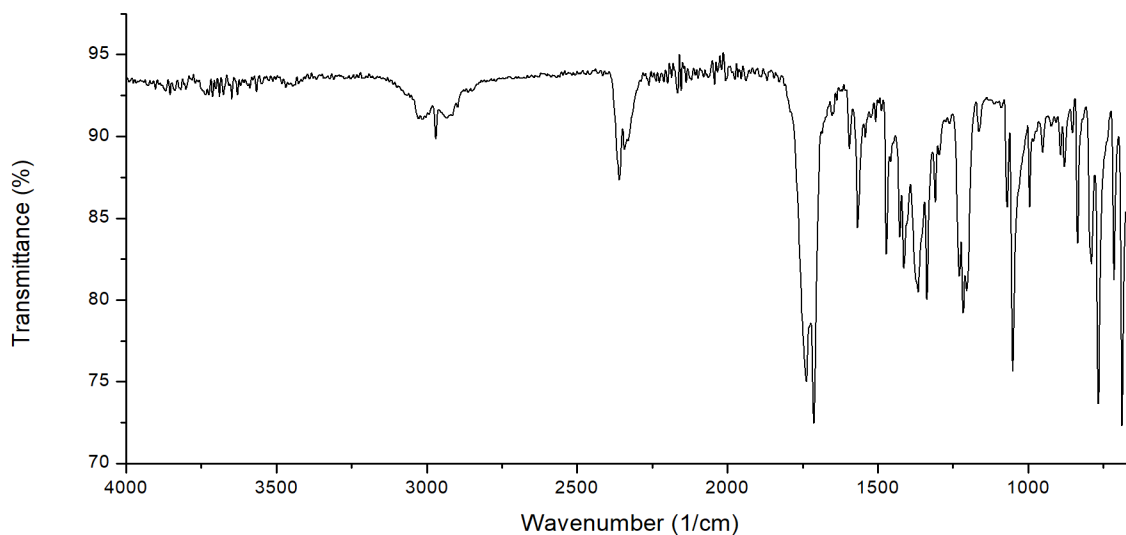


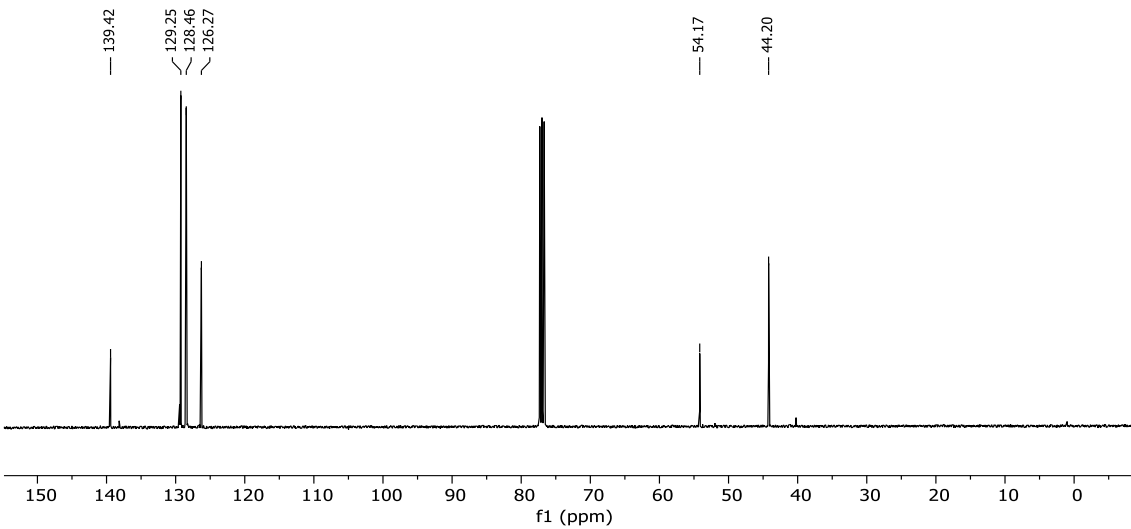
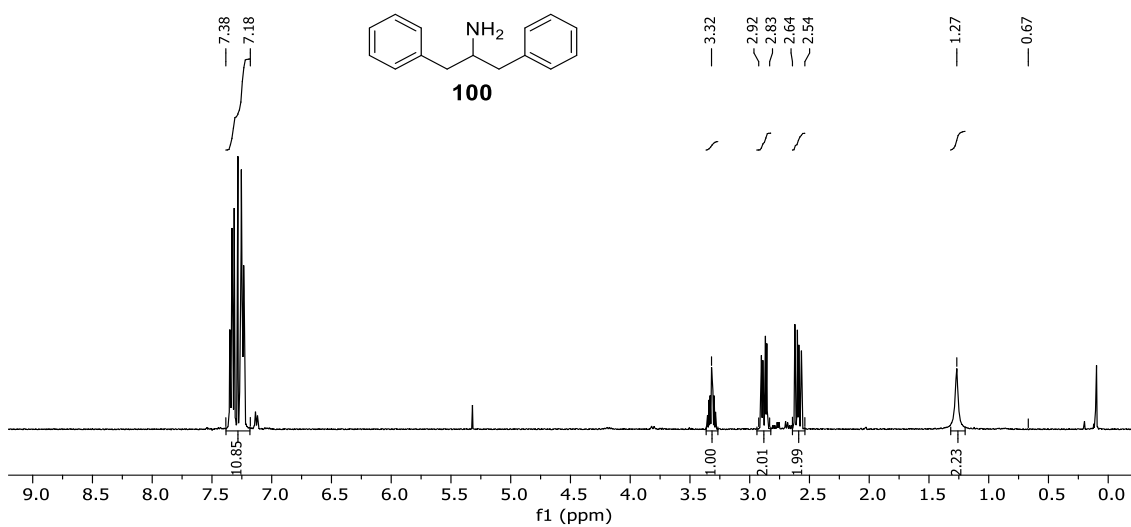
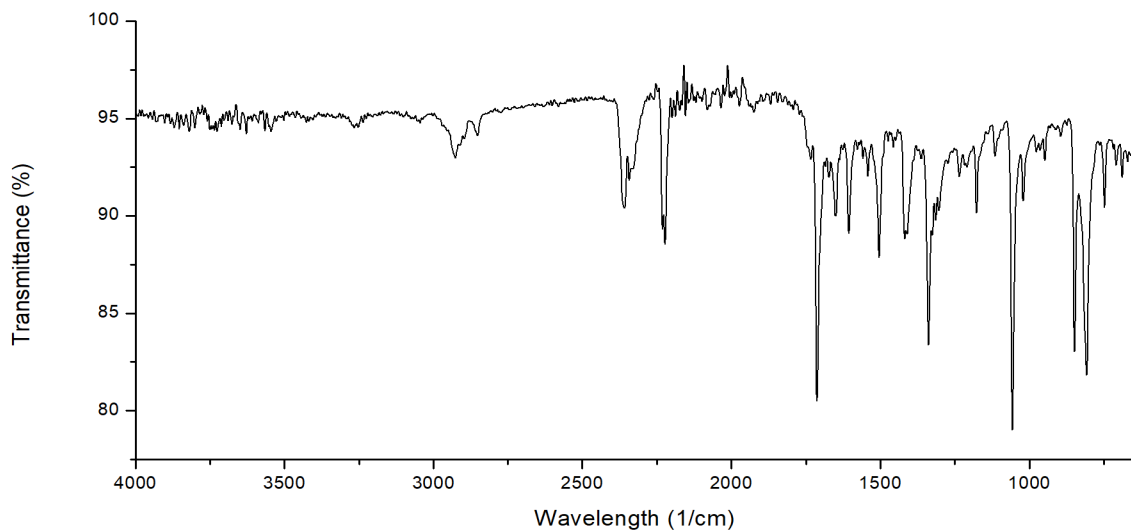


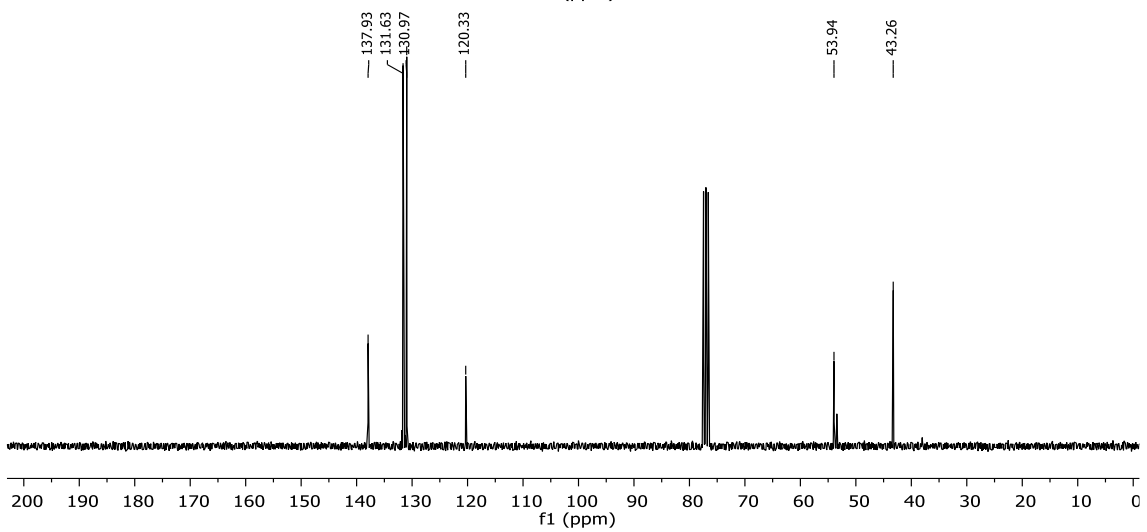
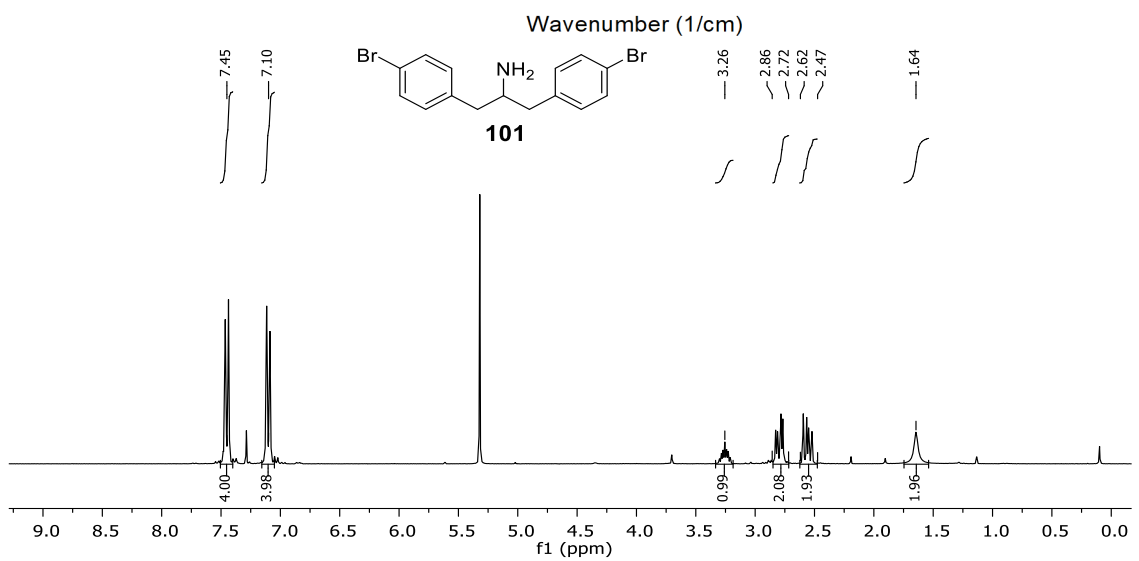
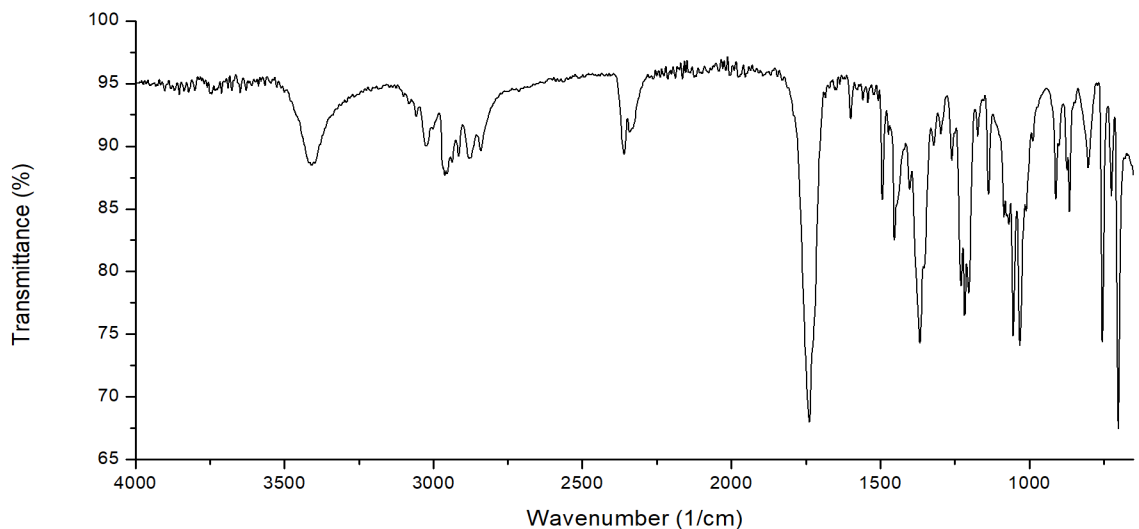


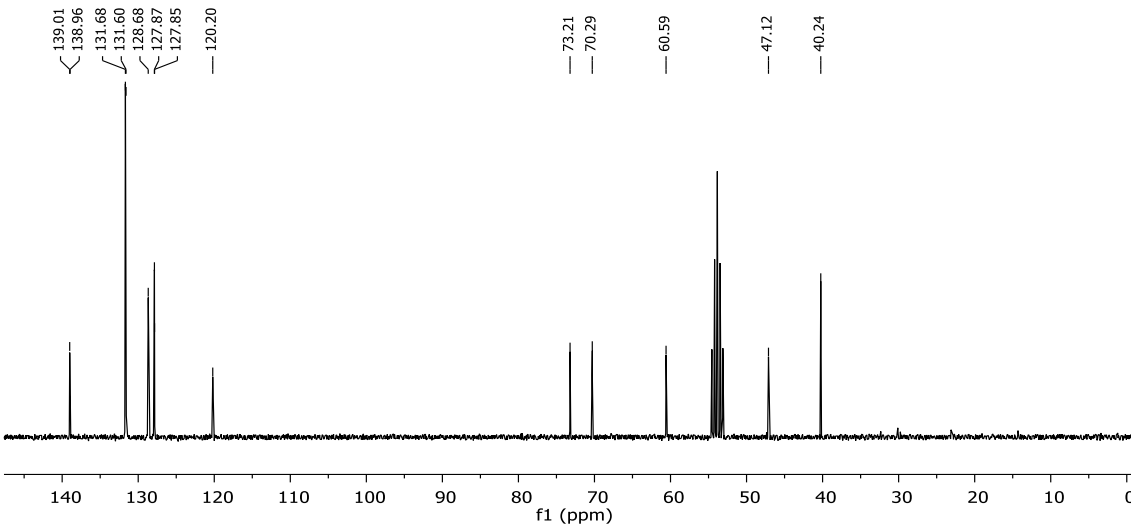
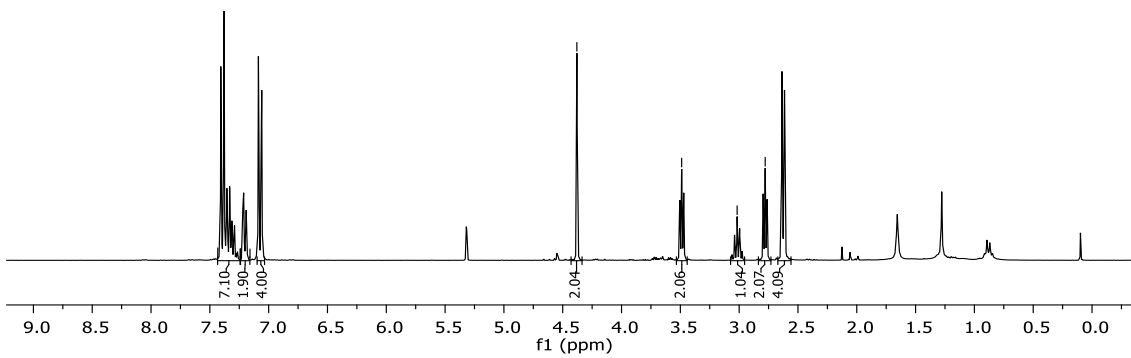
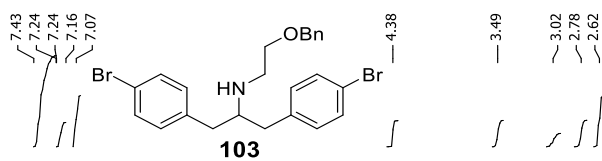
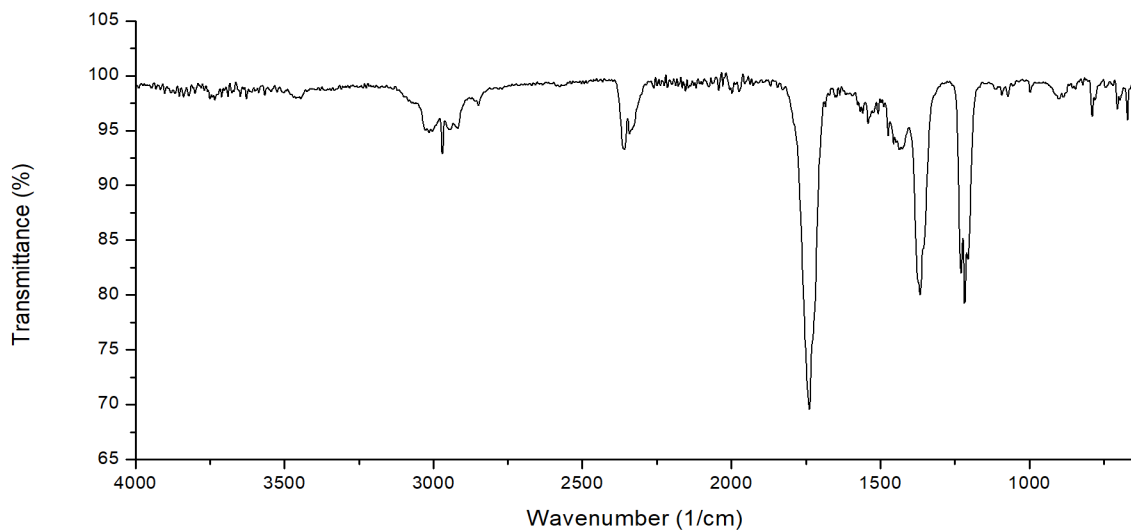
The shown spectrum is the crude spectrum after extraction. The approximate yields were calculated by comparing the backbone signal of the Furan (6.87 ppm) to the entire aromatic region of the two products, giving the ratio of both products.

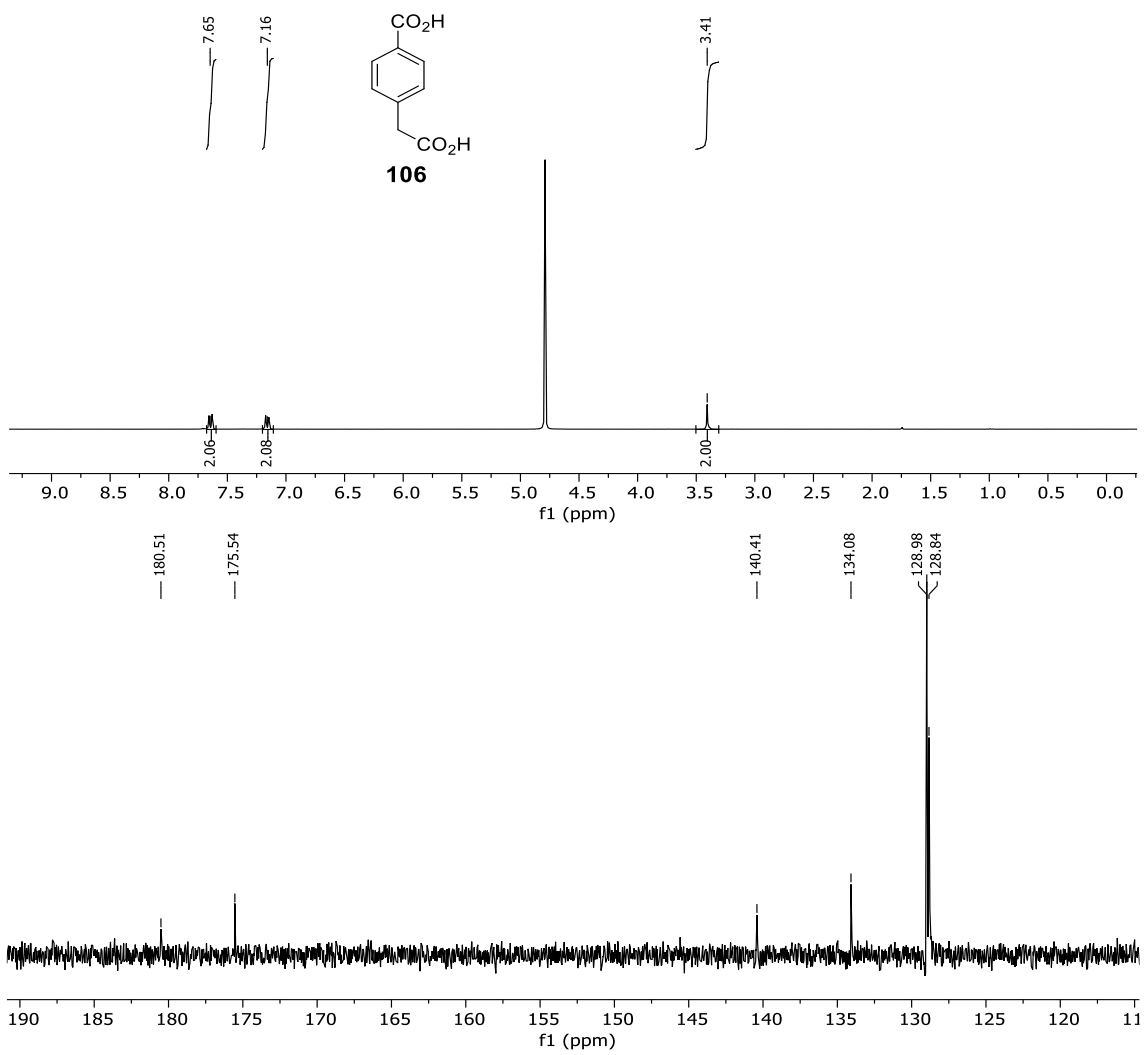
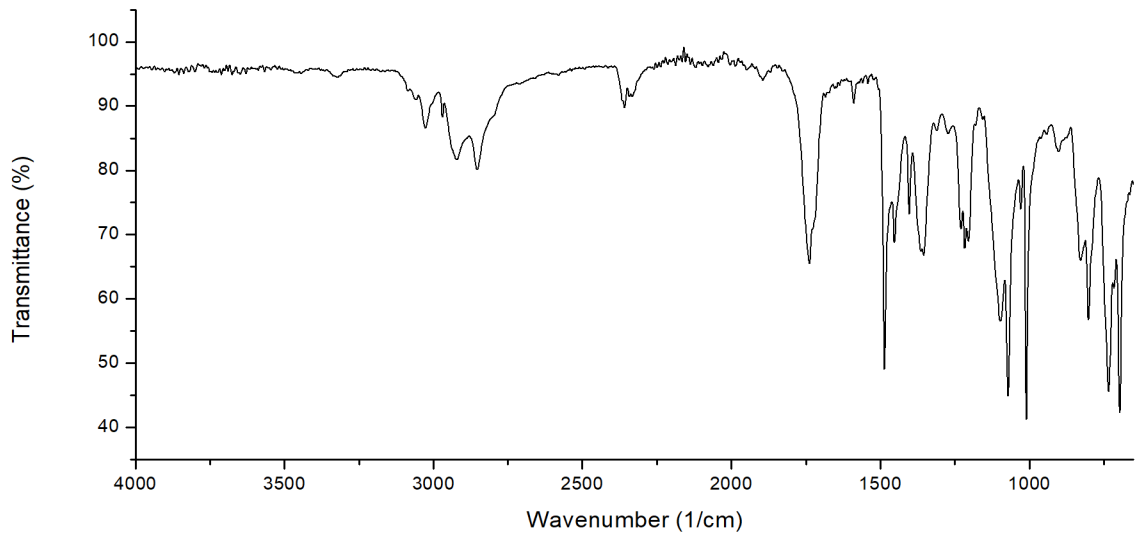


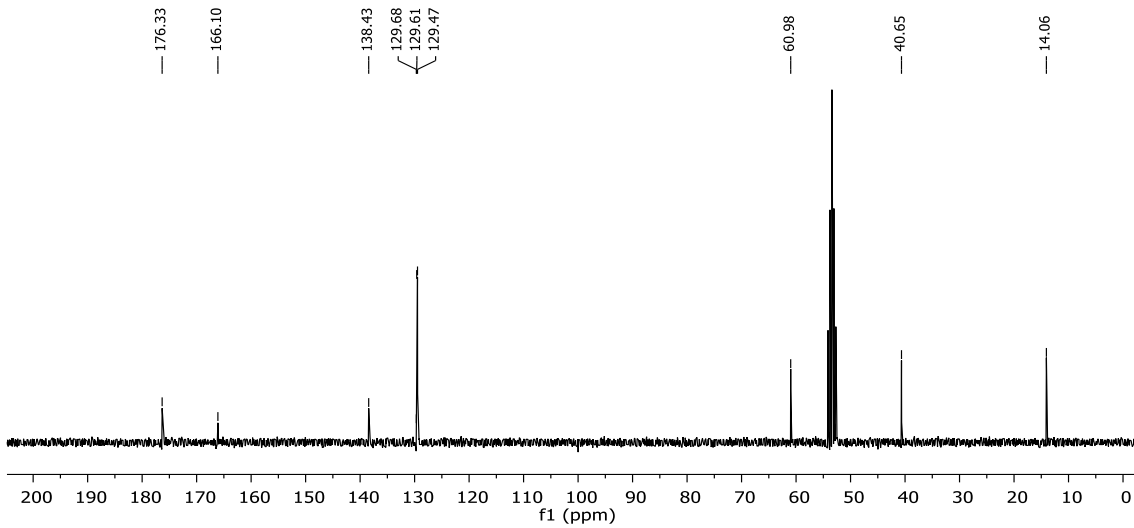
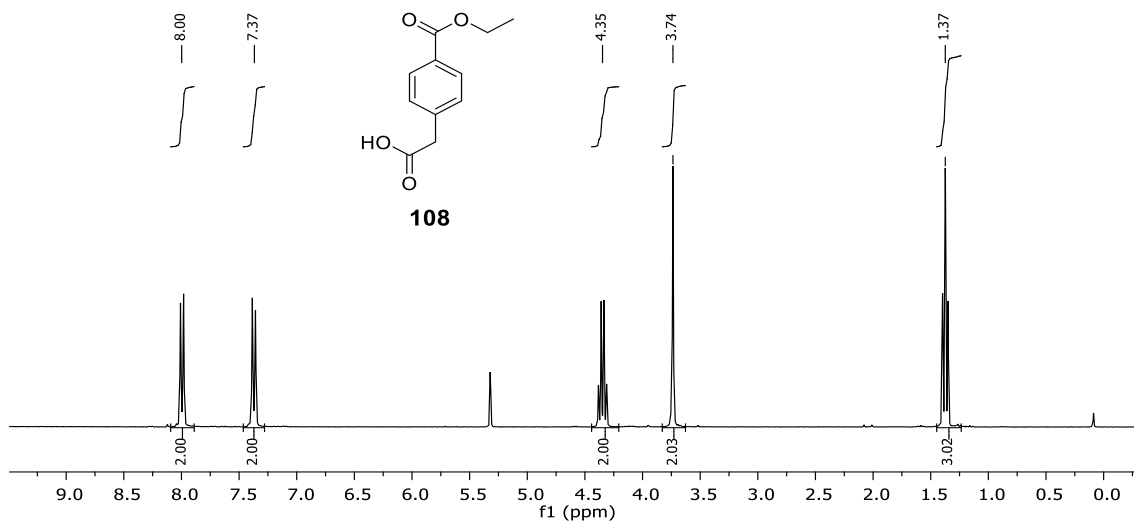
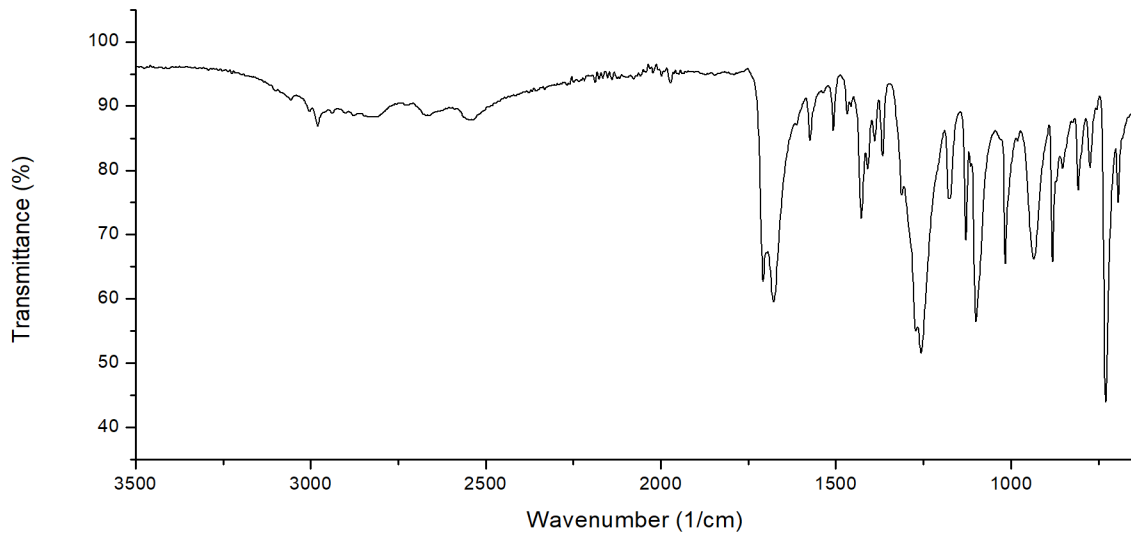


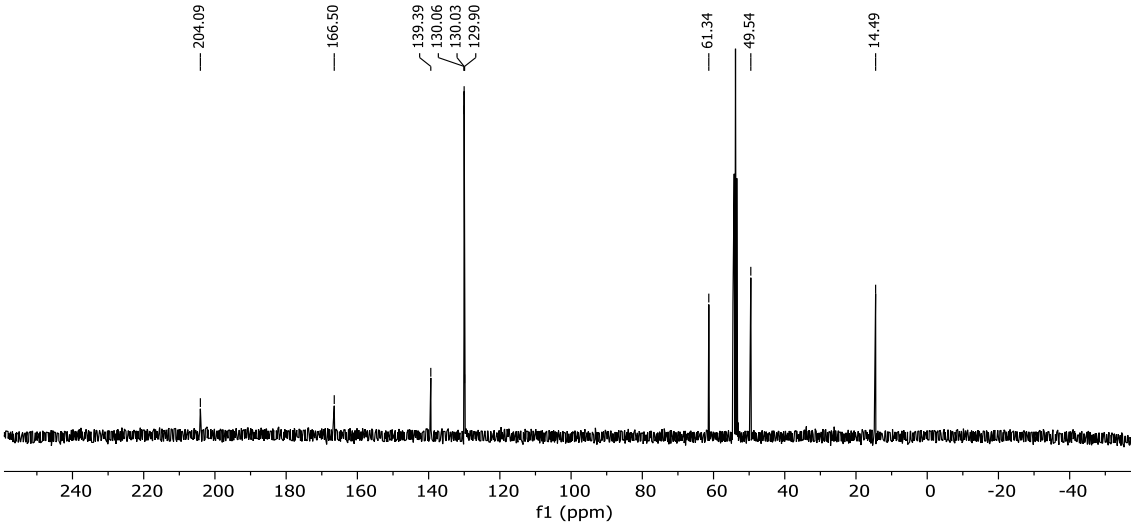
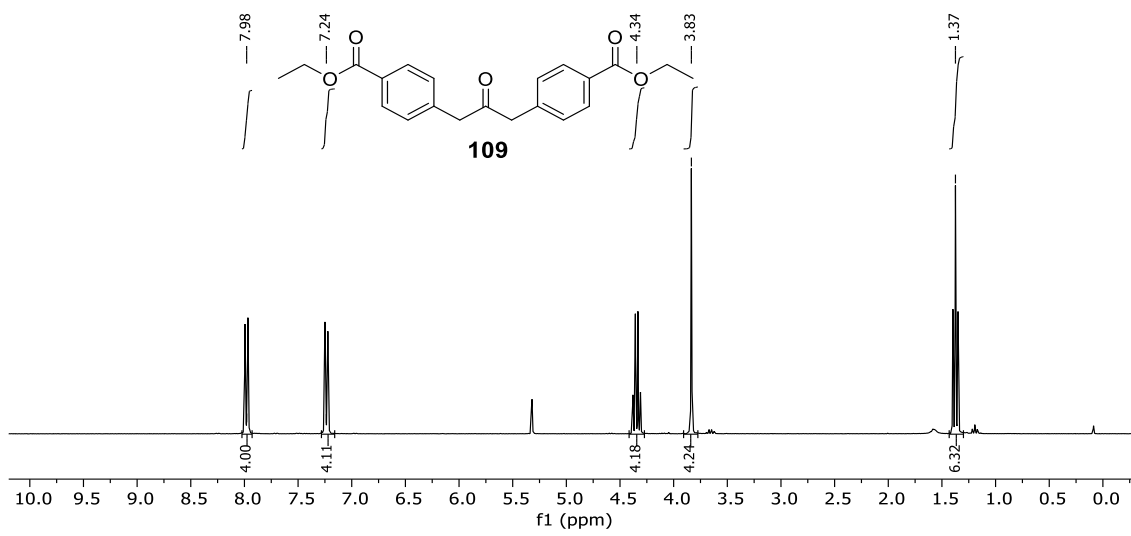
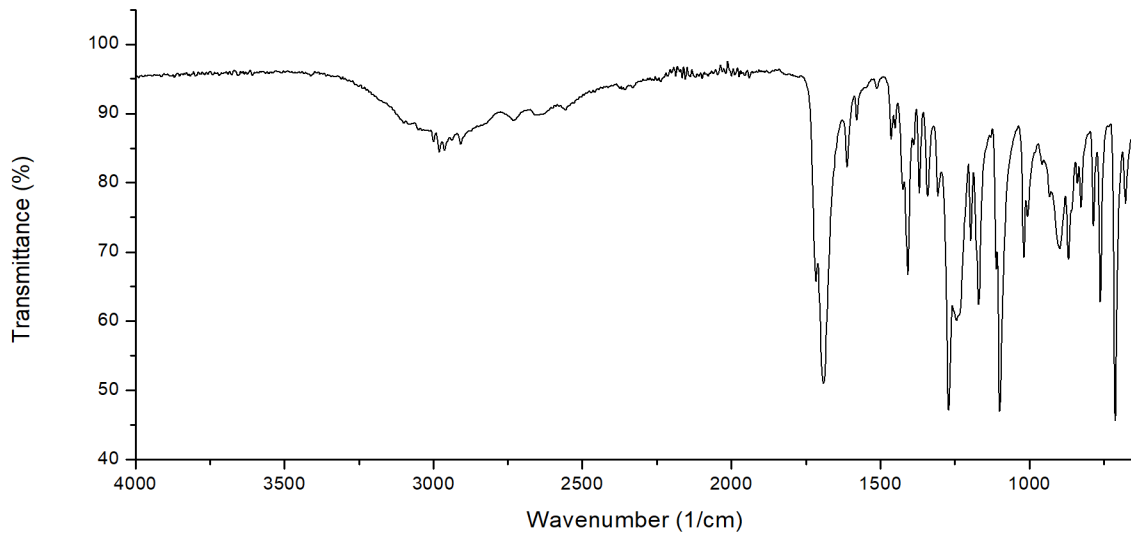


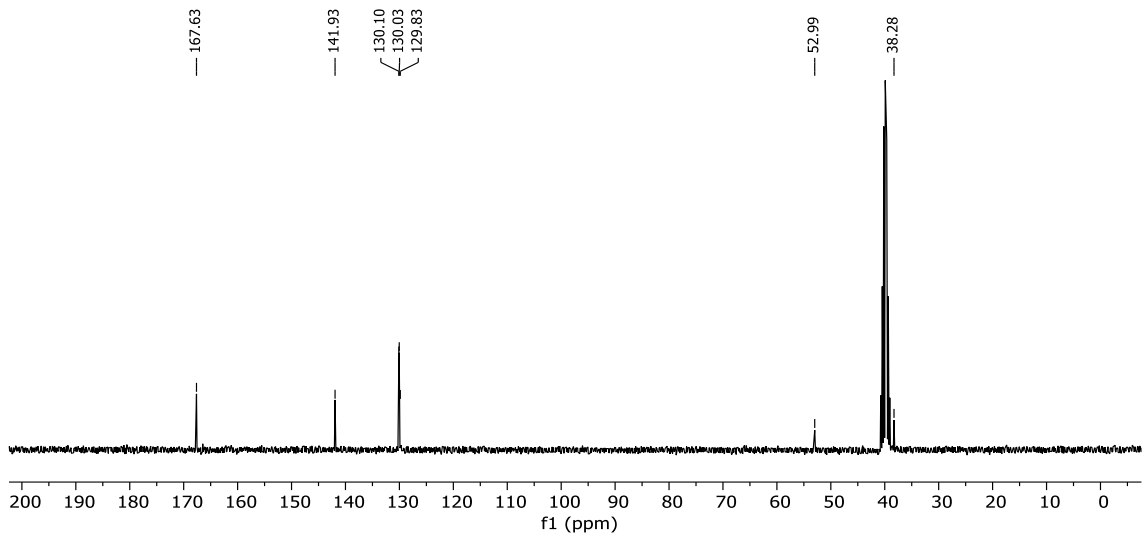
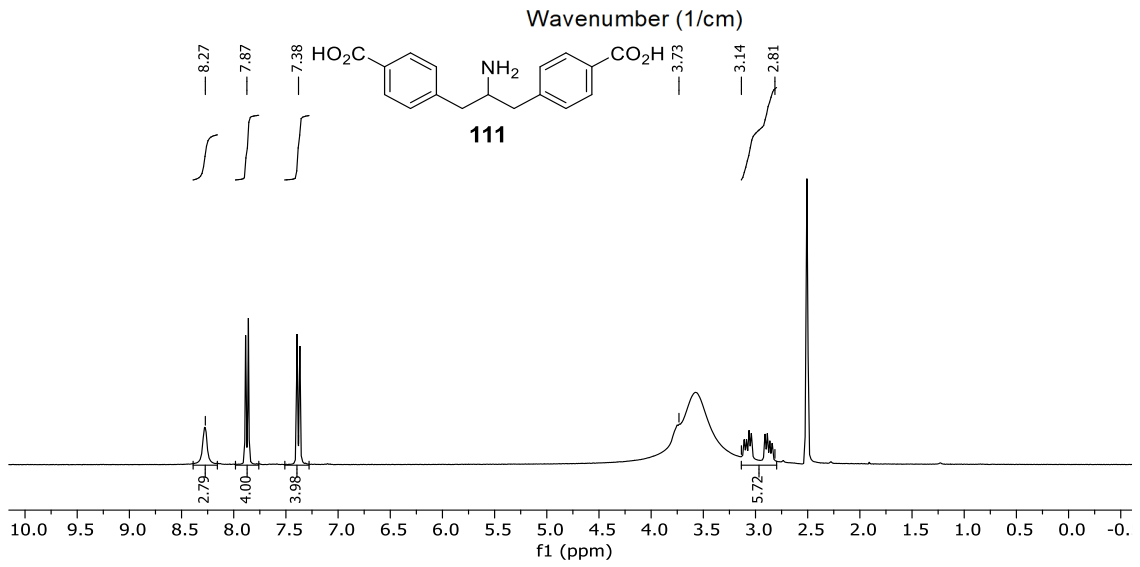
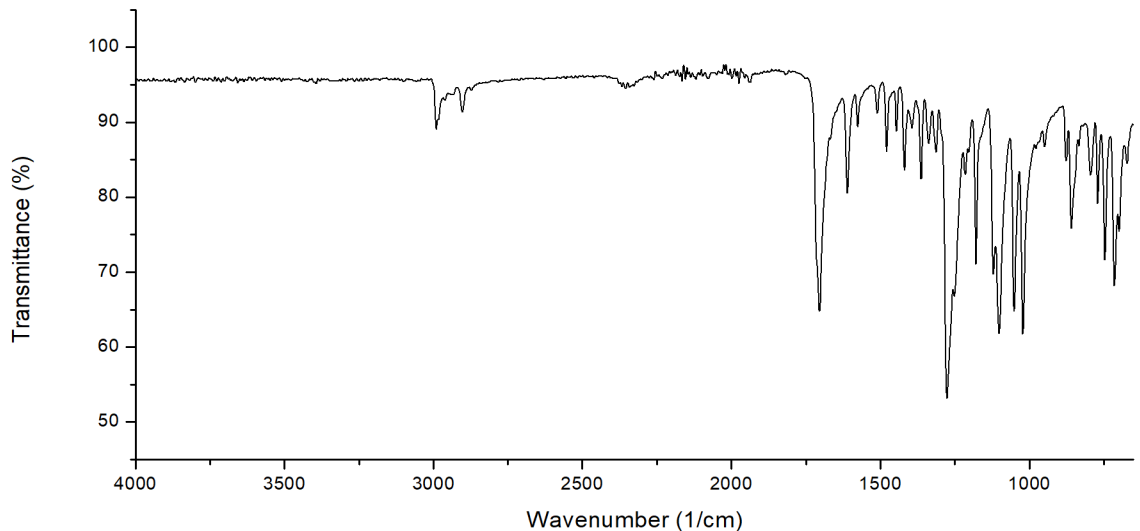


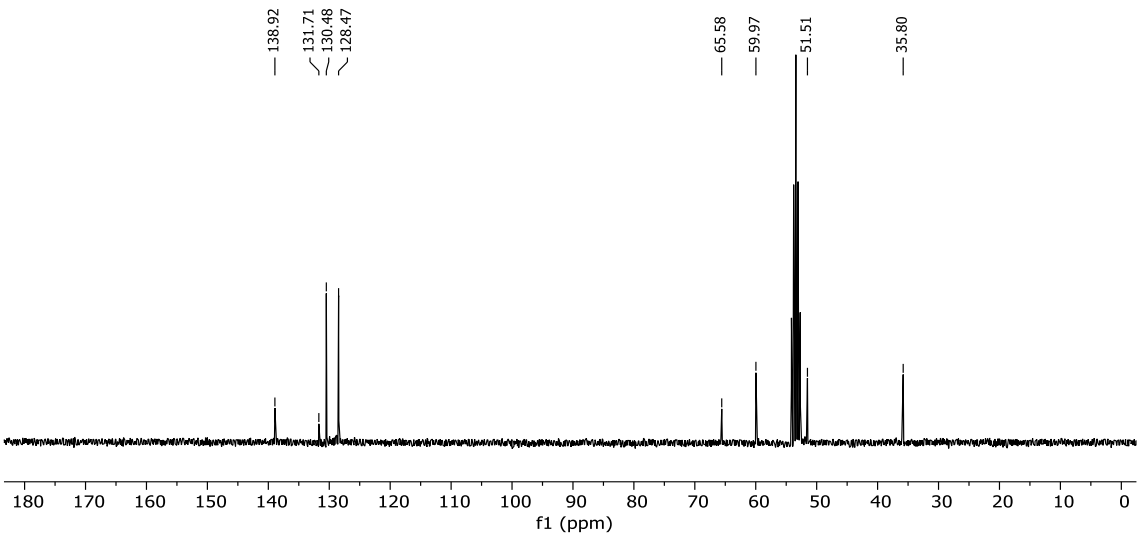
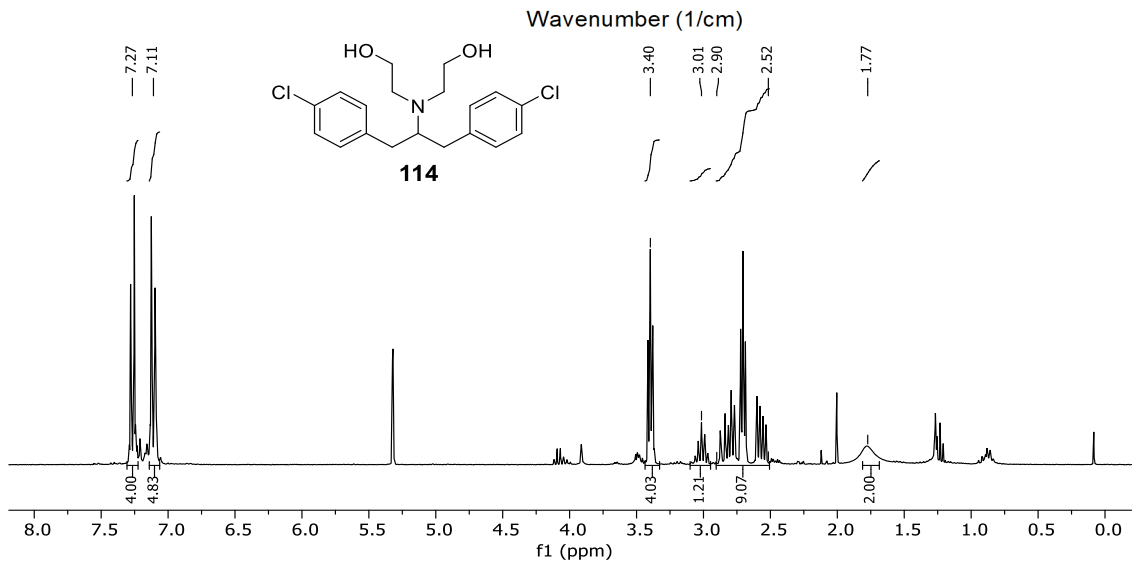
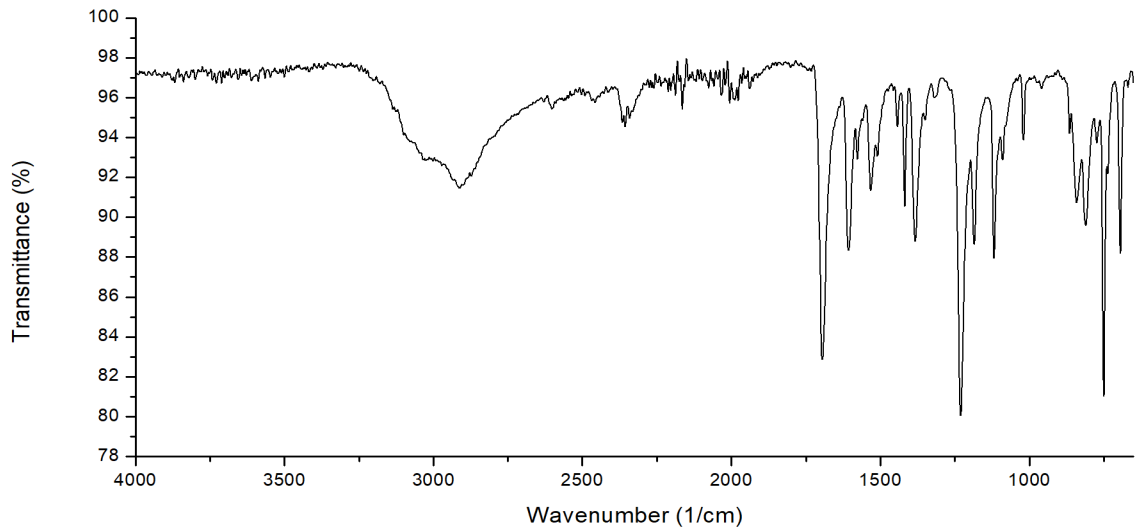


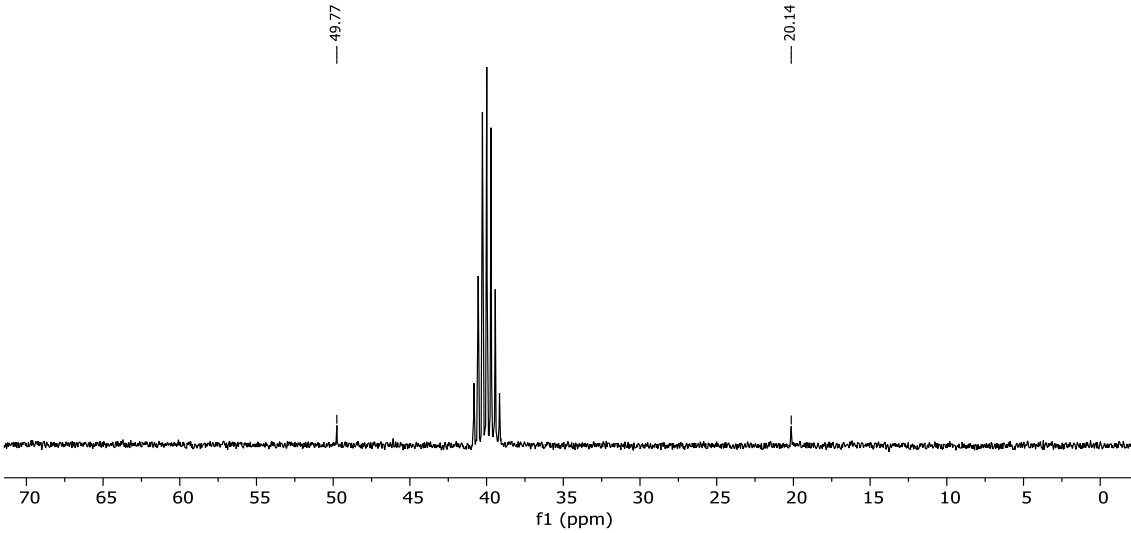
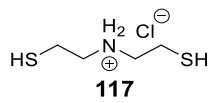
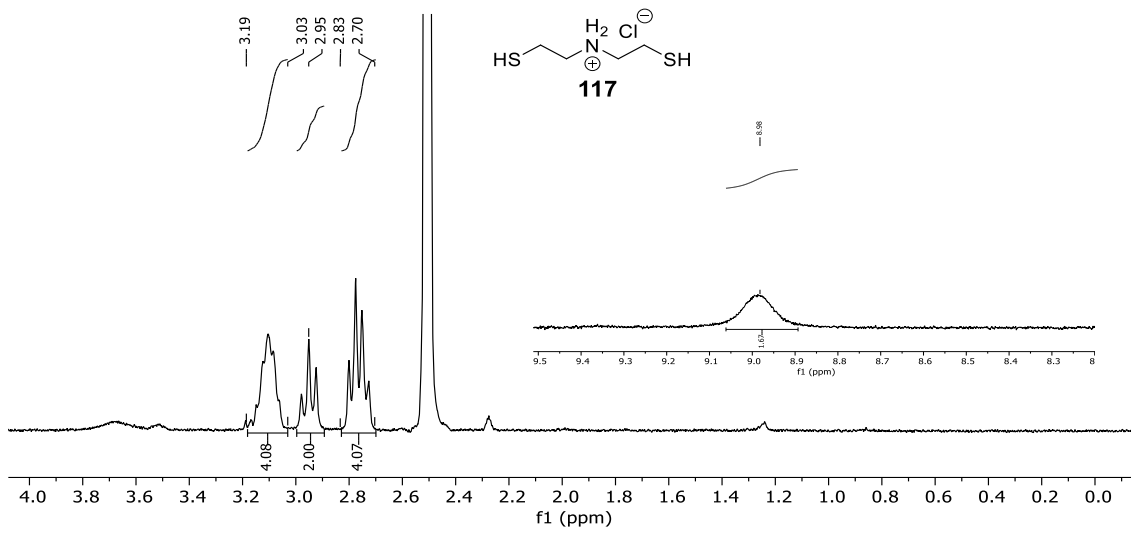
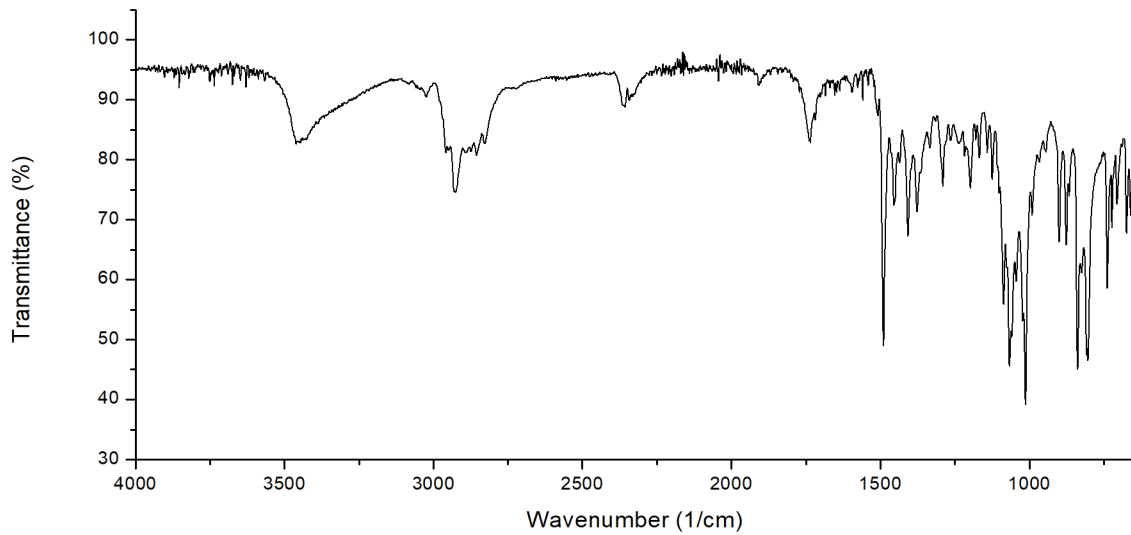


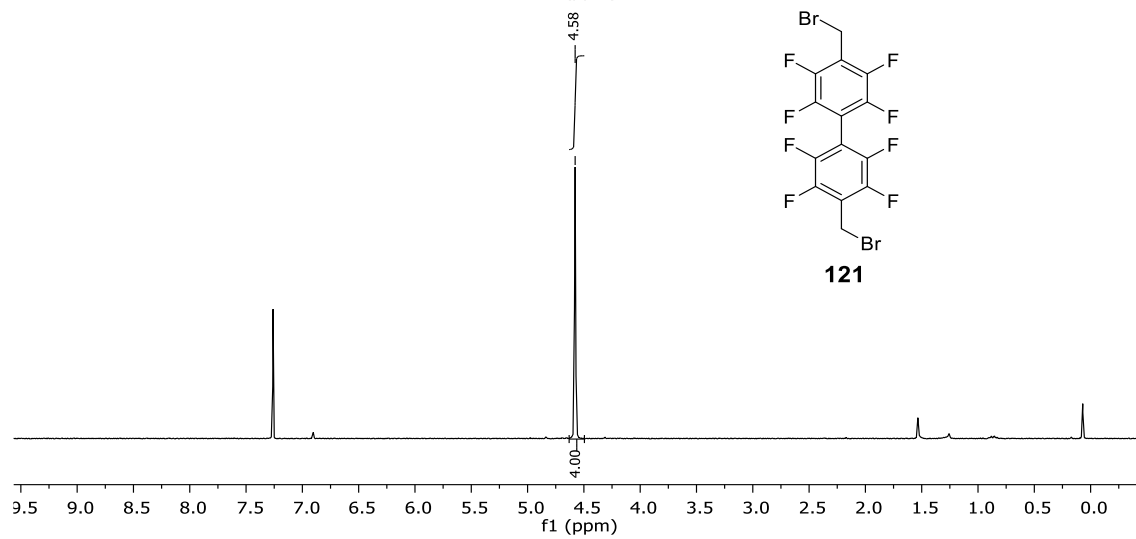
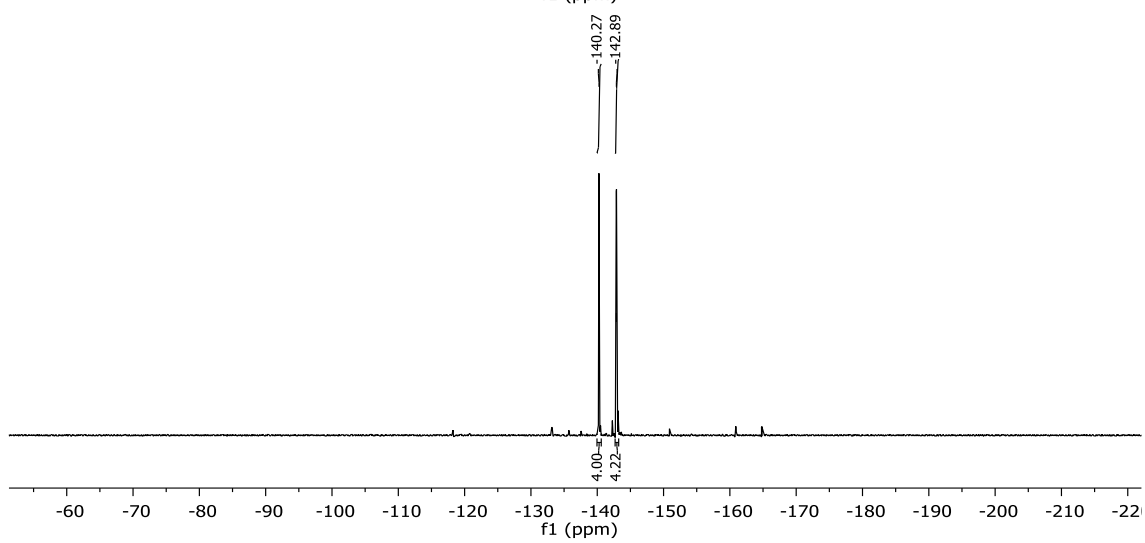
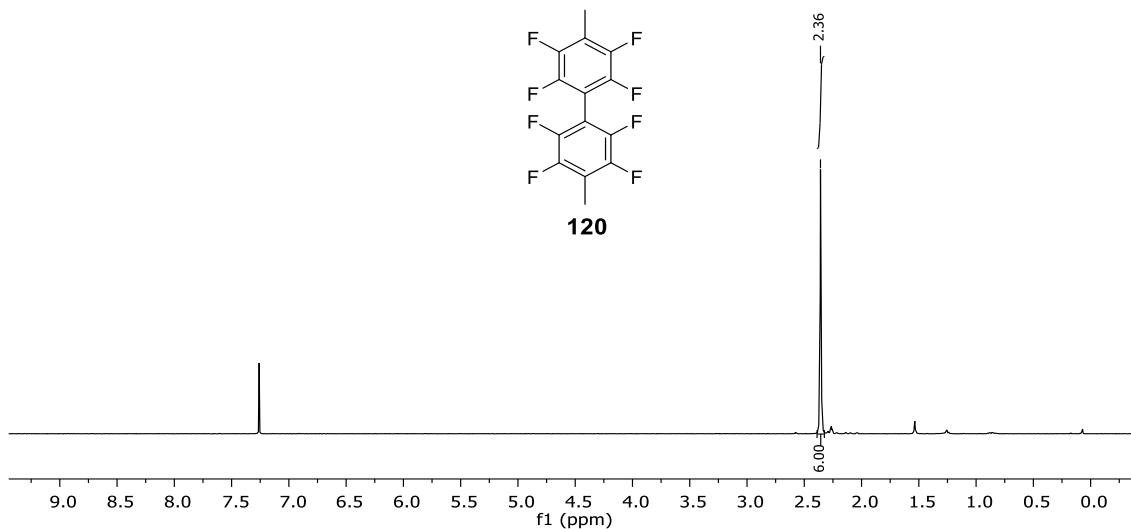


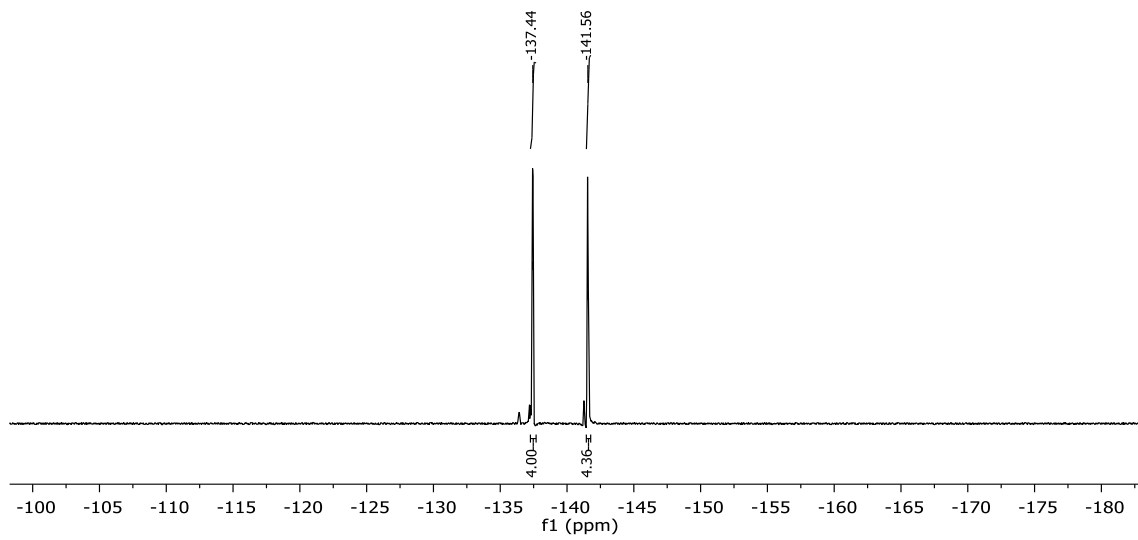






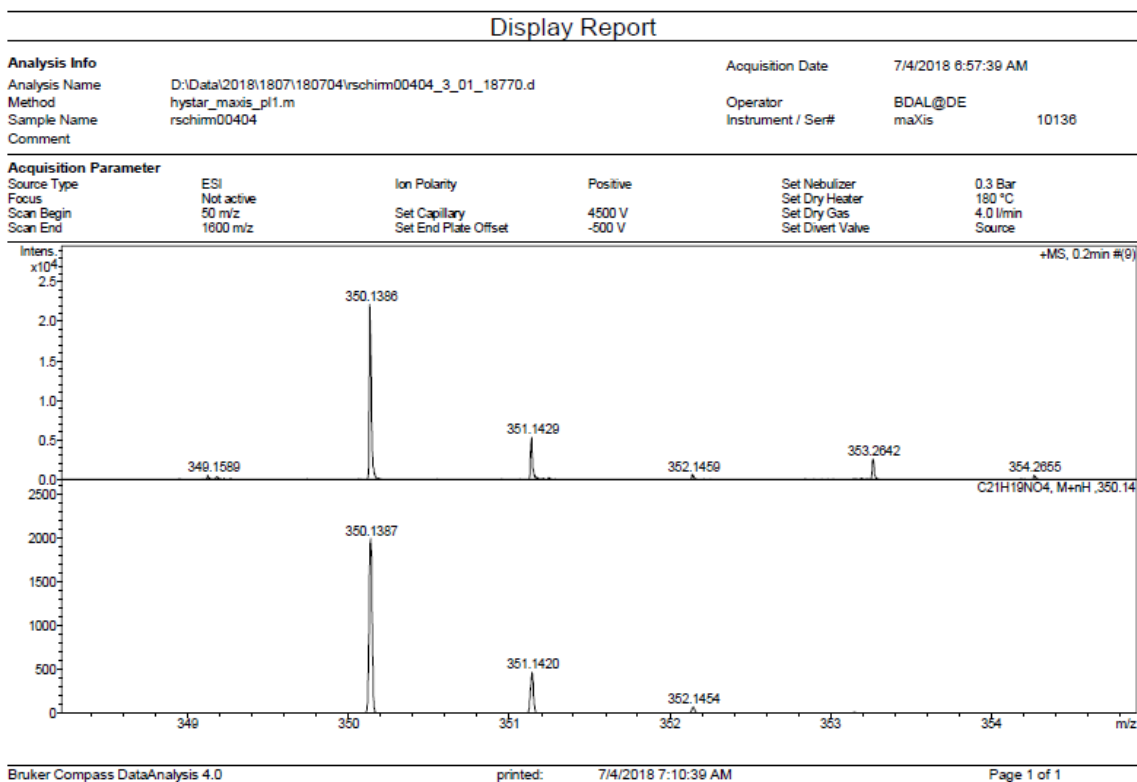




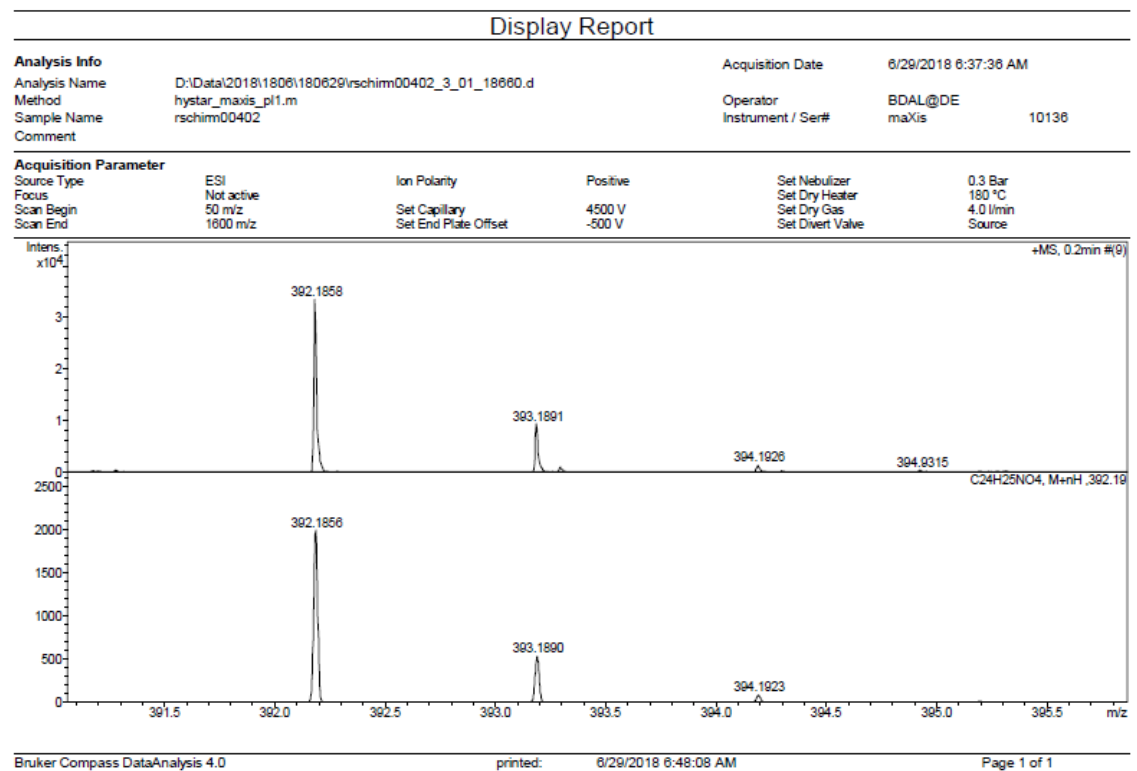


8.1.2 Mass spectra

1



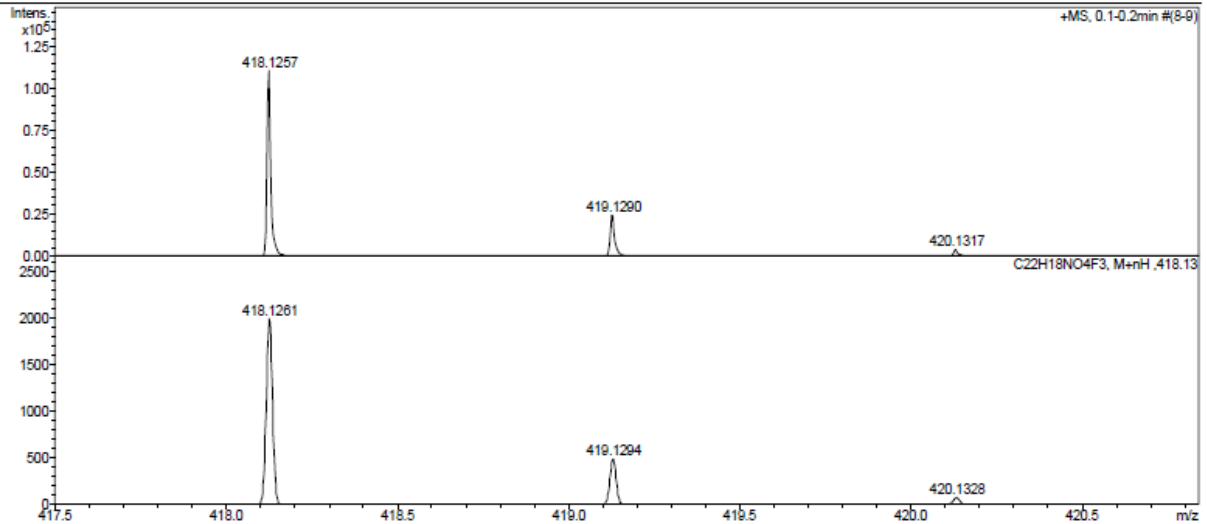
2



Display Report

Analysis Info		Acquisition Date	7/8/2018 9:02:44 AM	
Analysis Name	D:\Data\2018\1807\180706\rschim00410_7_01_18847.d	Operator	BDAL@DE	
Method	hystar_maxis_pl1.m	Instrument / Ser#	maXis 10136	
Sample Name	rschim00410	Comment		

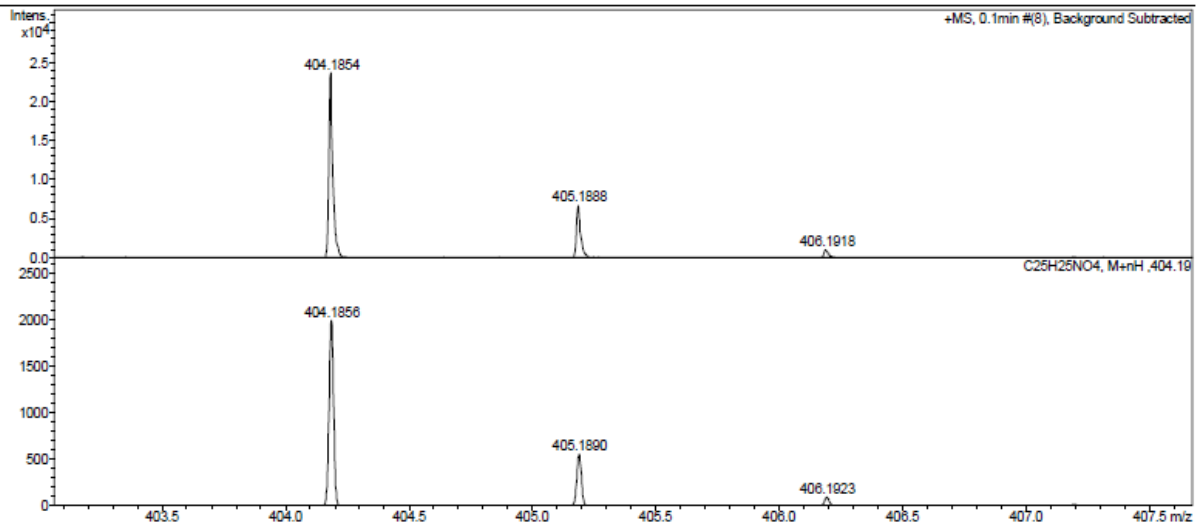
Acquisition Parameter					
Source Type	ESI	Ion Polarity	Positive	Set Nebulizer	0.3 Bar
Focus	Not active			Set Dry Heater	180 °C
Scan Begin	50 m/z	Set Capillary	4500 V	Set Dry Gas	4.0 l/min
Scan End	1600 m/z	Set End Plate Offset	-500 V	Set Divert Valve	Source



Display Report

Analysis Info		Acquisition Date	6/22/2018 7:31:17 AM	
Analysis Name	D:\Data\2018\1806\180622\rschim00399_5_01_18474.d	Operator	BDAL@DE	
Method	hystar_maxis_pl1.m	Instrument / Ser#	maXis 10136	
Sample Name	rschim00399	Comment		

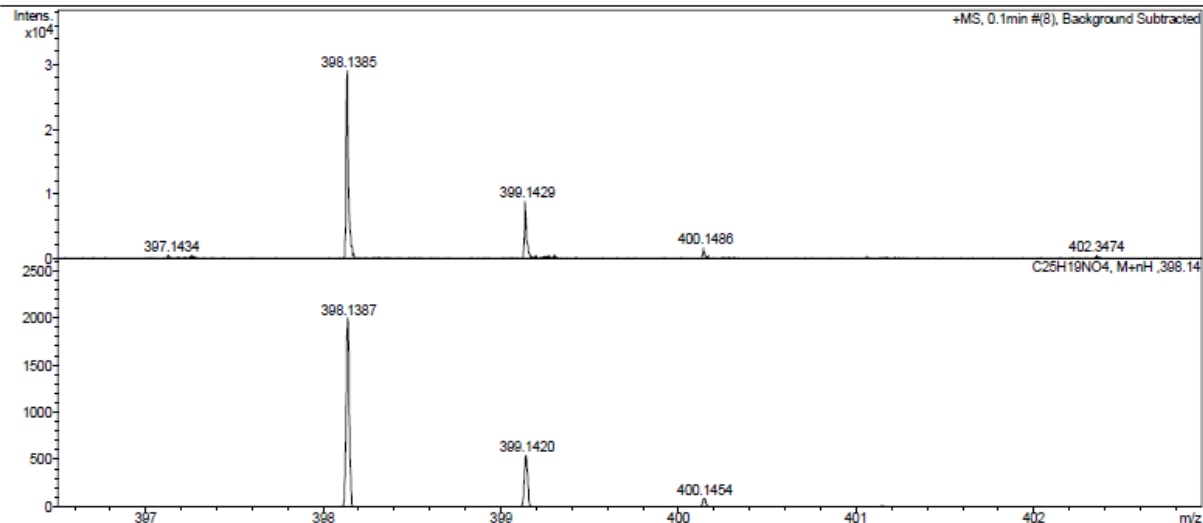
Acquisition Parameter					
Source Type	ESI	Ion Polarity	Positive	Set Nebulizer	0.3 Bar
Focus	Not active			Set Dry Heater	180 °C
Scan Begin	50 m/z	Set Capillary	4500 V	Set Dry Gas	4.0 l/min
Scan End	1600 m/z	Set End Plate Offset	-500 V	Set Divert Valve	Source



Display Report

Analysis Info		Acquisition Date	8/8/2018 9:50:25 AM
Analysis Name	D:\Data\2018\1808\180808\rschim00425_15_01_19739.d	Operator	BDAL@DE
Method	hystar_maxis_p11.m	Instrument / Ser#	maXis 10136
Sample Name	rschim00425		
Comment			

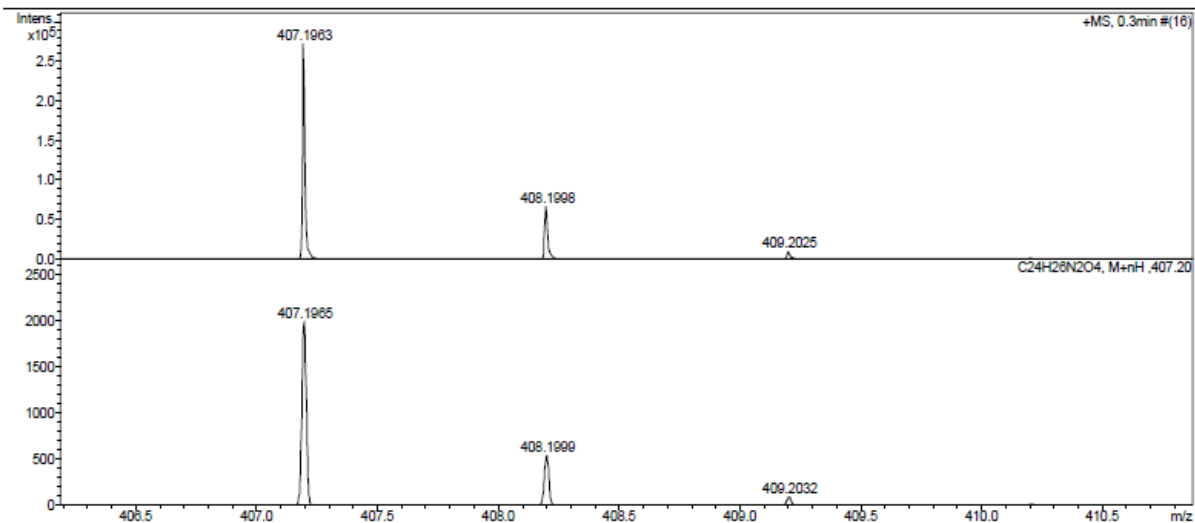
Acquisition Parameter					
Source Type	ESI	Ion Polarity	Positive	Set Nebulizer	0.3 Bar
Focus	Not active			Set Dry Heater	180 °C
Scan Begin	50 m/z	Set Capillary	4200 V	Set Dry Gas	4.0 l/min
Scan End	1600 m/z	Set End Plate Offset	-500 V	Set Divert Valve	Source



Display Report

Analysis Info		Acquisition Date	7/4/2018 8:02:30 AM
Analysis Name	D:\Data\2018\1807\180704\rschim00407_8_01_18775.d	Operator	BDAL@DE
Method	hystar_maxis_p11.m	Instrument / Ser#	maXis 10136
Sample Name	rschim00407		
Comment			

Acquisition Parameter					
Source Type	ESI	Ion Polarity	Positive	Set Nebulizer	0.3 Bar
Focus	Not active			Set Dry Heater	180 °C
Scan Begin	50 m/z	Set Capillary	4500 V	Set Dry Gas	4.0 l/min
Scan End	1600 m/z	Set End Plate Offset	-500 V	Set Divert Valve	Source

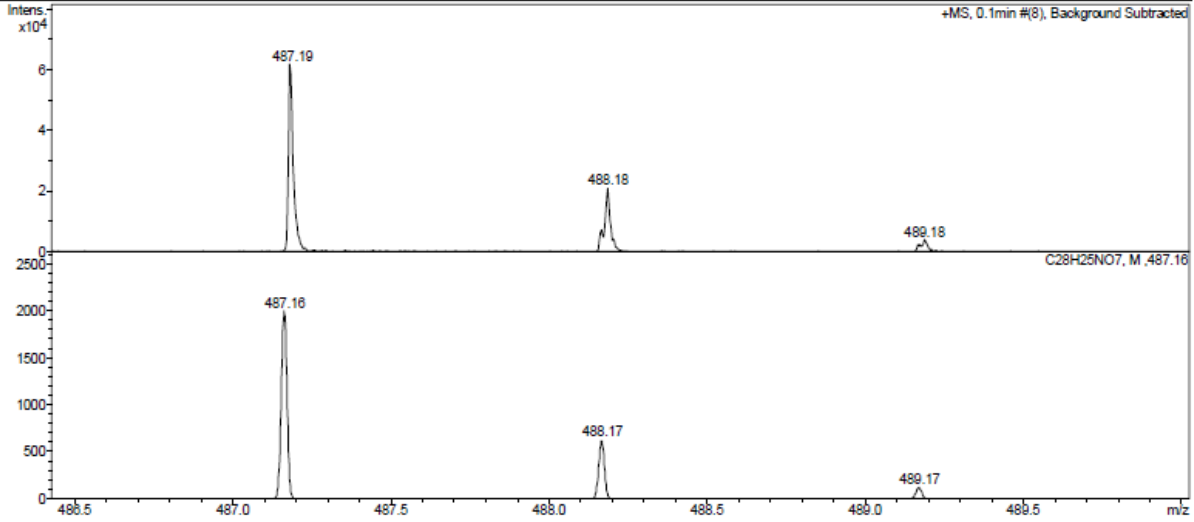


7

Display Report

Analysis Info
Analysis Name: D:\Data\2018\1808\180808\rschim00429_9_01_19730.d
Method: hystar_maxis_pl1.m
Sample Name: rschim00429
Comment:
Acquisition Date: 8/8/2018 8:07:12 AM
Operator: BDAL@DE
Instrument / Ser#: maXis 10138

Acquisition Parameter
Source Type: ESI
Focus: Not active
Scan Begin: 50 m/z
Scan End: 1600 m/z
Ion Polarity: Positive
Set Capillary: 4200 V
Set End Plate Offset: -500 V
Set Nebulizer: 0.3 Bar
Set Dry Heater: 180 °C
Set Dry Gas: 4.0 l/min
Set Divert Valve: Source

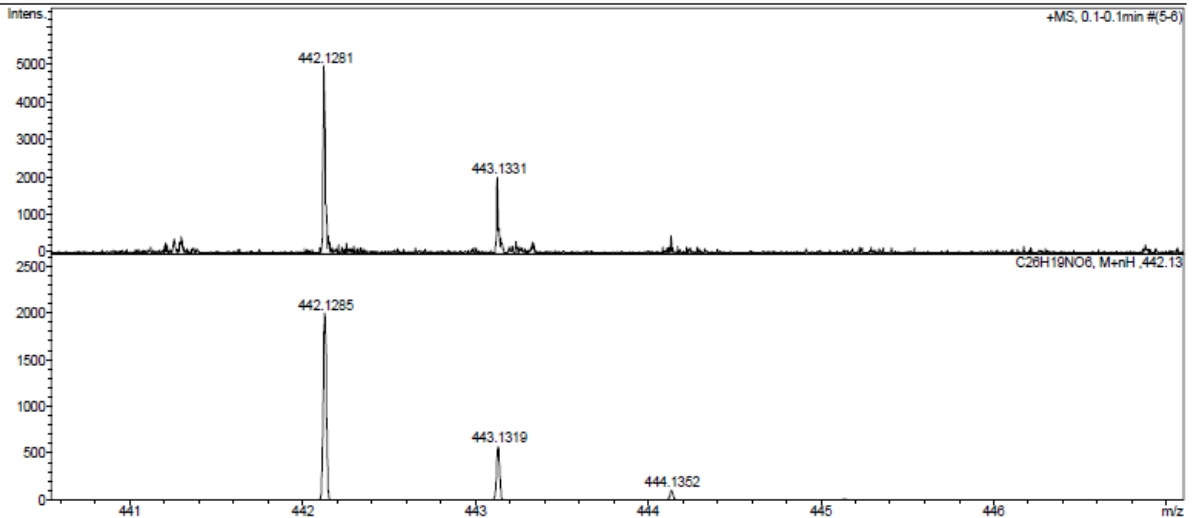


8

Display Report

Analysis Info
Analysis Name: D:\Data\2018\1808\180808\rschim00430_8_01_19729.d
Method: hystar_maxis_pl1.m
Sample Name: rschim00430
Comment:
Acquisition Date: 8/8/2018 8:03:06 AM
Operator: BDAL@DE
Instrument / Ser#: maXis 10138

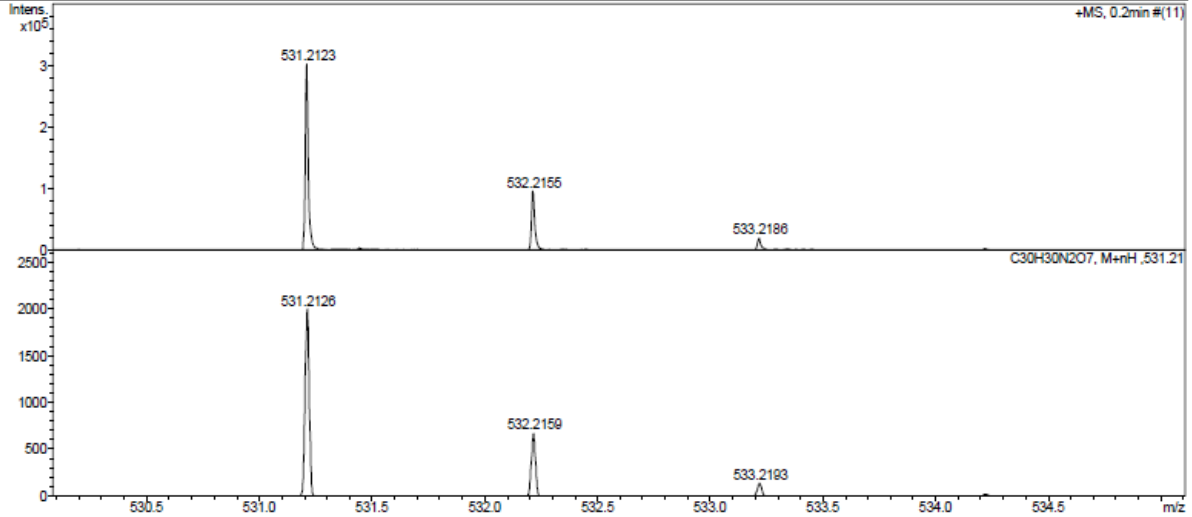
Acquisition Parameter
Source Type: ESI
Focus: Not active
Scan Begin: 50 m/z
Scan End: 1600 m/z
Ion Polarity: Positive
Set Capillary: 4200 V
Set End Plate Offset: -500 V
Set Nebulizer: 0.3 Bar
Set Dry Heater: 180 °C
Set Dry Gas: 4.0 l/min
Set Divert Valve: Source



Display Report

Analysis Info		Acquisition Date	7/25/2018 7:20:44 AM	
Analysis Name	D:\Data\2018\1807\180725\rschim00424_5_01_19341.d	Operator	BDAL@DE	
Method	hystar_maxis_p.m	Instrument / Ser#	maXis 10136	
Sample Name	rschim00424	Comment		

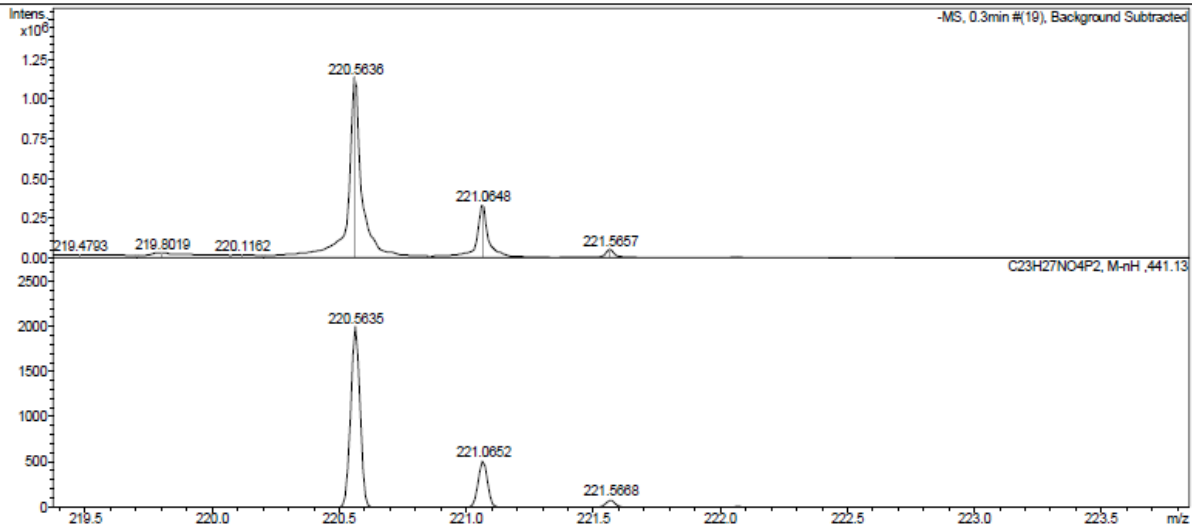
Acquisition Parameter					
Source Type	ESI	Ion Polarity	Positive	Set Nebulizer	0.3 Bar
Focus	Not active			Set Dry Heater	180 °C
Scan Begin	300 m/z	Set Capillary	4200 V	Set Dry Gas	4.0 l/min
Scan End	2900 m/z	Set End Plate Offset	-500 V	Set Divert Valve	Waste



Display Report

Analysis Info		Acquisition Date	21.11.2019 14:37:54	
Analysis Name	Z:\Data\2019\1911\191119\neg\rschim00574_9_01_108284.d	Operator	BDAL@DE	
Method	hystar_nLm	Instrument / Ser#	microTOF 10237	
Sample Name	rschim00574	Comment		

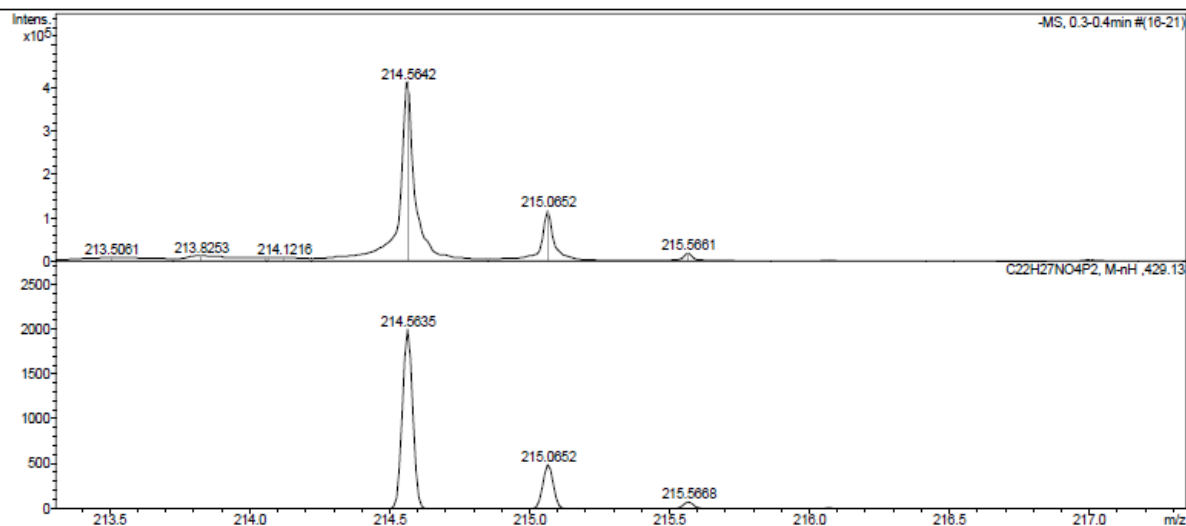
Acquisition Parameter					
Source Type	ESI	Ion Polarity	Negative	Set Nebulizer	1.6 Bar
Focus	Not active			Set Dry Heater	180 °C
Scan Begin	50 m/z	Set Capillary	3800 V	Set Dry Gas	8.0 l/min
Scan End	1600 m/z	Set End Plate Offset	-500 V	Set Divert Valve	Source



Display Report

Analysis Info		Acquisition Date	25.11.2019 08:58:04	
Analysis Name	Z:\Data\2019\1911\1sam251119\neg\rschirm00577_2_01_108307.d	Operator	BDAL@DE	
Method	hystar_n_lm	Instrument / Ser#	microTOF 10237	
Sample Name	rschirm00577	Comment		

Acquisition Parameter					
Source Type	ESI	Ion Polarity	Negative	Set Nebulizer	1.6 Bar
Focus	Not active	Set Capillary	3800 V	Set Dry Heater	180 °C
Scan Begin	50 m/z	Set End Plate Offset	-500 V	Set Dry Gas	8.0 l/min
Scan End	1600 m/z			Set Divert Valve	Source



Bruker Compass DataAnalysis 4.0

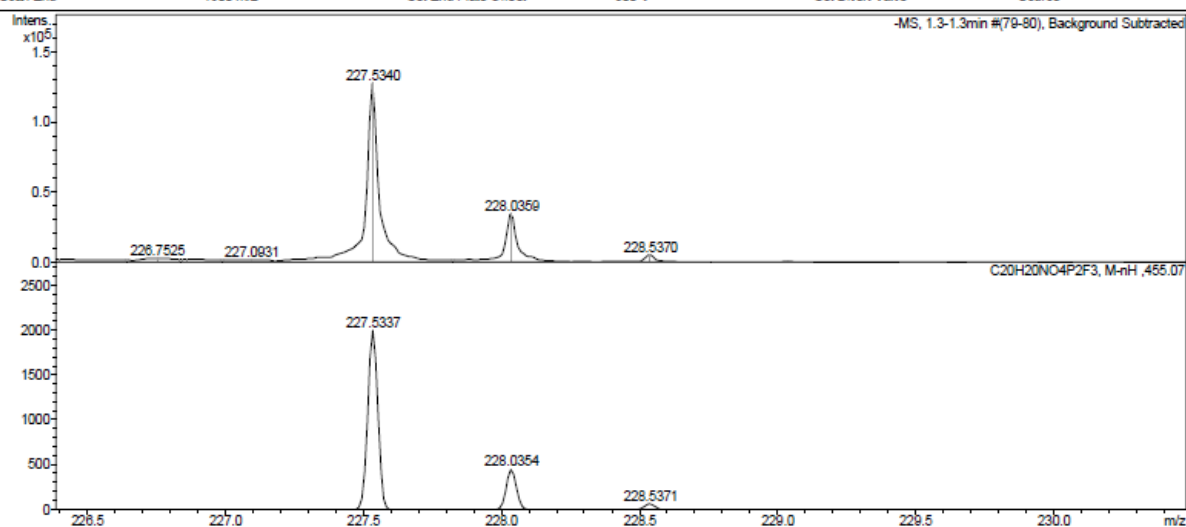
printed: 25.11.2019 09:55:43

Page 1 of 1

Display Report

Analysis Info		Acquisition Date	26.11.2019 07:30:07	
Analysis Name	Z:\Data\2019\1911\1sam261119\neg\rschirm00578_9_01_108323.d	Operator	BDAL@DE	
Method	hystar_n_lm	Instrument / Ser#	microTOF 10237	
Sample Name	rschirm00578	Comment		

Acquisition Parameter					
Source Type	ESI	Ion Polarity	Negative	Set Nebulizer	1.6 Bar
Focus	Not active	Set Capillary	3800 V	Set Dry Heater	180 °C
Scan Begin	50 m/z	Set End Plate Offset	-500 V	Set Dry Gas	8.0 l/min
Scan End	1600 m/z			Set Divert Valve	Source



Bruker Compass DataAnalysis 4.0

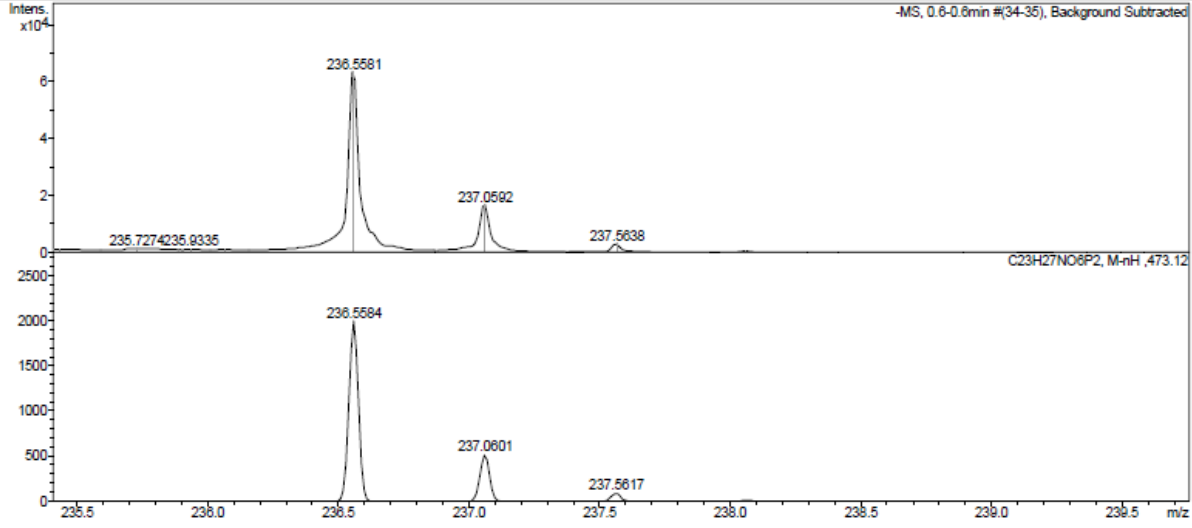
printed: 26.11.2019 07:08:06

Page 1 of 1

Display Report

Analysis Info		Acquisition Date	09.12.2019 06:57:02	
Analysis Name	Z:\Data\2019\1912\sam091219\neg\rschirm00579_1_01_108440.d	Operator	BDAL@DE	
Method	hystar_nLm	Instrument / Ser#	micrOTOF 10237	
Sample Name	rschirm00579	Comment		

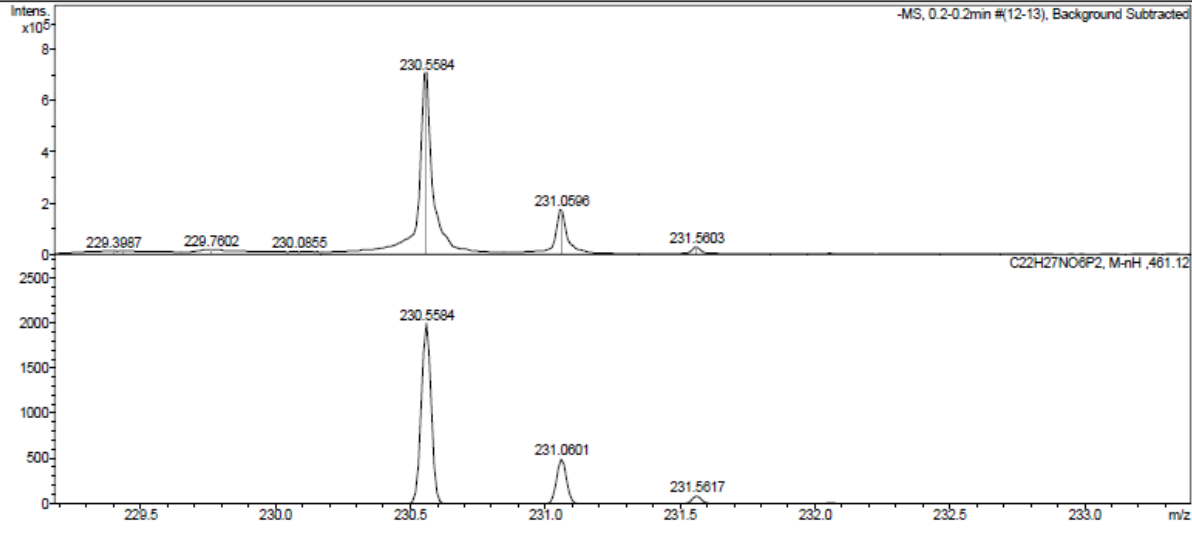
Acquisition Parameter					
Source Type	ESI	Ion Polarity	Negative	Set Nebulizer	1.6 Bar
Focus	Not active	Set Capillary	3800 V	Set Dry Heater	180 °C
Scan Begin	50 m/z	Set End Plate Offset	-500 V	Set Dry Gas	8.0 l/min
Scan End	1600 m/z			Set Divert Valve	Source



Display Report

Analysis Info		Acquisition Date	10.12.2019 14:13:55	
Analysis Name	Z:\Data\2019\1912\sam101219\neg\rschirm00580_29_01_108489.d	Operator	BDAL@DE	
Method	hystar_nLm	Instrument / Ser#	micrOTOF 10237	
Sample Name	rschirm00580	Comment		

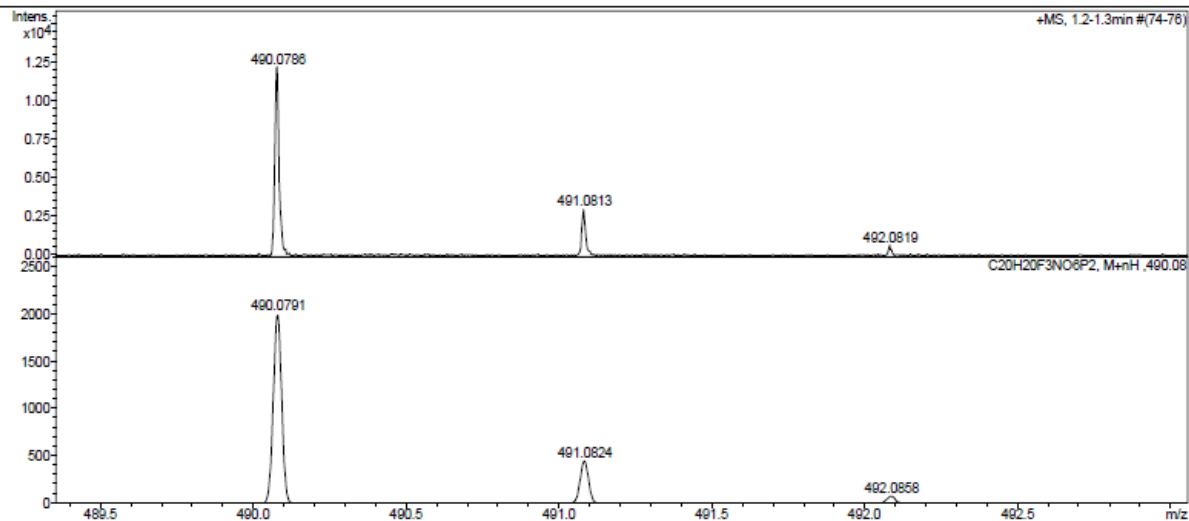
Acquisition Parameter					
Source Type	ESI	Ion Polarity	Negative	Set Nebulizer	1.6 Bar
Focus	Not active	Set Capillary	3800 V	Set Dry Heater	180 °C
Scan Begin	50 m/z	Set End Plate Offset	-500 V	Set Dry Gas	8.0 l/min
Scan End	1600 m/z			Set Divert Valve	Source



Display Report

Analysis Info		Acquisition Date	9/15/2020 11:15:10 AM	
Analysis Name	D:\Data\2020\2009\200915\rschim00613_20_01_30528.d	Operator	BDAL@DE	
Method	hystar_maxis_p.m	Instrument / Ser#	maXis	10136
Sample Name	rschim00613	Comment		

Acquisition Parameter					
Source Type	ESI	Ion Polarity	Positive	Set Nebulizer	0.3 Bar
Focus	Not active	Set Capillary	4200 V	Set Dry Heater	180 °C
Scan Begin	300 m/z	Set End Plate Offset	-500 V	Set Dry Gas	4.0 l/min
Scan End	2900 m/z			Set Divert Valve	Waste



Bruker Compass DataAnalysis 4.0

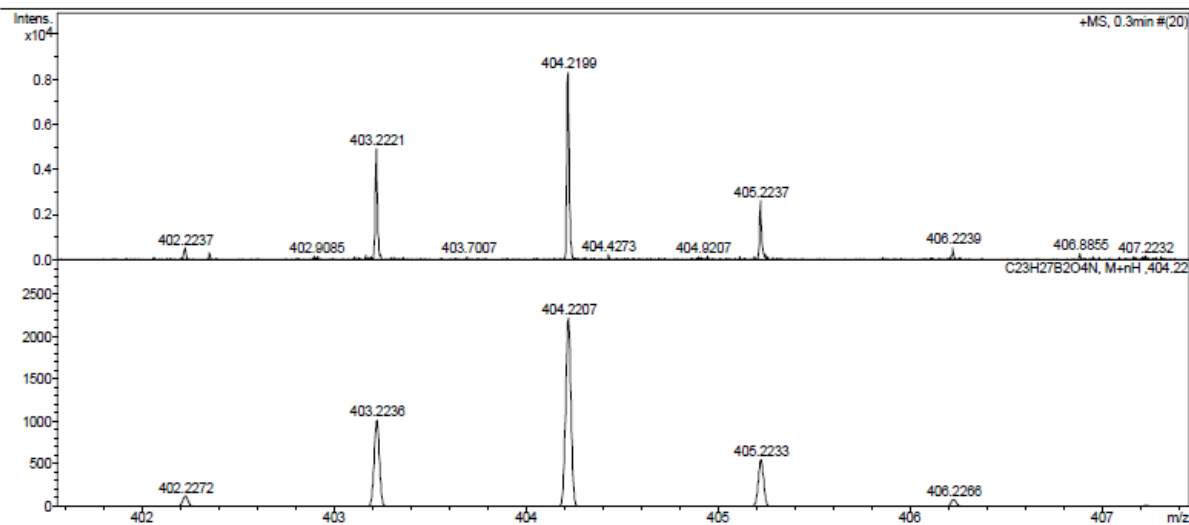
printed: 9/15/2020 11:22:18 AM

Page 1 of 1

Display Report

Analysis Info		Acquisition Date	9/15/2020 11:23:25 AM	
Analysis Name	D:\Data\2020\2009\200915\rschim00614_22_01_30530.d	Operator	BDAL@DE	
Method	hystar_maxis_p.m	Instrument / Ser#	maXis	10136
Sample Name	rschim00614	Comment		

Acquisition Parameter					
Source Type	ESI	Ion Polarity	Positive	Set Nebulizer	0.3 Bar
Focus	Not active	Set Dry Heater	180 °C	Set Dry Gas	4.0 l/min
Scan Begin	300 m/z	Set Divert Valve	Waste		



Bruker Compass DataAnalysis 4.0

printed: 9/15/2020 11:29:57 AM

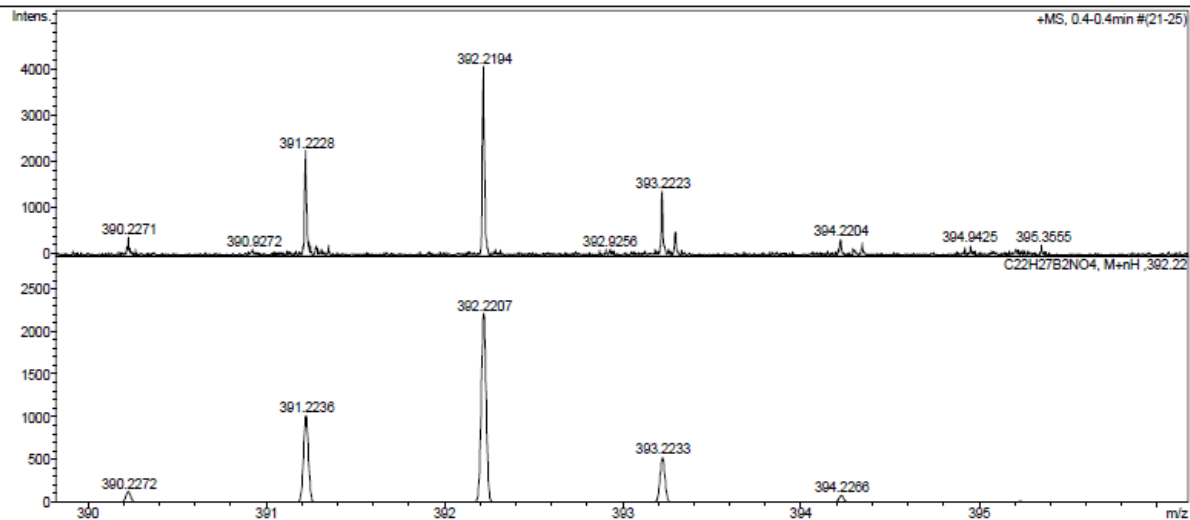
Page 1 of 1

Display Report

Analysis Info		Acquisition Date	9/15/2020 11:27:12 AM
Analysis Name	D:\Data\2020\2009\200915\rschim00615_23_01_30531.d	Operator	BDAL@DE
Method	hystar_maxis_p.m	Instrument / Ser#	maXis 10138
Sample Name	rschim00615		
Comment			

Acquisition Parameter

Source Type	ESI	Ion Polarity	Positive	Set Nebulizer	0.3 Bar
Focus	Not active			Set Dry Heater	180 °C
Scan Begin	300 m/z	Set Capillary	4200 V	Set Dry Gas	4.0 l/min
Scan End	2900 m/z	Set End Plate Offset	-500 V	Set Divert Valve	Waste



Bruker Compass DataAnalysis 4.0

printed: 9/15/2020 11:34:10 AM

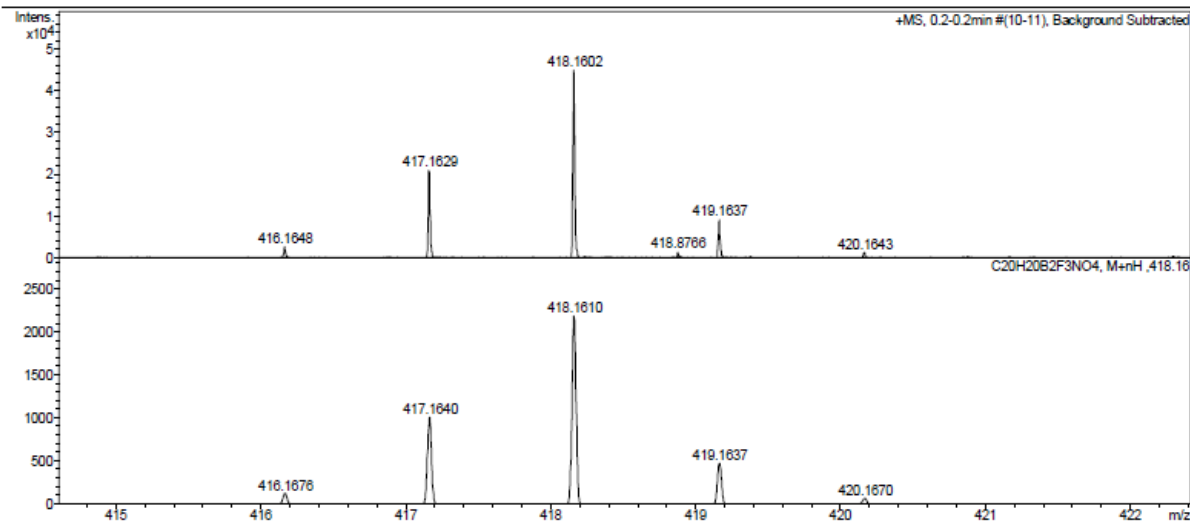
Page 1 of 1

Display Report

Analysis Info		Acquisition Date	9/15/2020 11:33:48 AM
Analysis Name	D:\Data\2020\2009\200915\rschim00616_24_01_30532.d	Operator	BDAL@DE
Method	hystar_maxis_p.m	Instrument / Ser#	maXis 10138
Sample Name	rschim00616		
Comment			

Acquisition Parameter

Source Type	ESI	Ion Polarity	Positive	Set Nebulizer	0.3 Bar
Focus	Not active			Set Dry Heater	180 °C
Scan Begin	300 m/z	Set Capillary	4200 V	Set Dry Gas	4.0 l/min
Scan End	2900 m/z	Set End Plate Offset	-500 V	Set Divert Valve	Waste



Bruker Compass DataAnalysis 4.0

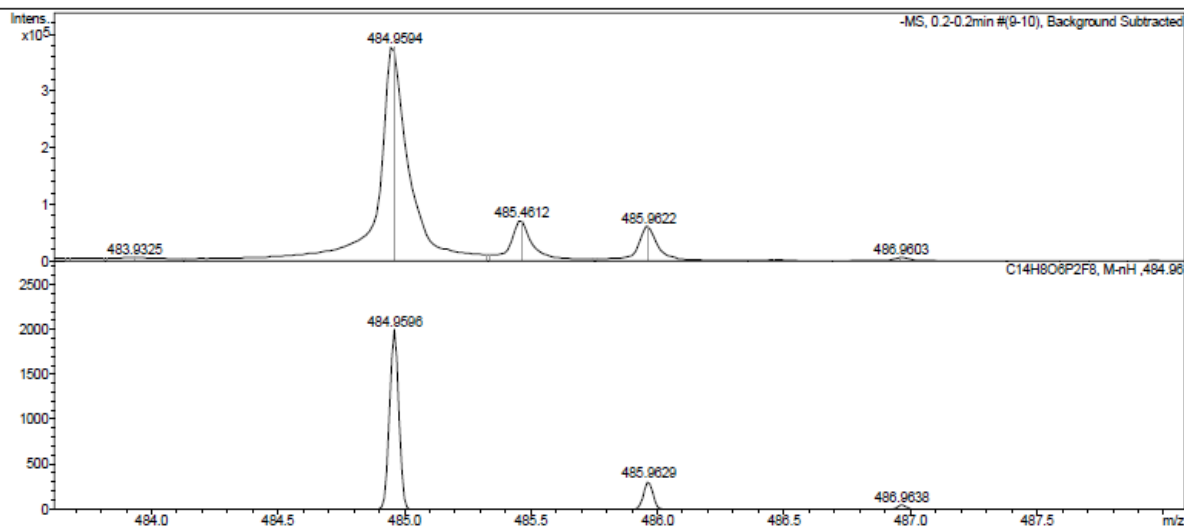
printed: 9/15/2020 11:37:50 AM

Page 1 of 1

Display Report

Analysis Info		Acquisition Date	25.09.2020 10:00:17
Analysis Name	Z:\Data\2020\2009\sam250920\neg\rschim00619_11_01_110020.d	Operator	BDAL@DE
Method	hystar_nlm	Instrument / Ser#	microTOF 10237
Sample Name	rschim00619		
Comment			

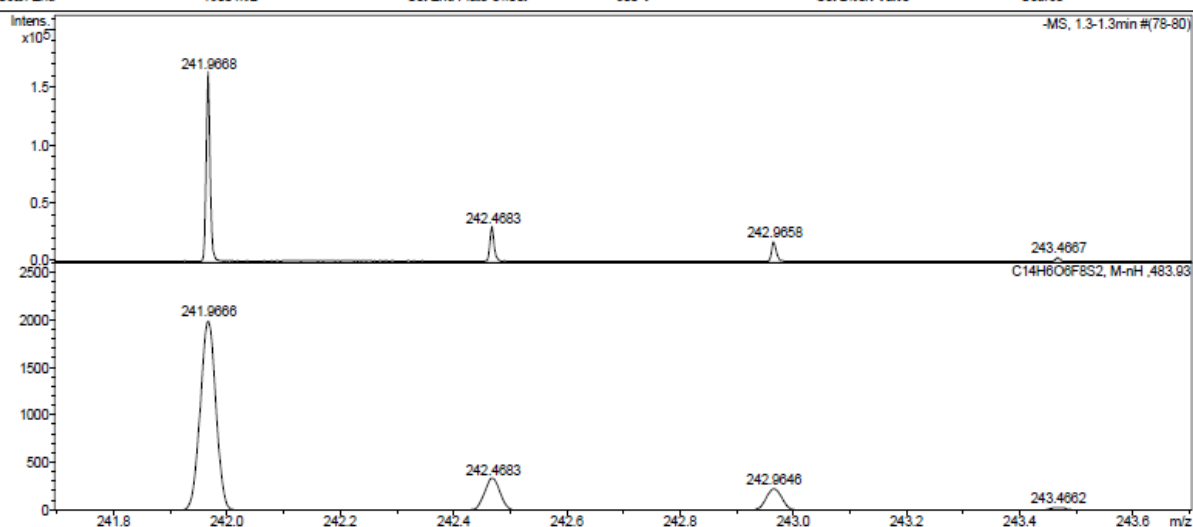
Acquisition Parameter					
Source Type	ESI	Ion Polarity	Negative	Set Nebulizer	1.8 Bar
Focus	Not active	Set Capillary	3900 V	Set Dry Heater	180 °C
Scan Begin	50 m/z	Set End Plate Offset	-500 V	Set Dry Gas	8.0 l/min
Scan End	1600 m/z			Set Divert Valve	Source



Display Report

Analysis Info		Acquisition Date	6/29/2020 11:57:37 AM
Analysis Name	D:\Data\2020\2006\200629\rschim00603_3_01_29360.d	Operator	BDAL@DE
Method	hystar_maxis_nlm	Instrument / Ser#	maXis 10136
Sample Name	rschim00603		
Comment			

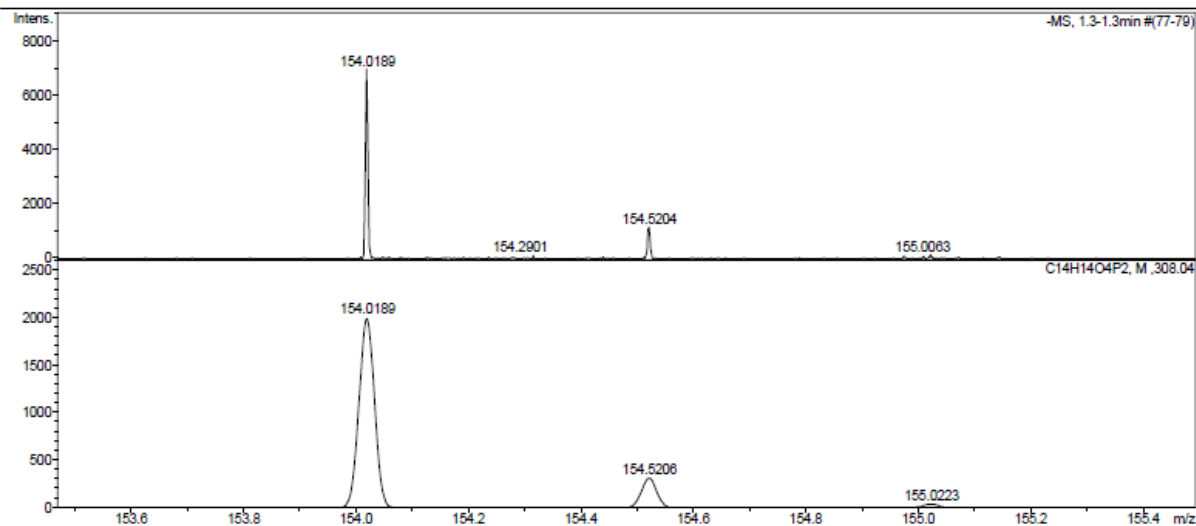
Acquisition Parameter					
Source Type	ESI	Ion Polarity	Negative	Set Nebulizer	0.3 Bar
Focus	Not active	Set Capillary	2600 V	Set Dry Heater	180 °C
Scan Begin	50 m/z	Set End Plate Offset	-500 V	Set Dry Gas	4.0 l/min
Scan End	1600 m/z			Set Divert Valve	Source



Display Report

Analysis Info		Acquisition Date	6/11/2020 1:37:29 PM	
Analysis Name	D:\Data\2020\2006\200611\rschim00601_37_01_29106.d	Operator	BDAL@DE	
Method	hystar_maxis_ni.m	Instrument / Ser#	maXis 10136	
Sample Name	rschim00601	Comment		

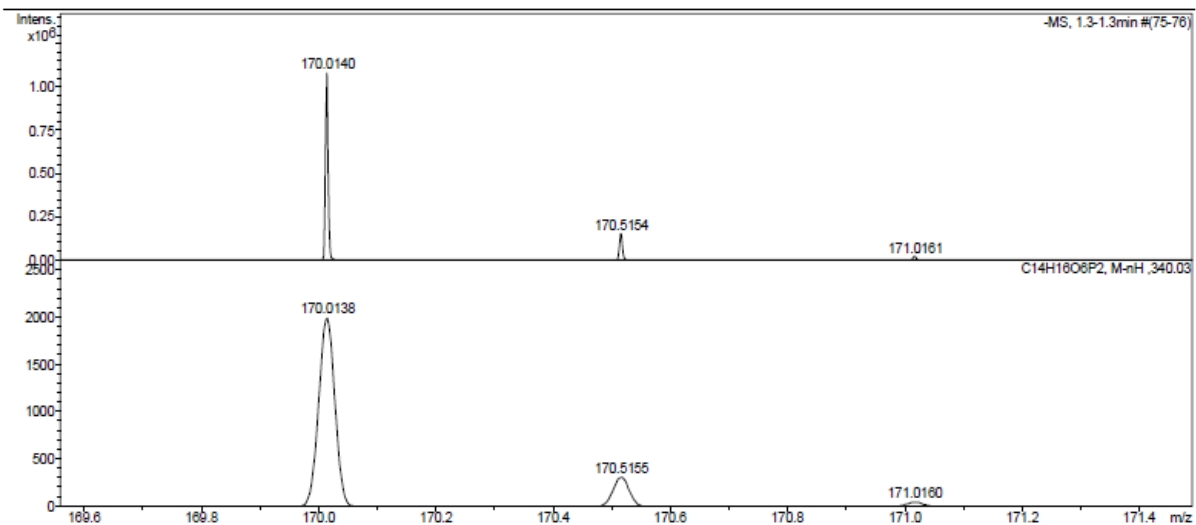
Acquisition Parameter					
Source Type	ESI	Ion Polarity	Negative	Set Nebulizer	0.3 Bar
Focus	Not active	Set Capillary	2600 V	Set Dry Heater	180 °C
Scan Begin	50 m/z	Set End Plate Offset	-500 V	Set Dry Gas	4.0 l/min
Scan End	1600 m/z			Set Divert Valve	Source



Display Report

Analysis Info		Acquisition Date	5/25/2020 4:13:36 PM	
Analysis Name	D:\Data\2020\2005\200525\rschim00595_29_01_28732.d	Operator	BDAL@DE	
Method	hystar_maxis_ni.m	Instrument / Ser#	maXis 10136	
Sample Name	rschim00595	Comment		

Acquisition Parameter					
Source Type	ESI	Ion Polarity	Negative	Set Nebulizer	0.3 Bar
Focus	Not active	Set Capillary	2600 V	Set Dry Heater	180 °C
Scan Begin	50 m/z	Set End Plate Offset	-500 V	Set Dry Gas	4.0 l/min
Scan End	1600 m/z			Set Divert Valve	Source

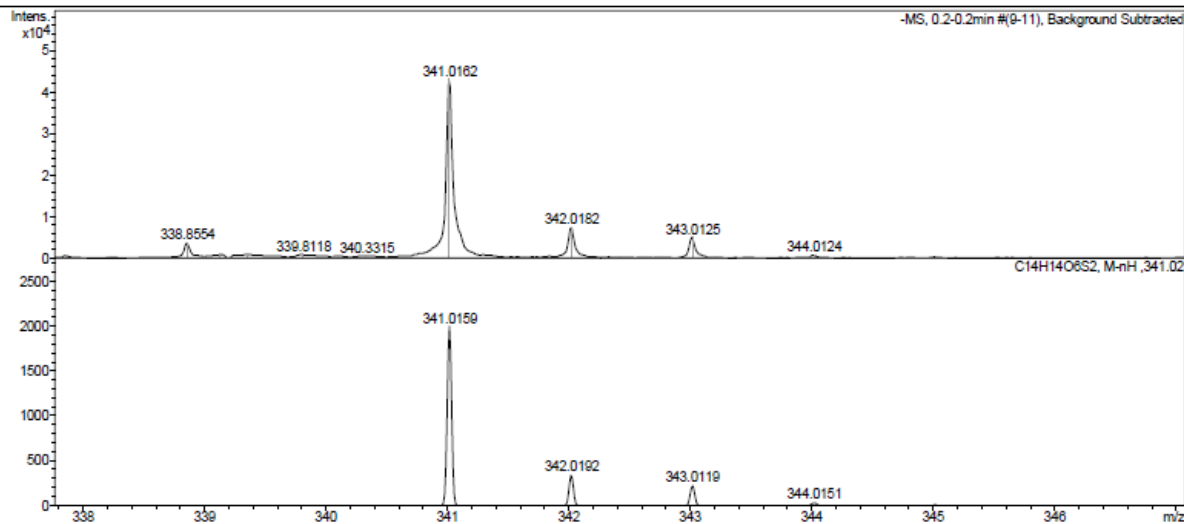


Display Report

Analysis Info		Acquisition Date	20.05.2020 09:51:45	
Analysis Name	Z:\Data\2020\2005\sam200520\neg\rschirm00594_18_01_109380.d	Operator	BDAL@DE	
Method	hystar_n1.m	Instrument / Ser#	micrOTOF 10237	
Sample Name	rschirm00594	Comment		

Acquisition Parameter

Source Type	ESI	Ion Polarity	Negative	Set Nebulizer	1.8 Bar
Focus	Not active	Set Capillary	3800 V	Set Dry Heater	180 °C
Scan Begin	50 m/z	Set End Plate Offset	-500 V	Set Dry Gas	8.0 l/min
Scan End	1600 m/z			Set Divert Valve	Source



Bruker Compass DataAnalysis 4.0

printed: 20.05.2020 10:32:21

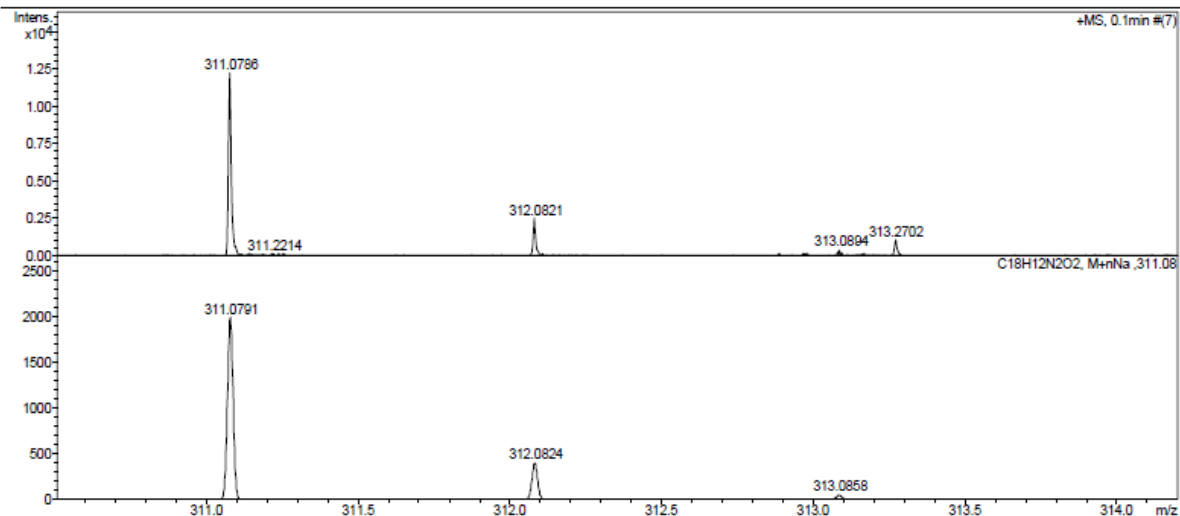
Page 1 of 1

Display Report

Analysis Info		Acquisition Date	7/6/2018 8:40:28 AM	
Analysis Name	D:\Data\2018\1807\180706\rschirm00413_4_01_18844.d	Operator	BDAL@DE	
Method	hystar_maxis_pl1.m	Instrument / Ser#	maXis 10136	
Sample Name	rschirm00413	Comment		

Acquisition Parameter

Source Type	ESI	Ion Polarity	Positive	Set Nebulizer	0.3 Bar
Focus	Not active	Set Capillary	4500 V	Set Dry Heater	180 °C
Scan Begin	50 m/z	Set End Plate Offset	-500 V	Set Dry Gas	4.0 l/min
Scan End	1600 m/z			Set Divert Valve	Source



Bruker Compass DataAnalysis 4.0

printed: 7/6/2018 8:46:35 AM

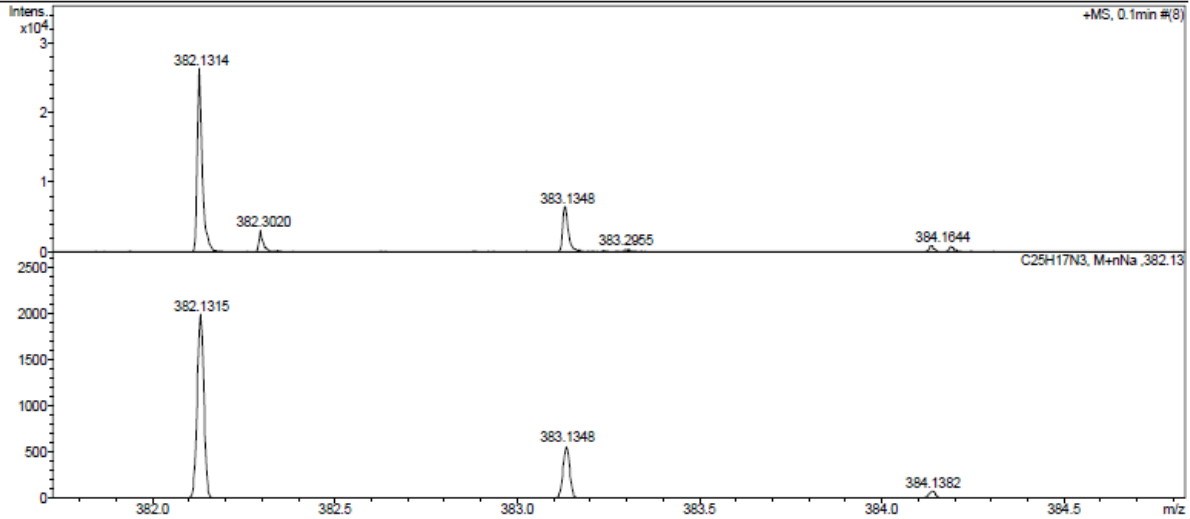
Page 1 of 1

35a / 43

Display Report

Analysis Info		Acquisition Date	6/26/2018 7:50:42 AM
Analysis Name	D:\Data\2018\1806\180626\rschim00400_4_01_18575.d	Operator	BDAL@DE
Method	hystar_maxis_pl1.m	Instrument / Ser#	maXis 10136
Sample Name	rschim00400		
Comment			

Acquisition Parameter		Ion Polarity	Positive	Set Nebulizer	0.3 Bar
Source Type	ESI	Set Capillary	4500 V	Set Dry Heater	180 °C
Focus	Not active	Set End Plate Offset	-500 V	Set Dry Gas	4.0 l/min
Scan Begin	50 m/z			Set Divert Valve	Source
Scan End	1600 m/z				

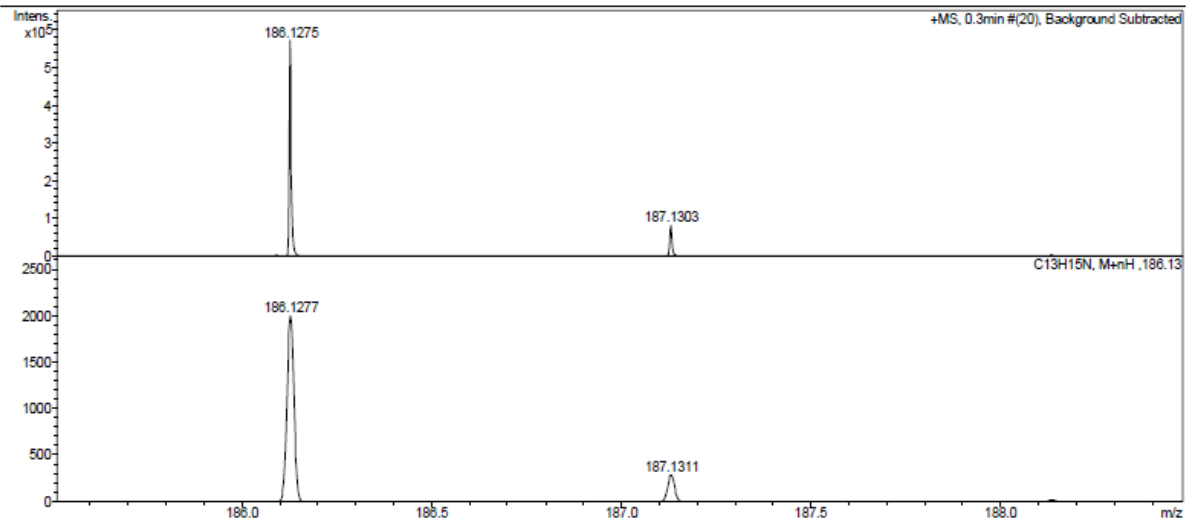


36a

Display Report

Analysis Info		Acquisition Date	9/17/2018 11:55:33 AM
Analysis Name	D:\Data\2018\1809\180917\rschim00445_12_01_20484.d	Operator	BDAL@DE
Method	hystar_maxis_pl1.m	Instrument / Ser#	maXis 10136
Sample Name	rschim00445		
Comment			

Acquisition Parameter		Ion Polarity	Positive	Set Nebulizer	0.3 Bar
Source Type	ESI	Set Capillary	4200 V	Set Dry Heater	180 °C
Focus	Not active	Set End Plate Offset	-500 V	Set Dry Gas	4.0 l/min
Scan Begin	50 m/z			Set Divert Valve	Source
Scan End	1600 m/z				

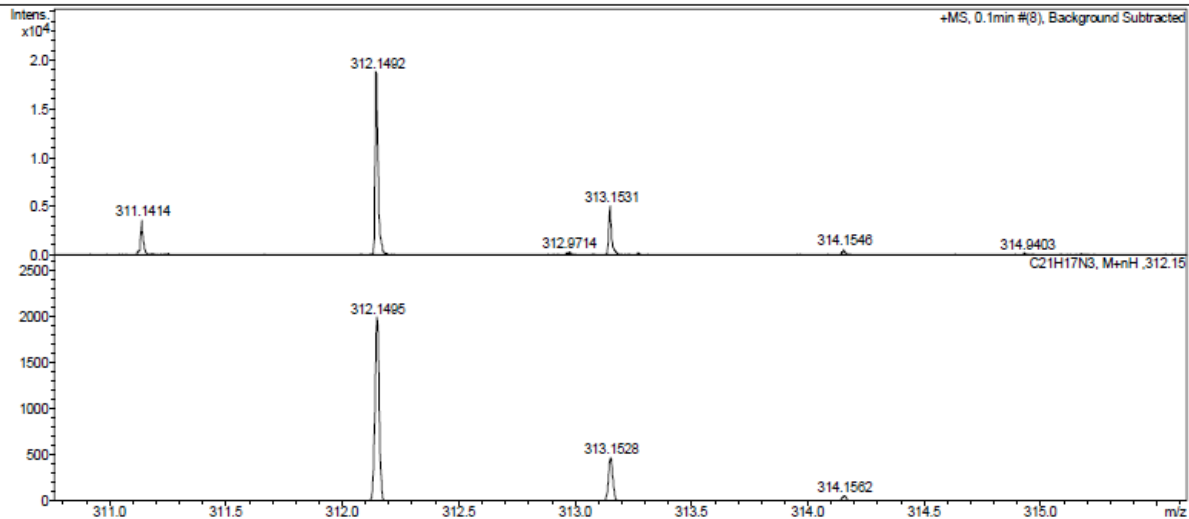


35b / 39

Display Report

Analysis Info
Analysis Name: D:\Data\2018\1806\180615\rschim00391_2_01_18292.d
Method: hystar_maxis_pl1.m
Sample Name: rschim00391
Comment:
Acquisition Date: 6/15/2018 8:25:01 AM
Operator: BDAL@DE
Instrument / Ser#: maXis 10136

Acquisition Parameter
Source Type: ESI
Focus: Not active
Scan Begin: 50 m/z
Scan End: 1600 m/z
Ion Polarity: Positive
Set Capillary: 4500 V
Set End Plate Offset: -500 V
Set Nebulizer: 0.3 Bar
Set Dry Heater: 180 °C
Set Dry Gas: 4.0 l/min
Set Divert Valve: Source

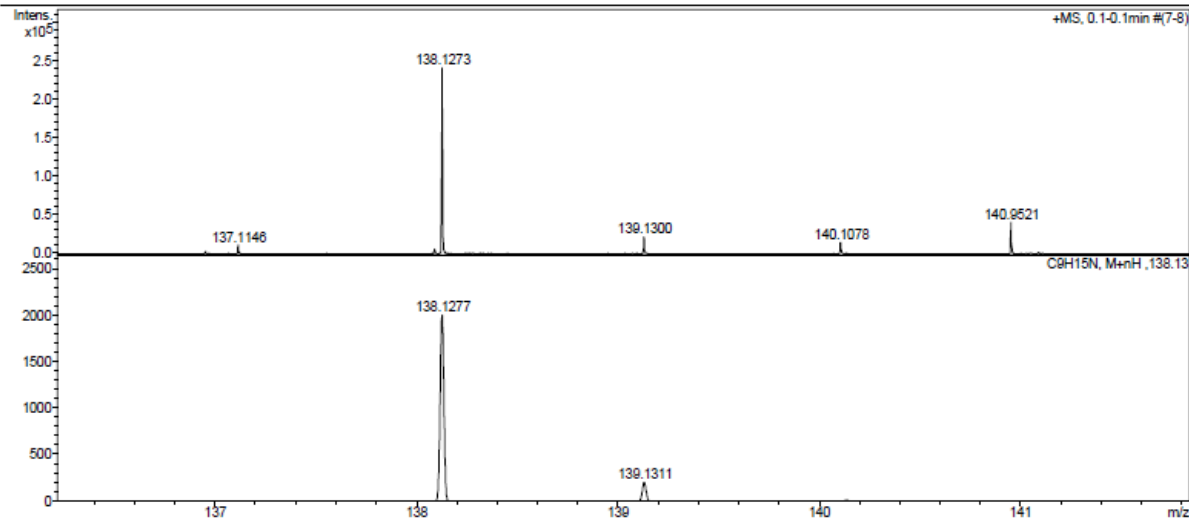


36b

Display Report

Analysis Info
Analysis Name: D:\Data\2018\1809\180917\rschim00440_10_01_20462.d
Method: hystar_maxis_pl1.m
Sample Name: rschim00440
Comment:
Acquisition Date: 9/17/2018 11:47:35 AM
Operator: BDAL@DE
Instrument / Ser#: maXis 10136

Acquisition Parameter
Source Type: ESI
Focus: Not active
Scan Begin: 50 m/z
Scan End: 1600 m/z
Ion Polarity: Positive
Set Capillary: 4200 V
Set End Plate Offset: -500 V
Set Nebulizer: 0.3 Bar
Set Dry Heater: 180 °C
Set Dry Gas: 4.0 l/min
Set Divert Valve: Source

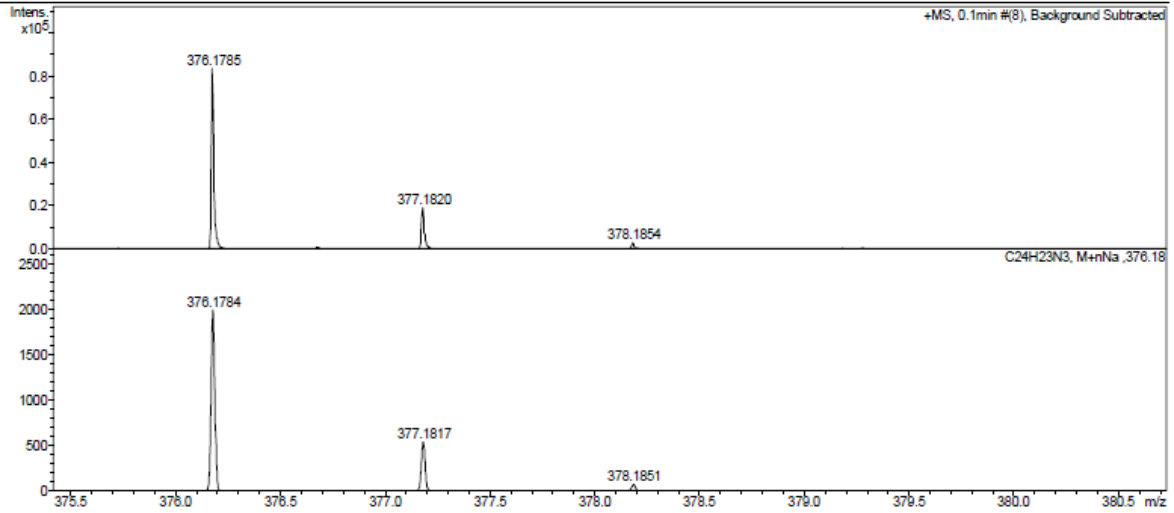


35c / 40

Display Report

Analysis Info		Acquisition Date	6/11/2018 7:48:22 AM
Analysis Name	D:\Data\2018\1806\180611\rschim00387_6_01_18126.d	Operator	BDAL@DE
Method	hystar_maxis_pl1.m	Instrument / Ser#	maXis 10136
Sample Name	rschim00387		
Comment			

Acquisition Parameter		Ion Polarity	Positive	Set Nebulizer	0.3 Bar
Source Type	ESI	Set Capillary	4500 V	Set Dry Heater	180 °C
Focus	Not active	Set End Plate Offset	-500 V	Set Dry Gas	4.0 l/min
Scan Begin	50 m/z			Set Divert Valve	Source
Scan End	1600 m/z				



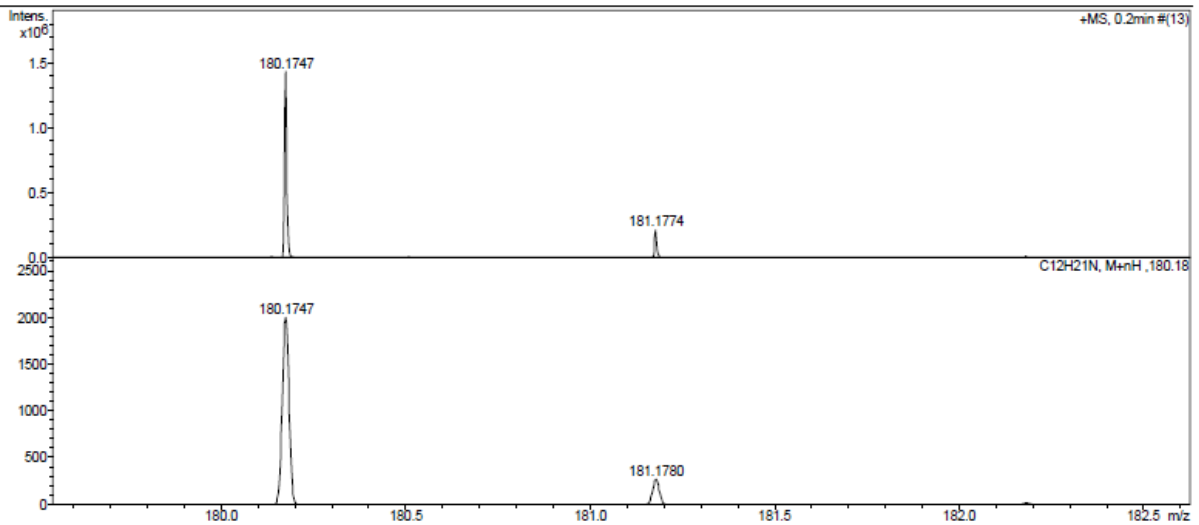
Bruker Compass DataAnalysis 4.0 printed: 6/11/2018 7:56:23 AM Page 1 of 1

36c

Display Report

Analysis Info		Acquisition Date	9/17/2018 11:38:42 AM
Analysis Name	D:\Data\2018\1809\180917\rschim00442_8_01_20460.d	Operator	BDAL@DE
Method	hystar_maxis_pl1.m	Instrument / Ser#	maXis 10136
Sample Name	rschim00442		
Comment			

Acquisition Parameter		Ion Polarity	Positive	Set Nebulizer	0.3 Bar
Source Type	ESI	Set Capillary	4200 V	Set Dry Heater	180 °C
Focus	Not active	Set End Plate Offset	-500 V	Set Dry Gas	4.0 l/min
Scan Begin	50 m/z			Set Divert Valve	Source
Scan End	1600 m/z				



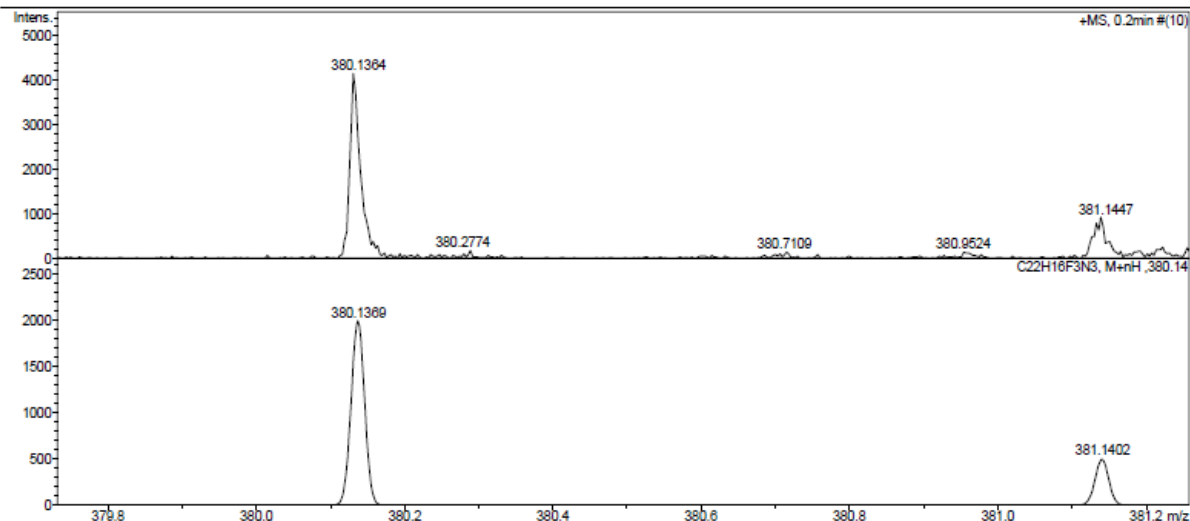
Bruker Compass DataAnalysis 4.0 printed: 9/17/2018 11:43:53 AM Page 1 of 1

35d / 41

Display Report

Analysis Info		Acquisition Date	6/12/2018 7:59:33 AM
Analysis Name	D:\Data\2018\1806\180612\rschim00389_1_01_18164.d	Operator	BDAL@DE
Method	hystar_maxis_pl1.m	Instrument / Ser#	maXis 10138
Sample Name	rschim00389		
Comment			

Acquisition Parameter		Ion Polarity	Positive	Set Nebulizer	0.3 Bar
Source Type	ESI			Set Dry Heater	180 °C
Focus	Not active			Set Dry Gas	4.0 l/min
Scan Begin	50 m/z	Set Capillary	4500 V	Set Divert Valve	Source
Scan End	1600 m/z	Set End Plate Offset	-500 V		

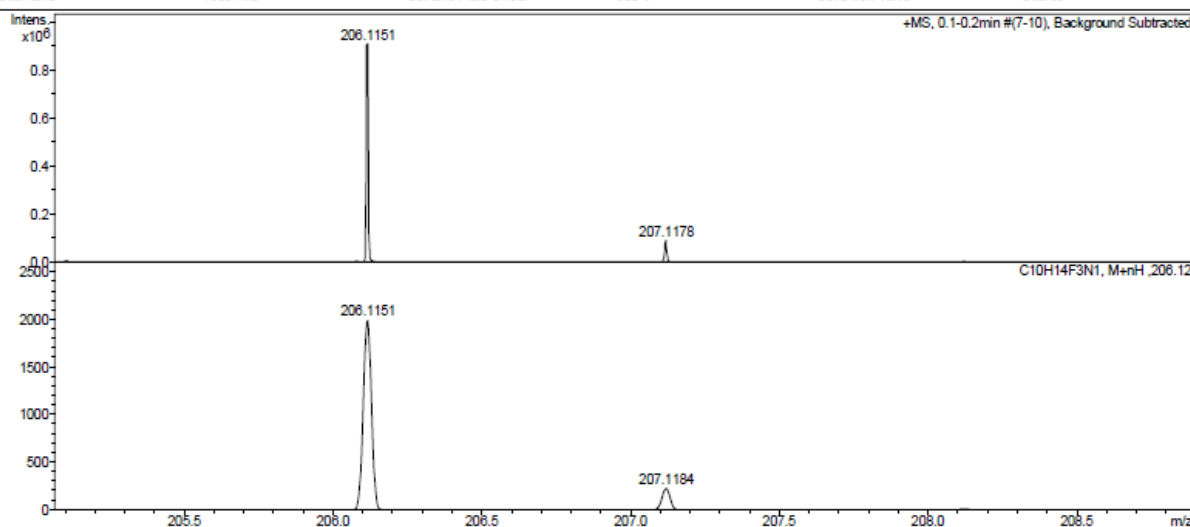


36d

Display Report

Analysis Info		Acquisition Date	8/4/2020 7:33:35 AM
Analysis Name	D:\Data\2020\2008\200804\rschim00609_3_01_29938.d	Operator	BDAL@DE
Method	hystar_maxis_pl1.m	Instrument / Ser#	maXis 10138
Sample Name	rschim00609		
Comment			

Acquisition Parameter		Ion Polarity	Positive	Set Nebulizer	0.3 Bar
Source Type	ESI			Set Dry Heater	180 °C
Focus	Not active			Set Dry Gas	4.0 l/min
Scan Begin	50 m/z	Set Capillary	4200 V	Set Divert Valve	Source
Scan End	1600 m/z	Set End Plate Offset	-500 V		

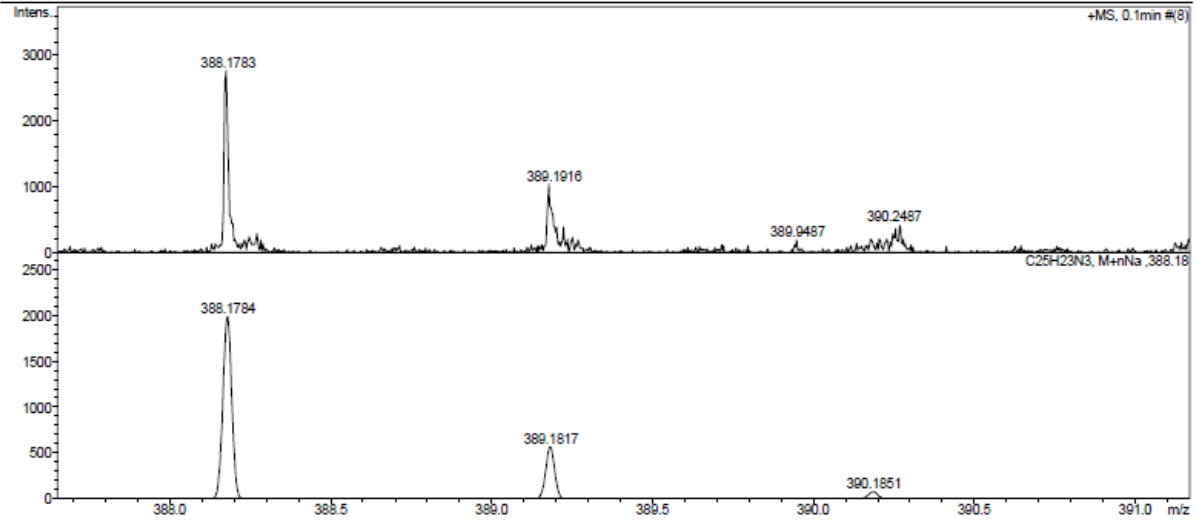


35e / 42

Display Report

Analysis Info		Acquisition Date	5/16/2018 8:10:02 AM
Analysis Name	D:\Data\2018\1805\180516\rschim00173_1_01_17579.d	Operator	BDAL@DE
Method	hystar_maxis_pl1.m	Instrument / Ser#	maXis 10138
Sample Name	rschim00173		
Comment			

Acquisition Parameter					
Source Type	ESI	Ion Polarity	Positive	Set Nebulizer	0.3 Bar
Focus	Not active			Set Dry Heater	180 °C
Scan Begin	50 m/z	Set Capillary	4500 V	Set Dry Gas	4.0 l/min
Scan End	1800 m/z	Set End Plate Offset	-500 V	Set Divert Valve	Source

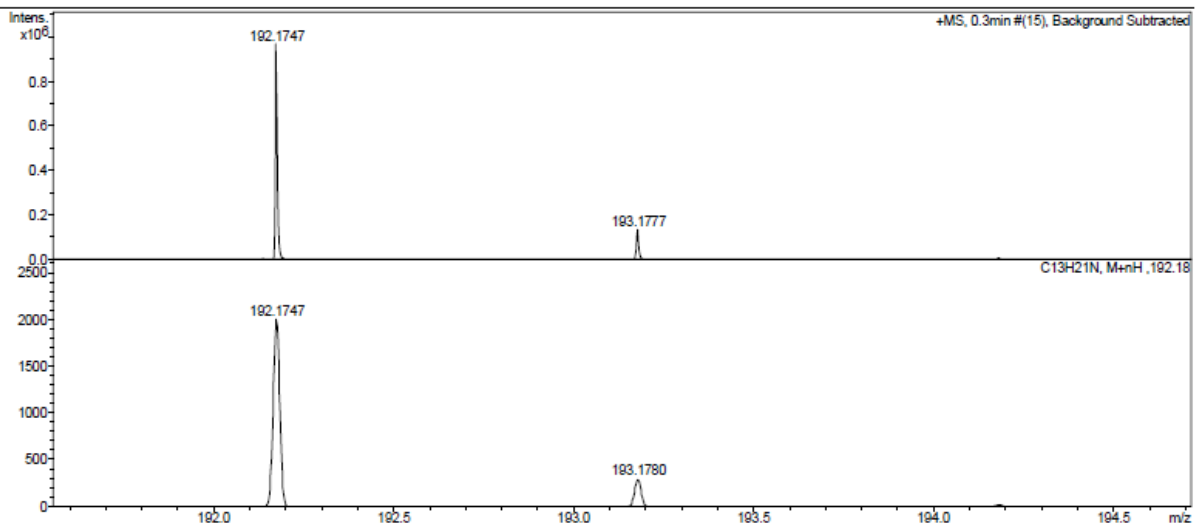


36e

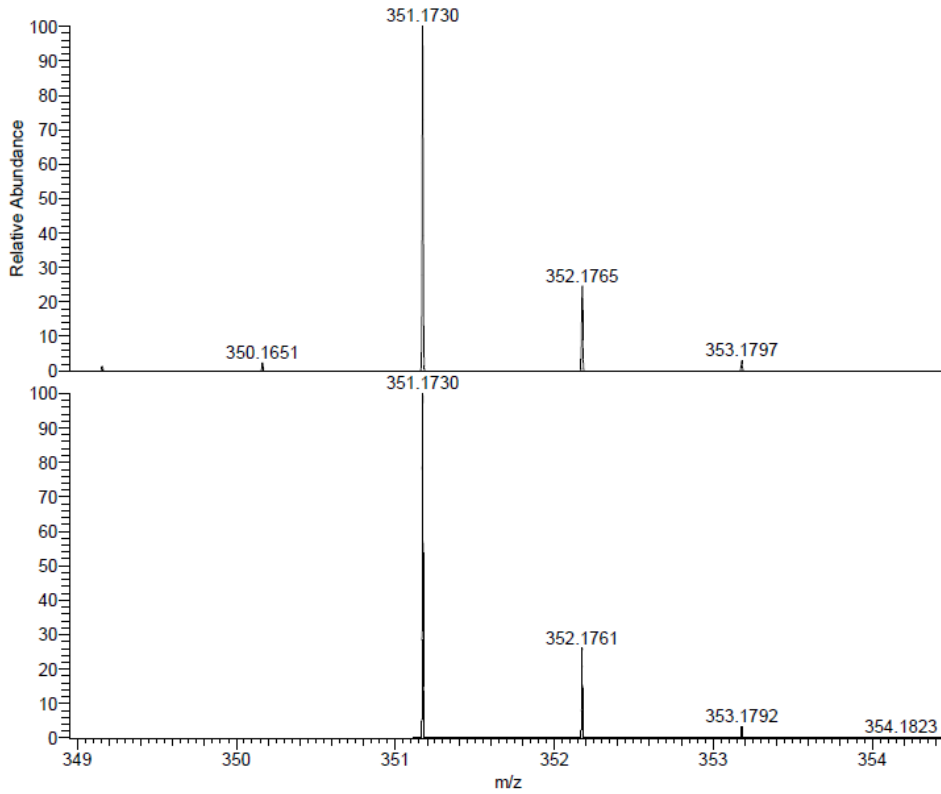
Display Report

Analysis Info		Acquisition Date	9/17/2018 11:59:19 AM
Analysis Name	D:\Data\2018\1809\180917\rschim00441_13_01_20465.d	Operator	BDAL@DE
Method	hystar_maxis_pl1.m	Instrument / Ser#	maXis 10138
Sample Name	rschim00441		
Comment			

Acquisition Parameter					
Source Type	ESI	Ion Polarity	Positive	Set Nebulizer	0.3 Bar
Focus	Not active			Set Dry Heater	180 °C
Scan Begin	50 m/z	Set Capillary	4200 V	Set Dry Gas	4.0 l/min
Scan End	1800 m/z	Set End Plate Offset	-500 V	Set Divert Valve	Source



35f



NL:
1.93E9
rschirm00583#272-285 RT:
0.71-0.74 AV: 14 SB: 1 1.50
T: FTMS + p EI Full ms
[60.0000-800.0000]

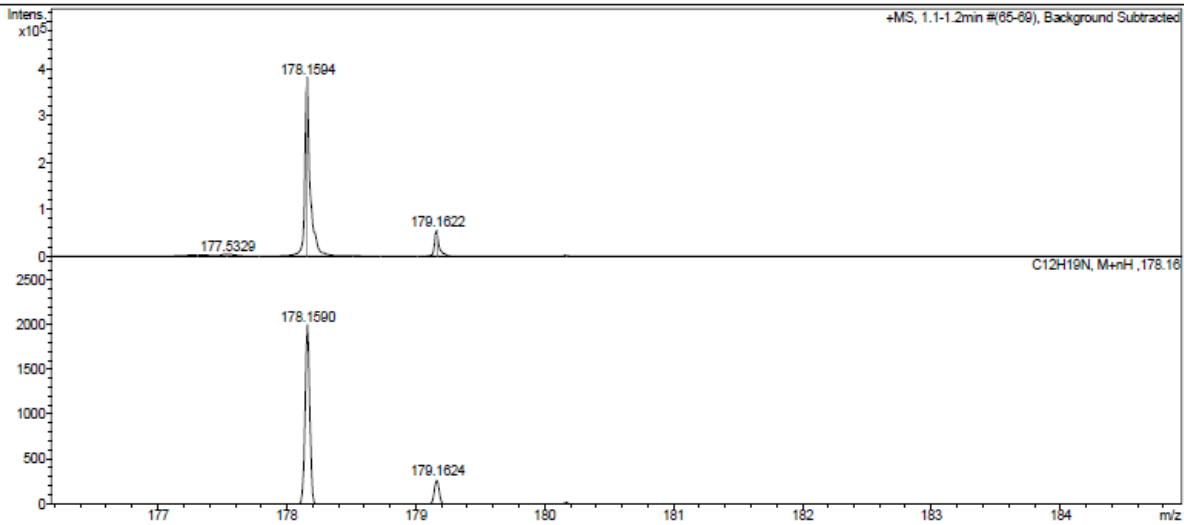
NL:
1.79E4
c₂₄h₂₁n₃
C₂₄H₂₁N₃
p (gss, s /p:40) Chrg 1
R: 60000 Res .Pwr . @FWHM

36f

Display Report

Analysis Info		Acquisition Date	18.12.2019 07:02:26
Analysis Name	Z:\Data\2019\1912\sam181219\rschirm00588_1_01_108575.d	Operator	BDAL@DE
Method	hystar_pl.m	Instrument / Ser#	micrOTOF 10237
Sample Name	rschirm00588		
Comment			

Acquisition Parameter					
Source Type	ESI	Ion Polarity	Positive	Set Nebulizer	1.2 Bar
Focus	Not active			Set Dry Heater	180 °C
Scan Begin	50 m/z	Set Capillary	4500 V	Set Dry Gas	4.0 l/min
Scan End	1600 m/z	Set End Plate Offset	-500 V	Set Divert Valve	Source

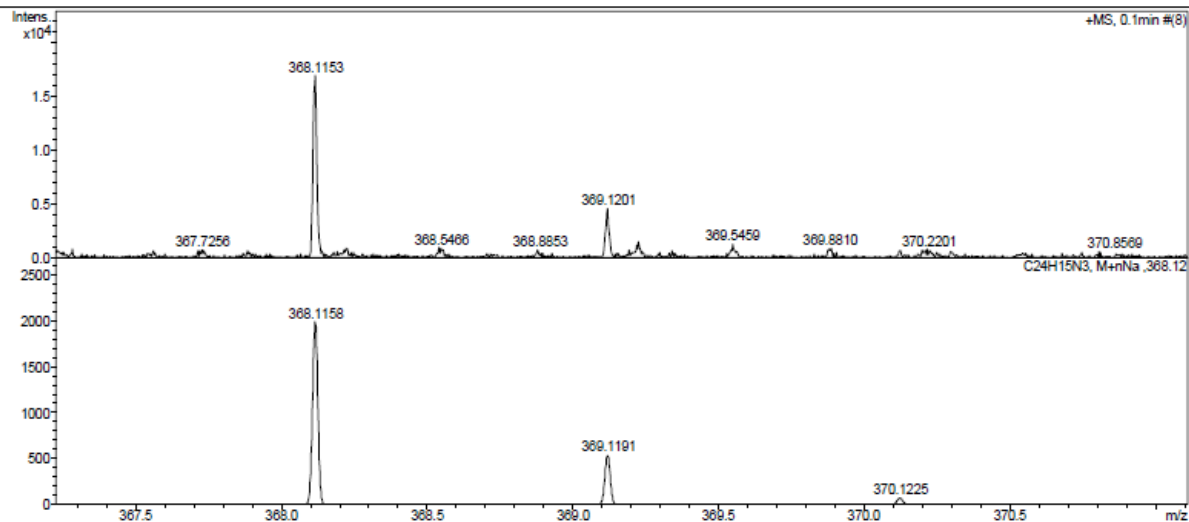


35g

Display Report

Analysis Info		Acquisition Date	12/10/2018 2:32:26 PM
Analysis Name	D:\Data\2018\1812\181210\rschim00456_23_01_21568.d	Operator	BDAL@DE
Method	hystar_maxis_pl1.m	Instrument / Ser#	maxis 10136
Sample Name	rschim00456		
Comment			

Acquisition Parameter					
Source Type	ESI	Ion Polarity	Positive	Set Nebulizer	0.3 Bar
Focus	Not active			Set Dry Heater	180 °C
Scan Begin	50 m/z	Set Capillary	4200 V	Set Dry Gas	4.0 l/min
Scan End	1600 m/z	Set End Plate Offset	-500 V	Set Divert Valve	Source



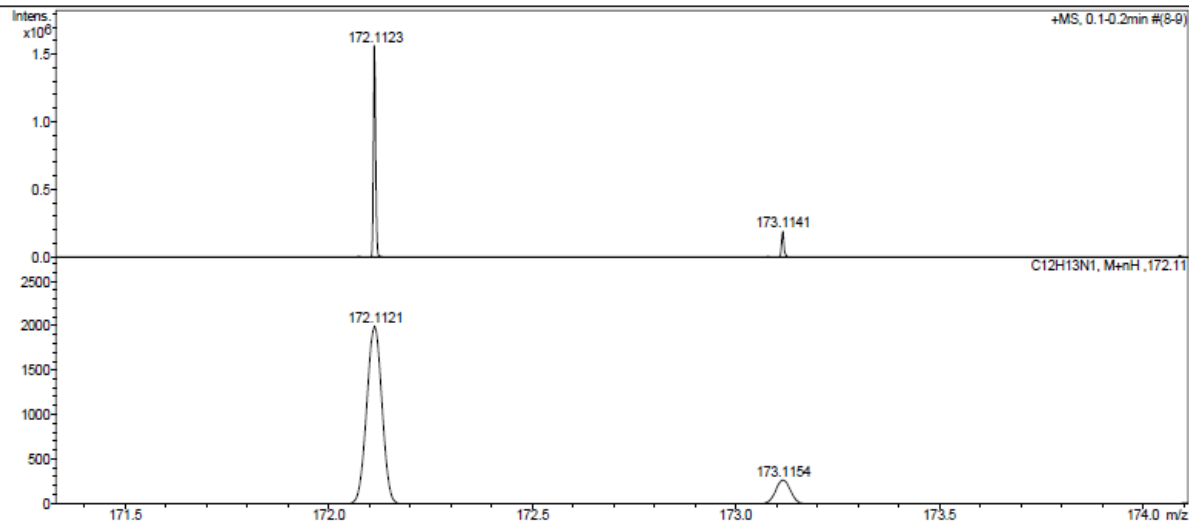
Bruker Compass DataAnalysis 4.0 printed: 12/10/2018 2:37:05 PM Page 1 of 1

36g

Display Report

Analysis Info		Acquisition Date	10/12/2018 11:35:45 AM
Analysis Name	D:\Data\2018\1810\181012\rschim00451_8_01_20833.d	Operator	BDAL@DE
Method	hystar_maxis_pl1.m	Instrument / Ser#	maxis 10136
Sample Name	rschim00451		
Comment			

Acquisition Parameter					
Source Type	ESI	Ion Polarity	Positive	Set Nebulizer	0.3 Bar
Focus	Not active			Set Dry Heater	180 °C
Scan Begin	50 m/z	Set Capillary	4200 V	Set Dry Gas	4.0 l/min
Scan End	1600 m/z	Set End Plate Offset	-500 V	Set Divert Valve	Source



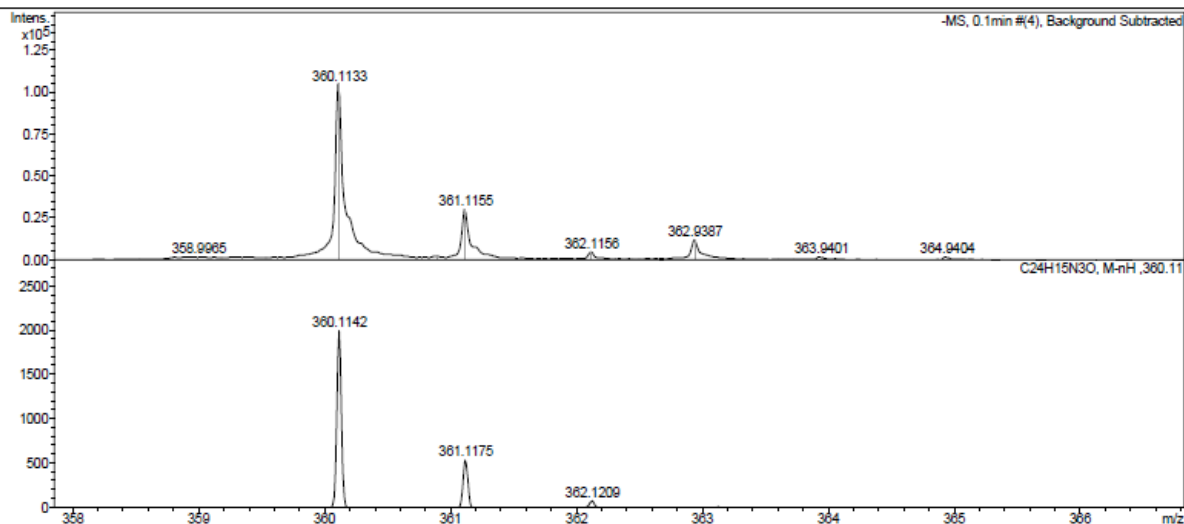
Bruker Compass DataAnalysis 4.0 printed: 10/12/2018 11:46:50 AM Page 1 of 1

35h

Display Report

Analysis Info		Acquisition Date	17.10.2018 13:51:55	
Analysis Name	Z:\Data\2018\1810\sam171018\neg\rschim00455_15_01_104040.d	Operator	BDAL@DE	
Method	hystar_nLm	Instrument / Ser#	microTOF 10237	
Sample Name	rschim00455	Comment		

Acquisition Parameter					
Source Type	ESI	Ion Polarity	Negative	Set Nebulizer	1.8 Bar
Focus	Not active	Set Capillary	3800 V	Set Dry Heater	180 °C
Scan Begin	50 m/z	Set End Plate Offset	-500 V	Set Dry Gas	8.0 l/min
Scan End	1600 m/z			Set Divert Valve	Source



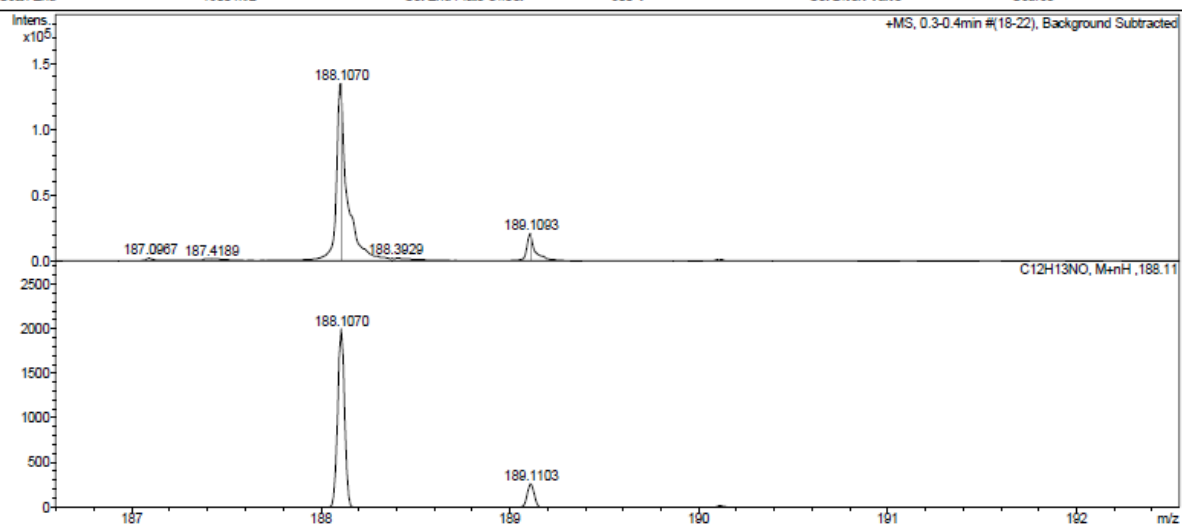
Bruker Compass DataAnalysis 4.0 printed: 17.10.2018 14:40:06 Page 1 of 1

36h

Display Report

Analysis Info		Acquisition Date	23.01.2019 09:40:32	
Analysis Name	Z:\Data\2019\1901\sam230119\rschim00466_9_01_105111.d	Operator	BDAL@DE	
Method	hystar_pLm	Instrument / Ser#	microTOF 10237	
Sample Name	rschim00466	Comment		

Acquisition Parameter					
Source Type	ESI	Ion Polarity	Positive	Set Nebulizer	1.2 Bar
Focus	Not active	Set Capillary	4500 V	Set Dry Heater	180 °C
Scan Begin	50 m/z	Set End Plate Offset	-500 V	Set Dry Gas	4.0 l/min
Scan End	1600 m/z			Set Divert Valve	Source



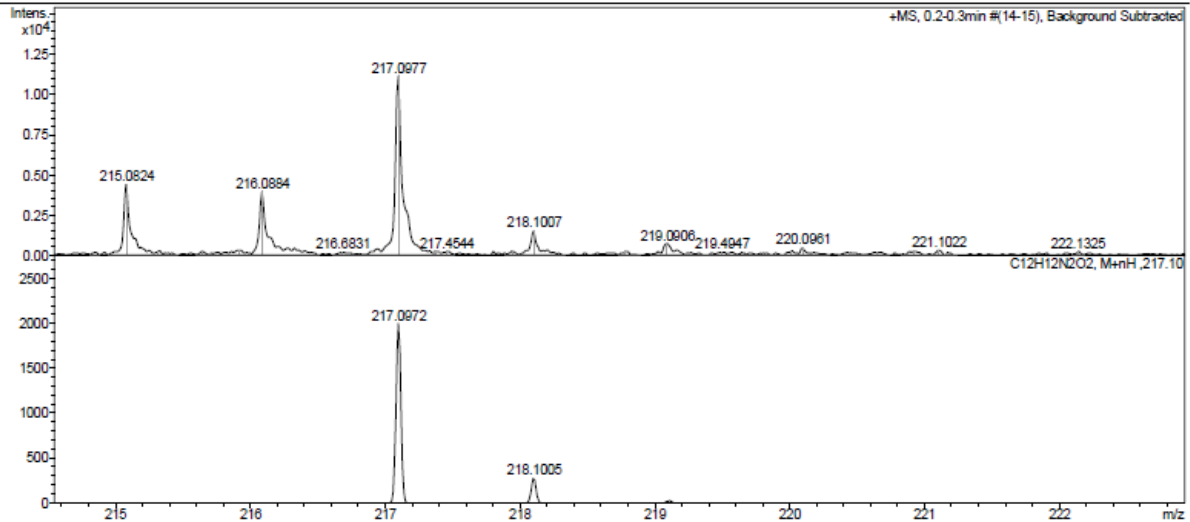
Bruker Compass DataAnalysis 4.0 printed: 23.01.2019 10:00:14 Page 1 of 1

36i

Display Report

Analysis Info		Acquisition Date	23.01.2019 09:28:22
Analysis Name	Z:\Data\2019\sam230119\rschim00464_6_01_105108.d	Operator	BDAL@DE
Method	hystar_pl.m	Instrument / Ser#	micrOTOF 10237
Sample Name	rschim00464		
Comment			

Acquisition Parameter		Ion Polarity	Positive	Set Nebulizer	1.2 Bar
Source Type	ESI			Set Dry Heater	180 °C
Focus	Not active	Set Capillary	4500 V	Set Dry Gas	4.0 l/min
Scan Begin	50 m/z	Set End Plate Offset	-500 V	Set Divert Valve	Source
Scan End	1600 m/z				

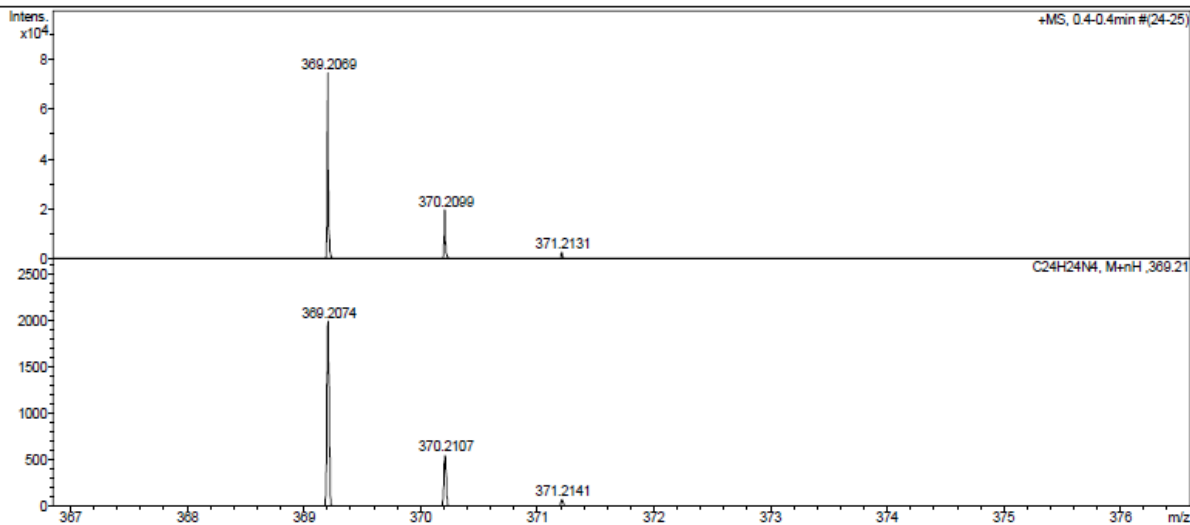


44

Display Report

Analysis Info		Acquisition Date	5/29/2018 2:57:09 PM
Analysis Name	D:\Data\2018\1805\180529\rschim00374_49_01_17854.d	Operator	BDAL@DE
Method	hystar_maxis_pl1.m	Instrument / Ser#	maXis 10136
Sample Name	rschim00374		
Comment			

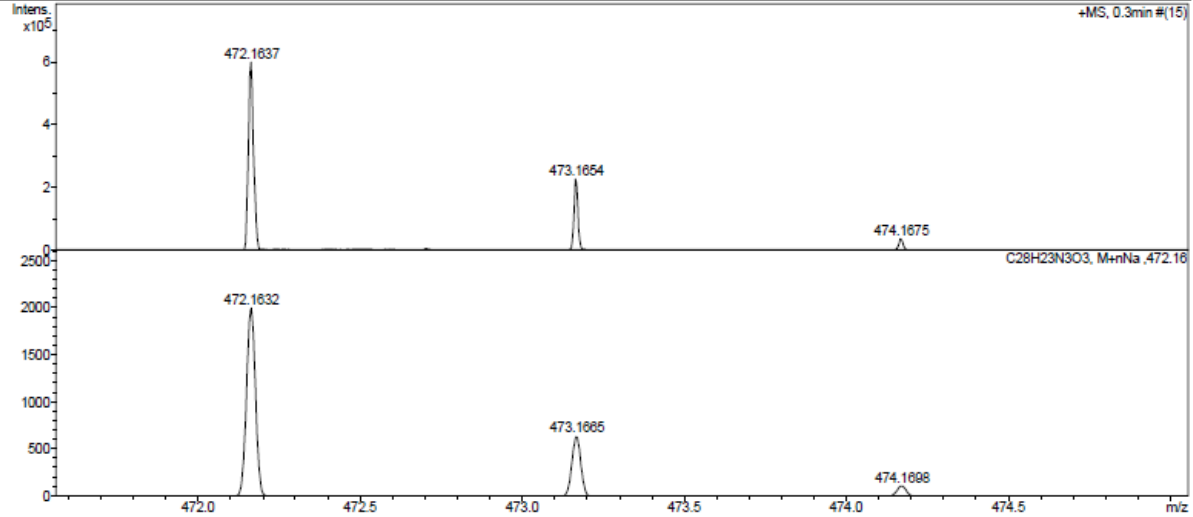
Acquisition Parameter		Ion Polarity	Positive	Set Nebulizer	0.3 Bar
Source Type	ESI			Set Dry Heater	180 °C
Focus	Not active	Set Capillary	4500 V	Set Dry Gas	4.0 l/min
Scan Begin	50 m/z	Set End Plate Offset	-500 V	Set Divert Valve	Source
Scan End	1600 m/z				



Display Report

Analysis Info		Acquisition Date	11/10/2020 10:37:12 AM
Analysis Name	D:\Data\2020\2011\201110\rschim00624_11_01_31336.d	Operator	BDAL@DE
Method	hystar_maxis_p.m	Instrument / Ser#	maXis 10136
Sample Name	rschim00624		
Comment			

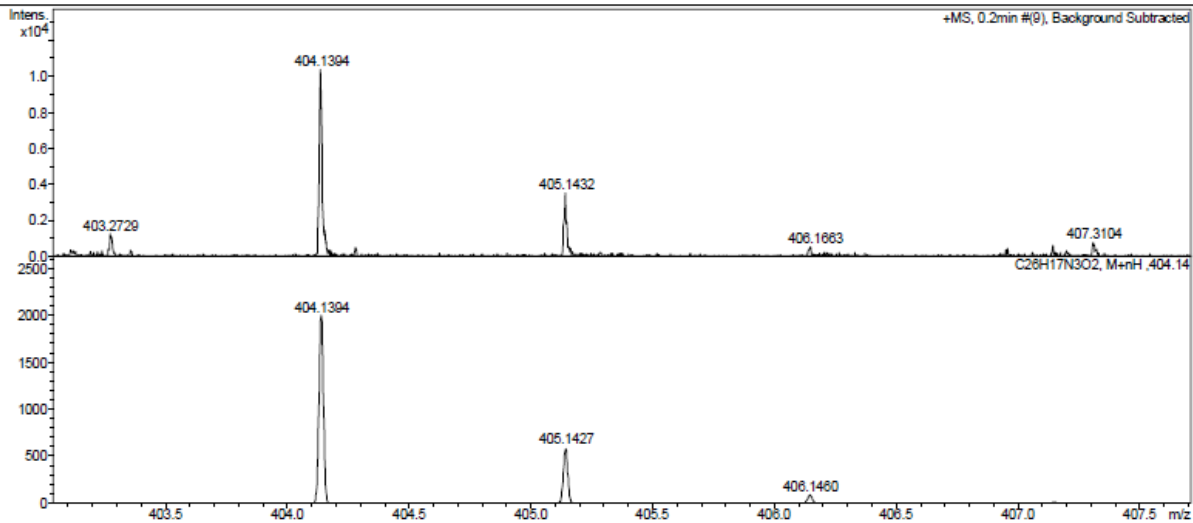
Acquisition Parameter					
Source Type	ESI	Ion Polarity	Positive	Set Nebulizer	0.3 Bar
Focus	Not active			Set Dry Heater	180 °C
Scan Begin	300 m/z	Set Capillary	4200 V	Set Dry Gas	4.0 l/min
Scan End	2900 m/z	Set End Plate Offset	-500 V	Set Divert Valve	Waste



Display Report

Analysis Info		Acquisition Date	8/8/2018 8:48:16 AM
Analysis Name	D:\Data\2018\1808\180808\rschim00426_12_01_19734.d	Operator	BDAL@DE
Method	hystar_maxis_pl1.m	Instrument / Ser#	maXis 10136
Sample Name	rschim00426		
Comment			

Acquisition Parameter					
Source Type	ESI	Ion Polarity	Positive	Set Nebulizer	0.3 Bar
Focus	Not active			Set Dry Heater	180 °C
Scan Begin	50 m/z	Set Capillary	4200 V	Set Dry Gas	4.0 l/min
Scan End	1600 m/z	Set End Plate Offset	-500 V	Set Divert Valve	Source

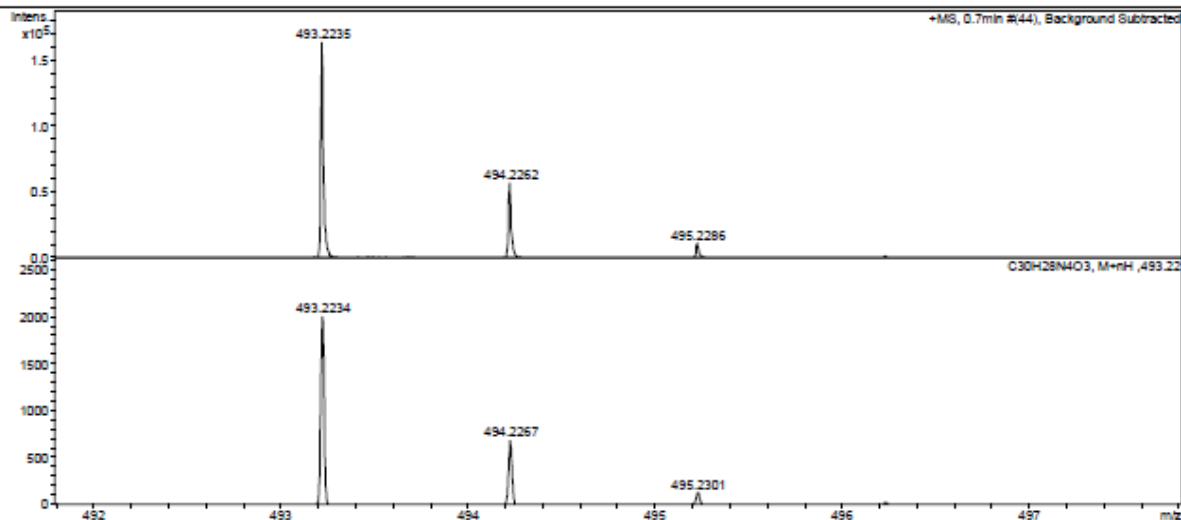


Display Report

Analysis Info		Acquisition Date	7/13/2018 7:48:30 AM
Analysis Name	D:\Data\2018\1807\180713\rschlm00418_7_01_19101.d	Operator	BDAL@DE
Method	hystar_maxis_p11.m	Instrument / Ser#	maXis 10136
Sample Name	rschlm00418		
Comment			

Acquisition Parameter

Source Type	ESI	Ion Polarity	Positive	Set Nebulizer	0.3 Bar
Focus	Not active	Set Capillary	4200 V	Set Dry Heater	180 °C
Scan Begin	50 m/z	Set End Plate Offset	-500 V	Set Dry Gas	4.0 l/min
Scan End	1600 m/z			Set Divert Valve	Source

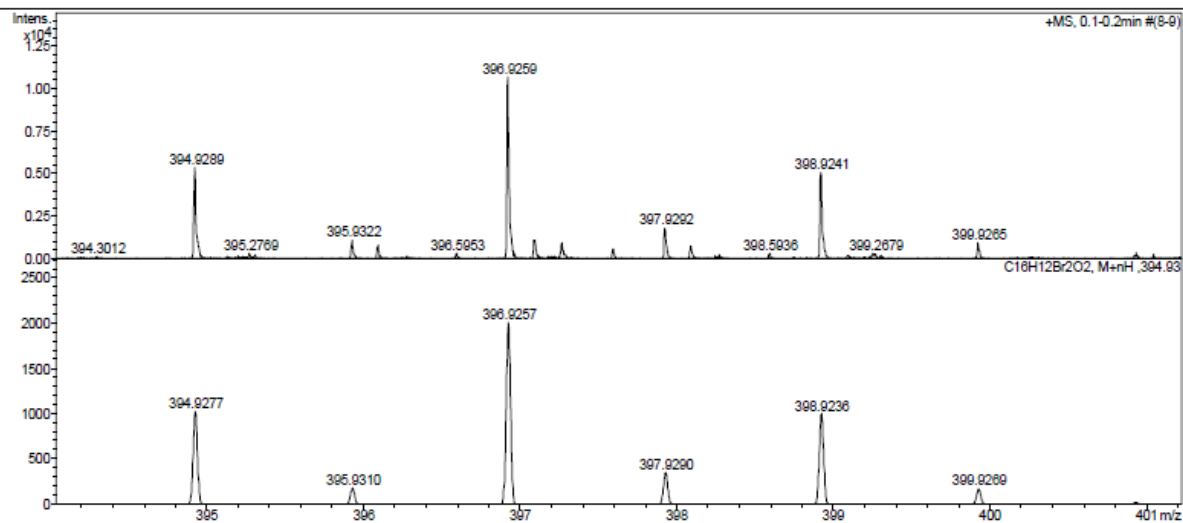


Display Report

Analysis Info		Acquisition Date	4/17/2018 10:23:55 AM
Analysis Name	D:\Data\2018\1804\180417\rschlm00160_13_01_18997.d	Operator	BDAL@DE
Method	hystar_maxis_p11.m	Instrument / Ser#	maXis 10136
Sample Name	rschlm00160		
Comment			

Acquisition Parameter

Source Type	ESI	Ion Polarity	Positive	Set Nebulizer	0.3 Bar
Focus	Not active	Set Capillary	4500 V	Set Dry Heater	180 °C
Scan Begin	50 m/z	Set End Plate Offset	-500 V	Set Dry Gas	4.0 l/min
Scan End	1600 m/z			Set Divert Valve	Source



51

Display Report

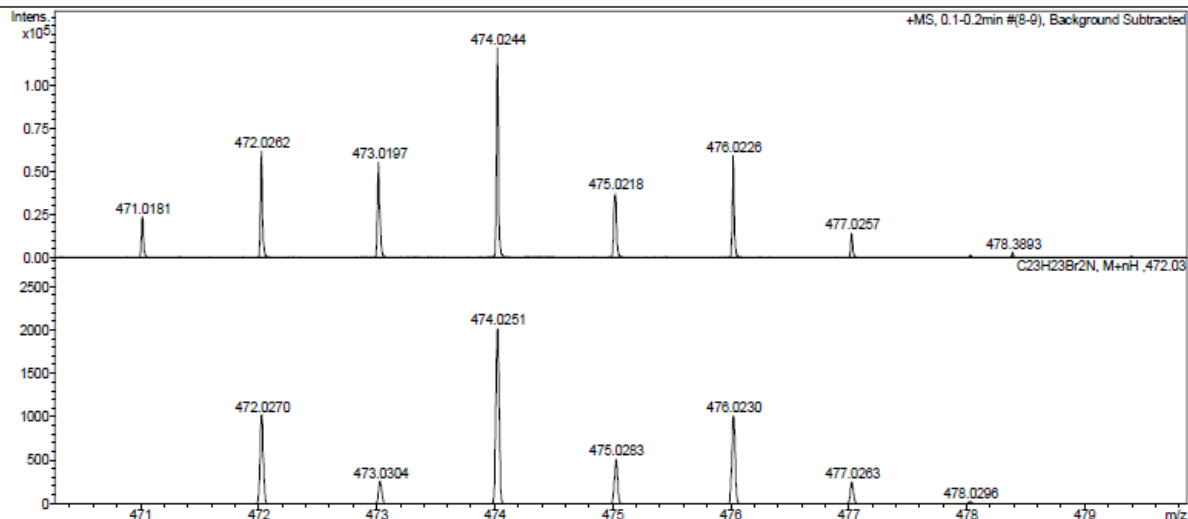
Analysis Info

Analysis Name: D:\Data\2019\1904\190424\rschim00509_14_01_23620.d
 Method: hystar_maxis_pl1.m
 Sample Name: rschim00509
 Comment:

Acquisition Date: 4/24/2019 12:22:30 PM
 Operator: BDAL@DE
 Instrument / Ser#: maxis 10136

Acquisition Parameter

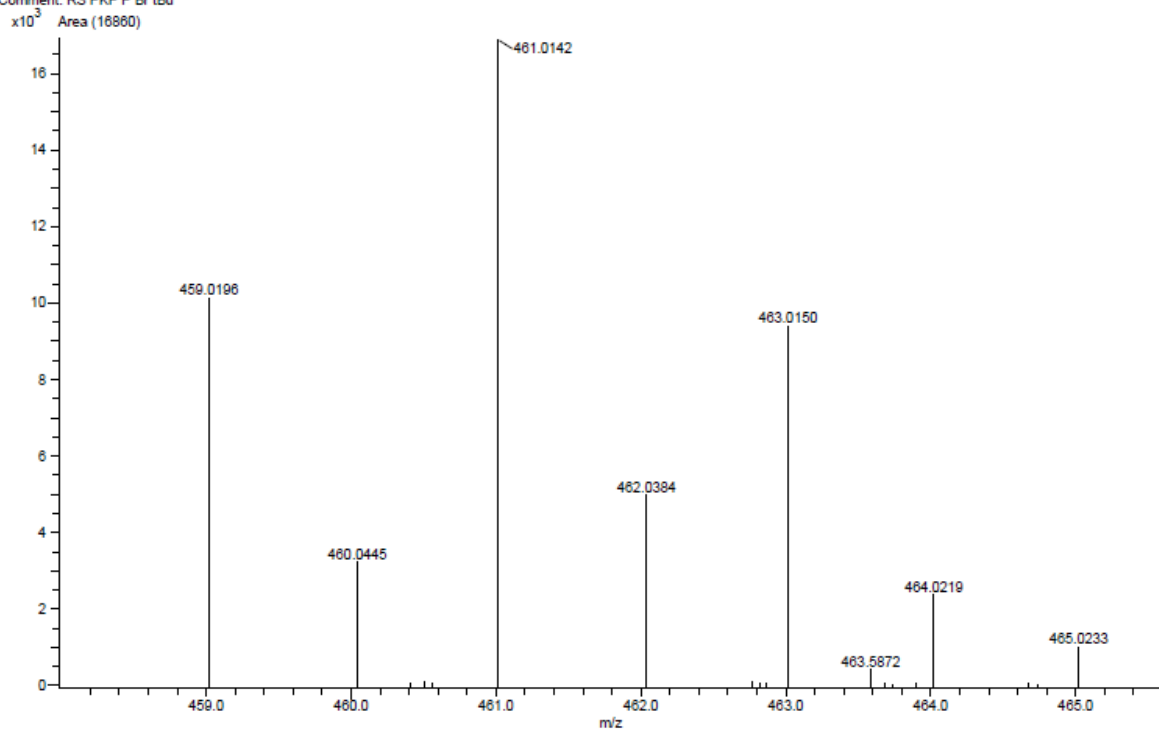
Source Type	ESI	Ion Polarity	Positive	Set Nebulizer	0.3 Bar
Focus	Not active			Set Dry Heater	180 °C
Scan Begin	50 m/z	Set Capillary	4200 V	Set Dry Gas	4.0 l/min
Scan End	1600 m/z	Set End Plate Offset	-500 V	Set Divert Valve	Source



52

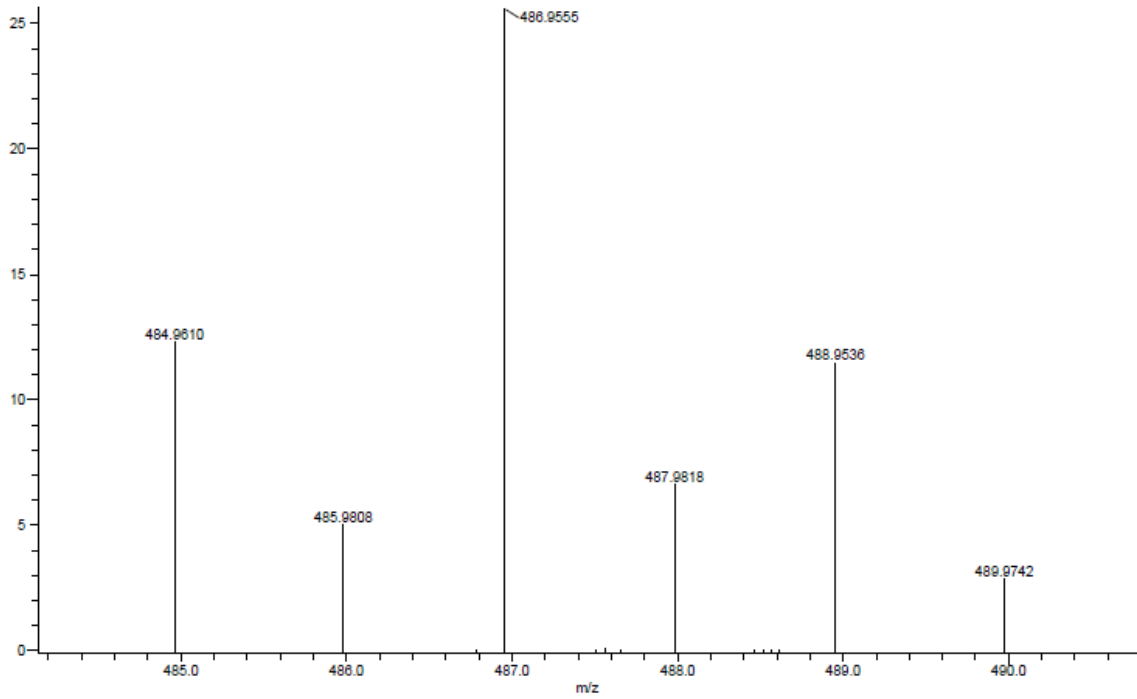
Acq. Data Name: rschim00528
 Creation Parameters: Average(MS[1] Time:0.39..0.39)
 Comment: RS PKP P Br tBu

Experiment Date/Time: 5/28/2019 11:17:43 AM
 Ionization Mode: EI+



Acq. Data Name: rschim00527
 Creation Parameters: Average(MS[1] Time:0.44)
 Comment: RS PKP P Br CF3
 x10³ Area (25556)

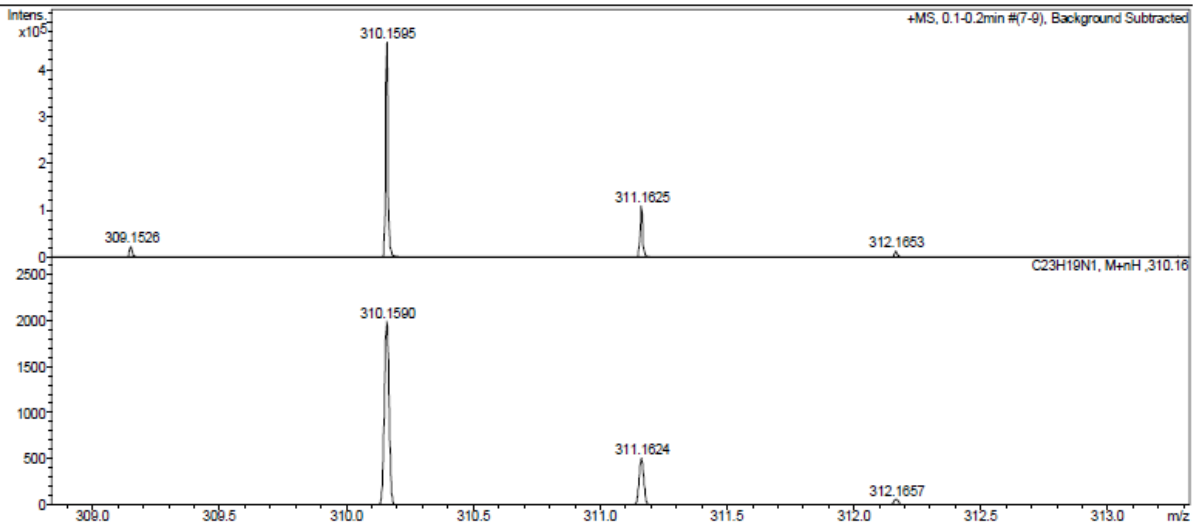
Experiment Date/Time: 5/28/2019 11:31:35 AM
 Ionization Mode: EI+



Display Report

Analysis Info		Acquisition Date	12/10/2018 2:40:03 PM
Analysis Name	D:\Data\2018\1812\181210\rschim00458_25_01_21570.d	Operator	BDAL@DE
Method	hystar_maxis_pl1.m	Instrument / Ser#	maxis 10136
Sample Name	rschim00458		
Comment			

Acquisition Parameter					
Source Type	ESI	Ion Polarity	Positive	Set Nebulizer	0.3 Bar
Focus	Not active			Set Dry Heater	180 °C
Scan Begin	50 m/z	Set Capillary	4200 V	Set Dry Gas	4.0 l/min
Scan End	1600 m/z	Set End Plate Offset	-500 V	Set Divert Valve	Source

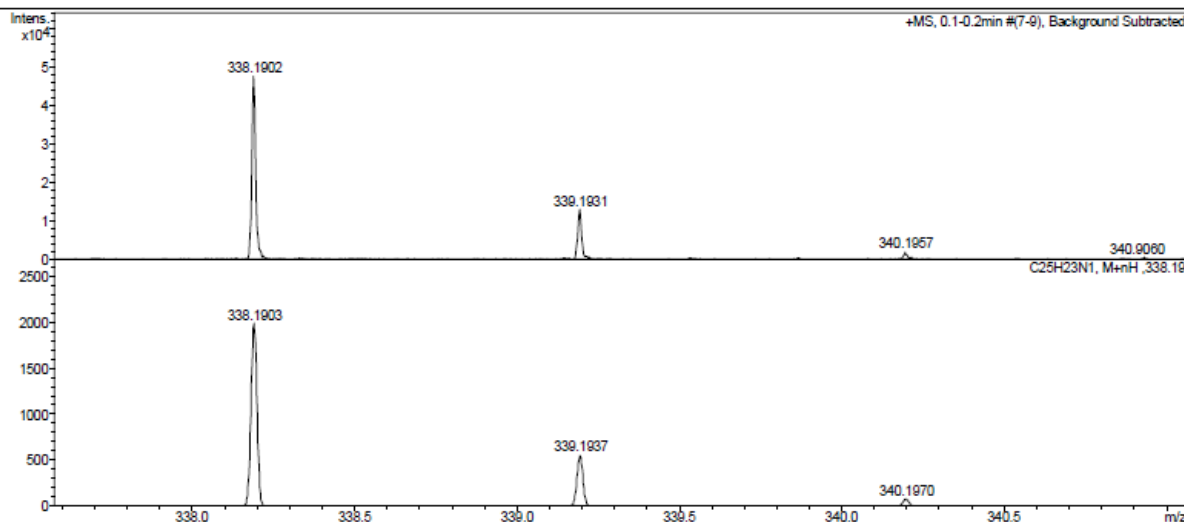


70

Display Report

Analysis Info
Analysis Name: D:\Data\2018\1812\181210\rschim00459_26_01_21571.d
Method: hystar_maxis_pl1.m
Sample Name: rschim00459
Acquisition Date: 12/10/2018 2:44:42 PM
Operator: BDAL@DE
Instrument / Ser#: maXis 10138

Acquisition Parameter
Source Type: ESI
Focus: Not active
Scan Begin: 50 m/z
Scan End: 1600 m/z
Ion Polarity: Positive
Set Capillary: 4200 V
Set End Plate Offset: -500 V
Set Nebulizer: 0.3 Bar
Set Dry Heater: 180 °C
Set Dry Gas: 4.0 l/min
Set Divert Valve: Source

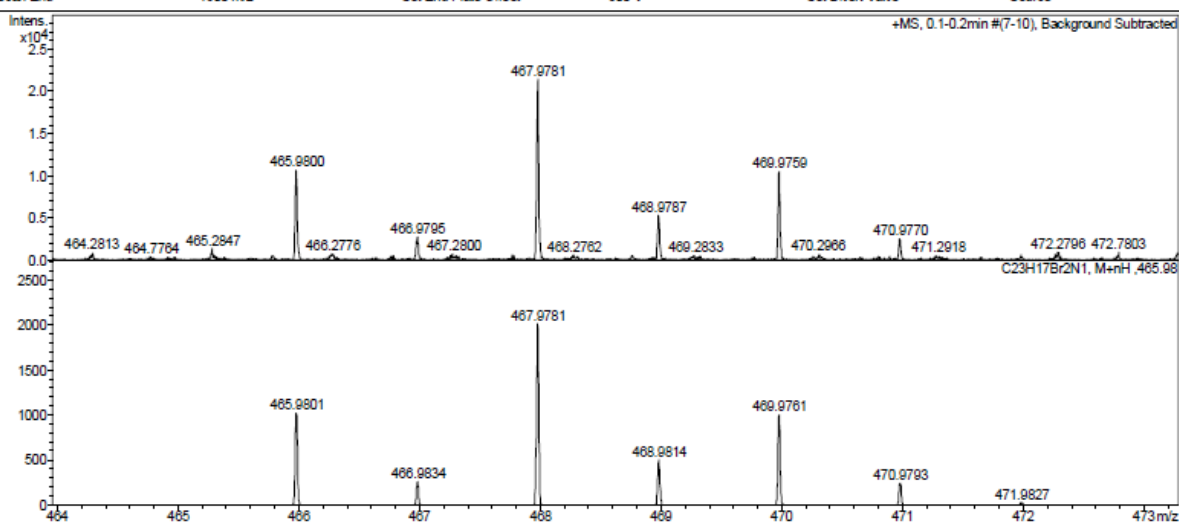


71

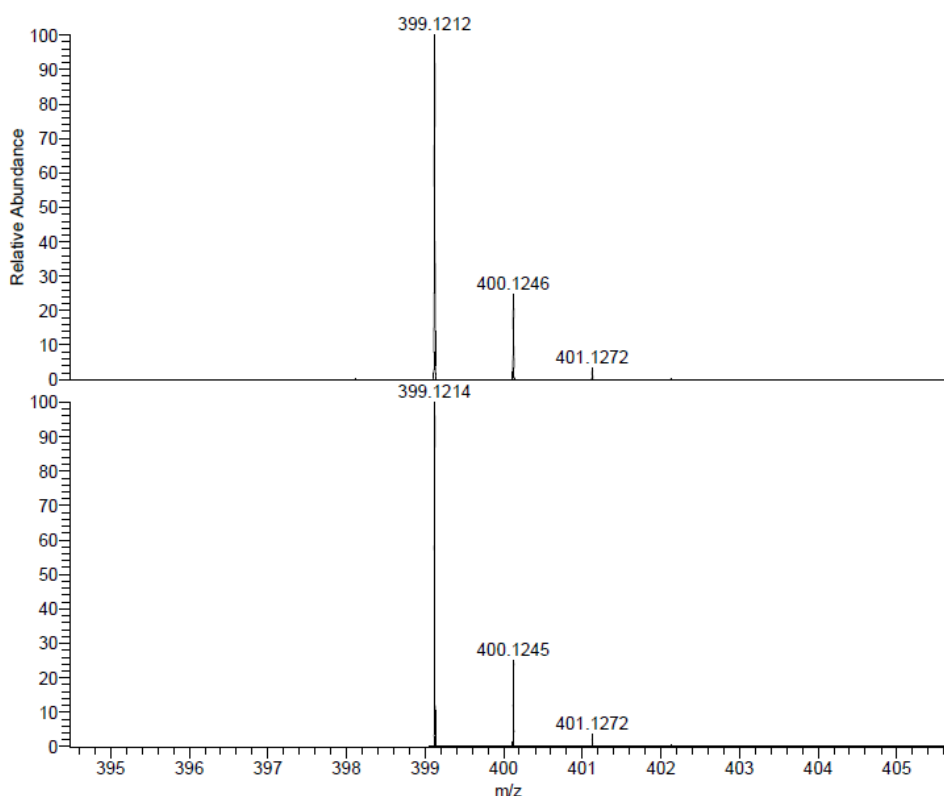
Display Report

Analysis Info
Analysis Name: D:\Data\2018\1812\181210\rschim00460_27_01_21572.d
Method: hystar_maxis_pl1.m
Sample Name: rschim00460
Acquisition Date: 12/10/2018 2:48:31 PM
Operator: BDAL@DE
Instrument / Ser#: maXis 10138

Acquisition Parameter
Source Type: ESI
Focus: Not active
Scan Begin: 50 m/z
Scan End: 1600 m/z
Ion Polarity: Positive
Set Capillary: 4200 V
Set End Plate Offset: -500 V
Set Nebulizer: 0.3 Bar
Set Dry Heater: 180 °C
Set Dry Gas: 4.0 l/min
Set Divert Valve: Source



72



NL:
6.28E8
rschim00584#156-160 RT:
0.45-0.46 AV: 5 SB: 1 1.50
T: FTMS + p EI Full ms
[60.0000-800.0000]

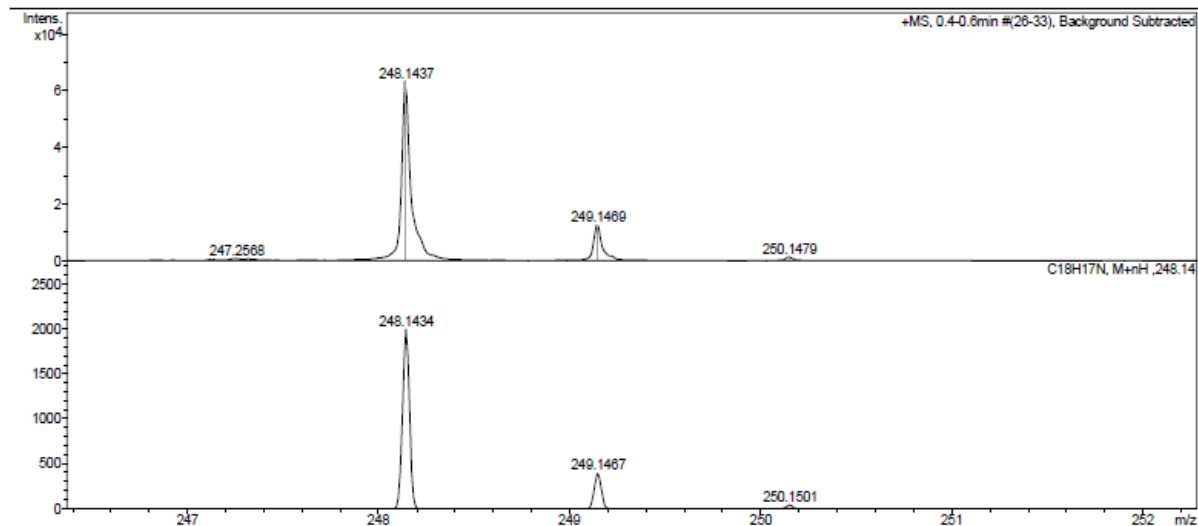
NL:
1.79E4
C₂₃H₁₇N₃O₄
C₂₃H₁₇N₃O₄
p (gss, s /p.40) Chrg 1
R: 60000 Res .Pwr . @FWHM

73

Display Report

Analysis Info		Acquisition Date	05.03.2019 08:14:56	
Analysis Name	Z:\Data\2019\1903\sam050319\rschim00471_2_01_105505.d	Operator	BDAL@DE	
Method	hystar_pl.m	Instrument / Ser#	micrOTOF 10237	
Sample Name	rschim00471			
Comment				

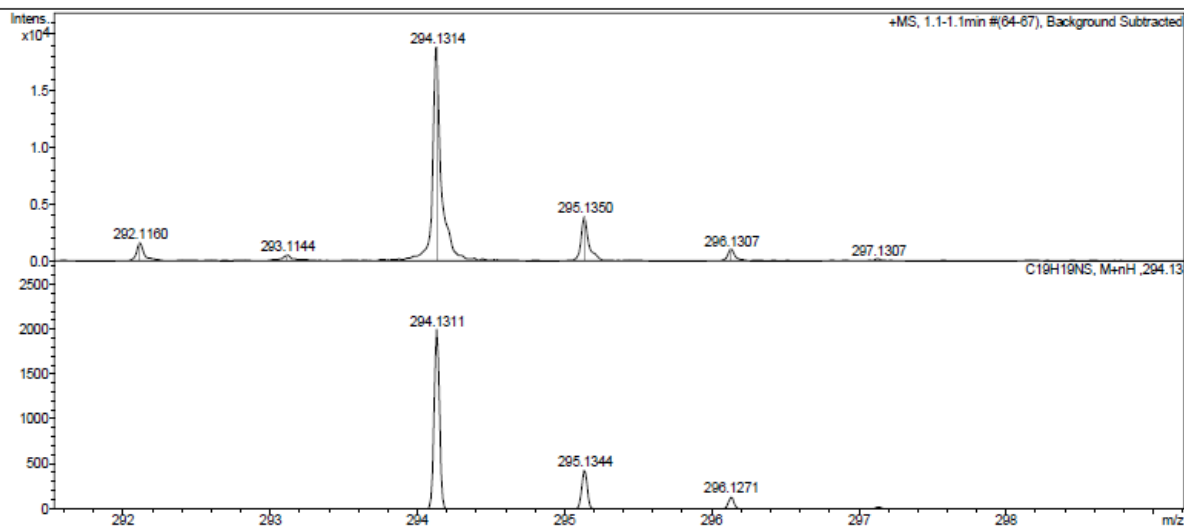
Acquisition Parameter					
Source Type	ESI	Ion Polarity	Positive	Set Nebulizer	1.2 Bar
Focus	Not active	Set Capillary	4500 V	Set Dry Heater	180 °C
Scan Begin	50 m/z	Set End Plate Offset	-500 V	Set Dry Gas	4.0 l/min
Scan End	1600 m/z			Set Divert Valve	Source



Display Report

Analysis Info		Acquisition Date	06.03.2019 09:46:30	
Analysis Name	Z:\Data\2019\1903\sam060319\rschim00473_1_01_105542.d	Operator	BDAL@DE	
Method	hystar_pl.m	Instrument / Ser#	microTOF 10237	
Sample Name	rschim00473			
Comment				

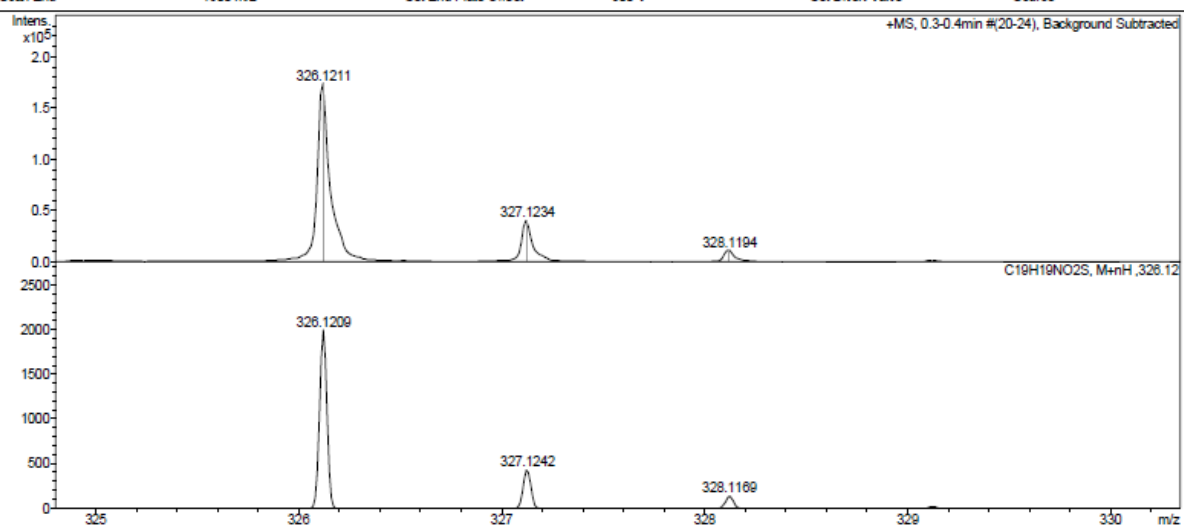
Acquisition Parameter					
Source Type	ESI	Ion Polarity	Positive	Set Nebulizer	1.2 Bar
Focus	Not active			Set Dry Heater	180 °C
Scan Begin	50 m/z	Set Capillary	4500 V	Set Dry Gas	4.0 l/min
Scan End	1600 m/z	Set End Plate Offset	-500 V	Set Divert Valve	Source



Display Report

Analysis Info		Acquisition Date	08.08.2019 11:13:52	
Analysis Name	Z:\Data\2019\1908\sam080819\rschim00536_7_01_107271.d	Operator	BDAL@DE	
Method	hystar_pl.m	Instrument / Ser#	microTOF 10237	
Sample Name	rschim00536			
Comment				

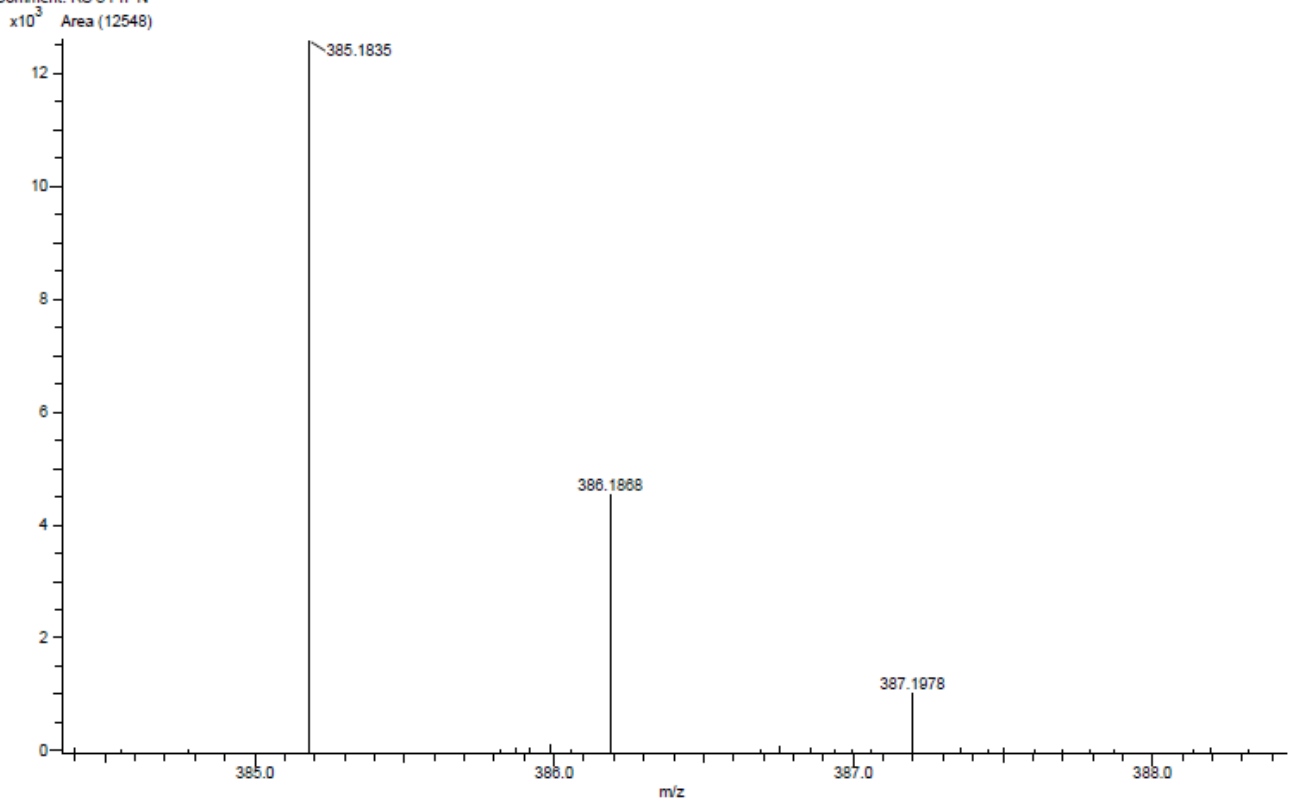
Acquisition Parameter					
Source Type	ESI	Ion Polarity	Positive	Set Nebulizer	1.2 Bar
Focus	Not active			Set Dry Heater	180 °C
Scan Begin	50 m/z	Set Capillary	4500 V	Set Dry Gas	4.0 l/min
Scan End	1600 m/z	Set End Plate Offset	-500 V	Set Divert Valve	Source



76

Acq. Data Name: rschirm00534
Creation Parameters: Average(MS[1] Time:2.72..2.78)
Comment: RS 3 Ph N

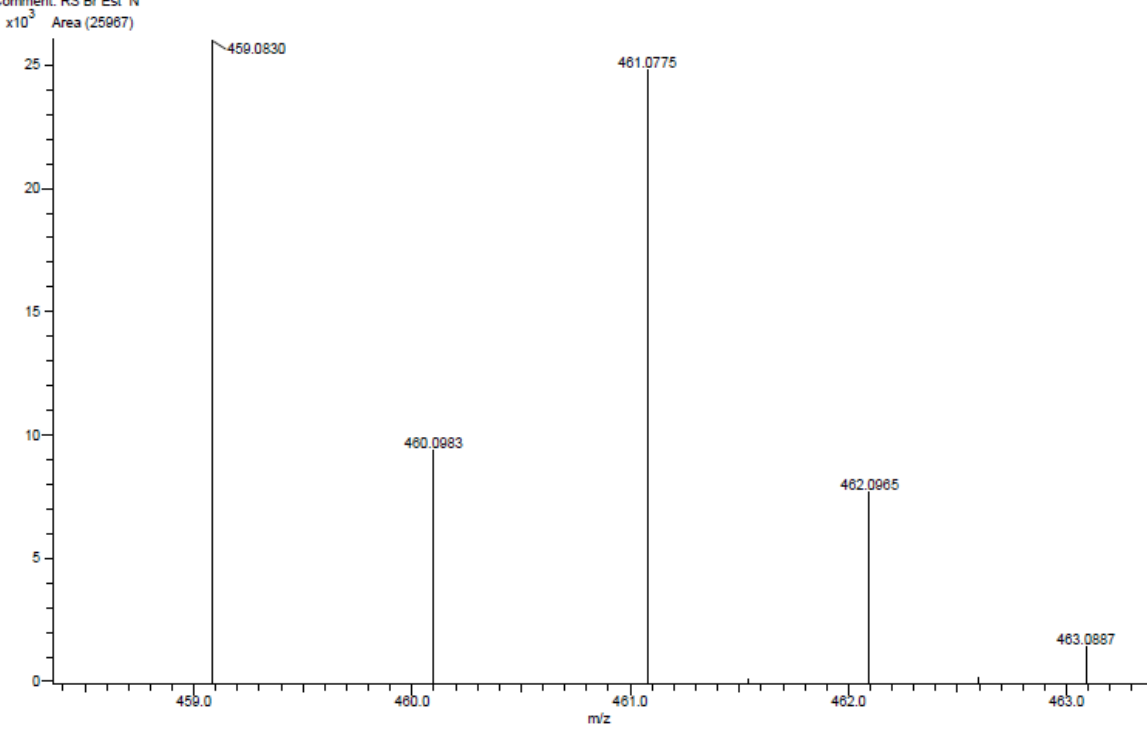
Experiment Date/Time: 8/8/2019 12:34:06 PM
Ionization Mode: EI+



77

Acq. Data Name: rschirm00535
Creation Parameters: Average(MS[1] Time:1.91..1.92)
Comment: RS Br Est N

Experiment Date/Time: 8/8/2019 12:45:53 PM
Ionization Mode: EI+

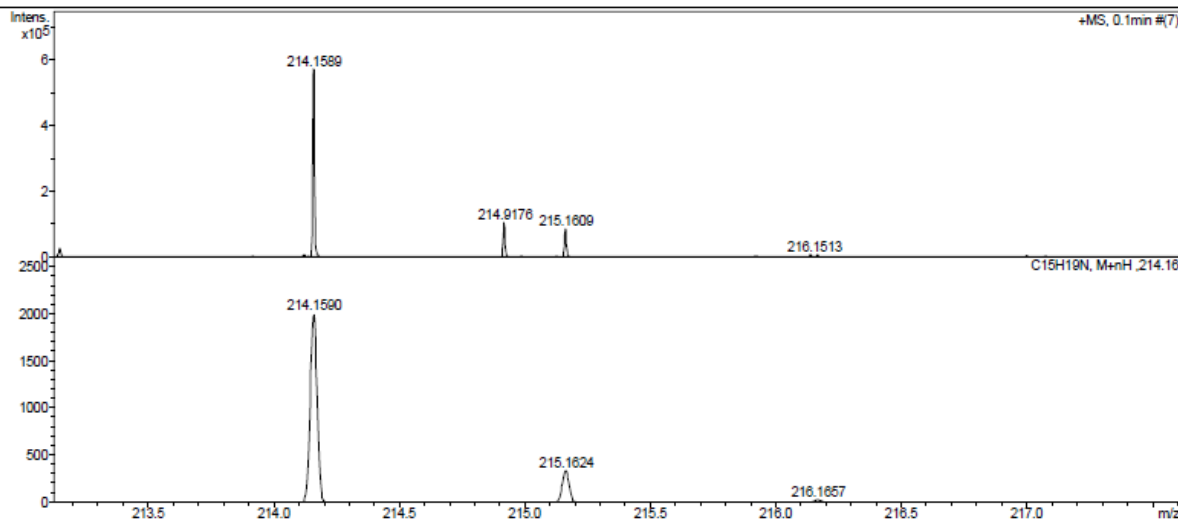


78

Display Report

Analysis Info
Analysis Name: D:\Data\2020\2001\200118\rschim00588_33_01_27372.d
Method: hystar_maxis_pl1.m
Sample Name: rschim00588
Acquisition Date: 1/16/2020 11:40:54 AM
Operator: BDAL@DE
Instrument / Ser#: maXis 10136

Acquisition Parameter
Source Type: ESI
Focus: Not active
Scan Begin: 50 m/z
Scan End: 1600 m/z
Ion Polarity: Positive
Set Capillary: 4200 V
Set End Plate Offset: -500 V
Set Nebulizer: 0.3 Bar
Set Dry Heater: 180 °C
Set Dry Gas: 4.0 l/min
Set Divert Valve: Source

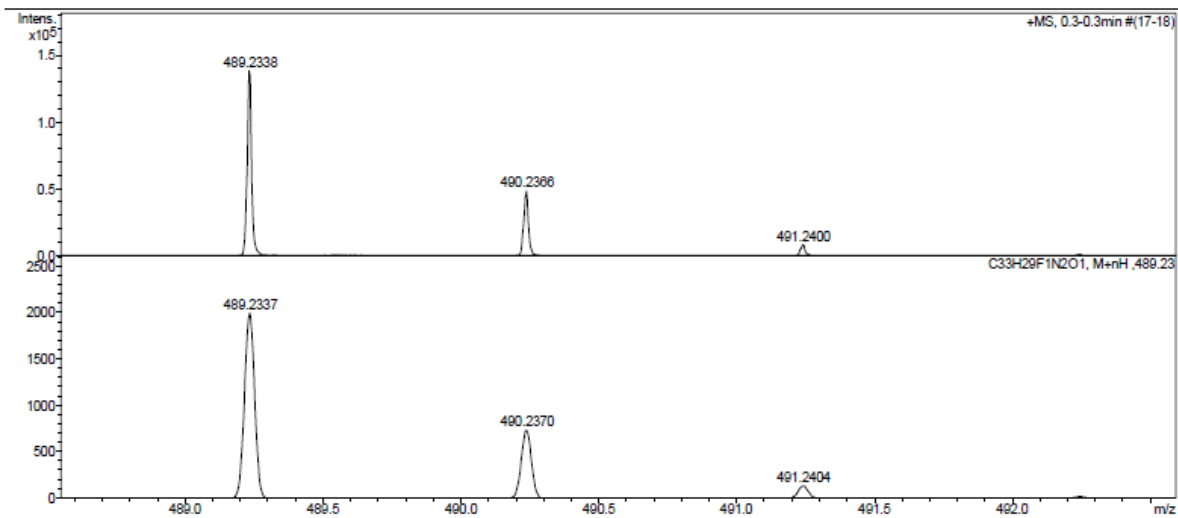


79

Display Report

Analysis Info
Analysis Name: D:\Data\2020\2006\200603\rschim00599_12_01_28871.d
Method: hystar_maxis_pl1.m
Sample Name: rschim00599
Acquisition Date: 6/3/2020 9:26:13 AM
Operator: BDAL@DE
Instrument / Ser#: maXis 10136

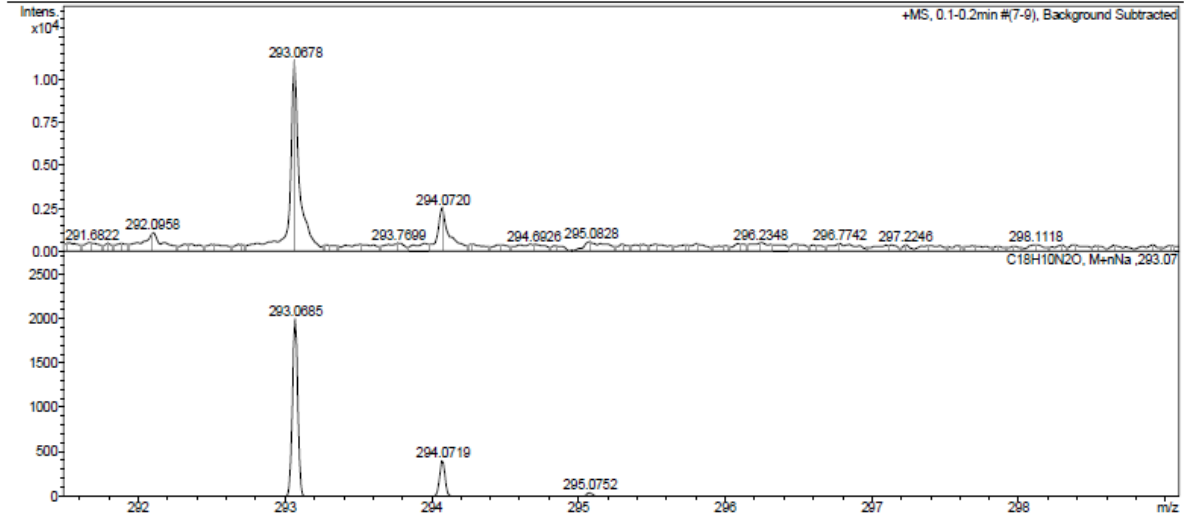
Acquisition Parameter
Source Type: ESI
Focus: Not active
Scan Begin: 50 m/z
Scan End: 1600 m/z
Ion Polarity: Positive
Set Capillary: 4200 V
Set End Plate Offset: -500 V
Set Nebulizer: 0.3 Bar
Set Dry Heater: 180 °C
Set Dry Gas: 4.0 l/min
Set Divert Valve: Source



Display Report

Analysis Info		Acquisition Date	08.08.2019 11:09:07	
Analysis Name	Z:\Data\2019\1908\sam080819\rschim00538_6_01_107270.d	Operator	BDAL@DE	
Method	hystar_pl.m	Instrument / Ser#	micrOTOF 10237	
Sample Name	rschim00538	Comment		

Acquisition Parameter					
Source Type	ESI	Ion Polarity	Positive	Set Nebulizer	1.2 Bar
Focus	Not active	Set Capillary	4500 V	Set Dry Heater	180 °C
Scan Begin	50 m/z	Set End Plate Offset	-500 V	Set Dry Gas	4.0 l/min
Scan End	1600 m/z			Set Divert Valve	Source



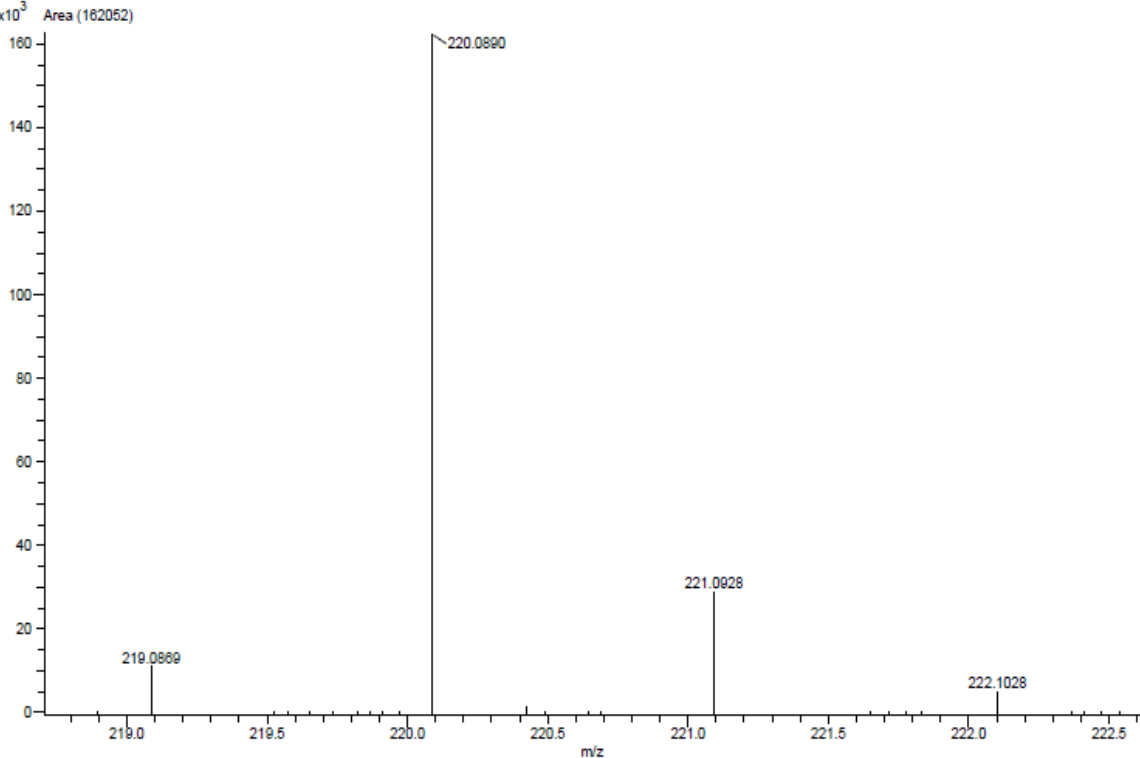
Bruker Compass DataAnalysis 4.0

printed: 08.08.2019 13:47:41

Page 1 of 1

Acq. Data Name: rschim00524
 Creation Parameters: Average(MS[1] Time:1.04..1.09)
 Comment: RS PKP Ph2 O

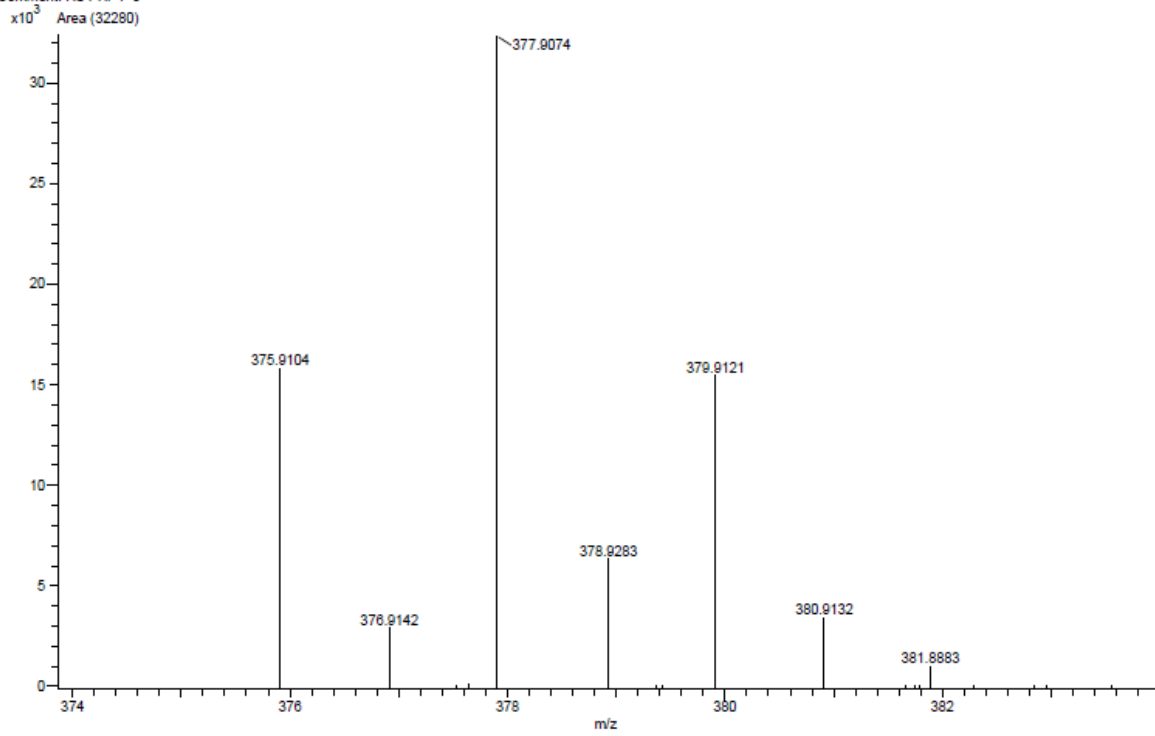
Experiment Date/Time: 5/23/2019 10:57:29 AM
 Ionization Mode: EI+



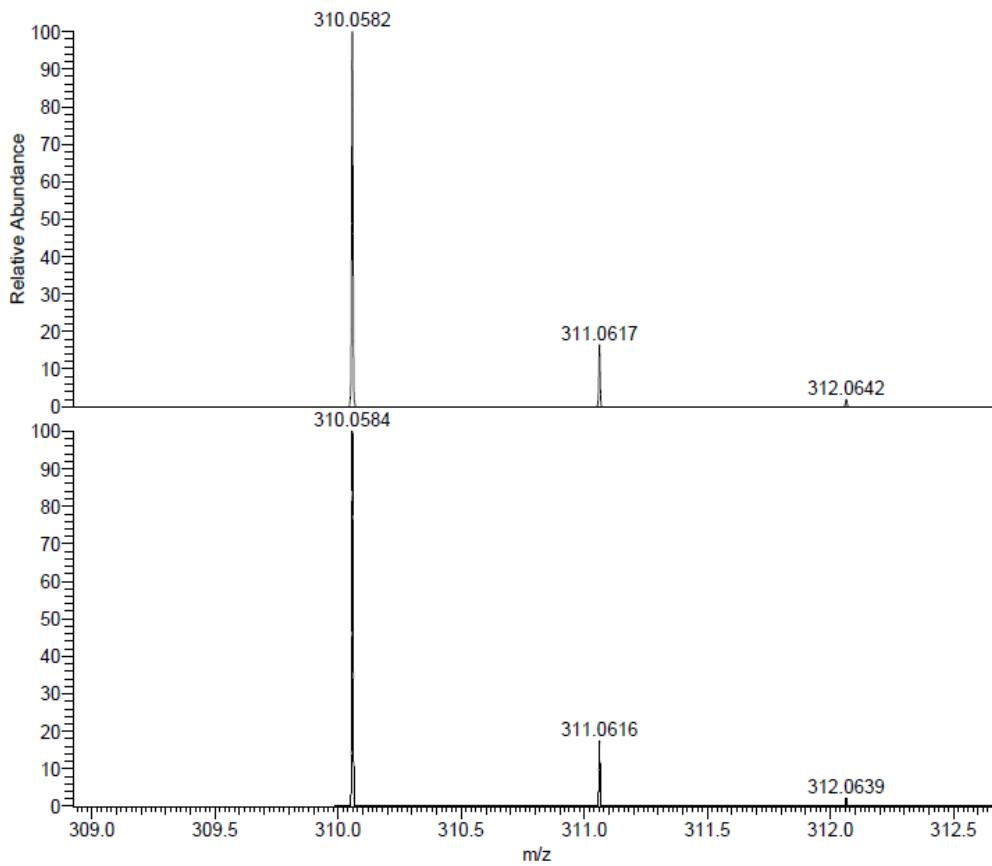
82

Acq. Data Name: rschirm00469
Creation Parameters: Average(MS[1] Time:0.31)
Comment: RS PKP F 3

Experiment Date/Time: 2/26/2019 12:51:18 PM
Ionization Mode: EI+



83



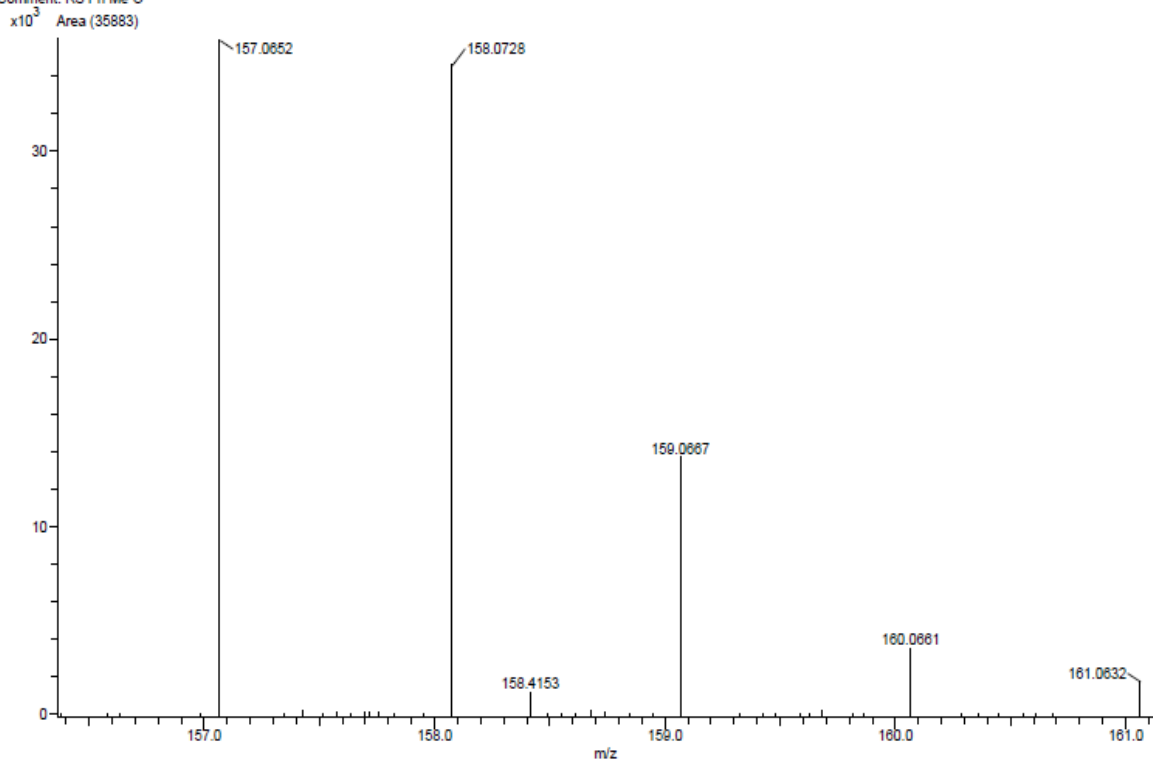
NL:
3.86E8
rschirm00585#174 RT: 0.49
AV: 1 SB: 1 1.50 T: FTMS +
p EI Full ms
[60.0000-800.0000]

NL:
1.94E4
C16H10N2O5
C16H10N2O5
p (gss, s /p:40) Chrg 1
R: 60000 Res .Pwr . @FWHM

84

Acq. Data Name: rschim00539
Creation Parameters: Average(MS[1] Time:1.08..1.20)
Comment: RS Ph Me O

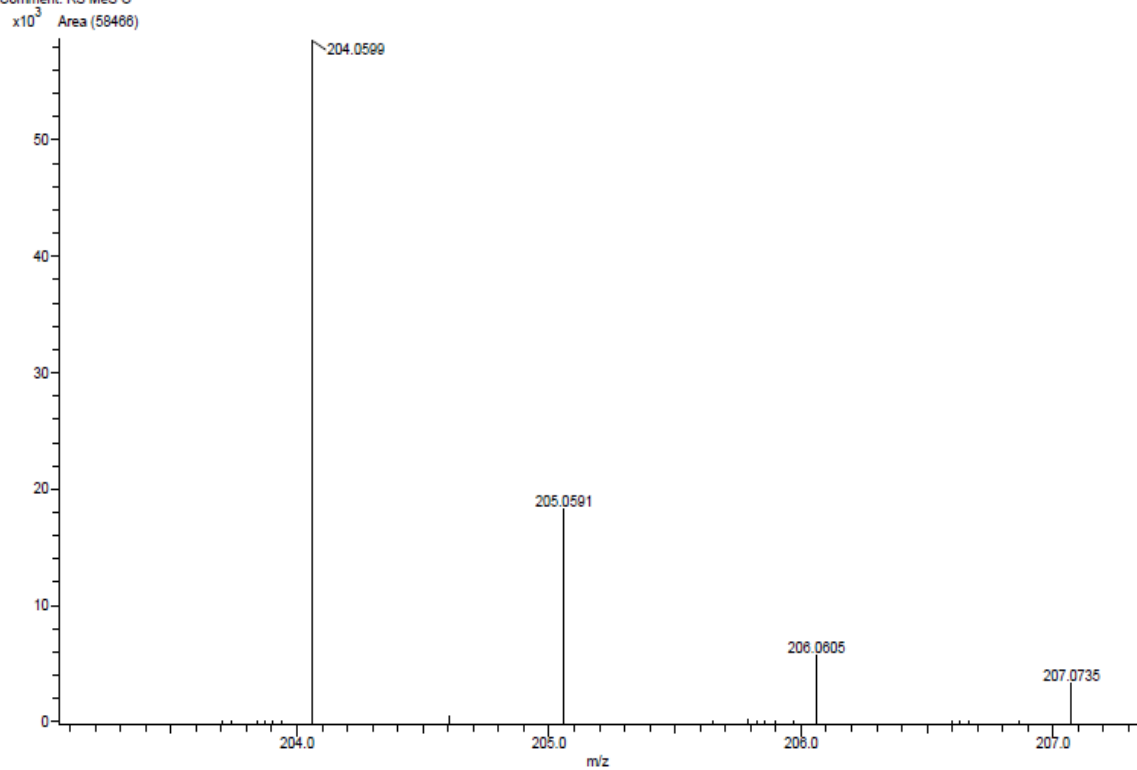
Experiment Date/Time: 8/8/2019 12:12:54 PM
Ionization Mode: EI+



85

Acq. Data Name: rschim00540
Creation Parameters: Average(MS[1] Time:0.23)
Comment: RS MeS O

Experiment Date/Time: 8/8/2019 12:01:49 PM
Ionization Mode: EI+



Display Report

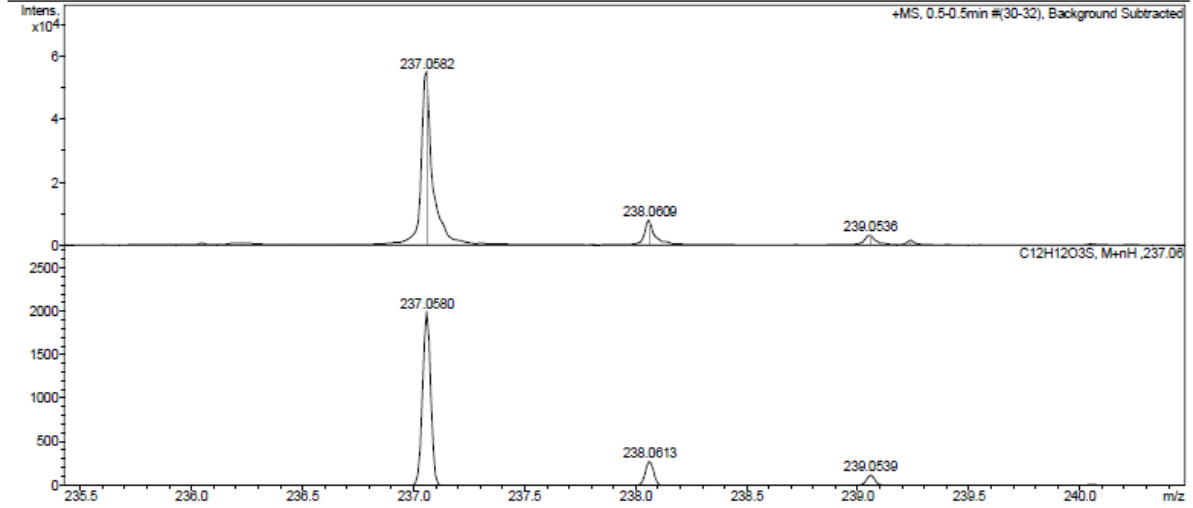
Analysis Info

Analysis Name Z:\Data\2019\1905\sam220519\rschim00525_7_01_106486.d
 Method hystar_plm
 Sample Name rschim00525
 Comment

Acquisition Date 22.05.2019 08:27:53
 Operator BDAL@DE
 Instrument / Ser# micrOTOF 10237

Acquisition Parameter

Source Type	ESI	Ion Polarity	Positive	Set Nebulizer	1.2 Bar
Focus	Not active			Set Dry Heater	180 °C
Scan Begin	50 m/z	Set Capillary	4500 V	Set Dry Gas	4.0 l/min
Scan End	1600 m/z	Set End Plate Offset	-500 V	Set Divert Valve	Source



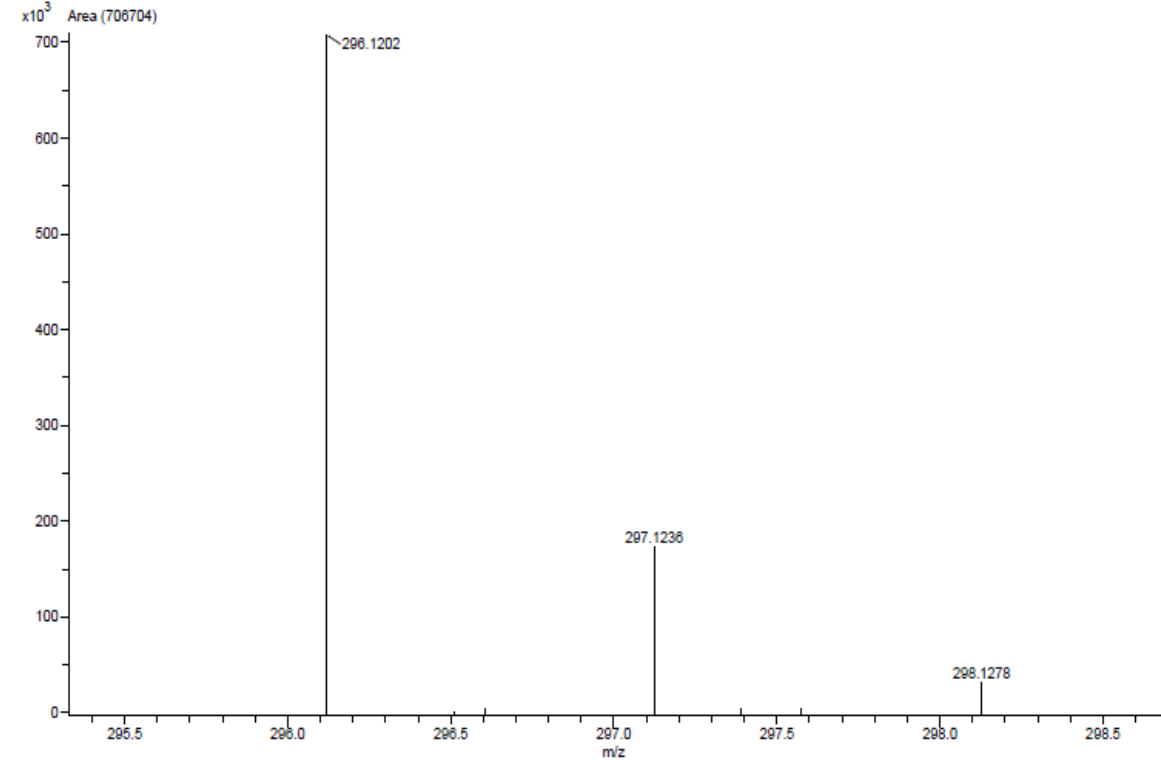
Bruker Compass DataAnalysis 4.0

printed: 22.05.2019 09:20:23

Page 1 of 1

Acq. Data Name: rschim00537
 Creation Parameters: Average(MS[1] Time:0.36..0.40)
 Comment: RS 3 Ph O

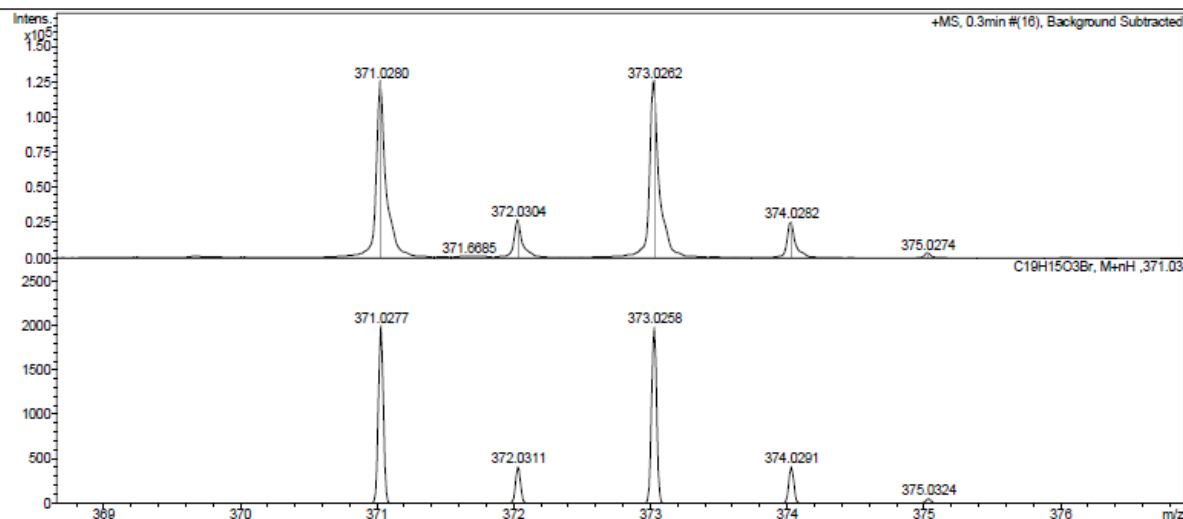
Experiment Date/Time: 8/8/2019 12:25:07 PM
 Ionization Mode: EI+



Display Report

Analysis Info		Acquisition Date	22.05.2019 08:58:08	
Analysis Name	Z:\Data\2019\1905\sam220519\rschim00526_13_01_106492.d	Operator	BDAL@DE	
Method	hystar_plm	Instrument / Ser#	micrOTOF 10237	
Sample Name	rschim00526	Comment		

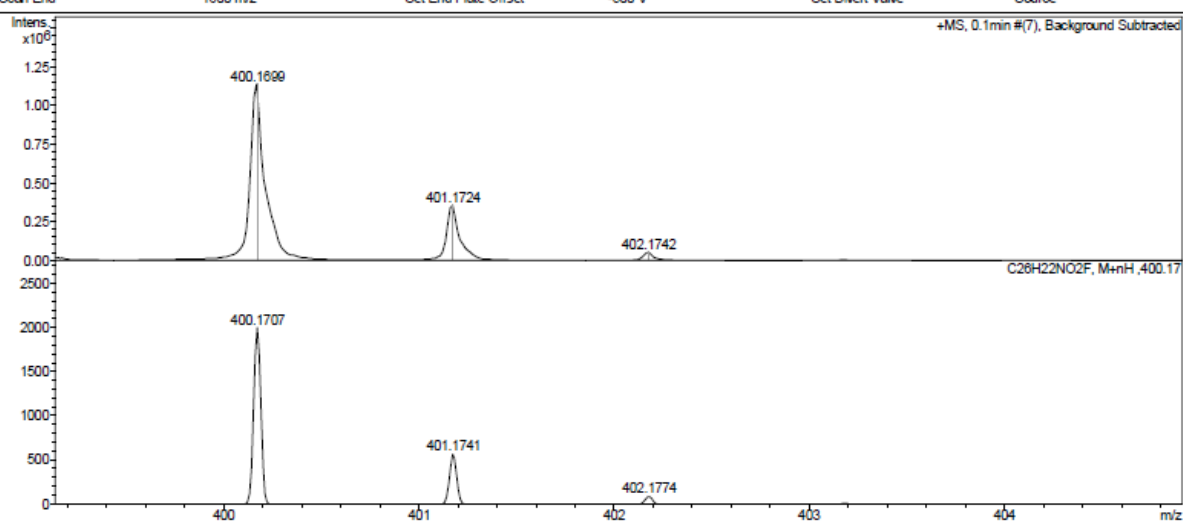
Acquisition Parameter					
Source Type	ESI	Ion Polarity	Positive	Set Nebulizer	1.2 Bar
Focus	Not active	Set Capillary	4500 V	Set Dry Heater	180 °C
Scan Begin	50 m/z	Set End Plate Offset	-500 V	Set Dry Gas	4.0 l/min
Scan End	1600 m/z			Set Divert Valve	Source



Display Report

Analysis Info		Acquisition Date	11.02.2020 14:15:57	
Analysis Name	Z:\Data\2020\2002\sam110220\rschim00589_18_01_109072.d	Operator	BDAL@DE	
Method	hystar_plm	Instrument / Ser#	micrOTOF 10237	
Sample Name	rschim00589	Comment		

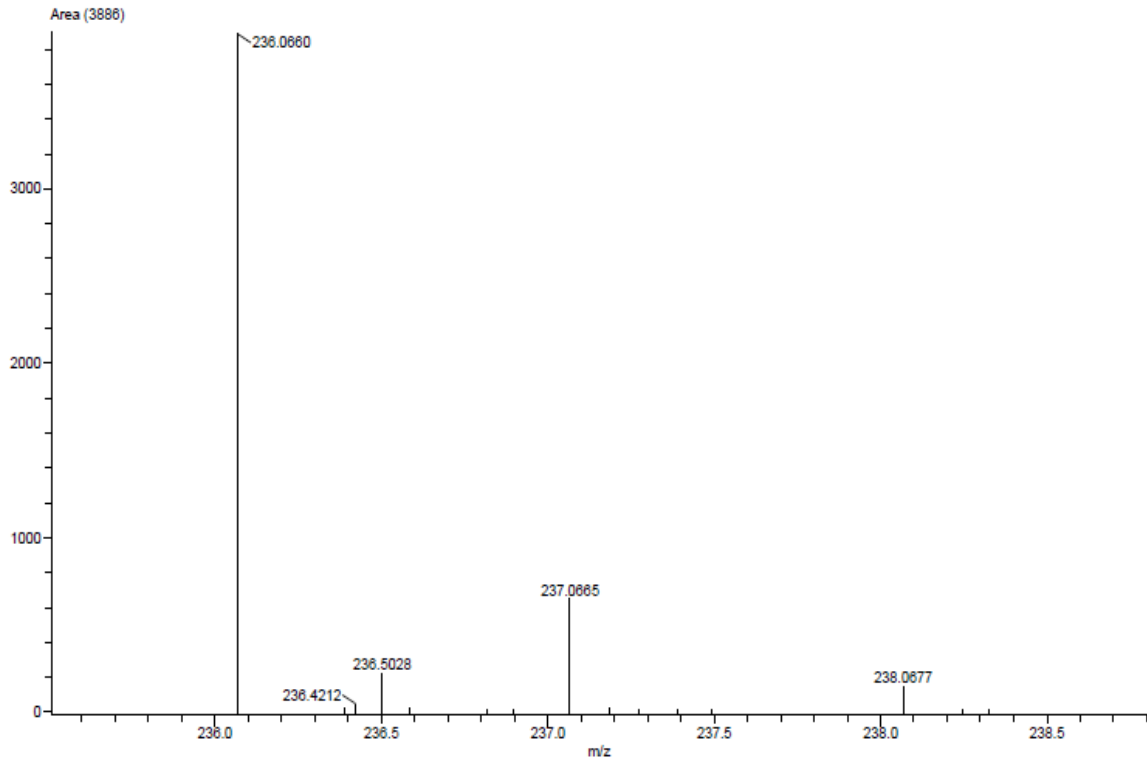
Acquisition Parameter					
Source Type	ESI	Ion Polarity	Positive	Set Nebulizer	1.2 Bar
Focus	Not active	Set Capillary	4500 V	Set Dry Heater	180 °C
Scan Begin	50 m/z	Set End Plate Offset	-500 V	Set Dry Gas	4.0 l/min
Scan End	1600 m/z			Set Divert Valve	Source



90

Acq. Data Name: rschim00497
Creation Parameters: Average(MS[1] Time:2.37..2.42)
Comment: dr20

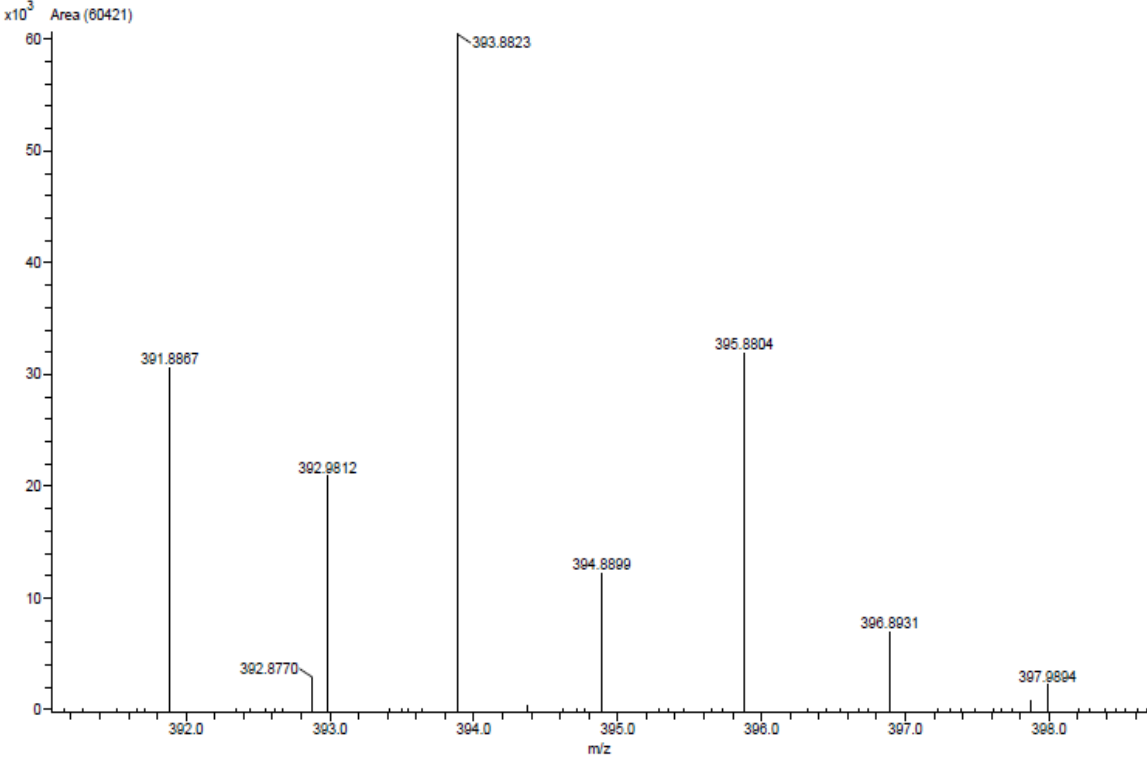
Experiment Date/Time: 4/16/2019 8:42:10 AM
Ionization Mode: EI+



91

Acq. Data Name: rschim00513
Creation Parameters: Average(MS[1] Time:2.32..2.39)
Comment: RS DR T Br

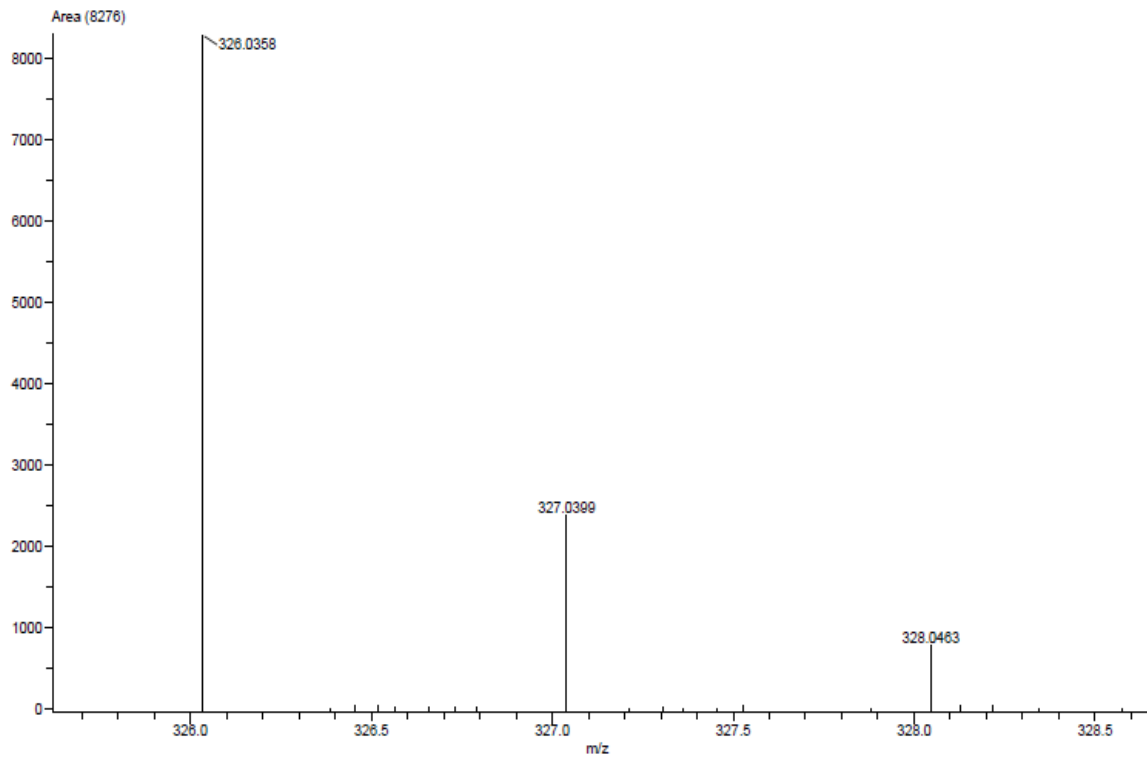
Experiment Date/Time: 5/15/2019 12:37:46 PM
Ionization Mode: EI+



92

Acq. Data Name: rschirm00512
Creation Parameters: Average(MS[1] Time:0.48..0.54)
Comment: RS DR T NO2

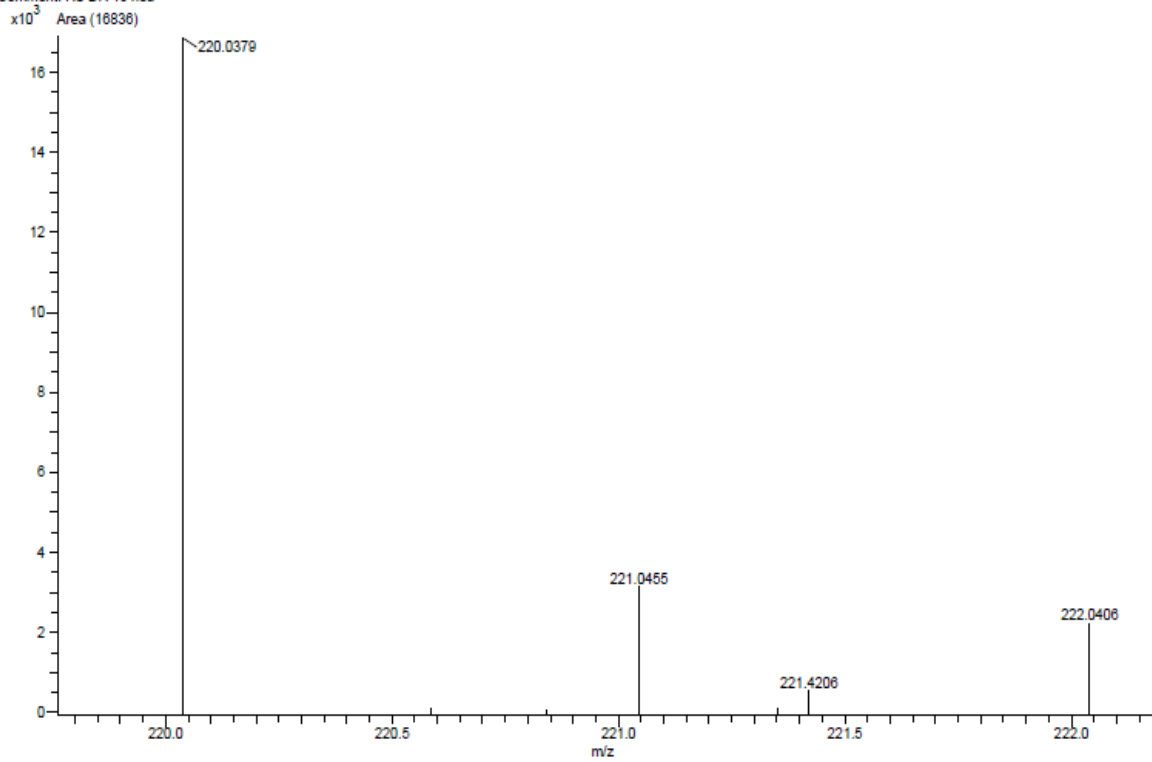
Experiment Date/Time: 5/15/2019 12:24:11 PM
Ionization Mode: EI+



93

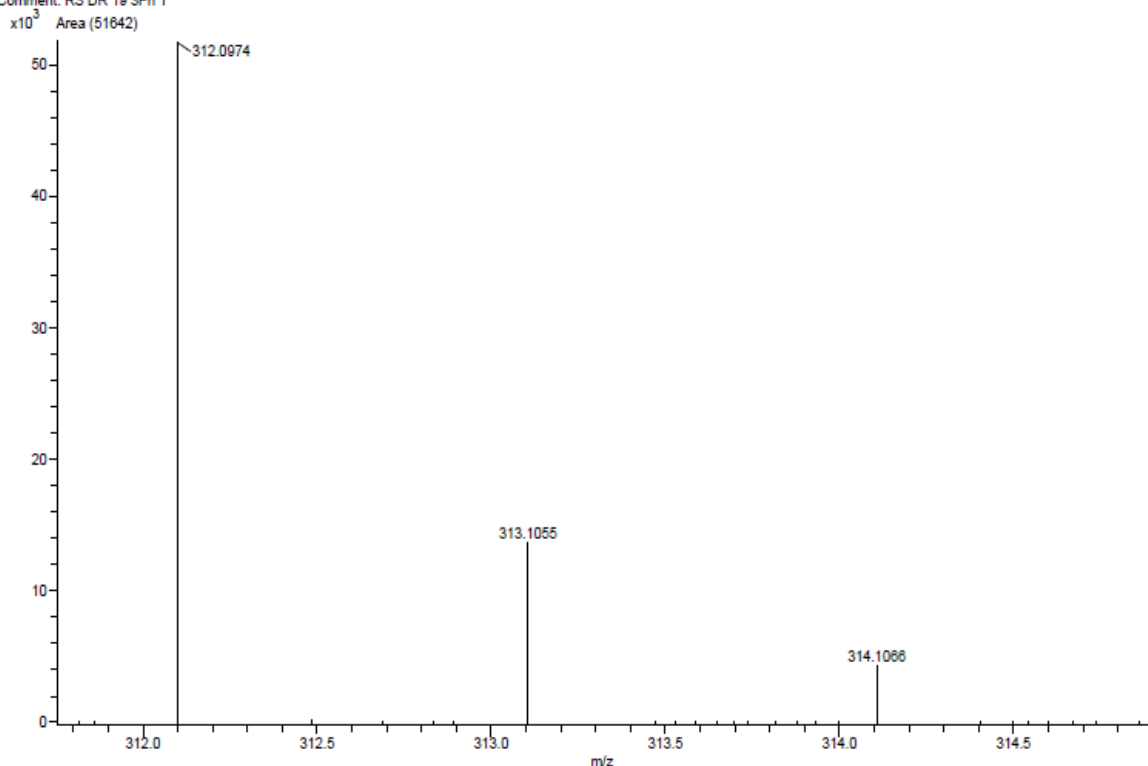
Acq. Data Name: rschirm00517
Creation Parameters: Average(MS[1] Time:1.13..1.13)
Comment: RS DR 19 neu

Experiment Date/Time: 5/20/2019 3:58:01 PM
Ionization Mode: EI+



Acq. Data Name: rschim00515
 Creation Parameters: Average(MS[1] Time: 1.11..1.21)
 Comment: RS DR 19 3Ph T

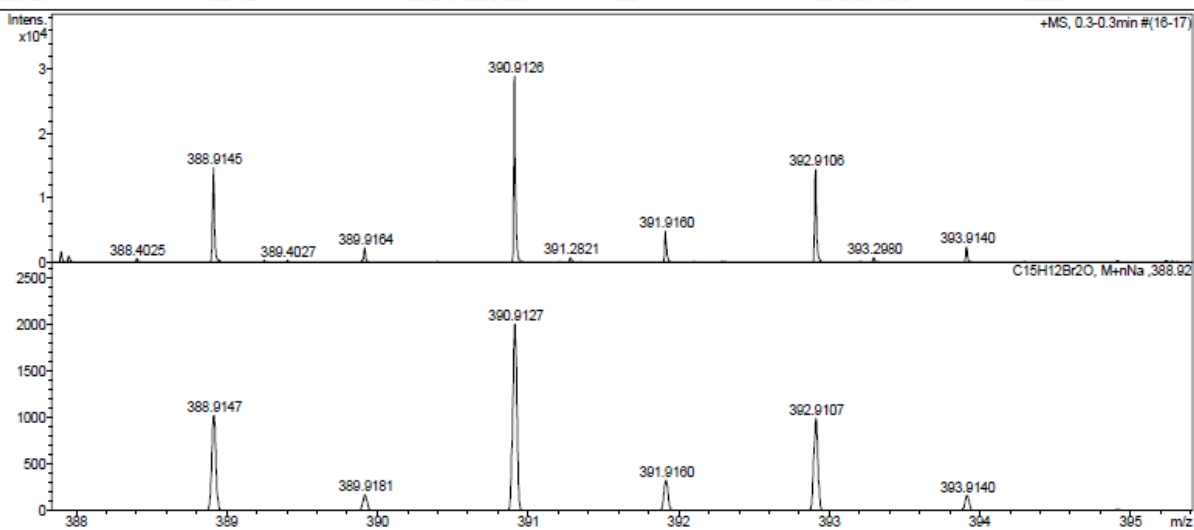
Experiment Date/Time: 5/20/2019 4:07:20 PM
 Ionization Mode: EI+



Display Report

Analysis Info		Acquisition Date	6/6/2018 6:48:23 AM
Analysis Name	D:\Data\2018\1806\180606\rschim00380_2_01_17994.d	Operator	BDAL@DE
Method	hystar_maxis_pl1.m	Instrument / Ser#	maXis 10138
Sample Name	rschim00380		
Comment			

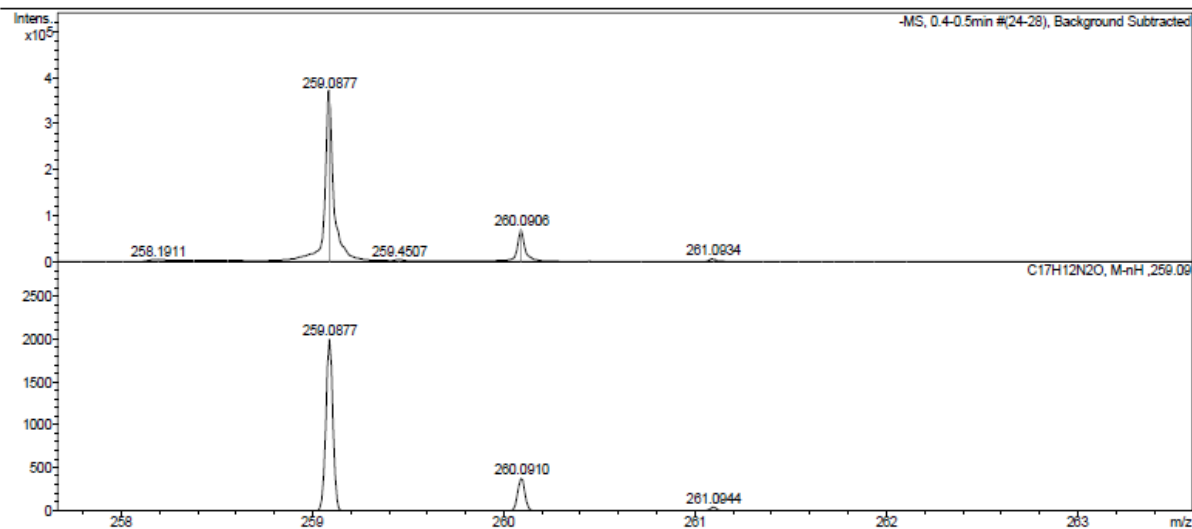
Acquisition Parameter					
Source Type	ESI	Ion Polarity	Positive	Set Nebulizer	0.3 Bar
Focus	Not active	Set Capillary	4500 V	Set Dry Heater	180 °C
Scan Begin	50 m/z	Set End Plate Offset	-500 V	Set Dry Gas	4.0 l/min
Scan End	1600 m/z			Set Divert Valve	Source



Display Report

Analysis Info		Acquisition Date	27.02.2018 08:29:40
Analysis Name	Z:\Data\2018\1802\1sam270218\neg\rschim00148_4_01_102284.d	Operator	BDAL@DE
Method	hystar_n1.m	Instrument / Ser#	micrOTOF 10237
Sample Name	rschim00148		
Comment			

Acquisition Parameter					
Source Type	ESI	Ion Polarity	Negative	Set Nebulizer	1.6 Bar
Focus	Not active			Set Dry Heater	180 °C
Scan Begin	50 m/z	Set Capillary	3800 V	Set Dry Gas	8.0 l/min
Scan End	1600 m/z	Set End Plate Offset	-500 V	Set Divert Valve	Source



Bruker Compass DataAnalysis 4.0

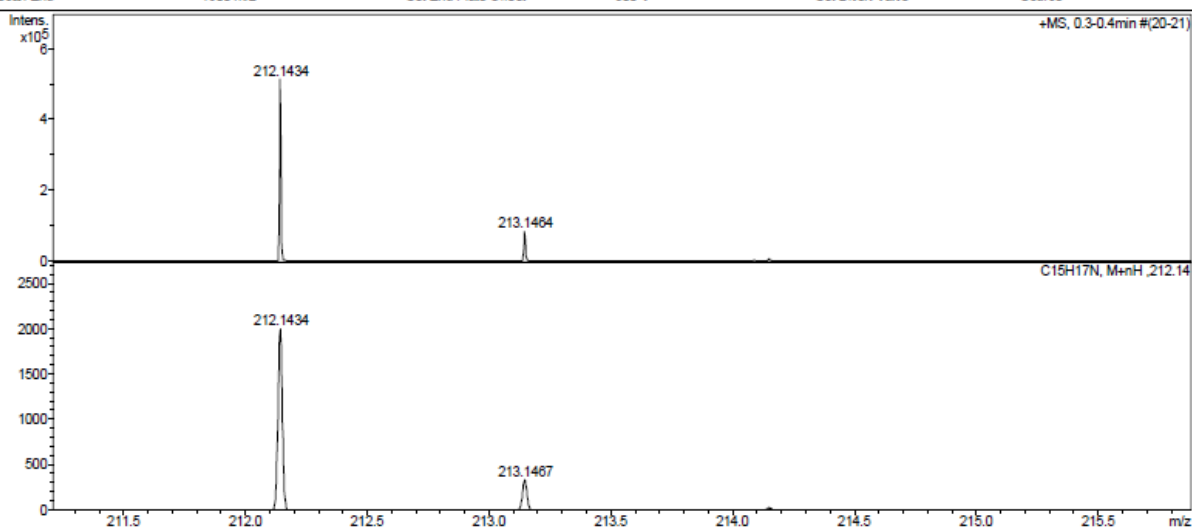
printed: 27.02.2018 08:36:26

Page 1 of 1

Display Report

Analysis Info		Acquisition Date	2/20/2018 7:50:45 AM
Analysis Name	D:\Data\2018\1802\180220\rschim00145_7_01_15864.d	Operator	BDAL@DE
Method	hystar_maxis_p11.m	Instrument / Ser#	maXis 10136
Sample Name	rschim00145		
Comment			

Acquisition Parameter					
Source Type	ESI	Ion Polarity	Positive	Set Nebulizer	0.3 Bar
Focus	Not active			Set Dry Heater	180 °C
Scan Begin	50 m/z	Set Capillary	4500 V	Set Dry Gas	4.0 l/min
Scan End	1600 m/z	Set End Plate Offset	-500 V	Set Divert Valve	Source



Bruker Compass DataAnalysis 4.0

printed: 2/20/2018 7:54:25 AM

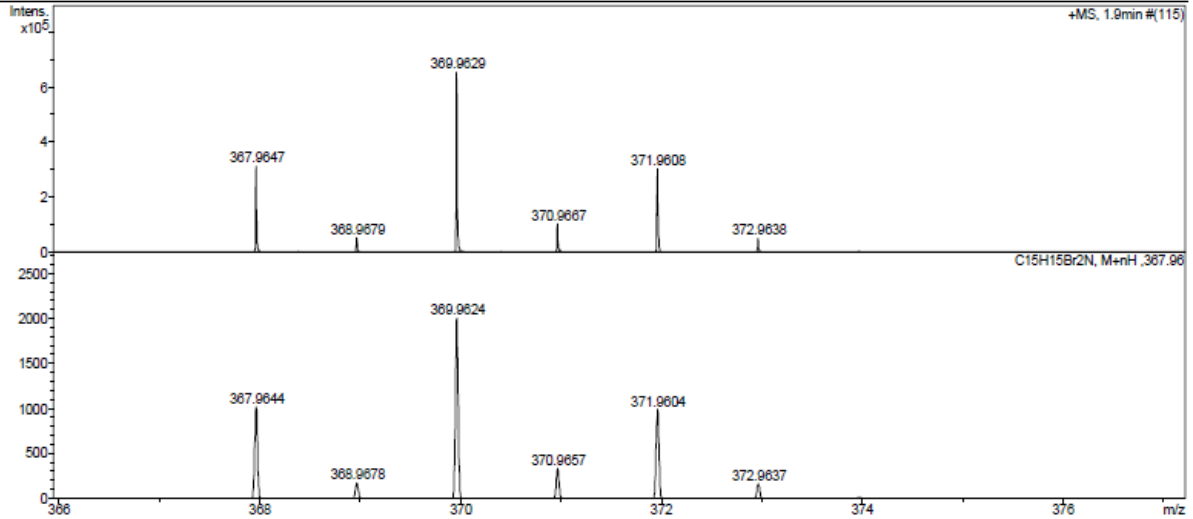
Page 1 of 1

101

Display Report

Analysis Info		Acquisition Date	9/5/2019 9:01:36 AM	
Analysis Name	D:\Data\2019\1909\190905\rschim00550_4_01_25956.d	Operator	BDAL@DE	
Method	hystar_maxis_pl1.m	Instrument / Ser#	maXis 10136	
Sample Name	rschim00550	Comment		

Acquisition Parameter					
Source Type	ESI	Ion Polarity	Positive	Set Nebulizer	0.3 Bar
Focus	Not active	Set Capillary	4200 V	Set Dry Heater	180 °C
Scan Begin	50 m/z	Set End Plate Offset	-500 V	Set Dry Gas	4.0 l/min
Scan End	1800 m/z			Set Divert Valve	Source

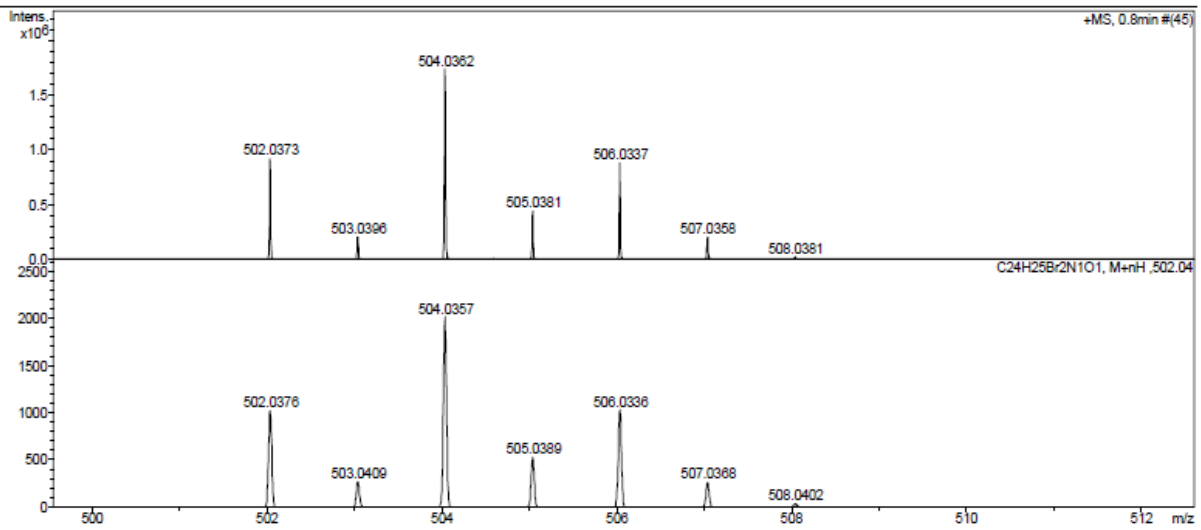


103

Display Report

Analysis Info		Acquisition Date	9/30/2019 9:36:29 AM	
Analysis Name	D:\Data\2019\1909\190930\rschim00561_1_01_26398.d	Operator	BDAL@DE	
Method	hystar_maxis_p.m	Instrument / Ser#	maXis 10136	
Sample Name	rschim00561	Comment		

Acquisition Parameter					
Source Type	ESI	Ion Polarity	Positive	Set Nebulizer	0.3 Bar
Focus	Not active	Set Capillary	4200 V	Set Dry Heater	180 °C
Scan Begin	300 m/z	Set End Plate Offset	-500 V	Set Dry Gas	4.0 l/min
Scan End	2900 m/z			Set Divert Valve	Waste

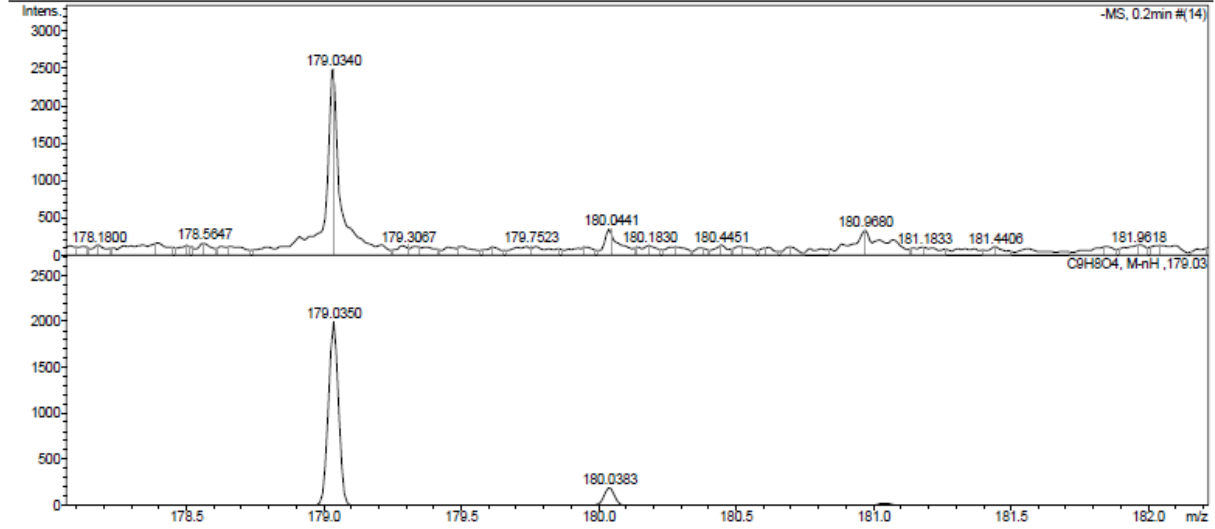


106

Display Report

Analysis Info
Analysis Name Z:\Data\2020\2011\sam041120\neg\rschirm00621_3_01_110579.d Acquisition Date 04.11.2020 15:10:03
Method hystar_nLm Operator BDAL@DE
Sample Name rschirm00621 Instrument / Ser# micrOTOF 10237
Comment

Acquisition Parameter
Source Type ESI Ion Polarity Negative Set Nebulizer 1.6 Bar
Focus Not active Set Dry Heater 180 °C
Scan Begin 50 m/z Set Capillary 3800 V Set Dry Gas 8.0 l/min
Scan End 1600 m/z Set End Plate Offset -500 V Set Divert Valve Source

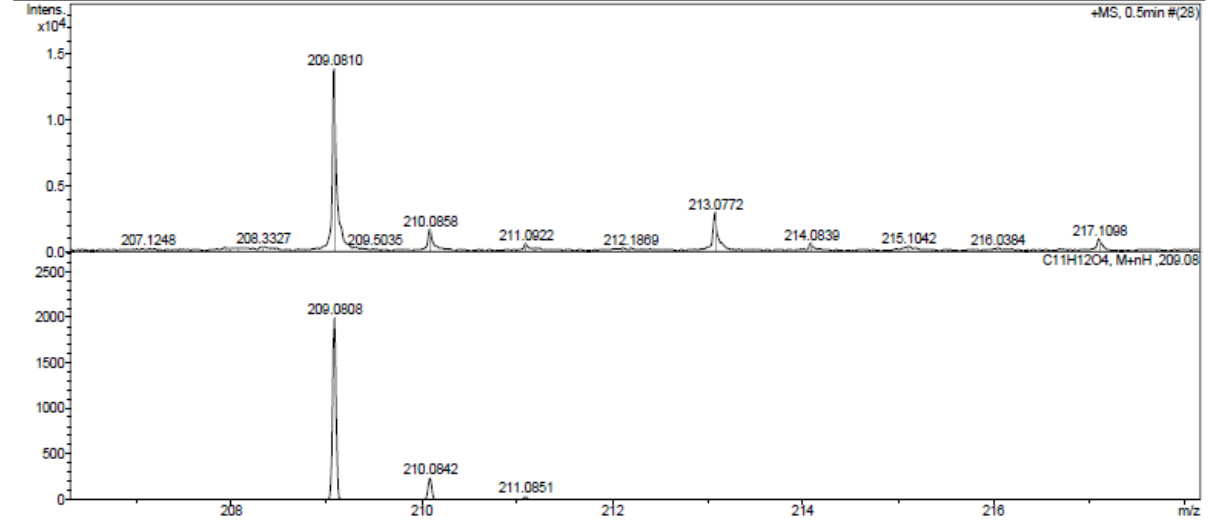


108

Display Report

Analysis Info
Analysis Name Z:\Data\2020\2011\sam061120\pos\rschirm00622_6_01_110630.d Acquisition Date 06.11.2020 11:56:24
Method hystar_pLm Operator BDAL@DE
Sample Name rschirm00622 Instrument / Ser# micrOTOF 10237
Comment

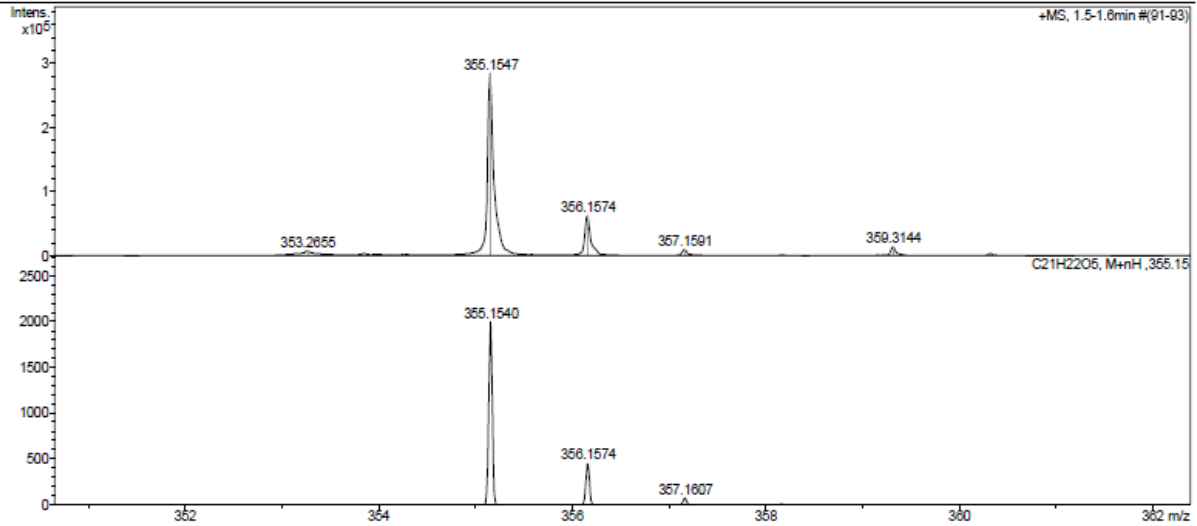
Acquisition Parameter
Source Type ESI Ion Polarity Positive Set Nebulizer 1.2 Bar
Focus Not active Set Dry Heater 180 °C
Scan Begin 50 m/z Set Capillary 4500 V Set Dry Gas 4.0 l/min
Scan End 1600 m/z Set End Plate Offset -500 V Set Divert Valve Source



Display Report

Analysis Info		Acquisition Date	09.11.2020 10:49:18	
Analysis Name	Z:\Data\2020\2011\sam091120\rschim00623_2_01_110839.d	Operator	BDAL@DE	
Method	hystar_plm	Instrument / Ser#	micrOTOF 10237	
Sample Name	rschim00623	Comment		

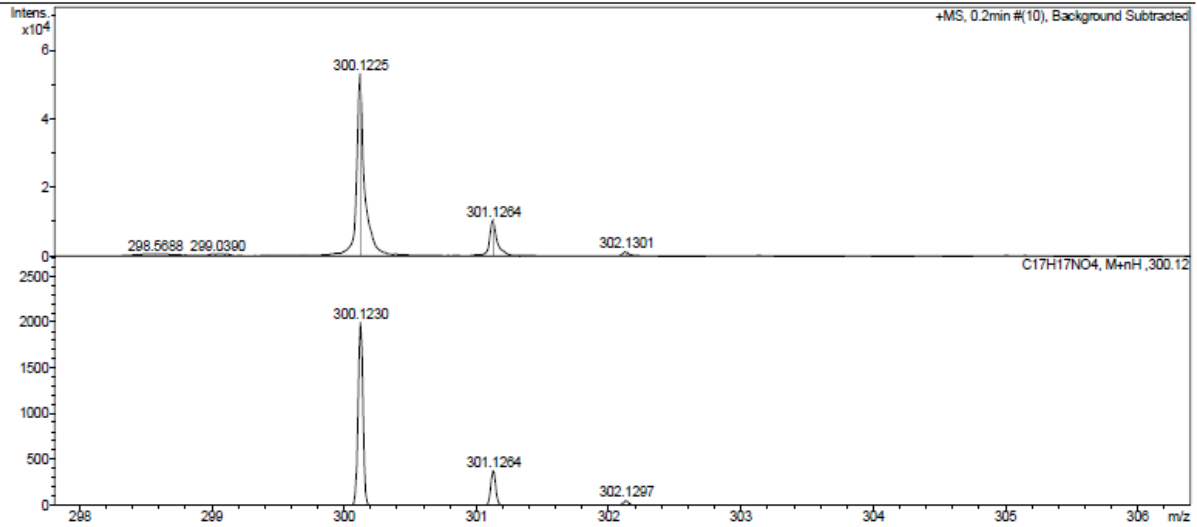
Acquisition Parameter					
Source Type	ESI	Ion Polarity	Positive	Set Nebulizer	1.2 Bar
Focus	Not active	Set Capillary	4500 V	Set Dry Heater	180 °C
Scan Begin	50 m/z	Set End Plate Offset	-500 V	Set Dry Gas	4.0 l/min
Scan End	1600 m/z			Set Divert Valve	Source



Display Report

Analysis Info		Acquisition Date	27.11.2020 07:27:28	
Analysis Name	Z:\Data\2020\2011\sam271120\rschim00625_4_01_110839.d	Operator	BDAL@DE	
Method	hystar_plm	Instrument / Ser#	micrOTOF 10237	
Sample Name	rschim00625	Comment		

Acquisition Parameter					
Source Type	ESI	Ion Polarity	Positive	Set Nebulizer	1.2 Bar
Focus	Not active	Set Capillary	4500 V	Set Dry Heater	180 °C
Scan Begin	50 m/z	Set End Plate Offset	-500 V	Set Dry Gas	4.0 l/min
Scan End	1600 m/z			Set Divert Valve	Source

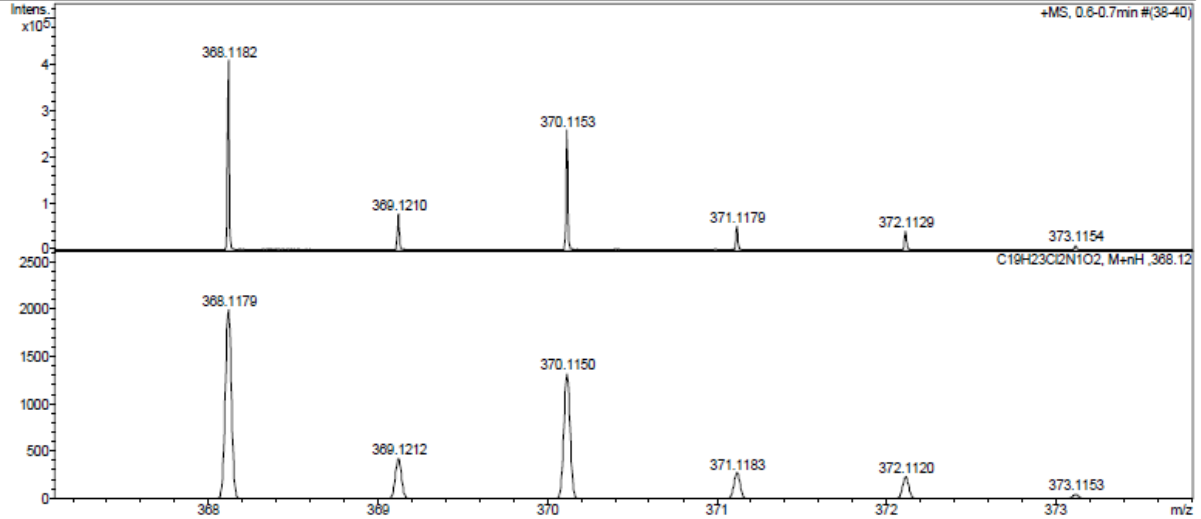


114

Display Report

Analysis Info
Analysis Name: D:\Data\2019\1909\190930\rschim00562_2_01_26399.d
Method: hystar_maxis_p.m
Sample Name: rschim00562
Acquisition Date: 9/30/2019 9:40:20 AM
Operator: BDAL@DE
Instrument / Ser#: maXis 10136

Acquisition Parameter
Source Type: ESI
Focus: Not active
Scan Begin: 300 m/z
Scan End: 2900 m/z
Ion Polarity: Positive
Set Capillary: 4200 V
Set End Plate Offset: -500 V
Set Nebulizer: 0.3 Bar
Set Dry Heater: 180 °C
Set Dry Gas: 4.0 l/min
Set Divert Valve: Waste

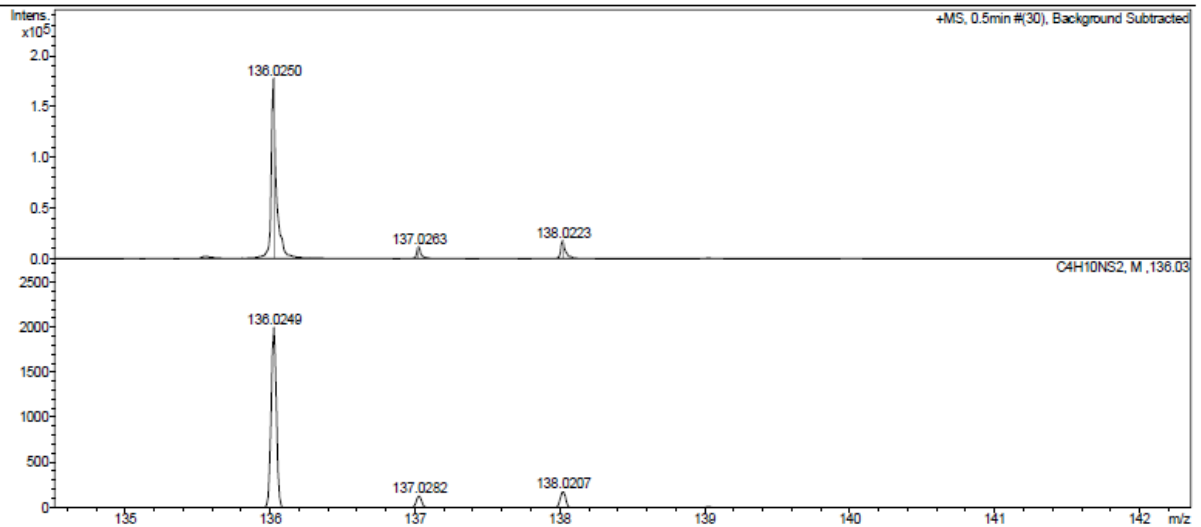


117

Display Report

Analysis Info
Analysis Name: Z:\Data\2019\1904\sam120419\rschim00498_9_01_106103.d
Method: hystar_pLm
Sample Name: rschim00498
Acquisition Date: 12.04.2019 07:55:28
Operator: BDAL@DE
Instrument / Ser#: micrOTOF 10237

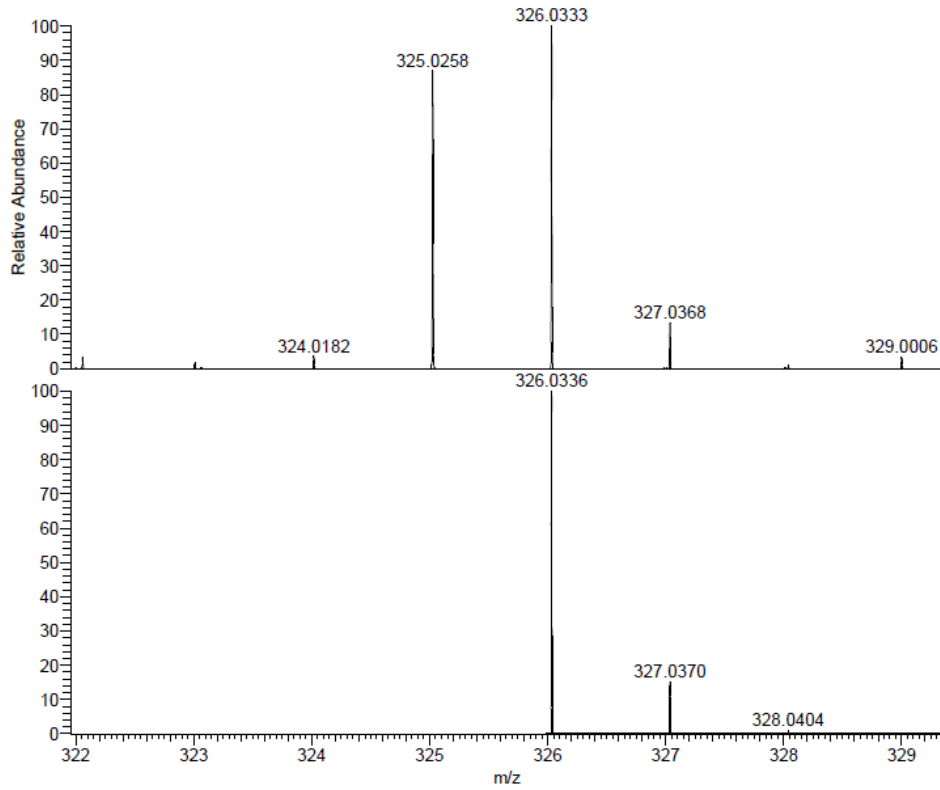
Acquisition Parameter
Source Type: ESI
Focus: Not active
Scan Begin: 50 m/z
Scan End: 1800 m/z
Ion Polarity: Positive
Set Capillary: 4500 V
Set End Plate Offset: -500 V
Set Nebulizer: 1.2 Bar
Set Dry Heater: 180 °C
Set Dry Gas: 4.0 l/min
Set Divert Valve: Source



120

C:\Xcalibur\data\rschim00602

06/29/20 08:24:09



NL:
2.13E9
rschim00602#169-176 RT:
0.48-0.50 AV: 8 SB: 1 1.50
T: FTMS + p EI Full ms
[60.0000-800.0000]

NL:
2.02E4
C₁₄H₆F₈:
C₁₄H₆F₈
p (gss, s/p:40) Chrg 1
R: 60000 Res .Pwr. @FWHM